Vern Dudley
EG&G
Div. 4721
Albuquerque, NM 87185

3008-2

Department of Energy
and
Sandia National Laboratories

Albuquerque, New Mexico 87185

Proceedings of the

LINE-FOCUS SOLAR THERMAL ENERGY TECHNOLOGY DEVELOPMENT

A SEMINAR FOR INDUSTRY

Albuquerque, New Mexico

September 9, 10, 11, 1980

Line-Focus Solar Thermal Energy
Technology Development Conference

Roscoe L. Champion, Conference Chairman
Component and Subsystem Development
Division 4722
Sandia National Laboratories

CONTENTS

Session I - Overview of Line-Focus Program

Virgil L. Dugan, Chairman
Solar Energy Projects Department 4720
Sandia National Laboratories

OVERVIEW OF LINE-FOCUS CONCENTRATOR PROGRAM

Virgil L. Dugan
Solar Energy Projects Department 4720
Sandia National Laboratories
Albuquerque, NM 87185

Background and Introduction

The Line-Focus Concentrator Program has emphasized the development and dissemination of solar technology in which the reflected sunlight is concentrated on a linear or line receiver. The primary objective of this program has been to assist in establishing viable solar resource options and a technological understanding which allows public decisions with high confidence.

The strategy for accomplishing this objective and for promoting the commercialization of line-focus concentrators involves improving the performance and the reliability of hardware at the component, subsystem, and systems levels; reducing the cost associated with installation of the systems; and allowing opportunities for increasing the production levels so that mass production technology can become a reality. A brief synopsis of activities and accomplishments relative to these strategies in fiscal 1980 is presented in the following sections.

Thermal Performance

In FY79, two engineering prototype parabolic trough modules were assembled at Sandia National Laboratories to provide a documented indication of the performance potential of parabolic trough solar collectors. One of these units was based upon an aluminum honeycomb sandwich structure manufactured by Hexcel and used mechanically formed, chemically strengthened glass as the reflector surface. The other unit was based upon a fiberglass honeycomb sandwich structure built by Custom Engineering and used thermally formed glass as the reflector surface. Both of these units demonstrated an ability to convert in excess of 60% of the incident sunlight to thermal energy at temperatures of 315°C. This demonstration provided a baseline for glass reflector technology and set a near-term performance goal for the collector manufacturing industry. Additional development activities sponsored through Sandia have established glass reflectors as viable alternatives for both present and future generations of parabolic trough collectors.

In FY80, many of the commercial parabolic trough manufacturers have approached or exceeded the near-term goal which had been established. One commercial parabolic trough collector tested has demonstrated performance approaching long term goals. With further improvements in the reflector structure manufacturing and alignment techniques and with additional improvements in glass technology, it appears that the near-term performance goal which was set will be consistently exceeded by commercial manufacturers in the near future.

Another class of line-focus concentrator which is termed a fixed mirror distributed focus (FMDF) collector or "bowl" has demonstrated a peak thermal efficiency in excess of 60% at an operating temperature in excess of 500°C and a pressure of 1000 psi. This test unit is operated by Texas Tech University at Crosbyton, Texas.

Current Cost Estimates

System demonstrations using parabolic troughs which were designed and built in the 1978 and 1979 time frames costed approximately 100 $\$/ft^2$ of installed collector aperture. In 1980, the detailed cost estimates for completely installed industrial process heat systems are running 40-50 $\$/ft^2$ of installed aperture; this is the complete cost for a turn-key system.

Figure 1 shows the progression of energy cost steps which are planned in the future technology development process. Note that the equivalent cost of energy from a current solar industrial process heat (IPH) system based upon an installed system cost of 40-50 $\$/ft^2$, nominal annual performance of 0.25 to 0.28 $MMBTU/ft^2/yr$, and current (not exaggerated) economic parameters lies in the range from 16 to 28 \$/MMBTU. This 1980 accomplishment is well within the window which had been previously defined. It is expected that the development of modular ΔT strings for line concentrator systems and of modular system designs will enable a great deal of the construction work currently done on-site to be done in a manufacturing environment and will significantly reduce the overall installation and construction cost. This step, which should begin in the early 1980's, should reduce the total installed system cost below the 30 $\$/ft^2$ level. With systems costing less than 30 $\$/ft^2$ and the development of a moderate set of financial incentives, midtemperature industrial process heat using line focus concentrators will be competitive with the upper ranges of heat provided by oil and natural gas in the mid-1980's.

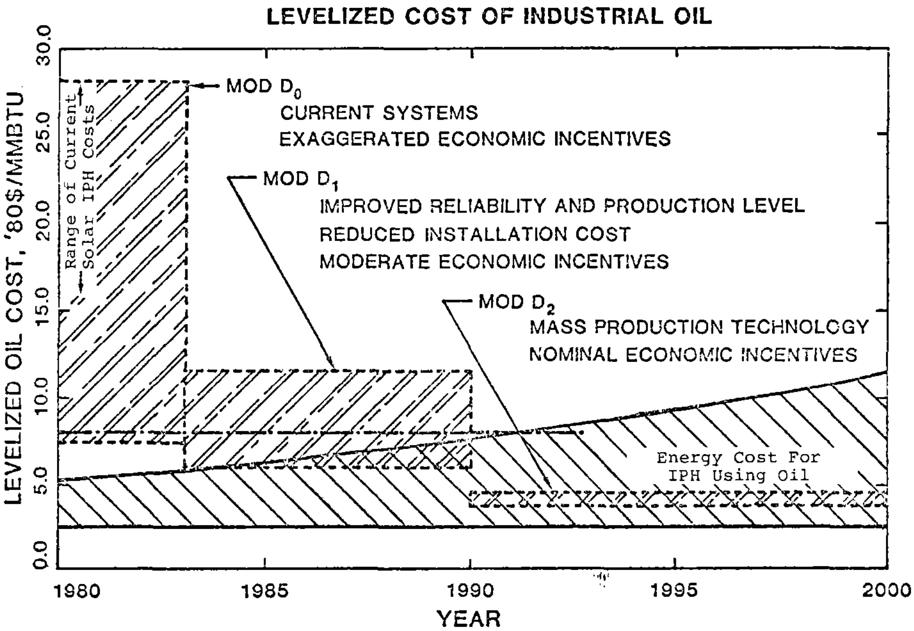

FIGURE 1

Systems Technology Demonstrations

Three operating solar electric systems which utilize parabolic trough technology have been built for irrigation pumping applications. Two of these, the Willard, New Mexico, system and the Gila Bend, Arizona, system have completed several years of experimental operation and have demonstrated both the feasibility of the technology involved in operating a combined solar thermal/organic Rankine-cycle turbine system and the procedures required for system control. Operation of the Gila Bend system was discontinued at the end of calendar year 1979 due to the completion of a set of experimental and operational exercises and because of the emergence of more current solar and engine technologies. Operation of the Willard system was discontinued in July of this year. Again, the technology base which is associated with this system has been fully explored and attention will be focused on the more recent systems applications.

The most recent demonstration of a system level technology for thermal-electric conversion has been a 23,000 ft^2 parabolic trough system installed at Coolidge, Arizona. This system powers a Sundstrand organic Rankine-cycle turbine which operates on a toluene working fluid at an input temperature of 290°C. The peak performance of this system is approximately 200 kWe. Dedication of this system occurred in November of 1979. An experimental program designed to completely characterize the system performance under a number of operating scenarios is currently underway.

There are currently nine industrial process heat systems which are in various phases of operational status or construction. The most recent of these is a system installed at the Johnson and Johnson plant in Sherman, Texas. The heat delivered by the system (350-370°F) provides steam for plant operations at approximately 100 psi. Additional industrial process heat systems using parabolic trough technology are in the final design stages, and construction of a number of these should begin sometime during 1980.

There are currently a number of operating oil companies who are considering the purchase of parabolic trough systems to provide process steam for enhanced oil recovery. This is being particularly emphasized by an incentives program designed for the expansion of enhanced oil recovery by any suitable means. This incentive program will be completed at the end of FY81.

Commercial Availability

Sandia National Laboratories has surveyed the potential set of line concentrator manufacturers in order to appraise the manufacturing capability which currently exists. In this exercise, at least 26 manufacturers of line concentrator technology have been identified. The designs of 15 of these manufacturers have been found to meet at least the minimum requirements for industrial process heat applications up to 350-400°F. The collector hardware from these 15 organizations is currently being evaluated at either the Midtemperature Solar System Test Facility at Sandia or at either DSET or Wyle Laboratories. Both DSET and Wyle Laboratories have been recently qualified as commercial testing laboratories for collector evaluation and characterization. This qualification was performed by Sandia in an effort to set up a completely independent test capability.

Present Technology Development Emphasis

As mentioned earlier, one key step in furthering the commercial progress of line concentrator technology is to reduce the installation cost for the systems. The key program element designed to accomplish this step is the Modular Industrial Solar Retrofit (MISR) Project. MISR is intended to allow the existing collector manufacturing complex to develop integrated, modular ΔT strings which can be fabricated within a production complex and installed at the site with a minimum of site labor. This project has been begun in FY80 and is intended to become fully operational in FY81.

In parallel with the effort to significantly reduce site installation and construction costs, there are a number of technology development activities which are intended to (1) allow improvements in the operational reliability and performance of current systems, and (2) allow for the emergence of more mass production oriented systems. Among these is the development of stamped sheet metal trough structures by The Budd Company, the development of sheet molding compound (SMC) trough structures by The Budd Company, the development of thermally formed glass laminate structures by Ford and PPG, and the development of aluminum honeycomb sandwich structures by Hexcel. Also, a new generation of system control technology is being developed by Honeywell; the Operational reliability and performance of black chrome selective coatings is being improved; receivers are being improved using better sealing techniques, thermocline storage techniques are being enhanced; pipe heat loss problems are being defined and eliminated; and optimal collector field layouts are being configured by Jacobs Engineering. Most of these technology endeavors will be demonstrated in the late FY80 and FY81 time frames.

It is the intent to publish a similar report of this type at this approximate date in FY81 to provide another update on the progress of line focus concentrator technology.

Session II - Line-Focus System Development

James A. Leonard, Chairman
Systems and Applications
Development Division 4725
Sandia National Laboratories

SOLAR ENHANCED OIL RECOVERY; A REVIEW OF CURRENT ACTIVITIES AND PROGRESS

Kenneth D. Bergeron
Systems Analysis Division 4723
Sandia National Laboratories
Albuquerque, NM 87185

I. The Prospects and Potential of SEOR

For more than 15 years, the production of many U. S. oil fields has been enhanced by the injection of huge quantities of steam, which permeates the reservoir, heating the heavy crude and reducing its viscosity. The idea behind Solar Enhanced Oil Recovery (SEOR) is simply that concentrating solar collectors are used instead of fossil-fired boilers to generate the steam. Recently, SEOR has received considerable attention as a favorable application of solar energy and as a potential early market opportunity.

A unique feature of SEOR, when it is considered as a solar industrial process heat application, is that the output of the "process" is oil, which is also the fuel being displaced by solar. For this reason, it is possible to identify several different competitive regimes, depending on the relative costs of solar and fossil energy and on the characteristics of the reservoir. This is illustrated schematically in Figure 1.

The quantity, b, plotted vertically, is the energy (expressed in equivalent barrels of oil) required to generate enough steam to produce one barrel of oil by steam EOR. This quantity varies from reservoir to reservoir, depending on the oil saturation and the physical properties of the producing formation. Clearly, the lower the value of b, the more profitable the operation will be. Conversely, if b is larger than some critical value, denoted b_c in the figure, a profit cannot be made with conventional steam EOR. (The value of b_c is a matter of judgement by the producer, but it clearly must be considerably less than one. Values of b ranging from .2 to .4 are typical of current projects.)

Along the horizontal axis is plotted the ratio of the levelized energy costs of solar and fossil fuels, taking account of operating expenses, taxes, etc. As this ratio decreases, solar EOR becomes more competitive, and the maximum value of b at which a profit can be made increases. We denote this solar breakeven value b_s, and a hypothetical curve is identified as the "Solar Profit Line" in the figure.

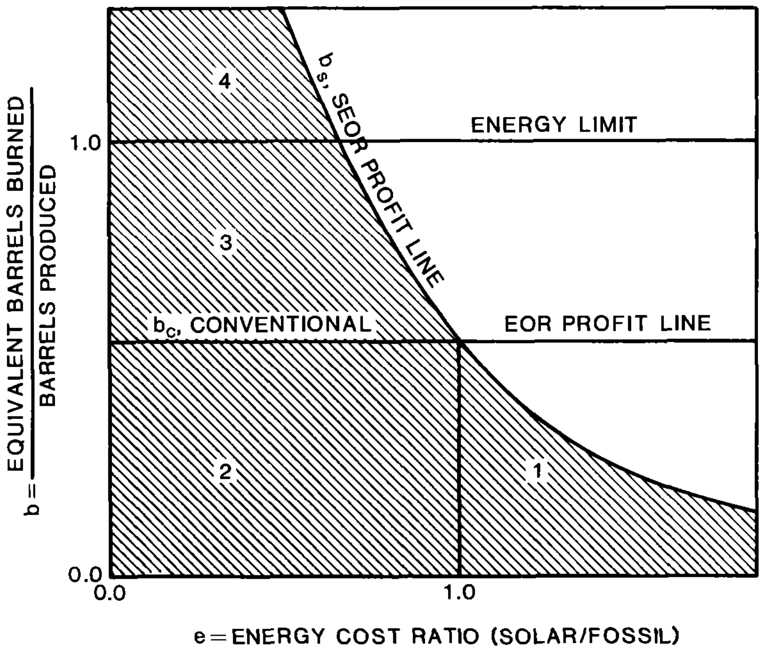

Figure 1. Regions of SEOR Profitability (Shaded Area) and Competitiveness with Conventional EOR (Regimes 1-4, Described in the Text)

Using this format, it is possible to identify different regimes of competition, corresponding to different economic conditions and reservoir types. The different cases result from the fact that not only must solar EOR make a profit ($b < b_s$), but also it must fare better than the competition. The different competitive regimes can be identified in the order in which they would occur in time (as the energy cost ratio decreases) as follows:

Regime 1: Constrained Competition--Since $e > 1$, solar would not compete in a free market for these conditions. However, one could imagine statutory restrictions which are so severe that the burning of liquid fuels for EOR would be effectively prohibited. If these conditions persisted, one might expect SEOR to be utilized. (Since $b < b_s$, it is a profitable venture.) The amount of such market penetration seems likely to be quite small, however, if only because most of the reservoirs with low values of b have already been depleted.

Regime 2: Direct Competition--Here, solar would be used for reservoirs which would have been steamed conventionally if solar were not more cost effective. The threshold, $e = 1$, at which SEOR breaks even was analyzed quantitatively in some detail in References 2 and 3. It is likely that fields with values of b less than

b_c will be the initial targets for SEOR, once cost competitiveness is established. This approach would minimize risk and maximize profits, but it is not a strategy which can be pursued indefinitely because the resource will eventually be depleted; the only reservoirs remaining will have values of $b > b_c$. For example, it is often predicted that the Kern River Valley (California) in which most of the current U. S. steam EOR production occurs, will be "steamed out" by some time in the 1990s. (Note that for simplicity we are discussing the cases of $b > b_c$ and $b < b_c$ as if they always correspond to distinct and different reservoirs. In actuality, a conventional steam drive has a value of b which slowly increases over time and is terminated when the economic limit b_c is reached. Another simplification is to treat b as if it is known in advance, when in fact it is often difficult to predict.)

<u>Regime 3</u>: <u>Extended Reserves</u>--The eventual exhaustion of the thermal EOR proven reserves (based on conventional EOR economics) is sometimes taken to imply that SEOR has a finite time window during which it must penetrate and exploit the market. This is a fallacy, however, because reservoirs with $b > b_c$ will not be steamed conventionally and will remain available as a potential resource for SEOR until the solar energy cost ratio has reached a value low enough to merit an SEOR operation. This is defined by region 3 on the figure, and it is important to note that this market will appear as soon as the cost breakeven point is reached.

<u>Regime 4</u>: <u>The Energy Limit; SEOR as Solar/Chemical Energy Conversion</u>--If all energy had equal value, it would never make sense to steam a reservoir with $b > 1$, because there would be a negative energy balance. However, liquid and gaseous chemical fuels are more valuable than their thermal energy equivalent because they are more versatile, transportable and storable. For this reason it is anticipated that an energy and economic price can rationally be paid to convert solar energy to chemical energy (e.g., hydrogen or alcohol). The same reasoning can justify SEOR in Regime 4, (though the additional cost of refining the crude oil to a premium fuel will have to be taken into account). Some unconventional resources, such as tar sand deposits, might also be included in this reservoir category. It will be many years before conditions such as these come to pass, but the existence of reservoirs in Regime 4 provides additional motivation to pursue SEOR as part of an energy policy which is oriented towards both near-term and long-term energy supplies.

II. Current Activities

Recently, the growing interest in SEOR has resulted in a number of activities, both in the private sector and by the Department of Energy and its contractors. Most of the private sector efforts have been exploratory studies by oil companies, both large and small. At the present time, results and details of most of this work have not been made public, but there is reason to believe that concrete decisions about whether or not to construct pilot SEOR systems will be made in the next several months. The principal reason for this timetable is the existence of a very favorable combination of solar tax credits and incentives from the Tertiary Incentives Program (TIP) established by the Energy Regulatory Administration (regulation 10 CRF 212). This program was established to provide incentives for all enhanced oil recovery, including chemical injections, in-situ combustion, etc. The provisions allow up to 75% of the capital costs of certain types of equipment to be recovered immediately by selling controlled (e.g., lower tier) oil at world oil prices. There are two important limitations to this incentive:

(a) not all oil companies have sufficient quantities of controlled oil to sell to be able to take full advantage of the TIP

(b) with oil price decontrol (scheduled for October 1981) the incentive disappears.

However, if full use of the TIP is made, and if the tax benefits of depreciation deductions, and federal and California solar investment tax credits are taken into account, the combined effect is to recoup 99% of the capital cost of the solar energy system.[4] Thirty-nine percent of this is from tertiary incentive revenues, so there is strong motivation to initiate the construction of SEOR projects within the next year.

The Department of Energy program on SEOR can be divided into two parts. First, there have been a number of preliminary feasibility studies undertaken by Sandia,[2,3] SERI,[5] Booz-Allen-Hamilton,[6] and others. Aerospace Corporation has recently been playing a leading role in coordinating this type of activity.

Second, two contracts were awarded for Feasibility and Design (Phase I) Studies of line focus solar energy systems at specific oil fields. The two contractors were Exxon, Inc., and the team of General Atomic/Petro Lewis Corporation.

The General Atomic system uses the Fixed Mirror Solar Collector (FMSC) concept which has been under development for several years. Heat transfer oil passing through the tracking receiver tube would be heated to 612°F and then pumped through a heat exchanger, generating steam at 700 psi, which is piped directly to the oil field.

The Exxon proposal utilizes a field of parabolic troughs to heat pressurized water to 250°F before being pumped into the fossil fired boiler. The reason the preheat mode was chosen is that the resulting low field temperature allows the collectors to operate at a higher efficiency (thermal losses are lower). Also, water at a relatively low pressure can be used as the heat transfer fluid, resulting in greater simplicity and presumably higher reliability.

Subsequent to the completion of their study, Exxon is considering the construction of a 100,000 ft^2 field of trough collectors without DOE support. The reason for choosing against direct federal support was simply that it would subtract from the other incentives mentioned above, resulting in an insignificant improvement in the economics of the project.

Exxon has also participated in a conceptual design study for a solar central receiver system for enhanced oil recovery. This was a collaborative effort with Martin Marietta as prime contractor, in response to a DOE Request for Proposals for Solar Repowering/Industrial Retrofit Systems. The proposed system would use more than 4. x 10^5 ft^2 of heliostats and a water/steam receiver. The design point output would be 29 MW_t of steam at 567°F (1200 psi).

III. Progress on Technical Issues

As with any new technological development, there are many unanswered questions concerning SEOR, making it difficult to assess its true potential. Many of these issues will take a long time to resolve, but some progress is being made in a few important areas. These include:

(a) Land Availability--As part of its study for the parabolic trough project, Exxon undertook a preliminary market study. One purpose was to estimate the size of the potential market for solar collectors for SEOR. In essence, this was a land availability study, because the approach was to identify the major California fields believed to be suitable for steam EOR and then to analyze each location very carefully for the availability of adjacent and suitable (e.g., flat) land. Using quite conservative criteria, it was estimated that the market potential for domestic SEOR was 325 x 10^6 ft^2 of solar collectors by 1990.

(b) Storage or Backup Requirements--An interesting possibility which has often been discussed in relation to SEOR is whether it is feasible to inject steam intermittently (when the sun shines) to achieve the same effect as the same average rate injected continuously. If this were possible, it would allow a stand-alone solar EOR system to be designed without the added cost of high temperature storage. A recent study at the University of Southern California has indicated that the effect of intermittency on oil production is small.[7] An experiment using scaled physical models compared the oil production of a continuous injection operation to the case when the injection rate was zero for half the "day" and twice the continuous rate the other half. (See Figure 2). It was found that after a delay period of about one year, the output from the diurnal operation matched the continuous one, and that eventually the total number of barrels recovered was approximately the same for the two cases.

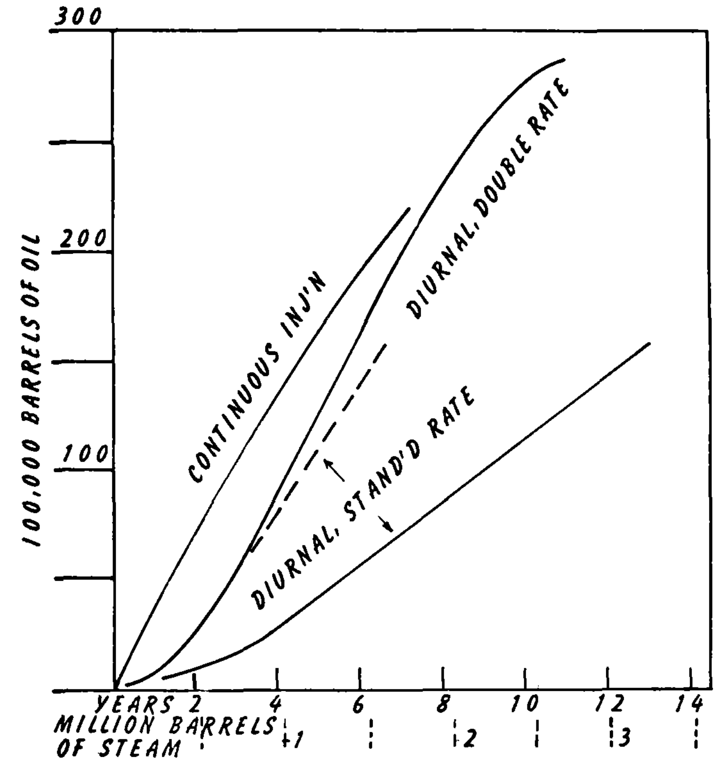

Figure 2. Cumulative Enhanced Oil Production Predicted by Scaled Physical Model Experiments (Ref. 7)

It remains to be proven, of course, whether this result will also occur in an actual petroleum reservoir. If it does, then fossil or thermal storage backup will not be necessary. However, it is important to keep this issue in perspective. As long as the energy cost ratio (see Figure 1) is not much less than 1, using a fossil backup may still be a cost-effective approach when all of the effects of daily cycling of steam injection are taken into account. There may also be a modified intermittent injection strategy (identified as "pressure maintenance" in Ref. 3) which has the advantages of continuous injection with a reduced consumption of backup fuel.

(c) Steam Pressure Requirements--An important question, which strongly impacts the role that line focus collectors can play in SEOR, is what the steam pressure requirements are. This is not the same question as what pressures do SEOR boilers typically operate at, because this pressure is often throttled down before the steam enters the injector well. There are two clear bounds on steam pressure at the bottom of the injector: it must be greater than the reservoir pressure and less than the pressure at which the formation will fracture and form channels (typically the lithostatic pressure). In many cases, these values bracket a broad pressure range (e.g., 50 psi to 900 psi). Unfortunately, the steam drive process is so complex and project time scales are so long (7 or more years) that the long-term response of the reservoir as a function different pressures within this range cannot now be accurately predicted.

Until a better understanding of the mechanisms of thermal EOR is obtained, perhaps the best way of estimating steam requirements would be to find out the wellhead pressures actually being used at conventional EOR facilities (though the possibility must be kept in mind that significantly reduced pressure may have a very small effect on performance). Most surveys (e.g., Exxon's market study and Ref. 2) indicate that there is a broad range of injection pressures, depending on the reservoir characteristics and on the oil company's standard practice (which can vary substantially from one company to the next). Average values of 400-500 psi are found, but there are some reservoirs with much higher (e.g., 900 psi) and much lower (e.g., 100 psi) pressures. Since parabolic troughs are capable of delivering thermal energy at 550°-600°F and since 450 psi steam corresponds to 450°F, it is clear that a large portion of the SEOR market is suited to trough collector systems. It is also clear that in some cases the steam pressures are too high and that only a point focus system would suffice. The logical conclusion is that both line focus and point focus systems are likely to have an important role to play in SEOR unless economics clearly eliminates one in favor of the other, a determination which should be made in the marketplace.

References

1. Solar Enhanced Oil Recovery Multi-Year Plan," (draft 7 July 1980), The Aerospace Corporation, El Segundo, CA.

2. K. D. Bergeron, "Solar Enhanced Oil Recovery: An Assessment of Economic Feasibility," Energy, 4, 1127 (1979); also SAND79-0787, Sandia Laboratories, Albuquerque, NM.

3. K. D. Bergeron, "Preliminary Assessment of Solar Enhanced Oil Recovery," Proceedings of the 2nd Miami International Conference on Alternative Energy Sources, Miami Beach, FL, December 1979.

4. R. Garman, "Potential for Solar Thermal Enhanced Oil Recovery," presentation to DOE/Fossil Symposium, August 1980.

5. P. deLeon, K. C. Brown, J. W. Margolis and L. H. Nasr, "Solar Technology Application to Enhanced Oil Recovery," SERI/TR-352-392, Solar Energy Research Institute, Golden, CO.

6. P. J. McCann, J. D. White and W. F. Adolfson, "Solar Steam Generation for Enhanced Oil Recovery," Proceedings of the 4th National Technology for Energy Conservation Conference, Albuquerque, NM, October 1979.

7. T. M. Doscher, F. Ghassemi and O. Omoregie, "The Anticipated Effect of Diurnal Injection on Steam Drive Efficiency," Society of Petroleum Engineers, SPE8885, April 1980.

A SENSITIVITY ANALYSIS OF SOLAR RANKINE COGENERATION SYSTEMS

Ralph R. Peters
Systems Analysis Division 4723
Sandia National Laboratories
Albuquerque NM 87185

Introduction

Sandia National Laboratories is evaluating a Performance Prototype Trough (PPT) Collector as a part of the Department of Energy's research and development program for solar-thermal energy systems. Included in this effort are analyses to determine the most advantageous use of second-generation trough collectors similar to the PPT. The sensitivity of the Solar Rankine Cogeneration (SRC) System design and economic feasibility to changes in system parameters has been investigated. SRC systems also were compared to Solar Process Heat (SPH) and Fossil Fuel Total Energy (FFTE) Systems. The results of this analysis are the subject of this paper.

Scope

Second-generation trough collectors similar to the PPT are expected to become operational in the near future (circa 1985). The scenario used in this analysis was chosen to be consistent with the projected date of availability. The user was assumed to be an industrial or commercial business which supplements its energy needs with solar energy from the SRC or SPH system. Since the energy requirements will probably be much larger than that which the SRC system can provide, the electrical-to-thermal (E/T) output ratio may be varied to produce the most economical system. The user may have to pay demand charges, so the SRC system must provide energy in a predetermined manner, not just when the sun shines. Thus, the system is a hybrid and the shape of the system output profile (or load) can become important. The percentage of this load, which is supplied by solar energy, will also be important. The orientation of the collector's axis of rotation (which affects the output profile) and the unit cost for collectors and thermal storage also affect system design and economics.

The particular cases investigated are listed in Table I. The load shape was considered important, so the effect of three different generic types was investigated. Plots of these loads can be found in Figures 1-4. These loads represent the electrical load requirement (peak value-200 kW) for the SRC systems with the thermal load of steam at 338°F (170°C) and 115 psia (0.79 MPa) essentially tracking it. The solar-based loads were designed to match the output profiles of the collector field on a certain clear day for each season. Because the output profile of a trough collector

TABLE I. Scope of Study

System Loads	Solar Fraction	Collector Orientation	System Cost
1. 24-hr load	1. 40%	1. N-S axis of rotation	1. Low cost [$208/m^2 of collector-dual media storage]
2. 8-hr load	2. 60%	2. E-W axis of rotation	2. High cost [$290/m^2 of collector-bulk fluid storage
3. Solar-Based load (one each for N-S & E-W axis fields)	3. 80%		
	4. Optimum		

SYSTEM CONFIGURATIONS

		Collector		Storage	Turbine		
Case	E/T	T_{Outlet} °F(°C)	$T_{Average}$ °F(°C)	ΔT °F(°C)	T_{Inlet} °F(°C)	P_{Inlet} psia(MPa)	Fluid
SRC-1	0.071	500 (260)	465 (241)	70 (39)	480 (249)	300 (2.1)	Caloria HT-43
SRC-2	0.097	600 (316)	524 (273)	152 (84)	580 (304)	400 (2.8)	Therminol MCS-2046
SRC-3	0.115	600 (316)	534 (279)	132 (73)	580 (304)	500 (3.4)	Therminol MCS-2046
SRC-4	0.128	600 (316)	544 (284)	112 (62)	580 (304)	600 (4.1)	Therminol MCS-2046
SRC-5	0.137	750 (399)	606 (319)	288 (160)	730 (388)	600 (4.1)	Syltherm 800
SRC-6	0.152	750 (399)	616 (324)	268 (149)	730 (388)	750 (5.2)	Syltherm 800
SRC-7	0.165	750 (399)	625 (329)	250 (139)	730 (388)	900 (6.2)	Syltherm 800
SPH	0.	460 (238)	409 (209)	102 (57)	-	-	Caloria HT-43
FFTE	0.202	-	-	-	1050 (566)	1000 (6.9)	-

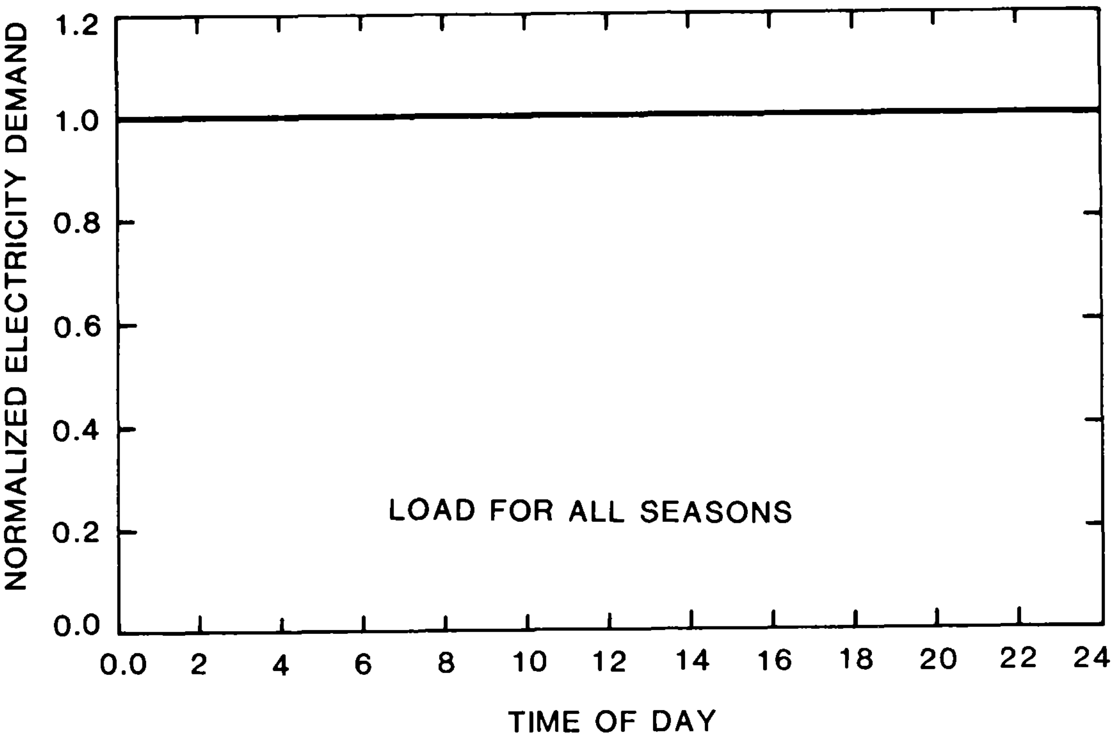

Figure 1. 24-Hour Load Profile

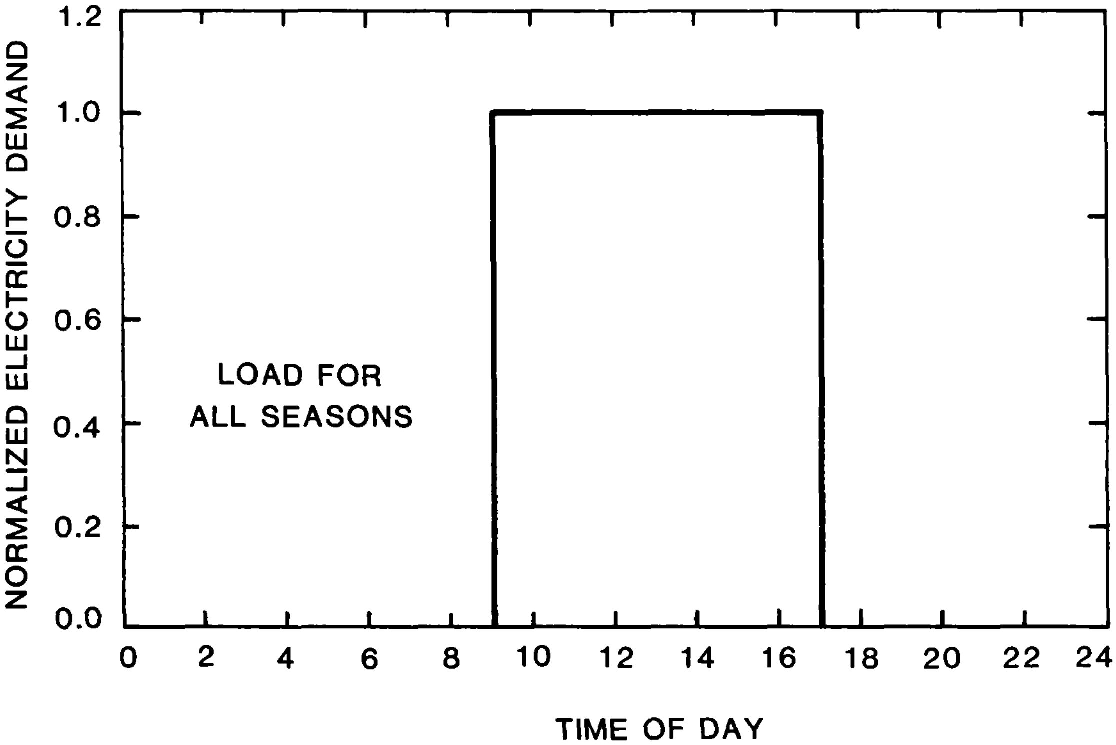

Figure 2. 8-Hour Load Profile

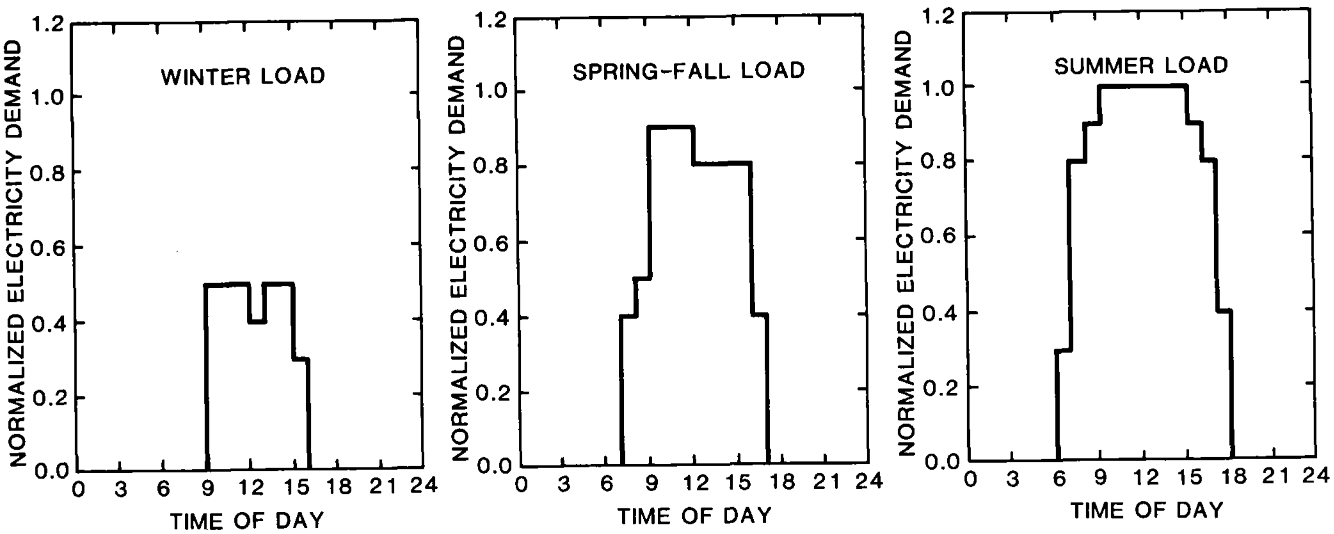

Figure 3. Solar-Based Load Profile for N-S Axis Collector Cases.

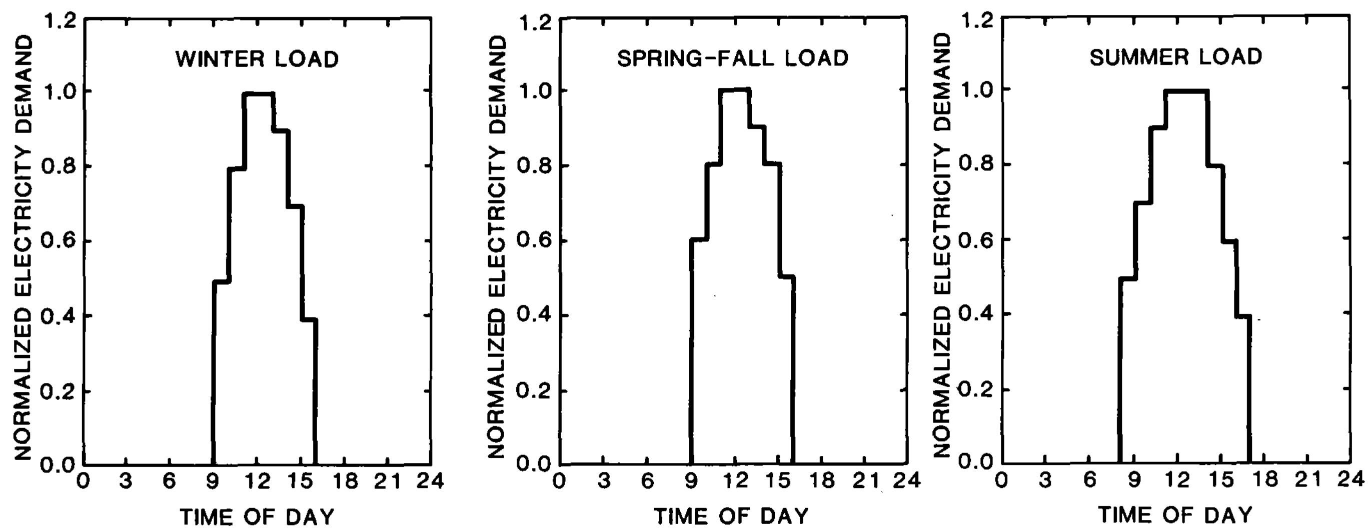

Figure 4. Solar-Based Load Profile for E-W Axis Collector Cases

is dependent on the axis of rotation, two different solar-based loads were defined. Because the fraction of the total load supplied by the collector field (the "solar fraction") has a large effect on system design and economics, four different cases were investigated. The optimum solar fraction for a particular case is that which produces the most economical system.

As previously mentioned, the orientation of the collectors affects their output profile on both a daily and an annual basis. Two different cases were examined: 1) North-South, and 2) East-West axes of rotation for the collectors. Samples of the PPT collector output profiles on three different clear days are presented in Figures 3 and 4. Two different system cost cases are identified in Table I. The two extremes presented correspond to somewhat optimistic and pessimistic costs for the collector field and thermal storage. The cost specifics will be discussed in a later section.

The electrical-to-thermal output ratio of the SRC system has a large impact on system design and economics. Increasing its value increases the value of the SRC system output because electricity generally costs more than thermal energy. In order to increase the E/T ratio, the turbine's inlet pressure and/or inlet temperature must be increased. These changes have many system ramifications which include:

1. Changing the collector average field temperature and, therefore, its efficiency.

2. Changing the temperature difference across thermal storage which changes the cost per unit of energy storage.

3. The possibility of a change in the heat transfer fluid which may have a different cost per unit with higher temperature fluids generally being more expensive.

The particular configurations investigated are listed in Table I. Information is also listed concerning the SPH and FFTE systems which were used in comparisons with the SRC systems. The SPH system provides only 338°F (170°C) - 115 psia (0.79 MPa) steam while the FFTE system uses fossil fuel to produce both electricity and thermal energy. The total matrix of cases investigated numbers about 400.

Methodology

The STESOPT computer code[1] was used to simulate the operation of the systems and optimize the system design (in this case the collector field and thermal storage size) such that the annualized cost of system operation is minimized for the case being considered. System simulation was done on an hourly basis for the entire year using a typical meteorological year [2] as input for weather and insolation.

The simulation of the major components was fairly detailed. The insolation available to a collector was modified by accounting for the sunlight's incidence angle and shadowing by adjacent collectors. The percentage of the ground covered by collectors (i.e., the packing factor) was assumed to be 30%. Thermal performance was estimated using the equation;

$$\eta = 0.76 - 0.0005\ (T_{avg} - T_{amb})/I_{av}$$

where T_{avg} is the average field temperature (°C), T_{amb} is the ambient air temperature (°C), and I_{av} is the insolation incident on the receiver (kW/m^2). Field pumping parasitics were also included as a loss mechanism. Two cost cases were considered: turnkey collector costs of $\$208/m^2$ and $\$290/m^2$ in 1980 dollars. The insolation data used in the simulations were that of the Albuquerque Typical Meteorological Year[2].

Thermal storage was assumed to be of a thermocline design with either bulk fluid or dual media energy storage. The two thermal storage energy loss mechanisms were those associated with overflowing the storage unit (i.e., the field is collecting more energy than can be used and storage is full) and thermal leakage. The leakage coefficient was chosen such that a full storage unit would lose 10% of the usable energy in 24 hours. The cost per MWh of thermal storage was estimated using the equation:

$$C = \frac{C_g \Psi}{\rho (C_p) \Delta T} \quad ,$$

C_g is the cost per gallon for the heat transfer fluid. The particular values used were: Caloria ~\$1.45/gallon, Therminol ~\$5.35/gallon, Syltherm ~\$23.76/gallon in 1980 dollars plus a 25% additional charge for tanks, controls, contingency, and indirect costs, etc. The term ρ is the fluid density, C_p is the heat capacity, ΔT is the temperature difference across storage and Ψ is the fluid fraction [1.00 - bulk fluid; 0.25 - dual media].

Simulation of turbine operation was accomplished by assuming the device operates in a classical thermodynamic cycle. The amount of shaft work which can be extracted is some fraction of the power produced by an ideal turbine operating in the same cycle. The specific expansion efficiency equation used was:

$$\eta = 0.45 + 0.3*L \qquad (0.3 \leq L \leq 1)$$
$$\eta = 0 \text{ for } L = 0$$

where L is the fraction of maximum power. The turbogenerator was sized such that the net output at maximum power was 200 kW and its cost was approximately $19,000. Costs for the associated components [pumps, heat exchangers, auxiliary heater, etc.,] were estimated using the STESOPT costing algorithms.

Economics

The optimum field design for a particular case was determined by minimizing the annualized cost of energy produced by the system. The annualized cost is a constant payment in current year dollars which pays for the capital equipment, backup energy costs, operation and maintenance costs, etc., over the lifetime of the system. This value is calculated using a discounted cash flow methodology similar to that presented in References 3 and 4. Values used in the economic analysis are listed in Table II. The cost figures for energy are those for an industrial user in Illinois purchasing electricity and light fuel oil in the 1985-2005 time period as predicted by Reference 5.

Results

The STESOPT code was used to design systems for the approximately 400 cases indicated in Table I. The results followed several definite trends so that the small sampling which follows gives an accurate representation of the overall results. Several terms must be defined before discussing the results. The first is the Service Cost Ratio (SCR) which is defined as the ratio of the annualized cost of the system under consideration (SRC, SPH, OR FFTE system) to the conventional system's annualized cost. The conventional system purchases electricity and fossil fuel to meet exactly the same load as that of the system under consideration. The fossil fuel is used to fire boilers which provide 338°F (170°C) steam to meet the thermal load requirements.

The Solar Fraction (SF) is defined as the reduction in the amount of fossil fuel purchased for the auxiliary heater from the case where there are no collectors or thermal storage:

TABLE II

ECONOMIC PARAMETERS

Year of Operation	1985
System Lifetime	20
Loan Lifetime	20
Depreciation Lifetime	7
General Plant O&M Cost	0.015
Collector Field O&M Cost	0.020
Property Tax and Insurance Rate	0.0225
Effective Income Tax Rate	0.50
Investment Tax Credit	0.25
Depreciation Method	Sum of the Year's Digits
General Inflation Rate	0.09
Discount Rate	0.15
Guaranteed Loan Interest Rate	0.11
Down Payment	1.00
Inflation Rate for Electricity	0.120
Inflation Rate for Fossil Fuel	0.115
Electricity Price (1985 Price in 1980$)	4.1¢/kWh
Fossil Fuel Price (1985 Price in 1980$)	$4.57/10^6$ BTU

$$SF = 1 - \frac{Q_{aux}}{Q_{aux\text{-zero solar energy}}}$$

This quantity may be defined on an annual or instantaneous basis.

In order to compare different loads, a quantity which will be referred to as the Average Hours of Solar Operation per Day (AHSOD) is defined as:

$$AHSOD = \frac{\int_{year} L(t)SF(t)dt}{\int_{year} dt}$$

where L(t) is the turbine's instantaneous fraction of maximum power and SF(t) is the instantaneous solar fraction. The maximum AHSOD value (SF(t) = 1 for all t) is defined by the loads.

Load	$AHSOD_{max}$
24 hr.	24.0
8 hr.	8.0
SB_{N-S}	6.9
SB_{E-W}	5.9

The Solar-Based loads' (SB) maximum AHSOD is small because the turbine operates only during the daylight hours and then at some intermediate power level for a considerable portion of the time.

The effect of collector orientation, AHSOD, and load on the SCR are illustrated in Figures 5-7. In all cases, it is observed that the SRC systems are competitive with the conventional systems. In general, the SCR starts at some low level for a small AHSOD value (SF $\simeq$ 40%) and then rises rapidly as $AHSOD_{max}$ (SF = 100%) is approached. The N-S axis systems have a smaller SCR than the E-W axis systems for small AHSOD values because an N-S axis collector field collects more energy per unit aperture area per year than an E-W axis field. Thus, a smaller field is needed for the N-S axis systems, and the corresponding SCR is lower than that of the E-W axis systems. As the maximum AHSOD value is approached, the shape of the annual collector output profile becomes important. Since the E-W axis annual profile more closely matches the 24-hour and 8-hour loads' annual profile, it is more economical for these loads if the system operates at large AHSOD values. The SB loads have been tailored to some extent to the collector output profiles, so in this case, the N-S axis systems are more economical than the E-W axis for all AHSOD values.

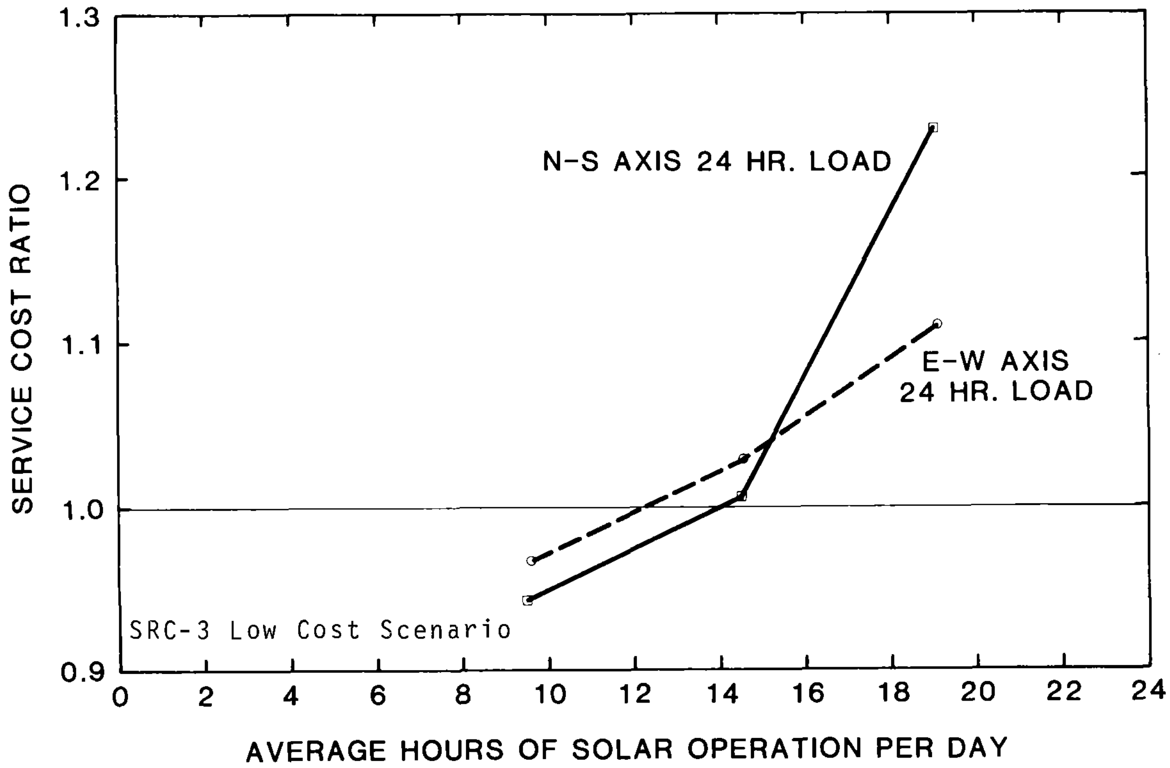

Fig. 5 Effect of Collector Orientation and Average Amount of Solar Operation Per Day on the Service Cost Ratio.

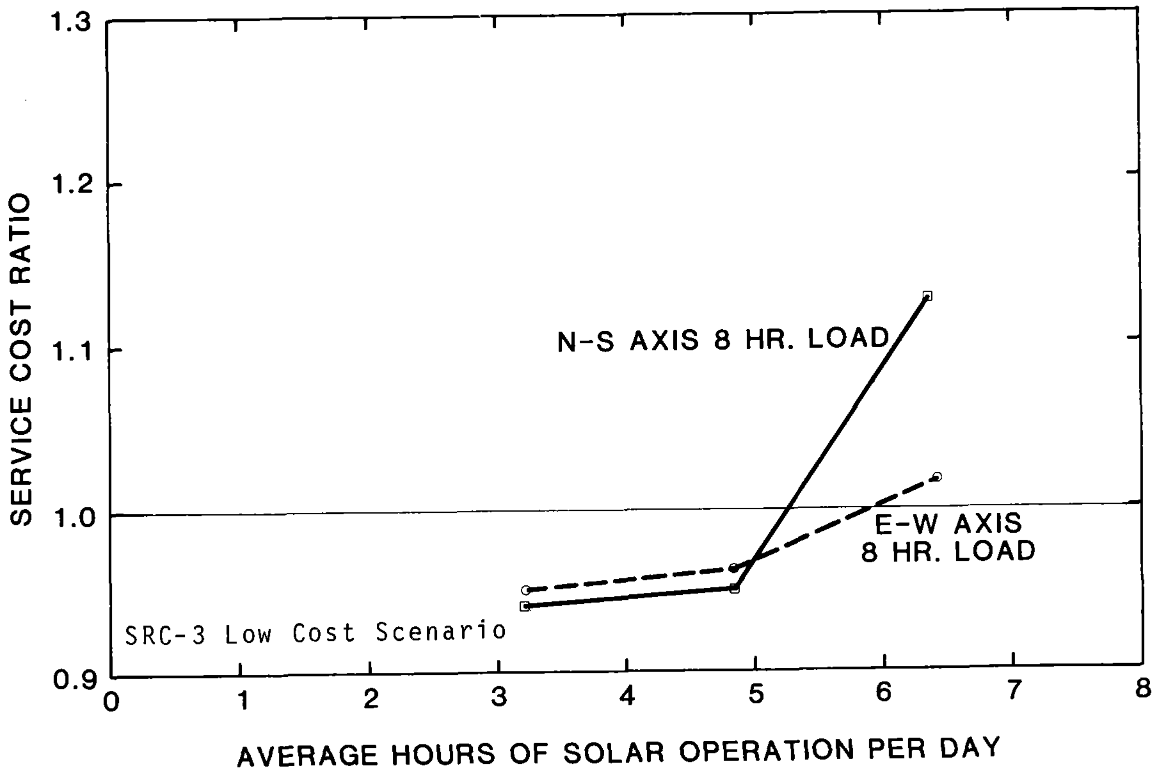

Fig. 6 Effect of Collector Orientation and Average Amount of Solar Operation Per Day on the Service Cost Ratio.

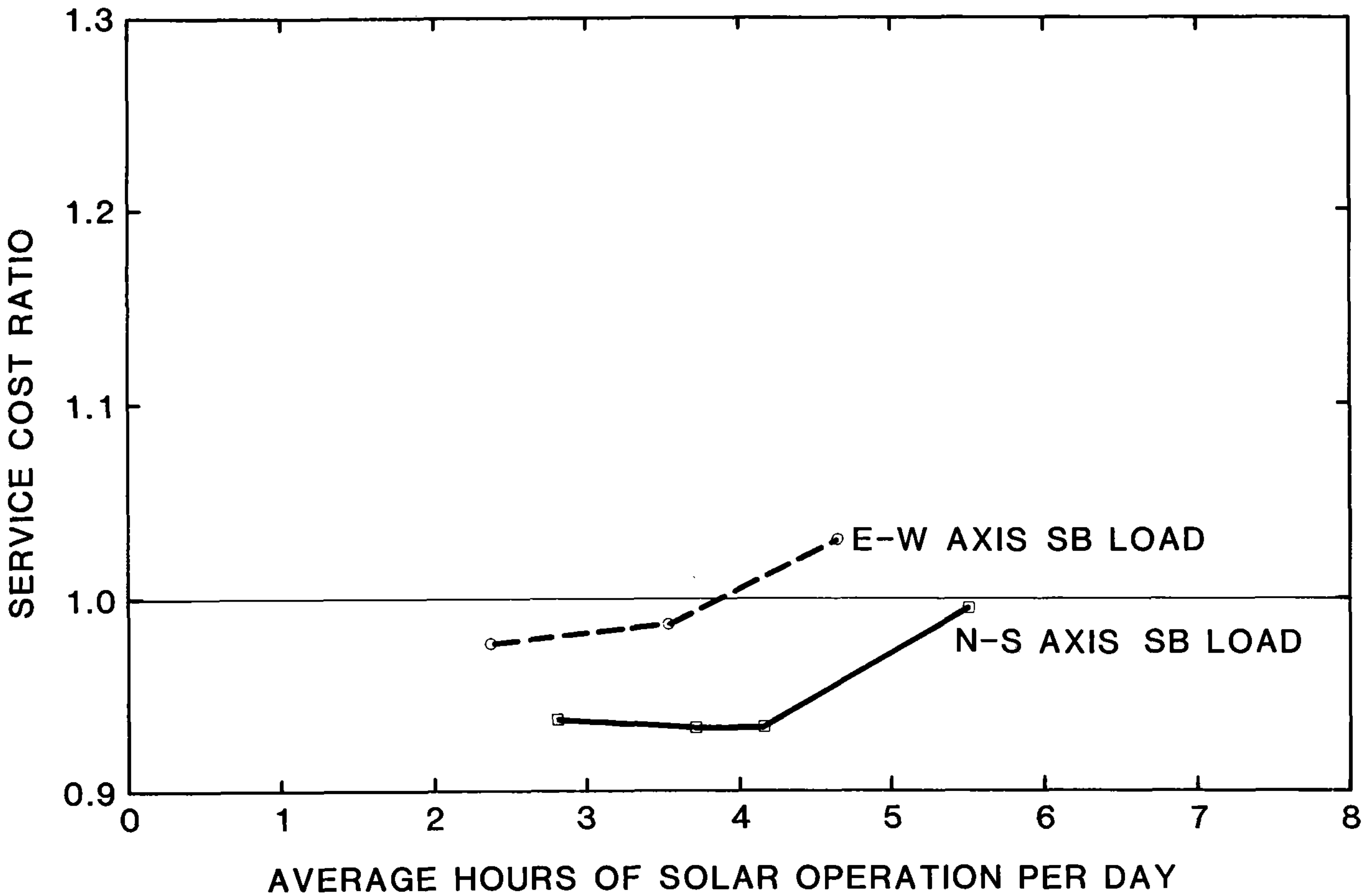

Figure 7. Effect of Collector Orientation and Average Amount of Solar Operation Per Day on the Service Cost Ratio for the Solar-Based Loads. Data for SRC-3 With the Collector and Thermal Storage Low Cost Scenario.

Figures 8-10 show the field and storage sizes for the cases previously discussed. These figures indicate that, as a result of a poor match between the N-S axis field's annual output profile and the 24-hour and 8-hour load annual profiles, the N-S axis system's field, which is at first smaller than the E-W axis field, becomes considerably larger at large AHSOD values. Since the field is an expensive item, the N-S axis system becomes more expensive at large AHSOD values. The storage size has been plotted in units of hours of turbine operation at full power, and it is seen that in all cases only daily storage (< 24 hours) is purchased. Systems designed for the eight-hour and SB loads have very little storage, less than two hours in most cases. Figure 11 illustrates the effect of moving from the low cost to high cost scenario. In this case, it means the SRC systems are no longer economical.

As previously discussed, the E/T ratio was varied in two manners. Figure 12 illustrates the effect of pressure for several 600°F (316°C) collector outlet temperature cases and indicates the effect is minor. The effect of varying the outlet temperature can be seen in Figure 13. The 500°F (260°C) and 600°F (316°C) systems have approximately the same SCR values indicating that, in this case, the benefit associated with moving to a higher outlet temperature (a higher E/T ratio) makes up for the increased costs (e.g., lower field efficiency, higher storage costs). The 750°F (399°C) systems are much more expensive than the others because their heat transfer fluid cost is disproportionately high and, therefore, thermal storage is more expensive. If a lower price heat transfer fluid capable of operation at elevated temperatures were identified, the 750°F (399°C) systems could be cost competitive.

A Solar Process Heat system seems to be a reasonable alternative to an SRC system because it is somewhat simpler. SPH systems were compared to SRC systems and one particular set of results can be seen in Figure 14 which indicates these two have essentially the same economic feasibility. The savings associated with deleting the turbogenerator and associated equipment, and reducing the average field temperature are thus nullified by the loss of electricity production. This particular result is based on the particular economic scenario assumed, especially that of the energy prices. One would like to determine whether this result is general or restricted to the particular choice of economic parameters. An examination of the ratio "SCR_{SRC}/SCR_{SPH}" indicates the absolute value of the annualized cost of electricity and fossil fuel is important as well as the ratio of the energy costs. It is, however, a fairly small effect. A simplified expression for this ratio, which assumes that all of the solar energy is used immediately to satisfy the load (i.e., flexible load-no storage) shows only the ratio to be important:

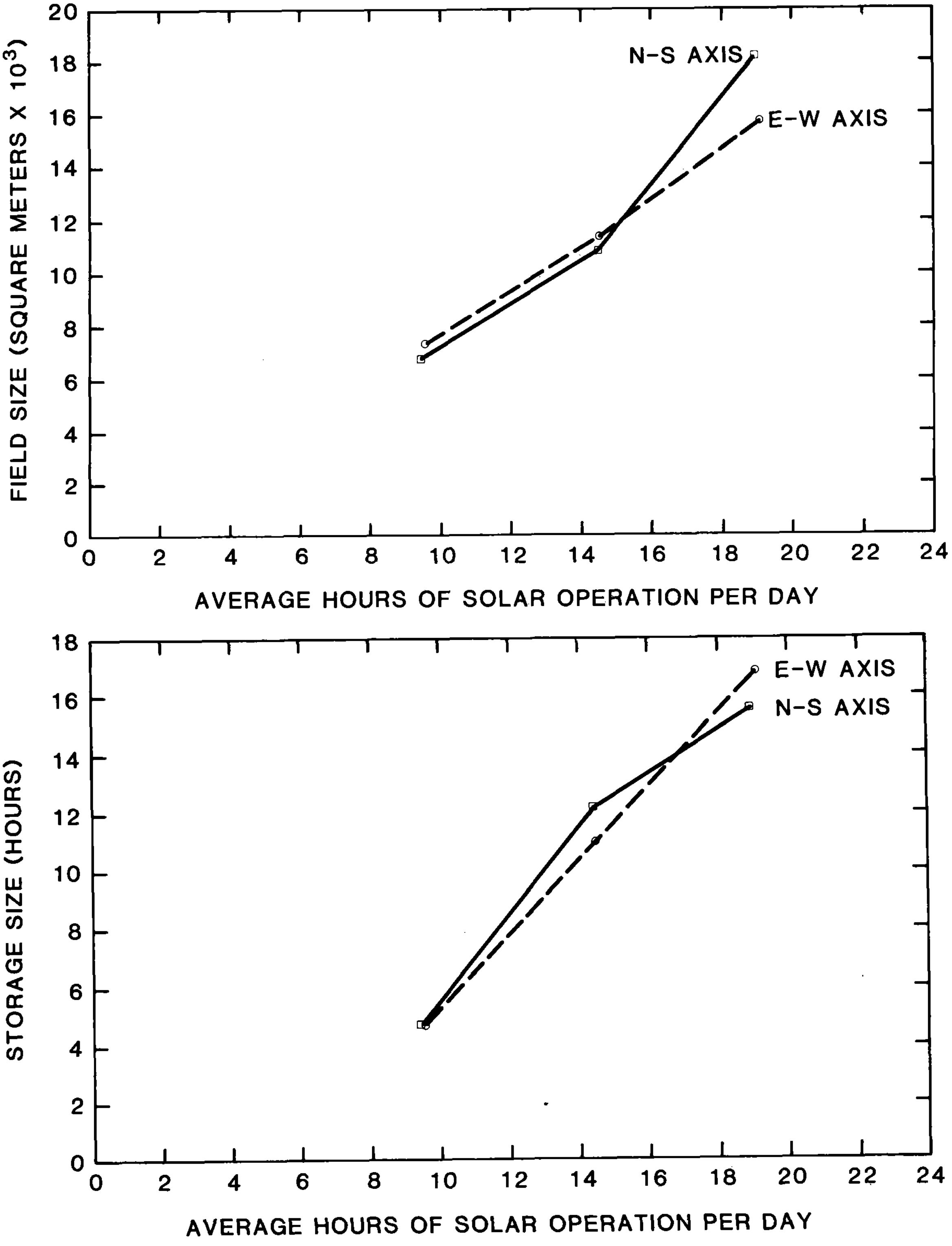

Fig. 8 System Design as a Function of Solar Operation Time for Case SRC-3 With a 24-Hour Load and the Low Cost Scenario.

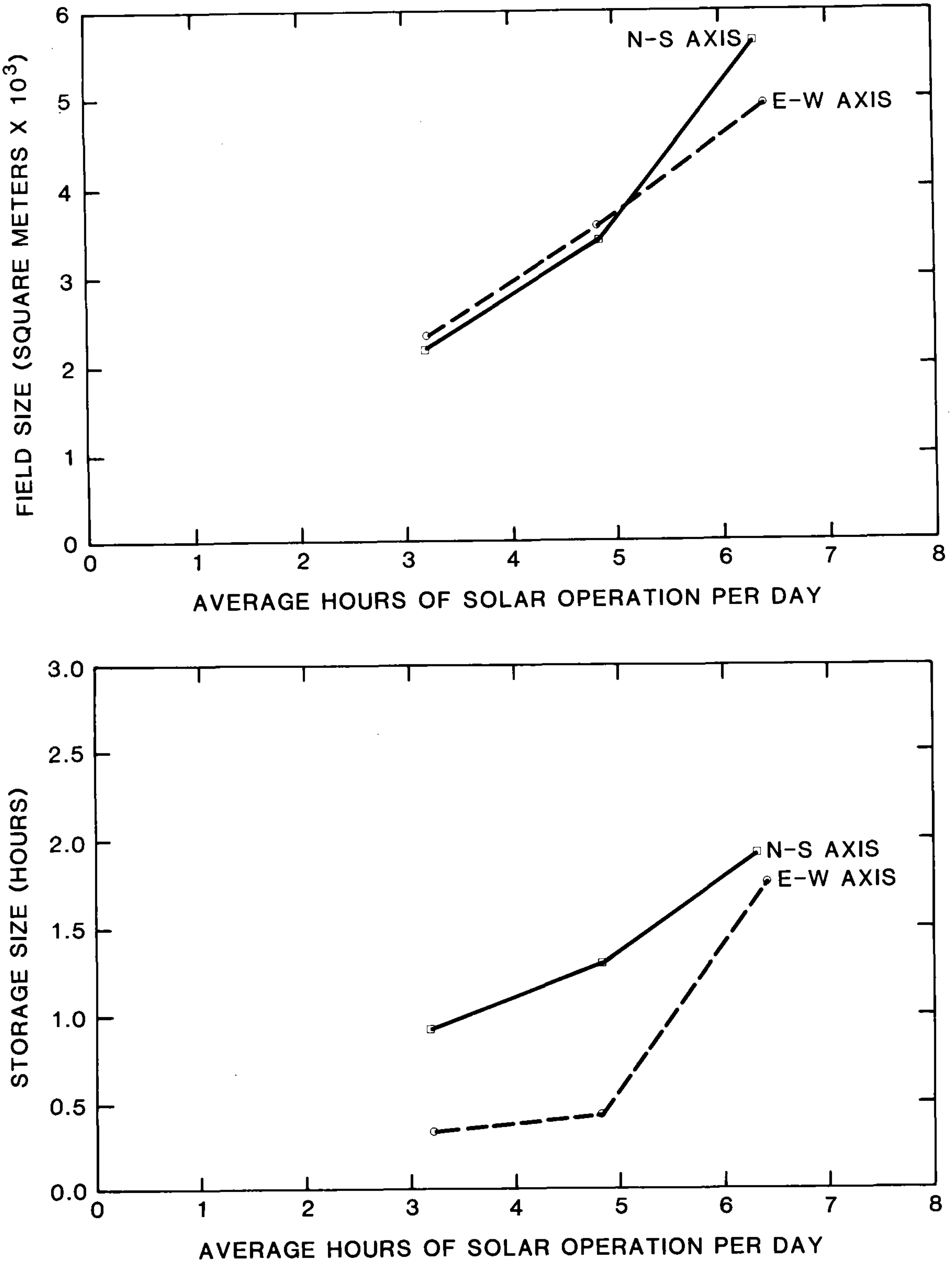

Figure 9. System Design as a Function of Solar Operation Time for SRC-3 With an 8-Hour Load and the Low Cost Scenario.

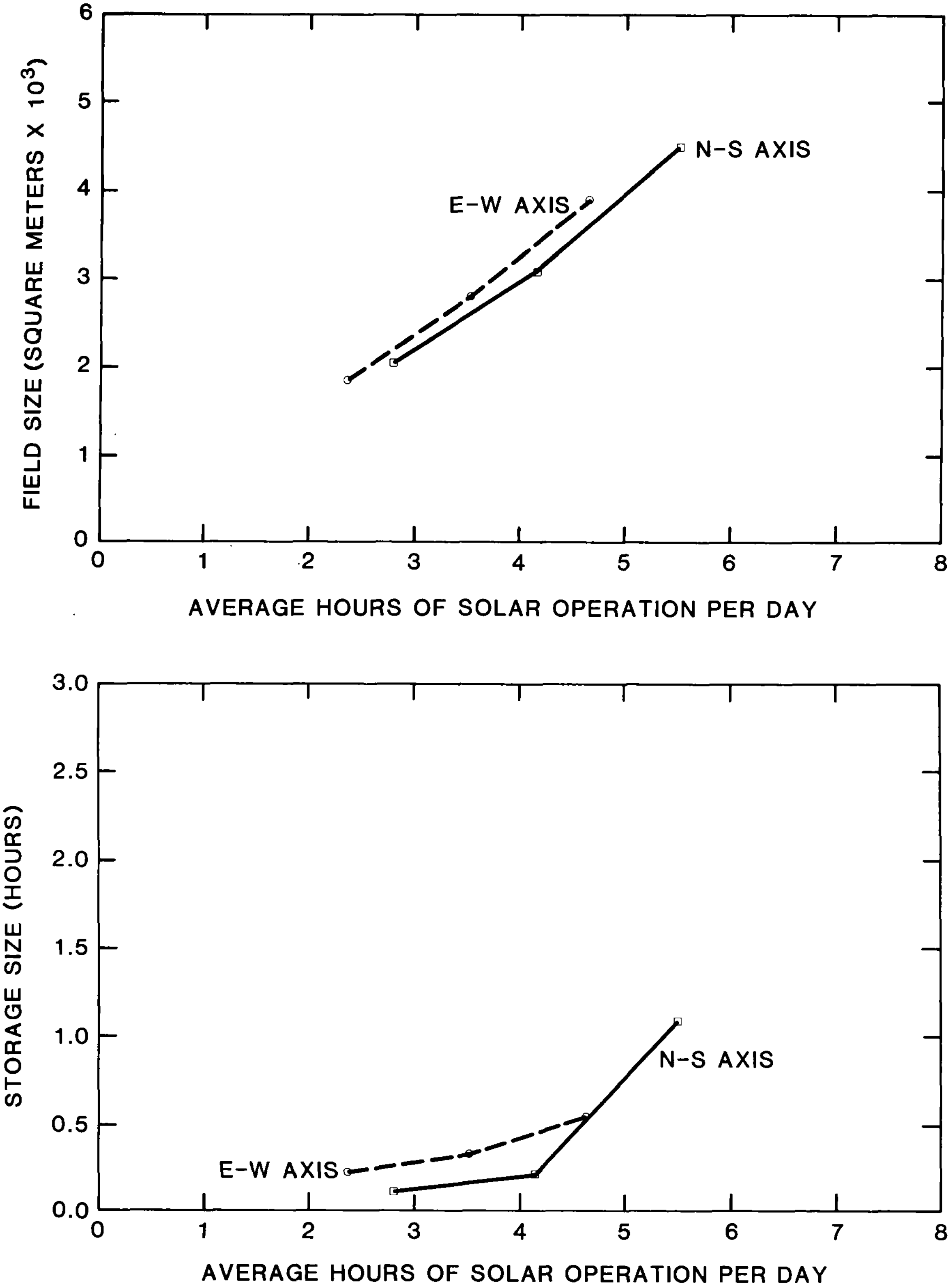

Fig. 10 System Design as a Function of Solar Operation Time for SRC-3 With a Solar-Based Load and the Low Cost Scenario.

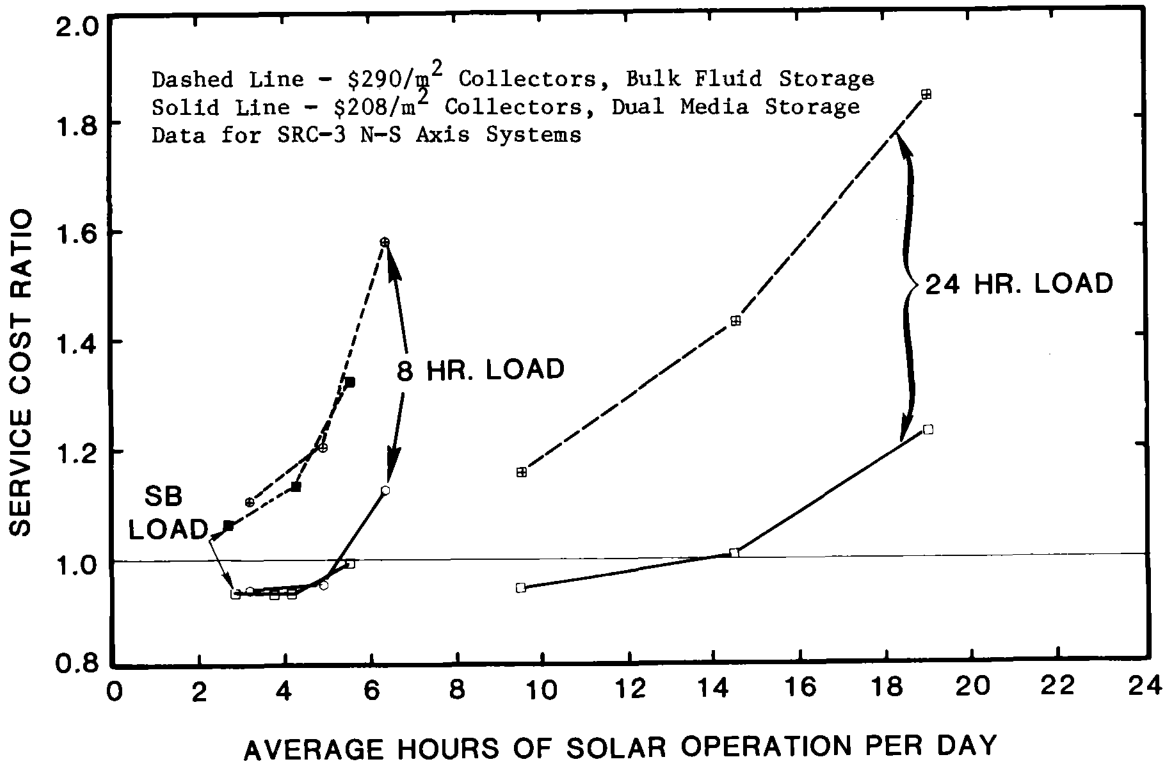

Fig. 11 Service Cost Ratio for Two Different Cost Scenarios

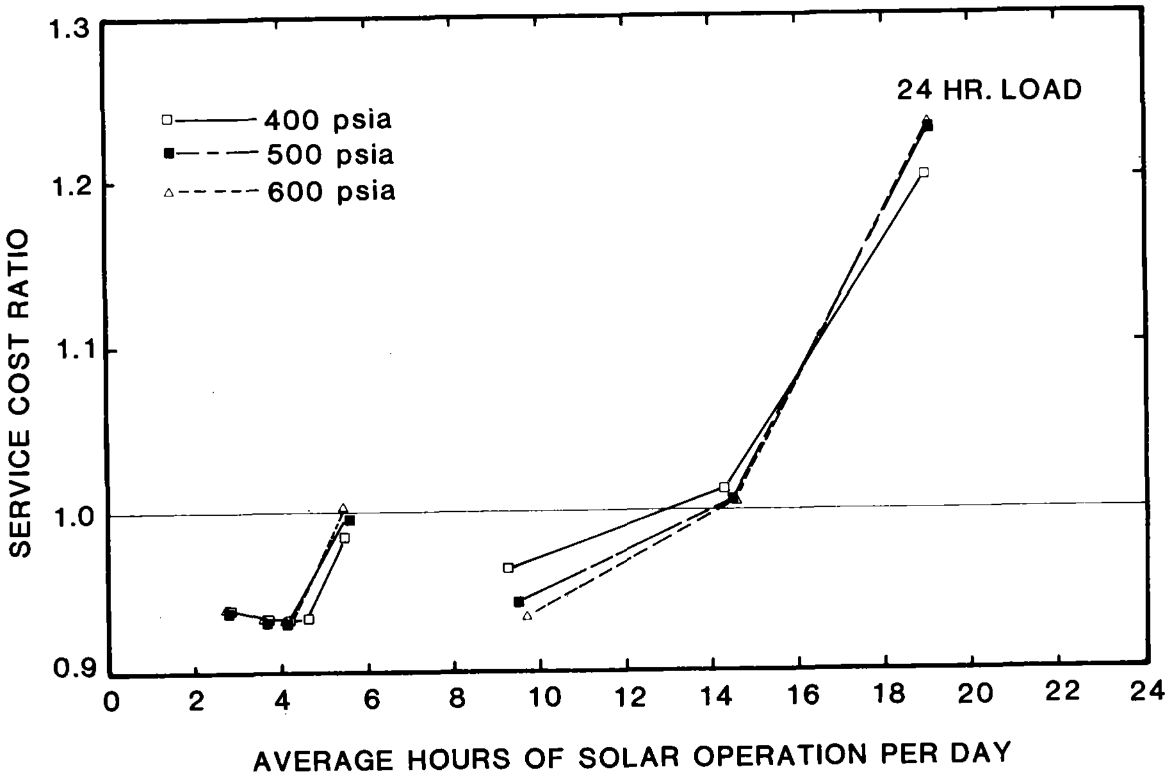

Fig. 12 Effect of Turbine Inlet Pressure on Economics. Data for 600°F Outlet N-S Axis Collector Field Systems, Low Cost Scenario.

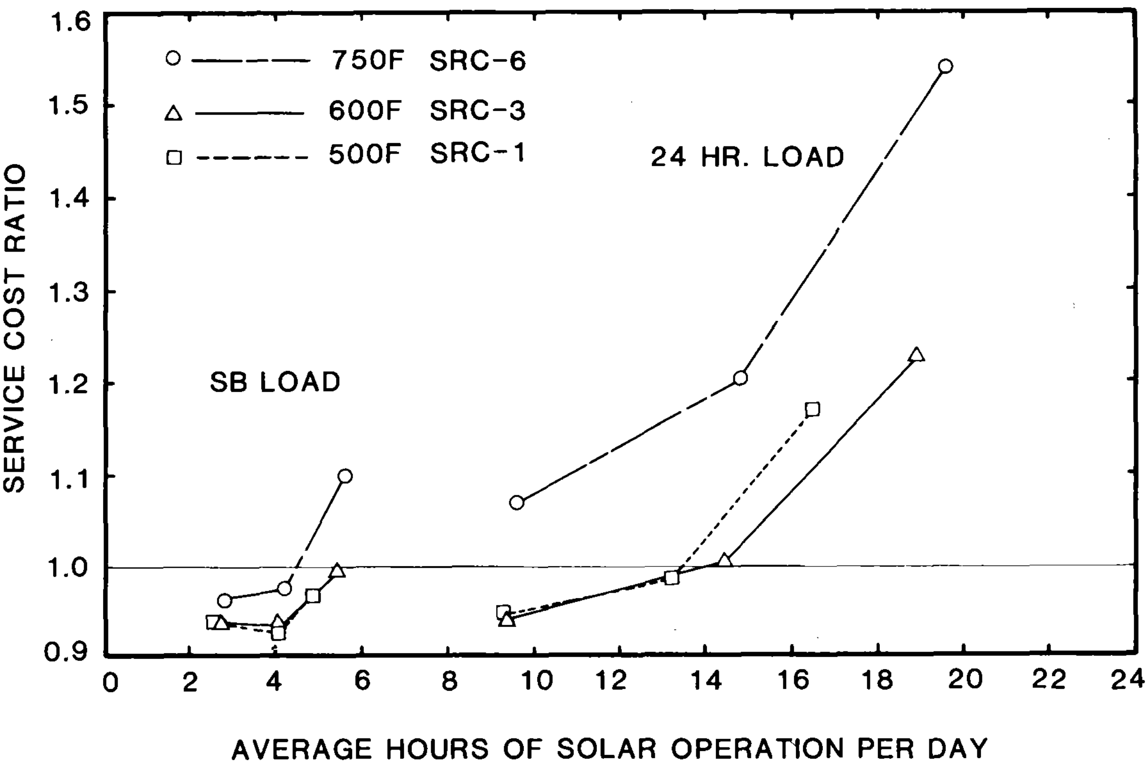

Fig. 13 Effect of Turbine Inlet Temperature on Economics. Data for Low-Cost Scenario with N-S Axis Collector Field Systems

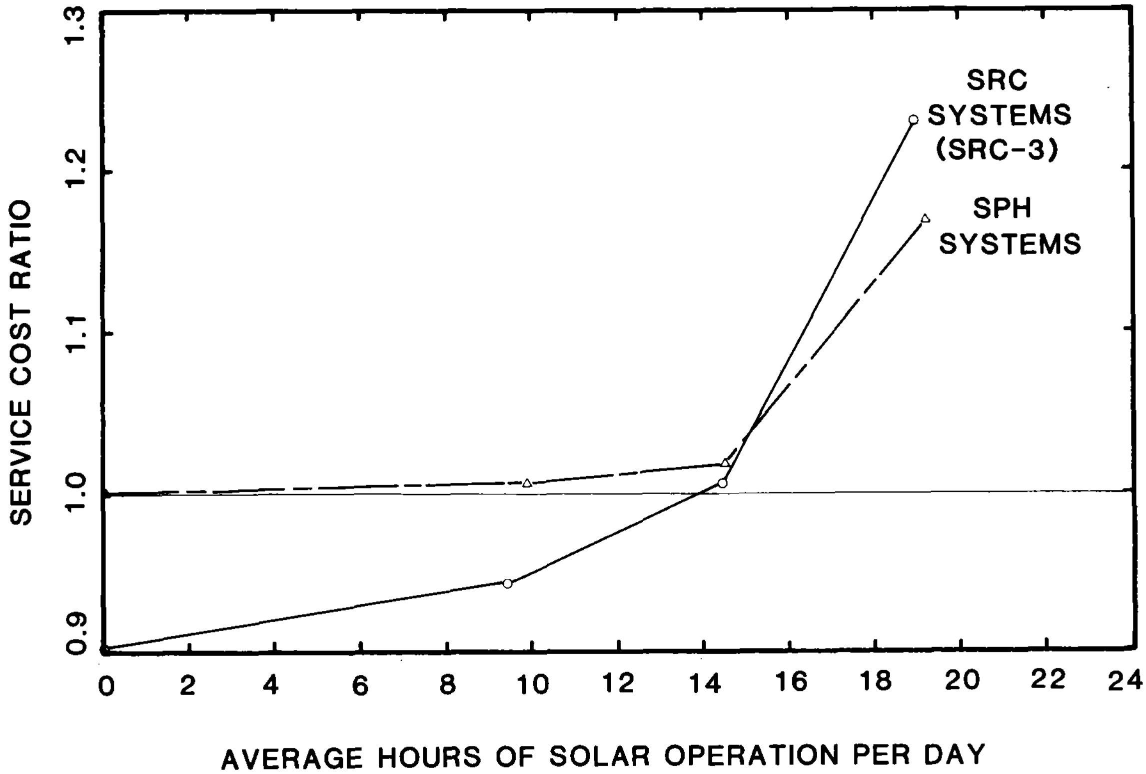

Fig. 14 Effect of Turbine Inlet Pressure on Economics. Data for 600°F Outlet N-S Axis Collector Field Systems, Low Cost Scenario.

$$\frac{SCR_{SRC}}{SCR_{SPH}} \simeq \frac{\eta_{F-SPH}}{\eta_{F-SRC}} \frac{1}{1 - \eta_c + \frac{C_E}{C_F} \eta_c \eta_B}$$

where η_F = Annual collector field efficiency

η_C = Cycle efficiency

η_B = Conventional boiler efficiency (0.85)

C_E = Annualized cost of electricity for the time period

C_F = Annualized cost of fossil fuel for the time period

Figure 15 plots the simplified equation's ratio value for N-S axis systems versus C_E/C_F for the three SRC field outlet temperature cases. Some data points corresponding to actual system designs are also plotted and indicate good agreement between them and the relevant simplified equation curve. This figure indicates SRC systems will have approximately the same economic feasibility as SPH systems over the range of C_E/C_F values which have been projected by various groups[5,6,7] (2.5-4.5). This analysis indicates it is difficult to make a decision concerning whether SPH or SRC systems are better on the basis of economic considerations alone.

Fossil Fuel Total Energy systems were also designed and simulated. The SCR values for these systems were in the range of 0.86 to 0.91 indicating no significant advantage over any of the other systems.

A simplified design procedure was developed to correlate the results of this study and thus aid in understanding them. This model simulated collector performance in the manner previously described. Thermal energy from the collector field was routed to the load which is either the turbogenerator (SRC systems) or the process heat demand (SPH systems). Excess collector output was routed to the thermal storage unit which was modeled as a box whose only loss mechanism was that of overflowing. The proper design for a particular case [e.g., SRC-3, N-S axis, 24-hour load, 40% solar fraction] then is that which has the same change in the solar fraction when another dollar is spent on either the collector field or thermal storage. In equation form:

$$\frac{\frac{\partial SF}{\partial C_S}(X_F,X_S)}{\frac{\partial SF}{\partial C_F}(X_F,X_S)} = 1 \quad \text{when } [X_F,X_S] \text{ is the proper design}$$

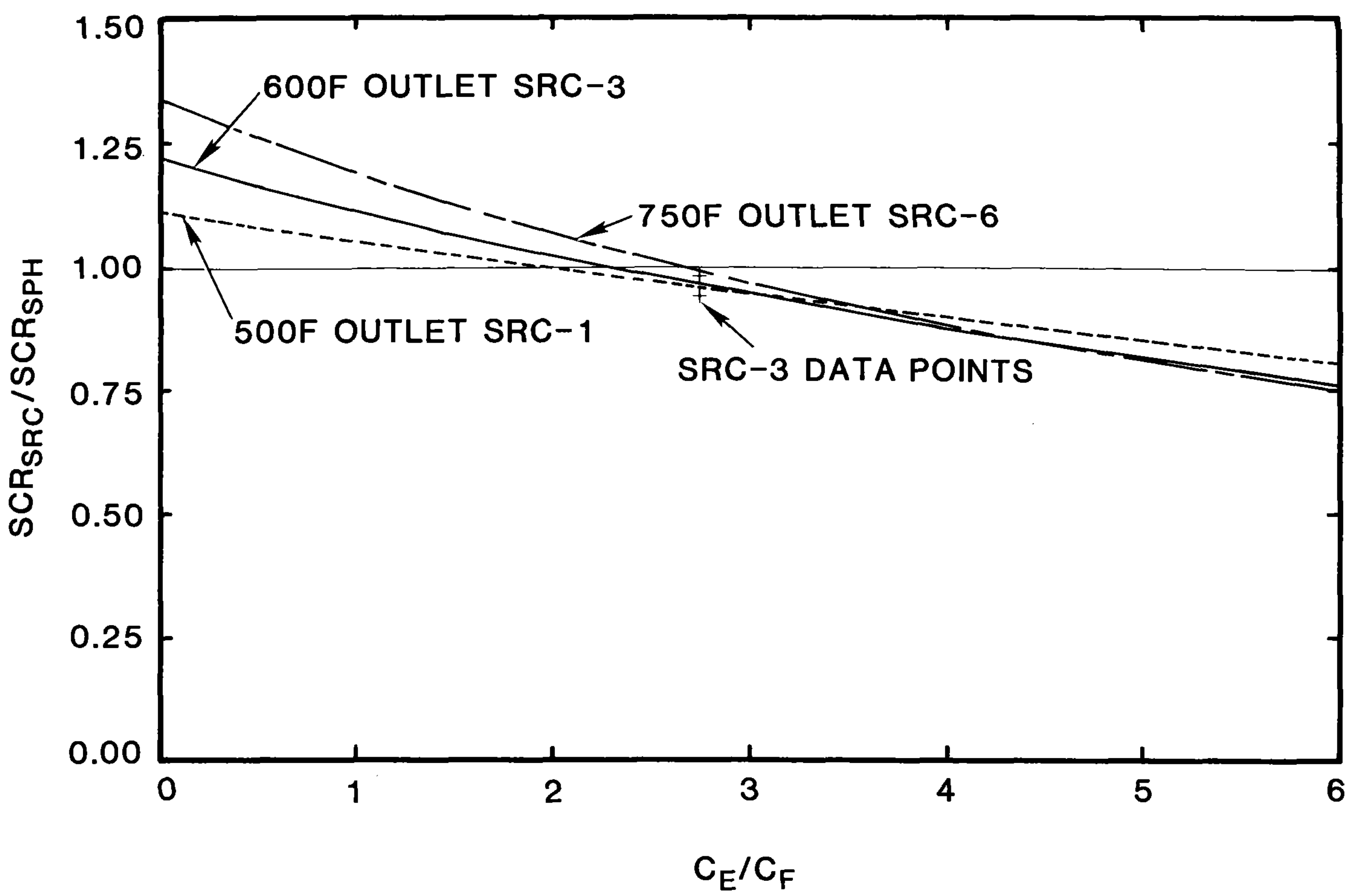

Fig. 15 Effect of the Ratio of Electricity to Fossil Fuel Cost on the Relative Economics of SRC and SPH Systems.

C_F and C_S are the annualized cost of the field and storage, respectively, and X_F and X_S are their sizes. The annualized cost of both subsystems takes into account the capital cost, operation, maintenance, property tax costs, etc. The simplified model's designs are plotted versus the STESOPT designs in Figure 16 for the approximately 400 cases investigated in this study and indicate the simplified model does a good job of designing the system. Investigation of off-design points (i.e., those not on the diagonal) indicate these are also fairly good designs with SCR values within a few percent of the corresponding STESOPT design SCR value.

Summary

The sensitivity of Solar Rankine Cogeneration and Solar Process Heat system design and economics to changes in the input parameters was investigated. The results indicate relative insensitivity to changes in:

1. Load shape for reasonable loads and intermediate solar fraction (≃ 50%).

2. Collector orientation.

3. Turbine inlet pressure.

System design and economics are relatively more sensitive to:

1. Component cost.

2. Collector field temperature.

The second case is really a subset of the first because the sensitivity to temperature results from the large increase in the cost in thermal storage as the field outlet temperature is increased above 600°F (316°c).

Solar Process Heat and Solar Rankine Cogeneration systems may be competitive with conventional energy sources in the near future if second-generation collectors can be built and installed for approximately $200 per square metre. Promising systems appear to be SPH systems which provide 338°F (170°C) steam and SRC systems which have a field outlet temperature of 600°F (316°C), and which produce electricity and 338°F (170°C) steam with an electrical-to-thermal energy ratio of about one-tenth.

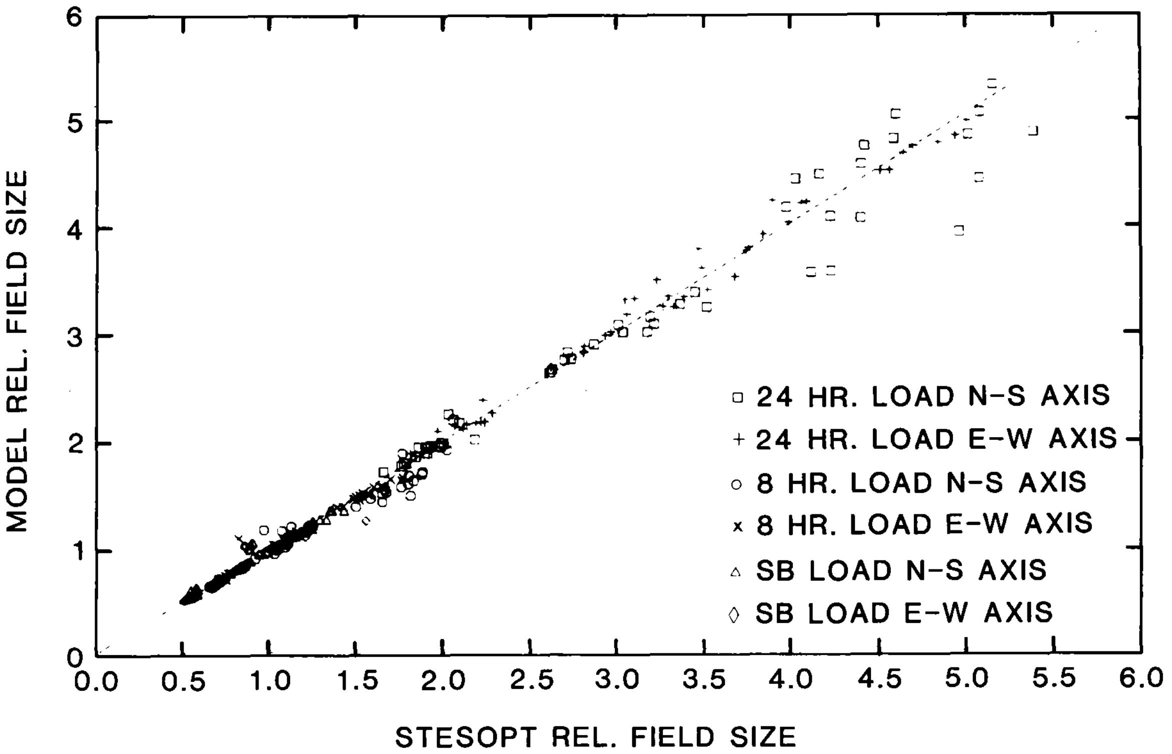

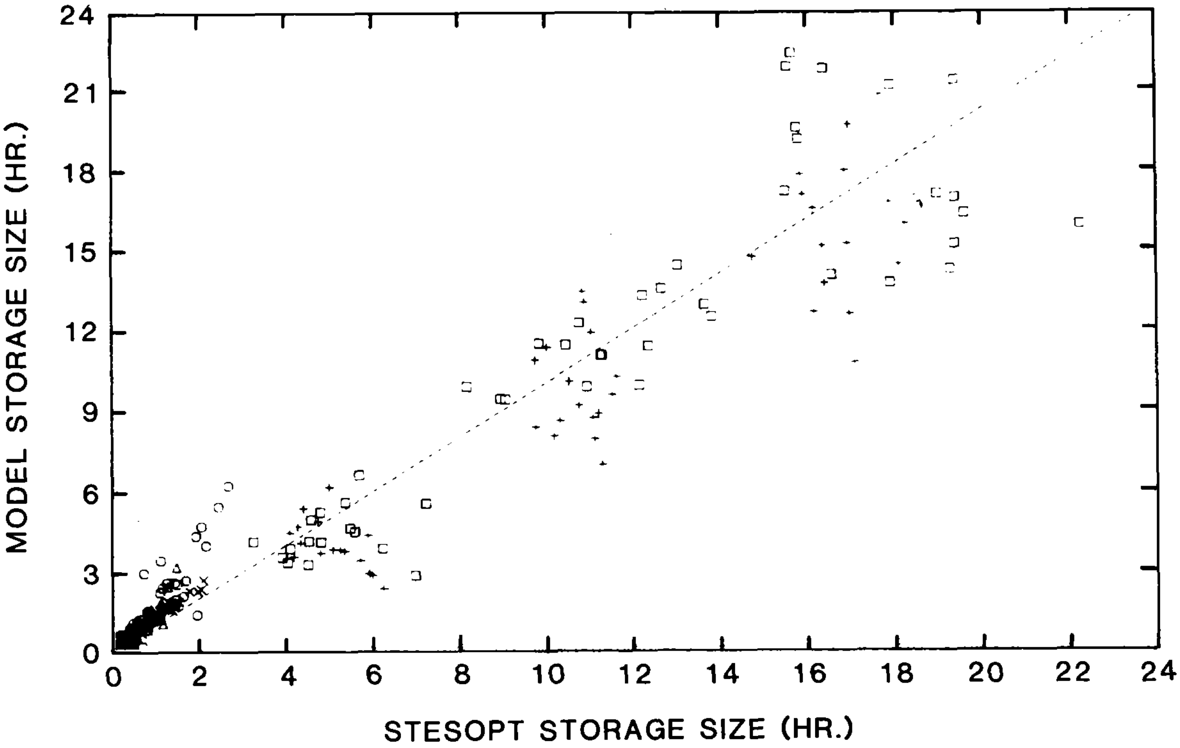

Figure 16 Comparison of STESOPT Code and Simplified Model Design for Approximately 400 Cases.

References

1. Peters, R. R., "A Methodology for Determining the Configuration of the Optimum Solar Total Energy System," SAND79-0422, Sandia Laboratories, May, 1979.

2. Hall, I. J., et al, "Generation of a Typical Meteorological Year for 26 SOLMET Stations," SAND78-1601, Sandia Laboratories, August, 1978.

3. Perino, A. M., "A Methodology for Determining the Economic Feasibility of Residential on Commercial Solar Energy Systems," SAND78-0931, Sandia Laboratories, January, 1979.

4. Dickinson, W. C., and Brown, K, C., "Economic Analysis of Solar Industrial Process Heat Systems: A Methodology to Determine Annual Required Revenue and Internal Rate of Return," UCRL-52814, Lawrence Livermore Laboratory, Livermore, CA, August, 1979.

5. Anon., "Solar Total Energy Systems Final Technical Summary Report--Volume II: Energy Use and Price Forecasts," ATR-78 (7692-01)-1, The Aerospace Corporation, El Segundo, CA, March, 1978.

6. Anon., "Institutional Applications of Solar Total Energy Systems," RA-78-1445, Resource Planning Associates, May, 1978.

7. Anon., "Application Analysis of Solar Total Energy to the Residential Sector--Quarterly Report for July 1 - September 30, 1977," Institute of Gas Technology, October, 1977.

SOLTES
(Simulator of Large Thermal Energy Systems)

Merton E. Fewell
Fluid Mechanics & Heat Transfer Division III 5513

and

Norman R. Grandjean
Component & Subsystem Development Division 4722
Sandia National Laboratories
Albuquerque, NM 87185

Introduction

SOLTES is a computer code that can be used to simulate a wide variety of thermal energy systems.[1] System models are modularly constructed from routines in a routine library. (This library may include user written routines.) Due to its software structure, SOLTES can be used, without penalty, to simulate small systems, individual components, and subsystems as well as large systems that may include Rankine-type power generation. Input to SOLTES is proportional to the size and complexity of the system model.

Quasi-Transient

Although the numerical approach used in SOLTES does not exclude transient component models, currently only thermal storage component models are transient; the other component models are steady state algorithms. The quasi-transient approach assumes that time variable data, weather and loads, change slowly relative to the time required for the components (other than thermal storage) to reach steady state operation, and, therefore, the transient behavior of thermal energy systems can be described by successively determining the steady-state response of the systems to time varying weather and loads. The frequency of these steady-state solutions are defined by a constant user-supplied time step.

Routine Library

The routine library from which appropriate algorithms are selected to model a thermal energy system, includes three types of algorithms--information, component, and system performance routines. Information routines supply time varying weather and load data and system performance routines calculate system performance. Component routines are mathematical models of controls or thermodynamic models of components in the thermal energy system. Controls may change the fluid flow rate, but do not change the thermodynamic state of fluids. Thermodynamic models may change the fluid flow rate or the thermodynamic states of the fluids flowing through them, and may include heat transfer and fluid mechanics effects.

Thermodynamic models currently exist for several types of solar collectors (both detailed models and efficiency models), pumps, thermal energy storage, thermal boilers, auxiliary boilers, heat exchangers, extraction turbines, extraction turbine/generators, condensers, regenerative heaters, air conditioners, space heater, etc. Control models currently exist for switches and flow controllers based on temperature, flow rate, insolation, etc.

Models of simple or complex Rankine-type power cycles can be modularly constructed from these routines and can be easily used for a large variety of working fluids. A load management component allows these cycles to simultaneously follow electrical and thermal loads that may be peak shaved and/or scaled.

Numerical Algorithm

Time varying weather and load data are supplied by information routines to component models requiring these data. (Component models separate state points in the system model.) Values of the fluid flow rate and thermodynamic state variables are stored at each point state in the system model. Sequential calls to each of the information and component routines are repeated until values of the fluid flow rate and thermodynamic state variables at each state point for two successive iterations are within user supplied convergence criteria. Upon convergence, the solution is advanced in time by the SOLTES time step and the procedure is repeated until the end of the simulation period.

Fluid Property Data

Fluid property data for heat transfer fluids are supplied as functions of temperature by polynomial fits. Power cycle/refrigeration working fluids are characterized by fourteen constants. The coefficients for the heat transfer fluid property data and the fourteen constants are provided in a fluid property data bank for many of the more commonly used fluids.

Input

SOLTES input includes fluid property data, values for information and component routine parameters, convergence criteria, and simulation period definition.

Output

Output is categorized as follows:

(1) Component/information routine input - values of the information and component routine input parameters.
(2) Convergence criteria and simulation period definition data - values defining convergence criteria and the simulation period.
(3) Values of the fluid flow rate and thermodynamic state variables at each state point.
(4) Calculated values of significant variables from each routine
(5) Energy accounting and system performance parameters.

Each of the categories are controlled by user input. The values of the significant variables and energy accounting and system performance parameters are available in tables and on a postprocessor file.

Unique Features

The overall modularity of SOLTES provides the system analyst with a framework so that he may concentrate on his particular applications without wasting time generating redundant software. A preprocessor aids the user in system model construction and modification and also generates a SOLTES program for the system model described by the input. SOLTES allows the simulation of two-phase flow and modular power generation.

Applications

SOLTES has been used for detailed studies of trough solar collectors, surface hydraulics for piping networks, pipe insulation studies, IPH systems simulation, and solar power system simulations.

Availability

CDC6600/7600 - Software and examples

Contact:
Julie M. Pietrzak
National Energy Software Center

Argonne National Laboratory
9700 South Cass Avenue
Argonne, Illinois 60439

Telephone: 312/972-7250

Documentation

Contact:
National Technical Information Service
U.S. Department of Commerce
5285 Port Royal Road
Springfield, Virginia 22161

Telephone 703/557-4600

Engineering Contact:	Software Contact
M. E. Fewell	N. R. Grandjean
Division 5513	Division 4722
Telephone: 505/844-3041	Telephone: 505/846-0024
FTS: 844-3041	FTS: 846-0024

Reference

1. M. E. Fewell and N. R. Grangjean, User's Manual for Computer Code SOLTES-1 (Simulator Of Large Thermal Energy Systems) SAND78-1315 (Revised), Sandia National Laboratories, Albuquerque, NM, June 1979.
(February 1980 revision to be published)

OPERATION OF THE WILLARD SOLAR IRRIGATION PROJECT

by

D. L. Fenton, G. H. Abernathy, G. A. Krivokapich, D. E. Ellibee, V. Chilton
New Mexico State University
Las Cruces, New Mexico 88003

ABSTRACT

The solar-thermal power system located near Willard, New Mexico is described including the modifications made during operation. Additionally, a maintenance summary is given. System operation results are given for the summer solstice, June 21, 1980.

INTRODUCTION

Whereas an estimated 20% of all agricultural production in the United States is produced through irrigation, agriculture's share of the total petroleum consumption is only 2.6%. Moreover, field-pumping of irrigation water requires approximately 20 percent of the total energy used for farm production in 1974 [1]. In New Mexico, 1,240,000 acres were irrigated in 1979 by 15,000 wells averaging 250 feet in depth and 8 inches in diameter. The distribution in fuel-type for New Mexico in 1979 was: 10%-diesel, 25%-electric, 5%-gasoline, 5%-LP gas and 55% natural gas [2].

In Curry county, New Mexico, natural gas over the past four years has increased in price over 300% [3]. The anticipation of rising fuel prices in 1975 precipitated the design and construction of the Estancia Valley Solar Irrigation Project completed in 1977. The project is located on a commercially operated farm managed by Paragon Resources*. The irrigation system is located approximately two miles southwest of Willard, New Mexico. The climate is characterized by low rainfall-- 12-25 inches per year--and a relatively high level of solar radiation during the growing season.

The power system designed involves the conversion of solar-thermal energy into mechanical energy by a Rankine cycle heat engine. Because off-the-shelf components were used to fabricate the system, peak solar collection temperature was limited to approximately 260°C (500°F) which bounded the overall system efficiency.

SYSTEM DESCRIPTION

Irrigation pumping provided a continuous load but necessitated the addition of a thermal storage system to meet the pumping demand. The power system can be divided into three subsystems--collection, storage and the heat engine. Collection of solar radiation was accomplished by trough-type, single-axis tracking collectors providing an aperture area of 1276 m^2

*Paragon Resources Inc., 4500 Borgan Road NE, Albuquerque, New Mexico 87109

(13,720 ft^2). The collectors were fabricated by two manufacturers-- Acurex Corporation and Solar Kinetics Incorporated. The thermal storage sub-system utilized a thermocline to effectively store useable energy. The organic Rankine cycle heat engine incorporated R113 as the working fluid and was fabricated by Barber-Nichols Engineering. The heat transfer fluid used throughout the power system was Caloria HT 43 manufactured by Exxon Incorporated. A belt-driven induction generator provided electrical power when mechanical power is not required. Table 1 summarizes the basic specifications of the system and Figure 1 is a shematic diagram showing the relative location of the components.

Table 1

GENERAL SPECIFICATIONS FOR THE WILLARD POWER SYSTEM

Location:	Estancia Valley, near Willard, New Mexico; latitude, 34.2°; elevation, 1835 m (6019 ft).
Irrigation:	Well-depth, 32 m (105 ft); irrigated area, 0.57 km^2 (140 acres); holding pond capacity, 5560 m^3 (4.5 acre ft).
Solar Energy Collection:	Parabolic trough, north-south axis, east-west tracking; Solar Kinetics Inc. collector field area, 651 m^2 (7000 ft^2); aperture width, 2.1 m (7.0 ft); Acurex Inc. collector field area, 625 m^2 (6720 ft^2); aperture width, 1.8 m (6.0 ft); heat transfer fluid, Caloria HT 43; maximum collector recirculation temperature, 216°C (420°F); storage tank (2) volume, 51.9 m^3 (13,720 gal).
Power System:	Barber-Nichols Engineering Rankine cycle engine with preheater and regenerator; working fluid, R113; peak boiler conditions, 163°C (325°F) and 1150 kPa (255 psia); condensing water, less that 16°C (60°F); condenser conditions, 30°C (86°F) and 55 kPA (8 psia); turbine single-stage, radial-inflow, reaction-type, 99 mm (3.9 in.) diameter, 36,330 rpm rotational speed; gearbox, two-stage, 1800 rpm output rotational speed.

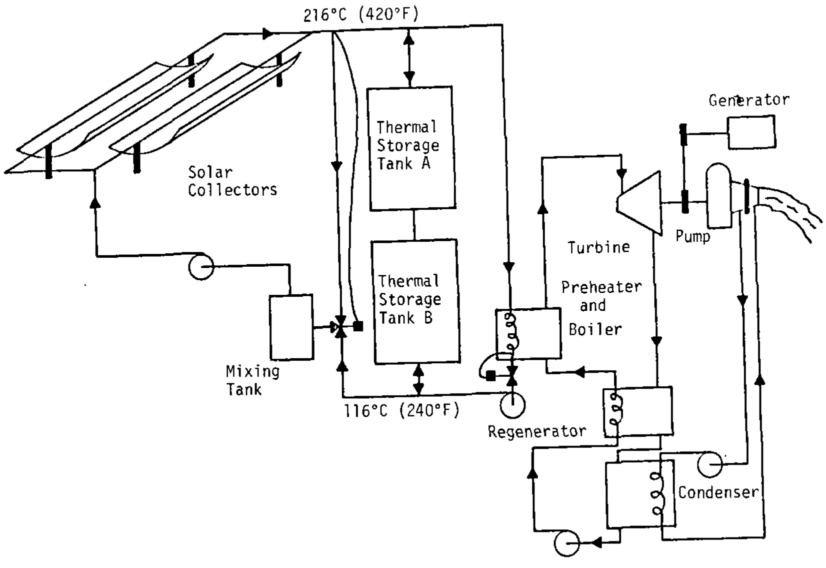

FIG. 1. SCHEMATIC DIAGRAM OF THE WILLARD SOLAR POWER SYSTEM

Although specific modes of operation can be discerned, a clear distinction among the modes does not exist. This feature is also exhibited with actual operation of the system. For example, hot oil from the collector field may have insufficient flow to satisfy the heat engine requirement. To make up the hot oil deficiency, hot oil is automatically drawn from the storage tanks. However, the points of "cross over" involve pure operational modes, but only exist momentarily. The four discernable modes of operation are as follows:

Mode Number	Mode Description
1	Collector Array Recirculation
2	Collector Array Recirculation and Hot Oil-to-Storage
3	Storage Hot Oil-to-Heat Engine
4	Hot Oil from Collector Array-to-Heat Engine and Hot Oil to or from Storage

Only the oil flow circuits define the modes of system operation.

OPERATIONAL SYSTEM MODIFICATIONS

With operation of the power system, modifications were made in several categories to improve overall system performance. However, in some cases, modifications were made in conjunction with component repair to regain system operation. This was particularly true with the turbine-gearbox assembly. The main categories of activity were: collector array, electrical controls and the heat engine.

Electrical Controls -- Several electrical control circuit changes were made to accomodate addition of the induction generator. Modified main control panel logic to conform to standard industrial practice and expanded control of collector arrays (wind switch and pyranometer controls applied identically to both arrays). Changes applied to electric well-pump to accommodate system automatic operation.

Collector Array -- Acurex: replacement of receiver tube cover glass, turbulator ribbon and improvement to the tracking mechanism and the pyranometer controlled "hold" function. Solar Kinetics: added "hold" function to tracking circuit, installed a desteer control, replaced mercury switches with limit switches for stow control and replaced east/west stow relays from 115 VAC to 24 VDC. As both collector arrays were first generation, the changes performed were not unreasonable.

Heat Engine -- More effective condenser pump control, addition of turbine-gearbox overspeed shut-down control, condenser float valve modified to provide a feed pump bypass. The turbine-gearbox was modified to increase the original critical speed of 36,000 RPM (near nominal operating speed) as follows: eliminated one of two high-speed turbine seals, shortened turbine wheel cantilever shaft overhang by 2.5cm (1 in) and eliminated the turbine wheel shroud.

A summary of the maintenance performed on the complete system normalized with respect to the total engine operational time of 1386 hrs is given in Figure 2. The maintenance items are classified as: collector field, thermal storage, Rankine cycle heat engine, agricultural or field work, data acquisition and the project site grounds. Major maintenance activities have included modification of the collector control equipment, receiver tube and glass cover replacement, removal and installation of the turbine assembly and leak repair and replacement of the R113 inventory.

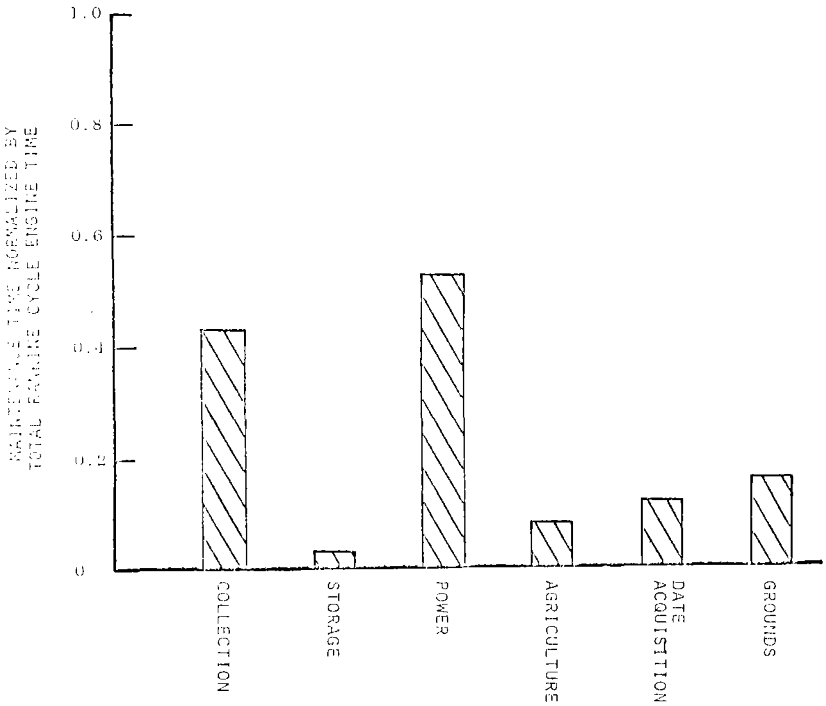

FIG. 2. MAINTENANCE SUMMARY OF THE WILLARD POWER SYSTEM FOR 1979

OPERATIONAL RESULTS

Operational characterization began in January 1980. Because the collector field was oriented for optimum collection during the summer months, the results of summer solstice are presented. Condition of the collector arrays affects operational performance and is therefore significant. The total reflectivity of the reflective surface was about 50% for Acurex (polished aluminum) and about 85% for Solar Kinetics (aluminized mylar) accompanied by an error band of $\pm$ 5% [4]. The reflectivity measurement was performed at the project site approximately a week before the data reported here. Additionally, the Acurex receiver tube cover glass exhibited no breakage compared to the 48% breakage (length basis) for Solar Kinetics.

Figure 3 shows the instantaneous solar radiation (direct and normal) for day number 173 which is the summer solstice, June 21. The morning was characterized by clear conditions and the afternoon by intermittant clouds. Figures 4, 5 and 6 give the instaneous efficiency for the total array, the Acurex array and the Solar Kinetics array respectively. Note that relatively steady operation occured in the morning in contrast to the afternoon. Indeed, the top-most points were restricted in value (direct beam radiation reduces to zero upon cloud passage but stored thermal energy in the collector flow loop releases a net thermal energy). The bars located about the collector efficiency data points indicate the uncertainty at the 95% confidence level. All other experimental uncertainties fall within the boundary of the data point itself.

Figure 7 and 8 show the variation of storage tank temperature and the total stored energy relative to 38°C (100°F). Observe that the thermocline or temperature gradient was stable throughout the day irregardless of the direction of oil (energy) flow. Figure 9 summarizes the energy transport rates occuring within the system. For example, note that between 9 and 12 o'clock, the collected thermal energy was divided such that 1/3 was delivered to the heat engine and the remaining 2/3 to storage. The mixing of operational modes due to clouds was observed in the afternoon. Figure 10 gives the instantaneous Rankine cycle heat engine efficiency for the

1980 summer solstice. Start-up transients persisted for almost an hour and during the period of active solar energy collection, operating conditions shifted. Later, upon heat engine operation from storage, operation was smooth and stable. On this particular day, parasitic electrical power consumption absorbed 18% of the output power (electrical) which was below the 27% average for this period. The total net electrical power produced this day was 243 KWH.

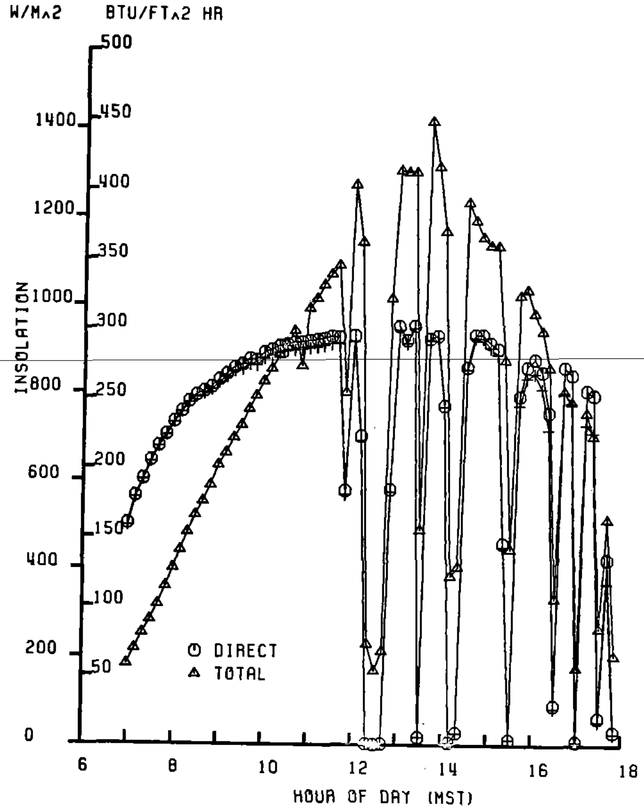

FIG. 3. INSTANTANEOUS SOLAR RADIATION FOR JUNE 21, 1980

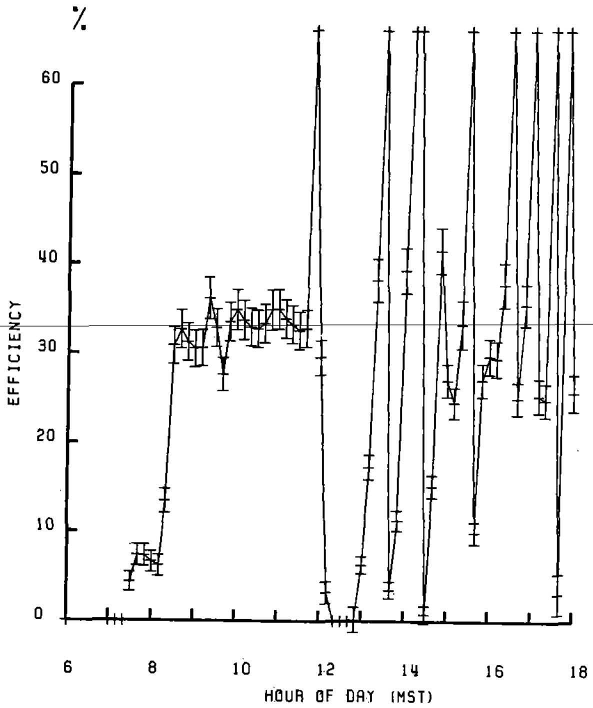

FIG. 4. INSTANTANEOUS TOTAL COLLECTING ARRAY EFFICIENCY FOR JUNE 21, 1980

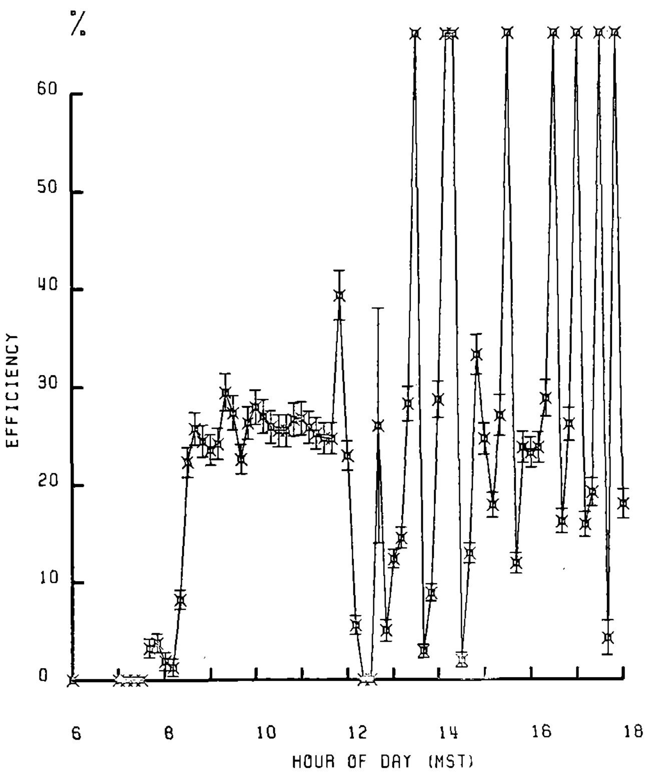

FIG. 5. INSTANTANEOUS ACUREX COLLECTOR ARRAY EFFICIENCY FOR JUNE 21, 1980

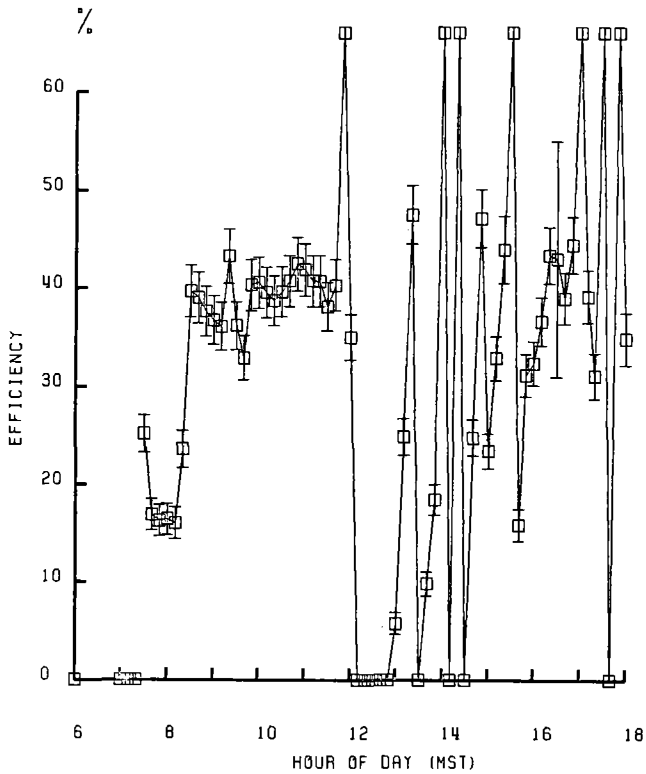

FIG. 6. INSTANTANEOUS SOLAR KINETICS COLLECTOR ARRAY EFFICIENCY FOR JUNE 21, 1980

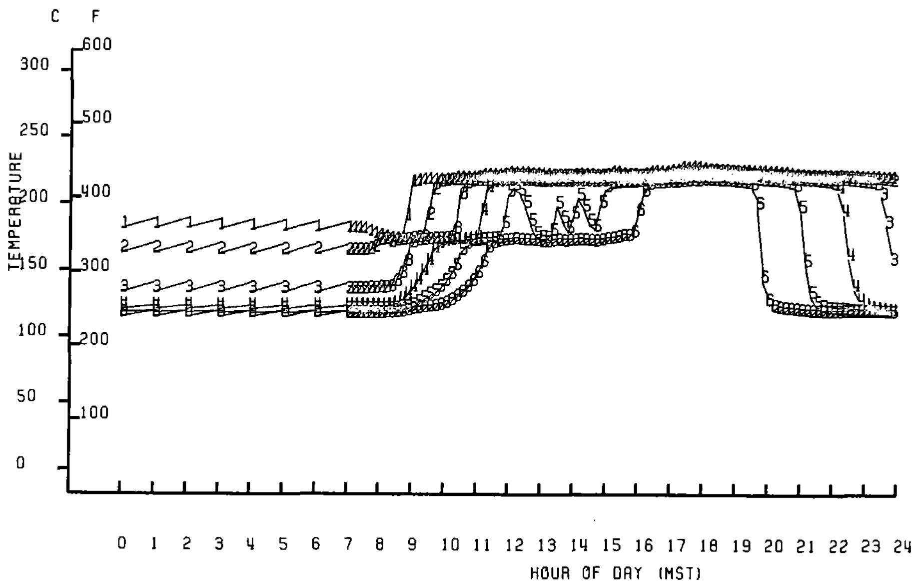

FIG. 7. VARIATION OF OIL TEMPERATURE IN TANK A FOR JUNE 21, 1980

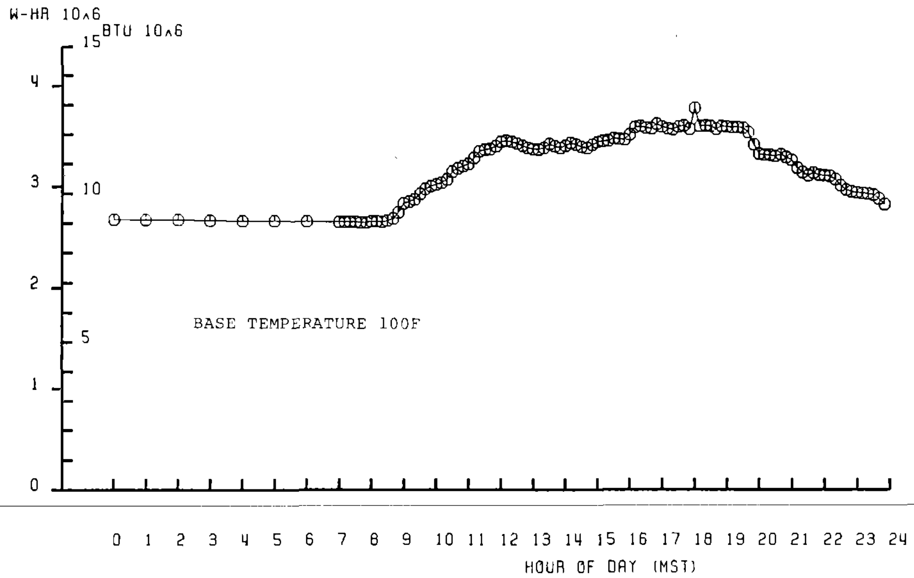

FIG. 8. VARIATION OF STORED THERMAL ENERGY FOR JUNE 21, 1980

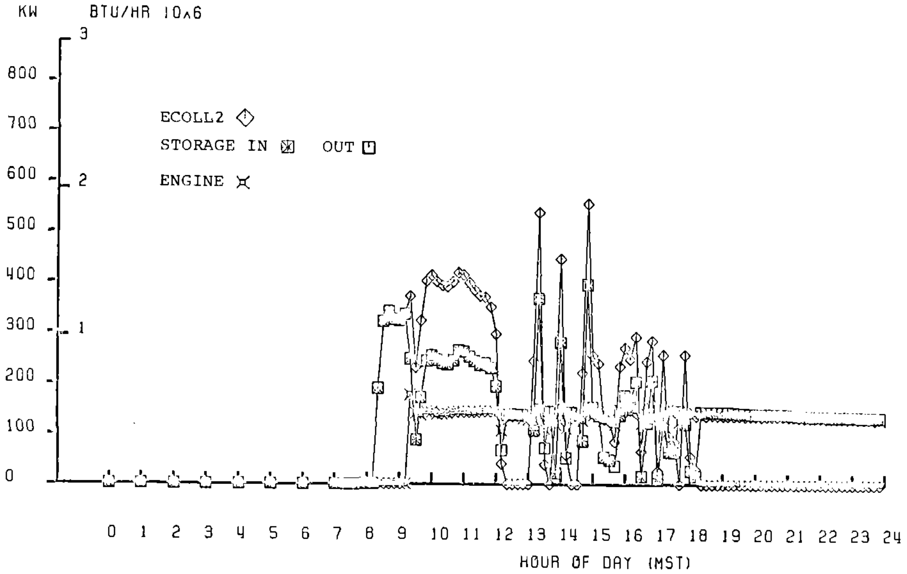

FIG. 9. ENERGY TRANSPORT SUMMARY FOR JUNE 21, 1980

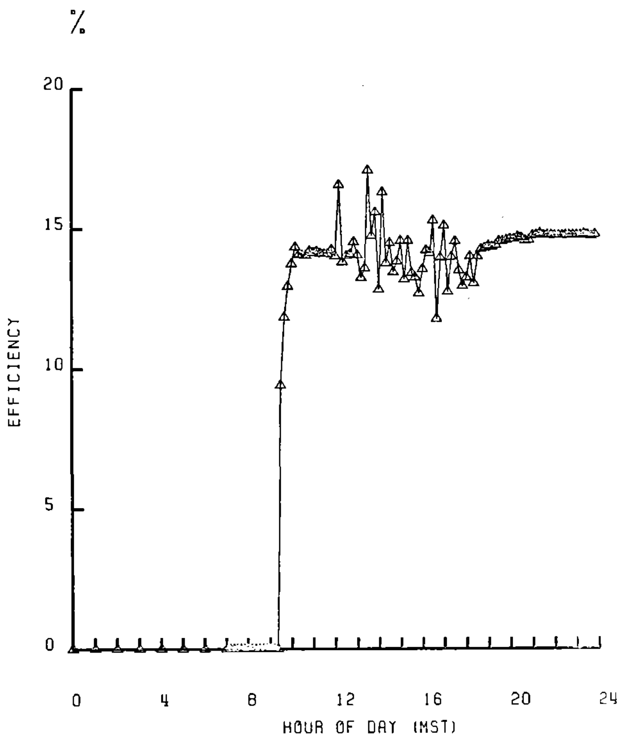

FIG. 10. INSTANTANEOUS RANKINE CYCLE HEAT ENGINE EFFICIENCY FOR JUNE 21, 1980

REFERENCES

1. Sloggett, G., "Energy Used for Pumping Irrigation Water in the United States", Agriculture and Energy, ed. by W. Lockerty, Academic Press, New York, pp. 113-147 (1977).

2. Anon., "Irrigation Survey 1979", Irrigation J., Vol. 29, No. 6, p. 58 (1979).

3. Abernathy, G. H., "Efficiency of Irrigation Plants Curry County", Cooperative Extension Service, New Mexico State University, Guide No. M-203.

4. Freese, J. M., "The Development of a Portable Specular Reflectometer for Field Measurements of Solar Mirror Materials", SAND 78-1918, Sandia Laboratories, Albuquerque, New Mexico (October 1978).

Coolidge 150 kWe Solar Irrigation Project

Dennis L. Larson
Soils, Water and Engineering Department
University of Arizona
Tucson, AZ 85721

Abstract

Construction of a 150 kW solar thermal-electric power plant on an irrigated farm near Coolidge was completed in autumn, 1979. The plant, designed by Acurex Corporation, includes over 2100 m^2 of Acurex-made parabolic trough type collectors and an organic Rankine cycle turbine engine built by Sundstrand Corporation. The plant is interconnected with the electrical utility grid. The installation is being operated by The University of Arizona with Sandia Laboratories direction. Operation is providing an evaluation of equipment performance and operating and maintenance requirements as well as the desirability of an on-farm location.

Background

In 1974, the magnitude of irrigation energy requirements, potential natural gas shortages and greatly increased energy costs motivated Arizona farmers to request an evaluation of the use of solar energy to drive irrigation pumps. A 1975-76 University of Arizona feasibility study listed a number of engineering and economic factors to be considered and conditions to be met for successful marketing and use of solar powered pumping plants (Larson et al., 1978). These included development of efficient, economical equipment, full utilization of the produced energy and availability of capital at a modest price.

In 1977, two solar thermal power plants were constructed on farms in the Southwest. Parabolic trough type solar collectors and Rankine cycle turbine engines are the principal components of both plants (Abernathy and Mancini, 1977; Alexander et al., 1978). The installations, a 50 kW unit located on a farm near Gila Bend, Arizona and a 25 kW plant constructed on a Willard, New Mexico farm, are directly coupled to pumps with backup electric motor drives. The Willard installation includes considerable thermal energy storage capacity for nighttime operation while the Gila Bend plant has none.

Later in 1977, three firms were contracted to develop conceptual designs of solar thermal-electric power plants by the U.S. Department of Energy. Honeywell proposed use of several large parabolic dish collectors, each supporting a small Brayton cycle turbine engine and generator set. The Black and Veatch design consisted of a field of heliostats, central receiver mounted on a tower and Rankine cycle engine. Acurex proposed a field of single axis tracking, parabolic trough type collectors and Rankine cycle engine. The Acurex concept was selected for construction, appearing to have the fewest technical unknowns and be most economical at that time. Procurement began in 1978; on-site construction later in the year. The operational plant was dedicated in November, 1979.

The chosen plant site is the Dalton Cole farm, located southwest of Coolidge in central Arizona. The power plant generates electricity since existing pumps were electrically driven and electricity could be readily used for other applications. Plant size was selected to meet the energy requirements of deep well pumping to provide irrigation water for a quarter section (160 acres or about 65 hectares) of Arizona cropland. The solar plant is being operated by the University of Arizona under contract with Sandia Laboratories.

Plant Description

The Coolidge power plant consists of solar collector, energy storage and energy conversion subsystems, Figure 1 and Table 1. The collector subsystem consists of 8 collector loops, each containing 48 collectors. Collector modules are 1.83m wide by 3.05m long (6 feet by 10 feet) and have reflective parabolic surfaces of polished aluminum. The solar concentration ratio is about 36 to 1. Collector receiver tube is coated with a selective black chrome surface and surrounded by a pyrex tube. The collectors, manufactured by Acurex, are arranged in a series of north-south oriented rows and track the sun from east to west. Present solar collector area is about 2130 square meters (23,000 square feet).

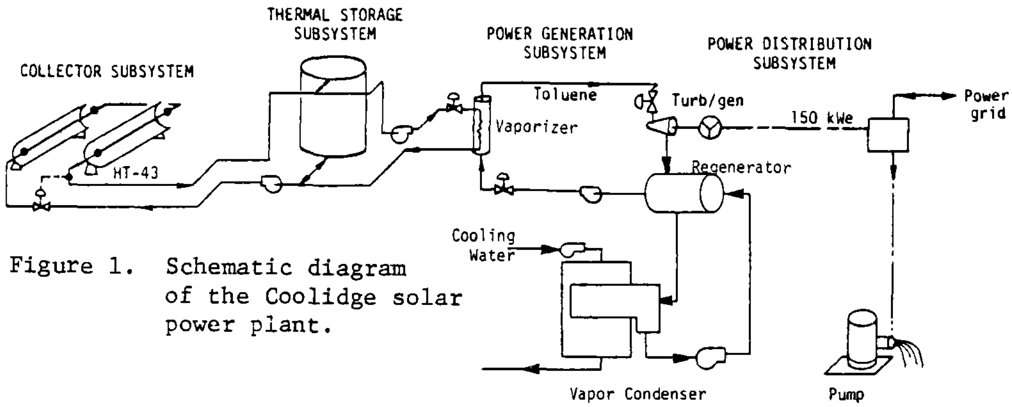

Figure 1. Schematic diagram of the Coolidge solar power plant.

A heat transfer oil, Caloria HT-43, is pumped through the receiver tubes at a rate controlled to obtain the desired outlet temperature, usually about 288°C (550°F). Energy storage is a 114 cubic meter (30,000 gallon) tank of hot oil, sufficient for approximately six hours of turbine generator operation. Present collector area can provide energy for up to eight hours of operation on a sunny June day. Additional collector area would increase the electrical generation period.

Energy conversion is accomplished by a Rankine cycle turbine engine through expansion of the organic fluid toluene. The engine, made by Sundstrand Corporation, is a scaled down version of one developed for other relatively low temperature applications such as conversion of power plant waste heat. The toluene is preheated in a regenerator, vaporized in a shell and tube heat exchanger and cooled in a condenser cooling tower. Nominal gross generator output is 200 kW; net electrical power produced is over 150 kW.

The plant is interconnected with the utility grid. Electric District Number Two, the local utility company, receives energy generated by the plant and supplies energy required to meet solar plant and irrigation pump needs. Generated energy surplus to plant requirements is purchased by the utility.

Table 1. Subsystem Description

Collector Field:		**Vaporizer:**	
Size	2140 m^2	Type	3-stage shell and tube
Orientation	N-S	Flowrates	Caloria HT-43: 15,740 kg/hr Toluene: 6305 kg/hr
Fluid	Caloria HT-43		
Temperatures	Inlet 200°C, outlet 288°C		
Design cond.	q_i = 599 W/m^2 $\dot{m}$ = 7575 kg/hr System eff. = 38.6%	**Turbine:**	
		Type	1-stage, impulse
		Inlet conditions	268°C, 1034 KPa
		Outlet conditions	41°C, 10 KPa
Thermal Storage:		**Electrical Generator:**	
Type	Thermocline		
Tank size	189 m^3 -- 4.2-m dia. x 14.9-m	Power rating	250 kVA
		Gross power	203 kW
Storage temp.	200°C to 288°C		
Storage medium	Caloria HT-43	**Controls:**	
Insulation	0.3-m, fiberglass	Collector cont.	Shadow band tracker
		Fluid temp	Variable flowrate, constant temp.
Cooling System:			
Type	Vapor condenser	Power generation subsystem cont.	Turbine speed, toluene flow
Water (makeup)	38ℓ/min		
Condensing temp.	41°C		
Power Generation:		**Auxiliary Oil Heater:**	
Type	Organic Rankine cycle		
Working fluid	Toluene	Type	Natural gas burner
Gross eff.	20%	Flowrate	15,876 kg/hr
		Inlet temp.	200°C
		Outlet temp.	288°C

Table 2. Cost Comparison of Solar-Thermal Electric Systems

	200 kW (Gross); 23,040 ft^2	
	Actual Cost of Current System \$000 (\$/ft^2)	Recurring Costs of Same System \$000 (\$/ft^2)
Installed collectors	810 (35) [a]	530 (23)
Construction and field installation	833 (36) [b]	645 (28)
Building	50	50
ORC subsystem	1068	650
Storage subsystem	209	150
Controls and data acquisition equipment	358	150
Design and field support	1493	150
Management	530	200
Total	5351	2525
\$/gross watt	26	12

[a] Collector hardware, installation on foundations and plumbing of the collector field.

[b] Site preparation and foundations, \$8/ft^2; mechanical on-site contract, \$15/ft^2; electrical on-site contract, \$10/ft^2; insulation on-site contract \$3/ft^2.

System Cost

The total cost incurred for the design, procurement, construction, and startup of the facility over the 2-year period ending 30 September 1979 was $5,351,000. Of this amount, approximately $2,023,000 was spent on labor and $3,328,000 on subcontracts, equipment, etc. These costs have been adjusted to exclude the expenses associated with site preparation and foundations installed for an addition to the collector field.

Table 1 presents a breakdown of costs and compares the actual system cost for the Coolidge plant with the estimated cost for building another similar installation. The same system, built today, would cost significantly less, only an estimated $2,525,000, due to nonrecurring costs of labor, engineering, management and data acquisition equipment, and experience with similar systems. An estimate by Acurex Corporation indicates that a modified system, containing more collectors and less thermal energy storage capacity, would result in lower power production costs. Mass production of equipment would further reduce costs.

System Performance

The Coolidge solar plant began operating early in October of 1979. Since January 1, 1980, the plant has operated daily except for a period from mid-February to early March. A fire in the shaft shroud area of the collector field pump necessitated pump removal and repair. Inclement weather delayed repair efforts. The collector system was operated 95 percent of the possible operating time during the months April through July. Repair and evaluation activities and weather conditions were responsible for inoperation. The power conversion system was operated 82 of the 92 days in May, June and July. Inoperative days were due primarily to insufficient energy availability.

Thermal energy gathered by the solar collector field is shown in Figure 2a as the cross hatched portion of the vertical bars. The bars also show solar energy availability and solar energy available during collector operation. Low solar energy availability during operation in February and March was due to the pump outage. Collected thermal energy, as a percentage of solar energy available during operation, ranged from 7.5 in January to 20.6 in March to over 32 percent in June and July.

The plant generated 22,000 kWh of electrical energy in June, the peak period. Output in May and July was nearly as large, Figure 2b. However, a natural gas fired boiler provided a large amount of the thermal energy required for turbine operation during the quarter surrounding winter solstice. Solar thermal energy collected during that period was too low temperature for efficient conversion.

Collector system efficiency was determined on clear days near the times of winter solstice, spring equinox and summer solstice. Collectors were washed prior to tests. Throughout evaluation, the Caloria flow rate was controlled to maintain the desired, constant collector system outlet fluid temperature. Collector system efficiency was computed as the thermal energy gained by Caloria during passage from inlet to outlet manifold locations divided by the total direct normal solar radiation intercepted by the collector area. Insolation received during the entire operating day was used in the computation of average system efficiency.

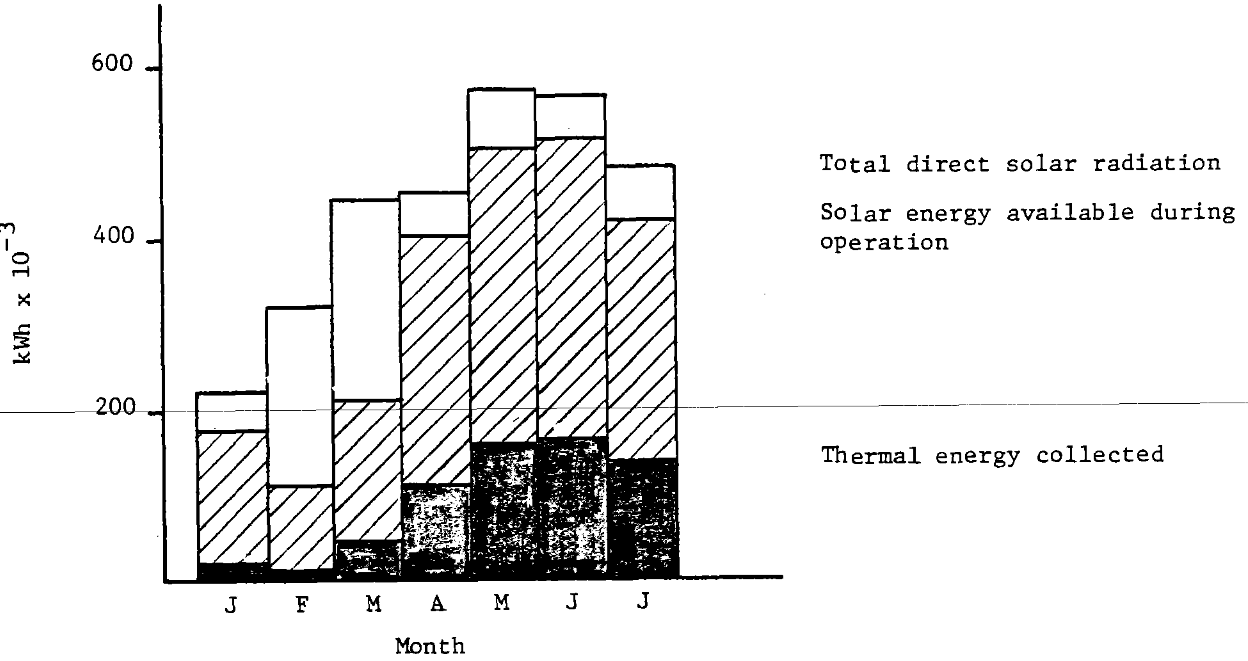

Figure 2a. Solar energy available and thermal energy collected by the plant from January through July, 1980. Low amounts of available insolation during operation in February and March are due to pump outage for repair.

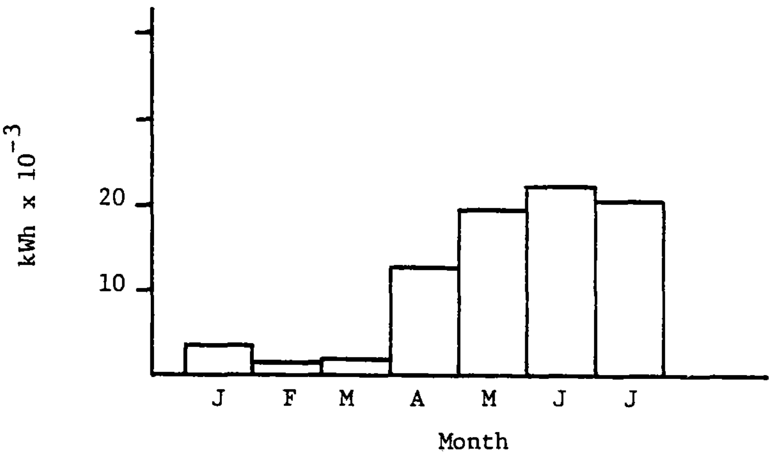

Figure 2b. Electrical energy generated by the plant from January through July, 1980.

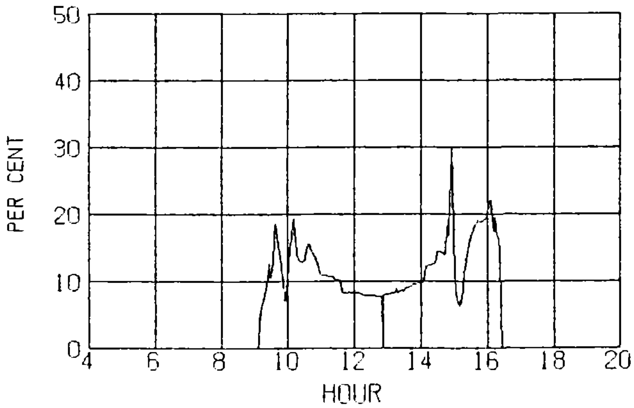

Figure 3a. Collector system efficiency on December 18, 1979. Inlet temperature $\simeq$ 192C, outlet temperature $\simeq$ 232C, peak direct solar radiation = 945W/m^2.

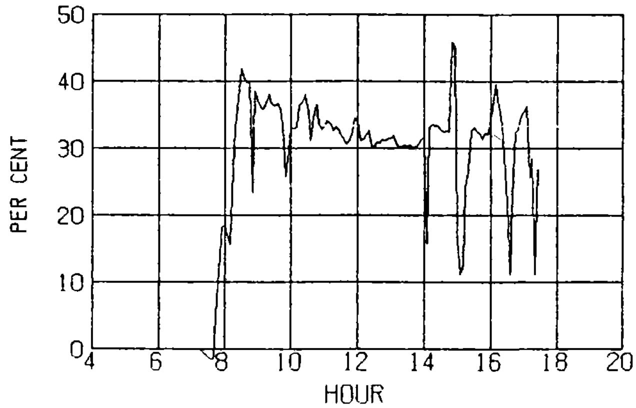

Figure 3b. Collector system efficiency on April 3, 1980. Inlet temperature $\simeq$ 189C, outlet temperature $\simeq$ 285C, peak direct solar radiation = 968W/m^2.

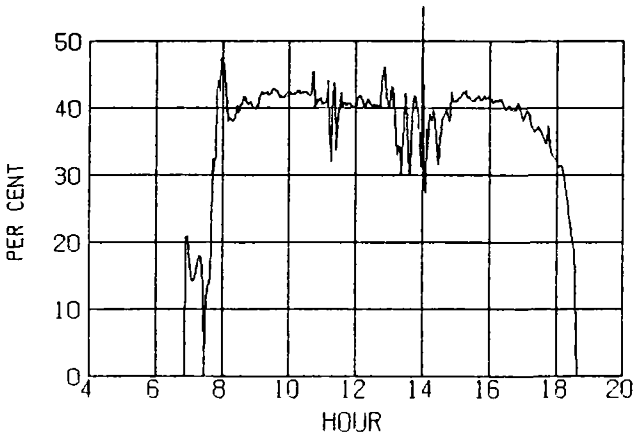

Figure 3c. Collector system efficiency on June 25, 1980. Inlet temperature $\simeq$ 187C, outlet temperature $\simeq$ 284C, peak direct solar radiation = 896W/m^2.

The mid-day collector system efficiency was 40-42 percent on June 25, 30-37 percent on April 3, and 8-15 percent on December 18, Figures 3a-c. Thermal energy collection rates were about 750 kW, 650 kW, and 200 kW on these three days respectively. Collector fluid outlet temperature was maintained at about 284C on June 25, 285C on April 3 and 232C on December 18; inlet temperatures were 185-200C during all tests. Too little energy was collected to conduct a stable, comparable evaluation at the higher temperature during the winter solstice period. Average collector system efficiencies were 36.9 percent on the summer test day, 30.1 percent during the spring test and 9.9 on the winter test day.

Summary

The Coolidge solar thermal-electric power plant was completed in October 1979 at a cost of 5.3 million dollars. Except for a late winter repair period, the plant has operated on a daily basis. Operation has characterized component and plant operation and determined repair and maintenance requirements. Operation in 1980-81 will obtain continued operational and maintenance data.

References

1. Abernathy, G.H. and T.R. Mancini. Design and installation of a solar-powered irrigation pump. Paper No. 77-4020, ASAE, St. Joseph, MI (1977).

2. Alexander, G., et al. Modification and 1978 operation of the Gila Bend solar-powered irrigation pumping system. Publ. No. SAND 79-7009, Sandia Laboratories, Albuquerque, NM (1978).

3. Larson, D.L., et al. Evaluation of solar energy for irrigation pumping. Trans. Am. Soc. of Agr. Engr. 21 (1978)110-115,118.

4. Larson, D.L. Utilization of an on-farm solar powered pumping plant. Trans. Am. Soc. of Agr. Engr. 22 (1979)1106-1109,1114.

5. Matteo, M.A. and D. Rafinejad. Design, construction and operation of a solar powered 150 KW irrigation facility. Proc., American Sec., Int. Soc. for Solar Energy Meeting, Phoenix, AZ. pp. 519-523 (1980).

6. Matteo, M.A. Personal correspondence, costs of the Coolidge and future similar solar power plants. Acurex Corp., Mountain View, CA (1980).

IEA/SSPS 500 kw DISTRIBUTED COLLECTOR SYSTEM

Hans Dehne
and
Don R. Duffy
Acurex Corporation
Mountain View, CA 94042

Introduction

The SSPS project, an IEA program, is directed at providing solar-electric system designs suitable for both industrialized and developing countries. Systems range from 50 kW to 5 MW and use a modular approach. Two demonstration plants (Figure 1) are presently under construction in the province of Almeria in southern Spain.

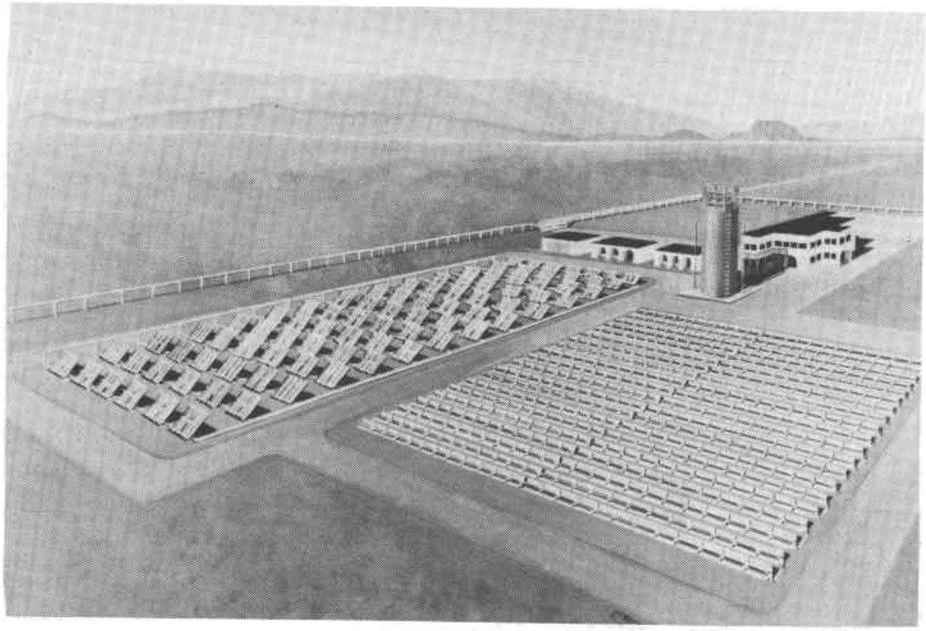

Figure 1. Model of SSPS Plants

The operating agent for the IEA on the project is the Deutsche Forschungsund Versuchsanstalt fur Luft-und Raumfahrt e.V (DFVLR), a scientific and research agency of the German government. A consortium of Acurex Corporation (U.S.) and Tecnicas Reunidas (Spain), supported by subcontractors from participating countries, conducted the Phase I design for DCS. An international consortium lead by Interatom (Germany) designed the CRS. DCS is being constructed by a consortium of Acurex Corporation (U.S.), M.A.N. Neue Technologie (Germany), and Tecnicas Reunidas (Spain), while a consortium of Interatom (Germany), Martin Marietta (U.S.), and SAIT (Belgium) constructs the CRS.

Buildings and infrastructure are being designed and built by the firms Initec and Laing (Spain). Subsystems for the two plants are being procured in participating countries.

The two adjacent plants are being constructed on the "Plataforma Solar" provided by Spain and will utilize a common building for power generation and to house control equipment. These facilities will allow easy comparison of economic, technical, and operational characteristics because solar conditions for each system will be identical at a given time. In addition to these two systems, a third CRS plant sponsored by Spain is being constructed nearby.

The major technical requirements for the SSPS plan designs are:

- o A net electric power output of 500 kW when the direct normal insolation at the site equals or exceeds 920 W/m^2 at equinox noon
- o An operational availability of 24 months after the contract begins
- o Maximum use of advanced but available and proven components
- o To the greatest extent possible, a capacity for scale-up to higher energy outputs or scale-down to lower energy outputs without major changes in the design principles
- o The possibility of operation both for delivery of power to an interconnected grid and for generating power at an isolated site
- o A design and technology suitable for utilization in both developed and developing countries which requires plants to be as simple as possible to allow operation with a minimum of personnel training and/or education

The two systems were optimized, taking into account finances, international requirements, and technical objectives.

500 kWe Central Receiver System (CRS)

A simplified process flow diagram for the CRS is shown in Figure 2. The heliostat field will consist of 93 units, each with a reflective surface area of 39.95 m^2. The receiver will be mounted on a tower south of the field at an elevation of 43 m. Sodium, the heat transfer medium, will be stored in a "hot" and a "cold" vessel. Hot sodium will be used to produce steam to drive a "spilling" steam motor.

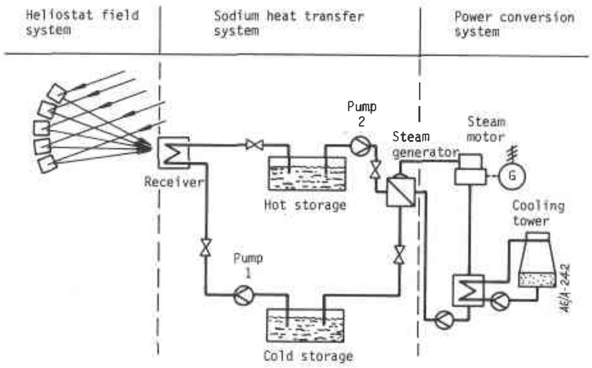

Figure 2. Simplifed Process Flow Diagram SSPS CRS

The main design data are presented in Table 1.

Table 1. Main System Design Data for CRS

Design point	Day 80, 12:00 (equinox noon) solar insolation, kW/m_2	0.920
Heliostat field	Total reflective surface area, m^2	4,000
Receiver	Aperture size, m^2	9
	Active heat transfer surface, m^2	16.9
	Inlet temperature, ^oC	270
	Outlet temperature, ^oC	530
Thermal storage	Storage medium	Sodium
	Thermal capacity, MWh	5.5
	Hot storage temperature, ^oC	530
	Cold storage temperature, ^oC	275
Steam generator	Sodium inlet temperature, ^oC	525
	Sodium outlet temperature, ^oC	275
	Water inlet temperature, ^oC	190
	Steam outlet temperature, ^oC	510
	Steam pressure, bar	100
Power (at design point)	Solar insolation, kW	3,675
	Thermal, kW	2,283
	Gross electric, kW	600
	Net electric, kW	517
Efficiencies (at design point)	Thermal/gross electric, %	26.3
	Thermal/net electric, %	21.9
	Insolation/net electric, %	14.1

500 kWe Distributed Collector System (DCS)

The major subsystems for the DCS include two collector fields, an energy storage system, a steam generator, a power conversion system, a control and data acquisition system, an electrical system, support equipment, and the infrastructure. The simplified process flow diagram in Figure 3 shows the general arrangement of these subsystems. The DCS plant design data are presented in Table 2.

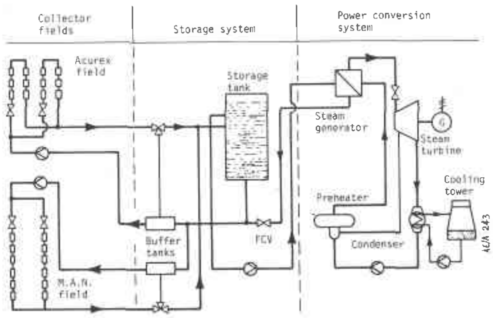

Figure 3. Simplified DCS Process Flow Diagram

As can be seen from the data in Table 2, two fields of approximately equal size are planned with a total collector area of $5{,}382 m^2$. One field is made up of 10 loops of four collector groups each designed and manufactured by Acurex Corporation, while the other field is made up of 14 loops of six collectors each designed and manufactured by M.A.N. Neue Technologie, a Germany company. The Acurex collectors are single-axis tracking with the rotational axis oriented east-west. The M.A.N. collector uses two-axis tracking. The entire plant including thermal storage and equipment, fits into an area 210 m east-west by 168 m north-south.

Table 2. DCS Plant Design Data

Design point	Day 80, 12:00 (equinox noon) solar insolation, kW/m^2	0.920
Collector fields	Total aperture area, m^2	5,362
	(M.A.N.: 2,688 m^2)	
	(Acurex: 2,674 m^2)	
	Collector input temperature, °C	225
	Collector output temperature, °C	295
	Heat transfer medium, Santotherm 55	
	M.A.N. collector, type 3/32 Helioman 64 modules in 14 loops	
	Acurex collector, type 3001, 40 groups in 10 loops	
Thermal storage	Storage medium, Santotherm 55	
	Capacity, equivalent to MWhe	800
Steam generator	Santotherm inlet temperature, °C	295
	Santotherm outlet temperature, °C	225
	Steam outlet temperature, °C	280
	Steam pressure, bar	25
Power (at design point)	Solar insolation, kW	4,933
	Thermal, kW	2,580
	Gross electric, kW	577
	Net electric, kW	500
Efficiencies (at design point)	Thermal/gross electric, %	22.4
	Thermal/Net electric, %	19.4
	Insolation/Net electric, %	10.1

The system has been designed with three heat transfer loops. The first loop extracts low-temperature heat transfer oil from the bottom of the thermal storage tank, circulates it through the collector fields, and returns it to the top of the storage tank; this decouples the solar fields from the power generation cycle. The second loop extracts hot oil from the top of the storage tank, circulates it through the boiler, and returns it to the bottom of the storage tank. The third loop circulates water through the boiler, expanding the steam through a turbine to extract energy for electrical power generation. The cycle is completed by condensing the expanded low-enthalpy steam then pumping the condensate back to the boiler. The thermal energy is converted to electrical energy using a steam turbine power conversion (PC) system.

The system design parallels that of the Coolidge, Arizona 150 kWe project; however, experience and improvements have been incorporated to gain higher efficiency, greater reliability, and lower cost. In this regard, the DCS plant brings the realization of economical solar energy another step closer. When this plant comes online, valuable operating experience will be gained for future improvements.

System Design

Collector Field Sizing Analysis

The collector field size was calculated using predicted efficiencies of the parabolic trough concentrating collectors; the M.A.N. collector has thick, sag glass reflective surfaces while the Acurex collector has thin, flex glass reflective surfaces. The collector efficiency parameters used in the analysis were later verified by tests which confirmed that the field sizing was sufficient to meet the energy delivery requirements. The analysis utilized the Soltan code with collector thermal performance curves and site weather data as input parameters. The analysis was carried out for both steady-state and transient behavior. Figure 4 shows the oil flow-rate into storage from the combined collector fields on the equinox day, as well as the start-up and operation of the PC system at the economical generation level of 500 kWe Net.

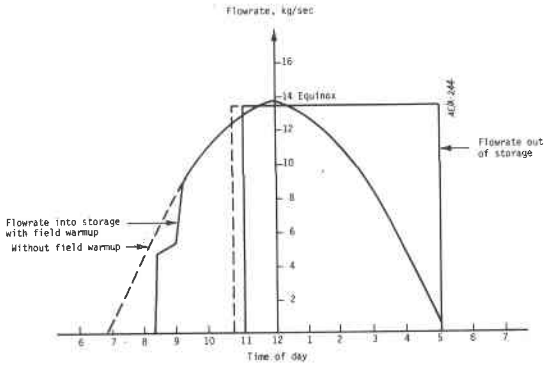

Figure 4. Storage of Thermal Energy (Equinox)

Collector Fields -- The layout of the collector fields depends on the type of collector used and often on the land available. Additionally, the field layout must minimize piping heat losses, pressure drop, transients, and parasitic electrical loads. These requirements are weighed against system inlet-outlet temperature requirements. The optimization for this plant resulted in 14 loops of M.A.N. collectors each with 192 m^2 gross collector area, and 10 loops of Acurex collectors with 257 m^2 gross collector area. The optimization was performed by assigning equivalent thermal units to pressure drop and electrical parasitics then looking for a minimum.

The Acurex collector will utilize thin, chemically tempered, laminated glass. Extensive tests conducted by Sandia Laboratories in support of this program showed the acceptability of thin glass bonded to a steel substrate by an acrylic film. This is a product developed by Glaverbel, Belgium. The SSPS project will benefit from the many improvements on the Acurex collector which have evolved from its use in various facilities. The Acurex as well as the M.A.N. collector had to qualify through tests prior to acceptance for this program. The Acurex collector is shown in Figure 5.

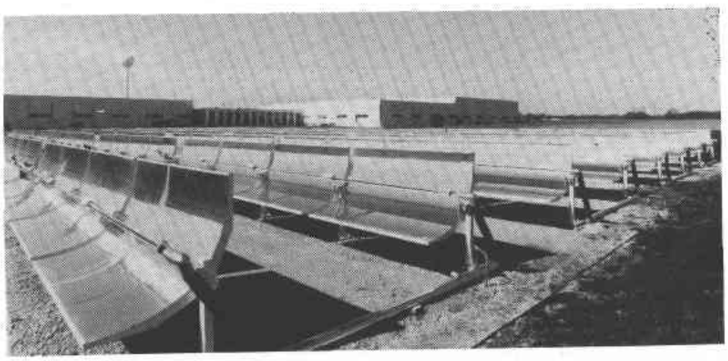

Figure 5. Acurex Collectors

The M.A.N. Collector is a double-axis tracking parabolic trough unit similar to a heliostat. The reflective glass is approximately 4 mm thick. This collector was tested in Madrid, Spain by an agency of DFVLR. Figure 6 shows the M.A.N. collector. Using two types of collectors (thin and thick glass, single- and double-axis tracking) within the same project was particularly attractive for purposes of performance and economic comparison.

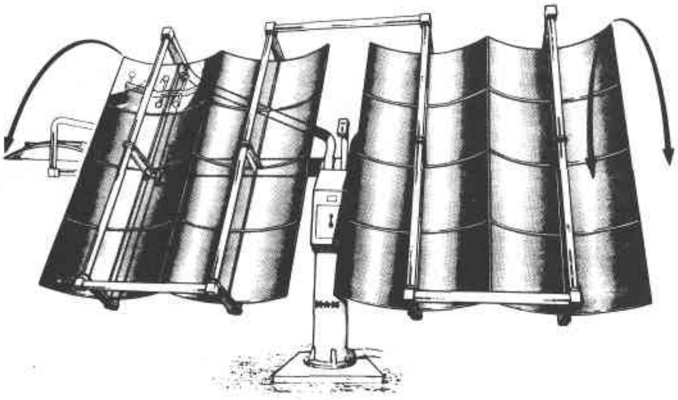

Figure 6. M.A.N. Collector Modulè Helioman

The temperature control system for both fields utilizes temperature control valves in each loop. Experience has shown that accurate temperature control cannot be assumed in each loop because the performance will vary with cleanliness, shading, and alignment. Accurate temperature control in this facility is important due to the high operating temperature which is near the acceptable bulk temperature limit for the heat transfer oil.

Storage System -- The thermal storage system consists of a thermocline scheme identical in size to the Coolidge tank but improved to enlarge its storage capacity, to reduce heat losses due to thermal syphoning, and to prevent leaks by eliminating flanged joints and minimizing the number of valves.

The pumps in the plant are centrifugal pumps, manufactured by Union Pump Company. Presently, only two or three pump manufacturers offer pumps with equivalent efficiencies and seals with high temperature capability. Careful attention must be paid to the seal configuration and possible flushing circuits if the seal area is to be kept clean and at an acceptable operating temperature.

Steam Generator -- The steam generator is comprised of two vessels. The evaporative incorporates the economizer by partitioning the oil flow in the vessel. A second vessel superheats the steam. The steam generator is oversized to accommodate large transients, and oil flow is controlled by a valve proportional to steam pressure and steam demand.

Power Conversion (PC) System -- The PC system selected for this plant consists of an eight-stage steam turbine coupled to a generator. The turbine auxiliary equipment includes the condenser, cooling towers, deaerators, ejector set, feed pump, feed water tank, and controls. This PC system offers high efficiency power conversion because of its multistage construction.

Control System/Data Acquisition System -- The control system combines a conventional analog control system and relay interlocks with a supervisory digital control computer produced by Hewlett-Packard. The multipurpose nature of the plant made a computer desirable, although plant operation is totally feasible with the computer shut down. The computer provides redundant safeguards, some automatic operations, and data acquisition. While unnecessary for operation in an undeveloped country, the computer in this application will aid in the test phases.

Auxiliary Systems -- The plant's remote location in Spain makes a certain independence necessary. For this purpose, a water treatment plant, fire-fighting system, emergency generator, uninterruptable power supply (UPS), and weather station are provided. The water treatment plant serves the boiler and collector cleaning needs. Critical areas are protected by the fire fighting system and hydrants. The emergency generator is sufficiently sized to start the plant and allows for startup during grid power failures, while the UPS provides uninterrupted operation should a power failure occur when the plant is operating. The weather station is used for plant control and anlysis purposes.

Piping Engineering -- Thermal systems employing heat transfer oils are subject to leakage. This plant therefore utilizes welded pipe joints and valves with a minimum number of flanges which are also a source of heat loss. Valve stems in hand valves are oriented to prevent oil leakage into insulation, while control valves employ bellows seals on the stem, backed by a packing. Pipes are kept to minimum lengths that can still accommodate thermal expansion movements while reducing heat losses; they are also oriented to prevent thermal syphoning from storage tanks.

Electrical and Instrumentation Engineering -- Standard electrical and instrumentation procedures were employed in the design. To make evaluations feasible, however, the plant is instrumented beyond the needs for operation.

Construction

Construction of the DCS plant is well underway. All equipment has been procured or is being manufactured. The infrastructure is complete, including buildings. Foundations for equipment have been laid, and collector installation has begun. Several preshipment tests have been concluded, with other tests imminent. Figures 7 through 11 show various construction activities at the site.

The schedule calls for completion and turnover of the plant by August 1, 1980. To date, no problems have surfaced with an impact on that completion date.

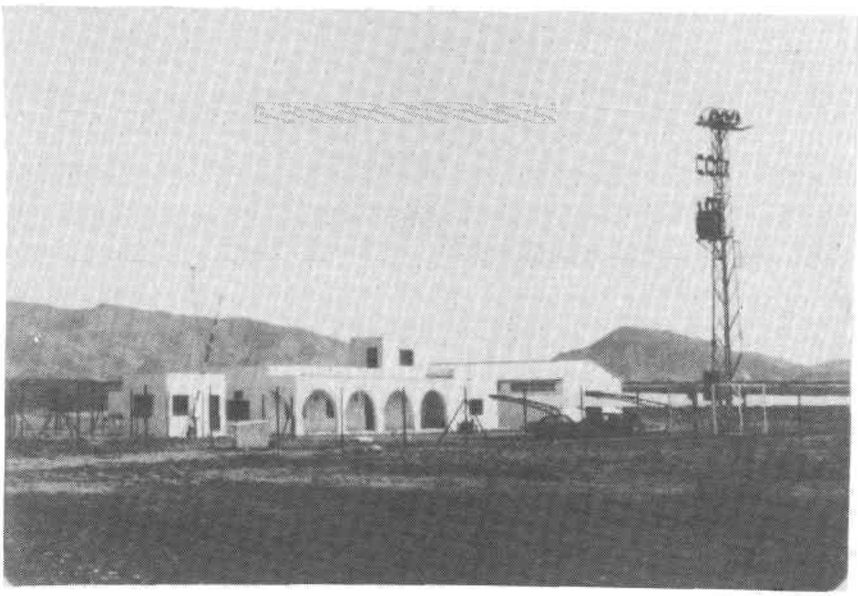

Figure 7. CEE Building

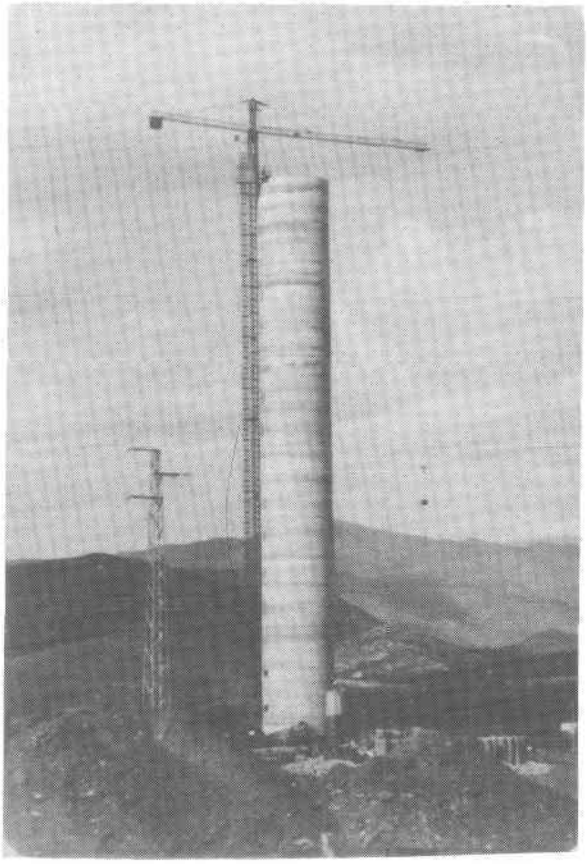

Figure 8. CESA-I CRS Tower

Conclusion

When completed, the SSPS power-plants will add valuable information to the area of solar energy technology; these systems which represent the latest technology applied in demonstration plants are in a unique configuration making comparison studies easier. Our energy needs demand that we pursue all avenues to improve the economics of solar energy and that we gain new information from every source. The SSPS plants offer the opportunity to advance the state-of-the-art in both design and operations.

Acknowledgements

DFVLR, M.A.N., Tecnicas Reunidas, S.A.

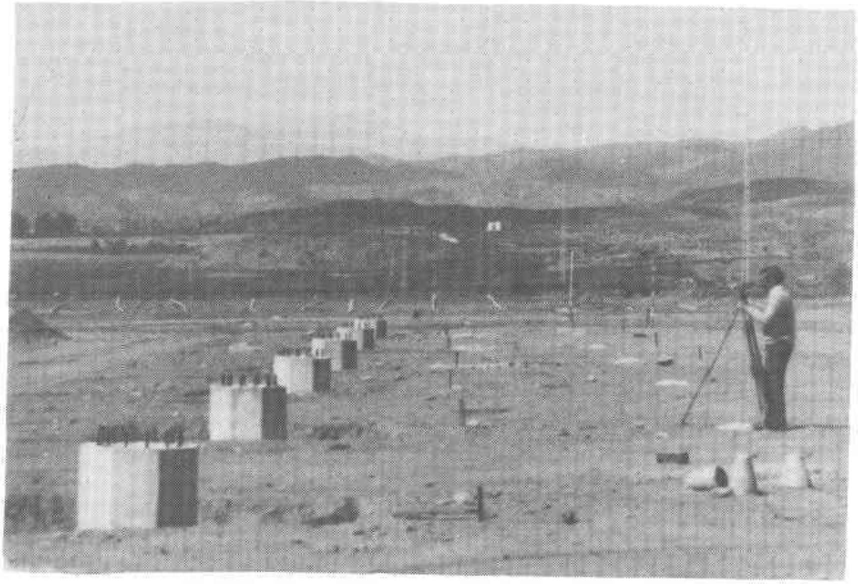

Figure 9. M.A.N. Collector Foundations

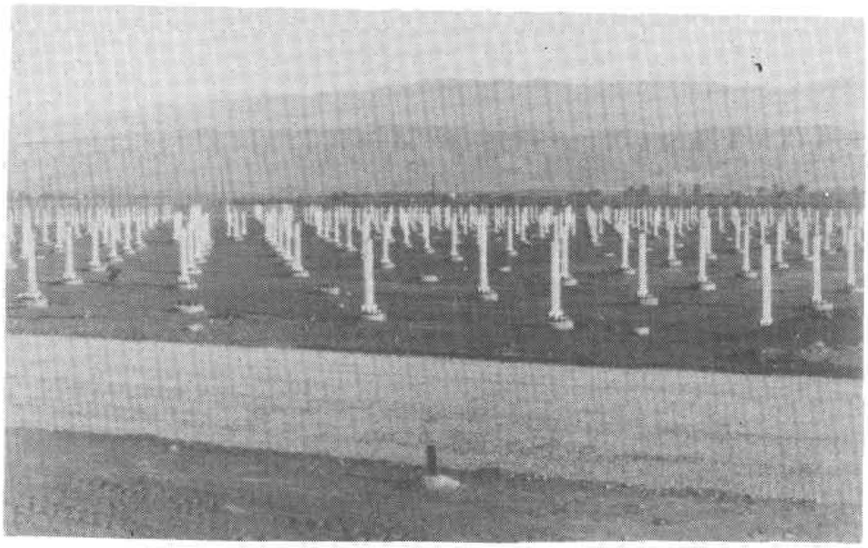

Figure 10. Acurex Collector Foundations with Support Posts

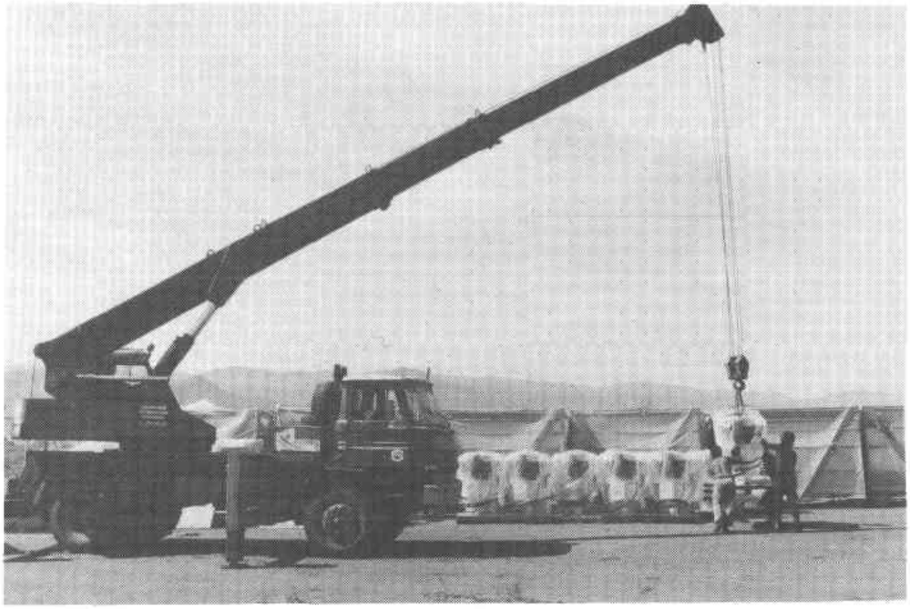

Figure 11. Unloading Collectors at Construction Site

References

1. IEA Small Solar Power Systems Project DFLAR (Status 1.9.1979)

2. "The DCS Solar Power Plant Within IEA's SSPS Project -- Aspects of the Final Systems Layout and the Component Selection." Dr. A. C. Kalt

AN OVERVIEW OF SOLAR INDUSTRIAL PROCESS HEAT

Kenneth D. Bergeron
Systems Analysis Division 4723
Sandia National Laboratories
Albuquerque, NM 87185

I. Industrial Process Heat as an Energy Market Sector

A useful first step in the process of defining an effective Solar Industrial Process Heat (IPH) program, and assessing progress in this area, is to describe in broad terms the characteristics of IPH as an energy market sector, and to compare it with other energy end use sectors which may be more familiar to the solar community (e.g., solar heating and cooling and solar thermal electricity). Some important characteristics are:

(1) Size--Approximately 19% of U. S. energy use, or about 15 quads, is consumed for IPH. By contrast, only 7 quads of electrical energy is used (requiring 20 thermal quads to produce). Since a significant fraction of IPH is at moderate temperatures, the potential market for solar thermal energy is extremely large.

(2) Competing Fuels--About 80% of conventional IPH is produced with premium fuels--oil and natural gas. By contrast, only 30% of the fuel used by electric utilities are premium fuels. If oil and gas prices continue to rise faster than the price of coal, this implies a clear economic advantage for solar IPH compared with solar thermal electric. It is also important that the risk of fuel curtailment is often perceived to be higher for industry than for other end uses.

(3) Industrial User Experience--Solar IPH has an advantage over solar heating and cooling because the typical industrial energy user is more adept than the homeowner at selecting, installing, operating and maintaining machinery for maximum economic benefit.

(4) Utilization--It is useful to define a characteristic of the thermal load called the "utilization factor," U, which is the ratio of the solar energy actually used divided by the energy which the solar energy system can deliver. Values of U are generally less than one because there are times when the solar energy is available, but not needed by the load. Since the important performance measure is the fossil fuel displaced annually, solar economics are often more strongly affected by U than by any other parameter. The economic advantage of solar IPH to solar space heating is simply that in the former, values of U approaching 1.0 are not uncommon (since the load is continuous and year-round), while in the latter, values of .3 or less are more typical (since only a small fraction of the annual insolation occurs during

the heating season).

(5) Heterogeneity--A wide variety of diverse applications come under the heading of industrial process heat, and there are broad ranges for all the parameters which influence system design and economics. One consequence is that it is more difficult to formulate an effective program to develop and stimulate solar IPH because there is no "typical" application, and there are special considerations which must be addressed for each of the many subsectors.

On the other hand, this heterogeneity can be an advantage for early market development, for reasons which are illustrated schematically in Figure 1.

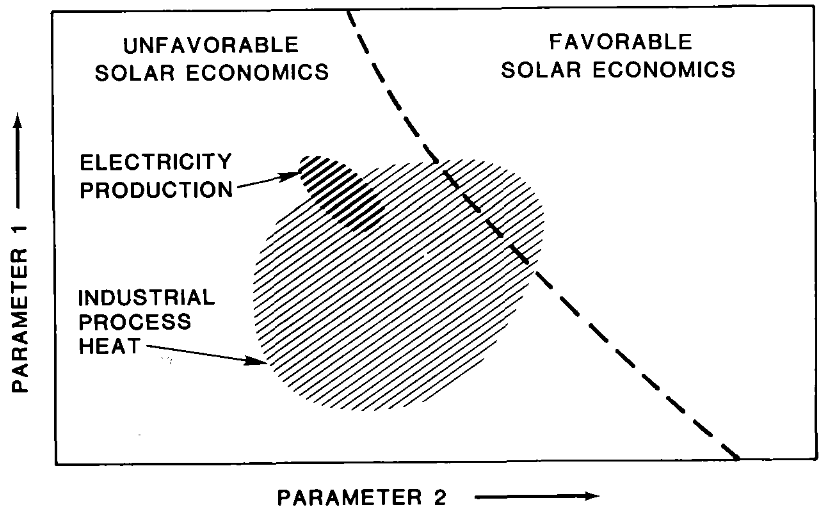

Figure 1. Hypothetical Distribution of System Parameters for Solar Energy Applications

Here, the heterogeneity of the IPH sector is manifested as a broad distribution of two hypothetical parameters affecting solar economics (examples: load temperature and land cost). By contrast, the values for applications in a more homogeneous sector like solar thermal electric production form a more dense and localized distribution in the parameter space. For a given choice of all the other parameters (e.g., fuel price) there is a boundary on this two-parameter plane which divides solar applications with favorable economics from those with unfavorable economics. Now, the point illustrated in the figure is that in the early years of solar energy development, it is reasonable to expect low levels of market penetration in the most favorable portions of the IPH spectrum long before significant penetration of the electricity market is seen. (Note also that the converse is also true: very high percentages of solar market penetration will be more difficult to achieve for IPH than for solar thermal electric.) Similar arguments lead one to expect a greater diversity of optimum system configurations and types (e.g., troughs, flat plates, central receivers, dishes) in the IPH sector than in the sectors with more homogeneous conditions.

II. The Department of Energy's Solar IPH Field Test Program

Against this background, the importance and the difficulty of the government's task of developing solar IPH become clear. An important part of this effort is the IPH Field Test Program, which consists of numerous solar facilities in a wide variety of configurations, industrial applications and geographic locations. The program has several purposes.

- It is the only realistic way to understand the interface between solar technology and the industrial energy user. Lessons learned in this regard may result in system or component design modifications, or in the development of procedures for the user to make the introduction of solar into his process more effective.
- It provides an effective minimal demand for collector manufacturers, encouraging innovation and progress in production techniques.
- It introduces and validates the idea of solar energy as a practical energy alternative to a wide variety of industries, so that when economics are more favorable, market penetration will proceed more smoothly and quickly.

Table I summarizes the projects which have been approved for construction to date. (The program has been in place for about three years.) Now shown on this table are five low temperature projects which have not completed the design and review process and have not been approved for construction. These projects, which average 50,000 ft^2 in size, are being managed by the Solar Energy Research Institute.

The Cycle 4 projects, which were very recently approved for construction, differ from the previous three cycles in two respects: (1) the fields are much larger--typically five times the size of the previous projects (which averaged 10,000 ft^2 of collector area); (2) the costs are shared between the government and the site owner. Table II lists some important characteristics of these latest three projects. All will use parabolic trough collectors.

At this early stage, it is difficult to measure the success of the Field Test Program in achieving its many purposes, but there is one encouraging trend to report. Figure 2 shows the installed system costs (in 1980 dollars) per unit collector area for all of the parabolic trough projects funded for construction. (These do not

		CYCLE 1 HOT AIR-HOT WATER 140-212°F	CYCLE 2 LOW TEMPERATURE STEAM 212-350°F	CYCLE 3 MID-TEMPERATURE STEAM 350-550°F	CYCLE 4 COST-SHARED STEAM 212-550°F	TOTAL
COLLECTOR TYPES	FLAT PLATES	4*	0	0	0	4
	EVACUATED TUBES	2	1	0	0	3
	PARABOLIC TROUGHS	0	3	5	3	11
	MULTIPLE REFLECTORS	1	0	0	0	1
	TOTAL SYSTEMS	7	4	5	3	19
STATUS	TO BE CONSTRUCTED	0	0	1	3	4
	UNDER CONSTRUCTION	0	2	4	0	6
	OPERATIONAL	7	2	0	0	9

*INCLUDES ONE COMBINATION FLAT PLATE/PARABOLIC TROUGH

Table 1. Solar IPH Field Tests

Site Location	San Leandro, CA	Haverhill, OH	Ft. Worth, TX
Industrial Partner	Caterpillar Tractor Co.	Columbia Gas Co. & U.S.S. Chemicals Co.	Bates Container, Inc.
Solar Designer	Southwest Research Institute	U.S.S.C./H. A. Williams & Assoc.	BDM Corporation
Thermal Load	235°F Pressurized Hot Water for Tractor Parts Washing	365°F Steam for Polystyrene Production	375°F Steam for Cardboard Corrugator
Collector Area	50,000 ft^2	50,400 ft^2	34,400 ft^2
Heat Transfer Fluid	Treated Boiler Water	Gulf Synfluid 4CS	Therminol T-60 (Monsanto)
Collector Layout	N-S Array on Roof of Factory	Ground Mount Along Line 65° East of North	Two Ground Mount Parcels, N-S

Table 2. Cycle 4 Solar IPH Field Tests

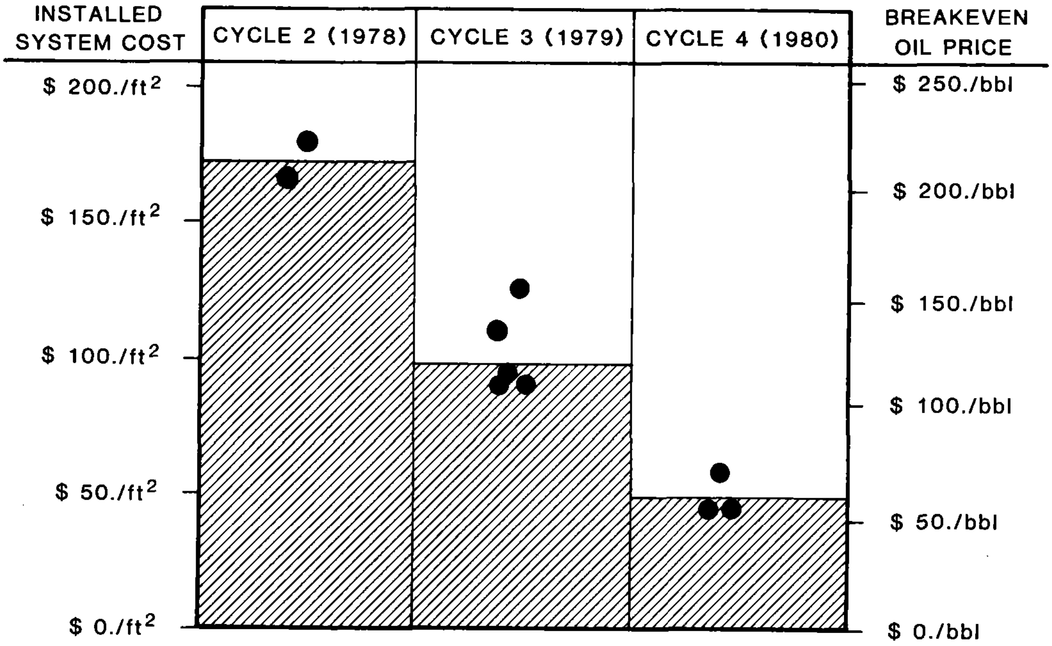

Figure 2. Cost Trends in Trough IPH Projects

include design costs, which for Cycle 4 amounted to about \$5 per ft^2.) The dramatic reduction in costs is due to a number of factors: (1) parabolic trough costs have been reduced substantially; (2) the larger field size for Cycle 4 introduced economies of scale; (3) it is probable that cost savings through improved design were achieved as a result of the learning process and competition among bidders. (Note added in proof: Final contract negotiations resulted in Cycle 4 costs about \$57/ft^2.)

On the right side of Figure 2 are given estimates of the initial year price of fuel oil at which the solar energy investment would break even. These are based on numerous assumptions about economics and system performance; for completeness, these are listed in Table III in the notation of Reference 3. As time goes on, if the demand for collectors increases, it is not unreasonable to expect this trend to continue to the point, eventually, of solar competitiveness with fossil fuel without federal support.

Table 3. Economic Parameters for Figure 2
(Notation of Dickinson and Brown, Ref. 3)

DP = 16 yr	N = 20 yr
$E_S = .304 \times 10^6$ Btu/ft^2	$OMPI_o = .025$
f = 1.	R = .15
g = .10	TC = .25
g' = .13	$\tau = .5$

III. Sandia's On-Site Materials Exposure Program

An important adjunct to the Field Test Program is the solar collector materials exposure program being conducted for Sandia by McDonnell Douglas Aeronautics Corporation at numerous proposed IPH sites around the country. Currently, there are nine exposure racks deployed at each of the Cycle 3 and 4 project sites. These contain specimens of various reflector and receiver materials whose optical properties are periodically measured after exposure to the natural environment. One purpose of this program is to identify major problems of collector materials degradation before the projects are constructed in order that timely action can be taken.

An example is the reflector soiling problem which was identified at the Henderson, NM, IPH site. Glass, acrylic and aluminum mirror samples showed a rapid loss of mirror reflectivity which could not be restored by non-abrasive washing. After five months of exposure, the reflectivity of the washed samples was less than 25% of the original value. The source of the problem was found to be the combined effects of a fine spray of water from a nearby cooling tower and wind-borne clay particles from the arid desert environment. As a result of these findings, the decision was made, prior to initiation of construction, to relocate the collector field a greater distance from the cooling tower, and it is now hoped that the soiling problem will be manageable with a reasonable schedule of collector cleaning.

Significant reflectivity losses are being observed at several of the other sites, also, although the problems are not in general as severe as at Lovington. In one location, a corrosive chlorine environment appears to pose a significant threat to mirror materials. In another, certain reflector specimens facing downward are losing reflectivity, possibly because of hydrocarbon outgassing from the tar roof. On the other hand, some sites appear to be very benign with respect to solar collector materials. An important conclusion is that the effect of the environment on collector performance depends strongly on the characteristics of the microenvironment. Thus, it is desirable to deploy exposure test racks at potential sites as early as possible, so that more accurate predictions of system performance are possible, and in order to develop a suitable cleaning strategy for that particular location.

References

1. "Putting the Sun to Work in Industry," SERI/SP-34-175, Solar Energy Research Institute, Golden, Colorado.

2. C. F. Kutscher and R. L. Davenport, "Preliminary Results of the Low Temperature Solar Industrial Process Heat Field Tests," SERI/TR-632-385.

3. W. C. Dickinson and K. C. Brown, "Economic Analysis of Solar Industrial Process Heat Systems," UCRL-52814, Lawrence Livermore Laboratories, Livermore, California.

MODULAR INDUSTRIAL SOLAR RETROFIT PROJECT (MISR)

Robert L. Alvis
Project Leader
Systems and Applications Development Division 4725
Sandia National Laboratories
Albuquerque, NM 87185

Introduction

The Department of Energy (DOE) has supported solar thermal energy development since the oil embargo. Parabolic trough type solar collectors were one of the first approaches tried, and much development progress has occurred. Several system experiments have been conducted to obtain realistic development status, and operational experience has been gained from them. The MISR Project represents a major thrust by DOE to bring solar thermal energy using line-focus solar collectors to commercial readiness. This paper describes the project and the approach being used to assure success in obtaining commercial readiness.

Background Information

The industrial sector of the U.S. is currently responsible for about 25% of the total U.S. energy consumption. Of this amount, 68% is used to generate heat for industrial processes.[1] Approximately 30% of all process heat requirements are with peak temperatures of 315°C (600°F) or less. This value increases to 52% when preheating is considered.[2] A significant amount of thermal energy is, therefore, used in industrial processes and at a temperature that can be supplied by parabolic-trough-type solar collectors. The President, in his June 20, 1979, address to Congress, declared that 20% of the domestic energy demand will be supplied by solar and renewable resources in the year 2000. A concerted effort will be required to meet this goal. MISR is such an effort. Much effort has gone into the development of the trough-type solar collector, and it is judged to be nearest to commercial readiness. These collectors operate more efficiently at lower temperatures, but can operate at about 60% efficiency at 300°C.[3] From thermodynamic theory, it can be shown that for maximum energy savings the displacement of fossil fuel should first occur at the the lower process temperatures. Yet, previous solar thermal experiments have indicated that the systems are more expensive and have more maintenance problems than the state of technology development would suggest. The MISR Project's main objective is to bring solar thermal systems, using line-focus solar collectors, to commercial readiness.

Commercial readiness will be considered to have occurred when solar thermal systems have been developed to fulfill a specific demand, operate reliably, produce reasonable cost energy, and a sufficient number of experiments have been conducted to lend credibility to the system's performance. In addition, it is considered necessary that system suppliers be developed which have proven solar system designs to supply the market as it develops. Commercialization, which would be the next logical development activity step, is not part of the MISR Project, but the MISR results will be useful in developing a proper plan.

MISR Project Description

The primary objective of the MISR Project is to develop a modular solar thermal line-focus system offering near-term commercial readiness with demonstrated reliability, and having definite market potential for industrial applications. A modular design approach offers the potential of minimizing system costs by reducing one-of-a-kind engineering and improving reliability by allowing the construction of the same system design many times. The cost of the first modular system is expected to be more than a conventional one, but the potential for cost reduction for follow-on systems is large.[4] This is one of the reasons for DOE assistance in the solar thermal system development. The MISR Project goals are to validate the potential of the modular design approach, reduce the solar system installation design costs to the typical 10% or less of system cost, and obtain a performance of \$10/MBTU (\$.034/kWh_t) by 1985.

The activities of the project are shown in Figure I. The inputs include the technology developed by both government and industry, the lessons learned from previous solar experiments, the industrial needs from industry, and the determination of modular size and

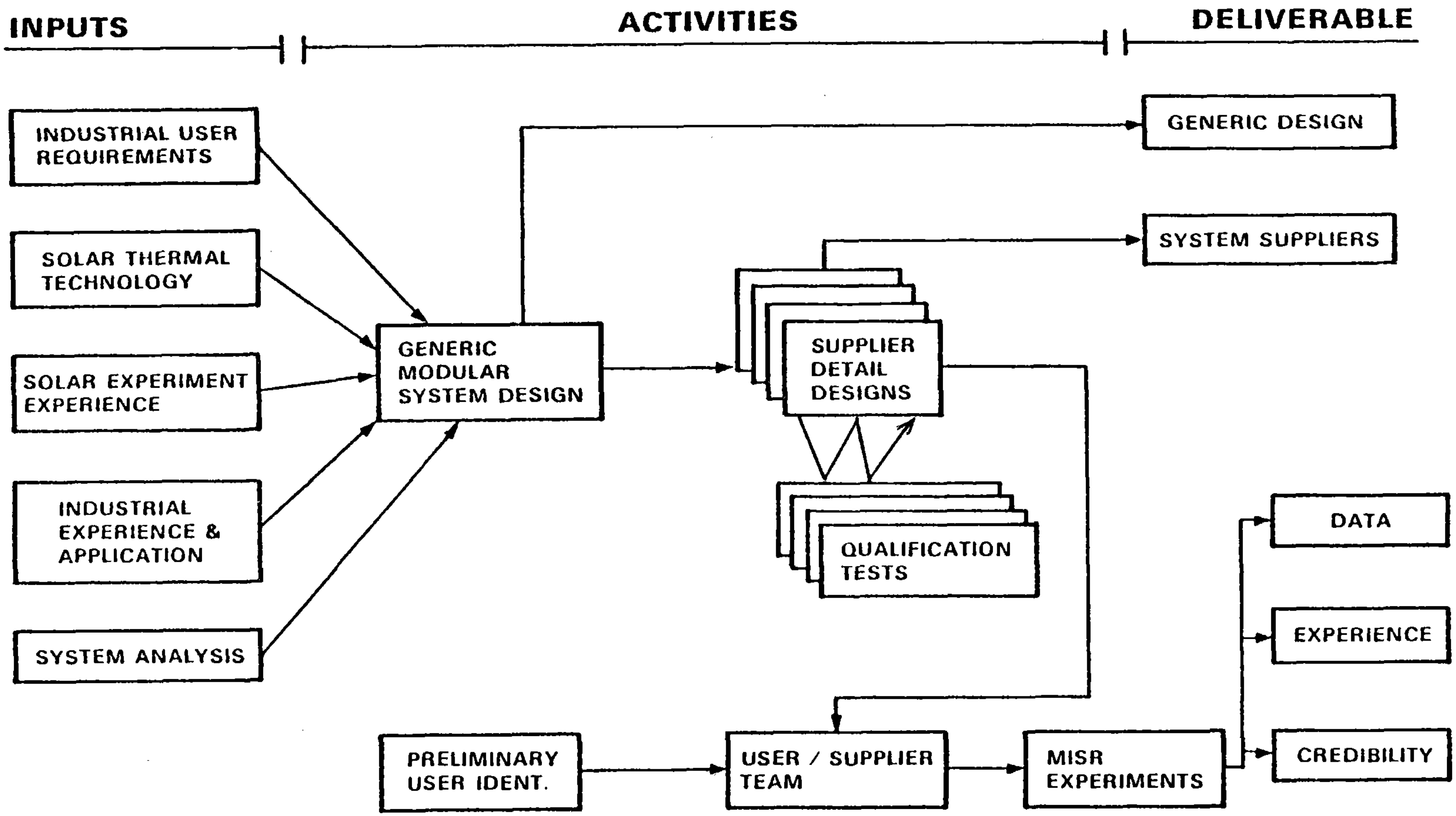

FIGURE 1. MISR PROJECT ACTIVITIES

operating characteristics which will serve a significant portion of the industrial need by market and system analysis. This information will be accumulated into a generic design by an A&E firm. This A&E will be responsible for incorporating standard practice into the design which will assure satisfactory construction at reasonable costs and will select design approaches that should result in high operation reliability. Once this information has been collected in the form of a generic design, it will be used as a technology transfer vehicle as it will become part of a Request for Proposal (RFP) for detailed modular system design and qualification hardware to industry. Up to six of the responses to the RFP will be selected for an award. Each modular concept, using a minimum amount of hardware which will be representative of a complete module, will be tested at Sandia National Laboratories. These tests will determine if the specifications of the RFP have been met. Only those modular systems meeting the specification will be acceptable for incorporation into the MISR experiment phase.

Experiment Phase

DOE will conduct joint solar thermal experiments using the qualified modular systems. DOE will first solicit industries which are interested in conducting such experiments. DOE will select approximately 15 industries desiring to conduct MISR experiments, furnish them with the list of qualified modular systems, and ask for a proposal for conducting the experiments. Industry will purchase the modular systems from the suppliers, have the systems installed, and will operate them for a minimum of two years. A data acquisition system will be furnished for collecting the data during the 2-year period. Up to 10 industries will be selected to conduct these experiments.

The experimental results will be evaluated to determine the modular system's degree of commercial readiness. If readiness is believed to have been reached, the MISR Project will terminate. If further improvement is warranted, and improvements are available, then a second experimental project cycle may be initiated.

Project Experiment Cycles

The MISR Project may incorporate up to three experiment cycles. The first cycle will use commercially available components, and if commercial readiness is demonstrated, the MISR Project will terminate. However, if improvements in the systems are required, a second experiment cycle of the same order of magnitude will be conducted using the same approach as before but with the available improved components. If commercial readiness is still lacking, a third experiment cycle using advanced components may be conducted.

Schedule

The MISR Project activity was initiated in March 1980. The Cycle-1 generic design is scheduled to be completed by February 1981. RFPs for industry-designed modular systems will follow immediately. Qualification tests of the accepted proposals should be complete by November 1981, and experiments at industries should be started in 1983. Results from Cycle-1 will be available in 1985. The second cycle will follow the first cycle by approximately 3 years, and the third cycle will follow the second cycle by another 3 years.

Conclusions

The MISR Project is considered a major thrust by the DOE in an effort to bring solar thermal energy systems to the point of commercial readiness. The modular systems developed will be designed, fabricated, and installed by industry. Therefore, solar thermal system suppliers will be developed. The system cost and performance data will be obtained by thermal energy users in real industrial environments. This data is expected to be useful to both industry suppliers, prospective system buyers, and be available to government commercialization planners. When commercial readiness is obtained, the MISR Project will terminate leaving industrial suppliers available to supply the market. Their marketing effort will be supported by credible cost and performance data.

References:

1. Energy Supply and Demand in the Mid-Term: 1985, 1990, and 1995, Energy Information Administration, April 1979.

2. Analysis of the Economic Potential of Solar Thermal Energy to Provide Industrial Process Heat, C00/2829-76/1, Intertechnology Corporation, February 1977, pp. 56-61.

3. Summary Report, Concentrating Solar Collector Test Results - Collector Module Test Facility, January - December 1979, SAND80-0846, (Albuquerque, NM: Sandia National Laboratories, August 1980).

4. L. B. Glaser, J. Kramer, and E. Causey; "Practical Aspects of Modular and Barge-Mounted Plants," Chemical Engineering Progress, Vol. 75, No. 1, pp. 49-55 (October 1979).

MIDTEMPERATURE SOLAR SYSTEMS TEST FACILITY (MSSTF)

Robert M. Workhoven
Experimental Systems Operations Division 4721
Sandia National Laboratories
Albuquerque, NM 87185

Introduction

The Experimental Systems Operations Division of Sandia National Laboratories in Albuquerque, New Mexico, operates the MSSTF shown in Figure 1. Work is sponsored by the Solar Thermal Program under the Division of Solar Thermal Energy Systems for the U.S. Department of Energy (DOE).

The MSSTF is primarily dedicated to support of the following projects and activities:

- Line Focus Component and Subsystem Development
- Line Focus System/Applications Development
- Commercial Products and Development Activities
- Thermal Storage Development
- Other development requiring unique capabilities, experience, etc.

SAND80-1681, Midtemperature Solar Systems Test Facility Program Status Report, by John Otts, describes the objectives, status and future activities as well as the responsible engineer and references for MSSTF programs. Copies of this report are available upon request. Many of the presentations of this seminar will review the status and results of these programs.

Two independent installations make up the MSSTF: (1) The Subsystems Test Facility (STF), and (2) The Collector Module Test Facility (CMTF).

The Subsystem Test Facility (STF)

The STF has completed its original objective as a Solar Total Energy Demonstration Facility and now operates as a Multipurpose Subsystem/System Test Facility. Specifically, it supports research and development, including service-life studies on components, subsystems, and systems. STF programs are listed in Figure 2 and are discussed in the SAND80-1681 report.

The Collector Module Test Facility (CMTF)

Figure 3 shows the CMTF as it looked a few months ago. The CMTF characterizes performance of collector components, subsystems, and system modules in support of commercial programs and line-focus collector development. CMTF programs are listed in Figure 4 and are discussed in the SAND80-1681 report.

DSET of Phoenix and Wyle Laboratories of Huntsville are now certified independent test laboratories and will conduct more commercial collector tests in the future. The CMTF will support component and subsystem development. However, some collector modules are still under test at the CMTF, as you will see later.

The CMTF is made up of three totally independent fluid-conditioning loops, summarized in Figure 5: (1) Loop No. 1, the Therminol 66 Loop; (2) Loop No. 2, the new higher-temperature loop; and (3) Loop No. 3, which uses water as the heat-transfer fluid.

Loop 1--In its six years of operation, the Therminol 66 Loop has logged over 6500 hours of operating time. Its configuration is continually changing, and now three collectors are connected to it so that any two can be tested simultaneously. This arrangement also uses the collectors to increase fluid-heating capacity and thereby reduce stabilization time at higher temperatures.

Loop No. 2--Loop No. 2, which has been operating since July, will soon become our primary test loop. It is connected to the Azimuth Tracking Collector Mounting Platform (Aztrak), but we plan to modify it so that it can also supply fixed-mount collectors for simultaneous testing with one that is Aztrak-mounted.

Line-focus collectors are unable to take advantage of this loop's expanded temperature capability because of the temperature limitations of black-chrome selective coating. The new Dow-Corning Heat Transfer Fluid Syltherm 800®. has opened the way for increased temperatures, however, and the loop hardware is consistent with this advance. Figure 6 is a schematic of Loop No. 2, which is our idea of what a high-performance fluid-conditioning loop for collector testing should look like. As we gained experience, we found elements that need to be changed in the next design, but we think this loop is adequate for now.

Loop No. 3--This loop, which has been operational for about three years, uses water as the heat-transfer fluid. In order to maintain a liquid state at temperatures up to 330°C, we must maintain pressures of 18.3 MPa (2700 psig). This means that construction of the loop, the interconnecting piping, and collectors is much different from that of the other two loops.

Maintenance is a serious problem with this loop. Daily temperature and pressure cycles involving water in the system cause many breakdowns. A high-pressure circulating pump failure has reduced current operating temperature limits to 220°C until more funds become available to buy a replacement, which is very expensive.

Figure 7 is a schematic of this loop, which has a pneumatically driven hydraulic intensifier to maintain the system's high pressure. The intensifier eliminates the need for a high-pressure vessel and reduces hardward costs and safety hazards.

Azimuth Tracking Collector Mounting Platform (Aztrak)

Figure 8 shows the Aztrak, a hydraulically driven structure that can track the sun's azimuth from sunrise to sunset on any day of the year. Loop No. 2 provides conditioned fluid to this platform, which can accommodate a 40-ft. string of parabolic troughs. Such a trough, with one-axis tracking, performs like a two-axis tracking collector on the Aztrak. It is controlled either manually or automatically by a microcomputer that calculates the sun's azimuth and keeps the platform within one degree of the correct position. The troughs use their normal tracking system for elevation control.

The original purpose of the platform was to allow us to run peak-efficiency (normal-incidence) tests any time of the day in which there was enough solar radiation, rather than just at solar noon. With this option, we normally have at least 4 hours test time available for recording data instead of only a few minutes. We now can drive the platform with the microcomputer to maintain a constant off-normal incidence angle along the axis of the trough. This capability permits us to achieve stable conditions at a given incidence angle instead of taking data "on-the-fly." For tests that are run in a fixed position, the higher incidence angles occur early in the morning and late in the afternoon, when radiation levels change rapidly. Figure 9 shows our first attempt at constant incident-angle tracking.

Since we can attain normal incidence in morning and afternoon when solar-radiation levels are lower, new data points are available. Here in Albuquerque, if the skies are clear around solar noon, the radiation is over 900 W/m^2. For this reason, our peak-efficiency results always have a high input level.

Another technique we hope to achieve is to simulate an all-day run in about 4 hours when solar-radiation levels are high and constant. This would eliminate the 12-hour days the CMTF crew does not enjoy.

Minicomputer Data-Analysis System

A minicomputer data-analysis system (shown schematically in Figure 10) will permit independent testing on all three collector loops simultaneously. This system provides real-time plots, as shown in Figure 11, with important data printed out in the form shown in Figure 12. All collected data are recorded and stored on magnetic tape for processing later.

Types of Tests at the CMTF

A variety of different experiments are run at the CMTF, but the three main collector module evaluation tests are: (1) peak efficiency, or normal solar incidence, (2) all-day efficiency, and (3) thermal loss rate. Other functional tests include power requirements, tracking, and control systems, and different receiver designs. Property measurements of reflectors and selective absorber coatings and a laser-ray trace of the troughs are made with instruments developed by other Sandia organizations for MSSTF use.

1. Peak-Efficiency Tests--These are run at four or five temperatures across the operating range of the collector. Flow rates are varied at one or more of these temperatures to determine the lower range of the turbulent-flow region. Valid data points are then generated with flow well into the turbulent region--i.e., Reynolds numbers of 10 000 or more. Figure 13 shows typical peak-efficiency curves.

2. All-Day Efficiency Tests-- The second type of test run at the CMTF is commonly called an "All-Day Run." In this case the fluid temperature and flow rate are held constant at the collector inlet for as long as possible through the day. Data from the first half-day are usually not valid because the fluid system takes several hours to stabilize at control temperature. If the sky remains clear in the afternoon, the test is continued until shadows fall on the collector in the evening. Figure 11 shows a good all-day run, including a peak-efficiency point. Incidence-angle modifiers are derived from these tests for each collector and are then used to predict annual performance.

3. Thermal Loss-Rate Tests--This third test measures the thermal energy lost by the collector receiver at various temperatures across its operating range. This test is run with the collector out of focus, usually after a peak-efficiency data point. Figure 14 shows the variations in different designs tested.

Recent Test Results

More than 20 collectors in various configurations and locations have been evaluated at the CMTF. Peak efficiecy is the most commonly discussed result, but it is by no means the only important performance characteristic. Tomorrow Tom Harrison will discuss monthly and annual performance or energy collection, which is really the end-product of a solar collector system. Still, peak efficiency is an indication of the quality of the materials used and of the effectiveness of the mechanical design. Figure 15 shows the results of several tests on the Acurex 3001-03 module with glass, FEK, and Coilzaic reflector materials. I cannot discuss collector costs because they vary according to the unique circumstances of each application.

A Solar Kinetics, Inc. Model T-700 trough was tested with a FEK film reflector. Another T-700 trough with Chemcor glass reflector is under test now. The FEK results and the projected glass results are shown in Figure 13.

A Suntec parabolic-trough module with sagged-glass reflector produced the results shown in Figure 16. Two different receiver designs are shown, although one was purely experimental and does not accurately represent a production model.

I have compiled these results and others on one plot that looks like Figure 17. Several points should be noted. Different types and compositions of glass are represented here, but only one acrylic film. Performance differences are caused by accuracy of focus on the receiver tube as acquired by general-trough conformity and reflector-panel continuity. Receiver design also affects efficiency, of course, especially as the operating temperature increases. This plot demonstrated how significant the differences in design and manufacturing are as compared with differences in materials. Specifically, glass usually has a reflectivity of about .93 compared to .85 for FEK; yet the peak efficiencies overlap. Analysts generated the long-term (5-yr.) goal shown on this plot about a year ago. At that time it was thought to be achievable with current materials and technology. As you see, the latest hardware is close to it already.

SUBSYSTEM TEST FACILITY PROGRAMS

I. PIPE HEAT LOSS
II. THERMAL SIPHON PROGRAM
III. PERFORMANCE PROTOTYPE TROUGHS
IV. PERFORMANCE PROTOTYPE TROUGH COMPONENT LIFE TEST
V. MODULAR INDUSTRIAL SOLAR RETROFIT SYSTEMS QUALIFICATIONS
VI. COLLECTOR DRIVE TEST PROGRAM
VII. FLEX HOSE TEST PROGRAM
VIII. LONG-TERM RECEIVER EVALUATION
IX. BLACK-CHROME SYSTEMS TEST
X. FLUID CONTROL SYSTEMS TEST
XI. PUMP HEAT LOSS
XII. PUMP POWER TEST
XIII. MIRROR CLEANING TEST SERIES
XIV. THERMOCLINE STORAGE TEST SERIES
XV. SHENANDOAH PROTOTYPE DISH EVALUATION PROGRAM
VXI. CUSTOM ENGINEERING TROUGH PROGRAM
VXII. RAYTHEON DISH PROGRAM
VXIII. FOUNDATION TESTS
XIX. HEAT TRANSFER OIL AGING PROGRAM
XX. GLASS REINFORCED CONCRETE STUDY
XXI. LARGE APERATURE PARABOLIC TROUGH
XXII. SOLAR INTENSITY PROFILE GAGE
XXIII. D-SHAPED RECEIVER TUBE AND RECEIVER TUBE SUBASSEMBLY
XXIV. MULTITANK STORAGE TESTS
XXV. ENERGY CONVERSION SYSTEM

REF: SAND80-1681, Midtemperature Solar System Test Facility Program Status Report, John Otts

COLLECTOR MODULE TEST FACILITY PROGRAMS

A. POWER REQUIREMENTS

B. COLLECTOR COMPONENT/SUBSYSTEM/SYSTEM

C. COMMERCIAL COLLECTOR EVALUATION (COMPOUND PARABOLIC COLLECTORS)

D. COMMERCIAL COLLECTOR EVALUATION OF PARABOLIC TROUGHS

E. TRACKER EVALUATION

F. RECEIVER EVALUATION

G. AZIMUTH TRACKING COLLECTOR MOUNTING PLATFORM (AZTRAK)

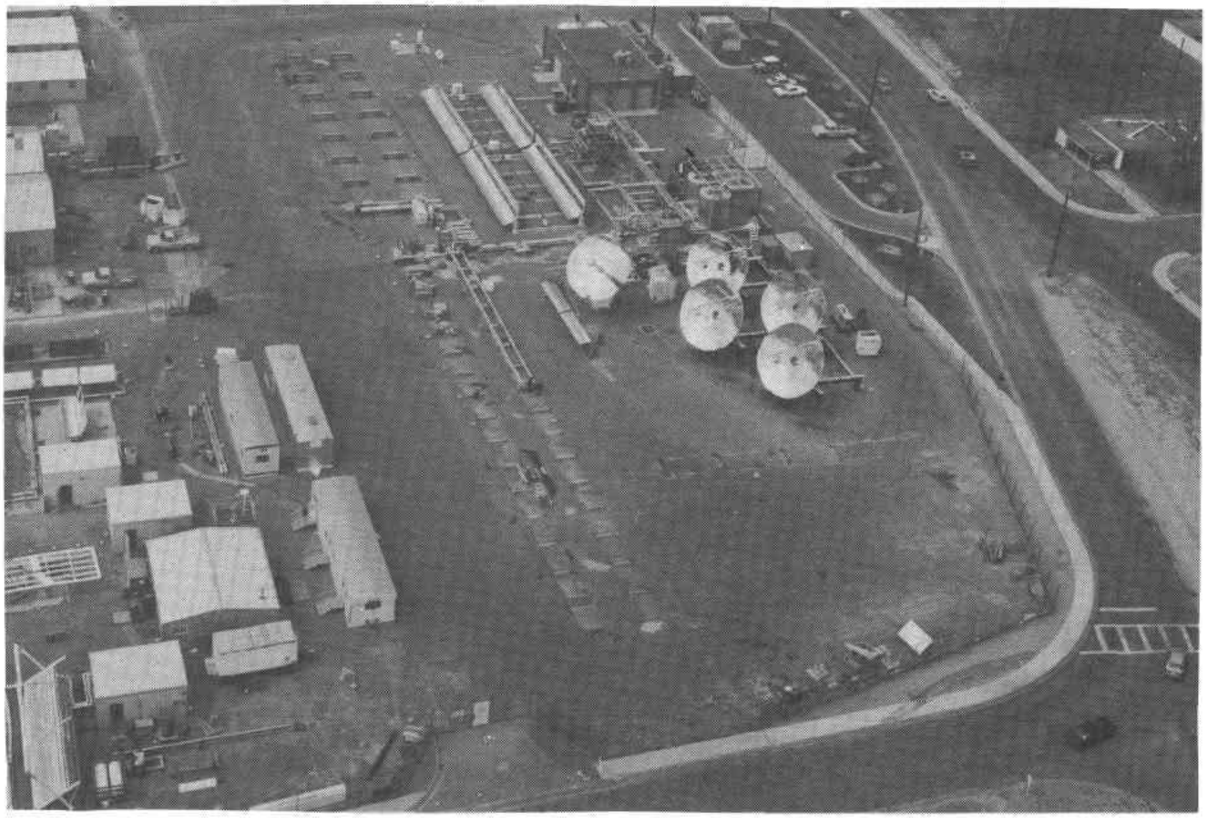

Figure 1. Midtemperature Solar System Test Facility (MSSTF)

SUBSYSTEM TEST FACILITY PROGRAMS

I. PIPE HEAT LOSS
II. THERMAL SIPHON PROGRAM
III. PERFORMANCE PROTOTYPE TROUGHS
IV. PERFORMANCE PROTOTYPE TROUGH COMPONENT LIFE TEST
V. MODULAR INDUSTRIAL SOLAR RETROFIT SYSTEMS QUALIFICATION
VI. COLLECTOR DRIVE TEST PROGRAM
VII. FLEX HOSE TEST PROGRAM
VIII. LONG-TERM RECEIVER EVALUATION
IX. BLACK CHROME THERMAL AGING STUDY
X. FLUID CONTROL SYSTEMS TEST
XI. PUMP HEAT LOSS
XII. PUMP POWER TEST
XIII. MIRROR CLEANING TEST SERIES
XIV. THERMOCLINE STORAGE TEST SERIES
XV. SHENANDOAH PROTOTYPE DISH EVALUATION PROGRAM
XVI. CUSTOM ENGINEERING TROUGH PROGRAM
XVII. RAYTHEON DISH PROGRAM
XVIII. FOUNDATION TESTS
XIX. HEAT TRANSFER OIL AGING PROGRAM
XX. GLASS REINFORCED CONCRETE STUDY
XXI. LARGE APERATURE PARABOLIC TROUGH
XXII. SOLAR INTENSITY PROFILE GAGE
XXIII. D-SHAPED RECEIVER TUBE AND RECEIVER TUBE SUBASSEMBLY
XXIV. MULTITANK STORAGE TESTS
XXV. ENERGY CONVERSION SYSTEM

REF: SAND80-1681, Midtemperature Solar System Test Facility Program Status Report, John Otts

Figure 2

Figure 3. Collector Module Test Facility (CMTF)

COLLECTOR MODULE TEST FACILITY PROGRAMS

A. POWER REQUIREMENTS

B. COLLECTOR COMPONENT/SUBSYSTEM/SYSTEM

C. COMMERCIAL COLLECTOR EVALUATION (COMPOUND PARABOLIC COLLECTORS)

D. COMMERCIAL COLLECTOR EVALUATION OF PARABOLIC TROUGHS

E. TRACKER EVALUATION

F. RECEIVER EVALUATION

G. AZIMUTH TRACKING COLLECTOR MOUNTING PLATFORM (AZTRAK)

Figure 4

CMTF TEST LOOP SUMMARY

LOOP	WORKING FLUID	MOUNTING	TEMPERATURE LIMIT	MAWP (PRESSURE)	FLOW RATE
1	OIL (T-66)	FIXED FOUNDATION	315°C (600°F)	.6 MPa (75 psig)	.06 - .6 L/s 1 - 10 GPM
2	OIL (SYLTHERM 800)	TURNTABLE	425°C (800°F)	1.4 MPa (200 psig)	.06 - .9 L/s 1 - 15 GPM
3	WATER	FIXED FOUNDATION	330°C (625°F)	18.3 MPa (2700 psig)	.06 - .6 L/s 1 - 10 GPM

DATA ARE ACQUIRED AND PROCESSED BY AN HP 1000 MINICOMPUTER SYSTEM.

Figure 5

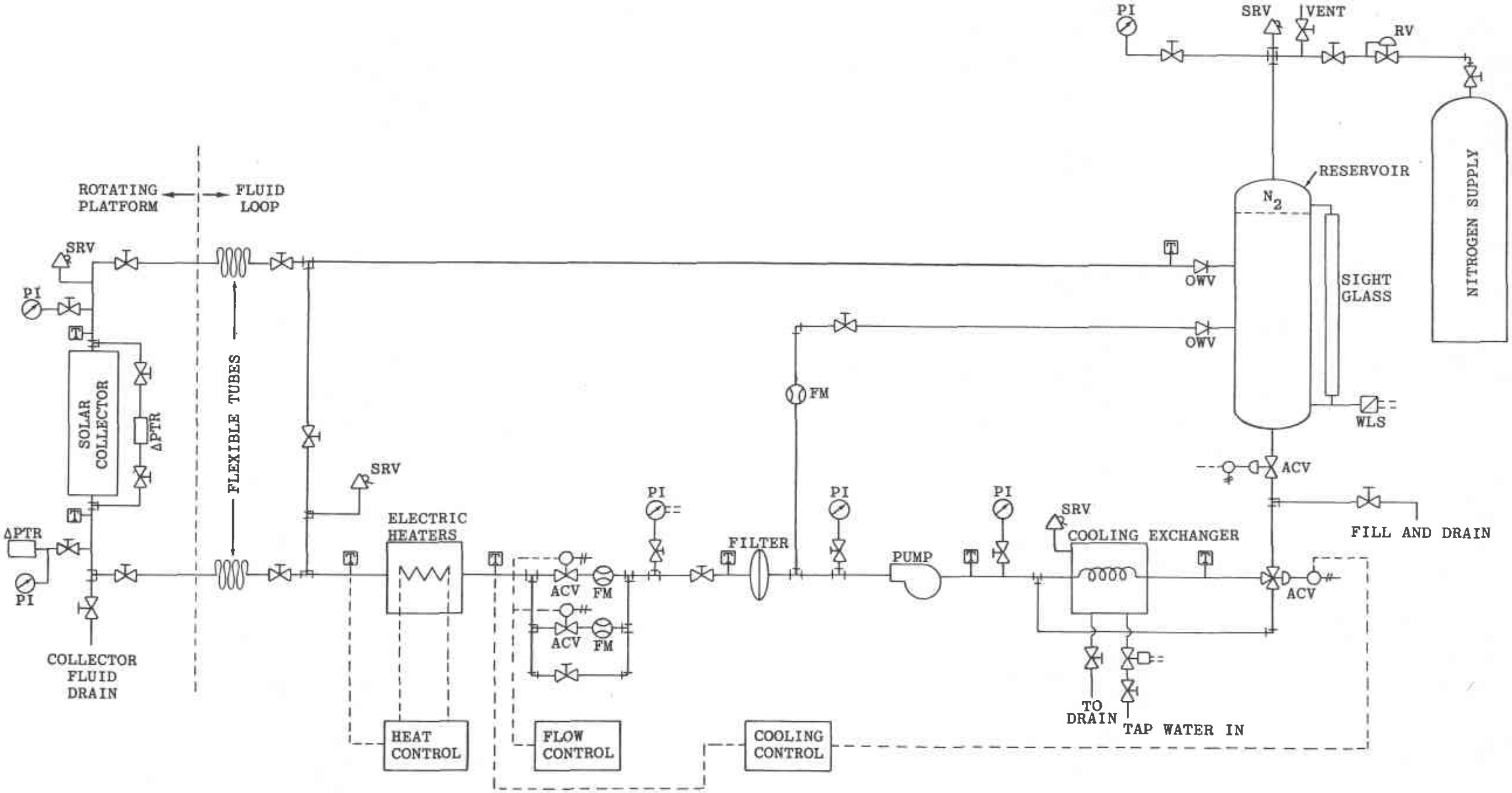

Figure 6. Schematic of Fluid Loop #2

COMPONENT DESCRIPTION

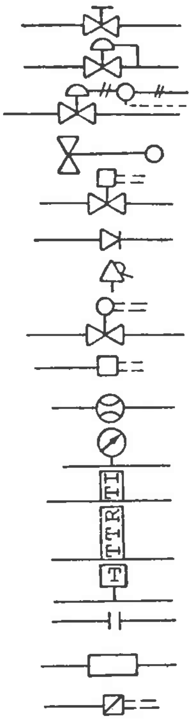

MV	Manual Valve
RV	Regulator Valve
ACV	Automatic Control Valve
LCV	Level Control Valve
SV	Solenoid Valve
OWV	One Way Valve
SRV	Safety Relief Valve
FS	Flow Switch
PS or TS	Pressure Switch or Temperature Switch
FM	Flow Meter
PI	Pressure Indicator
TI	Temperature Indicator
TTR	Temperature Transducer
T	Thermocouple
BD	Burst Disk
ΔPTR	Pressure Differential Transducer
WSL	Fluid Level Sensor

LINE LEGEND

—————————	High Pressure and/or Loop Path
—————————	Cooling System and Nitrogen Lines
----------	Electrical Lines
—//—//—//—	Air Pneumatic lines

Figure 6(a)

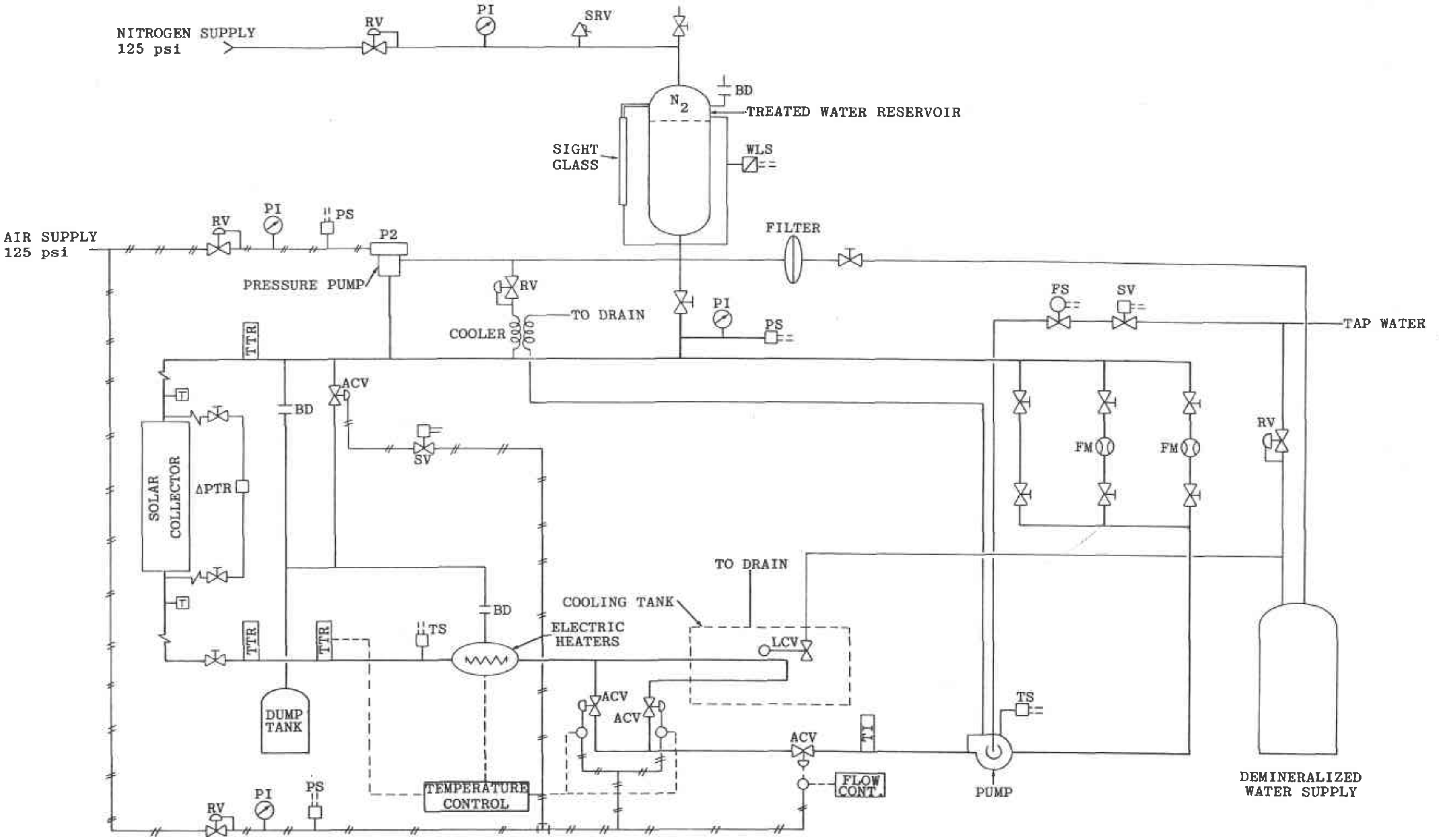

Figure 7. Schematic of Fluid Loop #3

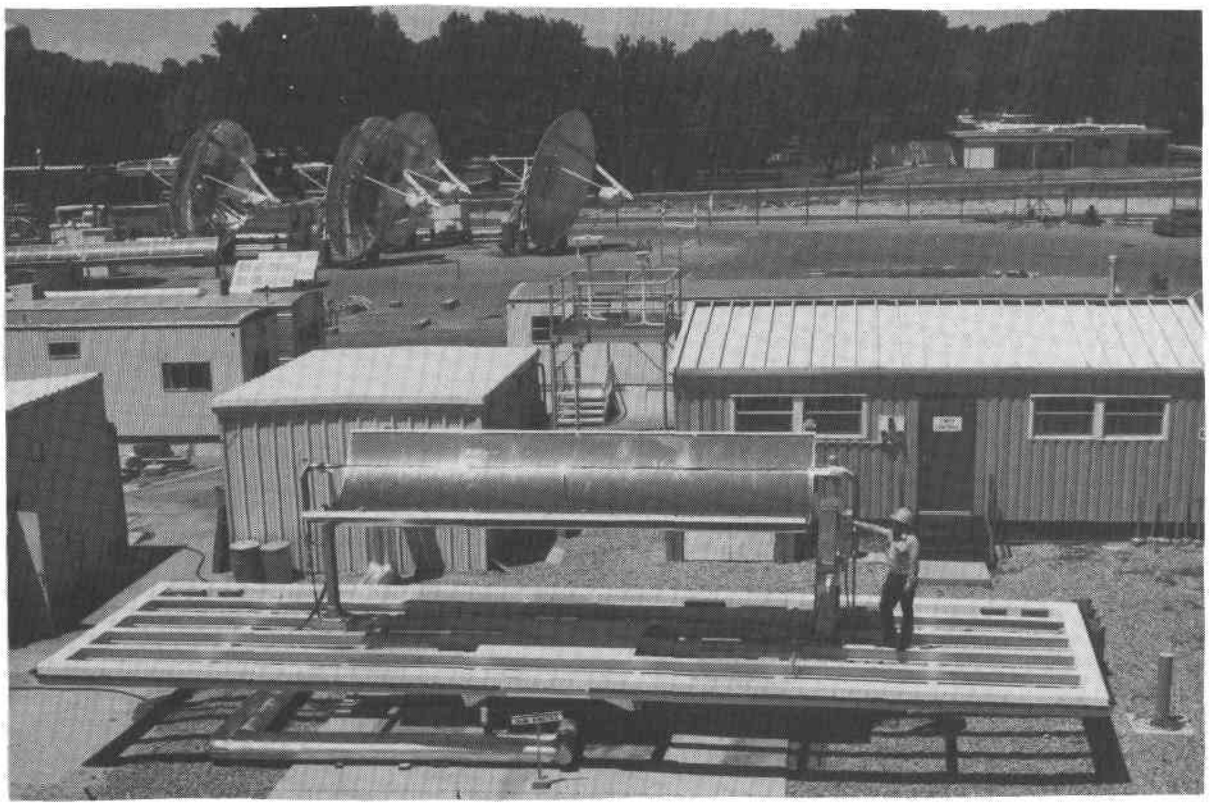

Figure 8. Azimuth Tracking Collector Mounting Platform (Aztrak)

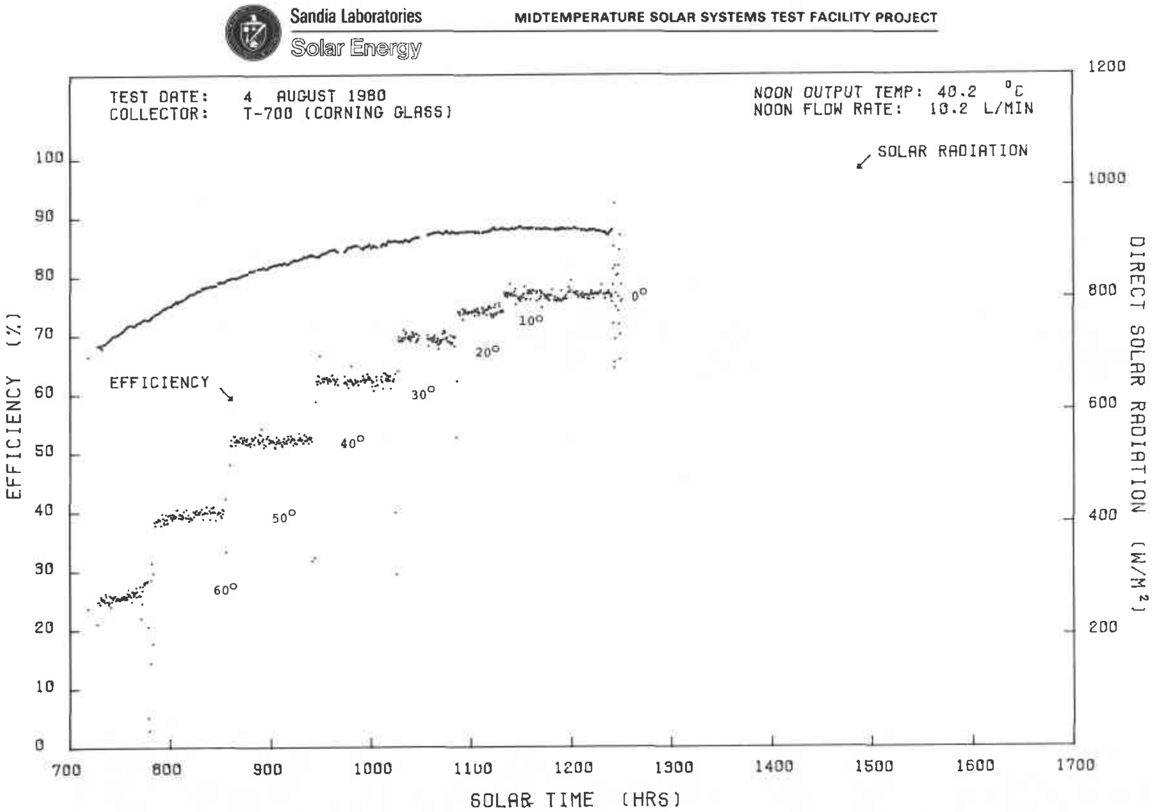

Figure 9. Solar Kinetics Parabolic Trough Efficiency Evaluation at 27.3°C Input. Constant Incident Angle Conditions.

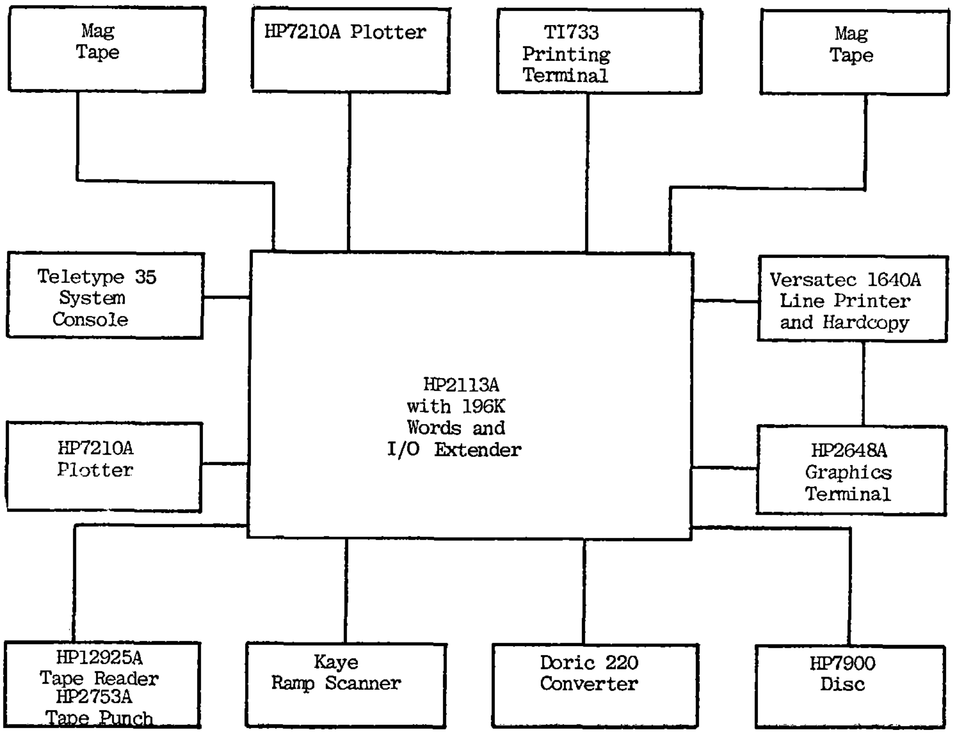

Figure 10. CMTF Data System

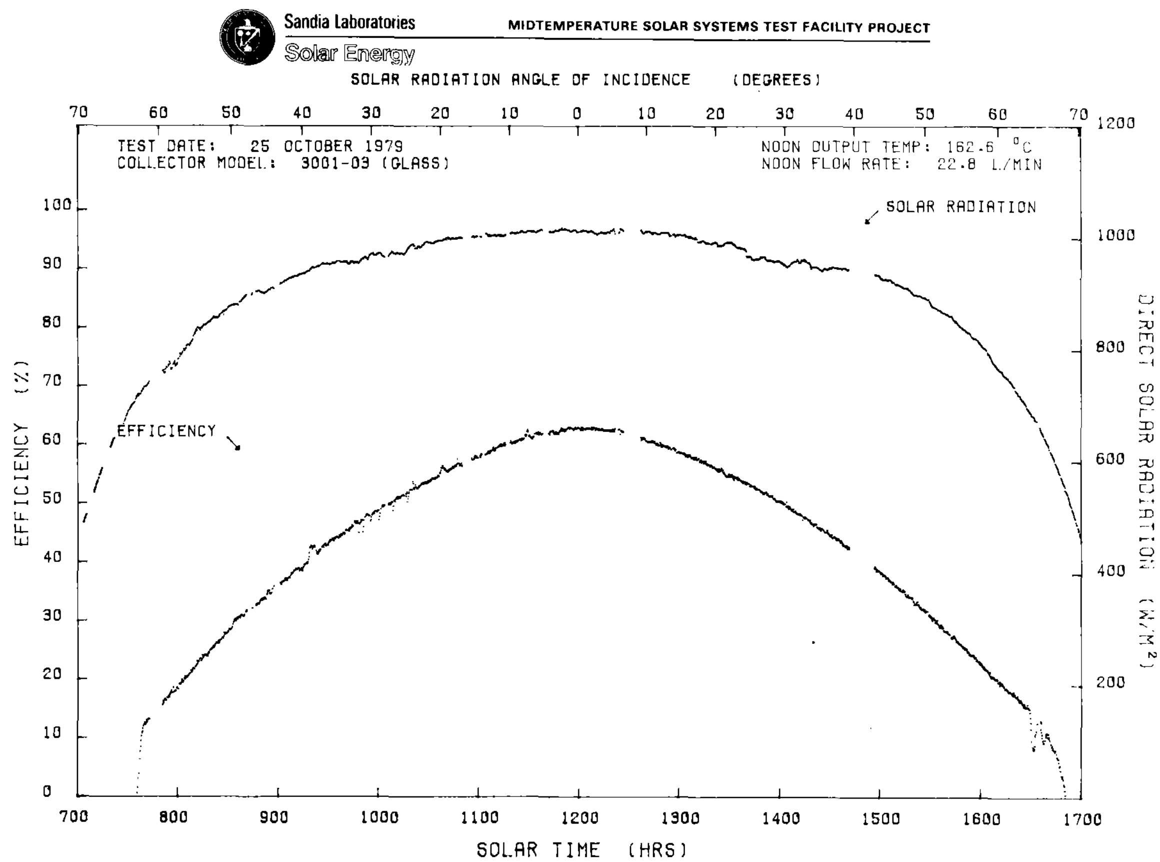

Figure 11. Acurex Parabolic Trough Efficiency Evaluation at 143.4° Input

**** SUNTEC PARABOLIC TROUGH EFFICIENCY TEST ****

TEST DATE: 13 AUGUST 1980 TIME: 11:14:51 (MST)
11: 3:59 (SOLAR)

26.38	(DEG C)	AMBIENT TEMPERATURE	(DEG F)	79.48
337	(DEGREES)	WIND DIRECTION		
.92	(M/SEC)	WIND SPEED	(MPH)	2.1

TEMP IN	TEMP OUT	SOLAR WATTS/M^2	DELTA TEMP	FLOW LITERS/MIN	EFFICIENCY PERCENT
296.76	308.74	938.7	11.97	18.24	50.4
296.77	308.76	939	11.99	18.29	50.6
296.78	308.78	939.5	11.97	18.25	50.4
296.75	308.79	939.9	11.99	18.23	50.4
296.8	308.79	940	12.01	18.33	50.8
296.75	308.81	940.4	12.03	18.35	50.9
296.74	308.81	940.1	12.04	18.31	50.8
296.79	308.82	939.9	12.03	18.31	50.8
296.76	308.83	940.1	12.03	18.34	50.9
296.8	308.84	939.1	12.06	18.34	51.1
		10 POINT AVERAGES			
296.77	308.797	939.67	12.012	18.299	50.71

50.77	AVG EFFICIENCY USING SUB. DELTA T
53.0701	AVG EFFICIENCY CORRECTED FOR OFF-NOON LOSSES
27888.6	AVG HEAT GAIN (KJ/HR)
476.546	AVG HEAT GAIN (W/M^2)
275.837	AVG RECVR TEMP MINUS AMB TEMP
.293546	(AVG TEMP-AMB T)/I
.781	AVG WIND SPEED (M/SEC)
11984.3	REYNOLDS NUMBER

END OF DATA BLOCK 101

**** SUNTEC PARABOLIC TROUGH EFFICIENCY TEST ****

TEST DATE: 13 AUGUST 1980 TIME: 11:16:50 (MST)
11: 5:58 (SOLAR)

26.71	(DEG C)	AMBIENT TEMPERATURE	(DEG F)	80.08
39	(DEGREES)	WIND DIRECTION		
1.05	(M/SEC)	WIND SPEED	(MPH)	2.3

TEMP IN	TEMP OUT	SOLAR WATTS/M^2	DELTA TEMP	FLOW LITERS/MIN	EFFICIENCY PERCENT
296.75	308.84	940.8	12.06	18.31	50.9
296.77	308.87	940.5	12.04	18.39	51
296.82	308.86	941	12.06	18.38	51.1
296.79	308.89	940.5	12.04	18.33	50.9
296.82	308.9	940.6	12.08	18.24	50.8
296.84	308.93	940.4	12.06	18.34	51
296.8	308.93	940	12.08	18.29	51
296.86	308.93	941.4	12.08	18.35	51
296.84	308.95	941.8	12.04	18.34	50.8
296.88	308.97	941.2	12.09	18.33	51
		10 POINT AVERAGES			
296.817	308.907	940.82	12.063	18.33	50.95

Figure 12. CMTF Data Printout

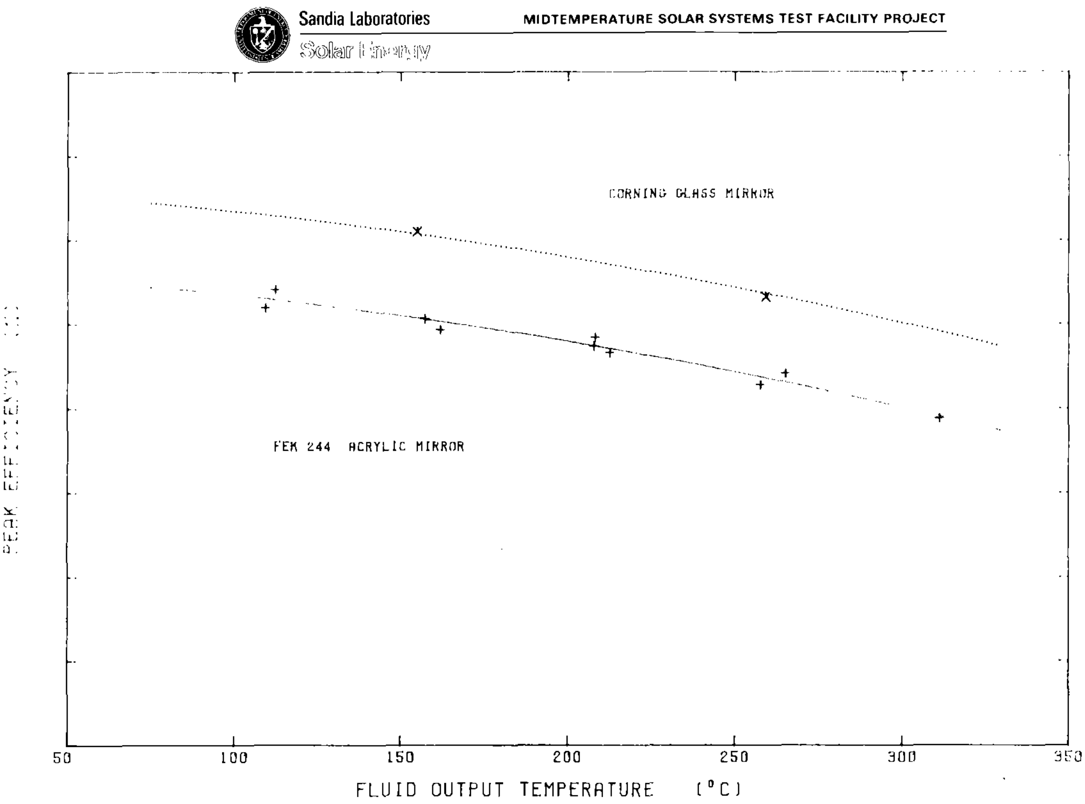

Figure 13. Solar Kinetics T-700 Efficiency Vs Output Temperature

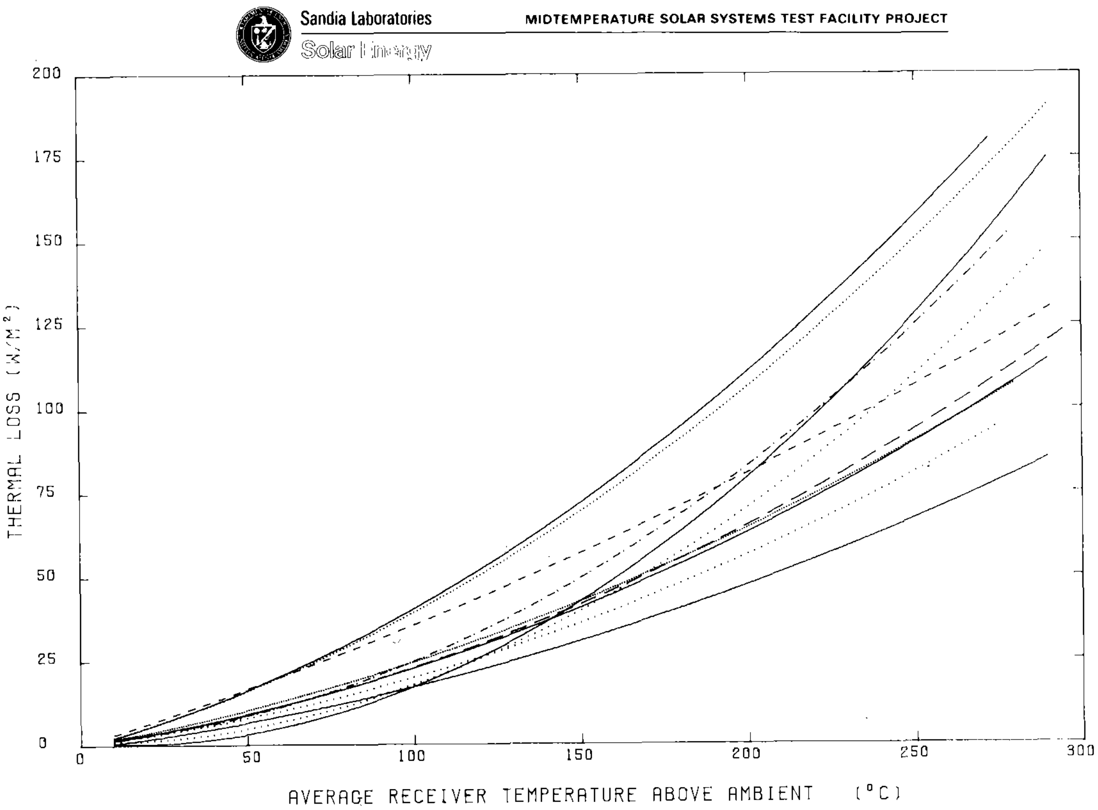

Figure 14. Comparison of Receiver Thermal Loss Per Unit Aperture Area

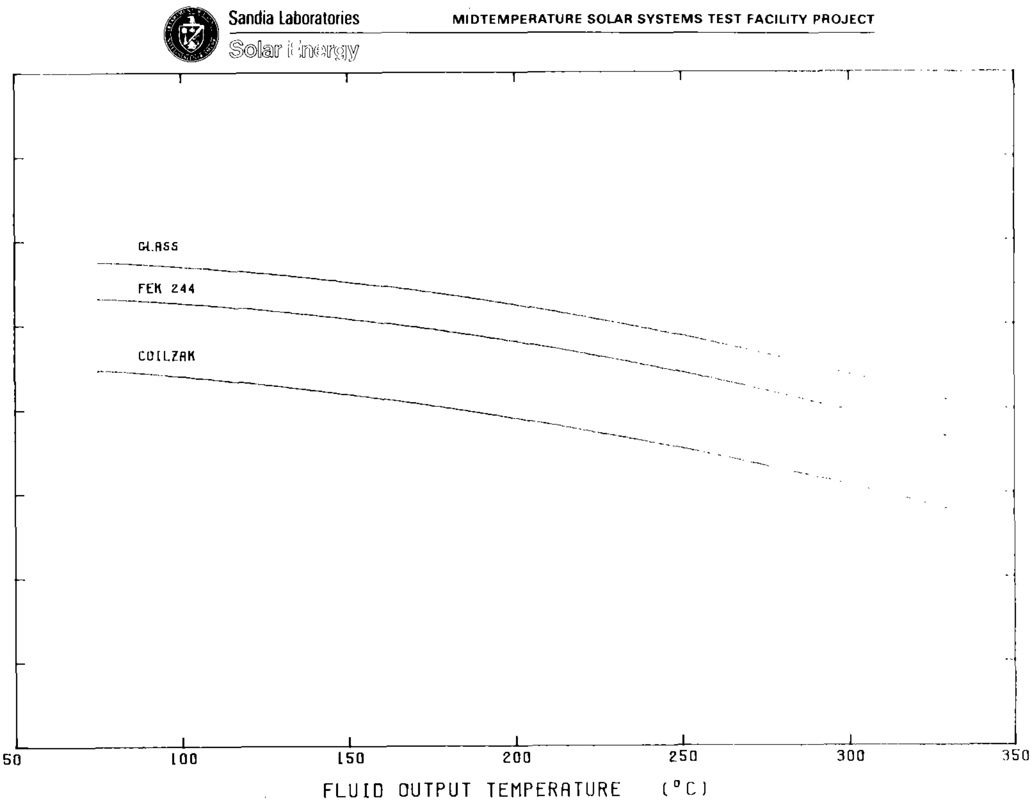

Figure 15. Acurex Efficiency Vs Output Temperature

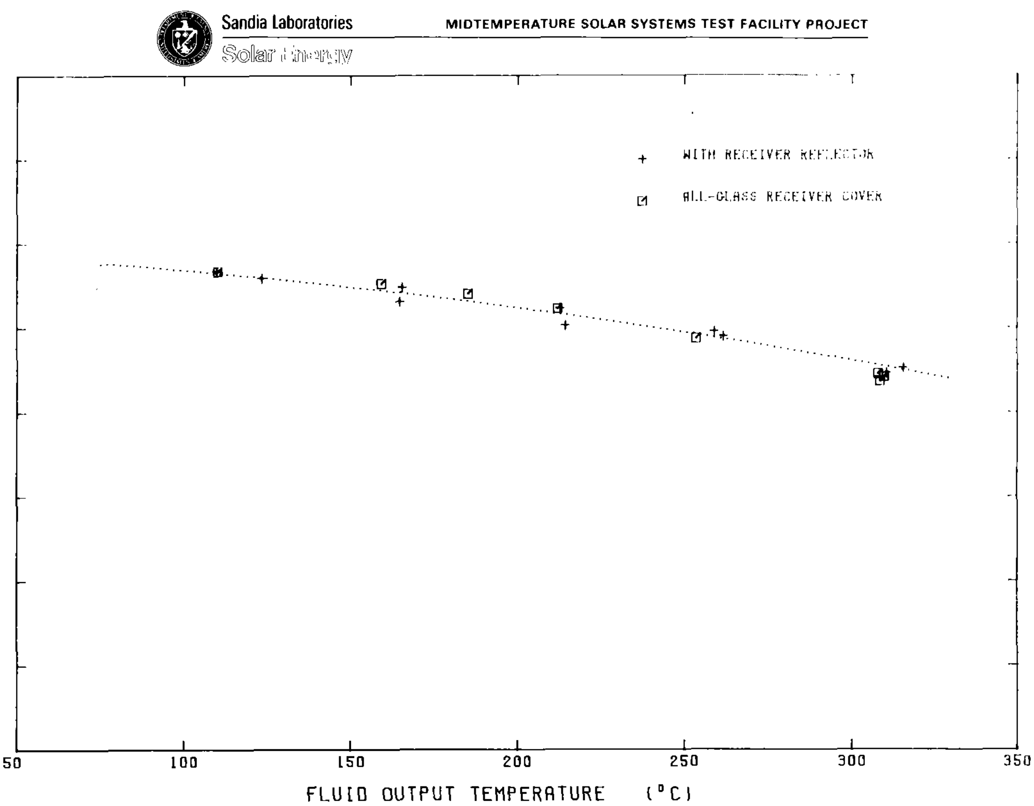

Figure 16. Suntec Glass Trough Efficiency Vs Output Temperature

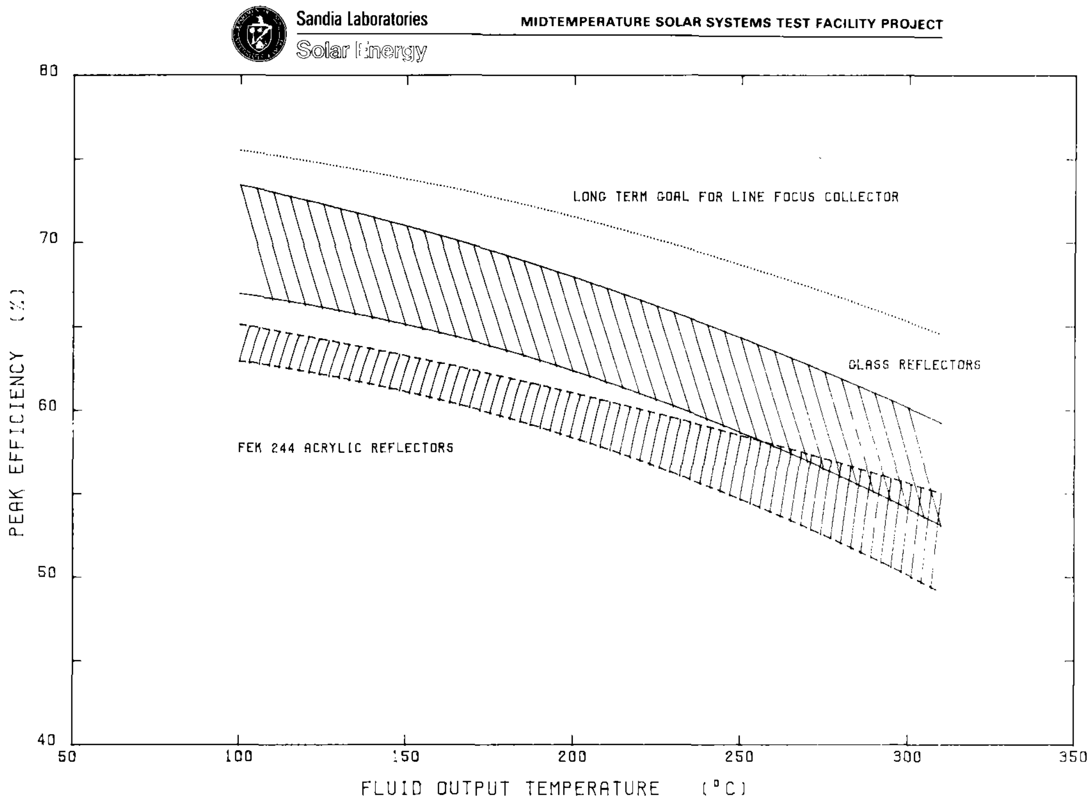

Figure 17. Performance of High Temperature Parabolic Trough Collectors

Session III - Tour of MSSTF

John V. Otts, Chairman
Experimental Systems Operations
Division 4721
Sandia National Laboratories

Reference

1. J. V. Otts, Midtemperature Solar System Test Facility Program Status Report, SAND80-1681, (Albuquerque, NM: Sandia National Laboratories, August 1980).

Sandia National Laboratories MSSTF/CMTF

LIST OF EXHIBITS

1. INCLINED TROUGH
2. SLATS
3. FIXED MIRROR SOLAR COLLECTOR
4. FRESNEL BELT
5. PARABOLIC TROUGH, INITIAL PROTOTYPE
6. CUSTOM ENGINEERING TROUGH
7. SOLAR COMPONENTS
8. SUNTEC TROUGH
9. ENGINEERING PROTOTYPE TROUGH
10. ACUREX TROUGH
11. TURNTABLE / SOLAR KINETICS
12. G.E. CUSP
13. CHAMBERLAIN C.P.C.
14. POLISOLAR TROUGHS
15. FLEX HOSE TEST STAND
16. COLLECTOR DRIVE TEST STAND
17. TOLTEC DUAL AXIS TROUGH
18. ALPHA SOLARCO SUNTREK-104
19. PIPE HEAT LOSS TEST
20. MIRROR EXPOSURE AND CLEANING TEST
21. BLACK CHROME THERMAL AGING TEST
22. SHENANDOAH PROTOTYPE DISHES
23. THERMOCLINE STORAGE TEST
24. THERMAL EXPANSION MECHANISM TEST

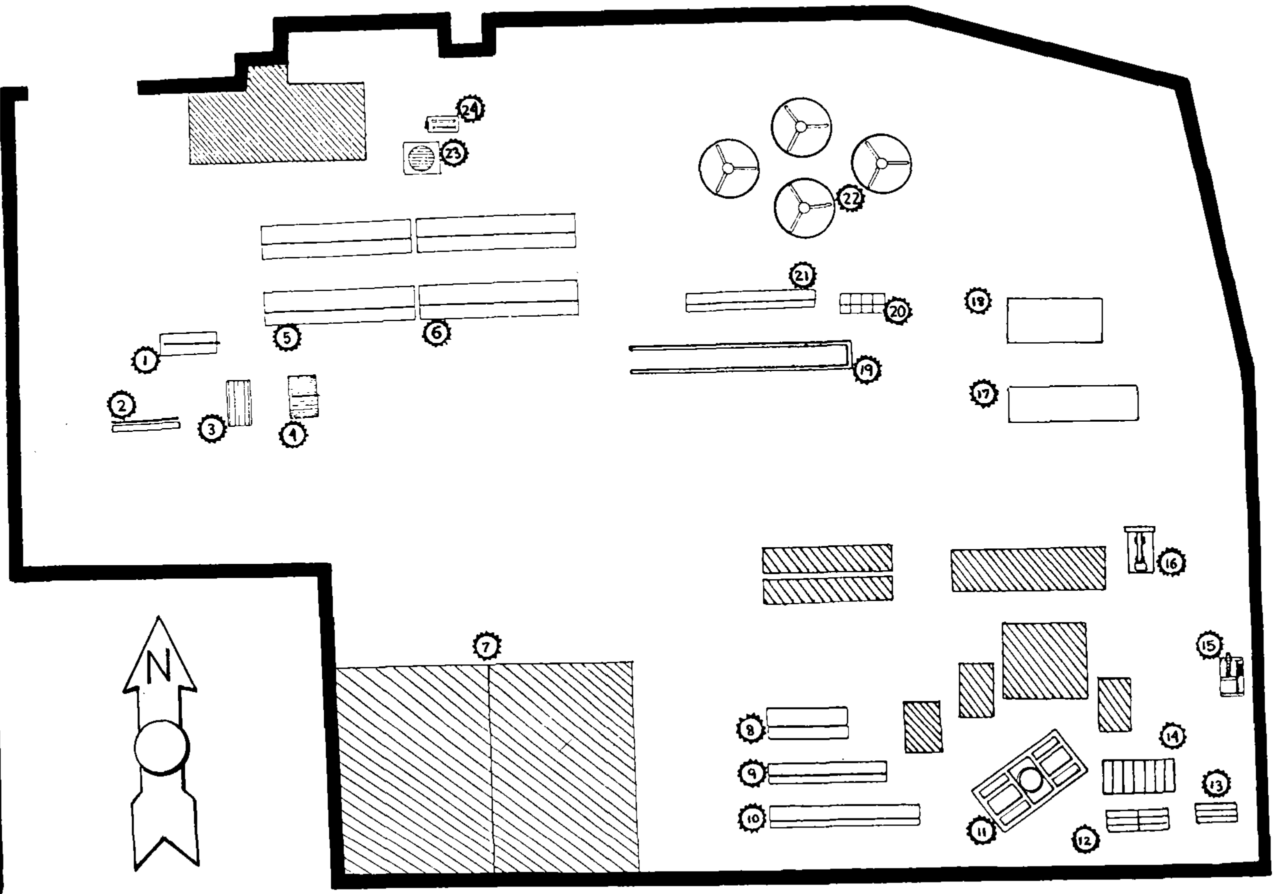

Session IV - Line-Focus Subsystem Development

Raymond W. Harrigan, Chairman
Component and Subsystems
Development Division 4722
Sandia National Laboratories

CROSBYTON SOLAR POWER PROJECT: REVIEW OF SYSTEM HARDWARE SERVICE

Dr. John D. Reichert
Project Director
Department of Electrical Engineering
Texas Tech University
P. O. Box 4709
Lubbock, Texas 79409

This is the Second of our semi-annual meetings on Buckets and Gutters. I had the privilege of hosting the First at Texas Tech in January, 1980. This time my privilege is to be a little more relaxed. Most of you were present at Crosbyton on January 23 at 3:30 p.m. to midwife the birth of our bucket, the ADVS, the largest single solar collector ever built. It was born before your very eyes and many of you helped the Exhausted Mothers do a little celebrating that night back in Lubbock.

We thought that such a birth should be attended by a little horn tootin', so we had borrowed some steam whistles from Santa Fe Railroad. On January 23, as you will recall, we slobbered a little wet steam through those old whistles and launched our party. Two days later, after you guys went home, on Friday, January 25 we got serious and sober and took the system on up to 1000°F at 1000 psi and achieved successful operation at design conditions, first try. [We disconnected the old whistles; they were not designed for high quality steam.]

Having found that the ADVS was easy to handle at design conditions, we proceeded to operate the system essentially all day, every day from then to now. Thus, we have about seven months of performance data (about 5000 hours on our feedwater pump). The system is solid and the results are good. The performance data is in exquisite agreement with design predictions. First cut results were reported to USDOE in our Crosbyton Solar Power Project Volume VI: <u>Analog Design Verification System Preliminary Performance Results</u>. We are now in the midst of preparation of a report giving more detailed results and analysis. This report will be available later this month (September, 1980), and I have no intention of preempting that event on the present occasion.

Thus, I am going to be a little backwards today. The good news will wait for a few days and will be good enough that I can afford to talk about the bad news today. This is, after all, the kind of occasion for which discussion of difficulties and problems is of greater value than celebrating good news. I want to talk about my troubles!

Most of our troubles have, ironically, had little to do with the solar specific portions of our system. It has been the "off the shelf" conventional components that have produced the most nuisance. For example, the solar boiler has given no trouble at all, but flow meters have failed repeatedly. I will spend the remainder of my time with warnings based on our recent experience.

Meters and Detectors. We built redundant metering and data acquisition into our system so we could live with failures. Flow meters have been particularly unreliable. We have been driven to remove all turbine meters from the system and to replace with bearingless optical meters. Even these have sporatic failures, but with two identical meters in series, we can usually deduce which is the better reading when they disagree. Pressure transducers have been replaced and have given erratic performance. The (type K) thermocouples, and there are about 60 of them, are arranged in pairs so that we get two signals from each location. Frequently, the two signals disagree. Leads pick up extraneous signals, must be guarded from cross-talk, and are subject to impedance matching problems. Some of these signals go to the control computer, to display devices, and to the data acquisition computer, and tend to give different readings at the different terminals.

Tracking pyrheliometers (for measuring solar brightness) are always a pain. We have two for redundancy because this data provides our primary normalization for efficiency. These have to be realigned several times each day. If the readings disagree, we use the larger of the two values for data analysis and go realign again.

Pumps, Valves, and Filters. We have had good service from our feedwater pump: 5000 hours of service to date. We have worried a great deal about components and parts made of 300 Series stainless steel, distributed throughout the system for corrosion resistance. Wet parts of aluminum, copper, or brass are strongly counterindicated in the presence of our high pH system water. For example, the system water quickly dissolved the aluminum body of a pressure regulating valve. The body was remade from a stainless steel block. Aluminum, copper, and brass wet parts cause two types of problems. In high pH environments these materials go into solution (erode) and lead to "bronze disease" or weakening: not good at 1600 psi. Downstream, nickel displacement and corrosion effects can be produced in our Inconel 617 boiler.

Series 300 stainless steels are vulnerable to "chloride stress corrosion cracking" in the presence of chlorides, oxygen, stress, and temperatures around 200°F. We have suffered no "chloride stress corrosion cracking" in our installed system, but observed the effect in preinstallation component qualification testing. Stainless 439 is resistant to this effect, as are other materials. However, Series 300 wet parts are already expensive and not readily available. Components of non-corroding, chloride proof materials such as 493 are not available and must be individually fabricated at the present time. Time and cost are nearly prohibitive. Thus, one must provide excessive water treatment.

Our original filter, upstream of our feedwater pump, was of ordinary steel, plated with a "corrosion proof" nickel layer on the wet surfaces. Such layers are unacceptable: they do not survive. Galvanic action and other corrosion moved at a swift pace and our system was quickly contaminated by rust particles. The filter housing was replaced (at a cost of over $1,000) by a stainless steel housing. Next problem: the metal retainers on the paper filter cartridges are made of highly corrodable metals and rust was produced again. We presently must use filters with no retainers! Filters do not appear to be available which are fully compatible with the purposes of stainless steel housings.

Our regulating valves, operated by automatic actuators, have been a major headache. Operating characteristics quickly change and decay. We simply replace our feedwater inlet valve whenever necessary. The steam exit control valves suffer from packing problems and from erosion of the regulating stem. Frequently, we must regrind stems and seats so that a new valve will meet manufacturers' specs. Erosion proceeds steadily in the presence of high flow, high quality steam. We replace the packings and stems as required. It is also unfortunate that steam control valves are not able to hold suitable pressure drops under liquid exit conditions.

Flex Hoses. Our system requires articulation of steam and water lines. We handle this with Series 300 stainless steel flex hoses which cost only about $80 each. Our fundamental worry that "chloride stress corrosion cracking" centers on these hoses. One has failed in service (with about 3 months of continuous service). Others have failed because they were not the right length and got pinched by some other component. Advice: use flex hoses of exactly the right length. Actually, we are quite pleased by the service we have received from our flex hoses, but regret the vulnerability to chloride.

Water Treatment. To avoid corrosion, scale, and damage to chloride senstive components, we have had to provide fairly elaborate water treatment. Water from our on-site well (390 ft.) is softened then sent through a reverse osmosis (RO) unit and deionization units (DI), and treated with hydrazine (oxygen scavenger). The hydrazine increases the pH to our required levels: 9.3 to 9.8. Additional pH increase, other than that provided by hydrazine can be achieved with ammonium hydroxide as required. The system reservoir is blanketed with nitrogen gas to avoid atmospheric oxygen. The point to most of this treatment is to protect our flex hoses and other stainless steel components from "chloride stress corrosion cracking".

We have incurred considerable nuisance in chloride level monitoring and from the ion exchange resin beds. Cation beds are frequently recharged with hydrochloric acid and, occasionally, are delivered full of this source of chlorides (pH 3 or less, sometimes). Cation and mixed beds must be tested before insertion into the system. Commercial water control service groups are geared to worry about calcium, iron, sulfates, and carbonates; they have no regard for nor useful experience with chlorides. At levels beneath 1 ppm chloride concentration, chloride monitoring is not, apparently, a science. No two labs or methods ever agree on the level. Puzzles, mysteries, and inconsistencies abound in the determinations.

The Inconel 617 Boiler Tubes. The boiler tubes are made of Inconel 617 because of its reputed resistance to "Creep Rupture". We are, so far, entirely satisfied with our Inconel 617 boiler. It is definitely a rugged material that will take a lot of thermal abuse. We have not installed the second boiler which was made of Inconel 625. The 617 boiler was slightly suspect because the thermocouples were silver brazed on. The Inconel 600 series is vulnerable to "silver stress corrosion cracking", and this boiler took damage during the course of thermocouple installation. The 625 boiler had it thermocouples installed by another technique, mechanical confinement with spot-welded foil strips, but the survivability of these thermocouples in service is not known at present. This will be determined when we install the 625 receiver. The 625 receiver has been on-site since early January, but we are reluctant to displace the 617 receiver, while its gives such good service.

System Computer Hardware. The system controller and the data acquisition system have given some problems. Dust conditions at the site have led to excessive cleaning and maintenance. We must clean the diskette and tape drives and heads very frequently (about fourteen day cycle). We are reluctant to dust proof the control room, because we wish the area to be accessible to our personnel and to visitors. There is a trade-off here between convenience/visibility and maintenance. We appreciate the great number of visitors at our facility and wish them to see all details of interest to them.

The system controller, in particular, is vulnerable to ambient temperature. Erratic behavior can occur outside the range: 54°F to 90°F. Thus we must guard the operability of our winter heating and summer air conditioning systems. Both computer systems suffer from component failure, particularly in keyboards, switches, and power supplies.

Motors. We have had to replace several motors on-site. Both of our small tracking drive motors have been replaced and repaired. Additionally our sump pump motor has failed and been replaced. Motors fail, and spares must be kept on hand at all times.

Mirror Panels. The one solar specific portion of our system which has produced failures has been our mirror panels. Space and time do not permit adequate discussion of the problem, but this topic is not of as much general interest because our panel concept is unique to our system. About 15% of our panels have failed (cracked) in service (actually, out of service; i.e., during times when the system was not operating) under conditions that they were designed and tested to endure. The cracked panels continue to give good service, but evaluation and redesign efforts are presently underway.

The present discussion has been somewhat generalized, because I did not wish to mention brand names for our components. However, the experience reported here is largely independent of manufacturer. Availability is severely restricted by time and cost in the "low flow, high quality regime" in which the ADVS test system operates. We will be happy to discuss our experiences more fully and specifically as you choose to contact us.

DEVELOPMENT OF THE T-2100 LINE-FOCUS SOLAR COLLECTOR

Gus Hutchison
Solar Kinetics, Inc.
Dallas, Texas 75247

The interest in concentrating solar technology has sharply increased since 1970. During that period, the first significant line focus concentrator to be fabricated and operated was at Sandia Laboratory in Albuquerque, NM. That version of the parabolic trough concept is fairly large with a nine foot aperture and a twelve foot module length.

The first commercial units were fairly small with a one foot by eight foot aperture for the collector by Del Manufacturing, followed by the Solar Kinetics, Inc. T-500 at 3½ x 20 foot aperture. The Acurex parabolic trough began with a 6 x 10 foot aperture and SKI responded with a 7 x 20 foot aperture in the T-700 model. The original Hexcel design, which was subsequently acquired by Suntec, offered up to an 8 x 20 foot aperture.

In each case the original Sandia nine foot collector was the largest of the first troughs since industry trended towards smaller models. SKI felt that larger aperture parabolic trough collectors should be considered in order to determine the optimum aperture size.

The concept first generated by SKI engineers for a large aperture collector was termed the T-1400. The idea was to build the collector in two 7 x 20 foot modules and assemble into a 14 foot wide module, on site. The main consideration was one of transportation due to ICC regulations restricting shipment on equipment wider than eight foot. However, many additional benefits began to emerge as the design concept unfolded.

A significant reduction in the number of parts is apparent for larger collectors. Quite often the size of a component has an economy of scale. For example, a fastener smaller than a ¼" bolt is seldom used since the care required during installation more than offsets the cost of the over-sized bolt. For larger units, the fasteners are optimized. The same argument holds for gauges and sizes. A smaller number of large units can require less handling and storage costs. SKI has found that a reduction in the number of specific items making up an assembly usually results in a cost reduction even though some items are larger and more costly.

The cost of installation, including the labor of actually mounting the collectors, could be reduced if the number of components could be reduced. The amount of insulated plumbing could be reduced with larger aperture collectors since the receiver serves as part of the fluid transport system. A reduction in the number, if not the size, of concrete foundations could also improve cost effectiveness. Many potentials for improved cost with larger collectors lead SKI to further investigate the T-1400.

Following this initial work, SKI entered into a contract with the BDM Corporation to investigate the feasability of a line focus thermo-electric power plant design, using the current production T-700 model. This 170 megawatt peak power plant design would require thirteen million square foot of collector or 96,000 T-700 modules. SKI Management decided to introduce BDM and D.O.E. to the T-1400 concept during this contract since a larger aperture collector would provide a more reasonable design for such a concept. It was then decided to optimize the design for size. Figure 1 indicates the various specifications for collectors of 7, 14, 21, 28 and 35 foot apertures; each increment representing one module width.

The design was optimized at three modules or a 21 foot chord with a 20 foot length. The primary consideration was ease of installation. A larger aperture requires elevated working conditions and higher costs. The 21 foot aperture collector was termed the T-2100. A comparison of the necessary components per million square feet of collector area is given in Figure 2. Figure 3 indicates the specifications for the T-2100. Figure 4 indicates the procedure for installation of the T-700 and Figure 5 shows the method used to install the T-2100.

A successful design will not require optical improvements over the T-700. The concentration ratio is planned to be similar. A geometric reduction in the surface area of the glass receiver cover will reduce the high temperature losses by 1/3 resulting in a net thermal efficiency improvement of up to three percentage points. Furthermore, the larger receiver will carry more thermal fluid per unit aperture per ΔP resulting in lower parasitic pumping losses.

The most dramatic impact on cost effectiveness is in the area of insulated plumbing. Figure 6 compares the plumbing for a nominal 80,000 square foot collector field, using T-700 or T-2100 collectors.

SKI is currently completing the T-2100 design and is fabricating four, 420 square foot modules for testing at Sandia Laboratory and BDM Corporation. Test data and cost estimates for future production will be available during the second quarter of 1981.

SPECIFICATIONS FOR LARGE APERTURE COLLECTORS

	APERTURE	NO. OF MODULES	ROTATION HEIGHT	RECEIVER HEIGHT AT STOW	FOCUS
T-700	7'	1	5'	3'	21"
T-1400	14'	2	9'	5'	42"
T-2100	21'	3	13'	7'	63"
T-2800	28'	4	17'	9.5'	84"
T-3500	35'	5	21'	12'	105"

FIGURE 1

T-700 VERSUS T-2100

	T-700	T-2100
NUMBER OF ROWS	1,190	238
HOSES	2,380	476
RECEIVERS	7,140	2,380
GLASS COVERS	14,280	4,760
GLASS COVER BRACKETS	15,470	4,998
RECEIVER BRACKETS	15,470	4,998
RECEIVER STANDS	15,470	4,998
MIRROR MODULES	7,142	2,380
BEARING ASSEMBLIES	8,330	2,618
CONCRETE FOUNDATIONS	8,330	5,236
ELECTRONIC TRACKERS	1,190	238
DRIVE PYLONS	1,190	238

FIGURE 2

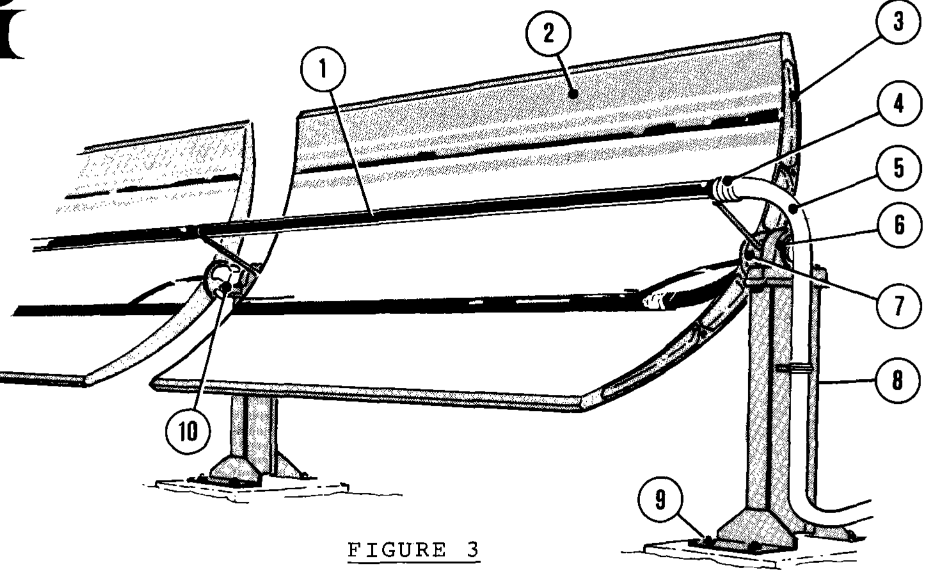

FIGURE 3

SOLAR KINETICS

SOLAR COLLECTORS FOR PROCESS HEAT UP TO 650°F

Solar Kinetics' rigid monocoque* mirror and no-lash hydraulic tracking* along with proven engineering concepts provide long life and low cost. Features of the system are:

1. The black chrome plated steel receiver tube is surrounded by a dry air annulus protected by Pyrex® glass tubing. Focus is adjustable during installation.
2. A precisely constructed mirror surface is covered with metallized acrylic film or glass combining weather resistance and high reflectivity.
3. The parabolic contour is N/C machine generated for an accurate focus.
4. The thermal expansion bellows allows for expansion of the receiver assembly and maintains a sealed, dry environment in the annulus.
5. An insulated stainless steel flex hose allows rotation of the collector with unrestricted flow.
6. Self aligning sealed ball bearings absorb structural loads maintaining collector motion without binding.
7. A steel flange carries torsional loads into the collector structure. Allows mirror installation with 10 bolts.
8. The steel support pylon is galvanized for corrosion protection.
9. Mounting studs are a standard pattern for each collector.
10. This load bearing joint* protects the collector structure from strains induced by misalignment from foundation shifts.

*PAT PENDING

SPECIFICATIONS	T-2100 *
MODULE WIDTH	22'
MODULE LENGTH	20 FT
MIRROR WIDTH	21'
SOLAR AREA	410 FT^2
REFLECTANCE	0.84/.96
MAX VERT HEIGHT	24'
ROTATION AXIS HT	13'
TRACKING ANGLE	270°
STOW ANGLE	HORIZONTAL
SYSTEM WEIGHT	5.0 LB/FT^2
RECEIVER TUBE	4.5" OD
ANNULUS MEDIUM	DRY AIR
SELECTIVE SURFACE	BLACK CHROME
ABSORPTIVITY	0.94-0.97
EMISSIVITY	0.18 @ 500°F
RECEIVER COVER	PYREX GLASS
MAX OPER TEMP	650 F
MAX OPER PRESS	250 PSI

SOLAR KINETICS, INC., 8120 CHANCELLOR ROW, DALLAS, TEXAS 75247 214-630-9328

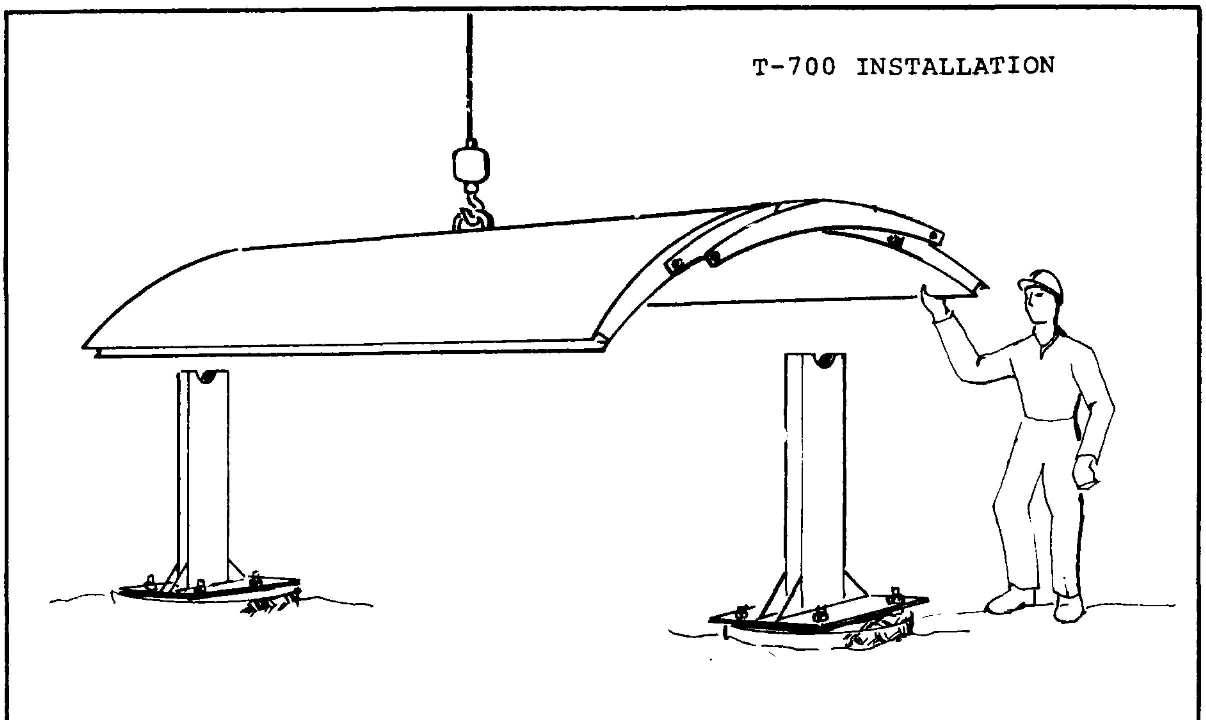

FIGURE 4

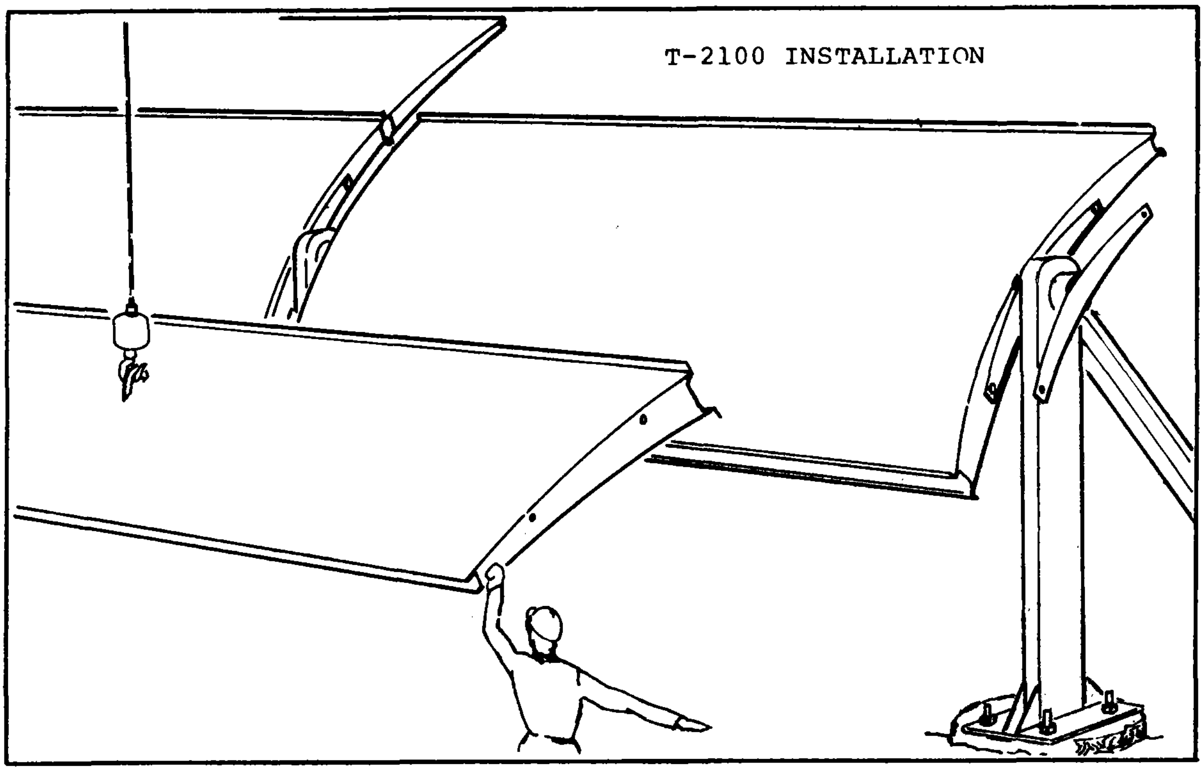

FIGURE 5

FIELD PLUMBING COMPARISON

	T-700	T-2100
Aperture	80,640	84,000
ΔT	200°F	200°F
Aperture/ΔT Loop	1680 ft^2	42,000 ft^2
ΔT Loops	24	2
Field Flow Rate	150 gpm	150 gpm
ΔT Loop Flow Rate	6.5 gpm	75 gpm
Receiver Fluid Velocity	1.5 FPS	1.8 FPS
Loop ΔP	5-10 PSI	3-7 PSI
Manifold ΔP	5.6 PSI	0.7 PSI
Volume of Pipe Insulation @3"	503 ft^3	109 ft^3
Insulation Skin Area	3,115 ft^2	628 ft^2
Active Thermal Mass	11,000 BTU/°F	27,000 BTU/°F
Passive Thermal Mass	4,700 BTU/°F	1,700 BTU/°F
Total Thermal Mass	15,700 BTU/°F	28,700 BTU/°F

FIGURE 6

PREDICTED PERFORMANCE OF LINE-FOCUSING, CONCENTRATING SOLAR COLLECTORS WITH POTENTIAL FOR USE IN INDUSTRIAL PROCESS HEAT APPLICATIONS

Thomas D. Harrison
Experimental Systems Operations Division
Sandia National Laboratories
Albuquerque, NM 87185

Introduction

Sandia National Laboratories (SNLA) is conducting a program to provide accurate predictions of the thermal performance of line-focusing solar collectors that have potential for use in producing industrial process heat (IPH). The program was authorized by the Department of Energy (DOE), Division of Solar Application through the Solar Energy Research Institute (SERI).

The predictions consider only the thermal performance. One should also consider the following factors:

1) Gaps and end losses
2) Cost of collector
3) Cost of installation
4) Cost of operation and maintenance
5) Losses in the energy transport system
6) System warmup penalties
7) Reliability
8) Durability
9) Degradation of performance
10) Wind effects
11) Parasitic losses

Qualifications for Commercial Laboratories

To ensure acquisition of valid performance data for solar collectors, the testing laboratories were required to:

1) Have a demonstrated expertise in solar collector testing,
2) Have the necessary instrumentation,
3) Be capable of testing at temperatures up to 300°C (572°F),
4) Be able to handle the collectors under consideration,

5) Operate under rules and procedures necessary for good testing practice, and
6) Be independent.

The two laboratories which met the qualifications were

1) DSET Laboratories, Inc., Box 1850, Black Canyon Stage, Phoenix, AZ 85029.
2) Wyle Laboratories, 7800 Governor's Dr. West, Huntsville, AL 35807.

Other commercial laboratories which believe themselves to be qualified are currently being evaluated.

Requirements for Collectors To Be Tested

By its charter, the testing program is limited to line-focusing collectors with potential for use in producing IPH. IPH consumes about 19 quads of energy annually, or about 25% of the total national energy consumption.[4] 40% of the IPH energy is consumed in the end-use temperature range 100°-175°C (212°-347°F), another 40% in the range above 590°C (1094°F), with the remainder in between.

Based on these figures, the minimum operating temperature was specified as 100°C (212°F). No maximum operating temperature was specified since the maximum testing capability would be 300°C (572°F) in any case. Size and weight limitations were set in order to ensure compatibility with the testing laboratory's collector mounting equipment.

Selection of Collectors

In order to assure that all eligible firms were given an opportunity to participate, a search was made to gather the names of firms which manufacture line-focusing, concentrating solar collectors. A list of 19 firms was prepared. Expressions of interest were followed by a visit from a Sandia representative to explain the program and to make judgment as to whether the collector actually met criteria. A formal agreement was established through Sandia's purchasing organization with qualified organizations.

Computer Program To Predict Performance

The performance prediction program developed by Sandia has two major inputs: the collector efficiency data obtained from the test program and meteorological data. The meteorological model chosen was the Typical Meteorological Year (TMY). The TMY tapes are available from the National Climatic Center, Asheville, North Carolina, for 26 sites in the U.S. A detailed description of the TMY selection method is given in Reference 5. Each TMY tape lists, on an hour-by-hour basis, an extensive array of meteorological parameters. The application in this project required the use of only the ambient temperature, the wind speed, and the direct normal solar radiation for input into the computer calculation.

An existing computer program was modified for making the solar collector thermal performance calculations for this project. No attempt was made within the computer program to simulate an actual IPH system application and, therefore, the collector fluid inlet temperature, $t_{f,i}$, can be arbitrarily selected. Low values of $t_{f,i}$ bias the performance predictions toward high efficiencies for the solar collector system. To assure the elimination of such bias, the highest possible value for $t_{f,i}$ was selected. This choice yields a conservative estimate for the amount of useful energy collected by the solar system. The general sequence of calculations performed by the computer program is shown in Figure 1. The calculation is repeated for each hour of the day through the entire year. The collector heat output for each hour is summed to provide daily, monthly, and annual totals. The entire calculation is repeated four times, once for each of four different collector output temperatures. The output temperatures selected were 150°C, 200°C , 250°C, and 300°C (212°F, 392°F, 482°F, and 572°F). Performance predictions were calculated for both N-S and E-W orientations of each collector. The five geographical locations selected were Fresno, California; Albuquerque, New Mexico; Ft. Worth, Texas; Charleston, South Carolina; and Boston, Massachusetts. The first four locations were chosen because they are at approximately the same latitude (32.5°N to 35°N) but in different zones of solar irradiation intensity. Boston (42.5°N) was selected because it is a highly industrialized area and a potential location for solar IPH installations.

The collectors for which predictions were made, listed according to the agency which tested them, are given in Table 1.

Error Estimate

Errors in the performance prediction estimate accumulate from both the collector testing program and the TMY data tapes. The maximum measurement errors in the testing program are listed in Table 2.

Assuming that the maximum error represents three standard deviations and that the errors are randomly distributed in time, the overall error in testing measurements is 2.56%.

No extensive validation has been performed for the TMY data. However, P. J. Hughes, formerly at the University of Wisconsin Solar Energy Laboratory, has assessed the TMY data for Madison, Wisconsin, by using the Transient System Simulation (TRNSYS) routine to compute the heat output for a solar collector system for the years 1953-1974. The standard deviation of the annual output compared to the mean of the 22-year data base was 4.44%. The heat output as calculated using the Madison TMY data tape was within the one standard deviation from the data base mean. For the purpose of this report the error contributed by the TMY data is assumed to be $\pm 4\%$.

Combining testing errors and meteorological errors yields a standard deviation for variations in energy output of 4.75%. A more accurate estimate of error will require a detailed comparison of the weather data for each locality against the TMY data for that locality.

Summary

Within the limitations previously noted, thermal performance predictions have been completed for 14 types of commercially available line-focusing collectors at 5 locations for 4 different collector output temperatures. The overall error in these predictions is estimated to be less than 5%. The TMY tapes provide typical long-term weather data, but short-term deviations are to be expected.

An example of the output of the computer program is listed in Table 3. A plot of the data for the E-W oriented collectors is shown in Figure 2, and for the N-S oriented collector in Figure 3.

References

[1] ASHRAE 93-77.

[2] Laboratories Technically Qualified to Test Collectors in Accordance with ASHRAE 93-77: A Summary Report, U.S. Department of Commerce PB 289 729 (Washington: National Engineering Laboratory [NBS], November 1978).

[3] Keith Masterson, Survey of Solar Thermal Test Facilities, SERI/TR-34-083 (Golden, CO: Solar Energy Research Institute, August 1979).

[4] D. W. Kearney, "Solar Industrial Process Heat Program," Solar Energy Research Program: FY Annual Report SERI PR 333--463, October 1979.

[5] Hall, I., Prairie, R., Anderson, H., Boes, E., Generation of Typical Meteorological Years for 26 SOLMET Stations, SAND78-1601 (Albuquerque: Sandia Laboratories, August 1978).

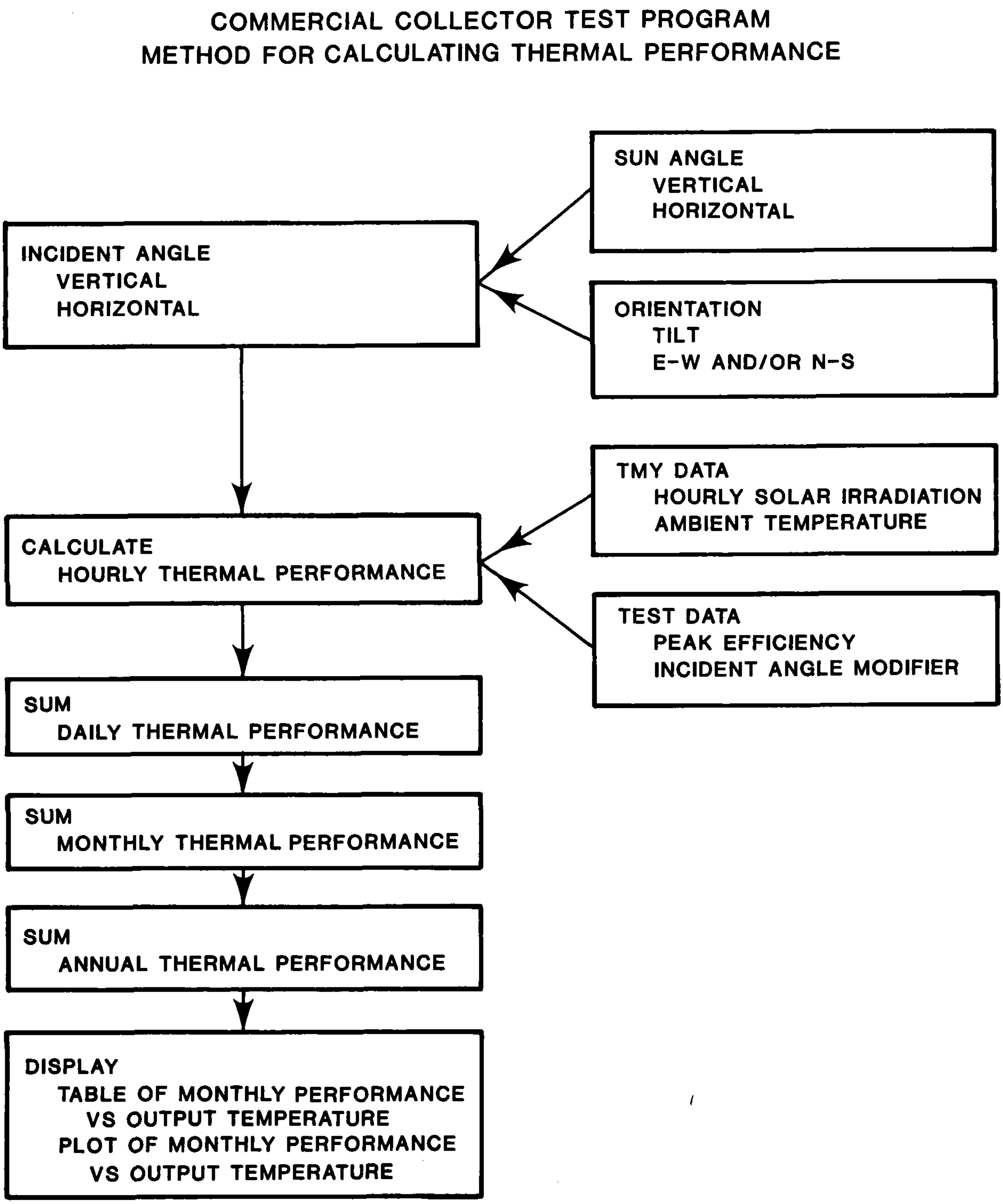

Figure 1. Method of Calculating Performance Predictions

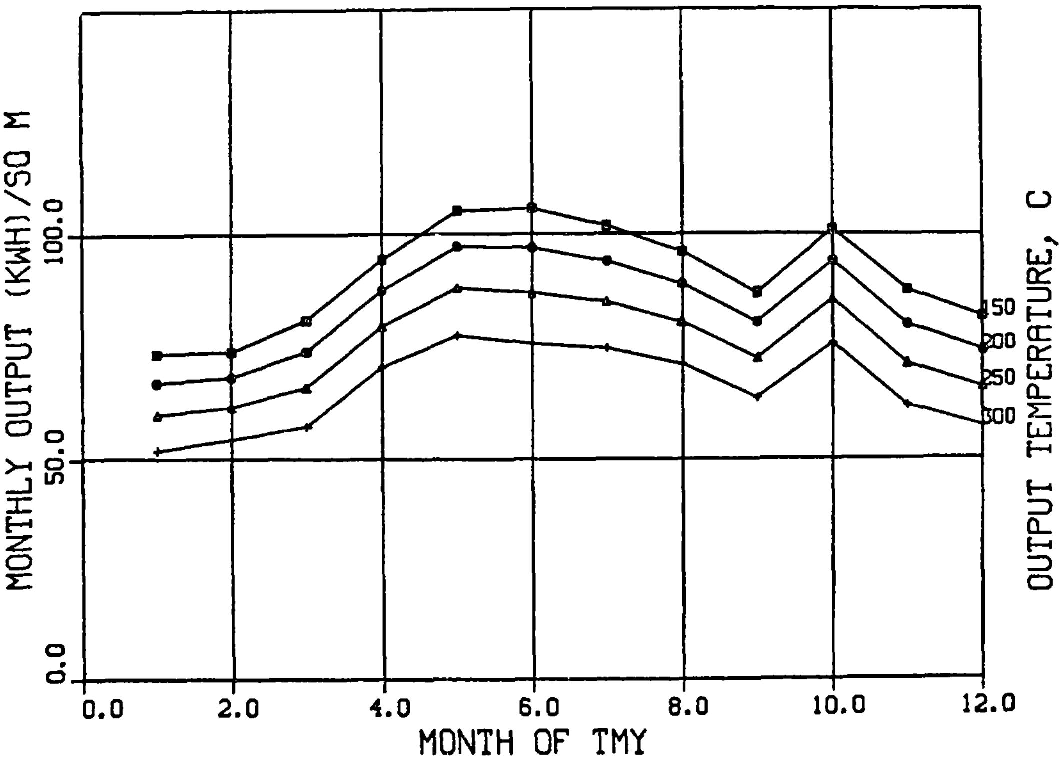

Figure 2. Thermal output of a typical high performance collector with E-W orientation and Albuquerque, NM, TMY solar data

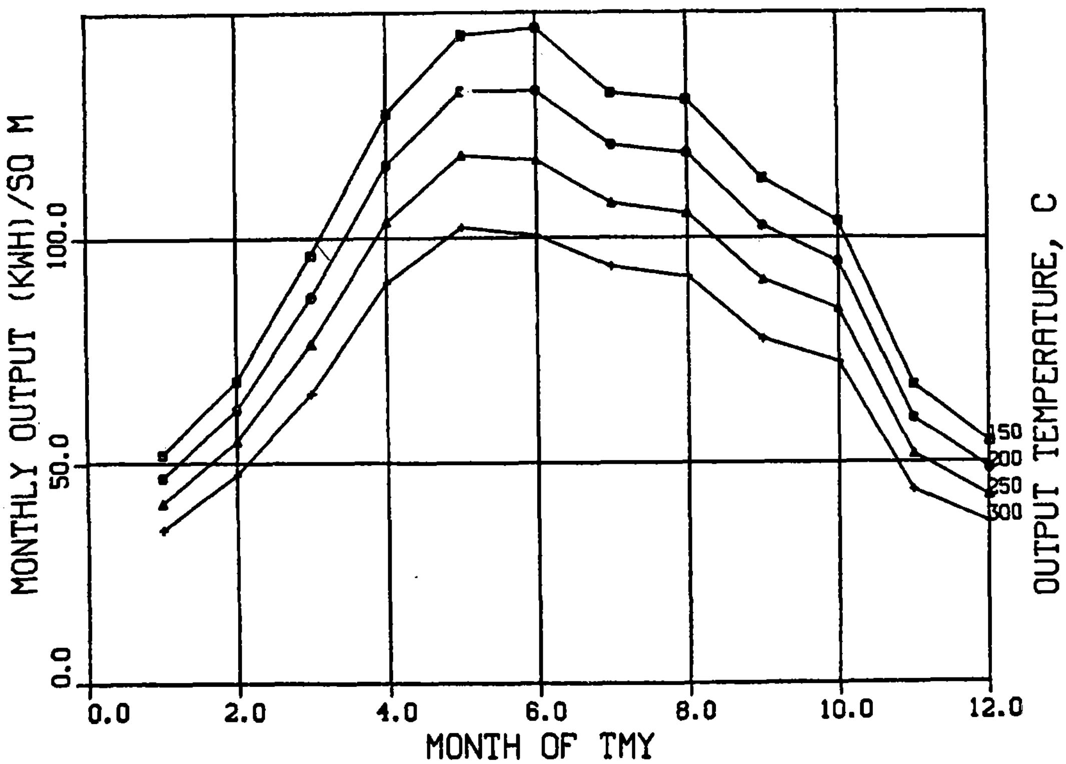

Figure 3. Thermal output of a typical high performance collector with N-S orientation and Albuquerque, NM, TMY solar data

Table 1

Collectors for Which Performance Predictions Are Being Made

Sandia	DSET	WYLE
Suntec	Alpha Solar	Toltec
Acurex (FEK 244)	Sun Heet	SKI (T-600)
Acurex (glass)	ZZ	AAI
SKI T-700 (FEK 244)	DEL	
SKI T-700 (glass)	Polisolar	
Custom Engineering	Viking	

Table 2

Maximum Errors in Measurement

Measurement	Maximum Error (%)
Differential temperature (Δt)	±2
Coolant mass flow rate (m)	±5
Optical properties (ρ, $\tau\alpha$)	±5
Tracking error (θ)	±1
Pyrheliometer (I_{DN})	±2

Table 3

Thermal Output for a Typical High-Performance Collector for Albuquerque, NM, TMY Data

Orientation	Output Temperature (°C)	Solar Energy Available (kWh/m^2)	Energy Collected (kWh/m^2)
E-W	150	2583	1088
"	200	"	1001
"	250	"	902
"	300	"	792
N-S	150	"	1236
"	200	"	1121
"	250	"	994
"	300	"	857

DESIGN OF COLLECTOR SUBSYSTEM PIPING LAYOUTS

Robert E. Morton
Jacobs Engineering Group
Pasadena, California 91101

Introduction

Review of current designs show that the process piping systems in solar collector arrays are being built around design criteria long established as acceptable by process industries. Although these criteria are known to be conservative when applied to solar collector fields, designers are still forced to use them because guidelines do not exist yet for solar applications. The use of conservative process piping design criteria undoubtedly increases capital and operating costs when used without consideration for the special nature of solar energy fields.

In early 1979, Sandia Laboratories commissioned Jacobs Engineering Group to study the piping criteria in depth as they apply to the design of solar field piping layouts. Field layout; optimum insulation type and thickness; method and frequency of pipe support; ΔT string length; pump type; driver type and many other related factors were to be studied. The long range goal of these studies is to develop special guidelines tailored to facilitate design of modular solar piping systems.

The initial design studies have been performed on a 50 thousand square foot solar collector field layout. As a result of these studies, recommendations for configuration; ΔT string length; header piping profile; and insulation material and thickness have been developed. The insulation recommendations can be applied to the design of any size solar array because it was possible to decouple the insulation study from the piping study. The other recommendations, however, apply strictly to the design of the 50 thousand square foot E-W collector array. Future studies should be made to determine the need to modify the piping recommendations for modular collector arrays which are larger or smaller than the one studied.

Design Criteria

The studies are based on certain design criteria established by Sandia. These are presented below in Table I.

Table I

Initial Design Criteria

Parameter	**Value**
Wind Velocity	5 ft/sec. normal to pipe
Size of collector field	50,000 ft^2
Drive string length	80 ft
Collector orientation	E-W
Collector spacing	15 feet
Heat transfer fluid	Therminol MCS-2046
Fluid ΔT	150°F
Fluid outlet temperature	600°F
Energy value out of collectors	$10 per million BTU
Annual capital charge	15% of initial investment
Foundation design	Optimum Sandia design
Minimum flow rate	50 gpm
Peak flow rate	300 gpm

Piping Study

Several alternative field layouts were proposed and, of these, two were selected for preliminary study. These are shown schematically in Figures 1 and 2. Heat transfer fluid enters and leaves the system via the center of the collector array in Figure 1, and via the edges of Figure 2.

Figure 1
Center Feed

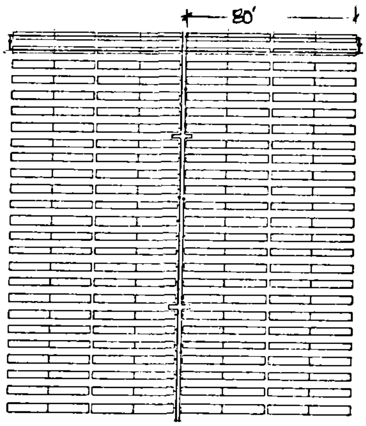

SOLAR ARRAY PLAN

Figure 2
Edge Feed

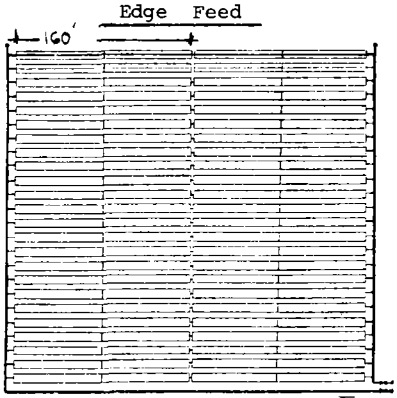

SOLAR ARRAY PLAN

The preliminary screening process consisted of a capital cost estimate, estimates of heat loss and a subjective critique of the arrays utility as a module in larger collector fields. It was found during this process that the capital costs of both configurations were about the same, however the center feed configuration of Figure 1 would not economically lend itself to larger modules. Each of the collector rows in Figure 1 requires two additional fifteen foot long 1" pipe return bends not required by the array in Figure 2. The extra pipe results in substantially higher heat losses for larger arrays. The edge feed configuration of Figure 2 was selected for detailed study for this reason.

Once the general configuration was established, cost comparisons were made of optimized edge feed 50 thousand square foot collector arrays to arrive at a recommendation for ΔT string length and receiver tube diameter. Four ΔT string lengths were considered. They ranged in size from 240' to 480' in length. Receiver tubes under consideration were 1" and 1.25" o.d. schedule 40 steel pipe. Each of the final candidate arrays evolved from optimization studies which considered the minimization of capital, heat loss and pumping cost in the piping size selection.

The results of the study indicate that the ΔT string length should be 320'. Receiver tube diameter can be 1" or 1.25" o.d.

Table 2 presents the total annual estimated operating costs for the range of ΔT strings studied. These costs are plotted in Figure 3. This figure shows the relative insensitivity of the estimated operating costs to ΔT string length and receiver tube diameter.

Table 2

Total Annual Operating Costs

Length of ΔT string	Receiver dia., in.	Pumping Cost, $/yr	Heat Loss Cost, $/yr	Capital Charge, $/yr	Total Cost, $/y
240	1.0	6800	9100	12900	28800
320	1.0	7300	8000	11250	26550
400	1.0	8550	7700	10400	26650
480	1.0	11300	7600	9900	28800
240	1.25	6400	9100	12900	28400
320	1.25	6540	8000	11250	25800
400	1.25	6950	7700	10400	25050
480	1.25	8300	7600	9900	25800

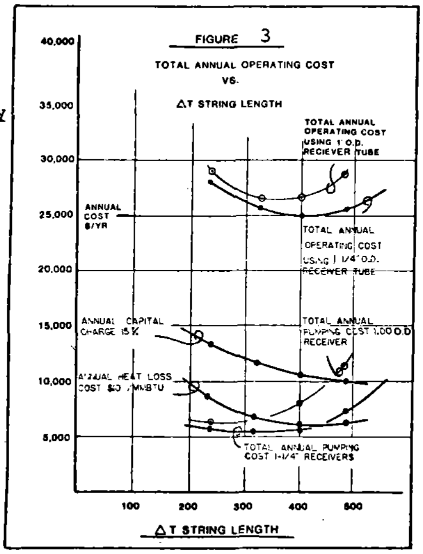

Figure 4 is a plan view of the conceptual 30 thousand square foot collector array developed in this project. The design is the result of otpimization studies made to find a design in which the pumping cost, heat loss cost and capital charge were minimized. This collector layout consists of twenty-four 320' long ΔT strings spaced at 15 foot intervals. Each ΔT string is composed of four 80' drive strings, a 1-1/4" o.d. receiver tube; two gate valves and

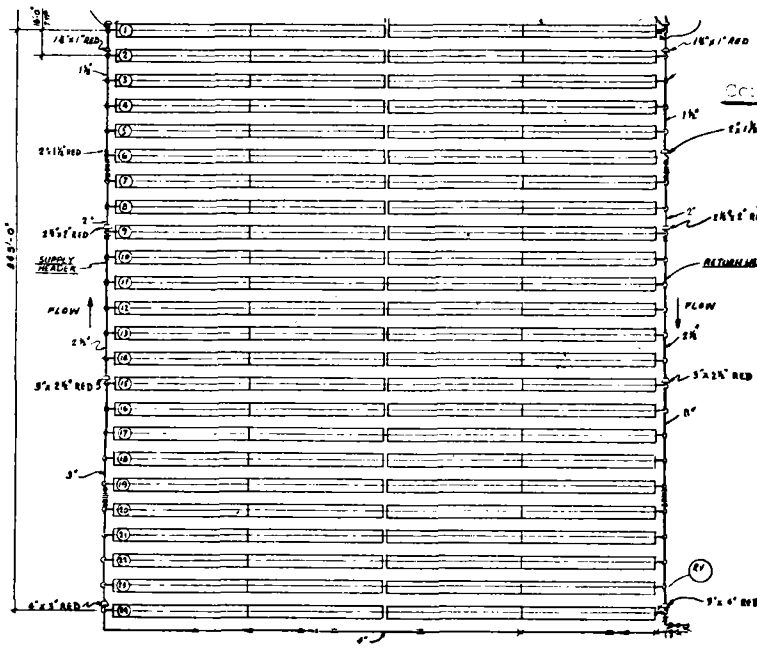

Figure 4

Conceptual Layout

a control valve. The telescoped header profile shown on Figure 4 results in the minimum overall operating cost, based on heat and power costs provided by Sandia. Heat is valued at $10/million Btu. Electric power costs 10¢/Kwh and the annual capital charge is 15 percent of initial capital investment. It has been shown by sensitivity study (see Figures 5, and 6) that these costs can vary substantially without affecting the design recommendation.

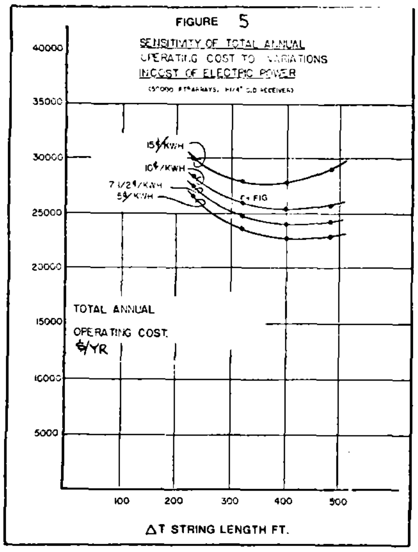

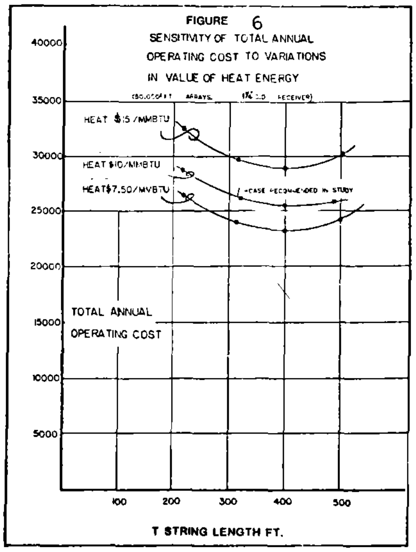

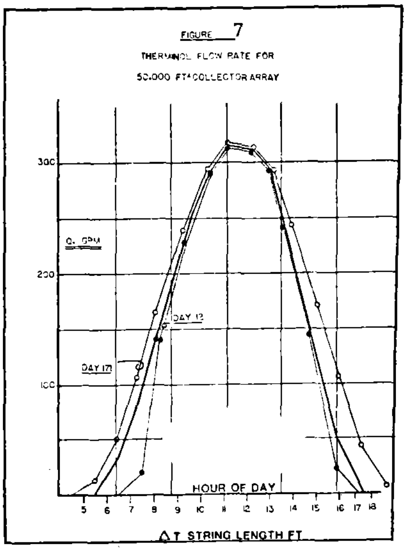

Pump Driver Study

Solar energy input to the collector is not constant over the operating day. Since it is desirable to maintain a constant fluid temperature rise across the ΔT string, the fluid flow must vary in proportion to the changing energy input. The flow rate in the ΔT string, and header piping, will rise from a minimum in the morning, peak at solar noon and fade off to a minimum value in the evening. The array will be shut down and allowed to cool overnight.

Various alternatives are available for pumping fluid through the collector piping. We have studied the use of centrifugal pumps in solar arrays. The pump is assumed to operate in one of three modes: continuous speed; two speed; and SCR drive variable speed. Annual operating costs were developed for each of the three modes in order to select the most economical. The pumping and capital costs were based on vendor pump price quotations, the pipe configuration shown in Figure 4, energy value of 10¢/Kwh and an annual capital charge of 15 percent of capital costs. Receiver tube o.d. was 1.25 inches.

FIGURE 8
ENERGY CONSUMPTION OF PUMP DRIVER ALTERNATES

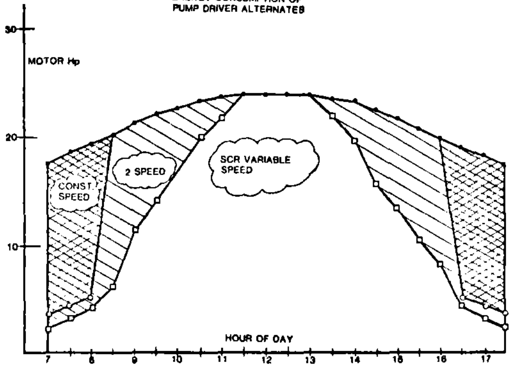

Energy consumption was estimated using the daily estimated flow curve shown in Figure 7. Using quantity-discharge curves provided by the pump manufacturer and calculated pipe system curves, estimates were made of pump BHP requirements. The BHP requirement was calculated over one operating day for half hour intervals. The calculated BHP values were then corrected for motor efficiency. The resultant gross Hp was converted to Kwh. The annual energy cost was based on the integrated daily energy consumption.

Figure 8 shows the calculated gross motor Hp for each of the three cases. The area under the curve is the total daily energy consumption for each case. Clearly, the continuous speed case uses the most energy, followed by the two speed case. It is evident from this figure that speeding up the pump impeller in proportion to energy input through the use of an SCR drive results in the lowest energy consumption.

Table 3 presents a breakdown of the total costs associated with pumping. The annual capital charge is 15 percent of the initial cost of the pump and controls. Even though the SCR drive is substantially more costly than the other two types of driver the energy savings justifies its selection.

Table 3

Total Annual Pumping Cost

Mode	Capital Charge,$	Energy Cost,$	Total,$
Continuous speed	1570	6540	8110
Two speed	1570	5510	7080
Variable speed	2730	3810	6540

Insulation Studies

Calcium silicate, mineral wool, fiber glass, and cellular glass were selected for study. These four were picked because they seemed to fulfill such basic considerations as cost, and resistance to high temperature and abuse. The optimum insulation material was found by weighing cost advantages of all four at their optimum thickness against ease in installation and service life. Part of the study consisted of evaluating insulation materials under changing conditions of heat loss and annual capital charge. To expedite the analysis one of the four materials (Base Case) was subjected to post-optimality analysis which showed the sensitivity of the calculated optimum thickness to changes in certain parameters. The behavior of the other three insulation materials to changes in the same variable was assumed to be consistent with the response shown by the Base Case. Calcium silicate was selected to be the Base Case because of its wide acceptance as an insulating material. As it turned out, fiberglass or mineral wool are preferred to calcium silicate.

Determining optimum insulation thickness for a given material involves the trade-off of insulation materials costs with the value of the energy saved. Estimating the energy savings requires calculating daily heat losses. The total heat loss calculated in this study was the sum of three individual component losses, the operating heat loss, the overnight cooldown heat loss and the startup heat loss. The capital cost of the insulation material and installation labor were obtained from insulation contractors. The cost data included the insulation material, vapor barrier, 0.016" aluminum covering, and all labor charges, installed in New Mexico.

The calculated optimum thickness of 4" for the Base Case (calcium silicate, over a 4" schedule 40 steel pipe) is shown by curve 3 on Figure 9 . The curve is relatively flat in the optimum region allowing a range of selection between 3" to 5" before significant change is made in overall annual costs. Curves 1 and 2 show the component capital costs and heat loss costs, respectively. Figure 10 shows the relative sensitivity of this optimum to energy costs of \$3, \$7.50, and \$10 per million btu; and three annual payback rates of 10, 15, and 20 percent. As expected, higher energy values tend to drive one to thicker insulation thicknesses.

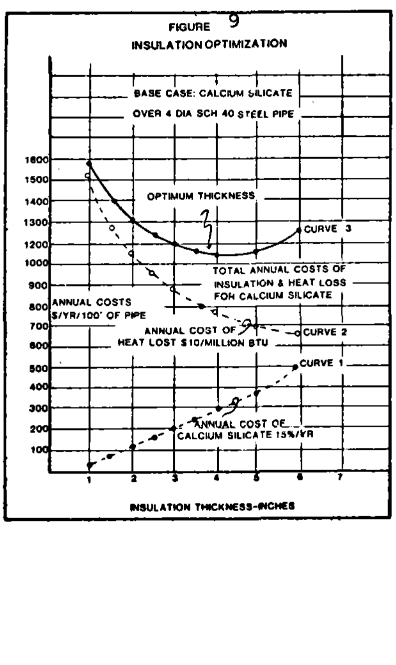

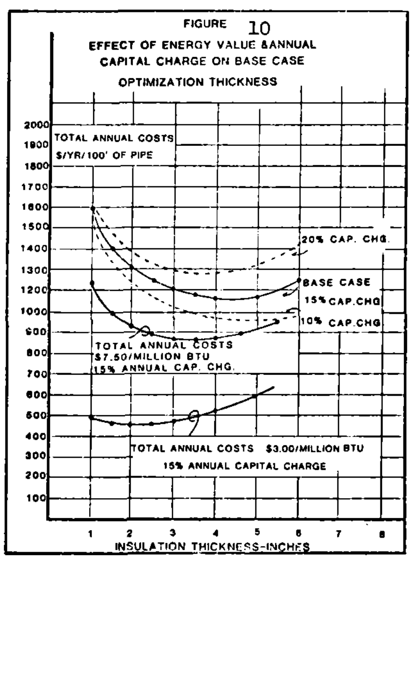

Figure 11 presents the relative performance of each of the four materials under Base Case conditions for a 4" pipe. Clearly, fiberglass or mineral wool have cost advantage over cellular glass or calcium silicate. The optimum thickness for all four is about the same. Figure 12 presents similar results for 2" and 8" pipes.

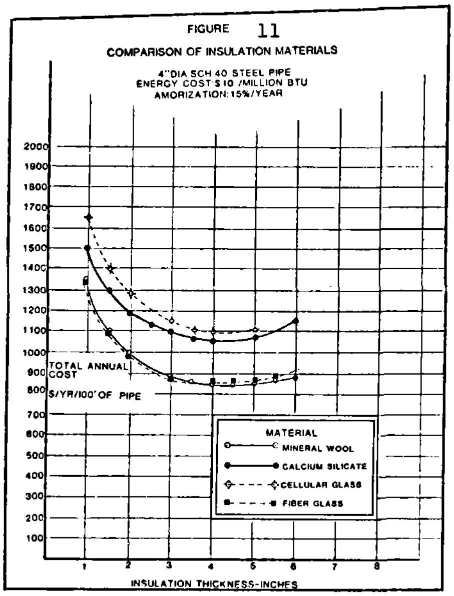

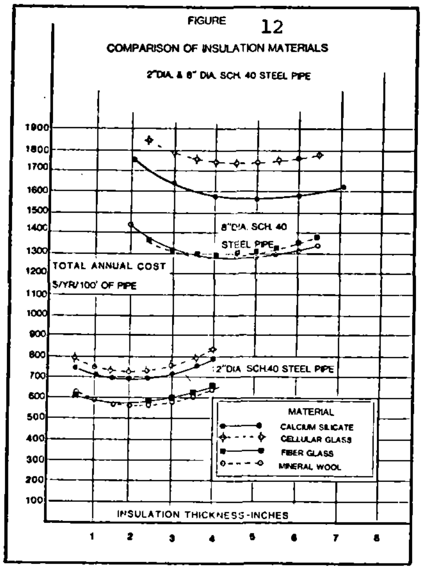

A schedule of recommended insulation thicknesses for various diameter pipes is presented below in Table 5. Preformed fiber glass or mineral wool insulation is preferred for those applications where physical abuse is not a problem. Calcium silicate can be used in combination with fiberglass in those areas of the array where the fiberglass could be damaged by rough treatment.

Table 5

Recommended Insulation Thickness
(Basis: $10/million Btu and 15% amortization)

Nominal Pipe Diameter, in.	Recommended Thickness, in.
1	1-2
1.5	1.5-2
2	2-3
2.5	3-4
3	3-4
4	4-5
6	4-5
8	6

DESIGN OF COLLECTOR SUBSYSTEM PIPING LAYOUT II
Evaluation and Extension of Standard Engineering Design Techniques

John Sharp
System Analysis Division 4723
Sandia National Laboratories
Albuquerque, NM 87185

Introduction

The thermal transport piping is one of the main components of a parabolic trough collector field. In designing the collector field piping, one must consider the effects of the layout on collector performance, thermal losses within the field, electrical energy for pumping, and the capital and installation costs of the piping network. For proper field design one should strive to minimize the total annual operation cost resulting from all of these factors. In the previous paper, Jacobs Engineering Group has developed a piping layout design using these ideas for a specific collector field located in Albuquerque, New Mexico. The objectives of the study described in this paper were to:

1. Verify the design techniques used by Jacobs.

2. Develop the tools needed to extend the analysis of piping field layouts to parameter values not evaluated by Jacobs.

Of particular interest were the Jacobs design criteria of decoupling the thermal and electrical parasitics and sizing field piping to provide equal fluid head loss through each manifold pipe size. The generalized computer optimization techniques developed as a part of this study confirmed these and other Jacobs design techniques.

Design Points

The design points of this initial study of piping layout subsystems were identical to those used in the Jacobs study(1) for verification. The collector area was approximately 50,000 square feet (4,600 square metres) provided by 7,680 linear feet (2,300 metres) of parabolic trough collector with a 6.6-foot (2-metre) aperture. Note that, since the size of the collector field was fixed, the amount and hence cost of the useful thermal energy from the field vary with location. The drive string length chosen was 80 feet (24 metres) with the ΔT string length some multiple number of drive strings. The receiver tube was assumed to be 1.00 inch (2.54 cm) ID steel tubing with a 1.25 inch (3.18 cm) OD and the heat transfer fluid selected for analysis was Therminol 66. The output temperature of the field was set at 600°F (315°C) with a 150°F (66°C) temperature rise across the ΔT string. The field was laid out in a perimeter flow scheme. The perimeter flow was chosen over center flow because it allows separate modular fields to be potentially connected with less piping [1]. The collector performance characteristics used were those of a parabolic trough representative of the design goals [2] for trough collectors. The value of energy was set at $10 per million BTU thermal and $0.10 per kWh electric with capital cost amortized at 15% per year.

Operation Costs

Electrical Parasitics--The electrical parasitics are the energy needed to pump the heat transfer fluid through the manifold piping and the parabolic trough receiver tubes. For a given size receiver tube, the velocity of the fluid is linearly dependent on the length of the ΔT string while the energy used to pump the fluid is approximately a cubic function of the velocity. Thus, when the ΔT string length is doubled, electrical energy consumption for pumping the fluid through the receiver tube increases by nearly a factor of eight. This cubic increase in pumping power limits the optimal length of the ΔT strings. The electrical parasitic consumed in the manifold piping remains nearly constant as the ΔT string length is varied. To decrease the electrical parasitic associated with the manifold piping, pipe sizes can be increased. However, increasing the pipe sizes also increases the thermal losses.

Thermal Parasitics--Thermal parasitics are divided into two general types: actual and potential. Actual thermal parasitics are the heat losses from the collector field. Both steady-state (operational) and overnight cooldown are considered. In distributed thermal solar energy systems such as those employing parabolic troughs, a considerable amount of energy is left in the field in the form of hot pipes and fluid when the system is shut down at night. Usable solar energy is typically available only six to eight hours a day which makes the duration of system cooldown more than sixteen hours on the average. The energy lost during overnight cooldown originates both in the manifold piping and the receiver tubes. Long cooldown times can make overnight cooldown a substantial portion of the total heat loss. In this analysis, steady-state heat loss is calculated only for the manifold piping since heat loss from the receivers is included in the normal collector efficiency used to compute collector output during operation. Piping heat losses can be reduced by using smaller pipe sizes or thicker pipe insulation, but smaller pipes require greater pumping power, and capital costs increase with thicker insulation.

Potential thermal energy is that energy lost due to the collectors shading each other at different times during the day. The closer the collectors are to each other, the greater the amount of shading. The shading penalty for collectors with a N-S tracking axis is larger than the penalty for collectors with an E-W tracking axis. Shading considerably reduces the annual 14% performance advantage that unshaded N-S fields have over unshaded E-W fields operating at 600°F in Albuquerque. To reduce shading, the collectors can be spaced farther apart, but doing so increases the actual thermal losses, the electrical parasitics, and the capital costs.

Capital Costs--The cost of manifold piping for the collector field must be included in selection of a field piping layout design. The capital costs considered include pipe, insulation, valves, fittings, welds, labor expenses, and overhead. The major trade-offs associated with capital expenses are insulation thickness versus heat loss, and spacing versus shadowing.

Field Optimization

Field design should minimize the annual operational cost which includes thermal and electrical parasitics and the capital costs of the manifold piping. The variables chosen to be minimized were the ΔT string length, row spacing, three manifold pipe sizes, the three associated insulation thicknesses, and the length of each pipe size. The ΔT string length was limited to fixed multiples of the drive string length, and continuous pipe size and insulation thicknesses are assumed. The annual parasitic cost is defined:

$$AC = \alpha * E + \beta * T + \gamma * C \qquad (1)$$

where:

$AC =$ Annualized operation costs [\$]

$\alpha =$ Cost of electricity (nominally @\$0.10 kWh)

$E =$ Electrical parasitics [kWh]

$\beta =$ Cost of thermal energy (nominally @\$10/10^6 BTU)

$T =$ Thermal parasitics [10^6 BTU]

$\gamma =$ Amortization rate of capital (nominally @15%)

$C =$ Capital costs [\$]

The optimization procedure used to find the minimum annual operation cost involves a random search of the variable space to find the best initial guess. Using this initial guess, a directed line search of the parameter space was used to find the minimum. At the minimum, the marginal cost of capital is equal to the marginal cost of the parasitics. Because of a difference in sun angles and shading, it was necessary to optimize fields with the E-W tracking apertures and N-S tracking apertures, independently.

East-West Field Results

East-west fields with ΔT strings of either 320 feet or 480 feet provided the lowest annualized operation cost. In Table I, the field designs for both ΔT string lengths are given. The minimum operation cost for both the 320- and 480-foot ΔT string designs was approximately \$21,500. The thermal parasitics were slightly less for the 480-foot ΔT string because of a small reduction in manifold piping. The electrical parasitics were substantially less for the 320-foot ΔT string because of the lower fluid velocity in the receiver tube. The increase in electrical parasitics is mainly offset by a decrease in capital costs for the 480-foot ΔT string. The total parasitics are between 9 and 10% of the energy collected in the receiver.

The optimum string spacing was 16.5 feet for both string lengths. The 16.5 foot spacing is equivalent to the aperture area being 0.4 of the total land requirements, which can also be defined as a packing factor of 0.4. The necessary number of collector strings for a 50,000 square foot field with 320- and 480-foot ΔT strings were 24 and 16, respectively. The manifold piping telescopes down through three sizes of pipes. For the 320-foot ΔT string design, there were 12 sections of large pipe or 198 feet of large pipe (i.e., row spacing times the number of sections) on each side of the field plus the 320 feet of return pipe, five sections of medium, and seven sections of small pipe. The number of sections of pipe for the 480-foot ΔT string design were 7, 7, and 2 for the large, medium, and small pipes, respectively. A large pipe size of 3.5 inches and insulation thickness of 4.7 inches to 4.9 inches are specified. A medium pipe size of 2.6 inches and insulation thickness of 4.0 inches are specified for both string lengths. The small pipe size is 2.0 inches with 4.0 inches of insulation for the 320-foot ΔT string, and 1.5 inches with 3.0 inches of insulation for the 480-foot ΔT string. The smaller pipe sizes for the 480-foot ΔT string design are a result of decreased fluid flow through the small pipes.

Figures 1 to 4 indicate the relative trade-offs between E-W collector field designs with different string lengths. In Figure 1, the minimum annualized parasitic cost is shown to increase for both short and long ΔT string lengths. In Figure 2, the accumulated thermal parasitics do not change radically as a function of the ΔT string length. The slight change initially is due to a reduction in the total footage of manifold piping. The overnight cooldown heat losses are approximately twice the steady-state heat losses. The shading loss is constant because the optimum packing did not change with string length. The accumulative electrical parasitics in Figure 3 increase rapidly as a function of ΔT string length. Electrical parasitics are the limiting factor for long ΔT strings. Capital costs initially decrease dramatically with longer ΔT strings in Figure 4. The reduction is mainly due to less pipe and fewer control valves. When the pipe sizes and insulation thicknesses are rounded off to available sizes, the piping layout design is very similar to the Jacobs design [1].

North-South Field Results

The suggested N-S field design is given in Table II. The minimum annualized operation cost is approximately $31,500. This cost is larger than the E-W field cost, but potentially more energy is available to the N-S field. The minimum cost ΔT string length is 480 feet. Due to increased shading, the optimum string spacing is 34.1 feet which is a 0.2 packing factor. The pipe sizes, insulation thicknesses, and numbers of sections are similar to the E-W 480-foot ΔT string values discussed previously. The total parasitics are almost 13% of the collected energy.

Figures 5 to 8 indicate the relative trade-offs between N-S collector field designs with different string lengths. The minimum annualized parasitic cost has a unique minimum at 480 feet in Figure 5. The shading heat loss in Figure 6 increases as the string length is reduced from 480 feet. This is because more rows are required with the shorter string lengths and the increases in manifold piping costs are so large, the row spacing must be reduced which in turn increases shading. The electrical parasitics in Figure 7 are very similar to those in Figure 4. Capital costs in Figure 8 are not noticeably reduced between 320-foot and 480-foot ΔT string lengths in Figure 8 due to the increase in the optimum row spacing.

Sensitivity Analysis

The most significant difference between the E-W and N-S field designs is the spacing between collector rows. For the E-W collector fields, the packing factor is 0.4, while the N-S field requires a packing factor of nearly 0.2. The change in packing factors is due entirely to the different sun angles and the associated shading resultant from the two orientations. In Figure 9, annualized cost is plotted as a function of string spacing for E-W collector fields of various ΔT string lengths. All of the other variables are those of the minimum cost layout. For the string lengths analyzed, all of the minimum annualized parasitic costs for E-W collectors occur at a string spacing of 16.5 feet. As the string spacing is reduced, the shading penalty increases the cost. Increasing the string spacing increases the total cost through higher heat losses and capital expenses. The total annualized parasitic cost for N-S collectors is shown in Figure 10. The minimum-cost N-S fields do not have the same string spacing for the different ΔT string lengths. When the string spacing is 16.5 feet, the total costs for the 320-foot and 480-foot ΔT string length N-S fields are nearly identical for the N-S and E-W fields.

Several sensitivity studies have been performed on the minimum cost field designs. The value of electricity, thermal energy, and capital were varied up to $\pm 50\%$. Simulations were run using the new energy and capital prices with the original minimum cost field design. Optimizations were run with the new prices, and the new minimum cost was compared with the simulation cost. For each price individually and in pairs, the annualized cost of the simulation was well within 5% of the new minimum cost for the E-W 320-foot ΔT string design. The individual thermal and electrical parasitics were also varied with similar results. These results were obtained because of the broad minimums associated with most of the cost factors. Because of these results, all of the pipe and insulation sizes can be replaced with the closest available size without noticeably changing the operation cost.

Conclusion

The principal objectives of this study have been successfully accomplished. The design techniques employed by the Jacobs Engineering Group have been verified and as a result can be used with confidence. The computer program used to assess these techniques is versatile enough to handle different locations, collectors, insulation materials, etc. Also, sensitivities of the field designs can be easily handled.

The sensitivity studies already completed have revealed the potential for modular design of parabolic trough collector fields. To obtain modularity, the field design must not depend on collector orientation. When the row spacing for N-S fields is reduced to 16.5 feet, the unshaded 14.1% advantage in yearly performance they have over E-W fields is reduced to 5.8%. Land restrictions would most likely restrict increasing the row spacing for E-W fields to 34.1 feet. Because of the nearly equal yearly performance, any collector orientation can be used. The penalty associated with a modular field, when compared to individually designed fields, is small. Modular fields can also potentially decrease the cost of installed parabolic trough collector fields, but local codes and land constraints may prohibit developing a prefabricated module.

Future work includes sensitivity studies which show the change in annual operation cost due to different locations and collector efficiencies. The calculated thermal losses are being compared with actual test results and the analytical models will be changed if needed.

References

1. Robert Morton, Interim Report, "Solar Collector Field Optimization Study," Jacobs Engineering Group, Inc., Pasadena, CA, September, 1979.
2. K. D. Bergeron, et al, "Line Focus Solar Thermal Energy Technology Development, FY79 Annual Report," Dept. 4720, April, 1980, SAND800865, Revised.

TABLE I

Minimum Annualized Parasitic Cost East-West Collector Field Design
(British units used for clarity)

ΔT String Length (ft)	320	480
Minimum Cost ($)	21,634	21,462
Thermal Parasitics (10^6 BTU)	1162.6	1101.5
Electrical Parasitics (kWh)	24,455	39,909
Capital Cost ($)	50,416	43,043
Thermal Parasitics (%)	8.2	7.8
Electrical Parasitics (%)	1.4	2.2
Total Parasitics (%)	9.6	10.0
String Spacing (ft)	16.5	16.5
Strings	24	16
Large Pipes	12	7
Large Pipe Size (in.)	3.5	3.5
Large Pipe Insulation (in.)	4.9	4.7
Medium Pipes	5	7
Medium Pipe Size (in.)	2.6	2.6
Medium Pipe Insulation (in.)	4.0	4.0
Small Pipes	7	2
Small Pipe Size (in.)	2.0	1.5
Small Pipe Insulation (in.)	4.0	3.0

TABLE II

Minimum Annualized Parasitic Cost North-South Collector Field Design
(British units used for clarity)

ΔT String Length (ft)	480
Minimum Cost ($)	31,658
Thermal Parasitics (10^6 BTU)	1,771
Electrical Parasitics (kWh)	50,162
Capital Cost ($)	59,578
Thermal Parasitics (%)	10.5
Electrical Parasitics (%)	2.4
Total Parasitics (%)	12.9
String Spacing (ft)	34.1
Number of Strings	16
Large Pipes	7
Large Pipe Size (in.)	3.6
Large Pipe Insulation (in.)	4.9
Medium Pipes	7
Medium Pipe Size (in.)	2.6
Medium Pipe Insulation (in.)	4.0
Small Pipes	2
Small Pipe Size (in.)	1.6
Small Pipe Insulation (in.)	3.0

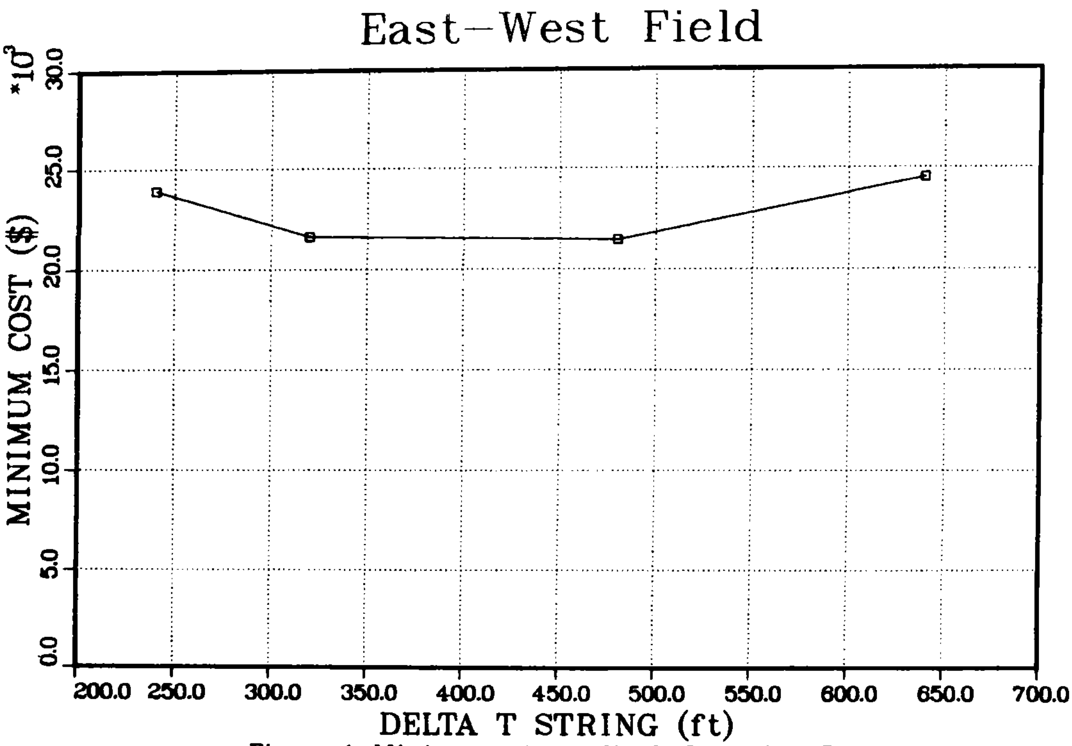

Figure 1. Minimum Annualized Operation Cost

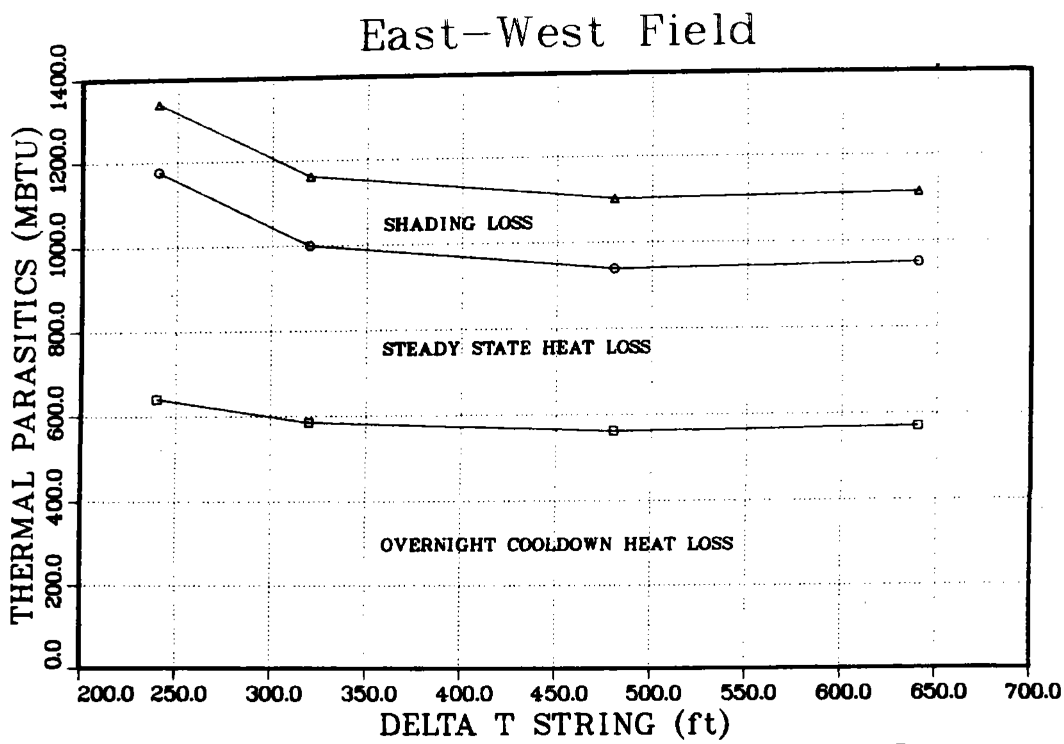

Figure 2. Accumulated Thermal Parasitics at Minimum Costs

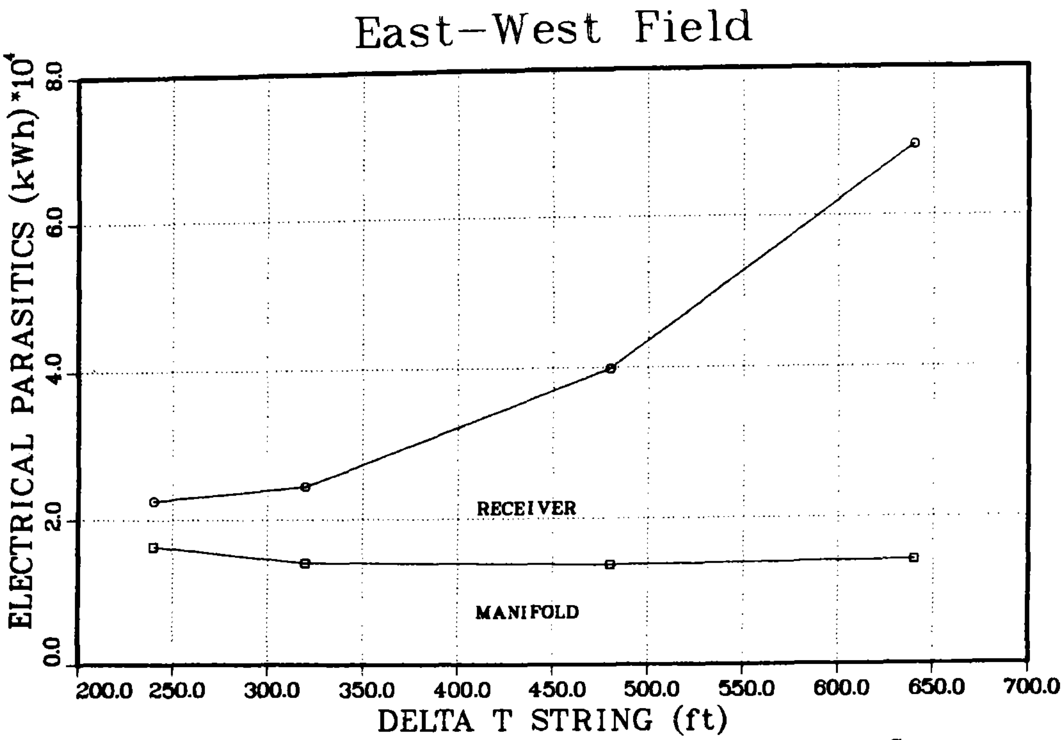

Figure 3. Accumulated Electrical Parasitics at Minimum Costs

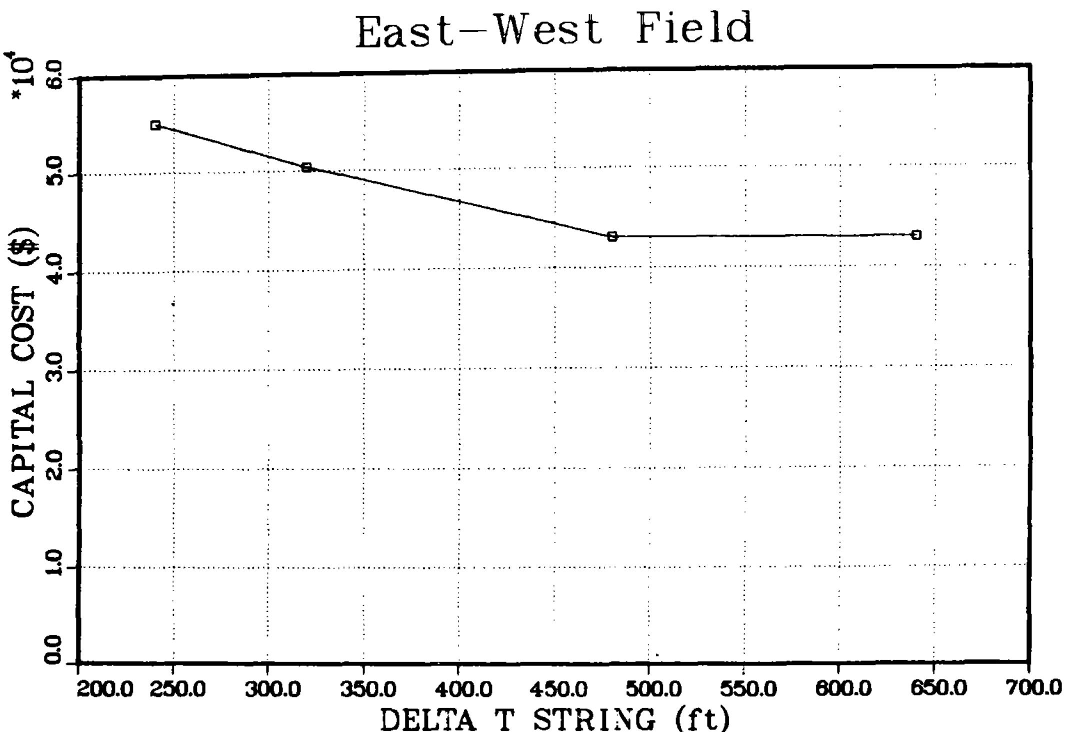

Figure 4. Manifold Piping Expenses at Minimum Costs

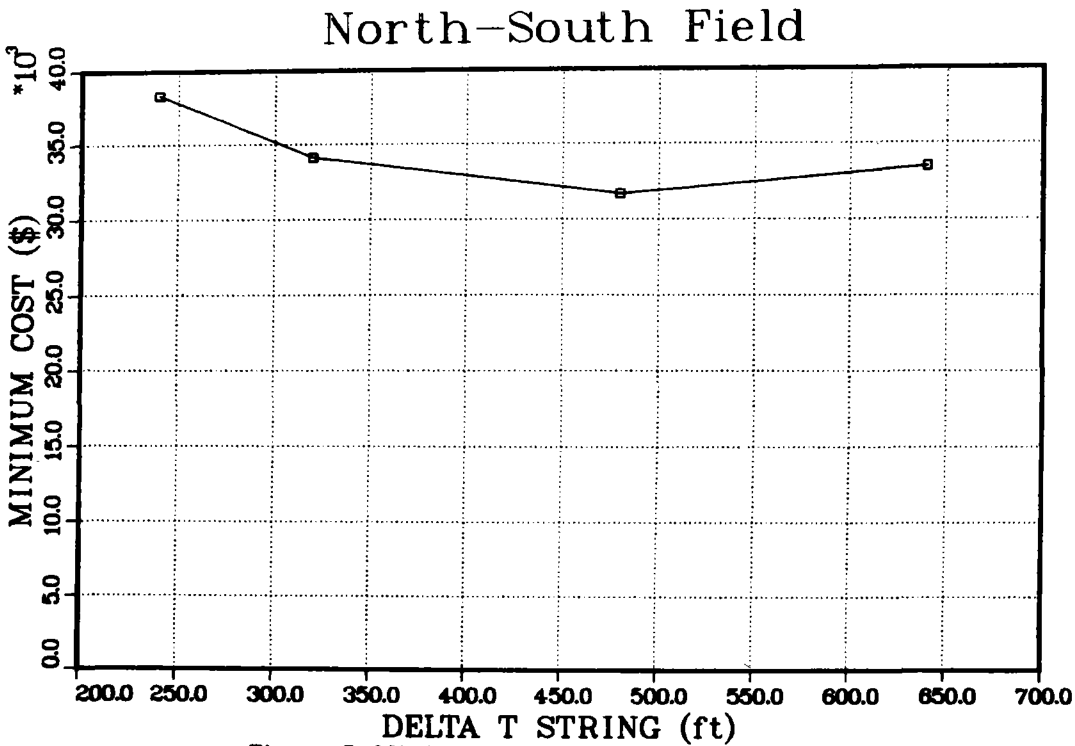

Figure 5. Minimum Annualized Operation Cost

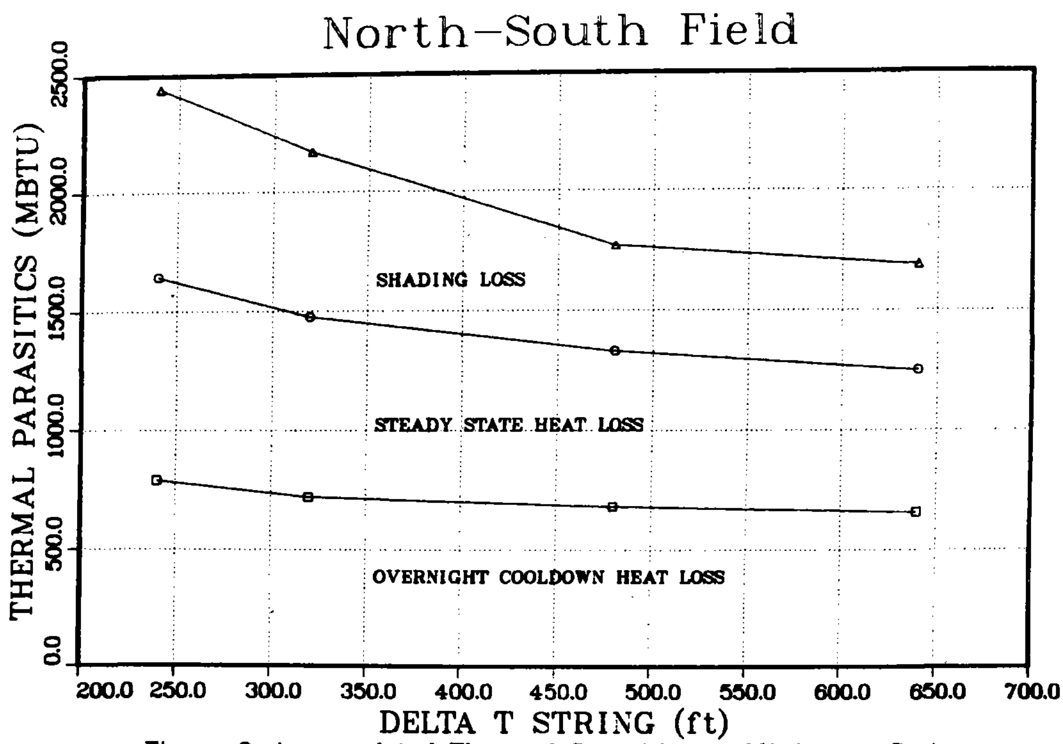

Figure 6. Accumulated Thermal Parasitics at Minimum Costs

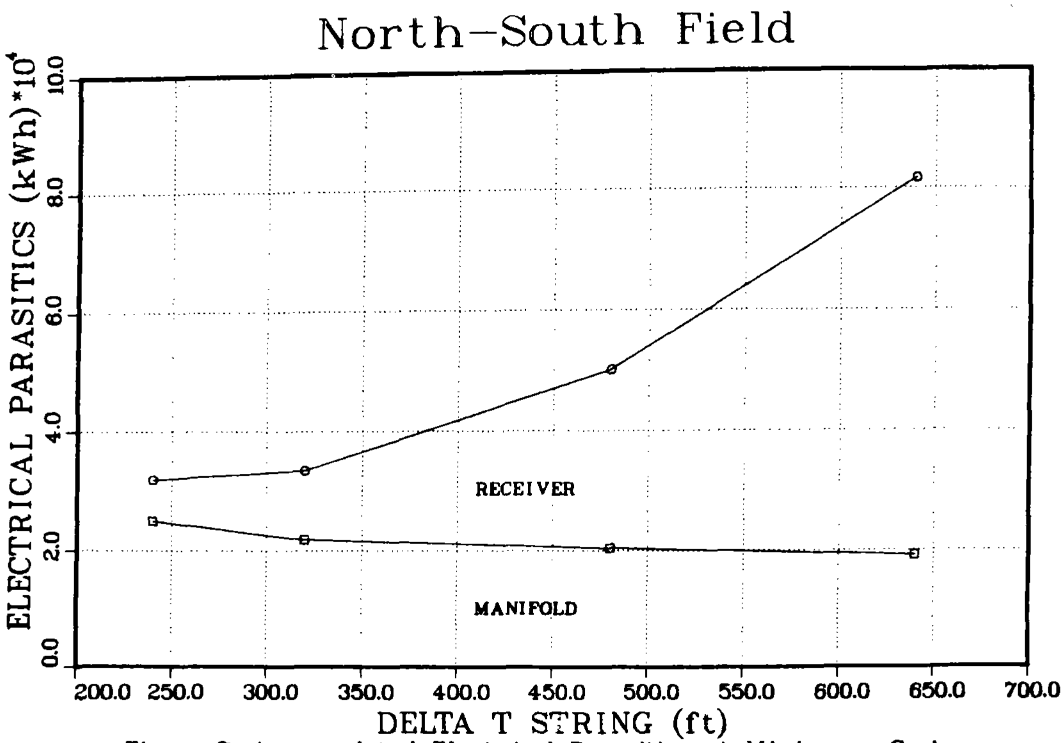

Figure 7. Accumulated Electrical Parasitics at Minimum Costs

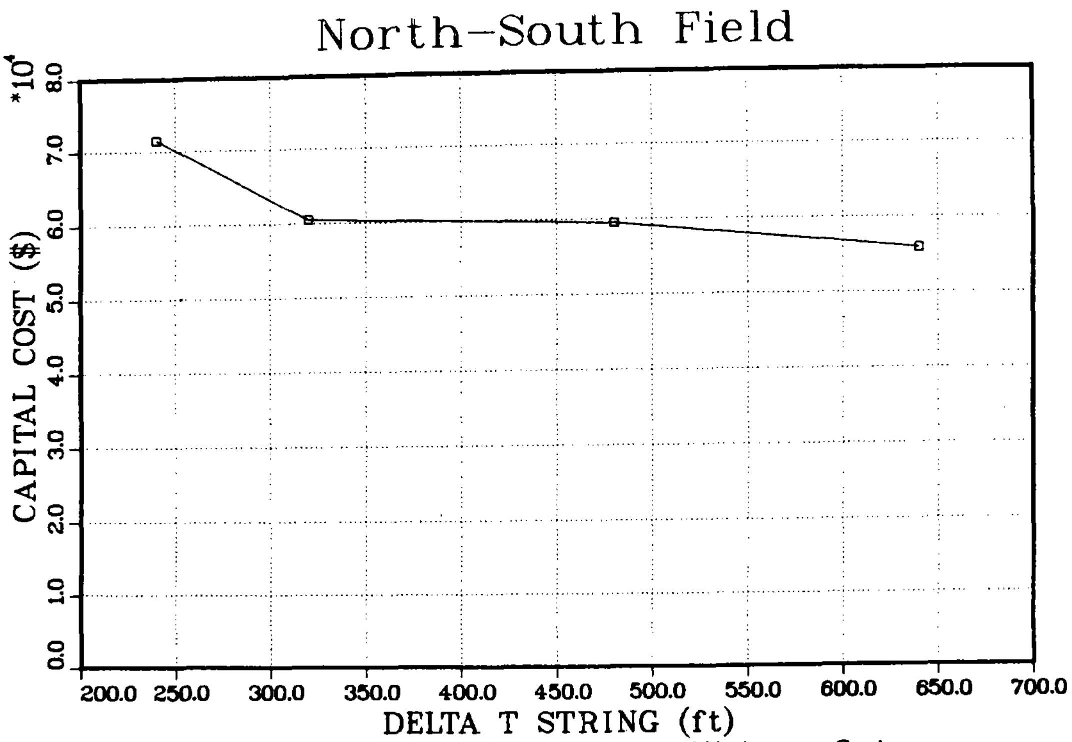

Figure 8. Manifold Piping Expenses at Minimum Costs

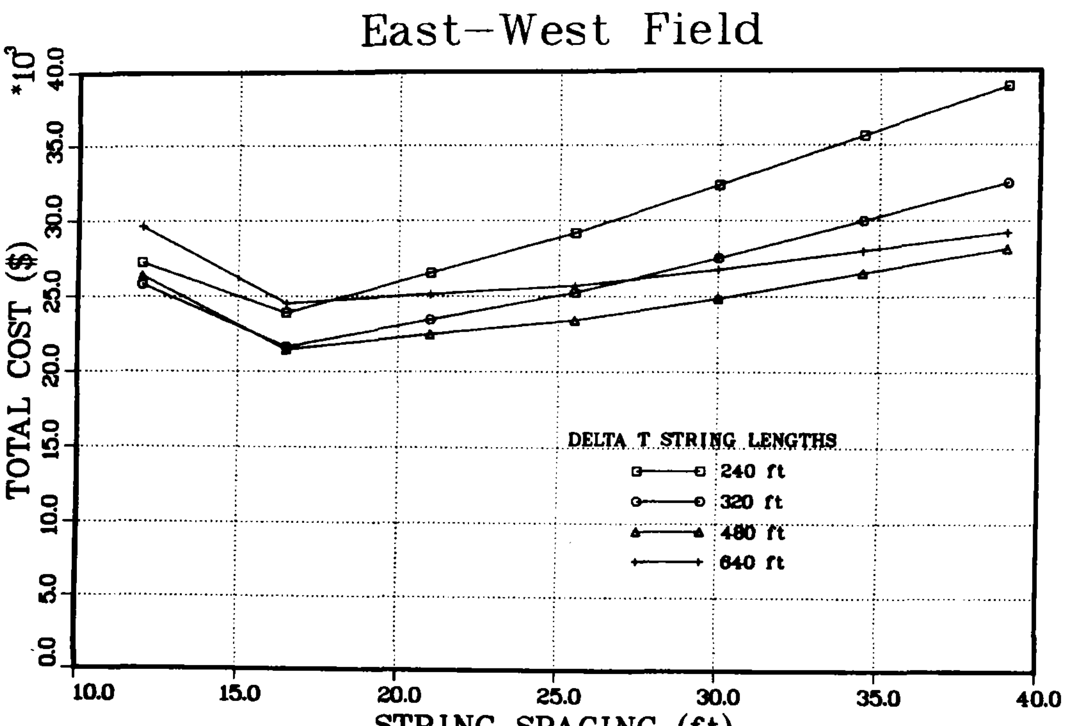

Figure 9. Annualized Operation Cost

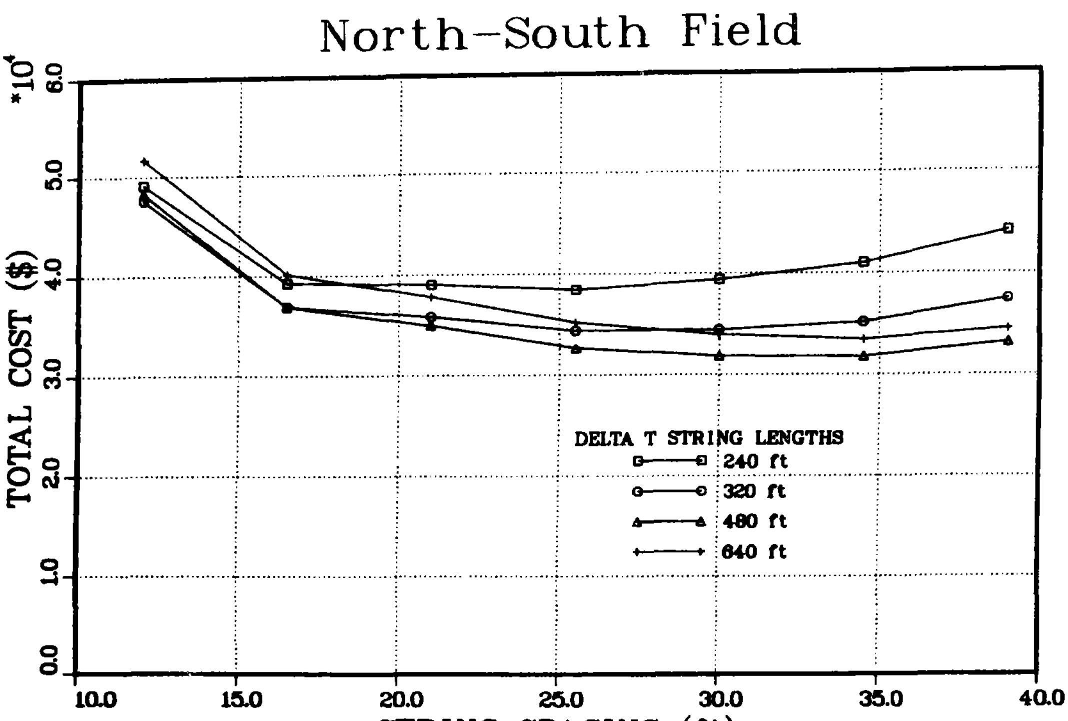

Figure 10. Annualized Operation Cost

SUBSYSTEM COLLECTOR PIPING HEAT LOSSES

Raymond W. Harrigan
Component and Subsystem Development Division 4722
Sandia National Laboratories
Albuquerque, New Mexico 87185

Introduction

Heat loss in piping manifolds is a principal parasitic decreasing overall thermal efficiency of parabolic trough collector fields. Computations of solar collector field performance typically underestimate the magnitude of field thermal losses because the computations usually ignore the effects of piping components such as valves and pipe anchors. These components can have large impacts since they typically represent highly conducting, uninsulated fins for thermal heat loss. In a well insulated piping arrangement, such components may, in fact, represent a dominant path for thermal energy loss in a collector field. In addition to strongly influencing thermal loss rates in operating solar collector fields, such piping components can accelerate thermal losses overnight as the collector field and associated piping cool down. A primary mechanism in accelerated thermal loss rates during overnight cooldown is convective transport of hot fluid, called thermosiphoning, to such components. Thermosiphoning from cold receiver tubes to hot insulated piping manifolds also contributes to increased heat loss from the collector field piping.

The effect of collector field components such as valves, pipe anchors and receiver tubes on daily integrated field heat loss is being quantitatively evaluated in the Midtemperature Solar Test Facility (MSTF) located in Albuquerque, New Mexico at Sandia National Laboratories (SNLA). The objective of these tests is to generate the data needed to allow proper trade-off evaluations of collector field heat loss and such effects as intercollector shadowing. Additionally, knowledge of heat loss from collector field components is imperative for field designers to be able to layout collector fields with the proper balance between the desire for enhanced fluid control and minimum valving to reduce thermal losses. The data from these heat loss tests will be factored into current efforts by Jacobs

Engineering[1] to define optimum field layouts for parabolic trough collector fields.

Current Status - Line Calibration Test

The calibration phase of the piping manifold heat loss tests has been completed. This phase involved the measurement of heat loss from an insulated section of pipe both during fluid flow through the pipe and overnight cooldown when there was no fluid flow through the pipe. The tests were formulated to duplicate, as closely as possible, the conditions modeled by the computer codes[2] used to compute heat loss due to overnight cooldown from collector field manifold piping. Excellent agreement was found between measured heat loss and computed heat loss. A complete description of the installation, instrumentation and, data acquisition system is available in an SNLA Test Report.[3] A photograph of the test manifold is shown in Figure 1.

Pipe Heat Loss Test Procedures

Heat loss tests were performed to measure the thermal losses from a 160 foot section of 2 inch Sch. 40 pipe designated as the Test Section in this report. The Test Section was insulated with 2 inches of fiberglass insulation with an outside layer of polyurethane insulation one inch thick. Heat loss during fluid flow conditions was measured at various flow rates. In all cases, turbulent flow conditions were maintained in order to minimize effects due to fluid film coefficients and provide tests which evaluated insulation effects only. An objective of the flow heat loss tests was to compare measured thermal conductance of the insulation with manufacturer's data. At high flow rates (e.g. 20 gpm) where turbulent flow conditions were clearly established, the temperature drop across the 160 foot length of pipe was small, magnifying the impact of any small instrumentation errors. At low flow rates, where the temperature drop along the pipe was large, nonturbulent flow conditions could occur, introducing errors due to the establishment of a fluid boundary layer with high thermal resistance. Measuring the fluid heat loss at several flow rates provided a mechanism for identifying these effects if they were occurring.

All temperatures during the flow heat loss measurements were monitored by thermocouples over a period of several hours during start up of the Test Section to insure achievement of thermal equilibrium. The Test Section was considered to be at equilibrium when the temperature drop across the line did not change by more than 5 percent over 30 minutes and the temperature profile through the insulation did not change. After a heat loss measurement was made, the direction of the fluid flow was reversed and the Test Section inlet and outlet temperatures and resultant heat loss were remeasured upon achievement of equilibrium. This provided verification of instrumentation accuracy.

Overnight cooldown tests were performed after flow heat loss tests at 600°F were run. The fluid flow to the Test Section was stopped and one end of the test section was valved shut. One end of the Test Section was left open to the fluid supply header to permit fluid to enter the Test Section as the fluid contracted upon cooling.

Results of Pipe Heat Loss Tests

The general procedure used in evaluating the results of the pipe heat loss tests was to compute an overall thermal conductance value (k-value) for the composite insulation on the Test Section using the temperature drop across the 160 foot line. This was done using fluid physical properties together with measured flow rates in the equation.

$$\text{Heat loss} = \dot{m}\ Cp\ \Delta T$$

where ΔT = measured temperature drop across 160 foot line
Cp = fluid heat capacity
$\dot{m}$ = fluid mass flow rate

The k-value thus obtained was

$$k = 0.019 \text{ BTU/FT HR}^{o}\text{F} \quad (\text{Fluid Temp.} = 600^{o}\text{F})$$

This value was found to be consistent with the composite k-value computed using manufacturer's published values for the fiberglass and urethane insulation.

This experimentally determined k-value for the composite insulation was then used to compute the expected fluid temperatures as the Test Section was allowed to cooldown. This calculated cooldown curve[2] is compared with the measured cooldown curve in Figure 2. As observed the results are in excellent agreement. The small discontinuities in the measured cooldown curve are due to subtracting the ambient temperature from fluid temperature without accounting for thermal lag. As the ambient temperature changes, the effect on the fluid cooldown curve will not be felt instantaneously as is shown in Figure 2. Figure 3 is the measured fluid cooldown curve without subtraction of the ambient temperature and is seen to be very smooth. The cooldown curve shown in Figure 3 is actually the temperature data from two immersion and two top and bottom pipe surface thermocouples located at the U-bend of the Test Section. The width of the cooldown curve in Figure 3 is due to slight thermal stratification in the line during cooldown. The magnitude of the stratification is shown in Figure 4 where the temperatures recorded by the bottom surface thermocouple and two immersion thermocouples is shown with respect to the top surface thermocouple. As indicated, thermal stratification varies from a maximum of about $8^{o}F$ to about $4^{o}F$ during the 20 hour cooldown period. Only the top surface thermocouple data were plotted in Figure 2 for clarity in comparing the experimental and calculated data. Thermocouples along the entire length of the Test Section were monitored to confirm that the entire section cooled uniformly during the test.

Tests In Progress -- Thermosiphoning

During August 1980, a series of tests to establish the effect of thermosiphoning from a simulated receiver tube on the rate of cooldown of the pipe heat loss loop will be conducted. The results of this test series will be reported at the conference. Preliminary tests on laboratory scale models has shown the presence of thermosiphoning in a two inch pipe. The test apparatus is shown in Figure 5 and consists of a two inch clear plastic tube connecting the right hot (160°F) and the left cold (34°F) tanks. The tube entrance into either tank was sealed with a copper plate and the presence of a thermal convection loop was visualized using dye injection techniques (see Figure 6). A u-trap in the 2 inch line (see Figure 7) was formed to effectively interrupt thermosiphoning in the laboratory apparatus. These observations prompted thermosiphon testing in the pipe heat loss loop.

Future Testing

Upon completion of the simulated receiver thermosiphon tests discussed above, the effect of valves, pipe anchors and other piping components on pipe heat loss will be evaluated. Pipe anchors, which are typically constructed of angle iron welded directly to the pipe, are of particular concern since they provide a direct thermal short to the environment. Anchor designs which are not directly welded to the pipe will be installed in the Test Section and evaluated together with various techniques for valve and anchor insulation. Changes in insulation characteristics due to aging at elevated temperatures and sagging of the insulation away from the pipe will also be studied.

Test Personnel

In order to facilitate transfer of information the following key people are listed in the event that questions should arise in the future concerning specific areas not completely described in this report.

Data Acquisition - B. J. Petersen
Thermocouple Installation - R. D. Meyer
Project Engineer - R. W. Harrigan

References

1. R. E. Morton, Progress Report of Solar Collector Array Piping Design Optimization Studies, Jacobs Engineering Group, Inc. (April 1980).

2. B. M. Bulmer, User's Instructions For Program Conduct, RS5511/1000 (Internal Sandia National Laboratories Memorandum) 1978.

3. R. W. Harrigan, Heat Loss In Collector Piping Manifolds: Test Status Report No. 1, Sandia National Laboratories, Albuquerque, New Mexico September 1980.

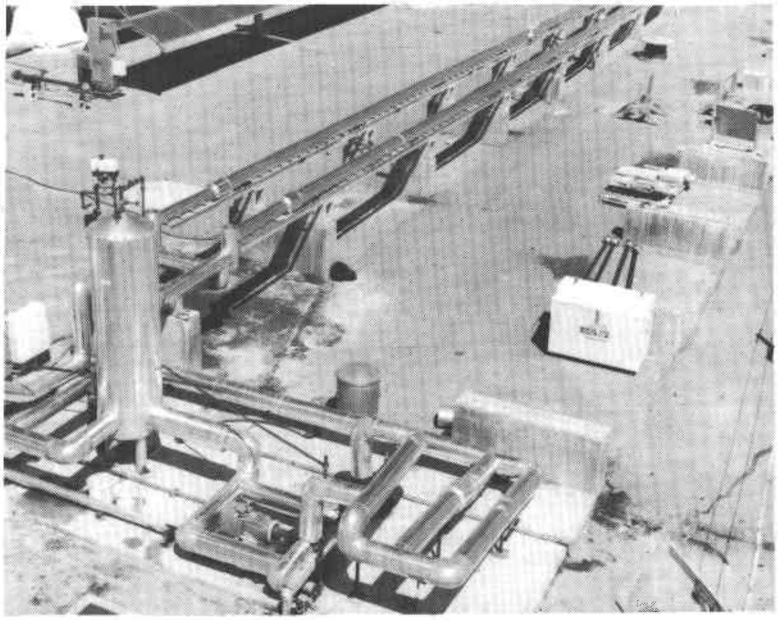

Figure 1. Pipe Heat Loss Loop

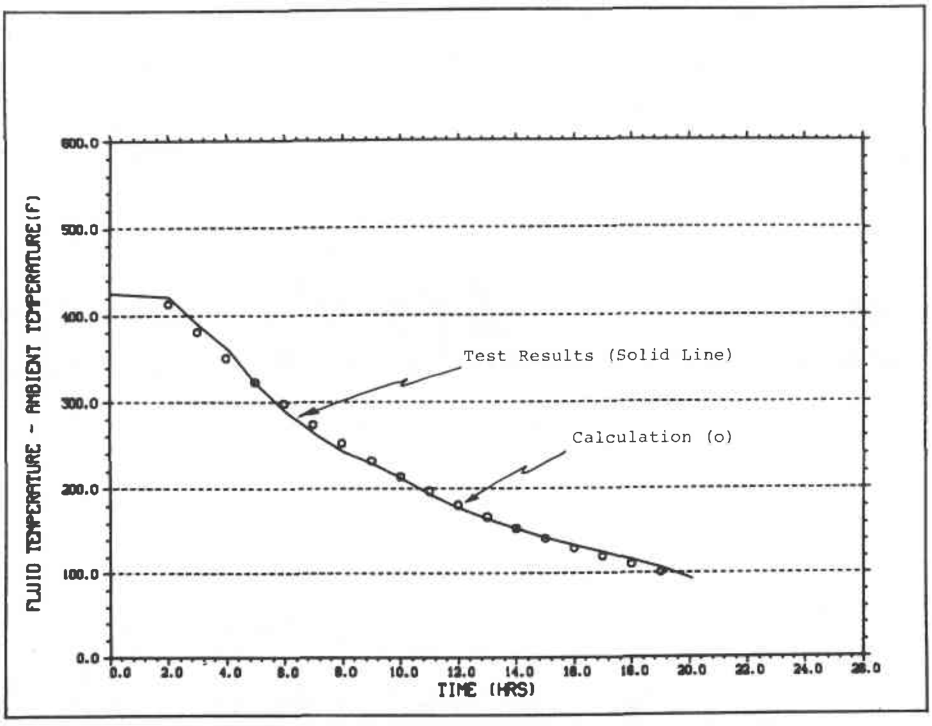

Figure 2 Cooldown of Pipe Heat Loss Loop
(Calculations vs. Test)

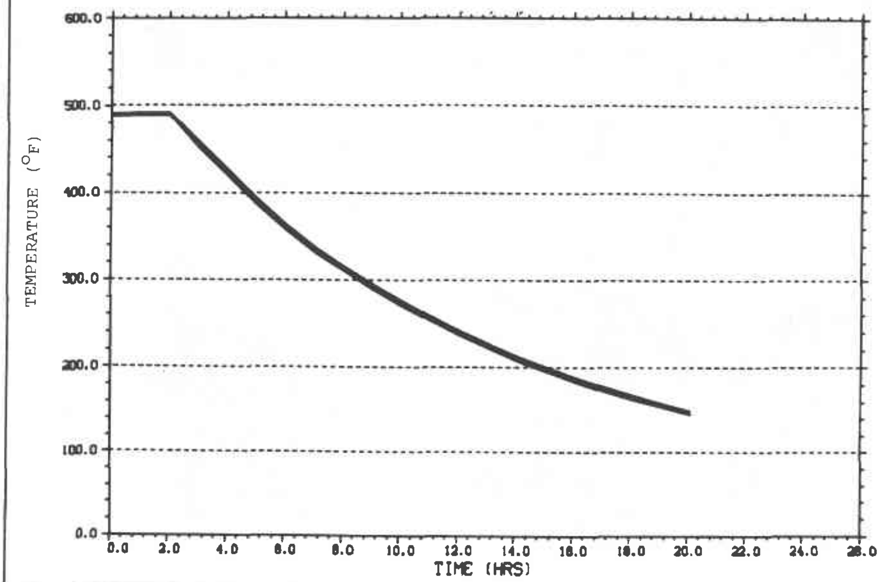

Figure 3 Cooldown of Pipe Heat Loss Loop (Ambient Temperature Not Subtracted)

Figure 4 Thermal Stratification In Heat Loss Loop During Cooldown

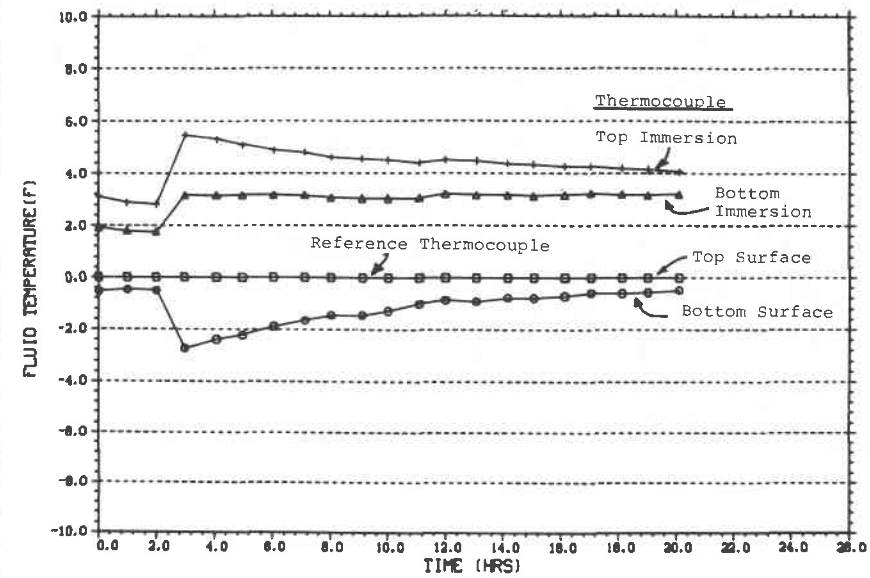

Figure 4 Thermal Stratification In Heat Loss Loop During Cooldown

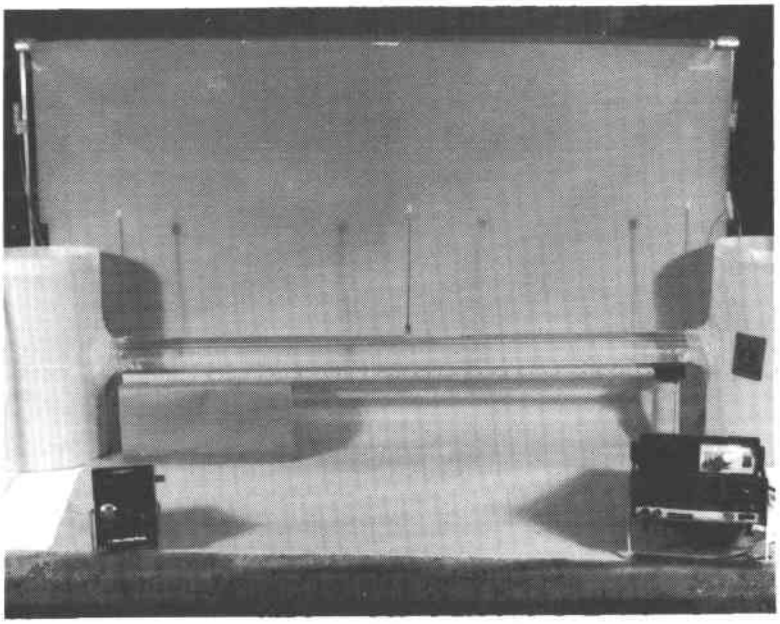

Figure 5 Laboratory Scale Thermosiphon Test Apparatus

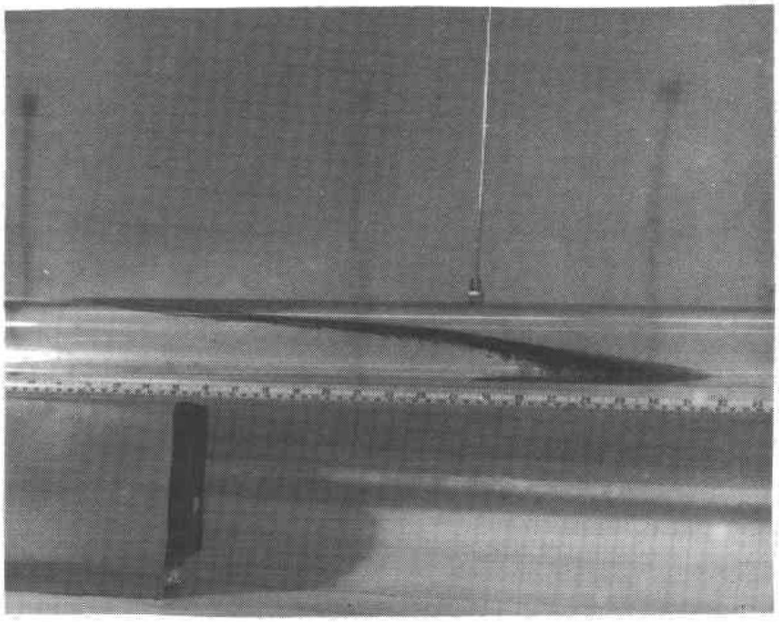

Figure 6 Dye Visualization of Thermosiphoning

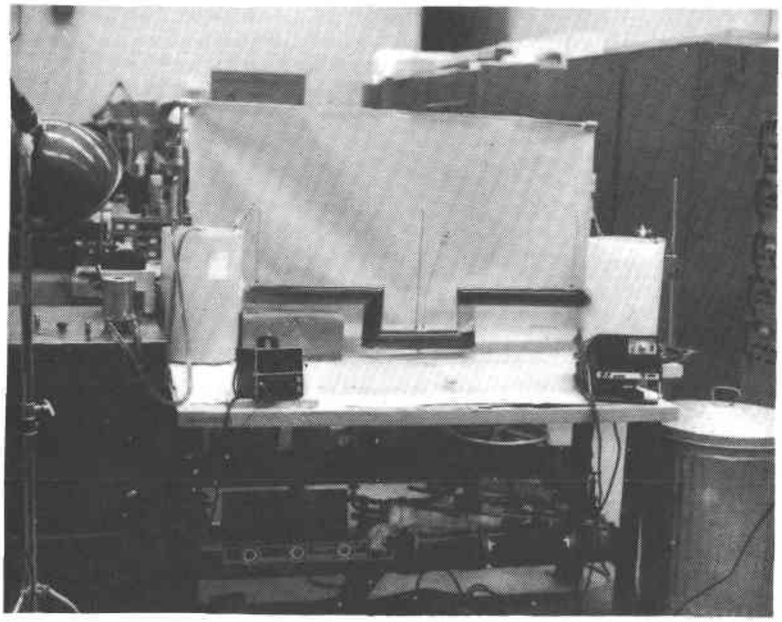

Figure 7 Effect of Trap on Thermosiphoning

FLUID CONTROL FOR PARABOLIC TROUGH COLLECTORS: SIMULATION STUDIES AND TEST RESULTS

Rudolph Schindwolf
Component and Subsystem Development Division 4722
Sandia National Laboratories
Albuquerque, NM 87185

Introduction

A significant problem that must be addressed in the design of a parabolic trough solar collector field is the control of the temperature of the heat transfer fluid. Fluid temperature control is required to prevent overheating and to maintain relatively constant output temperature for varying solar input conditions.

The complexity of the control system is highly dependent on the requirements of the process using the thermal energy. Of particular importance is the accuracy of temperature control required, and the temperature of the process relative to the maximum temperature capability of the collectors. Extremely simple fluid control systems can be used for industrial process heat systems operating at temperatures well below the collector capability. Figure 1 shows a solar system which supplements a fossil fuel system in the production of 100 psi steam (338^{o}F). The only control element required in this case is a check valve which prevents reverse flow of thermal energy back into the solar system when it is not capable of producing 100 psi steam. Variations in solar insolation and cloud cover transients are automatically accommodated by changes in the operating temperature of the field.

The other extreme of fluid control system complexity is required in systems used to generate electric power. In order to maximize heat engine performance, it is necessary to operate at as high a temperature as possible and with small variability. In this case the collectors will be operating near the maximum allowable temperature, and large variations in collector output temperature due to changes in solar insolation or other transients cannot be tolerated. Figure 2 shows a control system that will provide the required temperature control of the collector field as well as control of the field output. The output temperature of each row of collectors is controlled by modulating the fluid flow with a motor driven control valve operating off the output temperature of the row. The three-way valve at the output of the field prevents pumping cold fluid into the thermal storage tank or heat engine during startup.

This paper is primarily concerned with the latter rather stringent control problem associated with electric power generation. The temperature control system performance objectives were chosen to be $\pm 5^{\circ}F$ under steady state conditions and $\pm 50^{\circ}F$ during transients. Results of a computer simulation study of the fluid control system as well as test results obtained at the Midtemperature Solar System Test Facility (MSSTF) will be presented.

System Simulation

A digital computer simulation of the collector field and the fluid control system shown in Figure 2 was developed in order to study the dynamic behavior of fluid temperatures in the system. The pertinent parameters that describe the collector field considered for this study are given in Table I. A collector having a peak efficiency of about 60% is utilized in this study.

Table I

Total collector area	-	50,000 ft^2
Length of rows	-	320 ft
Number of rows	-	24
Output Temperature	-	$600^{\circ}F$
Temperature rise	-	$160^{\circ}F$

A major part of the simulation program is devoted to the temperature dynamics of the collectors and interconnecting piping. The partial differential equations that were solved to obtain the fluid temperatures in the system are given in Ref (1).

A proportional control algorithm operating off the output temperature of each collector row was used to operate the motor driven valves. The proportional gain was chosen to achieve the required static accuracy of $\pm 5^oF$. The significant control system parameters considered are given in Table II.

Table II

Proportional gain	-	.1 $ft^3/min/^oF$
Temp. sensor time constant	-	3 seconds
Valve slew time	-	15 seconds
Controller sampling time	-	1 second
Temp. sensor location	-	end of collector

Simulation Results

Two rather stringent transient conditions were considered in evaluating system performance. The first condition consists of starting the system by putting the collectors in focus with maximum solar insolation (300 BTU/hr-ft^2) and with all the fluid in the system at the normal field input temperature (440^oF). The second condition consists of the system operating normally at an insolation of 300 BTU/hr-ft^2 followed by a step change to 150 for 10 minutes followed by a step return to 300. The fluid output temperature response for these two conditions is shown in Figures 3 and 4. The startup transient shows an initial overshoot to 660^oF which slightly exceeds the allowable transient tolerance of $\pm 50^oF$. After the overshoot, the response is well damped and achieves the required temperature within four minutes. The response to the solar insolation transient is well damped with overshoots of about 2^oF, and with the steady state temperature for the two insolation levels within the $\pm 5^oF$ steady state accuracy requirement.

Simulations were performed for a wide range of values of the control system parameters in Table II in order to determine the system sensitivity to changes in these parameters. The most noticeable effect was that due to moving the temperature sensor location downstream from the end of the collector. Locating the sensor downstream is equivalent to introducing a transport delay into the system, which usually has a de-stabilizing effect. For a 20 ft sensor location, an overshoot to 715°F occurs which far exceeds the maximum fluid bulk temperature of 650°F. In addition, the damping after the overshoot is very poor and the system is on the verge of having a continuous limit cycle. Based on this data, it is obvious that the temperature sensor should be as close to the end of the receiver tube as possible. If it is not possible to place the sensor directly at the end of the receiver tube, it should be installed right after the flex tubing which will be about 5 ft from the end of the receiver tube.

The effect of partial cloud cover was also simulated, and it was found that a cloud cover of the type shown in Figure 5 was particularly troublesome. The response of the row output temperature to the last quarter of a row being cloud covered is shown in Figure 6. Under these conditions, the system is quite unstable with peak temperatures on the order of 750°F. This instability could have been expected since a section of a collector that is shaded behaves dynamically like a section of pipe, and previous results have shown that a significant length of pipe between the temperature sensor and illuminated collector will result in instability.

To overcome this partial shading problem requires anticipation of the high temperature condition before it arrives at the end of the collector. One technique which performs quite satisfactorily consists of using the simple proportional control algorithm, but with the additional capability of commanding maximum flow whenever the midrow temperature exceeds some preset value. The preset value was chosen to be 20°F above the normal operating temperature (520°F). The partial shading response for this algorithm is shown in Figure 7, which indicates that the overtemperature condition has been eliminated. The use of the midrow override is also effective in reducing the overshoot during startup, resulting in an overshoot of 630°F rather than the 660°F obtained previously.

Test Results

The recommended fluid control system was tested in a 240 ft collector string at Sandia's Midtemperature Solar System Test Facility (MSSTF). The first two collectors in the string were the old Sandia troughs which demonstrated a noontime efficiency of about 22% during the tests. The last two collectors were the new Custom Engineering troughs with mirrored reflectors, and these collectors demonstrated a noontime efficiency of about 52%. Both types of collectors have an aperture of 9 ft resulting in a total collector area of 2160 ft^2.

Figure 8 shows the output temperature response for slow variations in solar input. This data was taken on a day with high cirrus clouds, and has considerable direct normal insolation variation. It can be seen that the output temperature stayed within the required $\pm 5^{o}F$ from the set point as long as the insolation (component normal to the aperture) was greater than 600 W/m^2.

This 600 W/m^2 limitation would normally be a severe penalty since a considerable amount of energy remains to be collected between 600 and about 300 W/m^2. This limitation was, however, primarily due to the test setup, and should not be a problem when the proposed fluid control system is used in a more conventional configuration. The test configuration had a high minimum flow which resulted in a high minimum insolation. In addition, the low efficiency of the collectors required a lower flow than normal at minimum insolation.

Figure 9 shows the output temperature response when all the collectors are taken out of focus near solar noon for about 10 minutes and then put back in focus again. This transient simulates the conditions of a noontime startup or the effect of a cumulus cloud passing over the collectors on a bright sunny day. Both of these conditions are considered severe transients, and it can be seen that the output temperature response was well damped with practically no overshoot. This result is considerably better than expected, since the computer simulations showed that overshoots of about 50^{o} should be obtained. This difference in response can be explained by the low efficiency of the first two collectors in the string. Subsequent computer simulations have confirmed that a negligible overshoot will be obtained under these conditions.

Figure 10 shows the output temperature response while the fourth collector is out of focus. This test simulated the effect of a cloud shading the last collector. The test results indicate that the midrow override control is effective in keeping the temperature transient within the allowable $50^{o}F$. The system is obviously limit cycling under these conditions, but this is not objectionable since the cloud cover condition will not persist for any length of time.

Conclusions

The results of the simulation study show that a simple proportional control algorithm operating a motor driven flow-control valve on each collector row will achieve the required temperature control for the majority of transient conditions. Certain partial cloud cover situations can result in overtemperatures, but the addition of a simple override control operating off a midrow temperature measurement will correct the problem.

The results obtained from the MSSTF tests appeared to confirm the simulation study conclusions. Several discrepancies from expected performance were noted, but these have been attributed to test configuration peculiarities.

References

1. R. Schindwolf, Fluid Temperature Control for Parabolic Trough Collectors, SAND79-2006, Sandia National Laboratories, Albuquerque, NM 1979.

2. R. Schindwolf, "Fluid Control System Test Results", Sandia National Laboratories Internal Memorandum, Albuquerque, NM, May 15, 1980.

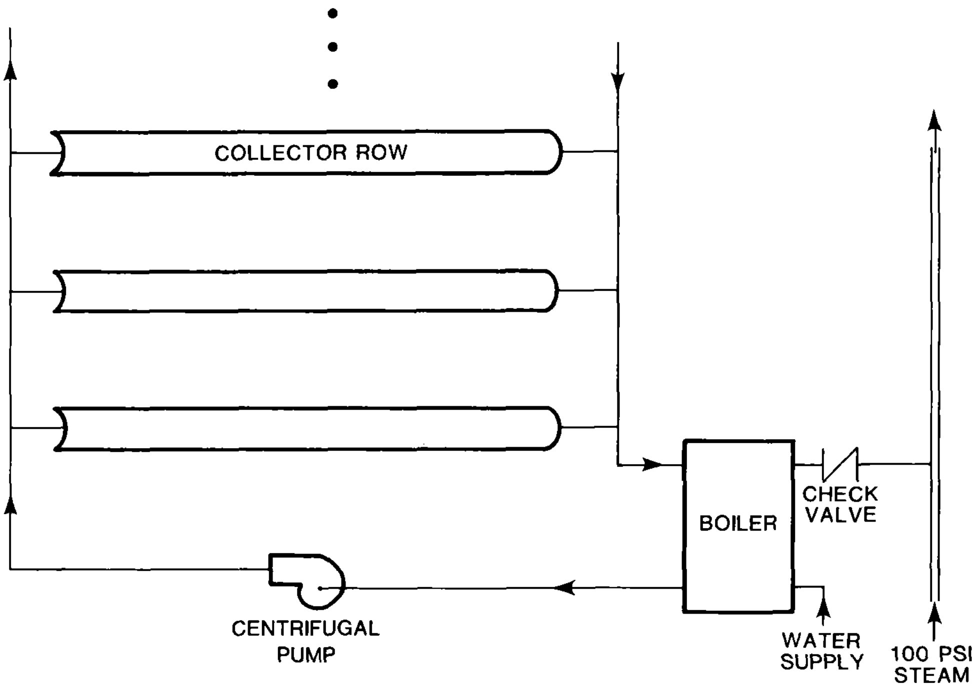

Figure 1. Industrial Process Steam System

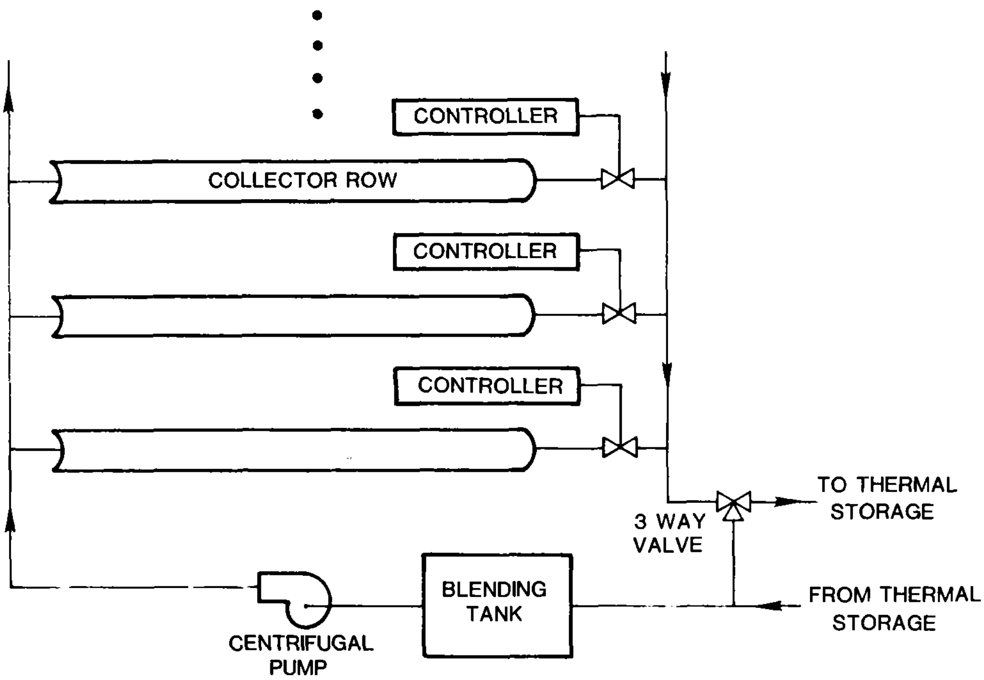

Figure 2. Electric Power Generation System

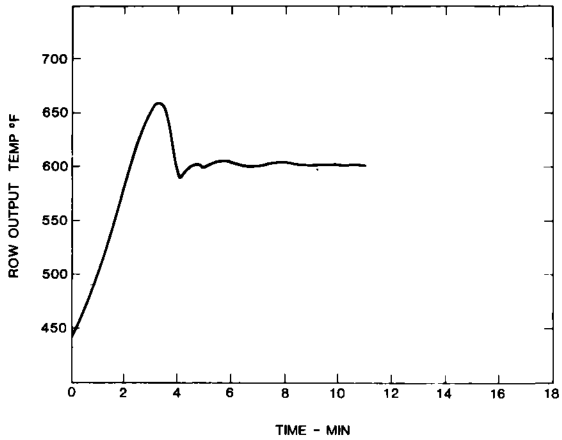

Figure 3. Startup Response

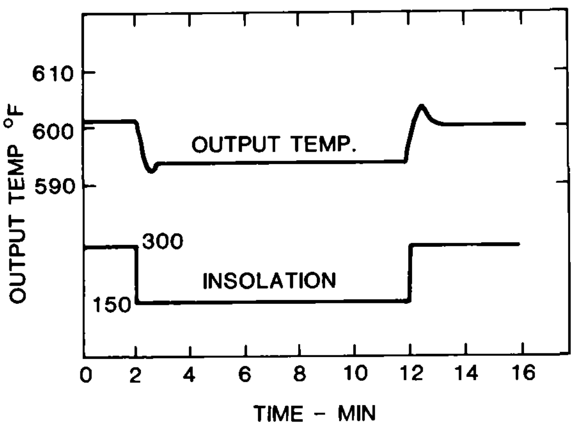

Figure 4. Insolation Transient Response

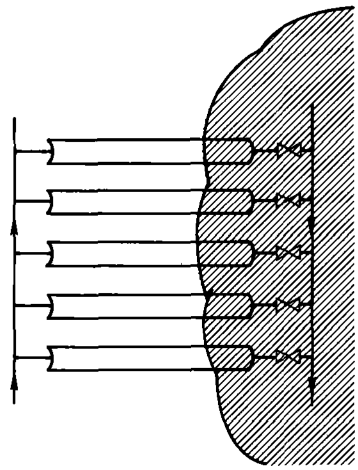

Figure 5. Partial Cloud-Cover Condition

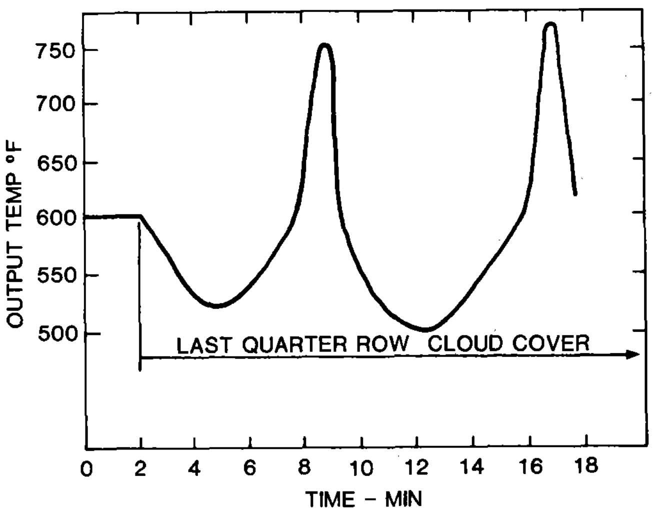

Figure 6. Partial Cloud-Cover Response

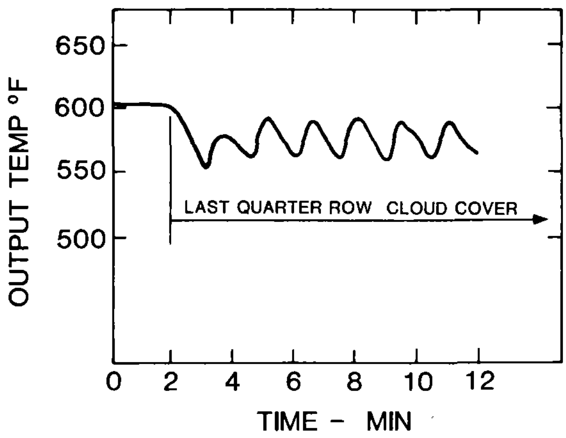

Figure 7. Partial Cloud-Cover Response With Midrow Override

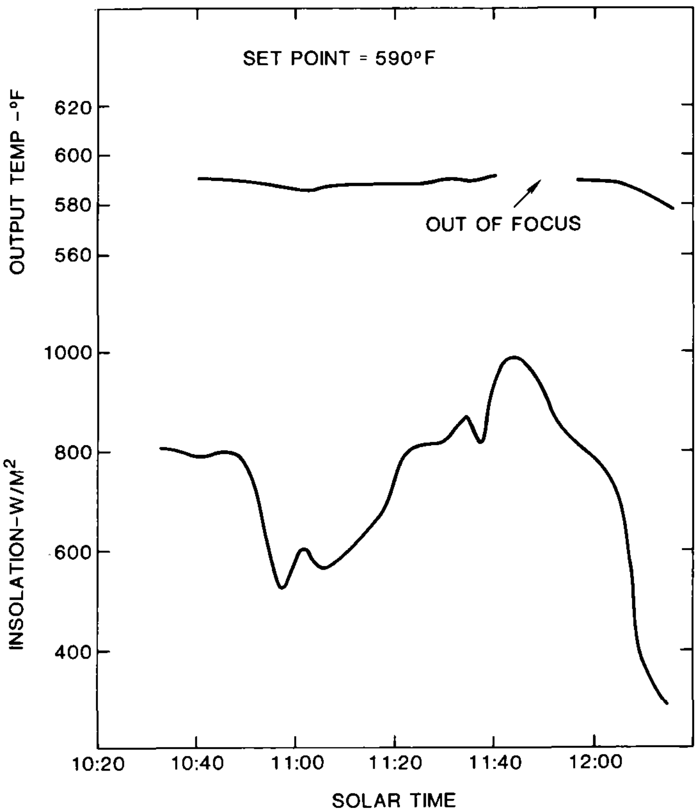

Figure 8. Test Results - Insolation Change Response

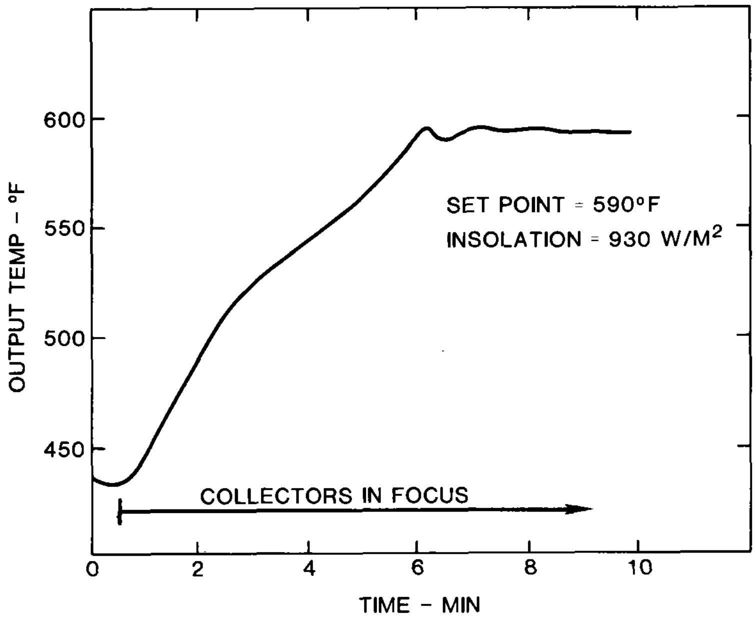

Figure 9. Test Results - Startup Response

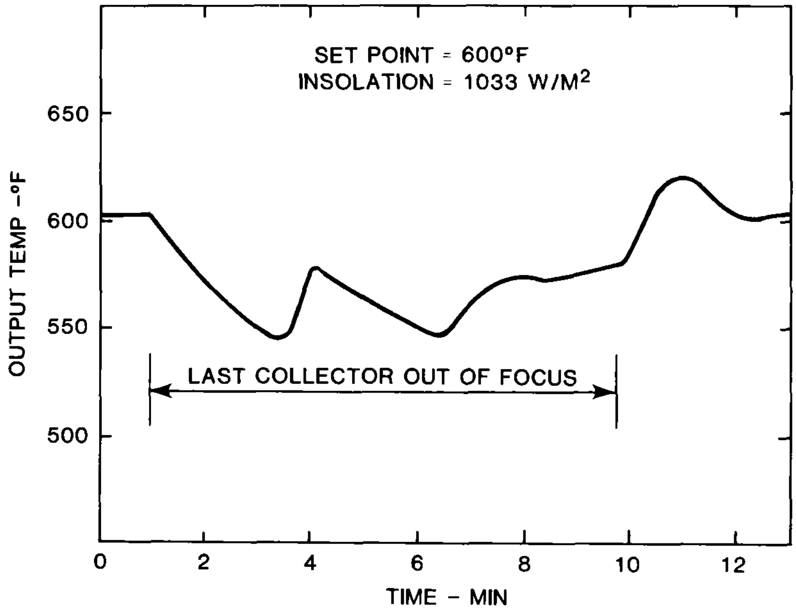

Figure 10. Test Results - Partial Cloud-Cover Response

SUBSYSTEM DESIGN HANDBOOK

Raymond W. Harrigan
Component and Subsystem Development Division 4722
Sandia National Laboratories
Albuquerque, New Mexico 87185

Introduction

In order to progress towards the near-term commercialization of solar energy, an extensive parabolic trough development program is underway which seeks to provide the technology readiness needed to support commercialization. This subsystem design handbook is being prepared as part of that effort. Handbook design procedures are needed to help instill reliability of design and lower costs resultant from custom designing. Development of standard design procedures is an evolutionary process and this project attempts to initiate that evolution.

The goal of this handbook is to provide easily used design techniques which will allow the execution of preliminary designs leading to the construction of solar thermal parabolic trough systems. In an effort to outline the contents in this brief paper, several areas have been selected to illustrate the type of material found in the handbook. The handbook by no means restricts itself to these design areas and attempts to address all areas pertinent to the design of operating solar thermal process heat facilities employing parabolic troughs. The handbook is structured to allow the designer to factor costs, which are current at the time of design execution, into the design process where needed. Thus, the design procedures are not limited by any assumed costs at the date of publication. Final design optimization and verification which may involve the use of computer simulation is beyond the scope of this handbook. The design procedures employ measured collector performance test data[1] and each of the 26 Typical Meterological Year[2] (TMY) sites is explicitly addressed. Publication of the handbook is anticipated in the Spring of 1981.

Collector Operating Temperature

The collector operating temperature is directly affected by the type of process with which it interfaces. There are basically two different types of industrial process heat demands. One type of demand is a sensible heating system in which the heat transfer fluid experiences large temperature swings and the second type of demand is a phase change system, such as steam, which tends to operate within rather narrow temperature limits. In addition, the presence of storage can have a significant impact on the selection of the collector operating temperature.

A sensible heat demand, in which the temperature of the process fluid varies over a wide temperature range, is perhaps the type of demand most easily serviced by a parabolic trough collector. Since a trough collector field collects thermal energy through a sensible heat mechanism, it is conceivable that the temperature in the collector field could be made to conform closely to the temperatures of the heat transfer fluid of the process. Conceptual design of the solar energy system can proceed in a rather straight forward manner since the average operating temperature of the collector field is approximately equal to the average process temperature. Such is not the case with steam systems.

The problem is illustrated schematically in Figure 1 for a hypothetical case in which 200 psi steam (380^{o}F) is desired. In transit to the point of use, the steam suffers a pressure drop resulting in 90% quality steam at 350^{o}F. This steam is then condensed at constant pressure. The condensate is reheated and vaporized to produce 200 psi steam to reinitiate the cycle. Sensible heat addition to the process steam generator is indicated on Figure 1 in the form of straight lines. As shown, several options are available with the constraint imposed by the second law of thermodynamics--the temperature of the collector fluid must, at any given point, be greater than the corresponding temperature of the process fluid in order for heat transfer from the collector fluid to the process fluid to occur. The different slopes for the collector fluid line represent different ΔT's across the collector field.

The design handbook provides the tools needed to choose the appropriate collector field ΔT through consideration of collector performance, pump power requirements, and storage costs.

Collector Performance

Parabolic trough collector performance is usually defined as a function of $\Delta T/I$ where ΔT is the difference between the receiver and ambient temperatures and I is the instantaneous direct normal solar flux passing through the collector aperture.[1] In order to use this performance data for system design the instantaneous performance data must be converted into an integrated performance over some period of time, typically a year. While some effort is being made to report predicted annual collector performance, the handbook provides nomographs for converting $\Delta T/I$ performance data into predicted integrated performance for use where annual performance has not been previously documented. The technique is based upon defining the performance of a hypothetical collector and then adjusting the integrated performance of this hypothetical collector for the difference between the $\Delta T/I$ data assumed for the hypothetical collector and the $\Delta T/I$ measured for the real collector. The performance data typically generated by this technique is illustrated in Figure 2 for an E/W oriented collector operating at the different average receiver temperatures indicated on the performance curves. Similar curves can be developed for collectors at any TMY site using the techniques developed in the handbook.

Collector Field Sizing/Storage Requirements

The determination of the proper collector field size to service a defined load is intimately tied to the amount of storage provided. Solar thermal process heat systems can operate without storage if the quantity of thermal energy delivered to the application is small compared to the demand but, for displacement of a large fraction of the fossil fuel demand, some storage is required. Both thermal energy demands which occur only during daylight hours (8 am to 5 pm) and demands which run 24 hours per day are considered in the handbook. In addition, the handbook examines both 7 days per week and 5 days per week demands to illustrate the effect on system design of a process heat application which shuts down on weekends. To do this, design tools were developed which examine the effect of variations in collector area and storage capacity on the utilization of the collected solar energy given that the demand for thermal energy is some fixed constant energy requirement. Figure 3 illustrates the use of the concept of energy utilization.

As shown in Figure 3, if nominal displacement is small (i.e. the ratio of collector field output to the application demand is small), it would be anticipated that the utilization of the collected solar energy would be near 100%. In other words, if the quantity of energy produced by the collector field is small compared to the demand, the application can accept any energy produced by the collector field and, as a result, all the solar derived energy is utilized in displacing the fossil energy normally used to meet the application's thermal energy demand. As the size of the collector field is increased, the utilization of the collected solar energy starts to decrease due to mismatches between the energy demand profile of the application and the energy supply profile of the solar collector field. Increasing the utilization of the collected solar energy requires storage.

As seen in Figure 3, the maximum demand displacement with near 100% utilization of the collected solar energy is about 80%. This requires storage of approximately 75% of the solar energy collected during the day. Increasing storage capacity beyond this does little to increase demand displacement beyond the 80% level. This is due to the seasonal variation of the output from an E/W solar collector in Albuquerque. Due to the greater seasonal variation in output of a N/S collector, a N/S oriented collector can displace only about 60% of a constant year-round demand without significant waste of the collected solar energy. Nomographs are presented in the handbook which allow choice of the most cost effective collector area/storage capacity combination.

Shadowing

The collector performance presented in Figure 2 is that of an isolated collector operating, as if, uninfluenced by its surrounding. Shadowing within the collector field will, however, reduce this performance as indicated in Figure 4. Shadowing will be dependent not only on the spacing between the collectors but also on collector orientation. As shown in Figure 4, a N/S collector suffers greater shadowing losses than an E/W collector in Albuquerque to the point where in situations of limited land availability the energy output from a N/S field begins to approach that of an E/W field. A general rule of thumb for spacing collectors is to provide a land area to collector aperture area ratio of 3:1.

There are frequently, however, good reasons for wanting to reduce this ratio. Often there is simply not enough land available and the resultant degradation in field performance needs to be evaluated. Additionally, the cost and thermal losses from interconnecting piping give rise to the desire to minimize collector spacing and a tradeoff analysis must be performed. Thus, for example, while a land area to collector aperture area of 3:1 may result in minimal shadowing losses in an E/W field, a ratio closer to 2:1 has been found to result in a more cost effective field layout due to reduced thermal losses in and capital costs of the field piping manifolds.[3] Tools to address these shadowing considerations for all TMY sites are presented in the handbook.

Additional Technical Design Considerations

The areas discussed above touch on some of the technical trade offs described in the handbook. The short space of this paper has allowed only a brief description of selected topics and how they are presented in the handbook. Other areas for which design techniques are being developed and incorporated into the handbook include determination of optimum piping insulation, heat loss (both steady state and overnight cooldown), fluid pumping parasitics, flow control, and, field start up. In short, the efforts presented in all the papers in this session need to be integrated into the handbook.

References

1. V. E. Dudley and R. M. Workhoven Summary Report - Concentrating Solar Collector Test Results Collector Module Tests Facility (CMTF) January December, 1978 - NTIS Report No. SAND78-0977 - (March, 1979).

2. I. Hall, R. Prairie, H. Anderson and E. Boes, Generation of Typical Meteorological Years for 26 SOLMET Stations - NTIS Report No. SAND78-1601 (August 1978).

3. R. E. Morton, Progress Report of Solar Collector Array Piping Design Optimization Studies, Jacobs Engineering Group, Inc. (April 1980).

Figure 1

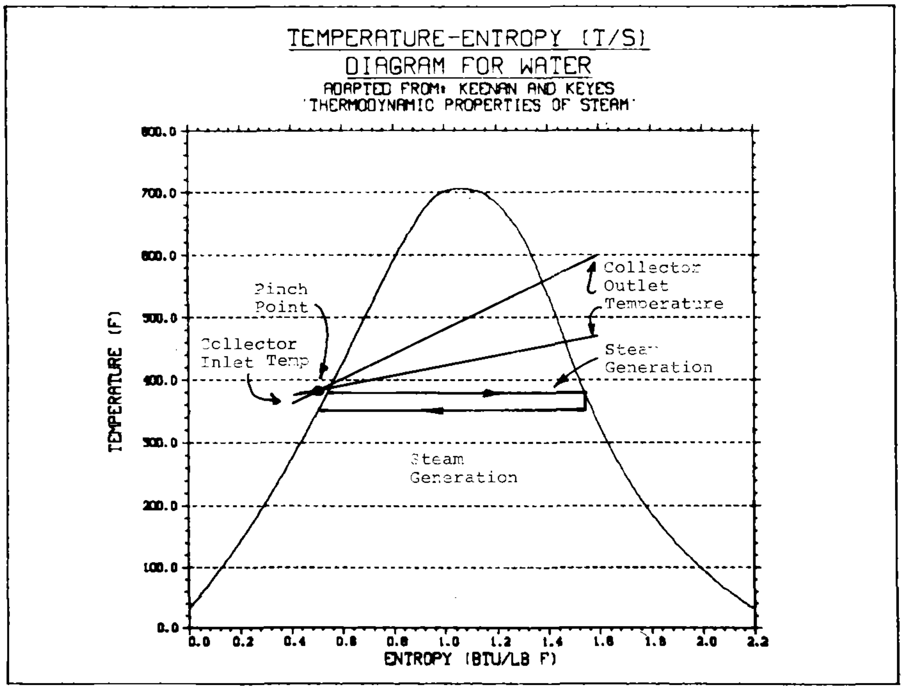

Figure 2

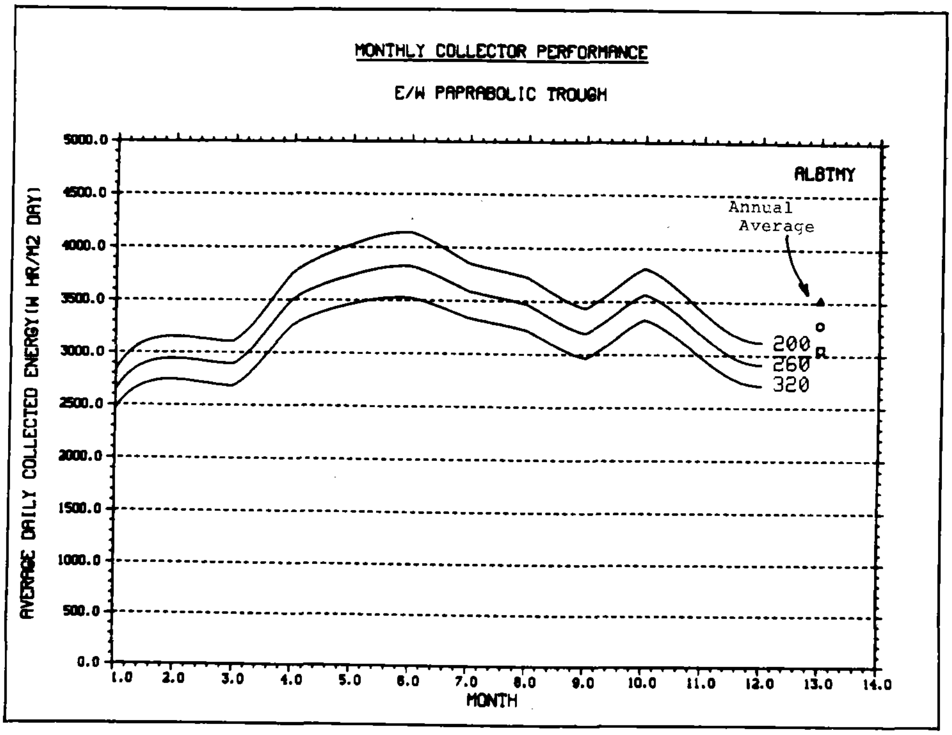

Figure 3

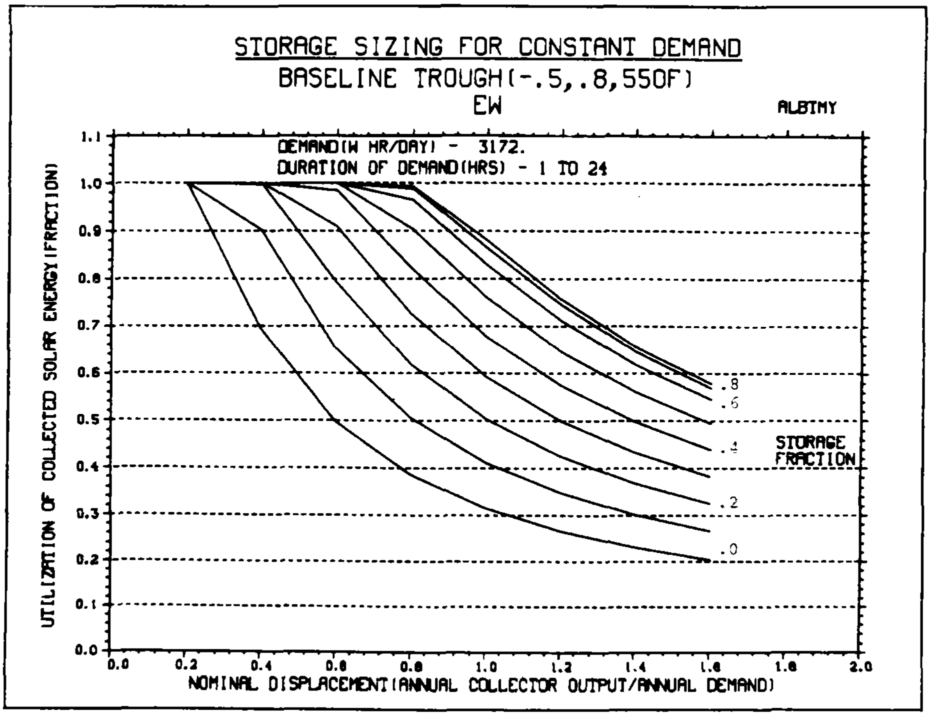

Figure 4

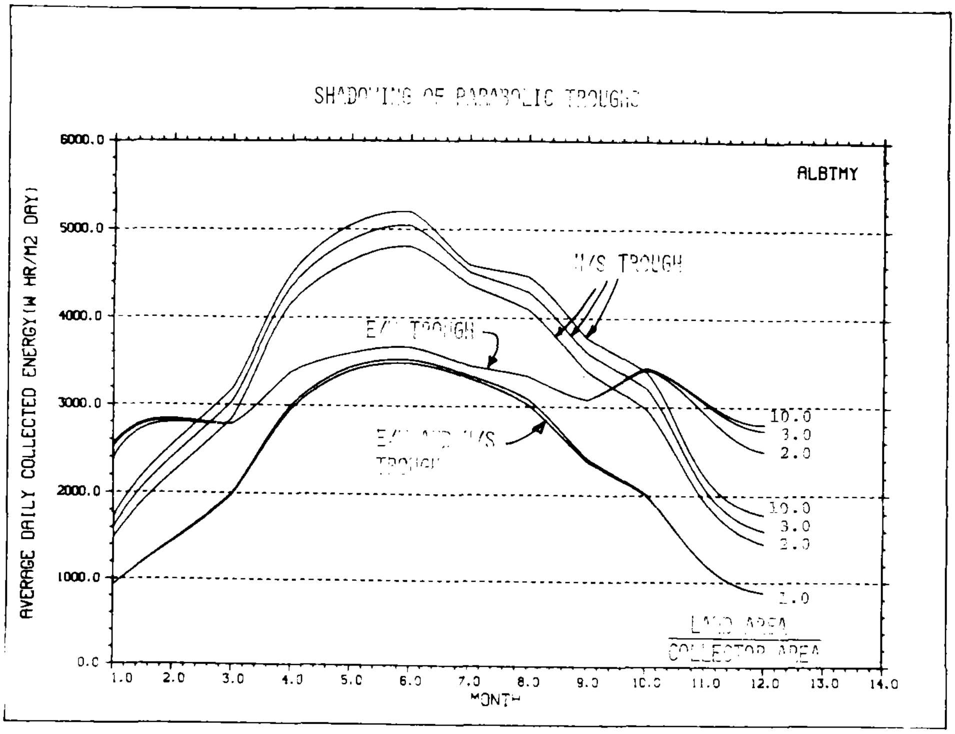

SOLAR COLLECTOR CLEANING STUDY

Lewis M. Larsen
Component and Subsystem Development Division 4722

and

James M. Freese
Thermophysical Properties Division 5824
Sandia National Laboratories
Albuquerque, New Mexico 87185

Introduction

Continuing studies at Sandia National Laboratories, Albuquerque (SNLA) on heliostats have indicated that degradation in reflectance does occur with time as a result of weathering (no cleaning). Inverted stow at night reduces the accumulation of this "weathering" soil, but it still progresses with time.(1) The same results have been obtained on sample mirrors that have been exposed to Albuquerque's ambient atmospheric conditions for 2.5 years.(2)

The purpose of the present study is to investigate a matrix of cleaning parameters, which include cleaning materials, sheeting agents, cleaning frequency, water pressure, water treatments, etc., and to identify good candidates. A longer term effort is aimed at developing cost-effective cleaning equipment, cleaning materials, and techniques for full scale systems.

McDonnell Douglas Cleaning Study

McDonnell Douglas (MDAC) conducted a cleaning study for Sandia National Laboratories with the following objectives:

1. to identify the nature of soil which adhered to silvered glass and aluminized acrylic mirrors after outdoor exposure
2. to determine the adhesion mechanisms which hold this soil on the mirror surface, and
3. to develop methods for removing the soil.

The description and the results of this effort have been previously published. A summary of the results of these studies are listed below.

A total of 350 test specimens were deployed at three sites for this work. The three locations were Shenandoah, Georgia, Daggett, California, and Albuquerque, New Mexico. The test specimens were 5" x 5" x 1/8" glass mirrors and 6" x 6" x 1/8" glass mirrors supporting a 5" x 5" x .003" square of FEK-244 (3M aluminized acrylic). The samples were soiled naturally and artificially. The artificial soiling was done by sprinkling material collected from the three sites onto a wet mirror surface and allowing it to dry in the sun. The materials were identified by optical and scanning Electron Microscopy.

The significant conclusions of this program were as follows:

1. Most of the surface contamination can be removed by the application of a 300 to 1000 psi tap water/mild detergent spray followed by a soft water rinse or by the application of a 300 to 1000 psi spray of ordinary tap water containing a sheeting agent (~200 ppm).
2. All glass and acrylic surfaces studied adsorbed some soil that could not be removed with the above cleaning technique. This tenacious layer is composed mainly of clays, micas, and barium or calcium carbonates.
3. This soil reduced the specular reflectance of glass mirrors 0.02 reflectance units, while acrylic mirrors were reduced 0.05 to 0.08 reflectance units.
4. Each cleaning activity restored the reflector to the same specularity - 98% of the original for glass and 92 - 95% for acrylic. Further soiling and rinsing exercises always regenerated the same specularity loss for both materials. No further degradation was noted after 30 soilings and washings.
5. A glass reflector could be restored to 100% of its original reflectivity at any time either by mechanical scrubbing with detergent, or by a 300 to 1000 psi spray and rinse with a 3% solution of a cleaning agent containing 5% hydrofluoric acid (CB 120) followed by tap water containing a sheeting agent. Acrylic reflectors could also be cleaned to 100% of their original specularity with this cleaning agent, however, scrubbing

is not recommended on acrylic surfaces because of low abrasion resistance of current acrylic reflective materials.

6. The attachment of the soil to the reflective surfaces was not the result of chemical interaction between soil and substrate, but was rather the result of intimate molecular contact between the two materials.
7. It was generally concluded from the above that the most cost effective method for solar collector cleaning is a monthly 1000 psi spray of tap water containing a sheeting agent, combined with an occasional (once every year or two) thorough cleaning either by scrubbing or using a pressure spray with the cleaning agent containing a small percentage of hydrofluoric acid.

Current Program

The current cleaning project was initiated in November 1979 at Sandia's Midtemperature Solar Systems Test Facility (MSSTF). Our study utilizes most of the recommendations that were made in the MDAC study in order to determine the effectiveness of these methods with Albuquerque city water in place of the Huntington Beach, CA. city water which MDAC used to clean the samples from the three sites.

Our test mirrors are two ft. by two ft. by 0.058 in. thick Corning 0317 glass samples silvered by Carolina Mirror Co. These samples are bonded to 16 gauge stainless steel sheets. Samples were mounted at a 45^{o} angle on exposure racks while individual wash stands were used for cleaning. Figures 1 through 6 show the exposure racks, individual wash racks, and some of the equipment being used in this study. The first eight samples were exposed in November 1979 but cleaning activities and reflectance measurements were not started until February 1980. Table 1 shows the cleaning procedures used on these samples.

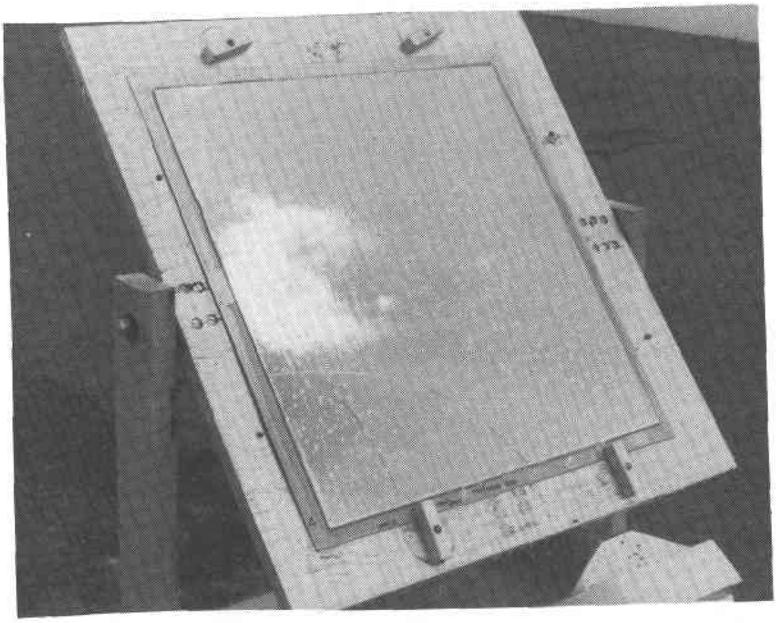

Figure 1. Sample #4-After Rinsing with Tap and 200 PPM Sheeting Agent

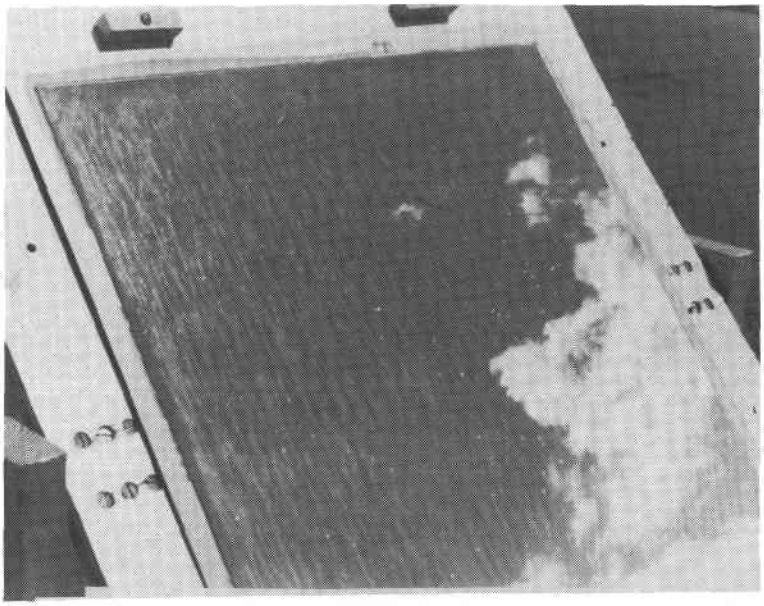

Figure 2. Sample #3-After Rinsing With Tap Water and 200 PPM Sheeting Agent

Figure 3. Individual Wash Stands - Rinsing With Tap Water and 200 PPM Sheeting Agent

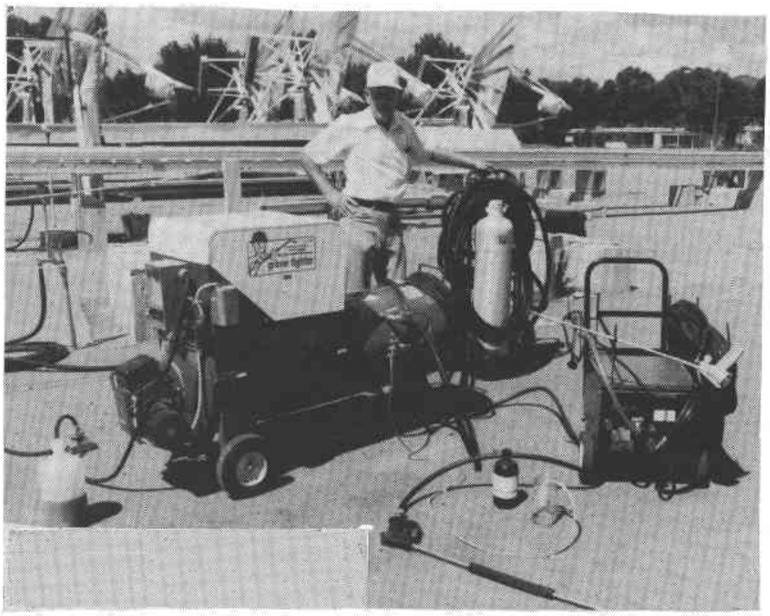

Figure 4. 100 PSI/4GPM Washer
500 PSI/3GPM Washer
Deionized Water Tank

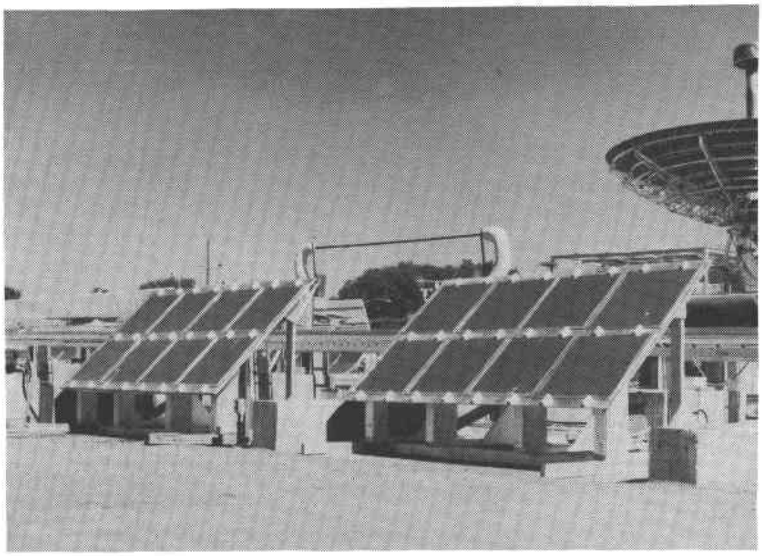

Figure 5. Exposure Racks

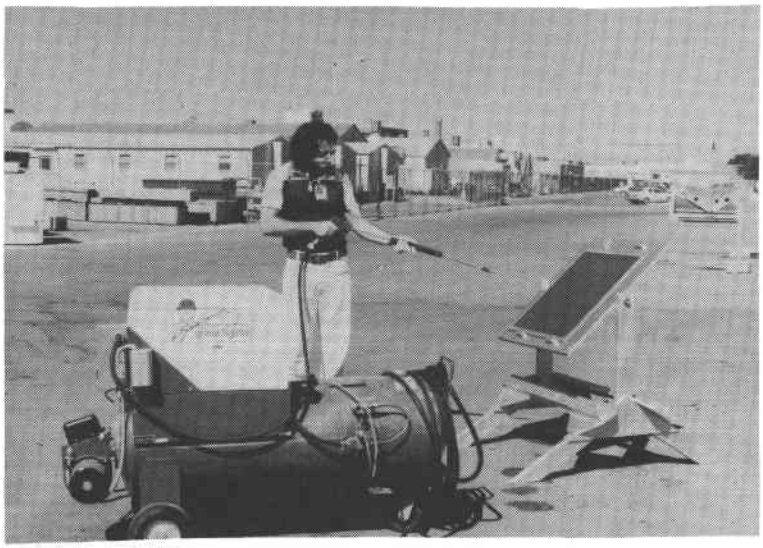

Figure 6. 1000 PSI/4GPM Washer and Individual Wash Rack

Table 1. Initial Cleaning Schedule
Rack #1

Sample No.	Pressure/Volume psi/GPM	Wash Cycle	Rinse Cycle	Cleaning Frequency
1,2	1000/4	Tap water/ Sheeting Agent	None	4 weeks
3,4	1000/4	Tap water/ Detergent	Tap water/ Sheeting Agent	4 weeks
5,6	1000/4	Deionized Water	None	4 weeks
7,8	1000/4	Tap water/ Sheeting Agent	None	8 weeks

After the first cleaning cycle in February, a severe wind storm overturned the exposure rack and cracked 6 of the 8 mirrors. The epoxy bonding held the glass in place so that reflectance measurements could still be obtained; however, the cracks could be responsible for some error in the reflectance readings. It was, therefore, decided that the cracked samples should be replaced. This was done in May 1980. At this time, a second 8-sample exposure rack was placed into service in order to evaluate some additional cleaning parameters. Table 2 shows the cleaning procedures used on the second set of eight samples, which include two aluminized acrylic samples (FEK-244).

Table 2 - Rack #2 Cleaning Sequence

Sample No.	Pressure/Volume PSi/GPM	Wash Cycle	Rinse Cycle	Cleaning Frequency
9,10	1000/4	Soft Water	None	4 weeks
11,12	500/3	Tap Water/ Sheeting Agent	None	4 weeks
13,14	500/3	Tap Water/ Detergent	Tap Water/ Sheeting Agent	4 weeks
15 (FEK-244)	1000/4	Dionized Water	None	4 weeks
16 (FEK-244)	1000/4	Tap Water/ Detergent	Tap Water/ Sheeting Agent	4 weeks

Portable Specular Reflectometer

Specular reflectance measurements were performed with a portable specular reflectometer developed by SNLA.[4] The measurement spectrum of the instrument has been limited to a range of 450-750 nm; thus, reflectance values do not represent solar averaged quantities. The absolute accuracy of the instrument is ±0.015 reflectance units. (1.00 reflectance units = 100% reflectance). However, the reproducibility of the instrument is better than ± 0.005 reflectance units so that changes in specular reflectance values greater than ± 0.01 reflectance units should be considered significant. Five locations were measured on each mirror and the average values were reported. Standard deviation values were typically less than ± 0.02 reflectance units for soiled mirrors and ±0.01 reflectance units for cleaned mirrors.

Cleaning Results and Discussion

Table 3 shows the results of specular reflectance measurements made on the initial 8 samples through May 21, 1980.

Table 4 shows the reflectance measurements taken after May 21, 1980 of the original two mirrors (Nos. 4 and 5), the six replacement mirrors (designated by the letter A), plus the additional eight samples that were added to the experiment at this time.

Table 3 - Reflectance Measurements Initial 8 Samples

SAMPLE NO	11/20/79 D	11/20/79 C	2/21/80 D	2/21/80 C	3/21/80 D	3/21/80 C	4/21/80 D	4/21/80 C	5/21/80 D	5/21/80 C	6/20/80 D	6/20/80 C
1		.944	.939	.926	.886	.915	.803	.885	.806	.876		
2		.944	.938	.946	.900	.918	.832	.899	.840	.891		
3		.943	.907	.938	.902	.917	.846	.901	.829	.897		
4		.944	.940	.943	.899	.931	.800	.890	.827	.891		
5		.944	.907	.920	.914	.933	.824	.926	.852	.921		
6		.944	.913	.937	.897	.923	.776	.909	.835	.913		
7		.944	.929	.936	.885	NC*	.816	.880	.826	NC	.794	.892
8		.944	.927	.945	.883	NC	.780	.880	.820	NC	.795	.896

*NC - Not Cleaned
D - Dirty
C - Cleaned

Table 4 - Cleaning Experiment - Reflectance Measurements

SAMPLE NO.	5/21/80 D	5/21/80 C	6/20/80 D	6/20/80 C	7/18/80 D	7/18/80 C	7/25/80 D	7/25/80 C	8/1/80 D	8/1/80 C	8/8/80 D	8/8/80 C	8/15/80 D	8/15/80 C	8/18/80* D	8/18/80* C	8/22/80 D	8/22/80 C
1A		.939	.851	.938	.820	.892	.862		.827		.875		.895	.875		.951	.908	
2A		.939	.843	.933	.824	.895	.855		.831		.878		.901	.891			.884	
3A		.951	.859	.951	.817	.929	.900		.846		.899		.922	.899		.959	.928	
4		.891	.829	.910	.810	.890	.813		.838		.872		.890	.865			.887	
5		.921	.843	.925	.795	.902	.854		.823		.864		.893	.905			.874	
6A		.941	.848	.940	.773	.920	.866		.805		.868		.888	.913		.949	.920	
7A		.943	.854		.799	.905	.855		.817		.867		.895	.895		.948	.918	
8A		.943	.840		.799	.912	.884		.793		.867		.895	.900			.891	
9		.939	.839	.944	.815	.923	.889		.825		.873		.893	.915		.949	.918	
10		.942	.860	.939	.805	.916	.886		.828		.883		.896	.917			.897	
11		.941	.892	.941	.824	.916	.889		.829		.878		.903	.879		.947	.924	
12		.945	.860	.939	.804	.911	.880		.843		.881		.902	.906			.880	
13		.949	.870	.933	.824	.925	.886		.842		.890		.904	.902			.899	
14		.948	.857	.937	.817	.915	.876		.836		.881		.898	.892		.948	.921	
15	FEK	.848	.712	.861	.708	.845	.787		.713		.785		.797	.818		.853	.828	
16	FEK	.852	.731	.853	.679	.808	.771		.728		.768		.792	.787		.854	.822	

D = Dirty
C = Cleaned
* - Cleaned with DI water and 3% CB120 - DI Rinse

The reflectance measurements from a representative number of the test samples have been plotted in Figures 7 through 11 to show graphically the effect of time on reflectance values. General comments regarding these tables and graphs are as follows:

1. The post-cleaning reflectance of all samples shows a gradual decrease with time.
2. The samples cleaned with deionized water only evidenced the smallest reflectance loss. (See Sample Nos. 5, 6, 6A, and 15.) This gradual decrease in reflectance is approximately 0.040 reflectance units for a 9-month period.
3. Samples cleaned with "soft" water exhibited a slightly greater reflectance loss than did the deionized water samples (See sample Nos. 9 and 10). The soft water samples have been exposed for only 3 months and additional experience is needed on these samples to verify this trend.
4. The samples washed with tap water and a 3% solution of detergent and then rinsed with tap water and a 200 ppm sheeting agent solution exhibited greater reflectance losses than either samples cleaned with deionized water or "softened" water (See Sample Nos. 3, 4, 13, 14 and 16). The increased reflectance loss experienced on these samples could be due to natural weathering, mineral accumulation or the presence of sheeting agent residue.
5. The samples, washed with tap water and a 200 ppm solution of sheeting agent in tap water exhibited the greatest loss of reflectance. (See Sample Nos. 1, 1A, 2, 2A, 7, 7A, 8, 8A, 11, and 12). These results indicate that the use of a detergent wash has some beneficial cleaning effect.
6. The samples that were cleaned at 4 and 8 week intervals indicated that the longer cleaning interval resulted in less reflectance loss. (See Sample Nos. 1, 1A, 2, 2A, 7, 7A, 8 and 8A). Additional data are needed in order to determine the optimum cleaning interval.
7. The samples that were cleaned in the same manner but with different water pressures exhibited no significant difference in cleaning effectiveness. (See Sample Nos. 1, 2, 3, 4, 11, 12, 13 and 14).

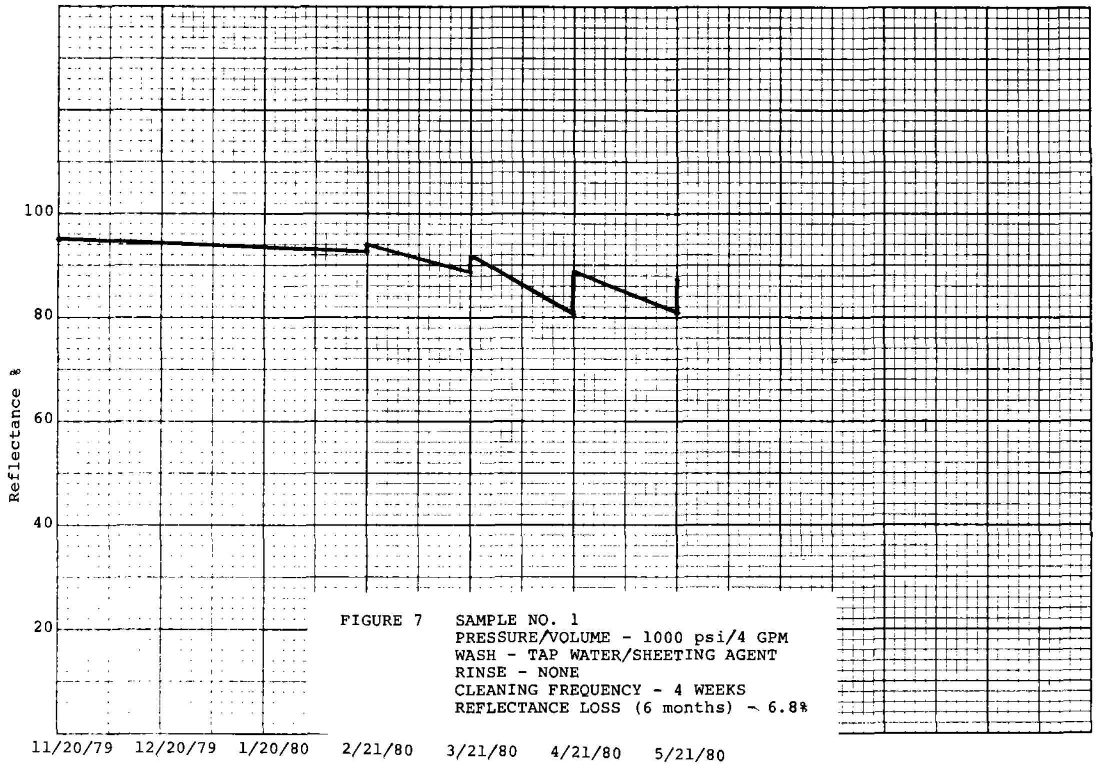

FIGURE 7 SAMPLE NO. 1
PRESSURE/VOLUME - 1000 psi/4 GPM
WASH - TAP WATER/SHEETING AGENT
RINSE - NONE
CLEANING FREQUENCY - 4 WEEKS
REFLECTANCE LOSS (6 months) ~ 6.8%

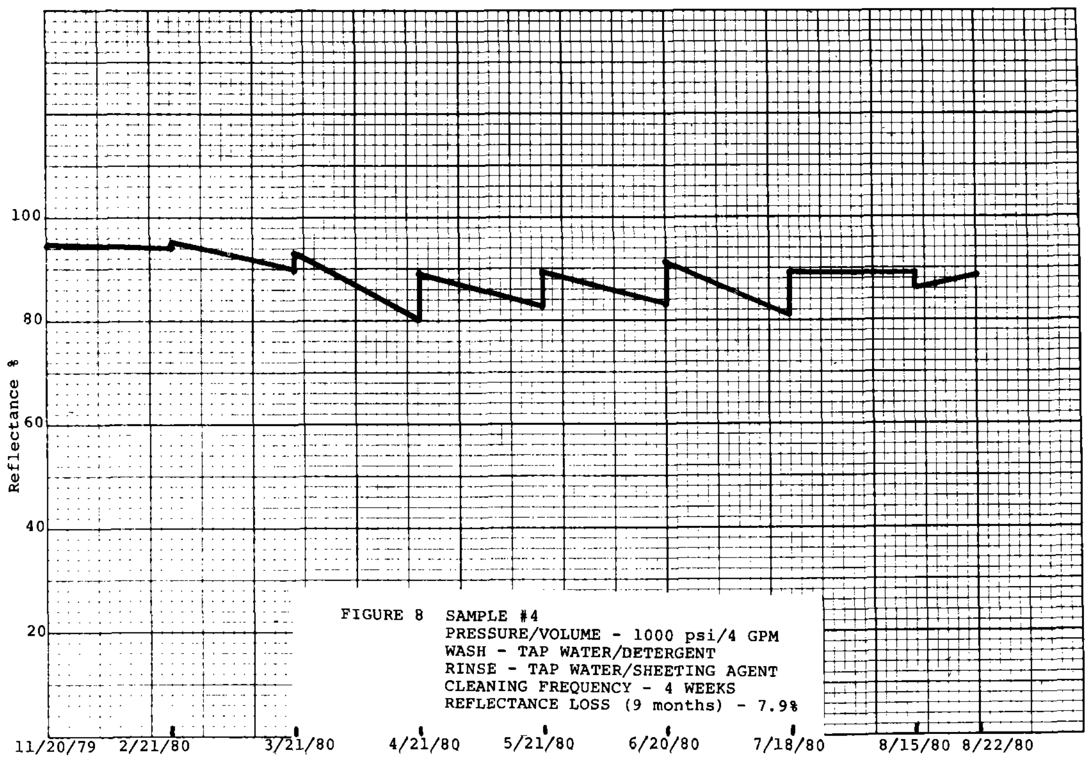

FIGURE 8 SAMPLE #4
PRESSURE/VOLUME - 1000 psi/4 GPM
WASH - TAP WATER/DETERGENT
RINSE - TAP WATER/SHEETING AGENT
CLEANING FREQUENCY - 4 WEEKS
REFLECTANCE LOSS (9 months) - 7.9%

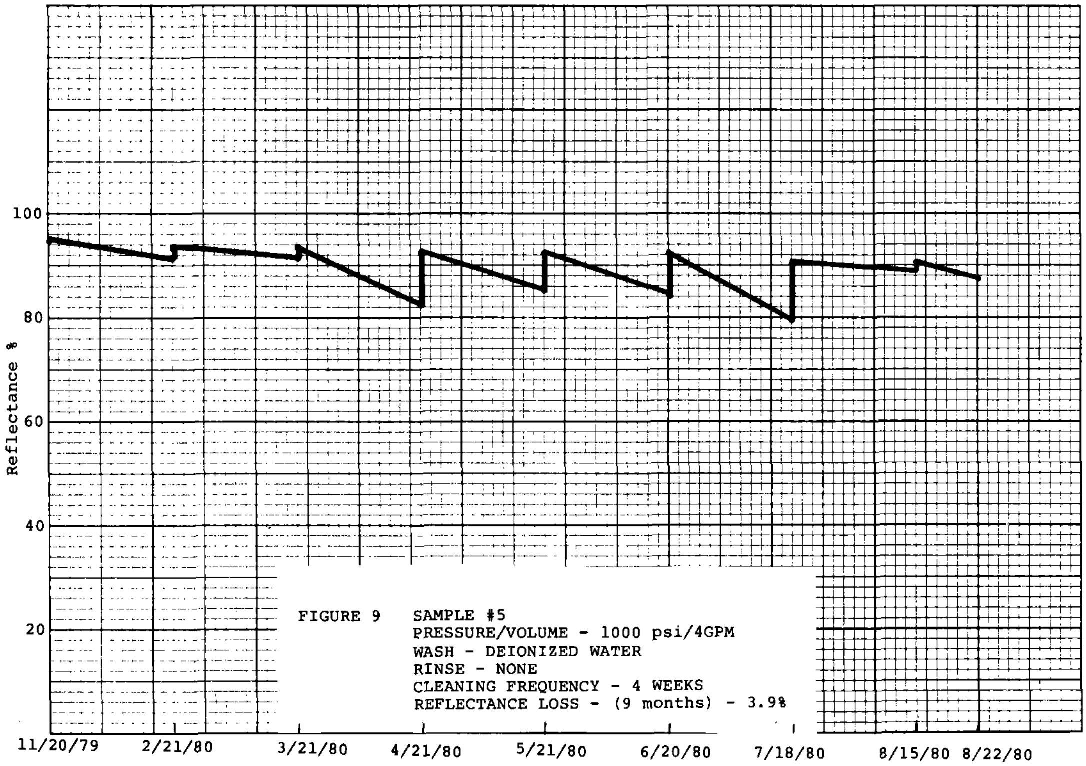

FIGURE 9 SAMPLE #5
PRESSURE/VOLUME - 1000 psi/4GPM
WASH - DEIONIZED WATER
RINSE - NONE
CLEANING FREQUENCY - 4 WEEKS
REFLECTANCE LOSS - (9 months) - 3.9%

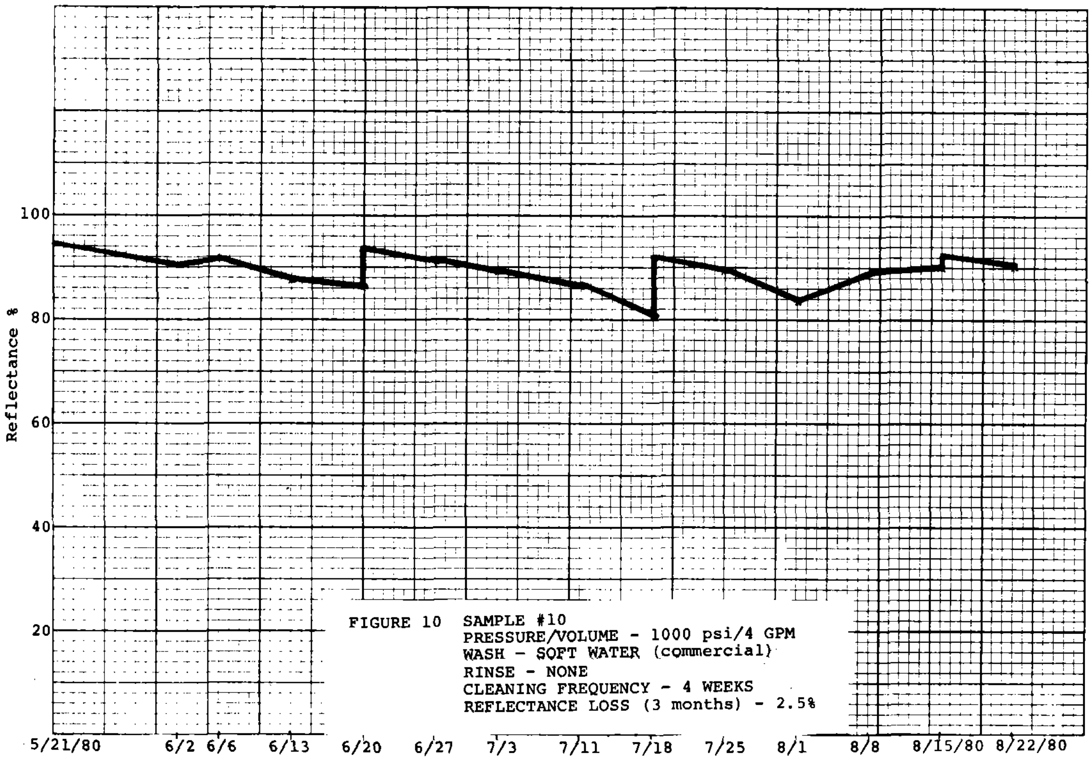

FIGURE 10 SAMPLE #10
PRESSURE/VOLUME - 1000 psi/4 GPM
WASH - SOFT WATER (commercial)
RINSE - NONE
CLEANING FREQUENCY - 4 WEEKS
REFLECTANCE LOSS (3 months) - 2.5%

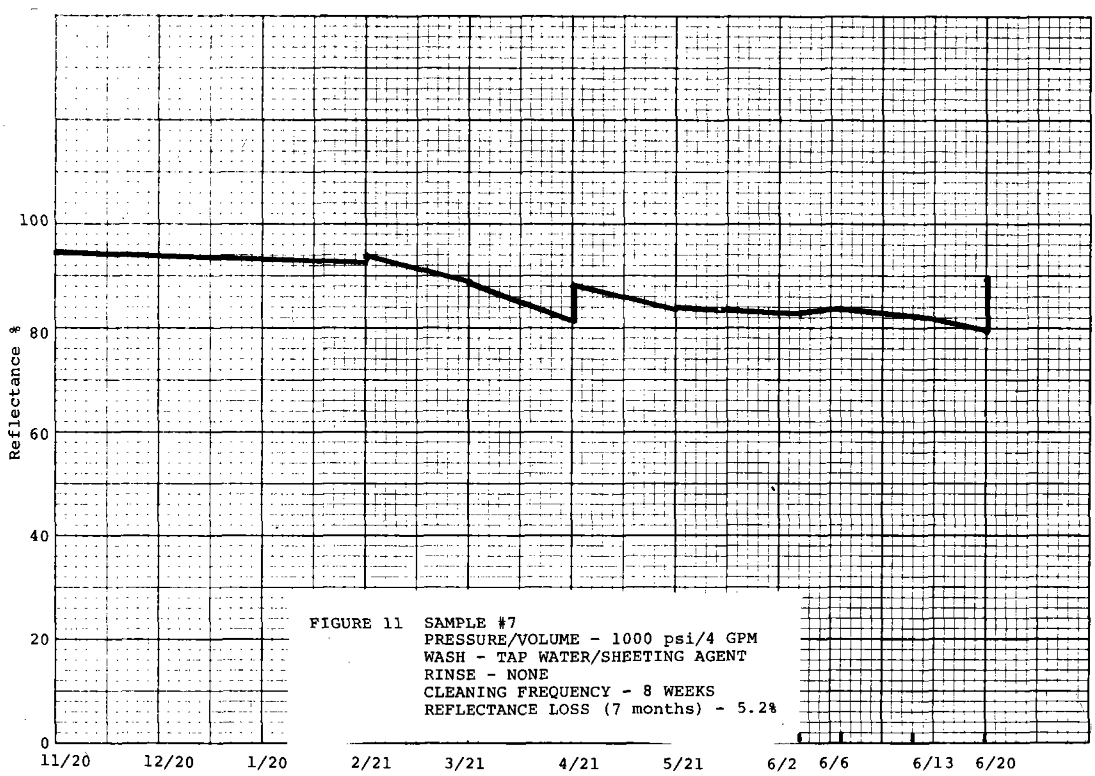

FIGURE 11 SAMPLE #7
PRESSURE/VOLUME - 1000 psi/4 GPM
WASH - TAP WATER/SHEETING AGENT
RINSE - NONE
CLEANING FREQUENCY - 8 WEEKS
REFLECTANCE LOSS (7 months) - 5.2%

8. To determine if the reflectance could be restored to 100% of its original value, 9 of the 16 samples were washed with a 3% solution of detergent containing a small percentage of hydrofluoric acid and deionized water. See Sample Nos. 1A, 3A, 6A, 7A, 9, 11, 14, 15, and 16). These samples were then rinsed with deionized water only. The reflectance of all these samples was returned to 100% of their original reflectance value (within experimental error.)

Conclusions

1. The results to date must be considered to be preliminary in nature. Additional cleaning cycles are required in order to definitely establish the most effective techniques.

2. No significant difference could be detected between cleaning with 500 psi (3 gal/min) and 1000 psi (4 gal/min) wash and rinse cycles.

3. There may be no significant differences in reflectance losses between the 4 and 8 week cleaning cycles. Additional data are needed in order to obtain an optimum cleaning interval.

4. It was verified that we can recover reflectance losses to 100% of original value by cleaning with a 3% detergent in deionized water cleaning solution in which the detergent contains 5% hydrofluoric acid, and then rinsing with deionized water.

5. We could not restore the reflectance value to within 2% for glass and 5 to 8% for acrylic of their original value by conventional techniques. A gradual decrease in reflectance with time has been observed.

6. The most effective cleaning we have observed involves the use of deionized water only. ("Soft" water may be a satisfactory substitute). In techniques involving the use of a sheeting agent, excessive foaming of the agent occurred and the expected sheeting action was not present. Further, the drying of the sheeting agent foam on the mirror surface left a film which probably reduced the reflectance.

Future Plans

1. In order to minimize the deposition of minerals contained in the local water supply, we shall investigate the use of compressed air to remove the wash-rinse water before it can dry on the mirror surface.

2. Since little difference in cleaning effectiveness could be detected at water-spray pressures between 500 and 1000 psi, additional cleaning studies will be conducted using available tap water pressures ($\leq$100 psi).

3. We shall attempt to determine the cause of the gradual degradation in reflectance with time, i.e., is it deposition of minerals from the tap water, residue from the sheeting agent foam drying on the surface, weathering (natural soil accumulation), or possibly a combination of all three?

4. Yet to be determined are cost-effective washing intervals i.e., regular intervals or wash only when the average reflectance measurements fall below a certain level.

5. The final procedures, equipment and cleaning materials will ultimately be evaluated on a field of advanced collector troughs scheduled for installation at SNLA.

References

1. D. L. King and J. E. Myers, Proceedings of the Society of Photo-Optical Inst. Eng. (SPIE), Los Angeles, CA (February 1980).
2. J. M. Freese, Effects of Outdoor Exposure on the Solar Reflectance Properties of Silvered Glass Mirrors, SAND78-1649 (September 1978).
3. M. B. Sheratte, Cleaning Agents and Techniques for Concentrating Solar Collectors, SAND79-7052 (May 1980).
4. J. M. Freese, "The Development of a Second Generation Portable Specular Reflectometer", Proceedings of Line-Focus Solar Thermal Energy Technology Development Conference, Albuquerque, New Mexico (September 1980).

THERMOCLINE THERMAL ENERGY STORAGE

Robert J. Gross
Fluid Mechanics and Heat Transfer Division 5513
Sandia National Laboratories
Albuquerque, New Mexico 87185

Introduction

To fully realize the potential of solar thermal technology, thermal energy storage (TES) becomes a necessity. Sandia National Laboratories, Albuquerque, (SNLA) is evaluating the thermocline TES concept to fulfill the needs of solar thermal systems.

Thermocline TES uses the system working fluid to store the thermal energy in a single, well-insulated tank. Use is made of natural buoyant forces and the extremely slow diffusive properties of liquids to keep the hot upper layer from the cold lower fluid layer.

The attractive characteristic of thermocline storage is that theory shows it has the potential of being a very efficient storage concept. Often when a claim is made concerning the efficiency of a storage system, the claim is based on the first law of thermodynamics (i.e., an energy balance). Availability and the second law of thermodynamics are not taken into account. However, if one examines TES systems from a second law standpoint, one fact is clear: the more heat that is transferred across a surface area with finite temperature differences, the lower is its overall second law efficiency. Thus the thermocline concept which has one phase that never transfers heat to other media will exhibit a large theoretical second law efficiency.

Thermocline storage is also economically attractive. A single-tank thermocline system consists of a tank filled with the system working fluid and two flow diffusers. With such a simple system, control, initial cost and maintenance cost could be minimal.

The objective of the thermocline project at SNLA is to determine the feasibility of thermocline TES from a theoretical, operational, and economic standpoint. This will be done by testing an engineering prototype (1200 gallon) storage tank, small-scale laboratory test programs, and development of analytical computer models.

Engineering Prototype Tank

A 1200 gallon engineering prototype storage tank has been installed at the Midtemperature Solar Test Facility located at SNLA. The oil storage tank design was constrained to be representative of standard commercial ASTM fabrication techniques and be compatible with a single media thermocline tank as shown in Figure 1. The tank has a removable top so that devices such as floating diaphragms, improved diffusers, etc. may be placed in the tank. The side walls of the tank were insulated with sixteen inches of fiberglass insulation. The top and bottom of the tank were also thoroughly insulated.

A primary goal of the instrumentation on the prototype storage tank is to provide accurate radial and axial temperature profiles of the tank and surrounding insulation. This has been accomplished with the placement of 384 thermocouples in the storage subsystem. Two vertical probes (See Figure 2) of sixty thermocouples each were installed to obtain accurate interior axial temperature profiles. On the inside tank wall, thermocouple rakes exist at eight locations (See Figure 3) to indicate the possibility of a boundary layer being formed. At twenty-five locations in the tank the radial temperature profile is defined from near the center of the tank to the outside tank wall by four thermocouples. At thirteen of these locations the radial profile is extended through the insulation. A photograph of the tank prior to installation is shown in Figure 4.

The prototype tank's status is that instrumentation checkout is essentially complete and test designed to characterize the heat loss from the tank is underway. The two heat loss testing techniques being used are a steady-state method with fluid flow and a transient ("cool down") method.

Analytical Investigation

Analytical work is being conducted to develop models and correlate data from the experimental program. The three sources of thermocline degradation which require consideration in the modeling effort are: natural convection induced by thermal losses at the tank wall, diffusion of heat from the hot layer to the cold layer at the thermocline interface, and mixing caused by the charging or discharging process.

It has been shown(1) that the diffusion of heat between layers is a small effect, which leaves the other two possible degradation sources to be dealt with.

When the tank is charging or discharging fluid, mixing at the inlet and outlet of the tank is the main source of thermocline degradation, while induced natural convection at the walls is a secondary concern. On the other hand, if a thermocline exists while the tank is in a static operational mode (no fluid flow), natural convection heat transfer induced by thermal conduction through the tank walls is a prime concern. Of course, the mixing process cannot occur when there is no flow.

Rahm and Walin[2,3,4,5] eveloped an analytical solution which applies during the charging/discharging process. Walin[2] derived a one-dimensional boundary layer method for a stably stratified fluid including heat loss or gain at the boundaries. The method is applicable to any geometry and can include mass flow into or out of the system. SNLA now has the capability to use this method. Though some experimental results by Rahm and Walin[5] indicate that the method can be accurate, their thermocline data is questionable. Thus, SNLA is performing small-scale laboratory experiments to verify the Rahm-Walin approach.

Hess and Miller[6,7] have thoroughly investigated the thermocline problem when the tank is in a static mode and thermal wall losses become the primary source of degradation. Miller[6] developed a two-dimensional computer model which solves the Navier-Stokes equations coupled to the energy equation relating to natural convection in a tank with highly conducting walls. Hess[7] performed well-designed experiments and confirmed the model's accuracy. This computer model is now in the process of being placed on the SNLA computer system.

Laboratory Investigation

The engineering prototype thermocline tank will provide information concerning subsystem operation and control as well as overall performance data as a a result of the extensive instrumentation. However, as is usual with such a large system, changing parameters and hardware is time-consuming and expensive. Thus, small-scale laboratory investigations are currently underway to complement the protoype tank testing and support the development of analytical tools. These investigations examine certain aspects of the thermocline phenomenon in detail.

One of the most important factors contributing towards thermocline efficiency during charging and discharging is the ability of the flow diffusers at the inlet and outlet to minimize turbulence and mixing. To focus on this important thermocline component, an experiment has been constructed to investigate diffusers designs. A diffuser design with diverter plates has been constructd and is prsently being installed in a small-scale glass tank. Flowmeters will measure flow rate in and out of the tank, and dye injection techniques will provide qualitative and quantitative data on the performance of the diffuser. This prototype diffuser and the entire experimental facility are designed so that flow configuration may be easily changed to facilitate optimization of the diffuser design. One design consideration is that the diffuser should have the shortest possible axial length to maximize the useful storage capacity of the tank. Low pressure drop through the diffuser is desirable also.

Another small-scale experiment is being conducted to investigate the applicability of the one-dimensional analytical method of Rahm and Walin (see Figure 5). The experiment consists of a small, plastic closed tank instrumented with 34 thermocouples. The tank will be filled with water at room temperature and then immersed in a hot water bath. This process will cause a thermocline to form at the top of the tank which will then commence to travel down to the tank bottom. If experiment confirms the Rahm-Walin theory, then the associated computer program will be modified to account more accurately for the thermal losses associated with a highly conducting wall.

References

1. Gosta Walin, "Contained Non-Homogeneous Flow Under Gravity or How To Stratify a Fluid in the Laboratory", J. Fluid Mech. (1971), vol. 48, part 4, pp. 647-672.

2. L. Rahm and G.Walin, "Theory and Experiments of the Control of the Stratification in Almost-Enclosed Regions", J. Fluid Mech. (1979), Vol. 90, part 2, pp. 315-325.

3. Lars Rahm, "Temperature Response by An Initially Homogeneous Fluid Subject to Thermal Forcing at the Vertical Boundary", Goteborgs Universitet Oceanogrofiska Institutionen, Report No. 28, 1978.

4. L. Rahm and G. Walin, "On Thermal Convection In Stratified Fluids", Geophys. Astrophys. Fluid Dynamics, (1979), Vol. 13, pp. 51-65.

5. Constance Miller, "Effect of a Conducting Wall on a Stratified Fluid in a Cylinder", Progress in Astro. and Aero. (1977), Vol. 60, pp. 190-208.

6. C. F. Hess and C. W. Miller, "Natural Convection in a Vertical Cylinder Subject To Constant Heat Flux", Int. J. Heat Mass Transfer (1979), Vol. 22, pp. 421-430.

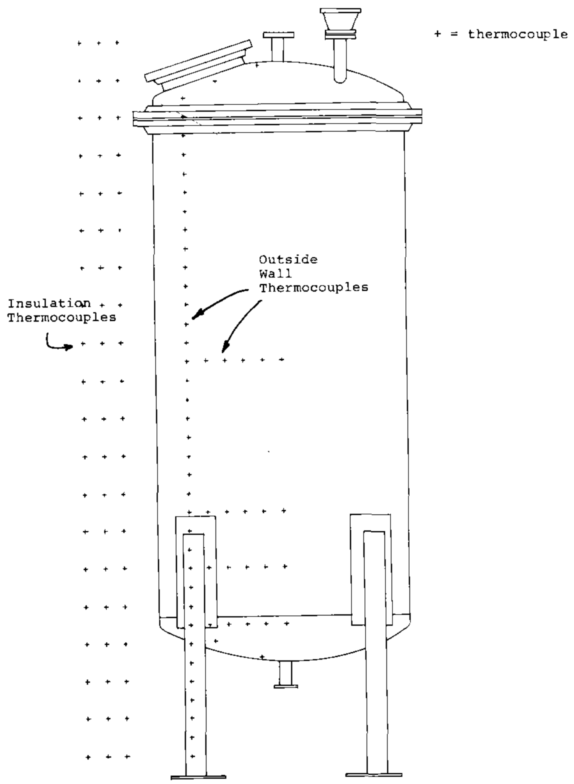

Figure 1. Thermocline Tank Show External Instrumentation

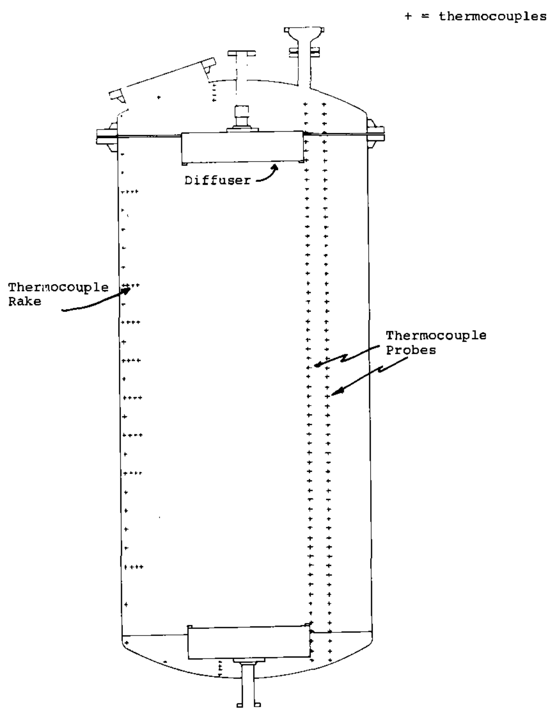

Figure 2. Internal Instrumentation of Thermocline Tank

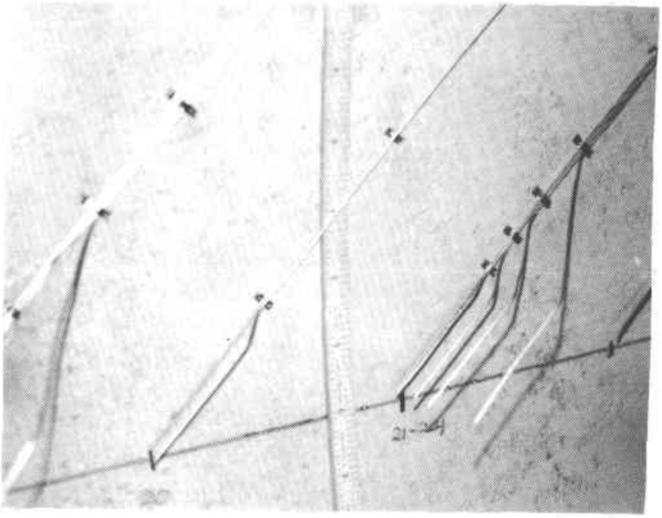

Figure 3. View of Thermocouple Rakes on the Inside Wall of the Engineering Prototype Tank

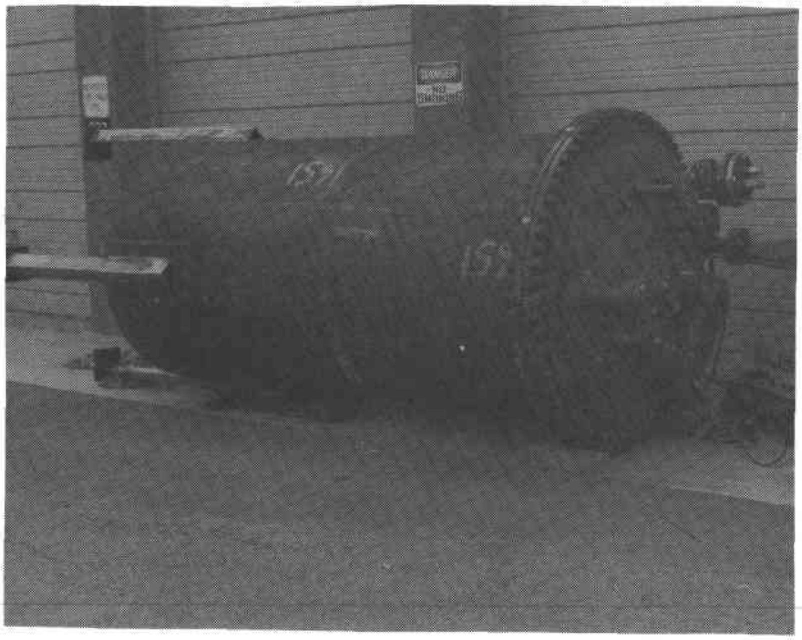

Figure 4. Thermocline Tank

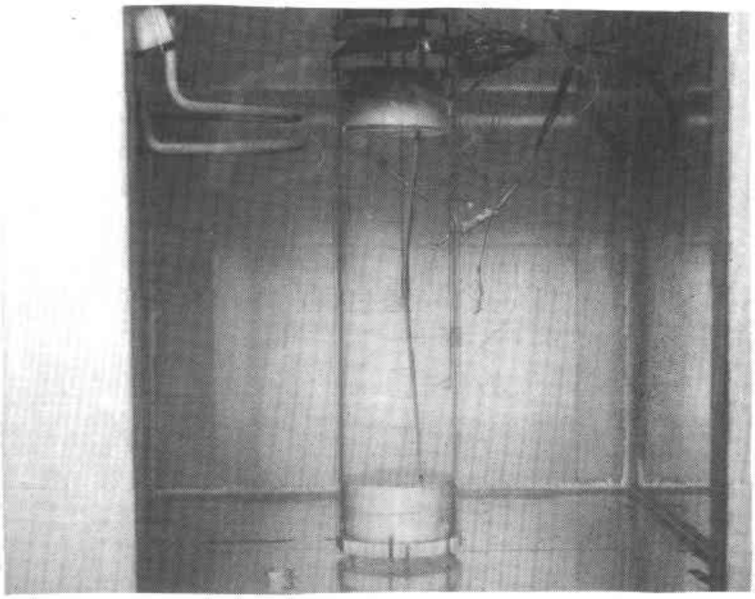

Figure 5. Rahm-Walin Experiment

Session V - Line-Focus Component Development

Siegfried Thunborg, Chairman
Component and Subsystem
Development Division 4722
Sandia National Laboratories

THERMOOPTICAL CONSIDERATIONS IN TROUGH DESIGN

George W. Treadwell
Component and Subsystem Development Division 4722
Sandia National Laboratories
Albuquerque, NM 87185

Introduction

Parabolic trough collector geometric configurations are significantly influenced by thermooptical considerations. From an elementary standpoint, the collector performance is determined by calculating the optical energy captured by the geometry and subtracting the thermal losses. In general, each of those features which influence optical capture and thermal losses will be described. For a proper geometric design, it will be shown that optical considerations are more dominant than thermal considerations.

Solar Coating

Experiments conducted in 1974 revealed that non-glazed and non-selectively coated receivers could not sustain 600°F operating temperatures. Figure (1) illustrates the test configuration. The use of receiver covers permitted positive efficiencies to be obtained. The configuration and test results are shown in Figures (2), (3) and (4). The results in Figure (4) were obtained with a modest evacuation of the annulus. As can be observed, only modest efficiencies resulted from the experiments.

Concurrent with the experiments, an analytical model was developed. This model analyzed the thermooptical characteristics depicted in Figure (5). With this model, analytical comparisons were made with some experimental results as portrayed in Figure (6). The excellent agreement has permitted the use of the computer to calculate thermooptical tradeoffs for other conditions.

The first thermooptical characteristic reviewed was the receiver absorber coating. For a given set of operating conditions, the absorptance-emittance tradeoff was conducted as shown in Figure (7). The negative slopes of the curves illustrate that changes in absorptance are far more effective in enhancing efficiency than are similar percentage changes in emittance.

An exhaustive examination of potential coatings of that era indicated that black chrome electrodeposited over dull nickel had the most desirable characteristics from a properties-cost standpoint. The typical properties are illustrated in Figures (8) and (9). Particular attention should be given to the absorptance decay illustrated in Figure (9) since the influence of that characteristic will be described later.

Sizing of Glass Annulus

The need for a receiver cover has already been illustrated. The size of the annulus gap is another thermooptical consideration. For a constant operating temperature, an energy balance results in the heat loss curves of Figure (10). It can be observed that if vacuum operation is desired, no annulus gap is desirable (Curve B). However, if the vacuum is lost, the losses are in accordance with the conduction and convection curve (Curve D). An optimum gap with minimum Curve B heat loss increase occurs at nominally a 1 cm gap. This result is essentially unchanged with regard to operating temperature and film coefficients.

Optics

Examination of the potential thermooptical losses in a collector design in Figure (11) reveals those categories through which improvements can be obtained in efficiency. That category most amenable to enhancement is the mirror reflectivity. The effect of enhancement of the optics is shown in Figure (12). With all thermooptical improvements, an efficiency of ~80% is possible.

Basic Receiver Sizing Techniques

With the foregoing as a prelude, a thermooptical design consideration is the receiver size. If it is desired to capture all of the energy reflected by a parabola, a sizing argument can be developed as shown on Figure (13). The receiver must be large enough to capture the sun and also to compensate for tracking and slope errors (assumed to be additive). Because of the incidence angle effect of the coating, the receiver must be increased in size to cause a maximum incidence angle of 60°. Given the resulting subtended angle of 1 3/4°, the receiver diameter is a function of the distance to the farthest point of the reflector. Since thermal losses are proportional to the receiver diameter, the farthest distance to the reflector should be the smallest possible. Examination of Figure (14) reveals a 90° rim angle to result in the smallest receiver for a given aperture.

Refined Sizing Technique

The development of a statistical energy deposition routine illustrated in Figure (15) allowed the thermooptical relationship between the rim angle and the receiver size to be investigated more thoroughly. For a 90° rim angle and approximately equal performance, the $\sigma = .01209$ curve on Figure (16) represents the previous strategy in receiver sizing. If the system errors are treated statistically, it should be possible to decrease receiver size in accordance with some selected error budget and achieve higher efficiency. A reasonable budget is approximately the $\sigma = .00772$ curve and the resulting receiver size is 1 inch OD for a two-meter aperture trough.

Rim Angle Re-Examination

A re-examination of the rim angle is shown in Figure (17). It can be observed that a rim angle of 105° results in the highest efficiency of those rim angles examined. However, a review of Table (I) indicates why a rim angle of 90° continues to remain a reasonable angle. Its arc length is not excessive and its accuracy is better maintained compared to the larger rim angles. Smaller rim angles suffer performance reductions due to the resulting larger diameter receivers, however, they involve less arc length (i.e. less material) and might be easier to fabricate.

The previous analysis and arguments have been based upon two axis tracking troughs (viz. normal incidence performance). From a cost-performance standpoint, it is more reasonable to use single axis tracking designs. Such designs have been analyzed with typical, meteorological year input data and the results substantiate the previous conclusions. The curve shapes on Figure (18) for Albuquerque illustrate that a 1 inch OD receiver is still optimum for a two-meter aperture trough. The same conclusion results from an examination of the Great Falls, Montana results shown in Figure (19).

Inexact Receiver Positioning

The focal line of a trough collector is an imaginary line in space. It is impossible, from a design standpoint, to precisely locate a receiver along the focal line when mechanical deformations and fabrication tolerances are considered. Figure (20) illustrates the influence of receiver off-axis mounting. It can be observed that as much as 2 mm departure from a theoretical focus results in only a nominal degradation. Unpublished work at Sandia suggested that a tracking bias of 4 mrad and a mislocation of 5 mm from focus at receiver support points can be tolerated without significant performance degradation for a 1-1/4 inch diameter receiver.

Practical Considerations

From these thermooptical considerations and others, criteria have been developed for the design of collectors. Practical design considerations, such as pylon gaps, receiver fittings, reflector coverage etc., will result in a decrease from the theoretical performance potential of the geometric configurations described in this paper.

References

1. G. W. Treadwell, Design Considerations for Parabolic-Cylindrical Solar Collectors, SAND 76-0082, Sandia National Laboratories 1976.

2. F. Biggs, EDEP: A Computer Program for Modelling the Parabolic Trough Solar Concentrator, TBP

3. G. W. Treadwell, et al., An Analysis of the Influence of Geography and Weather on Parabolic Trough Solar Collector Design. SAND 79-2032, Sandia National Laboratories, 1980.

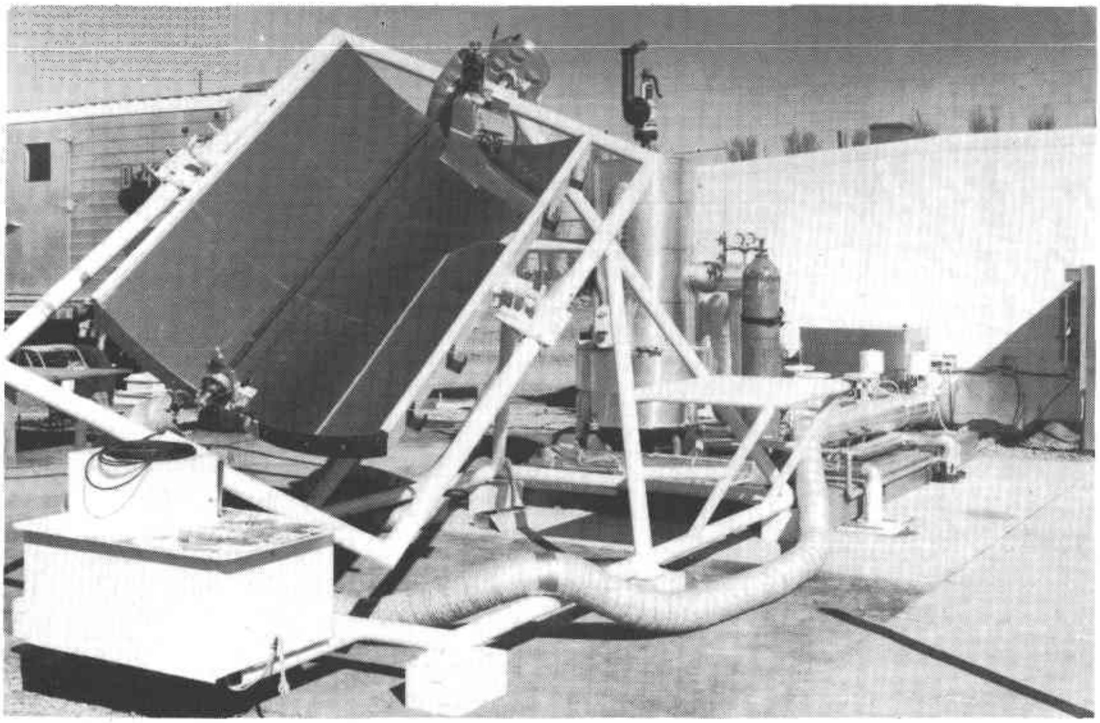

Figure 1 Reflector With Receiver Tube Suspended at Focal Line

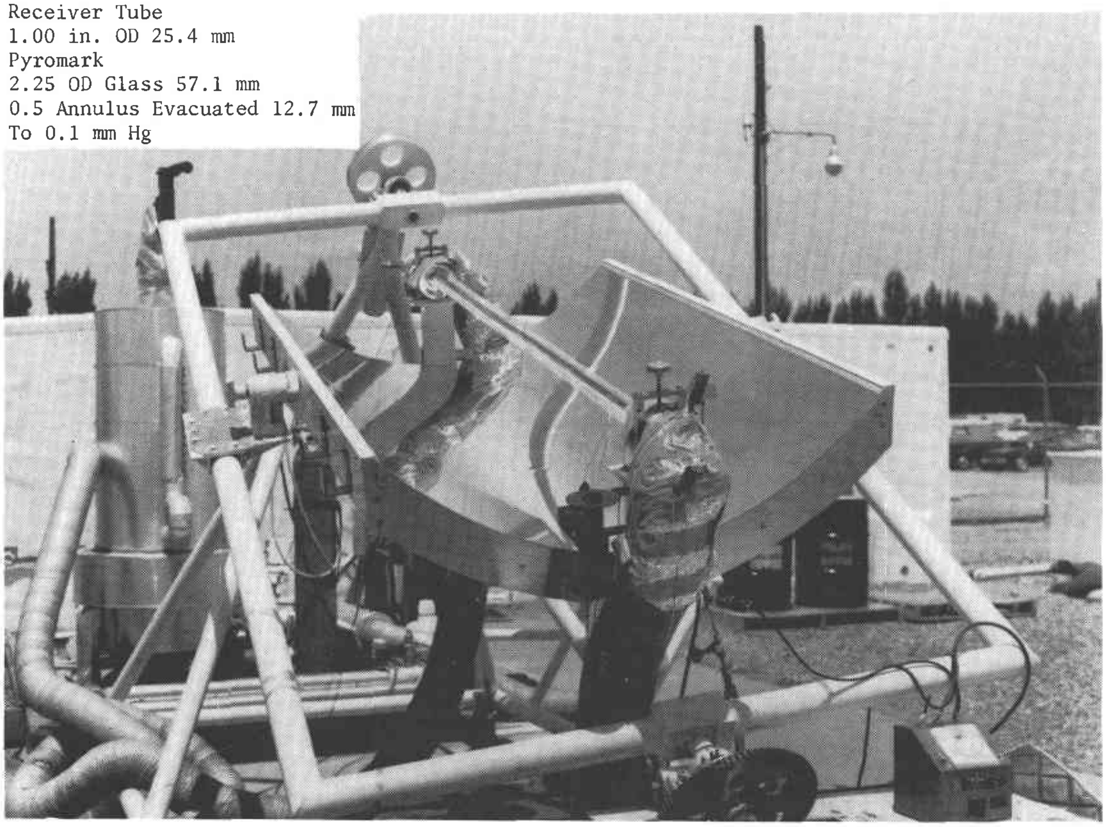

Figure 2 Reflector With Glass-Jacketed Receiver Tube Suspended

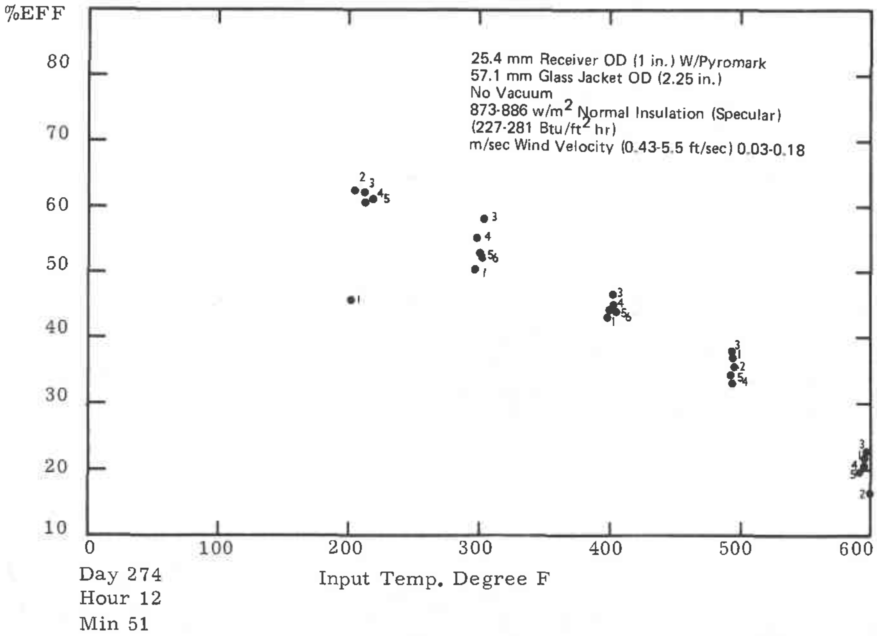

Figure 3 Input Temperature vs. Percent Efficiency for 25.4 mm OD Receiver With 57.1 mm OD Glass Jacket at No Vacuum

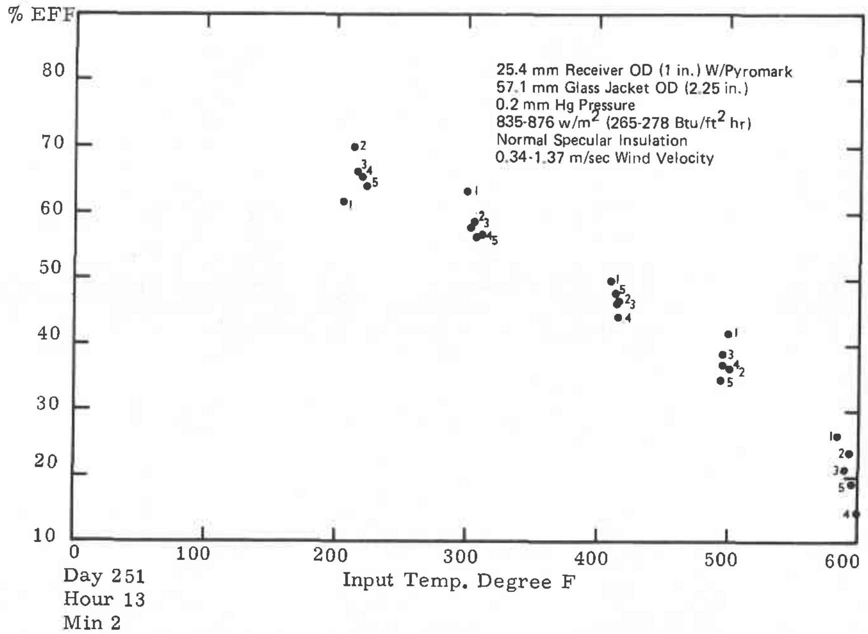

Figure 4 Input Temperature vs. Percent Efficiency for 25.4 mm OD Receiver With 57.1 mm OD Glass Jacket at 0.2 mm HG Pressure

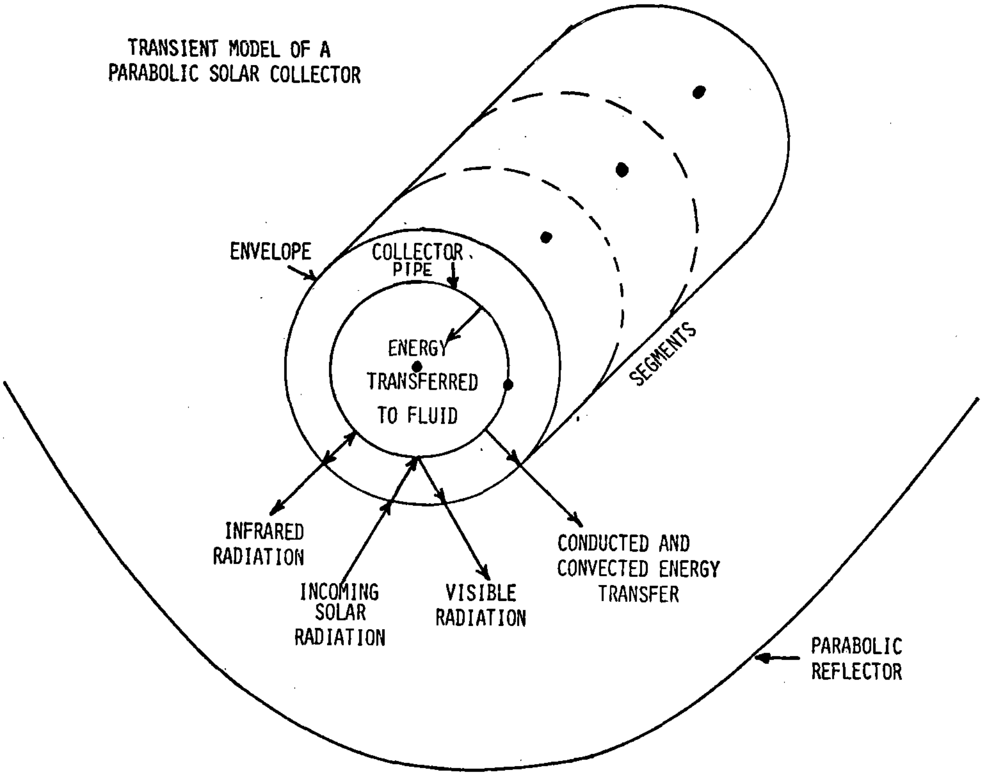

Figure 5 Trough Thermooptical Characteristics

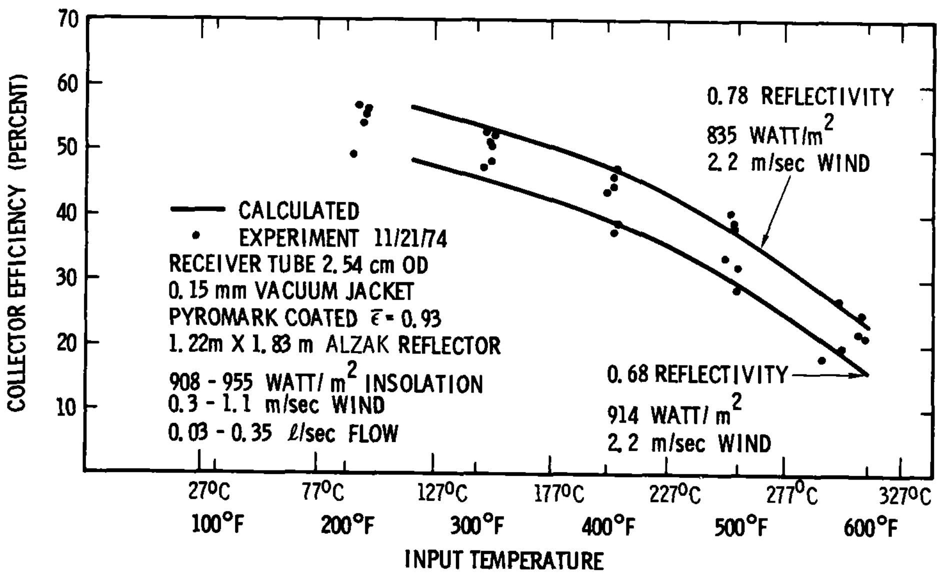

Figure 6 Solar Collector Test Results

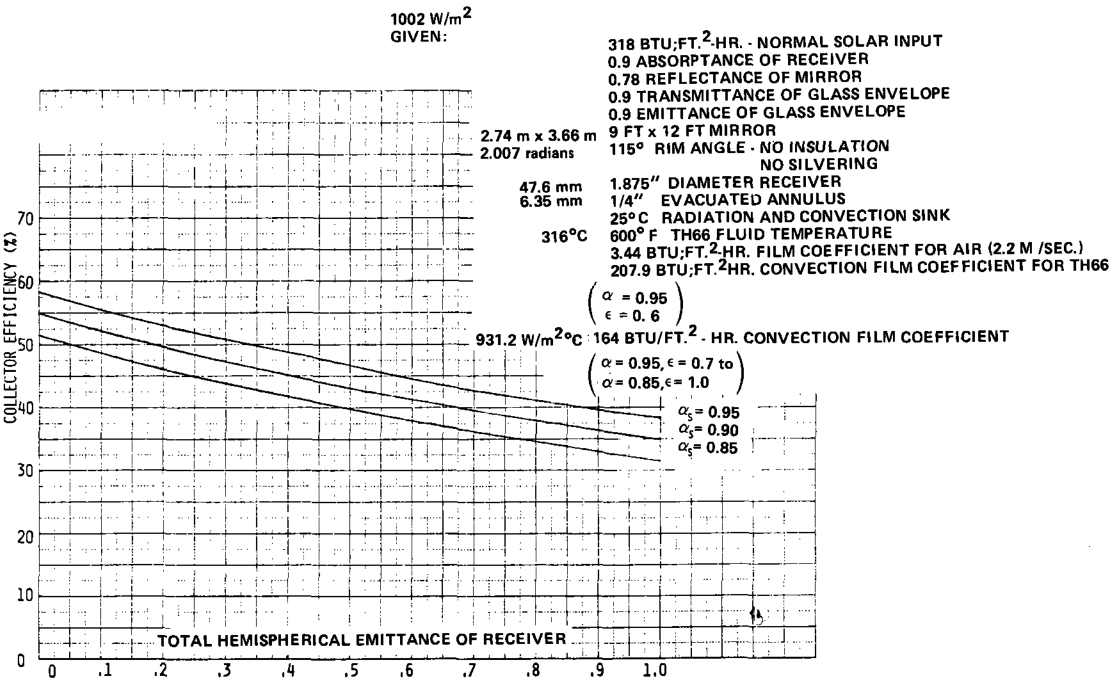

Figure 7 Total Hemispherical Emittance of Receiver vs. Collector Efficiency

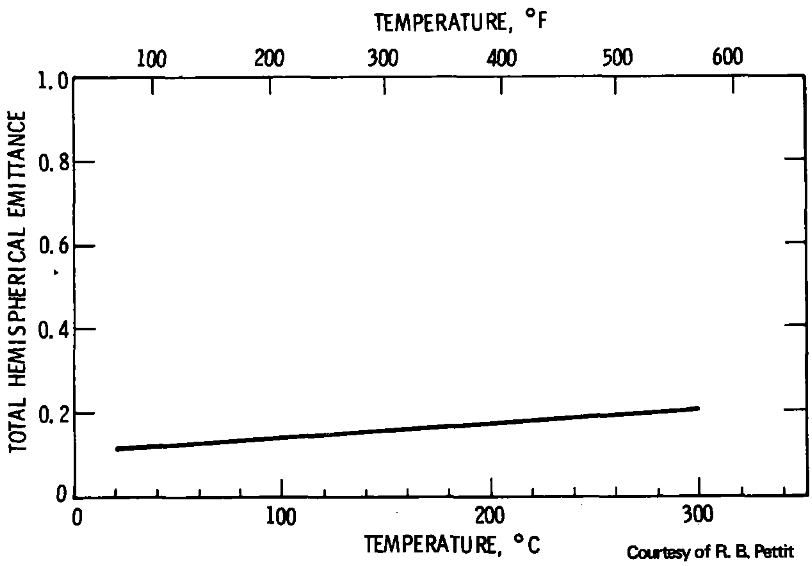

Figure 8 Harshaw Black Chrome on Electroplated Sulfamate Nickel (4 Minute Treatment Time)

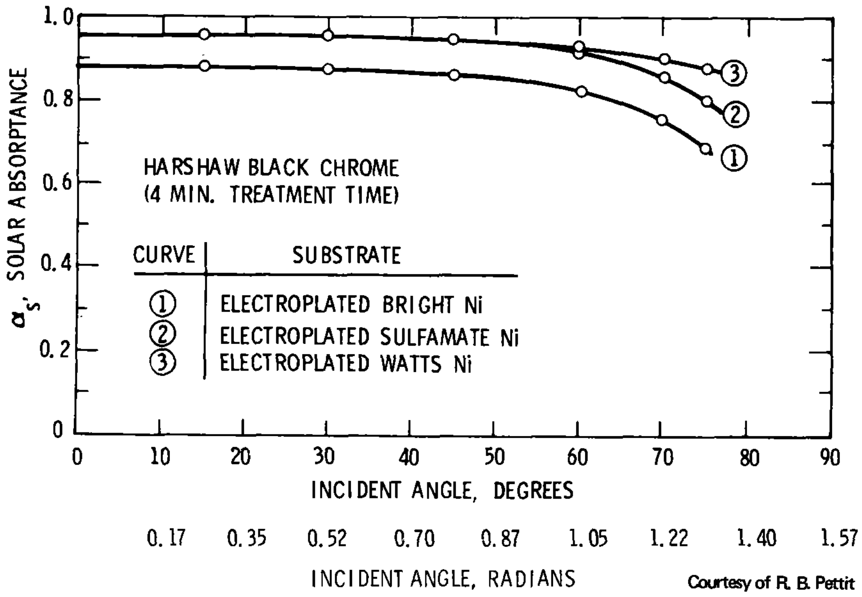

Figure 9 Harshaw Black Chrome (4 Minute Treatment Time)

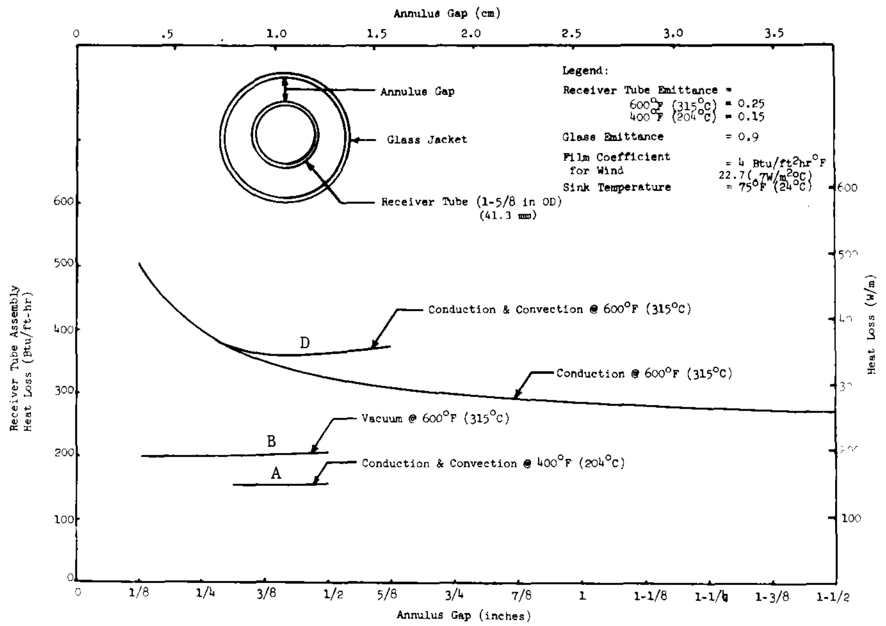

Figure 10 Results Obtained From Equation (1)

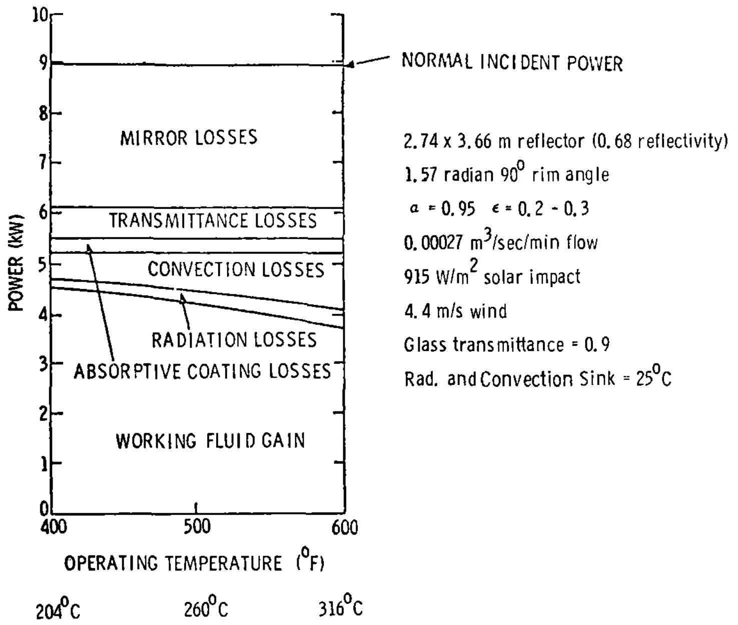

Figure 11 Collector Power Losses

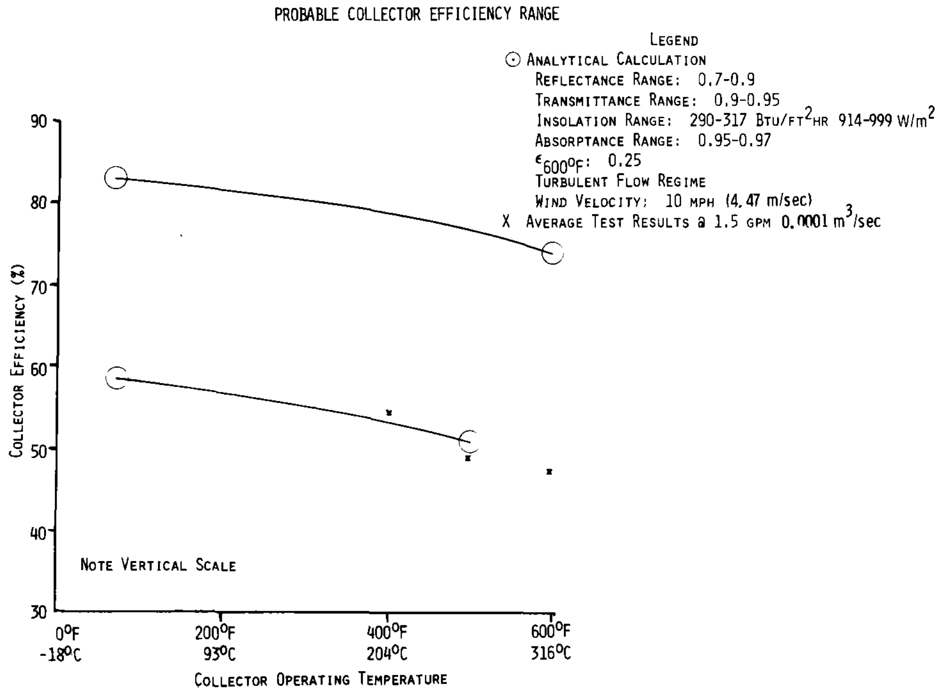

Figure 12 Probable Collector Efficiency Range

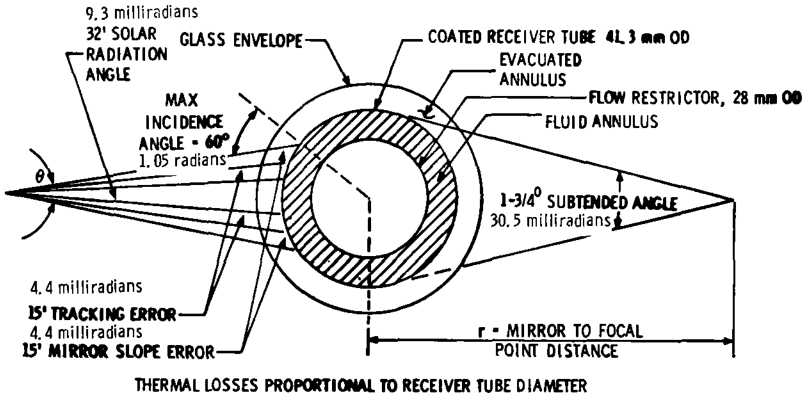

$$\text{RECEIVER TUBE DIAMETER} = \frac{2r \sin \theta/2}{\sin 60^{\circ} \sin (\text{RIM ANGLE})}$$

Figure 13 Receiver Tube Assembly Cross Section

RIM ANGLE SELECTION

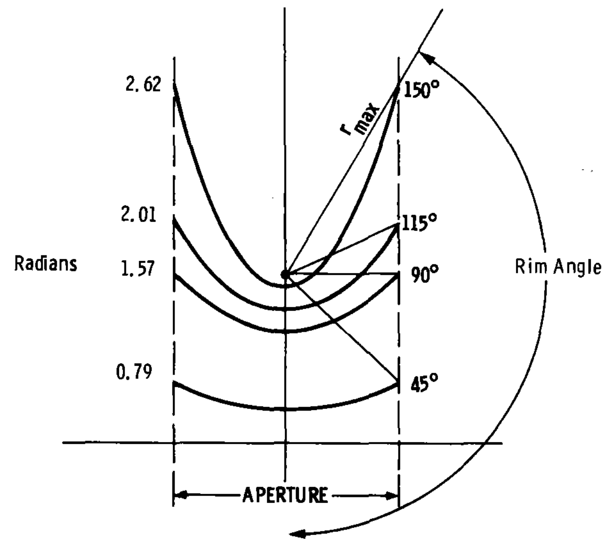

FOR COMMON FOCUS AND FIXED APERTURE:
r_{max} IS MINIMUM @ RIM ANGLE OF 90°

Figure 14 Various Rim Angles for Common Aperture

ENERGY DEPOSITION ROUTINE STATISTICALLY INCORPORATES:

- SUN'S SHAPE
- MIRROR SLOPE ERRORS
- SPECULAR SURFACE REFLECTIONS
- TRACKING ERRORS
- OFF-AXIS RECEIVER

$$\sigma^2_{SYSTEM} = \sigma^2_{SUN} + 4\sigma^2_{SLOPE} + \sigma^2_{AIM} + \sigma^2_{REFLECTOR}$$

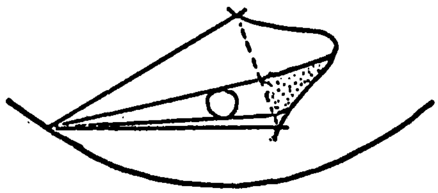

Figure 15 Energy Deposition Routine

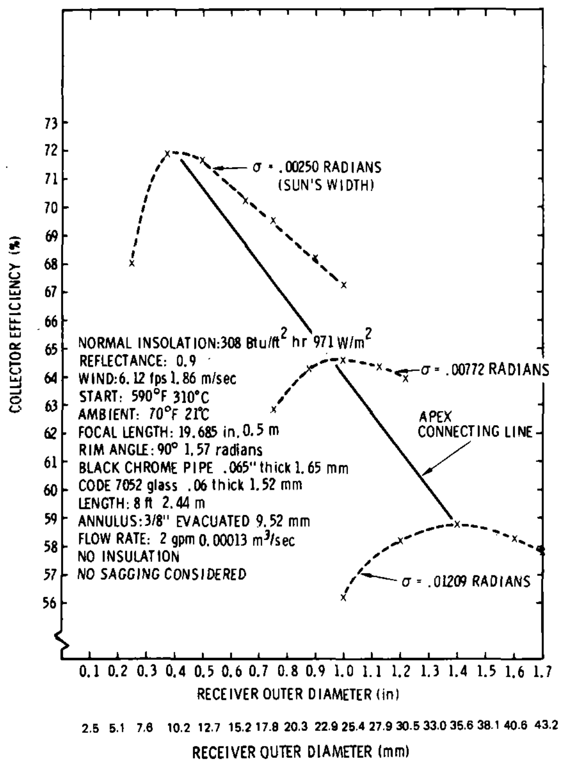

Figure 16 Energy Distribution vs. Collector Efficiency

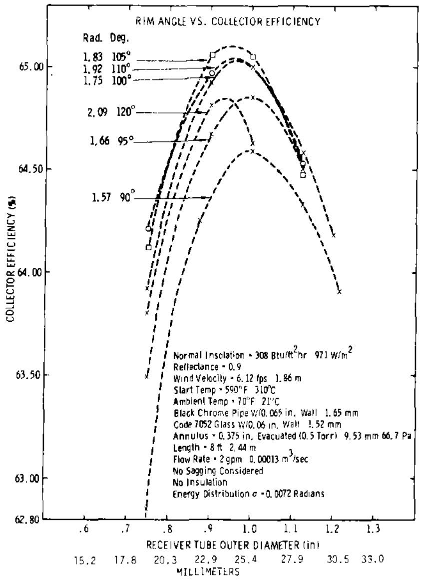

Figure 17 Collector Efficiency vs. Receiver Tube Outer Diameter

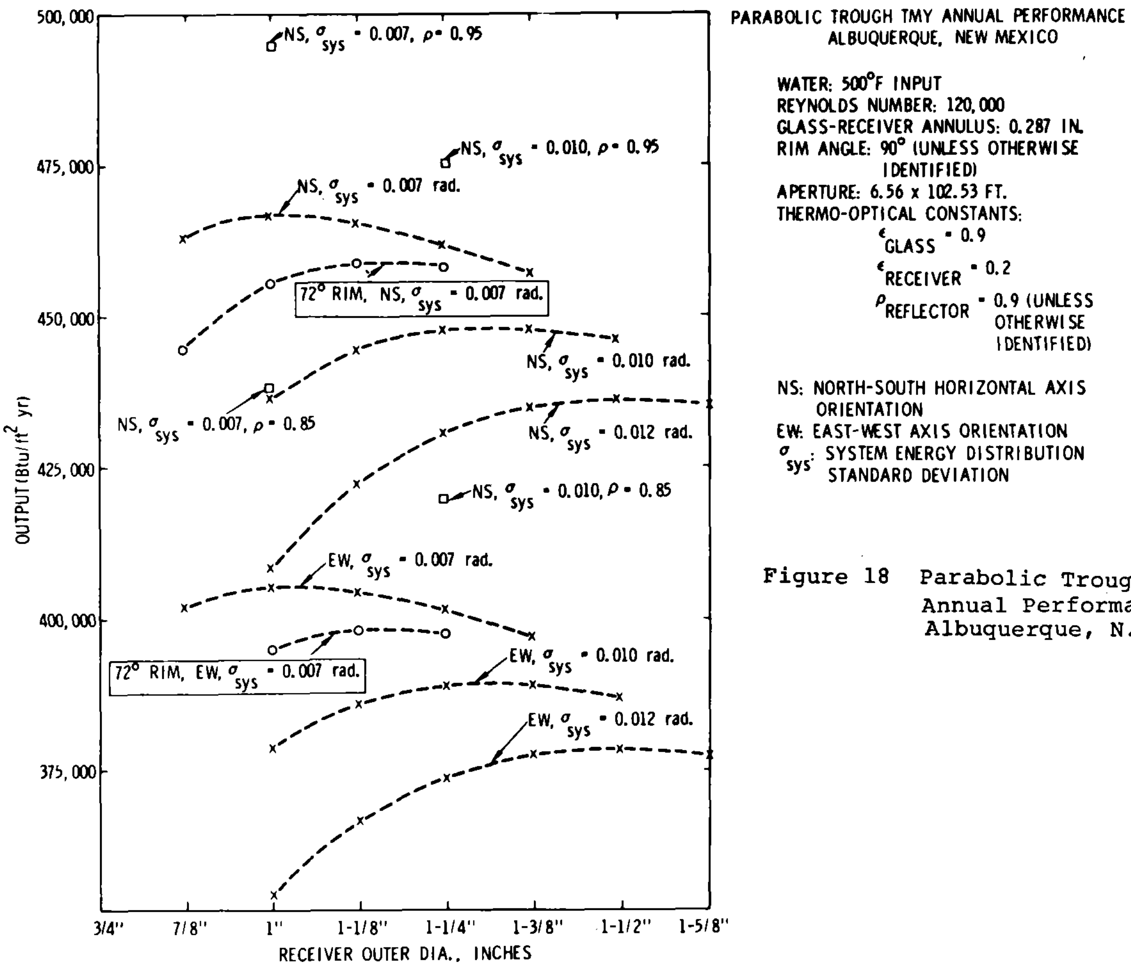

Figure 18 Parabolic Trough TMY Annual Performance, Albuquerque, N. M.

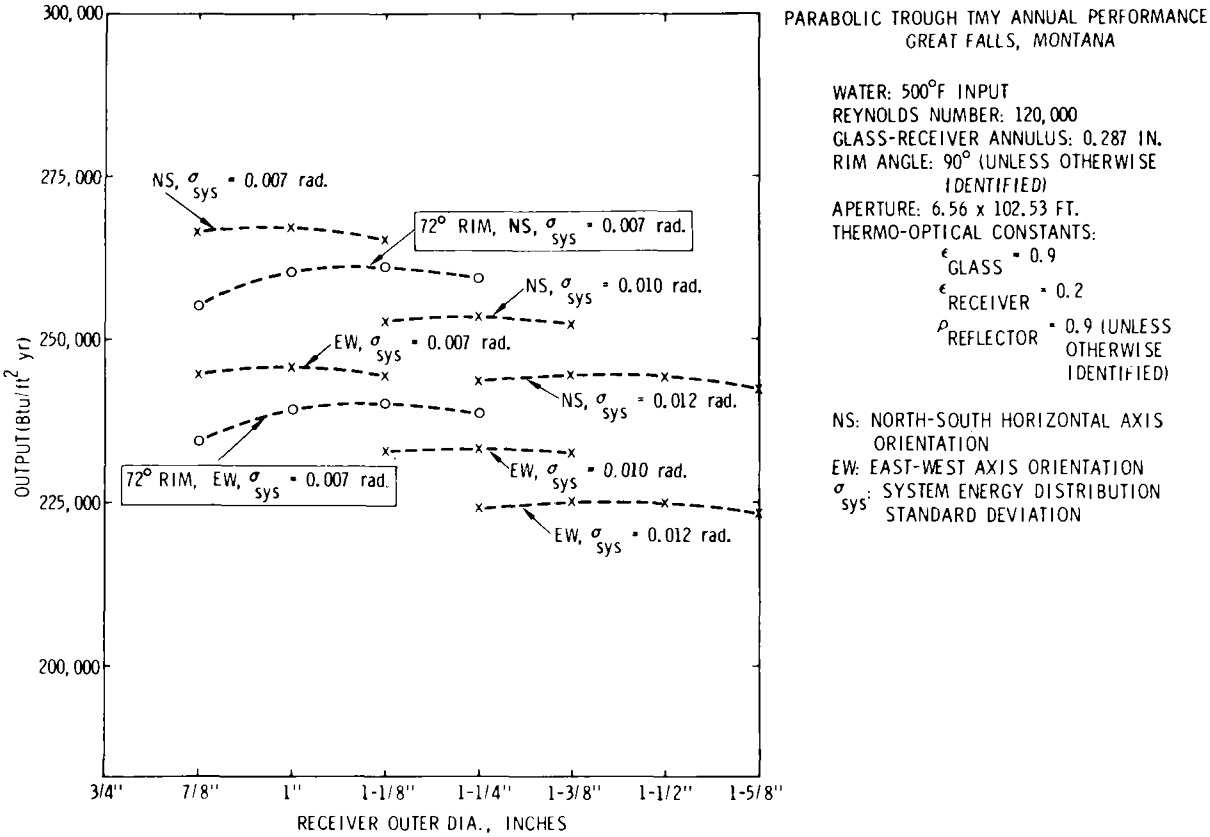

Figure 19 Parabolic Trough TMY Annual Performance, Great Falls, Mt.

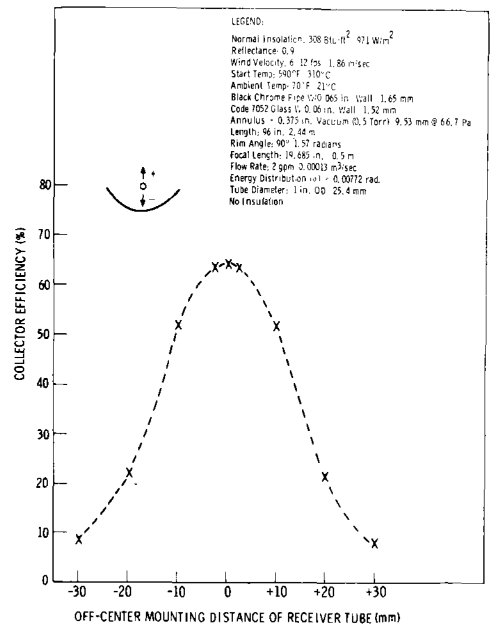

Figure 20 Influence of Off-Center Receiver Tube Mounting

TABLE I

Phase IVB Collector Sizing Considerations

Rim Angle (rad)	Rim Angle (deg)	Approximate Collector Efficiency (%)	Focal Length (mm)	Focal Length (in)	Approx. Optimum Receiver OD (mm)	Approx. Optimum Receiver OD (in)	Arc Length (mm)	Arc Length (in)	Remarks
1.22	70 (Trimmed 90°) 1.57 rad	63.7	500	19.68	22.9	0.9	1.51	59.36	90° Rim Angle Focal Length 1.57 radian 1.4 Metres Aperture
1.40	80 (Trimmed 90°) 1.57 rad	64.3	500	19.68	22.9	0.9	1.85	73.16	90° Rim Angle Focal Length 1.57 radian 1.678 Metres Aperture
0.79	45	55.97	1207	47.52	40.6	1.6	2.06	80.94	2 Metres Aperture
1.05	60	60.6	866	34.10	35.6	1.4	2.11	82.92	2 Metres Aperture
1.22	70	62.4	714	28.11	28.7	1.13	2.15	84.77	2 Metres Aperture
1.40	80	63.8	596	23.46	26.7	1.05	2.21	87.19	2 Metres Aperture
1.57	90	64.6	500	19.68	25.4	1.00	2.30	90.38	2 Metres Aperture
1.66	95	64.9	458	18.04	25.4	1.00	2.35	92.35	2 Metres Aperture
1.75	100	65.0	420	16.52	24.1	0.95	2.40	94.64	2 Metres Aperture
1.83	105	65.1	384	15.10	24.1	0.95	2.47	97.31	2 Metres Aperture
1.92	110	65.0	350	13.78	24.1	0.95	2.55	100.46	2 Metres Aperture
2.09	120	64.8	289	11.37	24.1	0.95	2.76	108.67	2 Metres Aperture

Normal Insulation - 308 Btu/ft^2 hr 971 W/m^2
Reflectance = 0.9
Wind Velocity = 6.12 fps 1.86 m/sec
Start Temp = 590°F 310°C
Ambient Temp = 70°F 21°C
Black Chrome Pipe W/0.65 m Wall 1.65 mm
Code 7052 Glass W/0.06 in. Wall 1.52 mm
Annulus = 0.375 in. Evacuated (0.5 Torr) 9.53 mm 66.7 Pa
Length = 8 ft 2.44 m
Flow Rate = 2 gpm 0.00013 m^3/sec
No Sagging Considered
No Insulation
Energy Distribution σ = 0.00772 Radians

TABLE I Collector Rim Angle Considerations

WIND LOAD DEFINITION FOR LINE-FOCUS CONCENTRATING SOLAR COLLECTORS

Duane E. Randall
Systems and Applications
Development Division 4725
Sandia National Laboratories
Albuquerque, NM 87185

Introduction

A multiplicity of experimental projects has demonstrated the technological feasibility of utilizing solar energy for mechanical and electrical power in addition to direct thermal energy requirements for applications in the low to intermediate temperature regime. However, the current economic characteristics of solar thermal energy sources preclude their widespread application and the commercialization of this technology through the private economic sector. One of the primary factors currently controlling this situation is the total installed cost of these energy systems. A prime contributing factor to this cost lies in the collector rigidity together with support structure and foundation requirements necessary to withstand adverse wind loading. A procedure is outlined herein to enable the designer to define peak wind loads which might be anticipated during the operational lifetime of a solar collector array.

This procedure is intended to provide the information necessary to the preparation of economical collector and foundation design characteristics while simultaneously meeting the necessary safety and reliability constraints for line-focus concentrating collector arrays.

Load Definition

The American National Standards Institute's A58.1-1972[1]* (Section 6) defines procedures for calculating minimum design

*The 1972 version is the latest revision currently in publication. However, the reader should be aware that a revised version is currently under review by the committee and is expected to be published in the near future.

wind loads on buildings and other structures subject to building code requirements. The major emphasis herein, and probably with good reason, appears directed at tall multi-story buildings. Generally included in the category of other structures are bridges, tall chimneys or smokestacks, and cranes. No specific provisions appear directed at low profile multiple module structures representative of line-focus solar collector arrays. However, alternate provisions are being incorporated in this standard whereby wind tunnel tests which provide an appropriately simulated test environment may be utilized to define loads for configurations and structures having unique characteristics which warrant special consideration.

The forces and moments experienced by a body immersed in a fluid flow are customarily defined by Equations (1) and (2):

$$F_i = C_i \, q \, A_R \tag{1}$$

$$M_i = C_{M_i} \, q \, A_R \, L_R \tag{2}$$

where

F_i = force component along coordinate i direction.

M_i = moment component about axis in coordinate i direction.

C_i, C_{M_i} = dimensionless force and moment coefficients, respectively, which are representative of the load characteristics of the body for coordinate direction i.

q = dynamic pressure of the flow field, generally representing the undisturbed state upstream or that state existing at the body location in its absence.

A_R = a reference area, generally selected to be representative of a plane area presented to the flow by the body, here chosen as the aperture area of a collector module = aperture width x length.

L_R = a reference length selected to be representative of a characteristic body dimension. Here chosen as the aperture width.

Dynamic Pressure

The dynamic pressure or velocity head of the flowing fluid is defined by:

$$q = 1/2 \, \rho \, V^2 \tag{3}$$

where

ρ = fluid density

V = fluid velocity

Reference (1) provides data and incorporates provisions for estimating the peak dynamic pressure to which a structure is likely to be exposed during its lifetime. Factors affecting the selection of an appropriate value include anticipated structure life, degree of risk to life and property, intended operational use, and degree of sensitivity to the wind. Based upon these factors, the standard requires a basic design wind speed based upon a 50-year mean recurrence interval for most occupied building structures and a 100-year mean recurrence interval for emergency facilities utilized for disaster recovery. A wind speed based upon a 25-year mean recurrrence interval is permissible for uninhabited structures or those offering negligible risk to human life.

Line-focus solar collector arrays of rather large area will be required in order to significantly impact the thermal energy requirements of anticipated commercial applications. Thus, a high probability exists for most arrays to be ground-mounted as opposed to roof-mounted installations. Special situations will exist where availability or cost of land or other circumstances may dictate roof-mounted installations.

Ground-mounted solar collector arrays present a negligible degree of risk to life and property under high wind conditions, have a significantly shorter economic life than most multi-story buildings, and would not be relied upon as an emergency energy source during or following severe storm conditions. Thus, a wind speed based upon the mean recurrence interval of twenty-five years, seems appropriate for line-focus solar thermal collector arrays. Where collector arrays are mounted on the roof of occupied buildings, more stringent requirements are appropriate, due to occupant risk, and a 50-year recurrence wind speed is suggested.

Figure 1 presents the annual extreme fastest mile wind speed at 30 feet elevation above terrain for the 25-year mean recurrence interval as presented in Reference (1). These data are based upon a statistical analysis of historical records of hourly observations at National Weather Service stations by Thom.[2] Recently Simiu[3] et al., have extended this data base to 129 stations in the contiguous U.S. adding later observations, correcting for certain instrument location errors present in the original data, and adjusting the data to the new standard anemometer height of 10 meters adopted by the National Weather Service. The data of Simiu covers observation intervals of 10 years to 54 years with the mean being 34 years. Eighty-four percent of these sites have observation intervals of twenty-five years or more. This review serves to reinforce the data illustrated in Figure 1 showing that: excluding the narrow coastal hurricane belt along the Gulf and Atlantic seaboards, the maximum 25-year recurrence fastest mile speed over the contiguous U.S. is 80 miles per hour at a standard 10 meter elevation. It should be pointed out that in addition to the hurricane belt, other special wind regions exist where, due to specific terrain features, flow channeling or focusing may lead to higher wind velocities in highly localized areas. However, the land area covered by these special wind regions together with the hurricane belt represents a very minor fraction of the contiguous U.S. Thus, to require all collectors to meet the design requirements for these areas would be an uneconomical alternative. A better solution would be to incorporate special protective features such as shielding or tie down provisions for installations in these areas. From this same data base the analogous 50-year recurrence fastest mile of wind speed at the standard 10-meter height show a 90 mph maximum again outside the hurricane belt. The use of fastest mile of wind speeds here implies an averaging period of t (secs) defined by:

$$t = 3600/V \qquad (4)$$

Thus, for the data presented in Figure 1, averaging periods are approximately one minute or somewhat less.

Finally, to complete the definition of the wind velocity experienced by collector arrays, a knowledge of the atmospheric boundary layer velocity profile is required. The character of the boundary layer, as defined by its total thickness and the velocity profile over that thickness, is determined by the surface roughness characteristics of the terrain and integral features such as natural growth or man-made structures in the upwind direction. Power law profiles as expressed by Equation (5) have been generally accepted as providing a satisfactory approximation to the atmospheric boundary layer velocity profile.

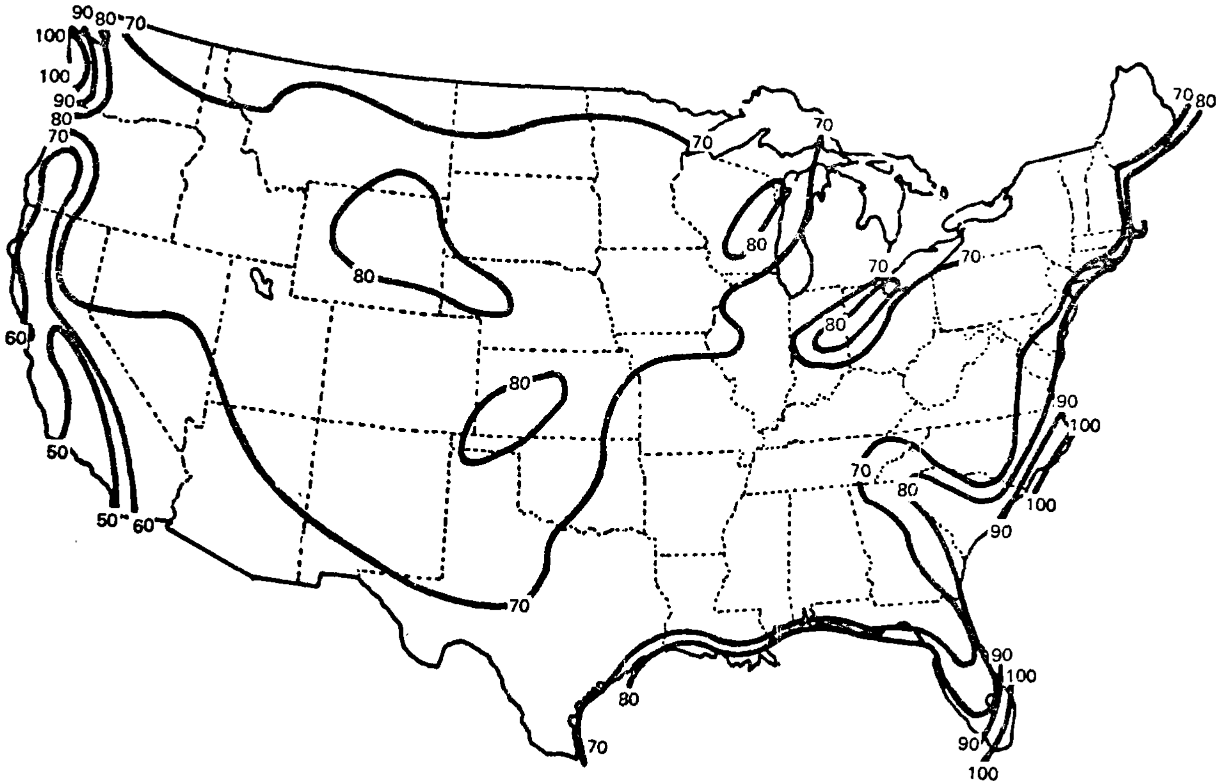

ANNUAL EXTREME FASTEST-MILE SPEED 30 FEET ABOVE GROUND, 25-YEAR MEAN RECURRENCE INTERVAL

Figure 1

Sandia National Laboratories

$$V/V_{ref} = (Z/Z_{ref})^n \qquad (5)$$

where

V = velocity at height Z above surface.

V_{ref} = velocity at a defined reference elevation Z_{ref}.

n = exponent for power law relation

A review and analysis of the literature and meteorological data on atmospheric boundary layers covering the 1880 to 1972 time frame has been summarized by Counihan.(4) His summary of the existing data on boundary layer velocity profile characteristics is summarized in Figure 2 which illustrates the power law exponent as a function of a surface roughness characteristic dimension. The proposed curve illustrated is the authors interpretation of the most accurate representation of all the data. The dashed lines represent his estimate of probable upper and lower scatter limits. The roughness length scale has been divided into four typical terrain categories to define useful boundary layer velocity profiles. These terrain categories together with representative descriptive features are:

I - Smooth surface: calm sea, ice, snow, mud flats.

II - Moderately rough: open flat terrain, rural grassland, and crops.

III - Rough: surburban with many houses, rural woods, or forested.

IV - Very rough: urban city centers, densely built up multi-story structures.

Earlier, Davenport(5) and Vellozzi and Cohen(6) had recommended values for the boundary layer thickness (δ) and the power law exponent (n) for terrain categories A, B, and C which correspond to categories II, III, and IV, respectively. A comparison of their values together with values calculated from Counihan's expression evaluated at the average roughness length for each terrain category is presented in Table I.

TABLE I

Terrain Category	I Very Smooth		II Open Flat		III Suburban		IV City Center	
	n	δ (meters)	n	δ (meters)	n	δ (meters)	n	δ (meters)
Davenport	-	-	0.16	275	0.28	400	0.40	520
Vellozzi & Cohen	-	-	1/7	275	1/4.5	400	1/3	460
Counihan	0.099	-	0.161	-	0.233	-	0.322	-

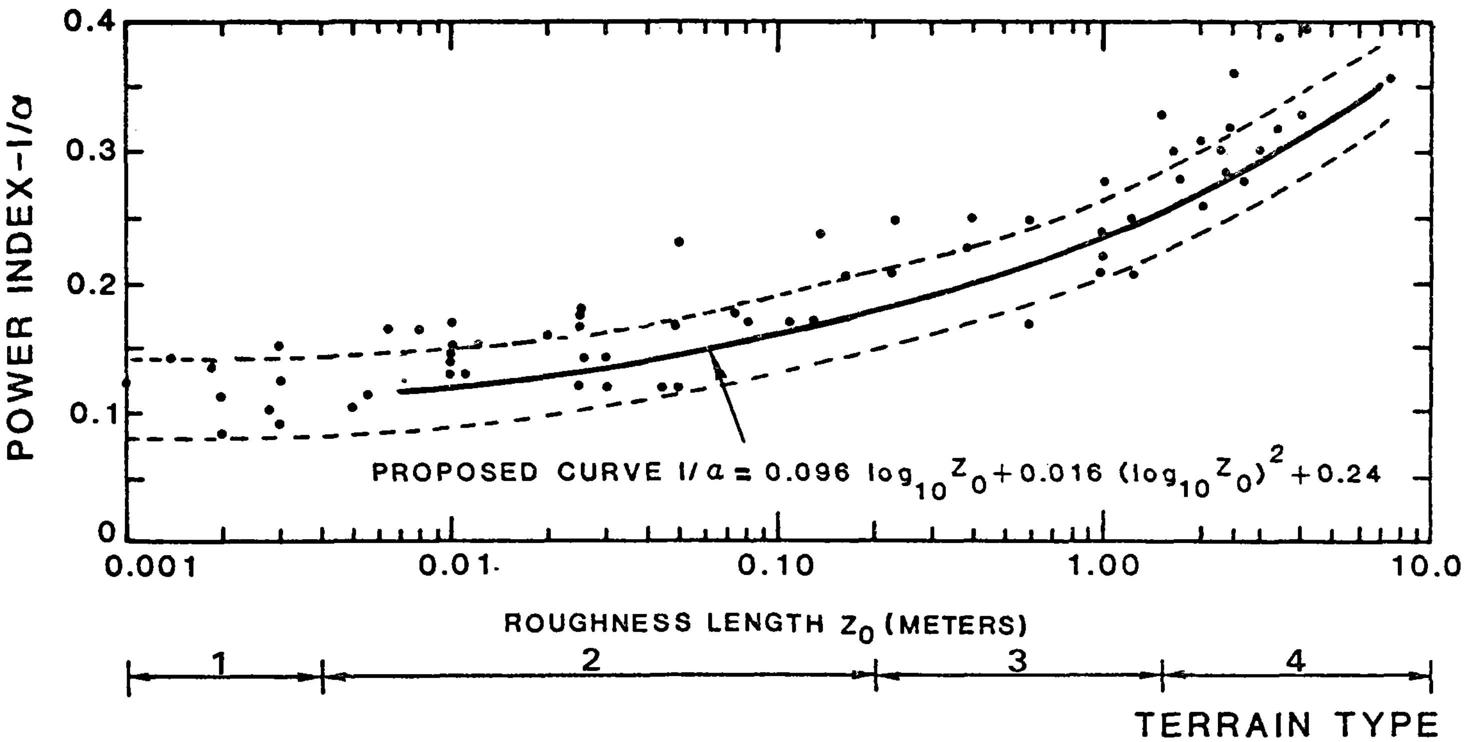

Figure 2

Sandia National Laboratories

These data exhibit good agreement with the curve of Counihan generally lying between the values recommended by the other two writers. Davenport's recommendations are incorporated in the Canadian standard while the American standard is based upon the values of Vellozzi and Cohen. Their values are slightly conservative (give a higher velocity and dynamic pressure) and will be utilized herein.

Dynamic pressure profiles for the first ten meters elevation based upon the power law exponents of References (5) and (6) are illustrated in Figure 3. The dynamic pressure here has been nondimensionalized by a 10-meter elevation reference value based upon the Vellozzi and Cohen category II (open flat) profile. The dynamic pressure profiles illustrated for the other terrain categories and for Davenport's power law exponents are based upon a constant geostrophic wind velocity; that is, the wind velocity existing at the upper edge of the boundary layer. Thus, the wind velocity existing at 275 meters over open terrain also exists at 400 meters over suburban terrain and at 460 meters over a city center area (520 meters for the Davenport profile).

Atmospheric density is a function of elevation from mean sea level and local weather conditions. A tabulation of air density versus elevation for standard atmospheric conditions is presented in Reference (7). Weather-caused variations are generally within $\pm$ 7.5% of these standard atmospheric values for elevations under 10,000 ft. The standard sea level value is recommended for collector design requirements. However, for certain site specific features of an installation, as perhaps foundations, advantage could be taken of a lesser value resulting from site elevation for instance.

These data permit the calculation of anticipated peak dynamic pressures to which a collector installation will be exposed over its lifetime. Few collector array installations are expected to be installed in locales representative of Category I. Category II, however, is appropriate for most irrigation applications as well as many process heat and other thermal applications. These array installations will typically be the ground-mounted variety. Rooftop collector array installations are expected to be located in more heavily built up suburban areas representative of Category III. It is not expected that any sizeable array installations will be found in locales

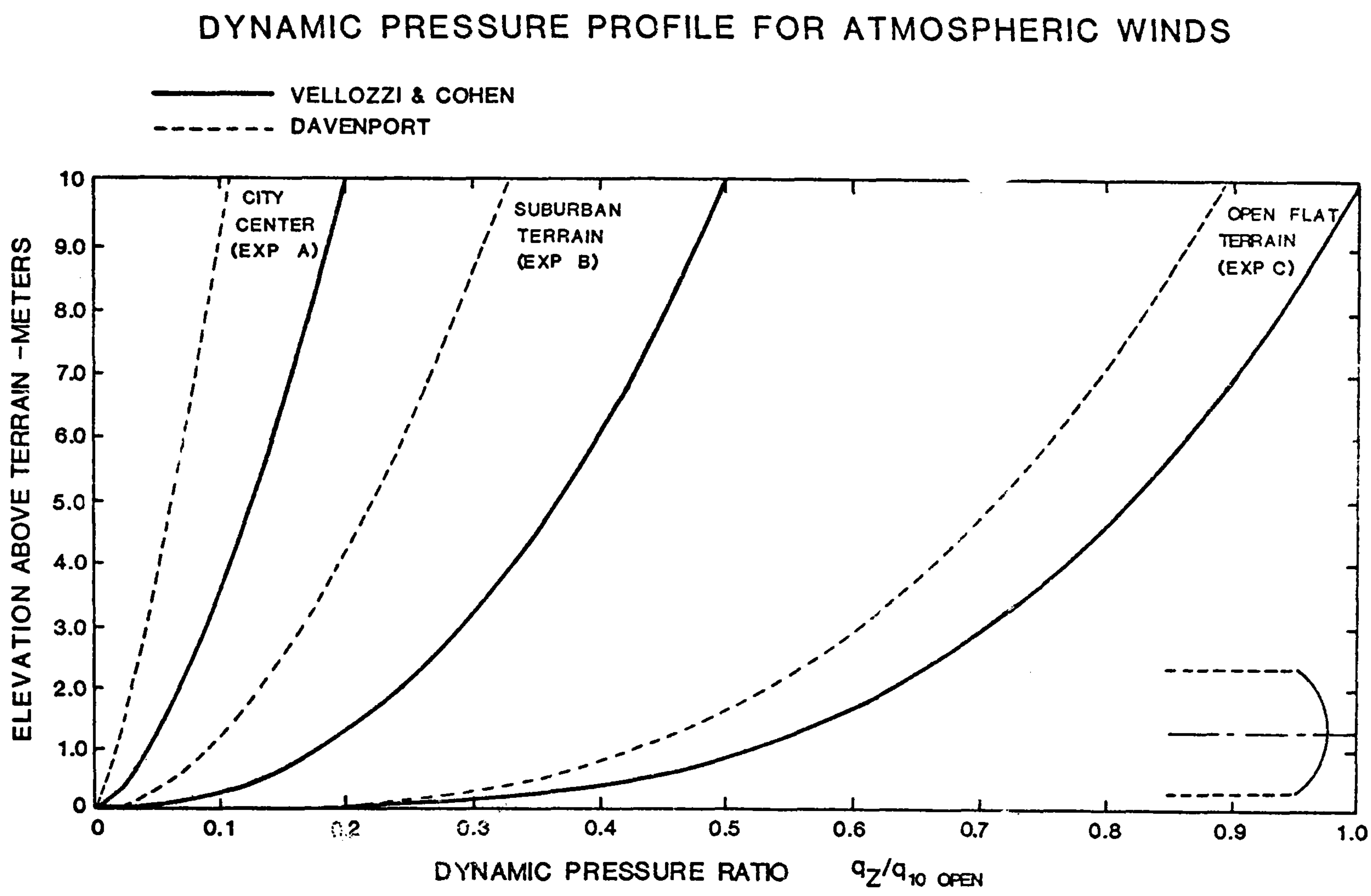

Figure 3

Sandia National Laboratories

representative of Category IV. Example calculations of dynamic pressure design values and the corresponding load levels for arrays representing a ground-mounted open terrain installation and a suburban roof-mounted installation have been carried out in the Appendix. The results of these calculations indicate that a dynamic pressure design value of 10 pounds per square foot serves suburban roof-top installations under 30 feet height as well as ground-mounted installations in open flat terrain.

Aerodynamic Load Coefficient

Experimental data representing the load characteristics of parabolic trough line-focus collector configurations has been obtained in two wind tunnel test series. The first test was conducted on single collector modules in the Vought Corporation Low Speed Wind Tunnel which provides an inviscid uniform flow field. A second test series was conducted on individual trough modules as well as multiple row array configurations in the Meteorological Wind Tunnel at the Colorado State University. This facility provides the capability of simulating the atmospheric boundary layer profile with respect to both velocity and turbulence intensity profiles. The influence of selected geometric design parameters for parabolic trough collector configurations has been established. Tabulations of the data are presented in wind tunnel test reports.[8][9] An analysis and summary of the lateral and lift force coefficient and pitching moment coefficient data for single trough modules as well as for trough modules embedded within a collector array is presented in References (10) and (11).

Gust Factors

The wind, particularly within the atmospheric boundary layer, is a highly variable commodity undergoing rapid fluctuations with respect to both speed and direction. The response of a structure to this cyclical loading is dependent upon the frequency of the applied loading, the natural vibrational frequency of the structural materials, and the structure's inherent damping characteristics.

The procedures of Reference (1) incorporates so-called gust factors to account for the structural response of buildings to the cyclical nature of the wind loading. These gust factors have been defined through a procedure based upon the calculation of deflections resulting from the imposition of a given kinetic energy spectrum to the building or structure. The gust factors of Reference (1) are based upon a kinetic energy spectrum selected to be a composite of typical spectra derived from wind records taken in the 15-meter (50 ft) to 152-meter (500 ft) height regime. The deflection calculation has been carried out for tall flexible buildings fixed at one end.

It is not currently clear to the writer that the configurations and the data base upon which the existing gust factors are evaluated are equally appropriate for multiply-supported multiple module collector rows within ten meters of the ground. Additional research is needed to validate the application of current gust factors to ground-mounted collector rows or to develop more appropriate values.

<u>Summary</u>

- o A procedure has been defined for calculating anticipated dynamic pressure design values and the corresponding wind loads experienced by line-focus concentrating solar collectors.
- o Experimental data defining the aerodynamic load characteristics for parabolic trough solar collector configurations has been obtained in two wind tunnel test series.
- o Additional research is needed in two areas to complete the definition of aerodynamic characteristics for parabolic trough solar collector configurations.
  - a) correlation of scale model wind tunnel test results to full scale collector load data.
  - b) definition of the aerodynamic pressure distribution over the parabolic trough reflector for structural design requirements.

  Two new test programs have been initiated to fulfill these requirements. A test to obtain pressure distribution data on scale collector models in the controlled environment of an atmospheric boundary layer wind tunnel facility has been undertaken. In addition, a full scale parabolic trough collector module with pressure and torque instrumentation will be deployed in a field experiment array to obtain field data on pressure distribution and pitching moments. Some field data on lateral and lift force components has recently been obtained at the Willard solar irrigation experiment.

- o Additional research is required to define appropriate values for gust factors which account for the cyclical nature of the wind loading for line-focus collector modules.

References

1) Building Code Requirements for Minimum Design Loads in Buildings and Other Structures, ANSI A58.1-1972, American National Standards Institute, Inc., 1972.

2) Thom, H.C.S., New Distributions of Extreme Winds in the United States, Journal of the Structural Division, ASCE Vol. 94, No. ST7, July 1968.

3) Simiu, E., Changery, M. J., and Filliben, J. J., Extreme Wind Speeds at 129 Stations in the Contiguous United States, NBS Building Science Series 118, National Bureau of Standards, March 1979.

4) Counihan, J., Review Paper, Adiabatic Atmospheric Boundary Layers: A Review and Analysis of Data From the Period 1880-1972. Atmospheric Environment, Vol. 9, 1975.

5) Davenport, A. G., The Relationship of Wind Structure to Wind Loading, Proceedings of the Symposium on Wind Effects on Buildings and Structures, Vol. I, National Physical Laboratory, Teddington, U.K., Her Majesty's Stationary Office, London, 1965.

6) Vellozzi, J., and Cohen, E., Dynamic Response of Tall Flexible Structures to Wind Loadings in Proceedings of the Technical Meeting Concerning Wind Loads on Buildings and Structures, Building Science Series 30, National Bureau of Standards, Washington, D.C., 1970.

7) 1962 U.S. Standard Atmosphere Washington, D.C., 1962.

8) Lindsey, J. L., "Force and Pressure Tests of Solar Collector Models in the Vought Corporation Systems Division Low Speed Wind Tunnel (LSWT 503)," SAND76-7007, May 1976.

9) Peterka, J. A., Sinou, J. M., and Cermak, J. E., "Mean Wind Forces on Parabolic Trough Solar Collectors," SAND80-7023, May 1980.

10) Randall, D. E., McBride, D. D., and Tate, R. E., Steady-State Wind Loading on Parabolic Trough Solar Collectors, ASME Century 2 Solar Energy Conference, San Francisco, CA, August 1980.

11) Randall, D. E., McBride, D. D., and Tate R. E., Steady-State Wind Loading on Parabolic Trough Solar Collectors, SAND79-2134, September 1980.

Appendix A

Two sample calculations are carried out to illustrate the application of the procedures and collector design philosophy outlined in this document.

Example I.

Given a ground-mounted array of 2 m x 6 m (6.56 ft x 19.69 ft) collector modules installed in Category II (open flat) terrain. Modules are installed with trough center line 1.5 m (4.92 ft) above ground.

Reference Area (A_R) = 2 x 6 = 12 m^2 (129.2 ft^2).
Reference Length (L_R) = 2 m (6.56 ft).
Basic Design Wind Speed* = 80 MPH (117.3 ft/sec) (at 10-meter elevation, 25-year recurrence).

$$\text{Velocity at Collector } ℄ = 117.3 \left(\frac{1.5}{10}\right)^{1/7} = 89.5 \text{ ft/sec.}$$

$$q_{10_{\text{open}}} = 0.5\,(0.002377)(117.3)^2 = 16.35 \text{ lbs/ft}^2.$$

$$q \text{ at Collector } ℄ = 0.5\,(0.002377)(89.5)^2 = 9.5 \text{ lb/ft}^2.$$

(Note: from Figure 3 $q_{1.5}/q_{10_{\text{open}}} = 0.5816$.)

$$\text{Geostrophic Wind Speed @ 275 m} = 80\left(\frac{275}{10}\right)^{1/7} = 128 \text{ MPH}$$
(188 ft/sec).

Assuming, for parabolic trough collector modules in an array protected with a wind screen fence, lateral and lift force, and pitching moment coefficients equal respectively to 0.5, ± 0.5, ± 0.35 these respective loads are:

---

*The 10-meter elevation basic wind speed data is based upon National Weather Service anemometer stations which, largely, are located at airfields. Thus, this data base, in general, has been accumulated for velocity profiles representative of Category II (open flat) terrain.

Lateral Force F_X = 0.5 (9.5) 129.2 = 614 lbs.
Lift Force F_Z = $\pm$ 0.5 (9.5) 129.2 = $\pm$ 614 lbs.
Pitching Moment M_θ = $\pm$ 0.35 (9.5) 129.2 (6.56) = + 2818 ft lbs.

Note: The loads calculated here do not include a gust factor to account for the cyclical nature of the wind about the fastest mile mean value.

Example II

Given the same collector array mounted on a building roof in a suburban area representative of Category III terrain. The collector centerline is 10 m (32.8 ft) above ground.

Basic Design Wind Speed* = 90 MPH (132 ft/sec) (at 10-meter elevation, 50-year recurrence).

Geostrophic Wind Speed @ 275 m = $90\left(\frac{275}{10}\right)^{1/7}$ = 144.5 MPH (212 ft/sec).

This geostrophic wind speed exists at 400 m over Category III terrain.

Velocity at Collector ℄ = $212\left(\frac{10}{400}\right)^{1/4.5}$ = 93.4 ft/sec.

q at Collector ℄ = 0.5 (0.002377) $(93.4)^2$ = 10.4 lb/ft^2.
(Note: from Figure 3, $q_{10_{sub}}/q_{10_{open}}$ = 0.50 @ 90 MPH $q_{10_{open}}$ = 20.7 lb/ft^3.

Thus, a rooftop installation at 10 m height in suburban-type terrain experiences a dynamic pressure only 9.5% greater than a ground-mounted installation at 1.5 m in open terrain and proportionately higher load levels.

---

*See previous footnote, pp. A1.

FOUNDATIONS FOR LINE FOCUSING SOLAR COLLECTORS

Harry E. Auld
Higgins, Auld & Associates, Inc.
2601 Wyoming Blvd., N.E., Suite H-1
Albuquerque, New Mexico 87112
(505) 296-5563

A line focusing solar collector system is subject to aerodynamic and mechanical (e.g., torgue from the drive mechanism) forces which result in fairly unique foundation loading conditions. These forces can be resolved into a single equivalent eccentric inclined load which is applied to the foundation-pylon system as illustrated in Figure 1. Note that the inclined load normally has an upward component. The design of foundations for the given loading environment is not straightforward and there are limited field test data available which is immediately applicable.

Because of these factors, as well as uncertainties associated with the magnitude of the applied aerodynamic forces, extremely conservative foundation designs have been executed for many of the solar collector systems built to date. These designs have historically resulted in foundation construction costs ranging from \$2-\$5 per square foot of collector aperture. A recent engineering estimate for a prototype collector field (Reference 1) indicated foundation construction costs of less than \$1 per square foot of collector aperture for foundations designed on the basis of the concepts presented in this paper.

A theoretical study was conducted for Sandia National Laboratories to determine the most cost effective foundation design for typical solar collector systems (Reference 2). The study concluded that a reinforced concrete cylindrical cast-in-place pier was the most economical configuration and recommended that this type of foundation be utilized whenever site conditions would permit. In addition, Reference 2 presented a rigid-pile theory which is applicable to the design of cost effective pier foundations.

The aerodynamic loads utilized for future foundation design should be based upon recent work accomplished by Colorado State University (Reference 3). Both theoretical and experimental research have been accomplished to take account of shielding from perimeter fencing and adjacent solar collector troughs. Equivalent design loads for a typical 6-1/2 ft x 80 ft (2 m x 24 m) drive string length are given in Table 1. It should be noted that the survival loads are calculated for a 50 year wind of 90 mph (this maximum design wind has been recently reduced to 80 mph). The survival loads may never occur during the lifetime of a system. In addition, they would probably result from wind gusts and would be applied to the structure for relatively short durations. Additional discussion of anticipated wind loads is presented in Reference 4.

The basic equations applicable to any rigid-pile theory are summarized in Figure 2. The ultimate vertical capacity (Q_{uv}) depends upon the buried surface area of the pier and the soil resistance (R). R is determined from basic soil parameters, as indicated in Figure 2. The ultimate horizontal capacity (Q_{uh}) depends upon the same basic soil parameters, the geometry (L, e, and D), and the assumed soil reaction distribution. Generally a rectangular distribution is utilized for cohesive soils and a triangular distribution is utilized for granular soils. Statics can be utilized to derive an equation for Q_{uh} for any assumed distribution. Recommended equations for both Q_{uv} and Q_{uh} are presented in Reference 2. Since the applied load has both vertical and horizontal components, an interaction equation is suggested for use in caluclating the combined capacity

$$\frac{P_{u\Theta} \cos\Theta}{Q_{uv}} + \left(\frac{P_{u\Theta} \sin\Theta}{Q_{uh}}\right)^2 \leqslant 1$$

A factor of safety of three (3) is normally utilized to calculate the ultimate load ($P_{u\Theta}$) from the design load (P_{Θ}).

Table 2 summarizes the foundation dimensions calculated for the design loads given in Table 1. A variety of soil parameters (Φ and c) were considered which might be encountered at typical solar collector sites throughout the United States. The cohesion values of 2500 and 1000 psf are associated with a range of clay materials which would be rated as typical and poor sites, respectively. The Φ angles of 42 and 30 degrees are associated with a range of granular materials which again would be rated as typical and poor sites, respectively. The material with both cohesion and internal friction values might be associated with a silty- or clayey-sand. Note that the lengths for all assumed conditions are quite short (< 9 ft).

Two experimental field test programs have been conducted to determine the capacity of reinforced concrete cylindrical cast-in-place piers which are directly applicable to the design of foundations for line focusing solar collector systems. The first program was conducted at the Collector Module Test Facility on Kirtland Air Force Base, New Mexico (Reference 5). The pier dimensions, predicted capacities, and measured capacities are summarized in Table 3. There was insufficient reinforcement provided to achieve the predicted horizontal loads. In every instance, the reinforced concrete section failed prior to the complete mobilization of the soil strength under the application of eccentric horizontal loads. The vertical capacity of the 18 inch diameter piers could not be determined because of equipment limitations, i.e., the load cell utilized could not accept a load in excess of 20 kips. Based upon these extremely limited experimental results, it can be concluded that it is imperative that the reinforced concrete section have sufficient strength to achieve the full capacity of the foundation system. In addition, the theory described is in good agreement with the measured vertical capacities.

The second program was conducted at a site in Shenandoah, Georgia where a double-axis-tracking solar collector system will be constructed (Reference 6). The pier dimensions, predicted capacities, and measured capacities are presented in Table 4. The predicted results are in good agreement with both the horizontal and vertical ultimate capacities. In two instances, the reinforced concrete section failed prior to the complete mobilization of the soil strength under the application of eccentric horizontal loads. It is interesting to note that the $L = 6.1$ ft pier provided a F.S. $\simeq 3$ for the horizontal survival load given in Table 1. The same pier provided a F.S. > 100 for the corresponding vertical survival load. It can be concluded on the basis of these results that the vertical load is unimportant to the design of foundations for the load combinations indicated in Table 1. Accordingly, the horizontal eccentric load will dominate the design and the interaction equation previously given need <u>not</u> be considered.

Another field test program has been planned and is awaiting execution. It will be conducted at a new location on Kirtland Air Force Base in the general vicinity of the Collector Module Test Facility. The approach presented in this papaer has been utilized to design pier foundations to resist the loading conditions given in Table 1. These results will be published in a forthcoming report.

The experimental field test programs confirm that the basic rigid-pile theory presented can be utilized, with appropriate soil parameters for the specific location of interest, to predict the ultimate capacity of pier foundations to both eccentric horizontal and axial vertical loads. The horizontal capacity controls the foundation design for loading conditions of typical interest. The corresponding vertical capacity is on the order of 100 times larger than the anticipated vertical load. The predicted horizontal capacities can be attained only if sufficient structural strength is provided to insure that the full soil strength is mobilized. Utilization of these principles, along with good interface management and construction practice, will result in cost effective foundations for line focusing solar collector systems.

Acceptance of these design concepts has been slow in spite of the good agreement between theory and field test results and the potential cost savings. A portion of the reluctance appears to be based upon the fact that it is easier to utilize the conservative approaches from standard codes instead of spearheading new approaches which can also be justified under the general code provisions. A technical paper is currently being prepared for publication in the ASCE Journal and continued emphasis is being placed upon presenting papers at symposiums, such as this one. Your help is required to insure that these concepts are accepted now.

---

1. Auld, H.E. and West, J.B., Solar Collector Foundation Design, SAND80-7070, Sandia Laboratories, Albuquerque, New Mexico, in publication.

2. Auld, H.E. and Lodde, P.F., Study of Low Cost Foundation/Anchor Designs for Single-Axis-Tracking Solar Collector Systems, SAND78-7048, Sandia Laboratories, Albuquerque, New Mexico, January 1979.

3. Peterka, J.A., Sinou, J.M., and Cermak, J.E., Mean Wind Forces on Parabolic-Trough Solar Collectors, SAND80-7023, Sandia Laboratories, Albuquerque, New Mexico, May 1980.

4. Randall, D., "Wind Load Data," paper presented at the Fourth Project Integration Meeting, Photovoltaic Concentrator Technology Development Project, sponsored by Sandia Laboratories, Albuquerque, New Mexico, 16-17 October 1979.

5. Auld, H.E., Analysis of Field Test Results for Single-Axis-Tracking Solar Collector Foundations, SAND79-7023, Sandia Laboratories, Albuquerque, New Mexico, July 1979.

6. Auld, H.E., Design of Field Tests and Analysis of Experimental Results for L.S.E. 7 Meter Collector Foundations, Shenandoah, Georgia, Sandia Laboratories, Albuquerque, New Mexico, November 1979.

TABLE 1. Typical Foundation Design Loads

Pylon Type	Load Component	Operational Loads (37.5 mph)	Survival Loads (90 mph)
Drive	P_h, lb*	655	3750
	P_v, lb**	-470	150
Interior	P_h, lb*	130	750
	P_v, lb**	-470	150

*P_h is assumed to act at an eccentricity of 53 in

**Up is assumed to be positive

TABLE 2. Summary of Foundation Dimensions for Table 1 Loading Conditions

Soil Parameters		Pylon	
Cohesion (c), psf	Angle of Internal Friction (Φ), Degree	Drive (D=18 in) Length, ft	Interior (D=14 in) Length, ft
2500	0	5.6	3.3
0	42	7.0	4.0
1500	35	6.0	3.5
1000	0	8.0	4.3
0	30	8.7	5.0

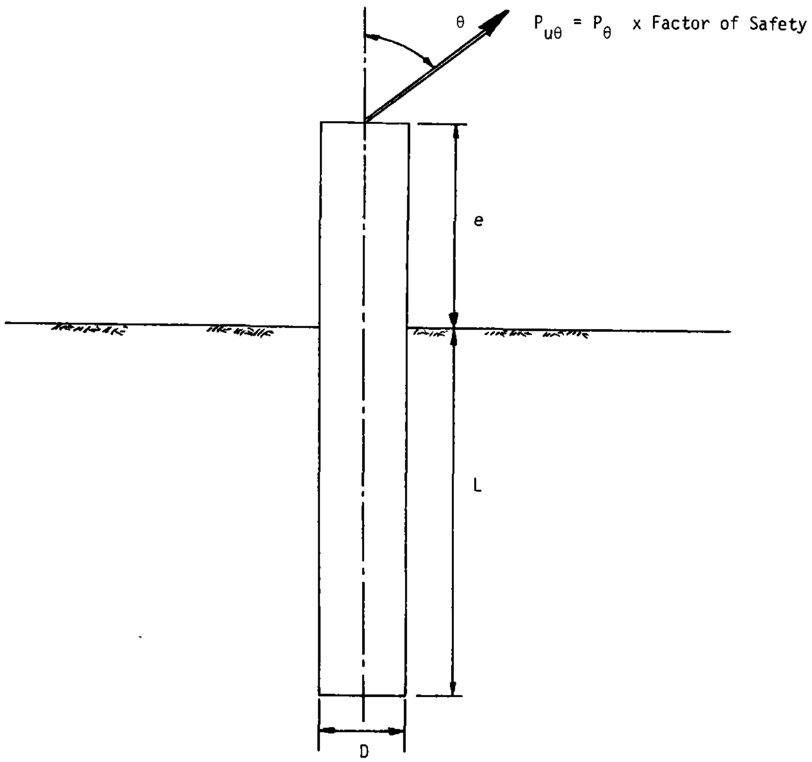

Figure 1. Typical Foundation Loads Resulting from Aerodynamic Forces

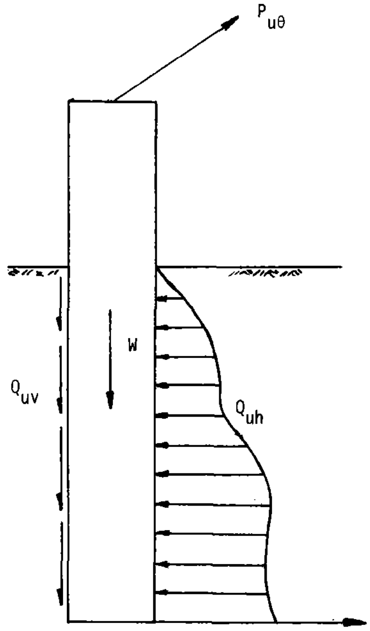

- $\dfrac{P_{u\theta}\cos\theta}{Q_{uv}} + \left(\dfrac{P_{u\theta}\sin\theta}{Q_{uh}}\right)^2 \leqslant 1$
- $Q_{uv} = R\,A_s + W$
- $R = f\,(c,\ \phi,\ \gamma,\ \&\ \delta)$
- $Q_{uh} = f\,(c,\ \phi,\ \gamma,\ L,\ e,\ D,$ & Soil Reaction Distribution$)$
- Statics Utilized to Derive Equations for Q_{uh}

Figure 2. Basic Equations of Rigid-Pile Theory

TABLE 3. Summary of Experimental Results (after Reference 5)

Diameter, in	12	18	18	12	12
Length, ft	7	20	29	12	21
Predicted Q_{uh}, kip	7	20	29	12	21
Predicted Q_{uv}, kip	16	41	50	21	31
Measured Q_{uh}, kip	4*	8*	7*	Not Tested	4*
Measured Q_{uv}, kip	15	>20**	>20**	19	Not Tested

Note: Eccentricity = 42 in, Φ = 35 degree, c = 1500 psf

*Failure load governed by reinforced concrete section

**Limited by test equipment capacity

TABLE 4. Summary of Experimental Results (after Reference 6)

Diameter, in	18	18	18	18
Length, ft	6.1	8.9	8.9	11.0
Predicted Q_{uh}, kip	9	23	23	37
Predicted Q_{uv}, kip	18	35	35	50
Measured Q_{uh}, kip	12	14*	26	29*
Measured Q_{uv}, kip	18	39	39	52

Note: Eccentricity = 51 in, Φ = 35 degree, c = 500 psf

*Failure load governed by reinforced concrete section

PYLONS

Theodore H. Reed
Electromechanical Subsystems Division 2323
Sandia National Laboratories
Albuquerque, NM 87185

Introduction

The component of the line focus collector which mounts the reflector structures and secures them to a suitable foundation is termed the pylon. The pylons also include bearings for rotation of the reflectors by the tracking drive system. When multiple collectors are combined end-to-end into a drive string row, the pylons at different positions provide certain functions which influence their design. The purpose of this paper is to address the design of the pylons. The major design factors will be defined and discussed.

Discussion of Design Factors

To point the discussion in a specific direction, assume a four-trough drive string which will rotate as one unit and which will require five pylons to support it. These five pylons do not share the loads and functions equally, so they need to be designed accordingly. The following sections will discuss the pylon requirements based on the design factors listed below.

Design Factors

1. Design Loads --
   - Static Weight
   - Wind Loads-Drag, Lift, Pitch Moments
2. Stiffness/Rigidity
3. Trough Gap
4. Tracking Center Location
5. Offset Bearing Mount
6. Thermal Expansion
7. Foundation Attachment
8. Bearings

Looking at Figure 1, it can be observed that the five pylons do not share equally in supporting the static weight of the four troughs. The pylons on the end of the row are supporting only half a trough, while the other three pylons must accommodate the static load of an entire trough. The second source of loads on the pylons arises from the wind. The wind, interacting with the four-trough structure, produces drag forces, lift forces, and pitch moments, i.e., rotational moments or torques that must be resisted by the pylons. Again, it may be observed that the end pylons of the row will see drag and lift forces associated with one-half a trough, while the interior pylons will be subjected to loads from an entire trough.

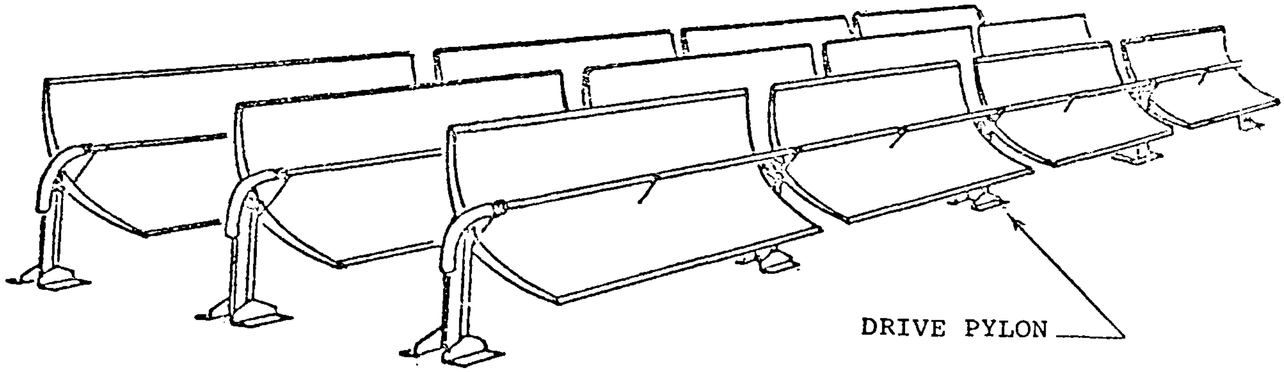

TROUGH COLLECTORS
FIGURE 1

The wind-induced pitch moment interacts with the pylons depending on the drive interface. Assume that the drive system is connected to the center of the drive string with a rigid shaft or torque tube connecting the row of reflector structures. This drive connection locks the rigid rotating system of four-troughs to the center pylon, while the other pylons do not apply any restraint at all on the rotating system. Therefore, the center pylon, termed the drive pylon, becomes unique in that it must sustain and resist the entire rotating structure static unbalance, if any, and the entire wind-induced pitch moment on the four reflector structures.

The rigidity of the pylons must be considered. When the collector is tracking the sun, the five pylons together must support the four troughs sufficiently rigid on a line under variable wind conditions such that the optical performance is not degraded. A second requirement is that the pylons must hold the system sufficiently rigid under survival wind conditions so that damage is not sustained by any collector components effected by flexure down the row.

Another requirement affecting the pylon design is the location of the bearing or tracking center relative to the reflector structure. A bearing center behind the trough would permit direct coupling of a bearing shaft to the trough structure. However, trade studies show that it is advantageous to support the four-trough system near the center of gravity to minimize the static load imposed on the drive system. This means that the bearing center falls inside the reflector contour.* The troughs must now be separated sufficiently for the pylon to have access to the bearing support center. It is desirable, however, to keep this trough gap to a minimum since it creates a cold spot on the receiver tube causing a thermal loss. The location of this bearing center relative to the reflector also affects the attachment of the trough structures to the pylon. The selection of a C.G. rotation center creates an offset mounting situation. Before considering this offset problem further, consider another factor. Ideally, the bearing centers of the five pylons should be assembled to lie on a straight line. Furthermore, straight and square reflector support structures and attaching hardware are needed so that there are no distortions induced during rotation of the system that might degrade the optical properties of the reflector system. Since some nonstraightness and nonsquareness is inherent in the field layout and the hardware, it is necessary to consider its magnitude and the need for compensating devices in the pylon attachment--such as spherical bearings, U-joints, and other flexible coupling devices. Interestingly, the offset mounting requirements between the bearing center and the trough structure does provide a link that might serve as a flexible coupling.

Another requirement on the pylon is to account for the thermal expansion of the reflector structures down the row over the climatic temperature extremes, i.e., from 115°F in the summer to -40°F in winter. A pylon design having high rigidity along the trough row axis to resist

*It is assumed that counterweights are not utilized to move the center of gravity.

high wind loads may require a slip joint at the bearing mount to alleviate this thermal effect. One consideration is that the designation of a center drive on the four-trough system provides a center reference so that only the linear expansion of two troughs each direction from the drive pylon must be considered.

Attachment features must be provided on the base of the pylons to tie them to the foundation. For economy of manufacture, the foundation features for mounting need to be given reasonable allowance on location. The pylon must also be assembled to be reasonably perpendicular to an average plane through the foundations, while the bearing centers are established on a line. A tight trough gap with close fit of the reflectors around the pylon makes the positioning of the pylon more critical on field assembly. It is apparent that some adjustability must be provided at the pylon base and perhaps at the bearing mount as well.

The pylon bearing is a design consideration. The resistance at the bearings to rotation of the four-trough assembly could be a factor in the sizing of the drive system. A choice needs to be made between a journal-type bearing or a rolling element type bearing. Dynamic loading certainly is not a factor. Tracking adjustments make for a continual starting friction situation, and the bearings see less than three quarters of a revolution in the application. Lubrication action could be a problem here, compared to more conventional bearing applications.

Description of Pylons

Proto-typical designs are presented for four of the five pylons needed for the four-trough drive string with a center drive. The drive pylon design is pending definition of the drive system and how it would interface to the pylon. However, a design choice on the drive pylon has been made that is a factor in the design of the other pylons. The drive pylon on its foundation is to have a sufficiently large moment of inertia longitudinally along the four-trough row to minimize that needed from the two pylons on either side of the drive pylon. This is advantageous in the design of the other pylons in two ways. One is that the other pylons can be made thin along the row. This provides a minimum trough gap at the intermediate pylons. The other advantage is

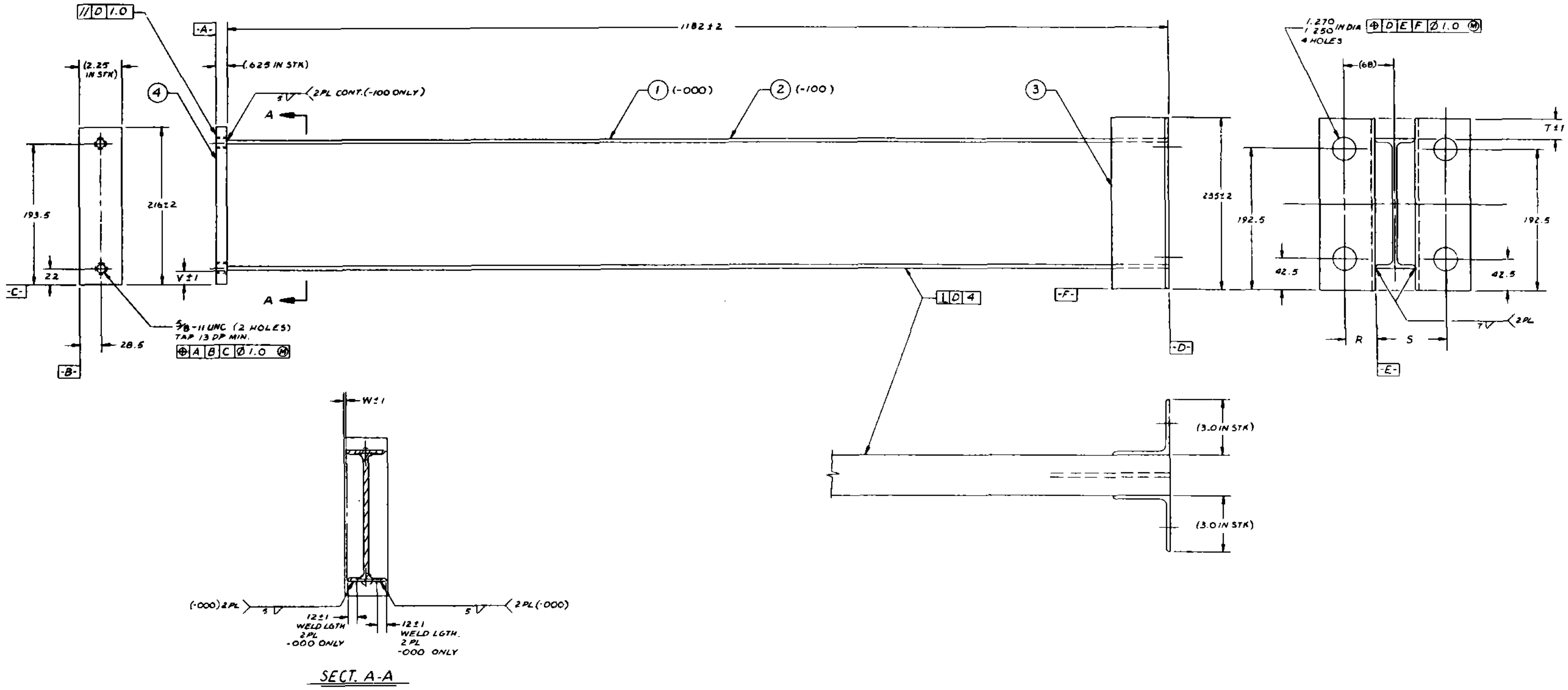

END & INTERMEDIATE PYLONS

FIGURE 2

NOTES:

1) End pylon - 6" junior beam
2) Intermediate pylon - 8" junior beam
3) Dimensions in millimeters unless otherwise noted

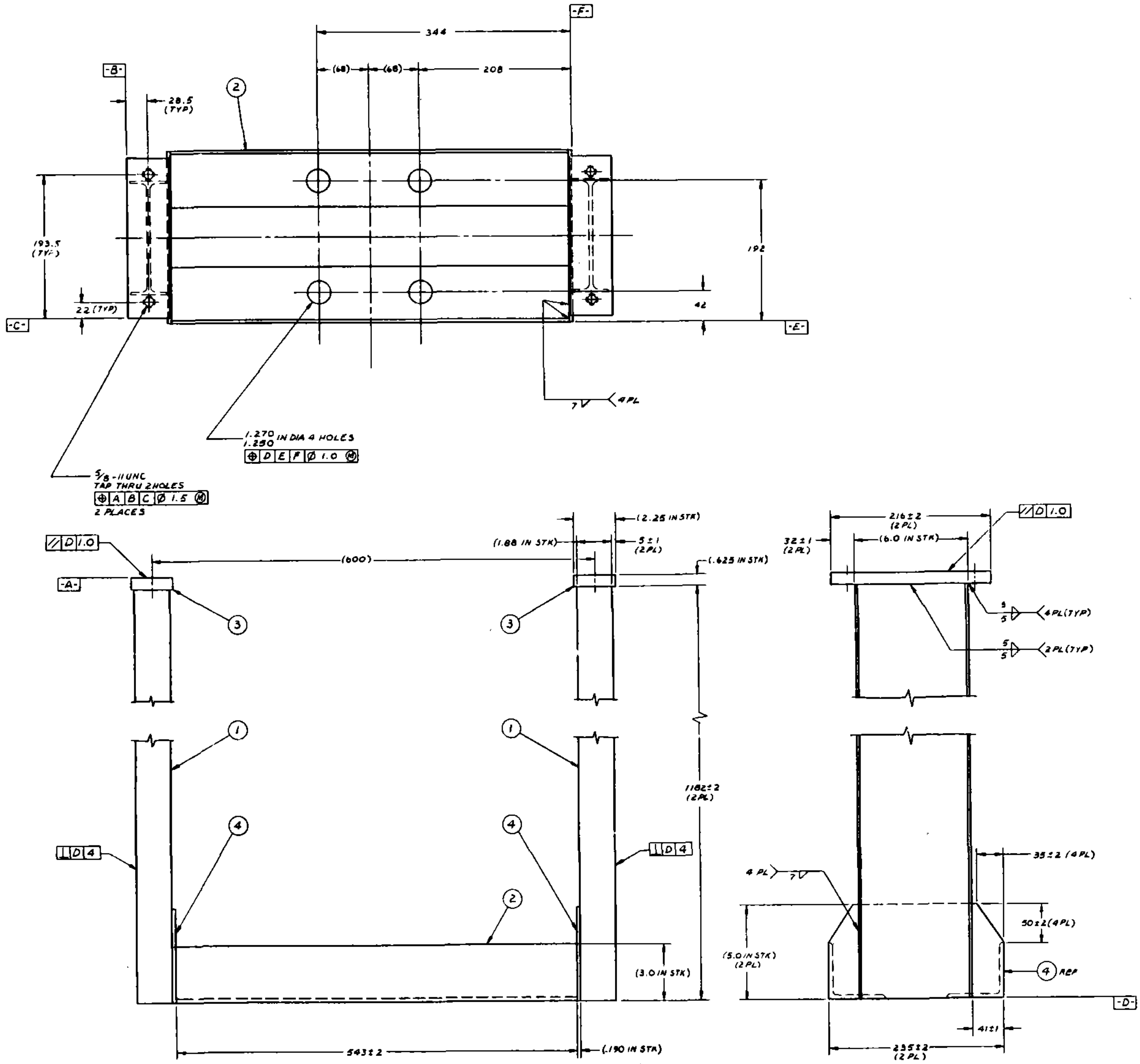

DOUBLE PYLON

FIGURE 3

NOTE: Dimensions in millimeters unless otherwise noted.

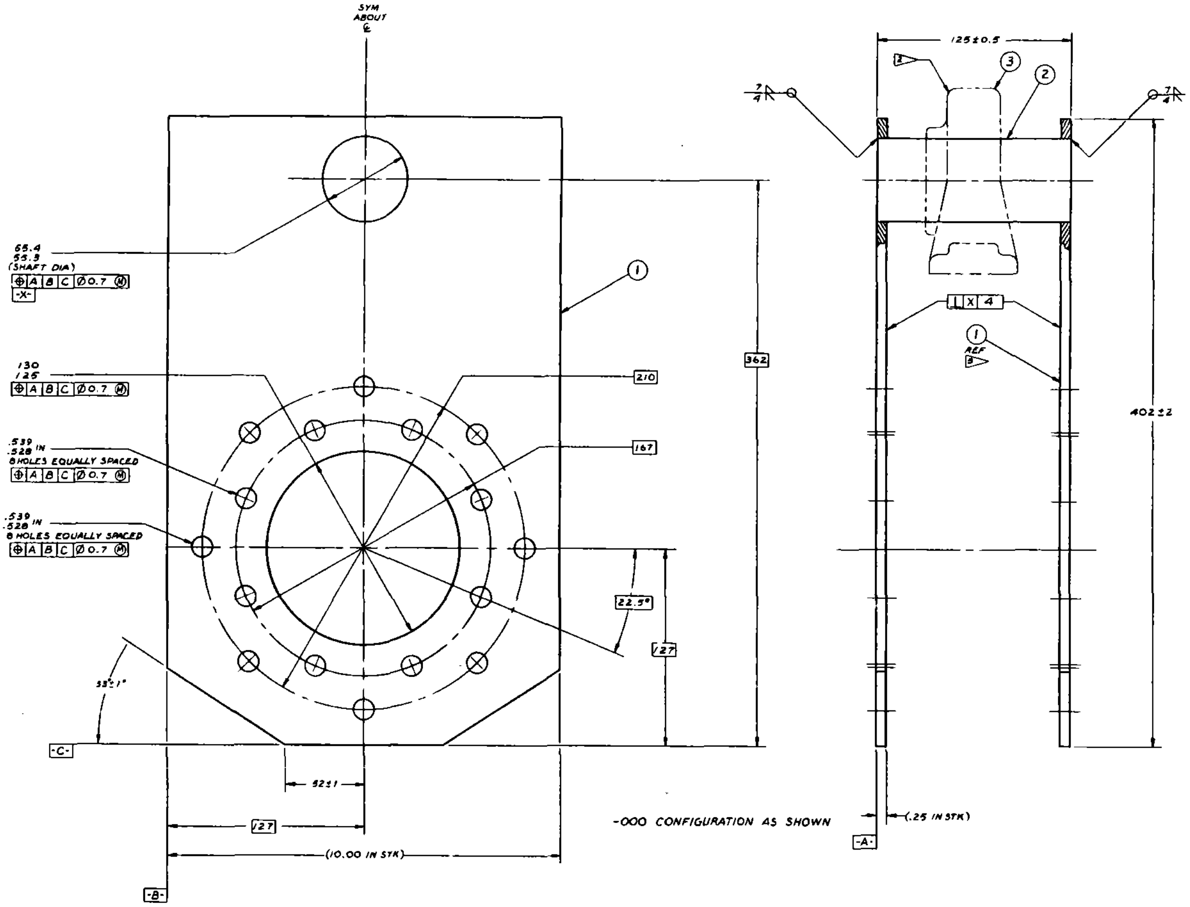

BEARING ASSEMBLY

FIGURE 4

NOTES: 1) A single plate only used with end pylons.

2) Dimensions in millimeters unless otherwise noted.

that the low moment of inertia of these pylons in the thin direction permits sufficient flexure to take care of the linear thermal expansion along the row. The associated bending forces acting on the bearings are acceptably small.

The material designated for the pylon designs is low carbon steel, generally ASTM Grade A36. The designs use standard structural shapes, i.e., beams, bars, angles, and plates in weldment configurations. The mounting of the pylons to the foundation is to be through a four-bolt array with 3/4-10 NC thread projecting 6 inches above the concrete on a 150 mm x 136 mm pattern (5.9" x 5.4" pattern). Attachment of the pylon is made using double nuts with washers to clamp the base of the pylon. Clearance holes of 1 1/4 inch diameter on the 3/4 bolts allows for some horizontal adjustment for variation on foundation features. The 3/4 diameter course thread bolt permits ample torque on tightening the nuts to clamp the pylon base securely.

Figure 2 illustrates the pylon designs for the intermediate row positions and the row end positions. These are weldments using the AISI standard junior beams 8" wide and 6" wide, respectively. The bases are 3 x 3 standard angles with the thicknesses being 1/4 inch and 3/8 inch, respectively. A plate welded to the top is drilled and tapped to attach a standard PB250 pillow block bearing.

Figure 3 illustrates a double pylon used to pick up the ends of longitudinally adjacent drive strings on a common foundation. This double pylon is cost advantageous since it eliminates one foundation. This again is a weldment using the 6" junior beams with 4 x 4 x 3/8 standard angles on the base. The interior space will be occupied by flexible hoses connecting the two adjacent receiver tubes. For all three pieces, hot dip galvanize is the selected finish.

Figure 4 is the bearing assembly with offset plates to reach below the reflectors to pick up the support structure. Two interface bolt patterns exist today to cover different reflector structure designs. The shaft is 2 3/16 inch diameter welded into 10 inch wide, 1/4 inch plates using both a groove weld and a fillet weld. The plates are believed to be adequate flexural elements to handle nonsquareness of the parts on assembly and axial alignment error through the five pylon bearing centers. The bearing selected for use with these designs is a standard PB250 pillow block with a spherical-mounted ball bearing. The bearing installation precludes the hot dip galvanize so this assembly must be painted. The square corners on the plates are planned to be used to mount the support for the receiver tube.

The design loads applicable to these designs are as follows:

1. Static Weight -- Range of four potential glass faced trough designs is 600 to 1100 lbs. Used 1200 lbs.

2. Wind Loads -- 80 mph (with wind fence)

   Horizontal - 650 lbs per trough
   Lift - ±650 lbs per trough
   Pitch Moment - 2860 lb-ft per trough

Static tests have been conducted on the designs. Prototypes that were tested had 3 x 3 x 3/16" stock thickness angles on the bases. The deflection at the bearing center for the end and intermediate pylons, respectively, were 1/4" and 7/16". The double pylon with 3/16" stock was unsatisfactory. At double the simulated wind load, deflections were excessive. The stock thicknesses have now been increased to 1/4 and 3/8 inch, respectively, on the end and intermediate pylons. The double pylon base angles have been changed to a 4 x 4 x 3/8 size. Confirmation tests are pending. The bearing assembly was tested to a 6000 lb-ft torsional load and the weld joint was sound.

The pylon designs are being evaluated for adaptation to stamping for lower cost manufacture. Recently, the designs were reviewed with three firms who are major fabricators of metal products. Suggestions for employing stamping techniques were solicited. Indications are that the structural shape weldment designs would be hard to replace with stampings economically unless the quantities become quite substantial. Additional review will be conducted.

INITIAL PARABOLIC TROUGH DESIGN AND PARAMETRIC EVALUATION

Robert C. Reuter, Jr.
Supervisor, Applied Mechanics Division III, 5523
Sandia National Laboratories
Albuquerque, NM 87185

Introduction

A parabolic trough is that portion of a parabolic, line focusing collector system which provides the correct optical shape for the reflective surface, maintains this shape to within acceptable tolerances during operation and protects the reflective surface during non-operating periods. In engineering terms this means that stresses and deflections experienced by the trough and reflector must remain below specified levels under various gravity, wind and thermal load environments and, at the same time, physical properties of the trough, such as size and weight, must be compatible with overall design objectives. With preliminary guidelines such as shape (parbola definition), aperture, deflection allowance under moderate wind (operating conditions), and no structural failure up to a specified wind speed (survival conditions), the designer proceeds to define construction concepts and materials for the trough. This task is not easy at first because of the many construction concepts (or designs) possible and the many materials available for each concept. The purpose of this paper is to outline the initial steps taken at Sandia: 1. to eliminate those materials and designs which have little or no chance for success, and 2. to provide preliminary guidance for design of those for which engineering development appears viable.

Early Design Elimination

Design concepts to be considered were placed into four categories: 1. slabs and laminates, 2. reinforced panels, 3. sandwiches, and 4. monocoque structures. Slabs and laminates are structural panels of single or multiple layers, unreinforced by periodic stiffeners and supported at their ends. A sheet of plywood formed to a parabolic cylinder is an example. To determine whether this design concept was worth pursuing, a figure-of-merit, F, was derived whereby the mechanical properties of the chosen material could be related to the structural properties required of the design. A slab "failed" if it did not satisfy the following inequality

$$\frac{E}{\rho^3(1 - \nu^2)} \geq F \tag{1}$$

where

$$F = \frac{12D}{\alpha^3}$$

In the above, E and ν are Young's modulus and Poisson's ratio, respectively, of the slab material (or equivalent properties in the case of a laminate) and ρ is the corresponding density. Structural properties are D, the flexural rigidity commonly used in plate and shell theory, and α, the areal weight of the panel. Structural property magnitudes represent fulfillment of trough strength, stiffness and weight requirements. Original values were $D = 0.5 \times 10^6$ lb-in and $\alpha = 3.0$ lb/ft^2. This yielded a value of F so that

$$\frac{E}{\rho^3(1 - \nu^2)} \geq 6.6 \times 10^{11} \ \frac{in^7}{lb^2} \tag{2}$$

No materials were found which satisfied (2), therefore, slabs and laminates were dropped from further consideration. There is an important message in the figure-of-merit, (2), which should be emphasized. It is not enough to find a material with high specific stiffness, (E/ρ), because of the cubic exponent of ρ in the denominator of (2). Low weight must be achieved. Halving the density is four times more effective than doubling the modulus. This result focused our attention upon the light-weight concepts categorized as the periodically reinforced, sandwich and monocoque designs.

Monocoque designs are those utilizing the stressed skin concept of construction. They looked promising from the figure-of-merit standpoint, but were eventually dropped in favor of other designs with potentially lower fabrication costs.

Analysis and Parametric Evaluation

In order to advance our evaluation and understanding of the light-weight designs remaining, an analysis based on methods of laminated plate and shell theory was developed. This capability permitted numerical evaluation of trough stiffness, strength, deformation and thermo-elastic behavior while using a variety of geometric properties as parameters. The net result was an understanding of the ultimate areal weight of a trough which had adequate stiffness, and how this weight varied as geometric parameters were changed. With the emphasis on low weight (and therefore, generally, lower costs), direct comparisons could be made among various designs once unit design costs were known. Examples of results of the structural analyses will follow.

Sheet molding compound (SMC) is a material which appeared practicable for a rib reinforced trough design[1,2]. With longitudinal rigidity supplied by the geometric stiffening of the parabolic shape, and torsional rigidity provided by a supplementary torque tube, only transverse ribs are required to stiffen a thin sheet of SMC against parabola geometry changes under load. Fig. 1 shows how the transverse flexural rigidity of a SMC trough varies with total thickness (equal to a fixed skin thickness, t_2, plus a varying rib depth) with rib spacing as a parameter. $(t/w)_1$ is the ratio of rib depth to rib width. The intersection of any of the curves with the horizontal line represents a set of geometric parameter values that will produce a trough with the required transverse rigidity of 0.5 lb-in. Figure 2 shows how the areal weight, or weight density, varies with total thickness, again using rib spacing as a parameter. If the intersections in Fig. 1 are replotted in Fig. 2, a curve is generated which illustrates how the areal weight varies with total thickness for all troughs that have the required 0.5×10^6 lb-in flexural rigidity. Other considerations, such as manufacturability and unsupported panel length, will place additional limitations upon rib depth and spacing, however, guidelines for their selection and their effect upon areal weight have been established. Areal weights significantly below the upper limit of 3.0 lb/ft^2 appear feasible. Similar results were obtained for a corrugated, (hat-section) reinforced skin made entirely of sheet steel[3]. These two concepts (the SMC rib reinforced trough and the sheet steel hat-section reinforced trough) were judged to be manufacturable, potentially low cost designs worthy of additional engineering development.

Another light-weight design concept we pursued, for the same reasons as stated above, is the sandwich concept[4]. This design utilizes two thin, high modulus sheets separated by a low density, shear resistant material, called the core. It is the two-dimensional analog of an I-beam. Proceeding with the analysis to generate numerical results as with the SMC design, Fig. 3 shows how the flexural rigidity of an aluminum honeycomb core/aluminum facing (skin) sandwich varies with facing thickness, with core thickness as a parameter. As before, intersections of these lines with the horizontal line in Fig. 3 represent designs which have the required 0.5×10^6 lb-in flexural rigidity. Fig. 4 shows how the areal weight varies with facing thickness, with core thickness as a parameter. Replotting intersections in Fig. 3 on Fig. 4 yields the curve representing the dependence of areal weight upon facing thickness for designs with the required flexural rigidity. Notice the existance of a minimum weight[7]. Additional results were obtained for other facing and core materials and combinations as shown in Fig. 5. Although it would be desirable to design for minimum weight, it may not be practical because of unreasonably thin facing thicknesses, as with steel. Fig. 5 provides a quick and convenient means of comparing the weights (and with a $/lb estimate, the costs) of a number of different sandwich materials. Figure 5 also illustrates the relative weight penalties associated with facing thicknesses in excess of those required.

Summary

Light-weight trough designs appear to have all the desirable characteristics necessary for a technically successful parabolic collector structure, and the potential for economic success. Only when heavy design concepts can be made inexpensively enough, and are not an unrealistic burden to support and control hardware, will they be competitive. One such concept is the glass laminate/space frame structure[5].

Structural analysis has become an important element in the development of our parabolic trough collector technology. Preliminary methods have contributed to our understanding of trough design capabilities, limitations, and mechanical behavior, and have aided in guiding early design. All of Sandia's trough designs chosen for further engineering development have been committed to finite element modeling[6] where a more refined, precise and detailed structural analysis can be achieved.

References

1. Reuter, R. C., Jr. and Allred, R. E., "Structural Optimization of SMC Line Focusing Collectors," SAMPE Series, Vol. 24, Book 2, 1979, p. 866.

2. Champion, R. L. and Kirsch, P. A., "Sheet Molding Compounds (SMC) Reflector/Structure," Proceeding of the Line-Focus Solar Thermal Energy Technology Development Conference, Sept. 9-11, 1980, Albuquerque, NM, Sponsored by the U.S. Department of Energy and Sandia National Laboratories.

3. Champion, R. L. and Biester, A. W., "Sheet Metal Trough Reflector/Structure," op cit.

4. McDowell, J. W. and Johnston, R. D., "Honeycomb Reflector/Structure," op cit.

5. Martin, S. B. and Lewis, I. E., "Glass Laminate Reflector/Structure," op cit.

6. Koteras, J. R. and Lewis, B. A., "Analytical & Experimental Studies of Some Parabolic Line Concentrator Design Concepts," op. cit.

7. Reuter, R. C., Jr., "Weight Minimization of Sandwich Type Solar Collector Panels," Proceedings of the 14th Intersociety Energy Conversion Engineering Conference, Boston, MA, Vol. I. p. 1., August 5-10, 1979.

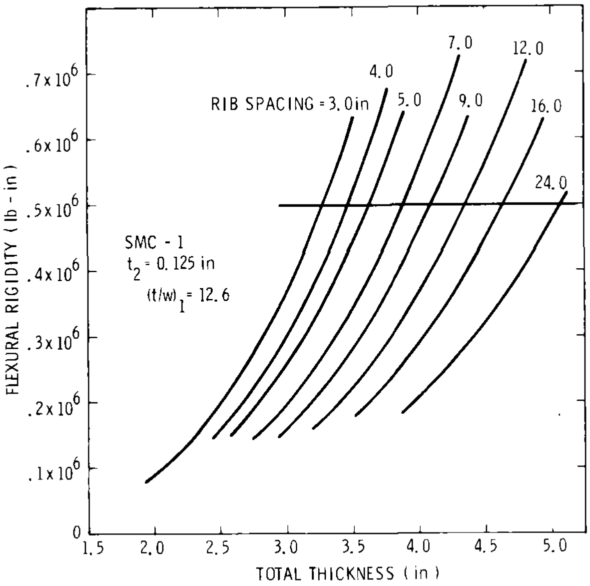

Fig. 1. Transverse flexural rigidity of rib reinforced SMC panel.

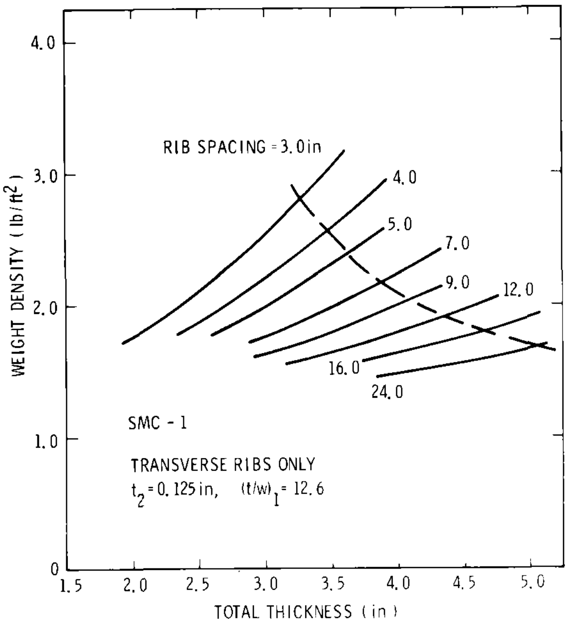

Fig. 2. Areal weight of rib reinforced SMC panel.

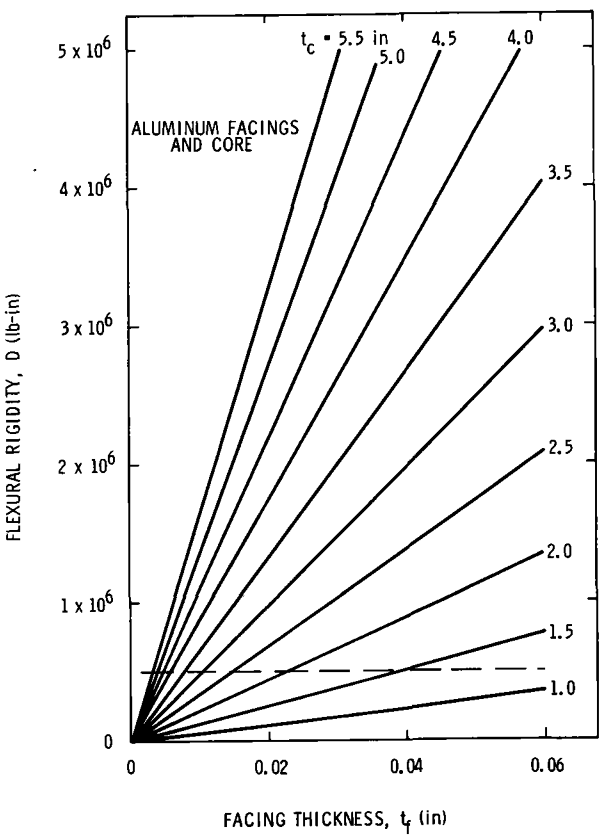

Fig. 3. Transverse flexural rigidity of aluminum honeycomb/aluminum facing sandwich panel.

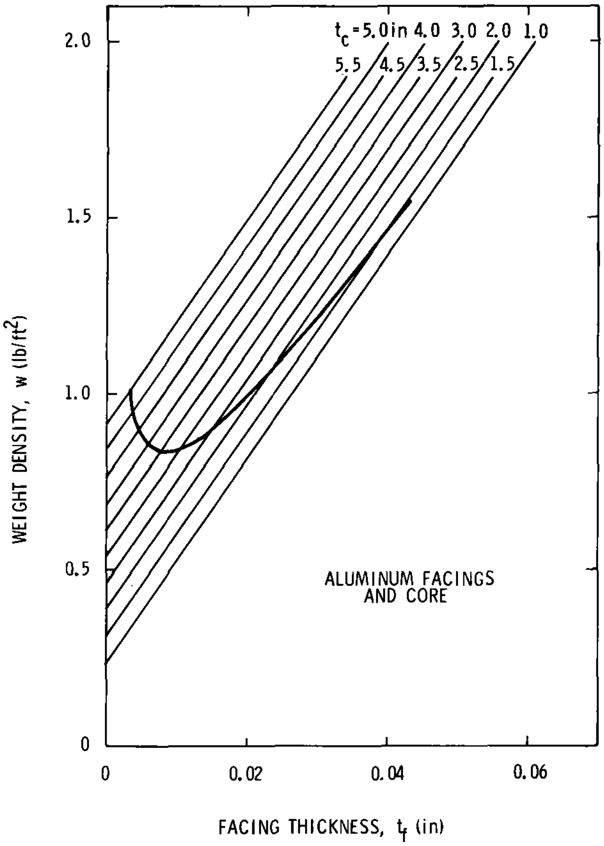

Fig. 4. Areal weight of aluminum honeycomb/aluminum facing sandwich panel.

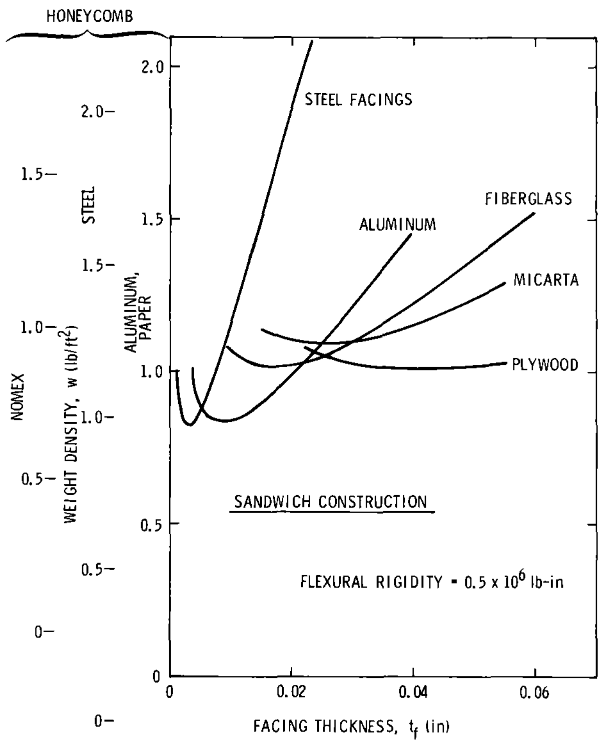

Fig. 5. Areal weights of sandwich panels constructed of various materials.

SHEET METAL REFLECTOR STRUCTURES

Roscoe L. Champion
Component and Subsystem Development Division 4722
Sandia National Laboratories
Albuquerque, New Mexico 87185

Introduction

Sheet metal, steel sheet metal, represents a low cost readily available material which has been incorporated into an endless array of products using high volume production techniques.

The adaptation of sheet steel technology to solar reflector panels appears very appropriate, but there remain questions regarding:

(1) The accuracy of stamped sheet metal panels

(2) Integration of the reflector material into the structure

(3) Environmental protection of the steel for long life

(4) Integration of the reflector/structure with the supporting torque tube.

The purpose of this paper is to describe the design requirements and material problems which might be encountered with sheet metal reflector structures. The following paper by The Budd Company will describe their effort in the development of tooling, and of fabrication and assembly techniques for stamped sheet metal reflector structures.

Project Scope

After a period of extended discussions with potential sources for a developmental effort, contact was made with the Budd Co. who had the capability, experience and interest in such a project.

Design Requirements

The design requirements for this reflector structure concept included:

1. Survival in 80 mph winds
   Drag, lift and torque loads
   1000 psi maximum stress in annealed glass.

2. Operation in 25 mph winds within specified deflection limits due to wind and gravity.
   Governing criterion has become the survival load; structures which survive 80 mph wind loads without damage are typically stiff enough to be within the 25 mph deflection limits.

3. Survival of other weather conditions including:
   - Diurnal and seasonal temperature cycling
   - Precipitation including rain, snow, and hail, and resultant snow or ice loads.

4. Contour accuracy of the reflective surface within an error budget of 3 milliradians rms.
   - Vital to collector performance
   - Has bearing on design and tolerances of tooling and assembly fixtures.

5. Long-term, low maintenance life of reflector structure in its outdoor environment.
   - Goal is 20 years
   - Factors include finishes, coatings, primers, adhesives, joining techniques, etc.

6. Low cost materials and fabrication.

Structural Concept Definition

The present design of a sheet metal reflector panel is shown in Figure 1 and 2, with its stamped frame panel on the back. Figure 2 illustrates the concept of an assembly of multiple panels on a torque tube. This design utilized Budd's stamping expertise in conjunction with structural analyses performed by Sandia. Metal thicknesses of .030 inch were based on their automotive experience. Analysis indicates a potential reduction of 20-25% with the use of thinner gages could achieve 2.0 lbs/ft^2 for steel structures. Stiffness requirements can still be met. Thinner sheets will require reconsideration of tooling design to achieve successful drawing of the panels in the thinner gage.

Reflector/Structure Concepts

Three configurations of reflector panels have been defined for fabrication and evaluation. They are:

I. Sheet metal structure consisting of a stamped frame (back) panel which is bonded or spot welded to the steel front panel.
. A sagged or chemically strengthened glass mirror is bonded to the steel assembly.

II. A combination structure consisting of the steel frame (back) panel bonded to a front panel which is chemically strengthened glass. The glass serves as mirror and front structural member.

III. An assembly in which the stamped back panel is bonded to a laminate front panel. The laminate is a chemically strengthened glass bonded in the flat to a thinner steel sheet.

IV. A fourth concept is a future possibility. It is an assembly with an annealed thin glass/steel laminate, should such a reflector material become available.

The advantages and disadvantages of each of these three configurations are as follows:

Configuration	Advantages	Disadvantages
I	1. Easy assembly of steel parts-bonded or spot welded	1. Difficult to bond large curved areas of glass with uniform adhesive layer and no bubbles
	2. Use sagged or chemically strengthened glass	2. Difficult to adapt for high production rates
		3. Requires two bonding operations, probably with different adhesives

Configuration	Advantages	Disadvantages
II	1. Eliminates one large area bonding operation	1. Requires expensive chem. strengthened glass Should have 8 ft length
	2. Eliminates front steel sheet	2. High stress on small areas of silver/glass interface
	3. Uses quick cure urethane adhesive. Short cycle times.	3. Differential expansion of glass and steel
		4. Corners and edges of glass vulnerable to chipping and dicing of entire part
III	1. Glass/steel laminate can be adapted to high production rates with good control	1. Probably requires chemically strengthened glass
	2. Could use thinner steel sheet, perhaps .015 or .022" thick	
	3. Potential use of thin (.020--.030") glass laminated to steel.	
	4. Adaptable to high rate processes	

Material Selection

The long-term life requirements for reflector panels dictate that corrosion protection must be an integral part of the design. Finishes for the steel under consideration include aluminized sheet, galvanized (in several types) and painted steel. The electrogalvanized and the aluminized materials have been successfully stamped. The aluminized steel appears to offer the advantages of long life and minimal primer or other coatings. Spot welded vs. bonded assemblies also must be evaluated, particularly from the corrosion viewpoint.

Adhesives for these various assemblies have been evaluated for their long term life capability as well as the processes by which they are applied and cured. Quick-curing urethane adhesives appear to be appropriate for the structural applications, i.e., between the two metal panels. At the present time, epoxies are the leading contenders for the glass-to-metal laminates. Additional work on adhesives is required.

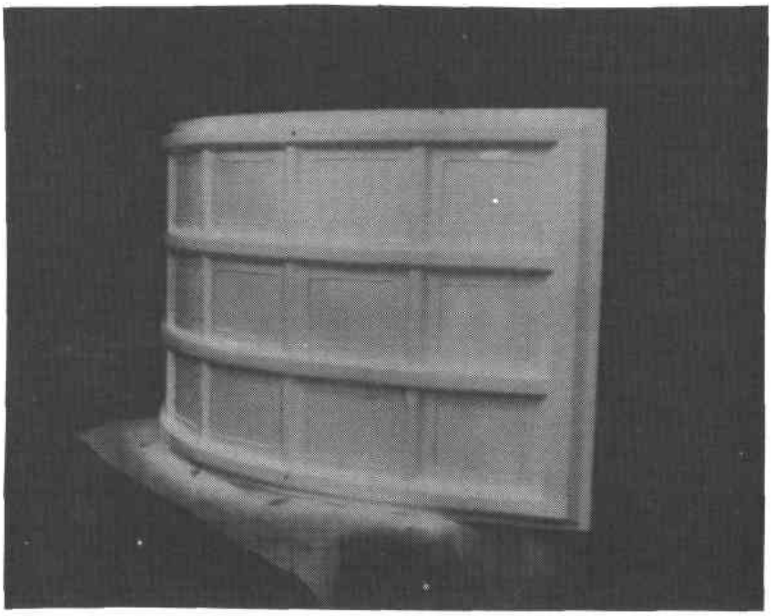

Figure 1. Assembly of Stamped Sheet Metal Panel

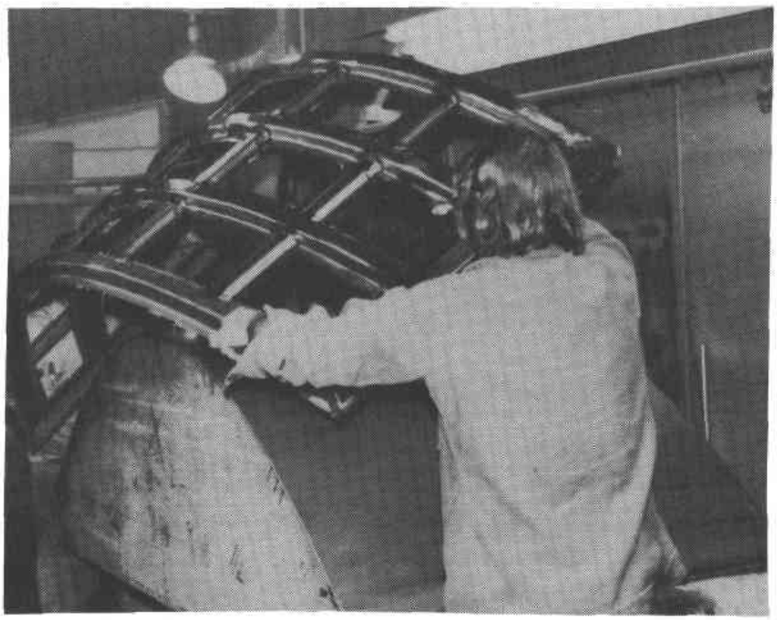

Figure 2. Sheet Metal Reflector Structure

2m X 6m PARABOLIC TROUGH MODULE DESIGN CONCEPT

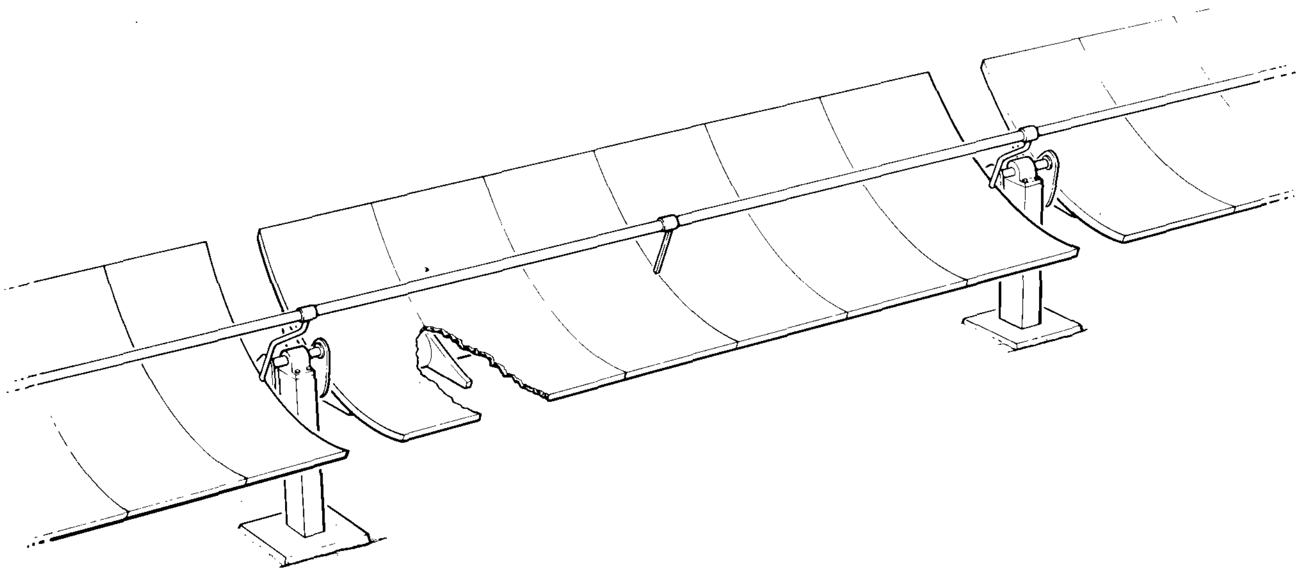

Figure 3. 2 x 6 m Parabolic Trough Concept

SHEET METAL TROUGH REFLECTOR/STRUCTURE

Albert W. Biester
The Budd Company Technical Center
Fort Washington, PA 19034

Introduction

In the search for a parabolic trough reflector structure which will be efficient, low cost, durable and suitable for mass production, many designs have been developed. The automobile industry, which is considered the model for high production of structural shapes, has long used sheet metal stampings to provide low cost structures. This discussion will describe how automobile production technology has been adapted to the development and prototype production of parabolic trough reflector structures.

Design Evolution

To provide for full understanding of the evolution of the reflector structure to be discussed here, it is desirable to briefly present some information regarding The Budd Company. Most people, if they are familiar with Budd, relate the company with passenger rail cars or highway trailers. What is not generally known is that Budd is the largest independent producer of automotive components in the country. Included in the automotive components produced by Budd are automobile frames and body panels, which are mass produced for various companies. This experience in the development and production of automotive parts, in discussions with Sandia, led to the concept of the sheet metal trough structure to be described.

Design Description

The design concept which has been developed will provide a parabolic trough structure which will meet the criteria for a low cost, accurate, durable structure with mass production potential. It is essentially a two piece sheet metal structure consisting of a formed frame or stiffening panel and a smooth contoured mirror panel. The two pieces can be bonded or spotwelded to form a rigid structure. An automobile panel analogous to this structure is a hood panel, which also

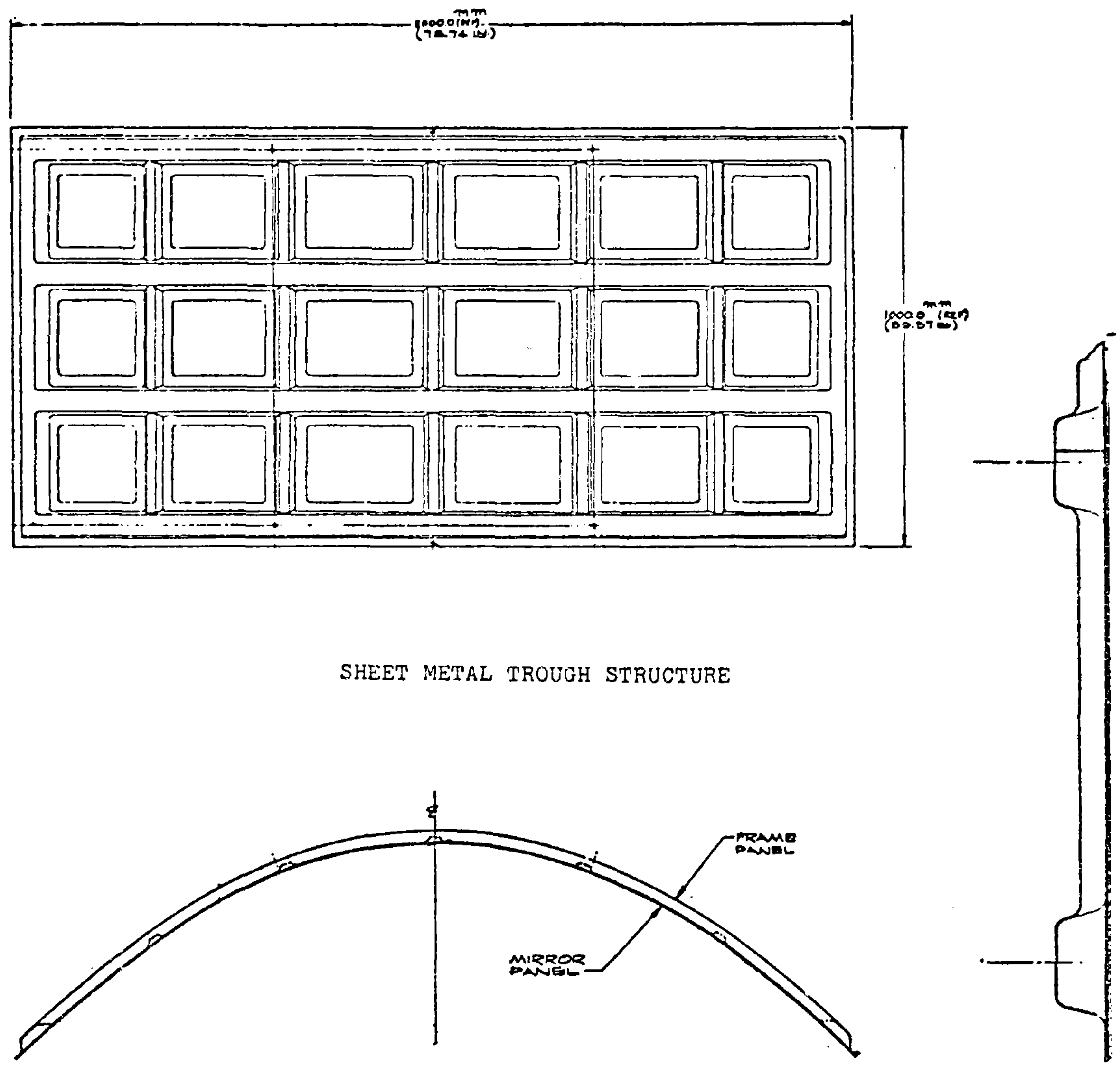

SHEET METAL TROUGH STRUCTURE

consists of a formed stiffener and a smooth, contoured skin. To provide the smooth exterior surface finish on the hood panel, the parts are joined by bonding. The reflective surface to be applied to the steel structure can be film, glass, or any of the presently utilized materials.

Material Selection

The material to be utilized in fabricating the structures must be low cost, formable, durable, particularly in corrosion resistance, and for the prototypes, must be available from warehouse stocks. The material choices for mass production are much broader than for prototypes since most materials are available in mill run quantities.

Various materials were considered for use. Aluminum and stainless steel are not low cost materials. Cold rolled steel is lowest in cost and formable but its corrosion resistance is poor. Aluminized steel is corrosion resistant but it is not recommended for severe forming and was not available in the sheet sizes required. The galvanized steel and galvannealed steel possess the corrosion resistance and forming characteristics but the spangled surfaces are not suitable for use with a film surface and they were also not available in the sheet sizes required. Zincrometal possesses the required properties but is only available in mill run quantities. This material has been widely used in the automobile industry. It is a cold rolled steel with a two part coating of Dacromet and Zincromet produced by various steel companies under license from Diamond Shamrock Corporation. The electrogalvanized steel has excellent surface finish, is formable and corrosion resistant, is reasonable in cost and is available in the required gage and sheet size required. It also has a phosphate coating which permits painting without further surface preparation. Therefore, electrogalvanized steel was used for the trough structures.

Adhesive Selection

A study was conducted to determine a suitable adhesive for bonding the structure. Information was gathered from various sources, including manufacturers and past experiments in Budd laboratories. The information obtained indicated that epoxy, urethane and acrylic adhesives all possessed the required properties although some seemed to be more suitable for the required application. A urethane adhesive with a long working life for prototype production was chosen and bonding tests were conducted, including shear pull tests, elevated temperature and water immersion tests. The chosen adhesive proved suitable for use in producing the prototype units.

Tooling Description

In producing the dies for forming the frame panels, normal automotive prototype production procedures were utilized. The dies were made of zinc alloy and are relatively inexpensive when compared with hard steel forming dies. The cutouts, trimming and drilling of the panels was performed manually using a template. In production, these operations would be performed in a blank and pierce die. The smooth mirrored panel was not pre-formed but obtained its contour on the assembly fixture.

To maintain the accuracy of the parabolic surface, it was recognized that the assembly fixture would be the most important tool. A fixture suitable for bonding or spotwelding the assemblies was designed and fabricated. For economy, the major portion of the fixture was made from an iron casting. It incorporates provision for vacuum hold down of the sheet for intimate contact with the parabolic surface. The machined parabolic surface of the casting was produced with a one-eighth inch offset to permit the use of one-eighth inch thick copper sheet to be the bottom electrode for spotwelding. In the event of possible damage to the copper sheet from spotwelding, an alternate aluminum sheet of the same one-eighth inch thickness was provided for the bonding operation. These sheets include holes for the vacuum hold down and are stretched over the iron casting. A bridge mounted on a parabolic track and incorporating a spotwelding head was provided. The panels are located on the fixture by two pins at the vertex on the datum line and are held in place and pressure applied by four straps over the longitudinal channels.

Assembly Procedures

Upon completion of the first stamped panels but prior to completion of the assembly fixture, two structural test units were prepared. These units were assembled using the same methods as planned for the prototype units except that they were assembled on a wooden fixture. The inside surfaces were prime painted and the smooth mirror panel was placed on the fixture. Adhesive was applied to the flanges of the formed panel and it was positioned on the mirror panel and strapped in

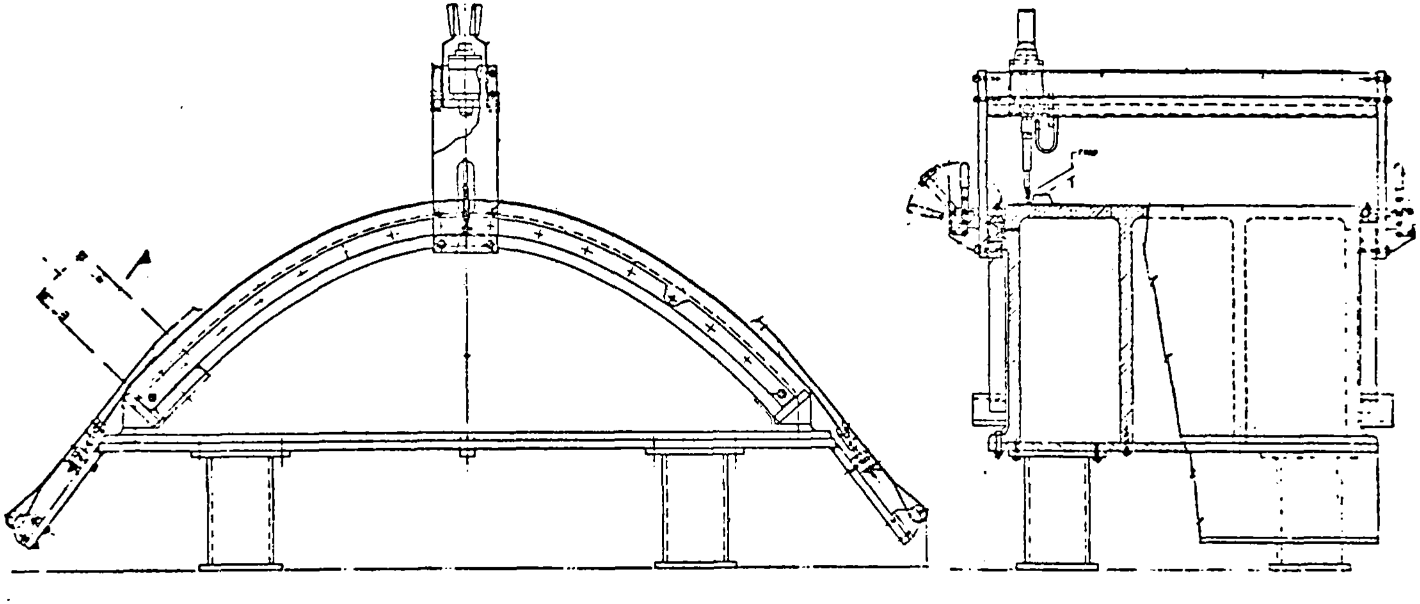

BONDING AND SPOTWELDING FIXTURE

place for curing of the adhesive. The assemblies were sent to Sandia for testing.

After completion of the assembly fixture, two structure assemblies were completed, one bonded unit and one spotwelded unit. The bonded unit was completed first, using the copper electrode sheet as the spacer. The bonded unit was produced using the same procedures previously utilized on the structural test units. The inner surfaces were primed and the parts assembled on the fixtures. After completion of the bonded assembly, sample spotwelding coupons were produced at various points on the fixture and the assembly was spotwelded, with welds on all flanges at two inch centers.

The assembled structures were measured by Budd on three dimensional measurement equipment to determine the deviation at specific points from the theoretical parabolic curve. One hundred thirty points on a specified grid pattern were measured and the results were gratifying. Laser tracing of the parabolic surfaces was performed by Sandia.

Mirrored Glass Assembly

The assembly fixture design was suitable for use as a fixture for installation of glass on the sheet metal structures. By replacing the one-eighth inch thick copper sheet with a one-sixteenth inch thick plastic sheet, the proper surface was provided for the glass. Using the bonded structure produced previously, a complete reflector was produced. Sag glass was used and held in place on the fixture using vacuum and locators for positioning. Adhesive was applied to the metal structure and spread using a doctor blade. The steel structure was then placed over the glass and strapped in place and held in the fixture for adhesive curing. The final operation in producing the structures was painting of the rear surface with primer and finish white paint, thereby adding to the corrosion resistance of the units.

Future Development Efforts

Future efforts in the development of this concept will consist of production and testing of additional bonded and spotwelded sheet metal structures, development of procedures for applying other reflective surfaces, such as chemically strengthened glass, production of variations in the configuration of the assemblies and development of the

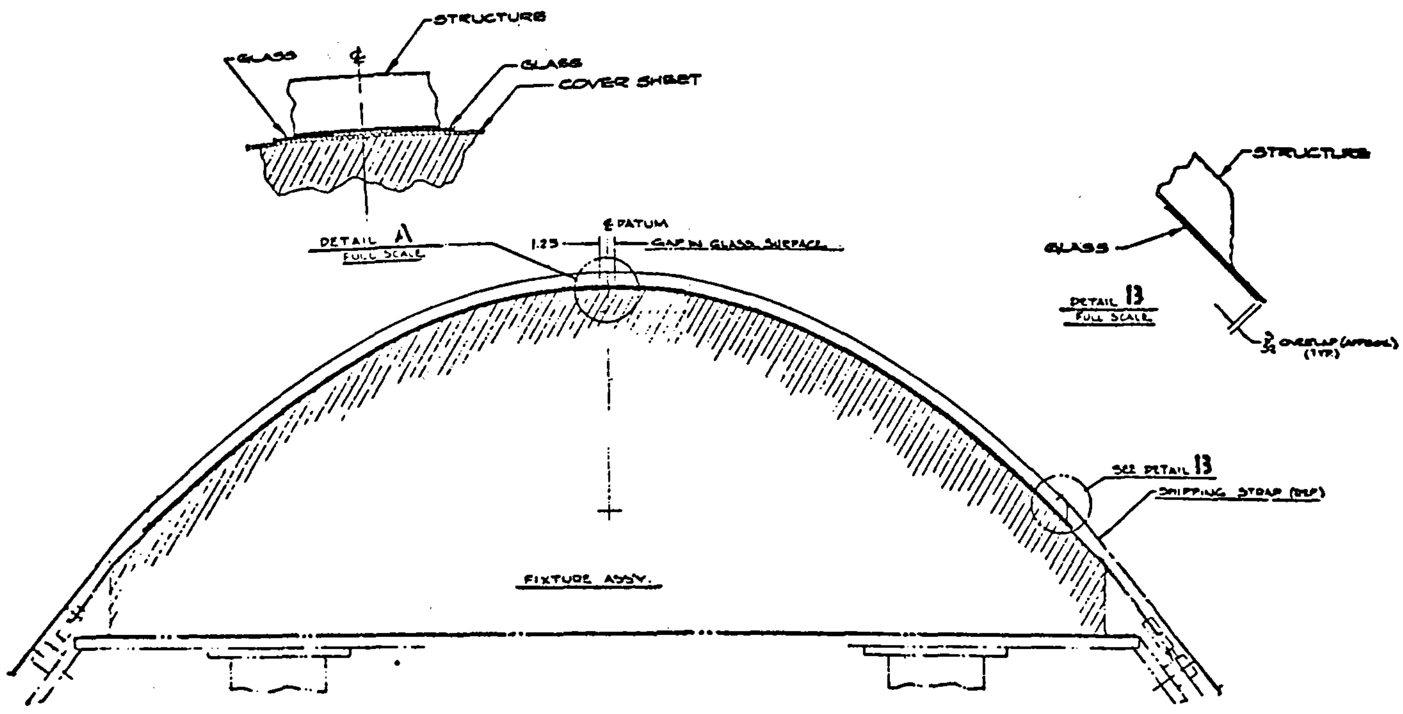

GLASS BONDING SET-UP

most desirable production techniques.

Conclusions

The results obtained to date from the prototype production of the sheet metal trough structures indicates that this design is a viable one for mass production. All of the manufacturing processes utilized are adaptable to high production. The forming operations are similar to those used for automobile panels and the stampings can be produced at extremely high rates. Spotwelding of the panels can be accomplished in production using gang welders or robots. Although a relatively slow cure adhesive was used for the prototypes, faster acting adhesives are available as are automated mixing and dispensing systems for the adhesives. Automated handling techniques can be developed for application of the reflective surfaces. For low cost, high production capability, it is difficult to visualize any system which can surpass the sheet metal concept.

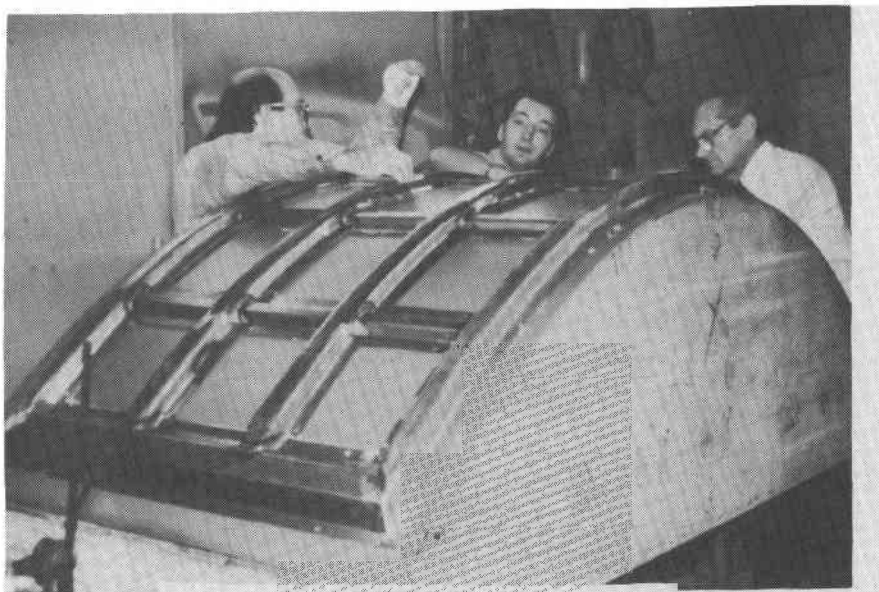

WOOD BONDING FIXTURE

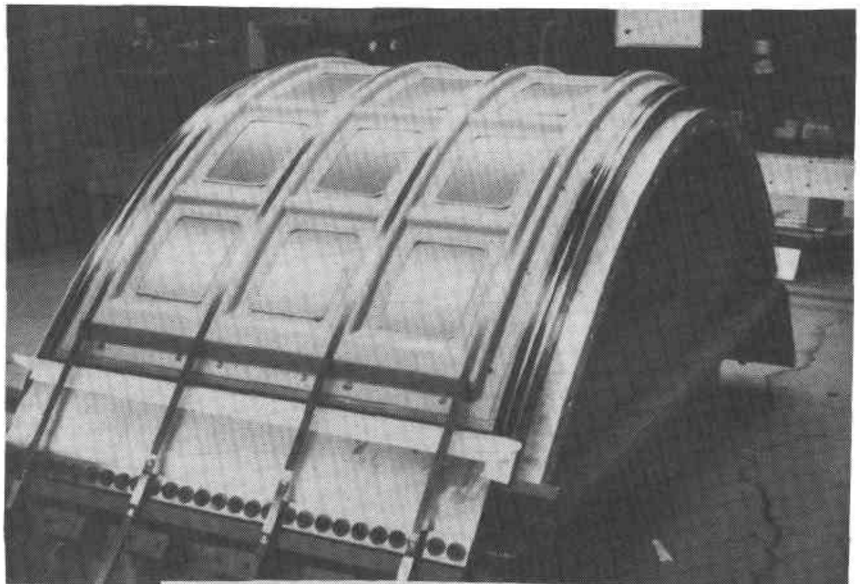

ASSEMBLY FIXTURE - BONDING SET-UP

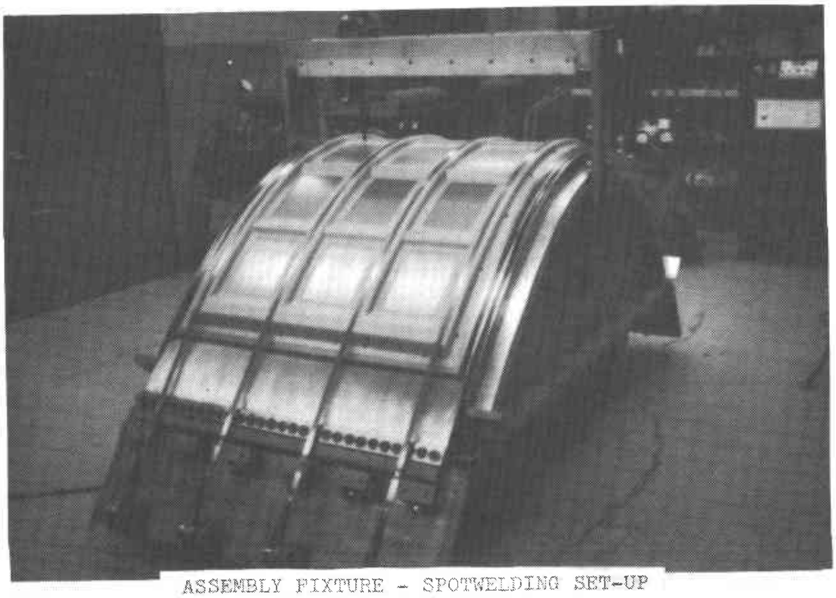

ASSEMBLY FIXTURE - SPOTWELDING SET-UP

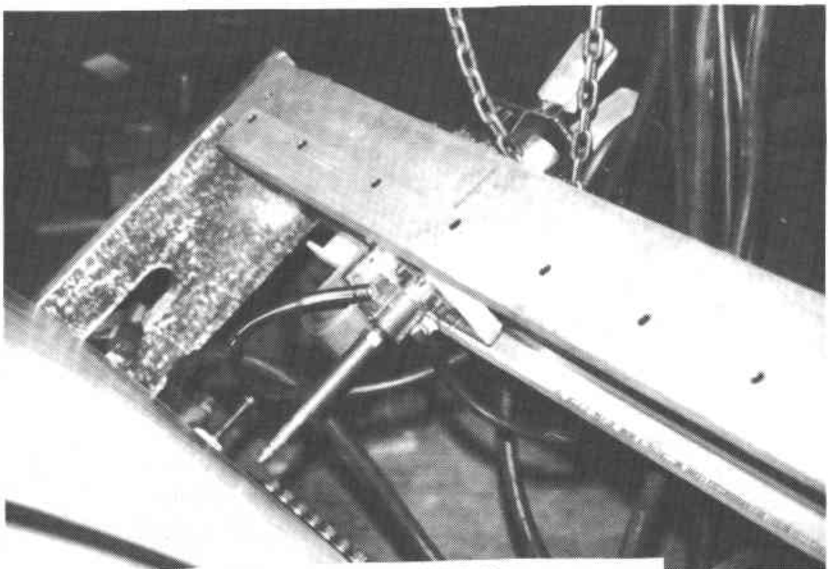

SPOTWELDING HEAD

SHEET MOLDING COMPOUND (SMC) REFLECTOR/STRUCTURES

Roscoe L. Champion
Component & Subsystem Development Division 4722
Sandia National Laboratories
Albuquerque, NM 87185

Introduction

Molding with sheet molding compound (SMC) is a potential fabrication technology for the manufacture of parabolic trough reflector structures. SMC is a polyester resin material with chopped fiberglass reinforcement along with appropriate fillers and modifiers. Parts of SMC are typically molded at 300°F and 600 to 1000 psi in 3 to 5 minute cycle times. SMC molding is a semi high volume production process. It offers potential for low cost.

Early investigations (Ref.1) of trough panels molded of SMC indicated that the slope error accuracy requirements, as well as stability requirements could be met. Analyses indicated that structural requirements could be met (Ref. 2). With this promise, a second development effort (Ref. 3) was undertaken in conjunction with Haveg Industries, Santa Fe Springs, California, to investigate the possibility of molding a silvered glass mirror into the panel as an integral part.

In several early attempts to mold flat glass mirrors into flat SMC parts, the SMC adhered to the protective paint coatings and the glass survived the molding pressures. Those attempts at molding flat annealed glass into curved sections by elastic deformation usually failed; the glass fractured. The availability of chemically strengthened glass mirrors offered new promise for SMC panels with glass reflectors.

Reflector trough panels of SMC and glass appear to offer two significant potential advantages over other fabrication techniques:

(1) The molding in of the reflector eliminates the secondary bonding operation,
(2) The encapsulation of the second surface silver provides significant improvement in long-term environmental capability.

The molding project at Haveg was initiated with the following objectives:

Primary: To determine the survivability of full size sheets of chemically strengthened glass and sagged glass in the molding process.

Secondary: To determine:

- Effects of molding on the silver coating of the mirror
- Bi-material response of glass and SMC which have different expansions
- "Sink" at the ribs
- Effect of the glass (a poor thermal conductor) on the flow and cure of the SMC
- Environmental stability and durability of the combination
- Processing parameters--how to handle the glass, pre-heating, and how to load the charge.

The purpose of this paper is to describe the results of the SMC development efforts at Haveg which led to the current SMC effort by The Budd Company and which is described in the paper following this one.

Design Description

The units molded at Haveg (Figures 1 and 2) were 2 x 4' in size with .050" and .060" thick glass mirrors. Rib height was 1 7/8" in a peripheral and centerline pattern. The thickness of the SMC face behind the glass was nominally .155" thick. The SMC material contained 30% chopped fiberglass. Glass sheets were slightly smaller than the 24 x 48" face dimension so that a narrow lip of SMC was molded all around the edge of the glass to provide a better grip on the glass and to decrease the shear stresses at the interface.

In the molding process, the glass was preheated to 260°F and placed in the mold; the SMC charge was set on top of the glass. The pressure produced by mold closure held the glass against the mold face and prevented resin from running under the glass. There was some concern regarding the effect of the glass (a poor thermal conductor) on the cure of the SMC adjacent to the glass.

Molding Results

Plans were to mold 18 units: six all-SMC, six with sagged glass mirrors and six with chemically strengthened flat glass mirrors. The all-SMC units were molded successfully. All of the four sagged glass units which were attempted resulted in major fracture of the glass. The mirror was molded in satisfactorily, but the glass was fractured. It would have functioned properly for a while, but its environmental capability would have been very short, primarily due to moisture penetration and deterioration of the silver on the mirror.

Eleven units were molded with chemically strengthened glass; one resulted in dicing of the glass, but that was due to grit underneath the glass during molding. Of the ten which survived the molding process, eight were unqualified successes. The glass was flush with the front molded surface; the SMC bonded to the protective paint over the silver and copper coatings on the back surface of the glass.

The remaining two units used a different SMC compound; both units molded with it had significant areas where the silver coating had delaminated from the glass. It was believed that this delamination was due to a higher expansion, higher viscosity SMC which used a rigid (non-flexibilized) resin.

Evaluation of Molded Units

The molded panels were evaluated in four areas:

1. Surface contour accuracy determined with a laser ray trace inspection.
2. Measurement of mechanical properties of the material, throughout the part.
3. Thermochemical analysis (degree of cure, component volume fraction, filament orientation and content, etc.)
4. Accelerated thermal cycling of some units.

The surface accuracy (slope error) of these units was determined with the laser ray trace system, which provides an accurate measurement of the focal length of the best fit parabola, the rms slope error (in milliradians) and essentially a contour map of the slope errors. We could thus establish the initial condition of a part and measure all subsequent changes quite accurately.

Initial focal lengths ranged from 31.1 to 32.0 in. Slope errors ranged from 1.52 to 3.0 milliradians rms (17mr = 1°). A slope error of 2.5 milliradian is within budget. The units were essentially very good except for variations in the focal length due to the bi-material effect of the expansion mismatch between glass and SMC.

Mechanical Properties

Samples were cut from various sections of the parts: the ribs, outer coaming, face sheet, etc. Test data on strength, modulus and expansion did not show any trends; data were relatively consistent. Expansion measured across the face sheet thickness indicated that the thermal barrier of the glass had only a very minor effect on the cure and the flow of the SMC over the back side.

Thermochemical Analysis

The thermochemical analysis showed nothing unexpected in the SMC; its flow and cure and properties were essentially within tolerance.

Bi-Material Response

The coefficient of thermal expansion of the glass is $5 \times 10^{-6}/°F$; the expansion of the SMC was about $10 \times 10^{-6}/°F$. This mismatch in expansion was expected to produce a bimaterial response in this molded part. Equations were developed to predict the amount of change in the focal length of the molded parts due to cooling from molding temperatures to room temperature. Correlation of the predicted values with actual focal lengths was fairly good for the first eight units. The last two units with a rigid resin did not correlate well.

This data were important in that it influenced the tooling design for the follow-on effort by The Budd Co. to mold 1 x 1 m panels with glass mirrors.

Environmental Testing

After laser ray trace (LRT) inspection of all units to establish their baseline condition, some units were subjected to accelerated thermal cycling between -20°F and + 130°F. These units were subsequently removed from the test chambers and reinspected with the LRT at weekly and, later, monthly intervals.

The thermal cycling produced an unexpected decrease in the focal length of the panels. In several weeks, a semi-stable state was reached at focal lengths of 30.9"; original was ~31.35". The cycling produced some type of stress relief or creep which allowed the change. This area is not understood.

With the feasibility of molding glass mirrors into SMC panels established, a contract was placed with The Budd Co. to scale up the 2 x 4' parts to a 1 x 1 m panel which could be assembled and tested in a 2 x 6 m collector unit. All of the problems had not been solved, but,

(1) Molding of strengthened glass was feasible
(2) The environmental capability looked very good
(3) Slope error accuracy was essentially within budget
(4) Bi-material and creep areas need additional investigation

The development effort by The Budd Co. on 1 x 1 m SMC panels is described in the following paper.

References

1. R. E. Allred, D. W. Miller and B. L. Butler, Environmental Testing of Solar Reflector Structures, Proc. 1979, International Solar Energy Society Congress, Atlanta, GA, May 28 - June 1, 1979, paper F-II-C-2.

2. R. C. Reuter and R. E. Allred, Structural Optimization of Sheet Molding Compound Line-Focusing Collectors, Proc. 24th National SAMPE Symposium, San Francisco, CA May 8-10, 1979, pp. 866-877.

3. R. L. Champion and R. E. Allred, Development of Sheet Molding Compound Solar Collectors with Molded In Silvered Glass Reflective Surfaces, SAND80-0702C, Presented at SME Composites Conference, Los Angeles, CA, June 1980.

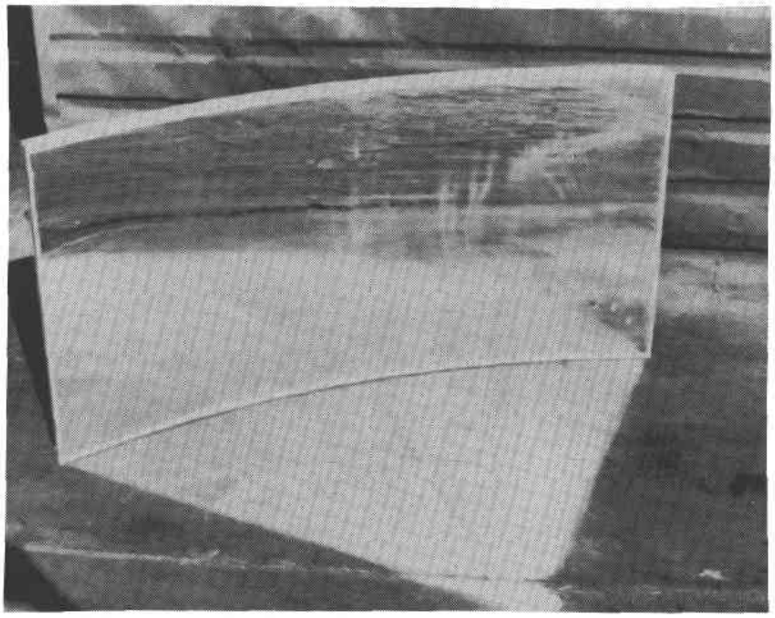

Figure 1. Front of 2 x 4 ft Haveg Panel

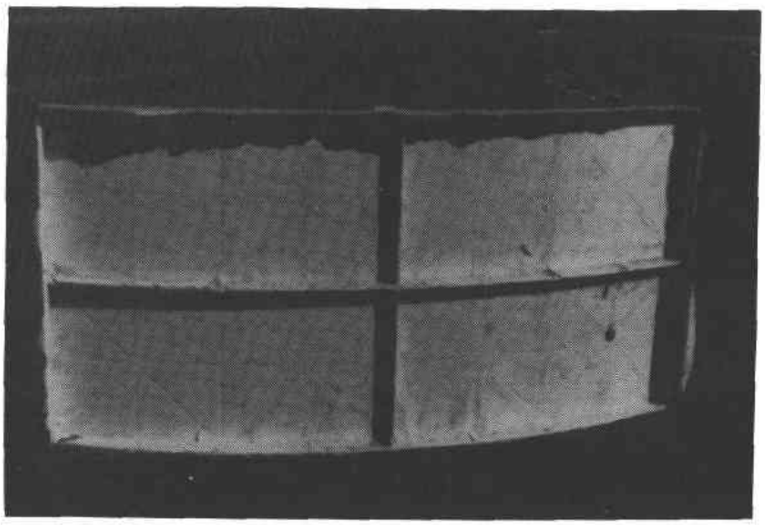

Figure 2. Back of 2 x 4 ft Haveg Panel

DEVELOPMENT EFFORT OF SHEET MOLDING COMPOUND (SMC) PARABOLIC TROUGH PANELS

Paul A. Kirsch
Advanced Materials Department
Budd Co. Technical Center
Ft. Washington, PA 19034

Introduction

The present development effort of sheet molding compound (SMC) parabolic trough panels is to develop molding techniques, provide information and demonstrate technical feasibility in the fabrication of SMC solar panels. The main thrust of the program is to successfully mold-in a mirrored glass sheet with the SMC, thus eliminating subsequent mirror to structure bonding operations and providing a good environmental seal for the silver coating on the molded surface of the glass. Co-molding of the mirror in the SMC also offers considerable potential in reducing the overall cost of such components.

Some of the problems that were expected to be encountered in this development program were:

(1) the adhesion capabilities between SMC and painted glass
(2) the positive positioning of the glass in the mold
(3) the survival of the glass and its silver, copper and paint coatings under pressure
(4) the development of uniform mechanical properties of SMC of the desired level
(5) the thermal expansion coefficient mismatch between glass and SMC

This paper will discuss these problems as well as the general progress of the program from initial panel design through to the molding of the trough solar panels.

Design and Fabrication of the Tooling

The finalized design of the Sandia trough panel is shown in Figure 1. Each panel extends from vertex to rim and two such panels, when fastened together at the vertex, form a one meter wide by two meter rim to rim reflector structure. It was decided early in the project to use ribs as the panel stiffening elements versus hat section braces to eliminate a separate press operation and a bonding operation. This change is expected to minimize the cost of the panel.

The major consideration in the design of the tooling was accounting for the thermal expansion coefficient (TEC) difference between glass and SMC. Because of the higher TEC of sheet molding compound when compared to glass, the trough panel's radius of curvature will increase when it is cooled from the molding temperature to room temperature. Equations predict that the "opened" shape of the panel remains parabolic, and these equations were used to calculate the smaller focal length needed for the tooling.

Positioning of the glass sheet in the die was another major consideration when designing the mold. The finalized panel design calls for the glass mirror to be held in the molded position by a constant thickness of SMC around the periphery. It was decided that the positioning of the glass sheet in the die could be accomplished by changing the angle of the rim coaming area to a nearly vertical position and by incorporating two vertical indentations on the vertex coaming (to be used also as locating devices when two panels are joined at the vertex). The chemically strengthened glass sheet can be over bent, placed in the mold, and allowed to spring back against the vertical surfaces, thus providing positive positioning of the glass sheet in the mold.

Other considerations in the design of the part and the mold included: (1) depth to width ratio of the ribs, (2) lead in radius to the ribs and (3) all other radii and draft angles. The ribs were designed to a depth of two inches, with a 1.5° draft on each side. The ratio of depth to average width is 12:1. To minimize the sink in the SMC panel and consequent read through to the glass mirror, the lead in radii to the ribs were kept at 0.010". If low strength or lack of fill occurred due to the lack of chopped glass fiber in the ribs, the radii could always be increased. Other radii in the corners were also kept at a minimum, nominally 0.010" internal radius and 0.020" external radius.

The completed zinc alloy tooling is shown in Figure 2.

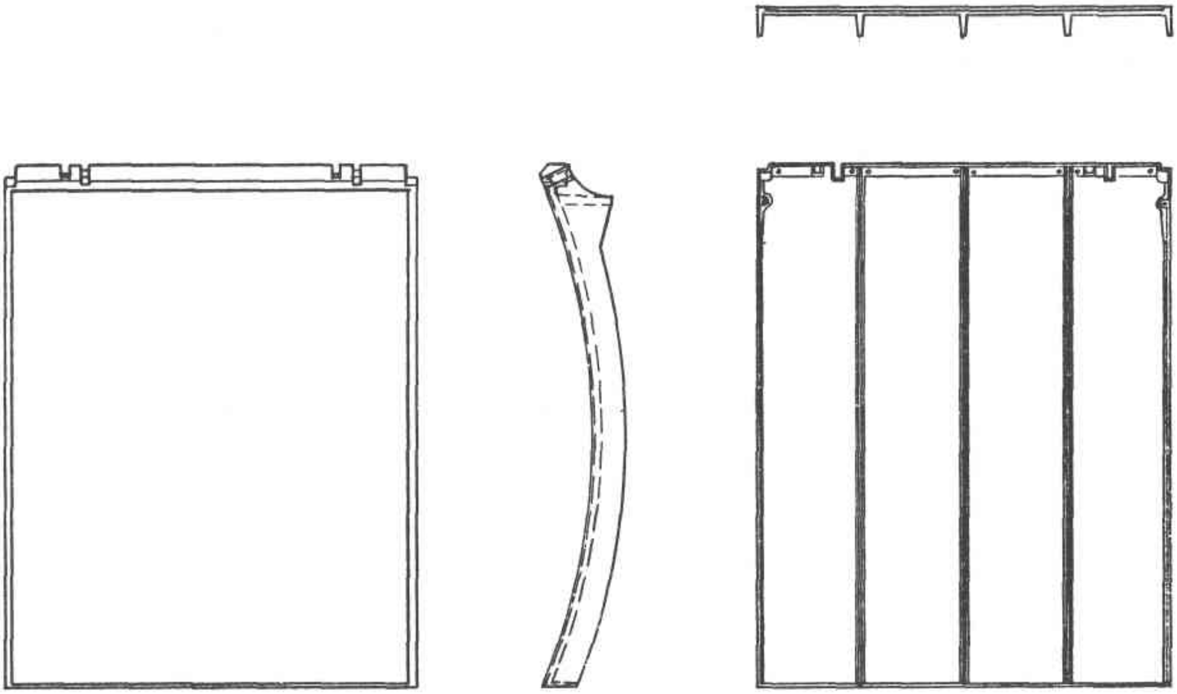

Figure 1 Finalized Panel Design

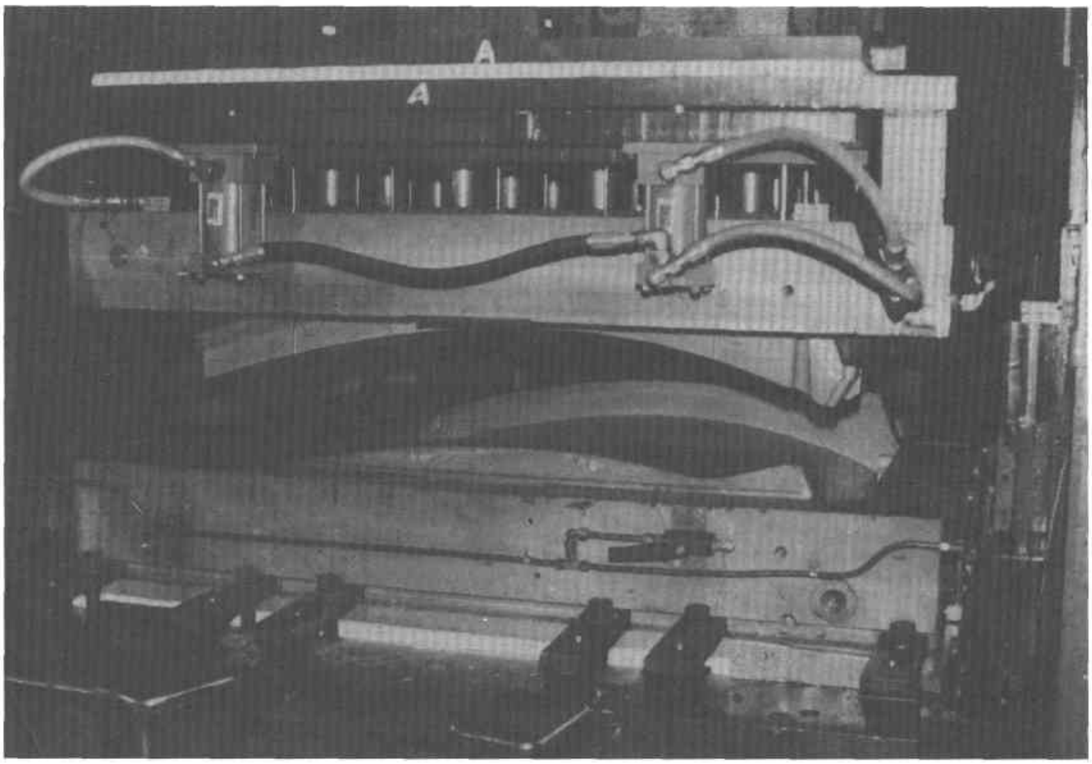

Figure 2 Solar Panel Mold

Material Selection

Sheet molding compound is a composite material consisting of chopped glass fibers combined with a resin and filler paste. SMC is manufactured by an automated continuous flow process which produces a reproducible sheet of uniform viscosity for molding. The SMC fabrication process is shown in Figure 3.

The desired material characteristics and properties for the panel are given in Table 1. From published papers on SMC properties and with Budd's experience in material properties versus glass content, it was decided that a 40% glass content SMC with an ultra-violet stabilizer added would satisfy the given material characteristics. The Budd Company's Plastic Products Division's formulation DSM 752 with UV stabilizer added was chosen for this project. The actual mechanical properties for this material, determined from samples cut from flat test plaques, are given in Table 2.

Mirrored Glass/SMC Adhesion

A program was devised to test for the adhesion between the mirrored glass sheets and the chosen sheet molding compound formulation. Moldings were made in a ten inch by twenty-four inch flat plaque mold mounted in a 150 ton hydraulic press. The glass, furnished by Sandia, was coated with a PPG Mirrochron 44410 paint, the same paint system used on the large glass sheets to be molded into the parabolic trough panels. Glass sheets with other coatings were also molded. The glass/SMC moldings were allowed to cool to room temperature at which time they were bent and twisted in an attempt to dislodge the glass from the SMC. While these tests were qualitative, the interface where failure occurred could be determined.

Two basic conclusions can be reached as a result of the adhesion tests. First, failure occurs at the paint/SMC interface when using the Mirrochron painted glass sheet. To increase the adhesion between the paint and the SMC, the paint should be wet-out with a system that is both compatible to the paint and the SMC. Examples are a thin coat of a polyester resin, the same used in the SMC, or a layer of an epoxy coating. The wetting-out of the paint transfers the failure from the paint/SMC interface to the copper/paint interface or to a cohesive failure in the paint. This coating technique seems to offer a short

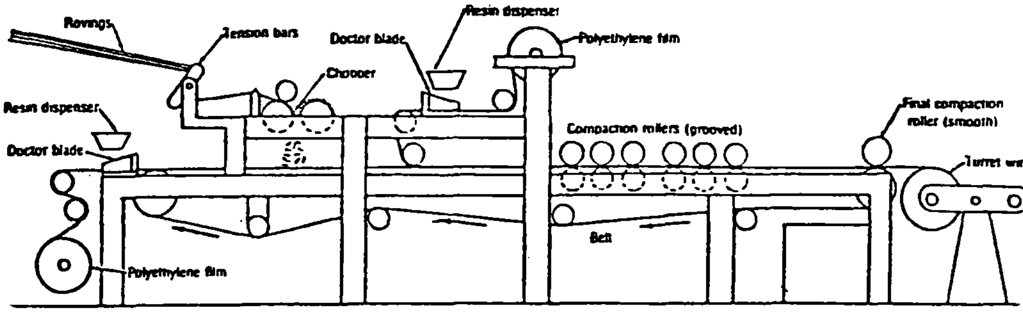

FIGURE 3 SMC PRODUCTION PROCESS

TABLE 1 - MATERIAL REQUIREMENTS

Low Shrink, Low Profile

Good Molding Characteristics

UV Stabilized Polyester Resin System

Young's Modulus - 1.5×10^6 PSI Minimum (1.8×10^6 PSI Desired)

Tensile Strength - 15,000 PSI

Flexural Modulus - 1.5×10^6 PSI Minimum (Higher Desired)

Flexural Strength - 25,000 PSI

Thermal Expansion Coefficient (TEC) 6 to 10×10^{-6} in/in/^{o}F

Mechanical Isotropy in the Plane of the Material

TABLE 2 - ACTUAL MATERIAL PROPERTIES

Young's Modulus - 2.19×10^6 PSI

Tensile Strength - 14,200 PSI

Flexural Modulus - 1.69×10^6 PSI

Flexural Strength - 29,400 PSI

Thermal Expansion Coefficient (TEC) 8.00×10^{-6} in/in/^{o}F
(over the range 0^{o}F to 200^{o}F)

term solution to the adhesion problem of SMC to the Mirrochron paint. Second, the adhesion tests show that a larger development effort is needed to understand the parameters that could affect the adhesion, such as mold closure, mold opening, material viscosity, abrasiveness, glass preheating, the application of the paint onto the glass, and the paint itself. A different paint may provide the best long term solution to the adhesion problem.

Molding of Trough Panels

The first consideration in the molding of panels was the determination of a charge pattern. To achieve uniform mechanical properties and complete rib fill-out, it was thought that the charge pattern should cover a large percentage of the total area with extra stacks of material around the rib areas. The total charge weight of twenty-five pounds included:

1 sheet - 37" x 44"
10 strips - 2" x 44", 2 each located over the 5 ribs
4 strips - 2" x 37", 2 each over rim and vertex coaming

Approximately 90% fill-out was achieved with this charge pattern. Succeeding charge pattern tryouts used the same basic pattern with variations in the width of the strips and in placement of material near the boss area. Complete fill-out has been achieved although material porosity and apparent air entrapment between the SMC and the glass can be attributed to this charge pattern. A different charge as shown in Figure 4 has been used successfully, providing complete fill-out, a marked decrease in porosity, and no air entrapment.

The loading of the glass in the mold was achieved by manually overbending the glass, lowering it within the vertical indentations and allowing it to spring back against these indentations. Since the Chemcor glass is very edge sensitive, special care was exercised when placing the glass against the rim and vertex sides since on these edges only 0.150" clearance exists between the molded glass and the edge of the panel. Sliding and turning of the glass on the die, resulting in the glass shattering, was of major concern.

After the glass was placed in the die the charge pattern was located on top of the glass and the panel was molded for a total of three minutes. A typical pressure-time curve is shown in Figure 5. After

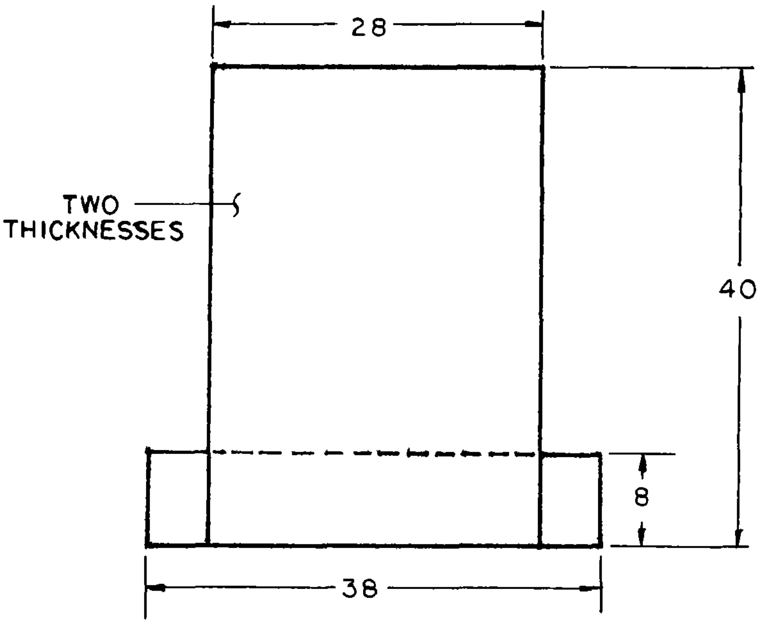

FIGURE 4 CHARGE PATTERN

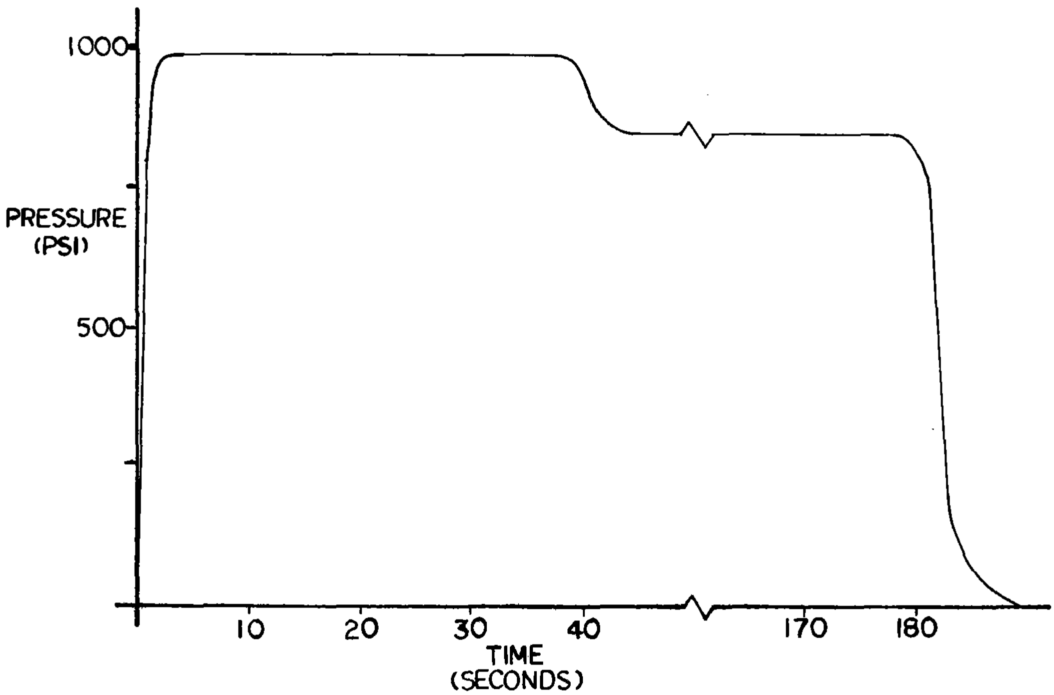

FIGURE 5 PRESSURE-TIME CURVE FOR SMC TROUGH PANEL

the initial high pressure needed for mold fill-out, the pressure was reduced for the remainder of the cure cycle.

Fifteen panels have been molded with the Chemcor glass sheets. Of these, three of the sheets broke because the glass hit an edge and shattered, two broke because of a piece of grit in the mold, and two broke on ejection. The opening velocity of the ram has been slowed to alleviate the glass breakage on ejection. Placement of the glass and cleaning of the mold continue to be critical items.

The eight panels that survived the molding have indicated some areas of concern that were foreseen and some that were not foreseen. The bimetallic action of the glass and SMC has caused the panel when cooling to increase in focal length, an expected result. However, the bimetallic action also develops a curvature across the width of the panel, resulting in a separation between the glass and the SMC at the rim and vertex corners. It is believed that this problem is a combination of the bimetallic action and insufficient adhesion between the glass and the SMC as the panel cools to room temperature. A possible solution is to clamp the panel to a fixture immediately after ejection and allow the glass to SMC adhesion to develop its full strength before removing the clamps.

Some of the panels have shown a delamination of the reflective silver surface and the glass surface, with sizes ranging from pencil point to four inch diameter areas. The silver delamination areas show no consistency in location from panel to panel and do not occur on every panel. The silver delamination could be caused by high local viscosity areas of the SMC, flow of the SMC, or poor silver to glass adhesion strengths.

Some panels have shown a gaseous bubble trapped between the glass and the SMC, which would indicate no glass/SMC adhesion in these areas. It is believed that the charge pattern is the main cause for this problem and that with the pattern as shown in Figure 4 the air entrapment problem, although still a cause for concern and something to be watched, has been minimized.

The molding of the panels has shown success in many areas of initial concern. A definable edge of SMC, although only 0.150" thick on the rim side, has been molded on every part where the SMC was given enough time to flow around the glass. Complete rib and boss fill-out has occurred even with only a 0.010" lead in radius. There has been no noticeable read through of the ribs onto the glass surface.

Material property tests have been performed on samples cut from a trough panel, with the following results:

(1) the flexural strength of the rib areas is greater than the required value

(2) the flexural modulus of the rib areas is greater than the required value

(3) the glass content of the rib areas is equal to the glass content of flat plaque samples

(4) the insert pull out strength of the bosses is greater than the required strength

Conclusion

A greater understanding of the problems that were expected to be encountered in this development program has been attained. The positioning of the glass in the mold, the survivability of the glass, complete part fill-out and the achievement of the needed strength and stiffness have provided a firm foundation on which to gain confidence in the molding of glass/SMC trough panels. However, problems do remain. Present areas of concern are the adhesion between the glass and the SMC and the silver delamination.

It is believed that SMC/mirrored glass solar panels can be developed for co-molding at rates similar to those available in automotive applications. This method of fabricating such panels will minimize their cost and make their application in solar systems cost competitive as the cost of fossil fuels increases.

Acknowledgements

Work on the development effort of SMC parabolic trough panels is being performed under contract to Sandia Laboratories, Contract No. 13-8720.

HONEYCOMB REFLECTOR/STRUCTURE

Joseph W. McDowell
Electromechanical Subsystems Division 2323
Sandia National Laboratories
Albuquerque, NM 87185

Introduction

The Engineering Prototype Trough (EPT), described in the FY1978 Annual Progress Report "Midtemperature Component and Subsystem Development Project" SAND79-0800, was an earlier attempt to use a honeycomb panel fabrication for a reflector structure. It was 75 3/4" across and 20' long, or 2 m x 6.1 m.

With mirrored glass added to this structure, it gave an enticing peak performance of 60% at 316^{o}C. However, this was achieved by blocking out 4" bands along each rim in order to eliminate zones of excessive slope error. This error was induced by a fabrication technique. A preassembly of the face skin with joined honeycomb panels and the rim rectangular tubing was made in the flat. As this large preassembly was stretched over a forming tool, the stiffness of the rim edges was impossible to overcome. Hence, large slope errors resulted in the rim areas.

Yet the whole concept appeared promising and had the potential for mass production if processing techniques were revised. This led naturally to the current design for a honeycomb reflector module.

Design Lessons Gained From the EPT

The first EPT and subsequently some slightly modified troughs were made by Hexcel, Inc. at the Casa Grande, Arizona plant. The success of these troughs in both laser tracing and performance testing was fundamentally due to an excellent forming tool. This tool, which provided an inverse shape of the fabricated part parabolic contour, was made from dense core honeycomb milled in a five-axis mill to the exact inverse contour of the $x^2 = 4$ (19.01") y. While it was never formally checked, it did match an accurate template extremely closely. This tool, which was adhesively assembled, was used in a room temperature process for trough fabrication since no ovens of this size were available.

If any springback did occur in the assemblies produced on this tool, it is our opinion that this was in the order of a 1/16" at the rims and appeared to be systematic from vertex to rim. Larger deviations than this were measured near the rims, but this appeared to be the result of the stiffness already described. So with the materials and processes involved with the EPT and the future honeycomb reflector, the amount of error caused by springback was and will be small. In that event, the error in focus will really be small enough to be compensated by a slight change in the location of the receiver. (See Figure 1)

For some time now, the EPT has been showing signs of rust corrosion in the interior of the sandwich. The face sheets used in its fabrication were 26 ga cold rolled steel. While we attempted to seal the structure at all steps, we now believe that we should not have allowed mounting bracket holes, receiver support holes and locating and aligning rivets used in the initial assembly to intrude into the interior. These may be the sources of moisture intrusion. In any case, the steel is rusting, particularly in the bonded areas using a Hexcel proprietary sheet adhesive. We can only speculate on this, but recent comments by Hexcel lead us to believe that better cleaning and pretreatment of the steel has improved this bonding process on current panels.

Design Description of an Improved Prototypical Trough

Each reflector module is approximately 2 m x 6 m aperture fabricated as a single unit with a 19.01" focal length, consisting of the following material: (See Figure 2)

1) 26 ga (0.019") aluminized steel face and back skins
2) 1" thick x 3/4" cell overexpanded, .005 aluminum honeycomb core
3) 12 panes of .050" thick, chemically strengthened glass 39 1/4" x 44 7/8" with silver mirror on second surface
4) 4" wide, 26 ga aluminized steel double strips of steel for face sheet joints and back sheet vertex joint
5) 26 ga aluminized steel sheet filler/compensation strips

MIRROR NO. ..., YR,MO,DA,TEST NO: ...
NOMINAL Z INCREMENT (M)=.04
SLOPE ERROR SCALE IS 20 MILLIRAD. PER Z INCREMENT

ADV. TROUGH IN FIELD, LIGHT BREEZE--TRANSIT/TAPE MEAS. ALIGN
LEFT HALF, FIRST SCAN 4CM TO RT OF L EDGE, SET. 18 TO 7F

Figure 1

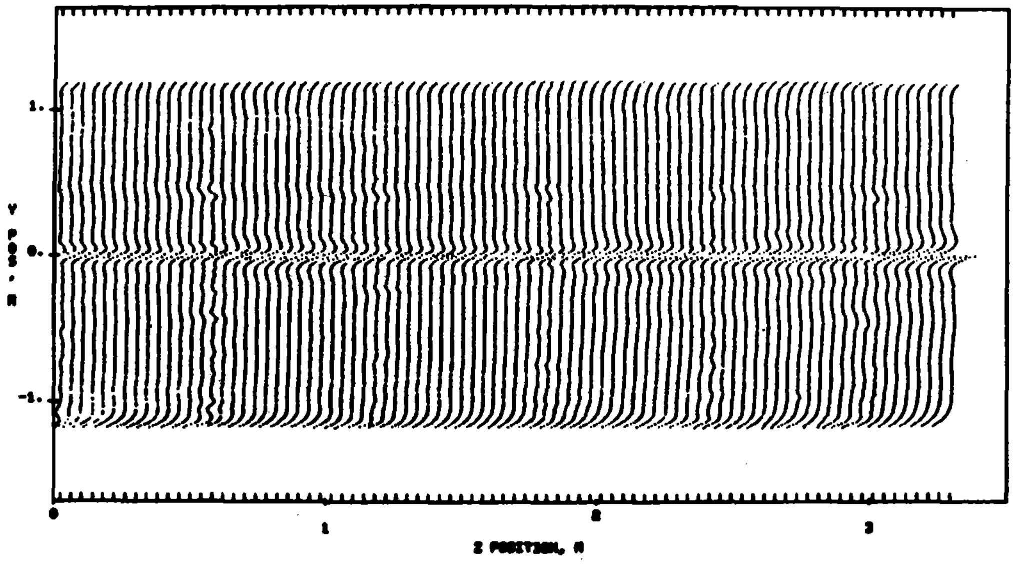

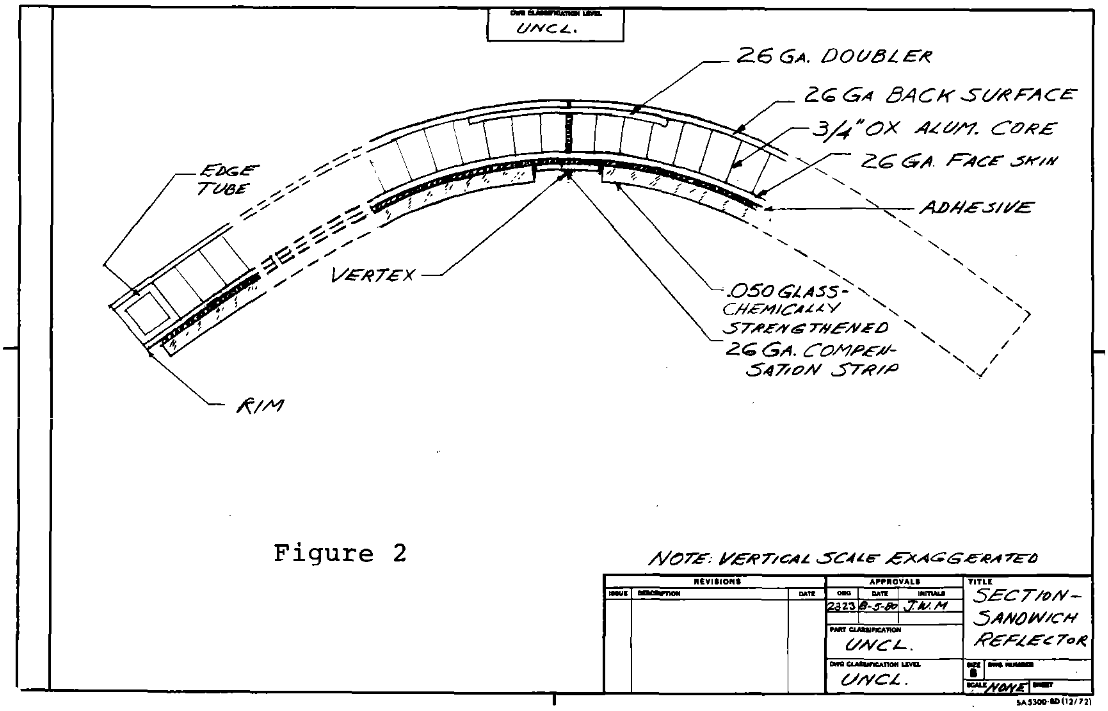

Figure 2

6) Mounting pads and edge closures

7) Adhesives

<ins>Design of Steel/Mirrored Glass Face Laminate</ins> -- It is proposed that the reflecting face of the module be made from six subassemblies that are rim to rim laminates of two chemically strengthened mirrored glass panes which are essentially one-half parabolas in length and a rim to rim 26 ga steel sheet. Such laminates will be made in the flat with the adhesive cured in a press and then stretched over the final assembly/tooling for the final assembly fabrication. Experience in assembly of the EPT showed that pushing a flat sheet of chemically strengthened glass into position to match a previously built trough contour lacked control, consumed manpower, caused voids in the bond line and made adhesive control and cleanup difficult. Other early experience with sagged glass panels, which are not chemically strengthened, showed many difficulties when the slightly differing trough and glass contours were brought together with a few mils of adhesive between since local stress areas occurred and glass fractured.

The 26 ga steel sheet for skins was chosen because it provides more than adequate strength for sandwich skin stresses and in combination with the honeycomb provides the rigidity required for the 2 m x 6 m structure. It is also a practical gauge for availability and can be handled (with difficulty) in large panels through processing operations. Further, it droops under gravity into the curvature required.

The laminate combination of 26 ga steel and .050 glass, however, is not ideal. A glass of approximately .035 would be better, but this is not available in the 0317 nor in chemically strengthened condition. While not ideal, the laminate of 26 ga and .050 glass can be stretched onto an inverse parabolic tool form with low force. A theoretical glass to steel laminate does have its neutral axis approximately .010 into the glass, but the chemically strengthened glass outer layers permit this without fracture. An adhesive with some small amount of flexibility helps to move the neutral axis toward the bond line, which would be the ideal condition. It is hoped that a warm temperature cure for the laminate can be developed such that additional compression pre-stress can be imparted to the glass, thus effectively moving the neutral axis toward the bond line. The additional forces needed to make this laminate lay on and conform to the tooling may inhibit this approach.

The principal problem which needs to be solved in the laminate assembly is the elimination of large air entrapment zones as the sheets are brought together. A method of feeding both sheets simultaneously through a slight pressure zone provided by rollers as the sheets come together onto the adhesive layer have been tried. Also, a few experiments at Sandia have shown that a widely spaced pattern of small perforation holes in the steel can provide the relief for entrapped air and surplus adhesive as well.

The adhesive used for joining the laminate will most likely be an epoxy system which is formulated 60 parts of Epon 828, 40 parts Versamid 140 and 10 parts ATBN. While the perfect adhesive is yet to be discovered for this task, this blend has achieved an excellent bond, providing weathering protection and it is compatible with the silver/copper mirror and mirror paint layers as shown by extensive simulated environment exposure and field exposure of the EPT.

Trials with PVB film, acrylic systems and proprietary adhesives will continue to be made in search of perfection. Future sessions such as this should be able to report the progress with processing and aging results of these alternatives.

<u>Design for Long-Life Corrosion Protection</u> -- Here the overriding design objective is to maximize the sealing of the internal cavity of the structure and then, realizing that this will not be perfect, to offer barriers to the progressive corrosion attack. The choice of materials is almost as important as the sealing. The main surfaces of the structure will be aluminized steel to slow the moisture attack and <u>solid web</u> aluminum honeycomb core has the usual anti-corrosion properties while acting as barriers. The edges will be adhesively sealed with either square tubing or channel section with at least 1/2" of adhesive-filled lap joints. All doublers will also feature wide lapping areas to present long leak paths. No holes for any reason will intrude into the internal cavity of the structure. Mounting pads and later receiver supports will be adhesively attached only.

The outermost barrier to attack from the elements will be paint.

Because of the aluminum coating on the steel, an aluminum primer will be necessary, this is to be followed with a urethane base white gloss-coat. The paint coating is essential in all zones where steel substrate is exposed by cutting. Also, all bond lines, be they edges of a bonding layer or squeeze out between sheets or filets such as will be found around the boundaries of individual glass panes will be painted to provide UV protection. Finally, the paint will provide protection for potential pin holes or thin spots of the aluminized coating on the steel faces.

Design for Minimizing Section Modulus Transitions -- From the aggregate of errors affecting components of the total collector system, the contour of the trough structure has been assigned a target of 2.5 milliradian scope error at one standard deviation. The slope referred to in slope error is the angle of tangency to the curvature of the trough at any point and the error is a measure of the amount that the slope angle deviates from the theoretical line of tangency of a perfect parabola at that point. Unfortunately, it is an immutable law of optics that error of a reflected ray is twice the error of the slope such that a 2.5 mr slope error means a 5.0 mr error for the reflected or aimed ray.

While this measure of error is at first thought unfamiliar and dimensionally vague, it is really a quite useful concept. A 1 mr angle is 0.0570°, a small number. But at such small angles it is valuable to remember that at one inch from the apex a milliradian angle has a span of .001". At 40 inches, the offset is .040". So for $1\sigma = 5$ mr, the aiming error at 40 inches is ±.200" and for 3σ the error is ±.600. From this, it is quickly apparent that slope errors at the vertex of a parabola with a focal length of 19.01" are half as important as rim errors. Because of this, structural details which affect slope will, if possible, be concentrated at the vertex. At present, both the honey-comb and the mirror glass must be discontinuous at the vertex.

It may be thought that quality of a curved surface formed on an inversely curved tool is controlled by the contour quality of the tool. This is true in a large sense, but not true if the section modulus of the formed assembly changes. This introduces local stresses which distort the zone of transition. For example, on the EPT it was agreed that the honeycomb for want of larger panels would have to be joined at the vertex. Unfortunately, due to schedule, this size was not available in time and three pieces were joined to form a rim to rim sandwich. This fabrication process caused two contour affected zones 3-4" wide in which the slope error was estimated to average 3-4 milliradian with peaks of error as great as 10 milliradian (remember: aiming error is 2 x slope error). (See Figure 3.) To put this another way, the added stiffness of the honeycomb in the zone where it was preassembled with butted edge joints caused distortion of the formed surface, yet the tool to which this contour was formed was much better.

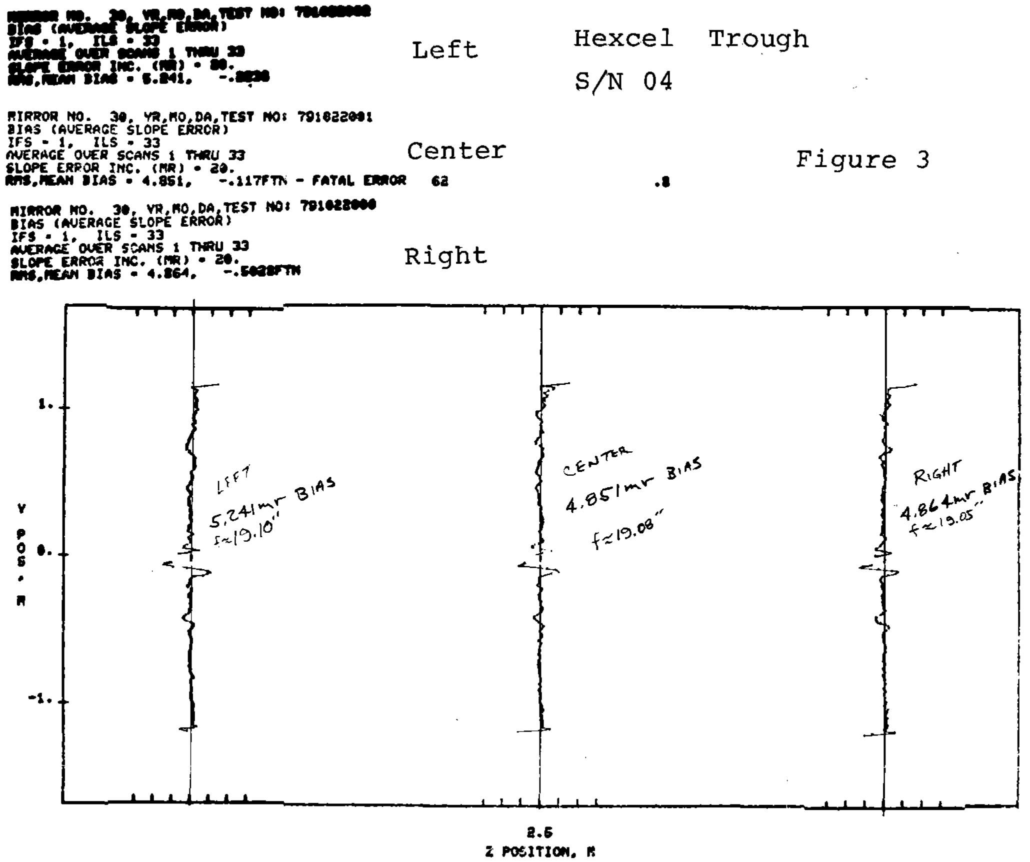

Figure 3

One of the potential distortion zones in the honeycomb structure is found in the face sheet laminate. In the description of the laminate, you will recall that each is made from a rim to rim 26 ga aluminized steel sheet, but two pieces of approximately half parabolic chemically strengthened glass panes. In some early experiments here at Sandia, it was found that butting the two panes of glass at the approximate vertex was not completely satisfactory when the curved laminate was stretched over a tool form. As the ends of the laminate were pushed down against the tool, the discontinuity in section modules at the butt joint caused the steel to yield and linear bulge was formed. In order to avoid this, the chemically strengthened glass panes for the final design have been sized to provide a gap between glass pane edges. This gap of approximately one inch will be spanned by an aluminized steel 26 ga strip. This strip will be adhesively attached to the rim to rim face sheet as the laminate is fabricated. The strip provides a section modulus similar to the glass-steel-laminate modulus. As such, it has proven in limited experiments here that less yielding occurs and this source of distortion is minimized.

Alternate Reflector Surface

Recently, a domestic source for sheets of .040" nonstrengthened glass has come to our attention. These sheets are large enough to be cut to 39 1/4" x 89 7/8" and thus provide a rim to rim laminate of the 1 m x 2 m aperture size. While we have not yet made a laminate of this size at Sandia, others have handled this process successfully which is encouraging. Unless some unusual problem of cutting, mirroring and handling occur, a laminate of this design will provide a constant modulus in bending and should make the vertex joint distortions and subsequent slope errors minimal. Here again, future sessions such as this and informal contacts by telephone should serve to keep you advised of our progress.

GLASS LAMINATE REFLECTOR/STRUCTURE

Samuel B. Martin
Electromechanical Subsystems Division 2323
Sandia National Laboratories
Albuquerque, NM 87185

Introduction

A straightforward concept for a parabolic trough solar collector utilizes thermally formed and laminated glass mirrors which are supported by a steel structure. Automotive windshield technology demonstrates that glass can be thermally formed to shape and laminated using high volume production techniques. Relative to potential application to solar collectors, laminated mirrors for heliostats at the CRTF have indicated excellent protection of the silver from the environment. Metal stamping technology appears applicable for fabrication of the support structure because of good contour accuracy and potentially low costs in production.

The purposes of this paper are to describe the concept; to present evaluation results on prototype thermally formed glass mirrors; and to describe design, fabrication, and assembly considerations for the concept. The following paper will describe manufacturing development and costing of thermally formed glass.

Concept Description

A mockup of the concept is shown in Figure 1. The glass mirrors are approximately 1 m x 1 m aperture. Twelve mirrors will be mounted on a steel support structure to provide a 2 m x 6 m aperture trough. The support structure will consist of a thin walled torque tube with sheet metal ribs to support the glass. It is currently planned to bond the glass directly to the support structure with a resilient adhesive. An alignment fixture will be required to position the glass during bonding.

Most glasses currently available will require a relatively thin second surface silvered front sheet to minimize absorption. The mirror is laminated to a thicker back sheet of glass to provide structural support and to protect the silver.

Thermally Formed Glass Reflectors

Ford and PPG have recently completed developments to thermally form glass to a two meter parabola. Ford gravity sagged 2.2 mm thick Ford low iron float glass from the Barstow heliostat glass run and 1.5 mm thick Corning 0317 glass. PPG gravity sagged and also press formed PPG glass in thicknesses of 2.3 mm and 1.5 mm. Glass sheets in these thicknesses are not self-supporting and must be supported on a substrate to evaluate the accuracy. Average 1σ slope errors were approximately 3 mr (milliradians) for the PPG press formed glass, 4 mr for the Ford gravity sagged glass, and 7 mr for the PPG gravity sagged glass which had long wavelength errors.

Indications are that improved optical surface accuracy could be achieved with continued development. The scope of the recently completed development efforts pertained primarily to concept verification and involved limited runs of parts relative to more typical manufacturing development volumes. A sample of glass from each group was bonded to a honeycomb trough segment and showed slope errors of less than 2.5 mr which is the design goal. Accuracy of the present glass appears adequate for low pressure bonding.

Large area void free bonds of curved glass to parabolic trough sections have proven to be difficult to make. The most successful effort to date was made by Custom Engineering using an accurate male mold to support the glass during bonding with a relatively thick adhesive line to fill gaps between the trough and the glass. Automotive windshields have long demonstrated that large area void free bonds can be made using sheet polyvinyl butyral (PVB) as the adhesive. Both sheets of a windshield are sagged as a matched pair so that uniform thickness void free bonds are obtainable. It is this technology which is being applied to laminated parabolic trough mirrors. PPG is currently under contract to make prototype laminated glass mirrors.

Solar averaged reflectivity is approximately 0.89 for the Ford glass and 0.87 for the PPG glass. This is less than the 0.94 desired and available in the Corning 0317 and the Schott B270. Ford demonstrated that the Corning 0317 glass can be sagged on the same tooling. However, the softening temperature is higher than for ordinary float glass which presents problems for sagging matched pairs. The Schott B270 glass has sufficiently low absorption that 6 mm glass could be used directly without laminating.

Structural Design

The primary function of the support structure is to accurately align and hold the individual glass panels without introducing excessive stresses into the glass. A panel size of 1 m wide by 1.1 m arc length was selected as a reasonable compromise between fabricating and handling requirements versus minimizing the number of panels to be aligned. For this panel size, a thickness of 6 mm provides reasonable rigidity and handling strength. The design limit for tensile stress in the glass is 1000 psi long-term and 2000 psi short-term. Bonded line supports using a resilient adhesive were chosen to spread the loads and to accommodate the thermal mismatch between the glass and steel. Silicon rubber was used for the heliostats and the trough mockup, but urethanes and polysulfides are being investigated to obtain shorter cure times. Average normal stresses in the adhesive from wind and gravity loads are very low (< 10 psi).

Twelve mirrors are required to provide a 2 m x 6 m trough. A thin walled 250 mm diameter tube will be used to carry the bending and torque loads. Sheet metal ribs will be fastened to the tube to support the glass. Initial designs were based on longitudinal supports which were bonded to the glass and then bolted to the support structure. See Figure 2. Stresses and slope errors were evaluated with a finite element analysis and found to be acceptable for attaching at either three or four points as shown on the trough mockup. However, stability is much better for the four-point mounting. Tolerancing the parts to provide proper alignment proved to be difficult, and individually adjusting the panels did not appear desirable for production. Bonding of the glass directly to the support structure and allowing the adhesive to compensate for tolerance buildups at the final assembly stage appears to be desirable. An alignment fixture will be required to position and hold the glass during bonding.

Both longitudinal stringer and parabolic rib approaches are being investigated. Figures 3 and 4 show the basic concepts, respectively. The longitudinal stringer approach offers the potential for easier alignment of relatively noncritical parts. The parabolic ribs conceptually require fewer, but more critical parts. The Budd Company has demonstrated the capability to stamp accurate parabolic sections from sheet metal. (See proceedings paper by Champion and Biester.) It is important for both concepts that the design is able to accommodate normal tolerances for tube straightness and that welding locations and sequences be chosen to minimize warping of the final assembly.

It should be noted that bonding the glass to steel structural members, in general, limits the working stress in the steel to 3000 psi to keep the stress in the glass below 1000 psi. There is a reluctance at this point to allow the glass to take significant portions of the trough assembly structural loads. This requires two independent ribs per panel and limits the maximum stress in the rib when the glass is bonded directly to the rib. When the glass is bonded to the longitudinal stringers, it is possible to share ribs, but the stress in the stringers must be limited to be compatible with the glass. In either case, the glass will take the bending loads between supports imposed by wind and gravity.

Conclusions

A collector made with a glass laminate reflector is very simple in concept. There is an existing mass production industry which has the capability to manufacture glass laminates with only normal improvements required. Silvering of the curved glass is the major step not demonstrated on a production basis. Improvements in accuracy and reflectivity would be expected as the market develops.

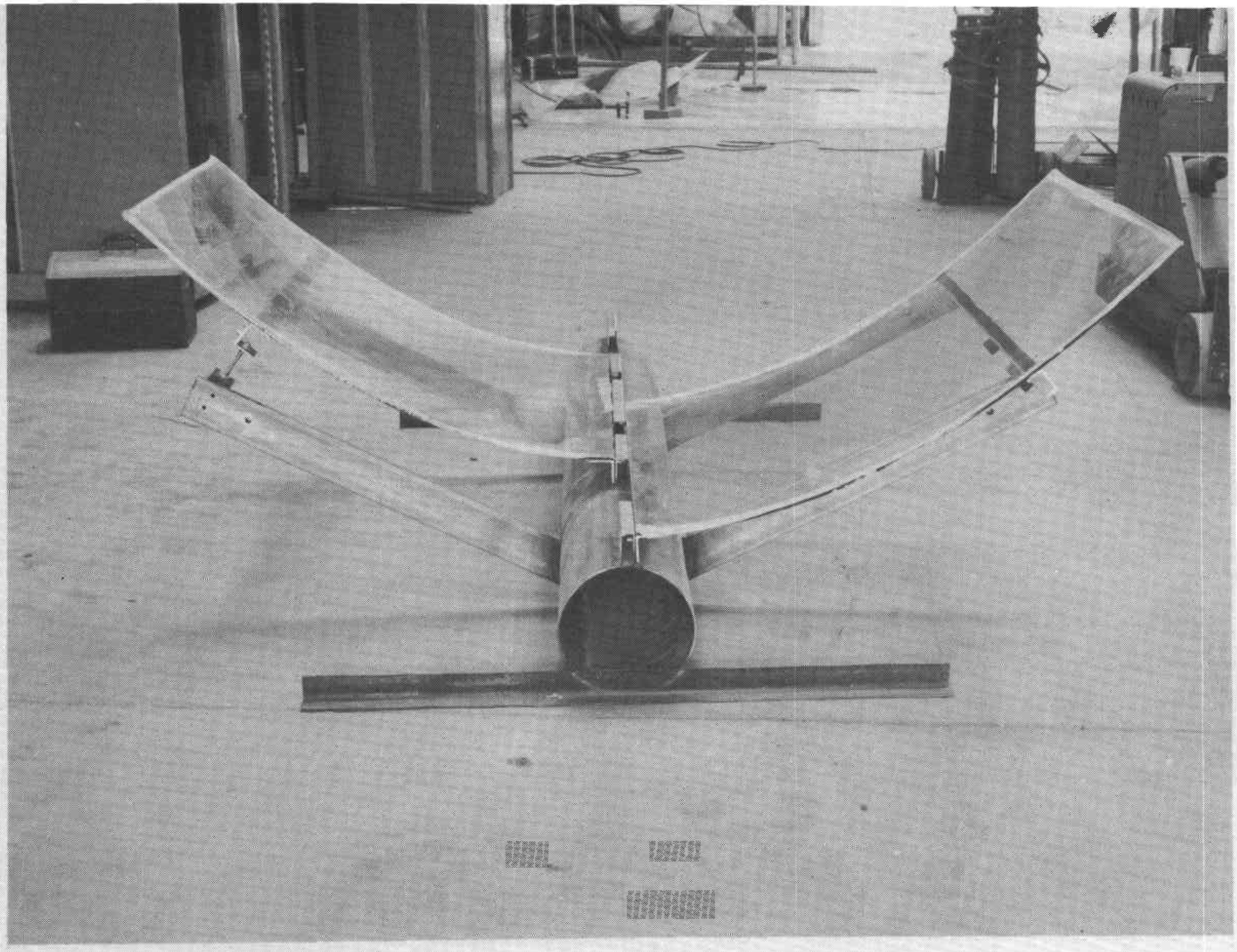

FIGURE 1 - GLASS LAMINATE MOCKUP

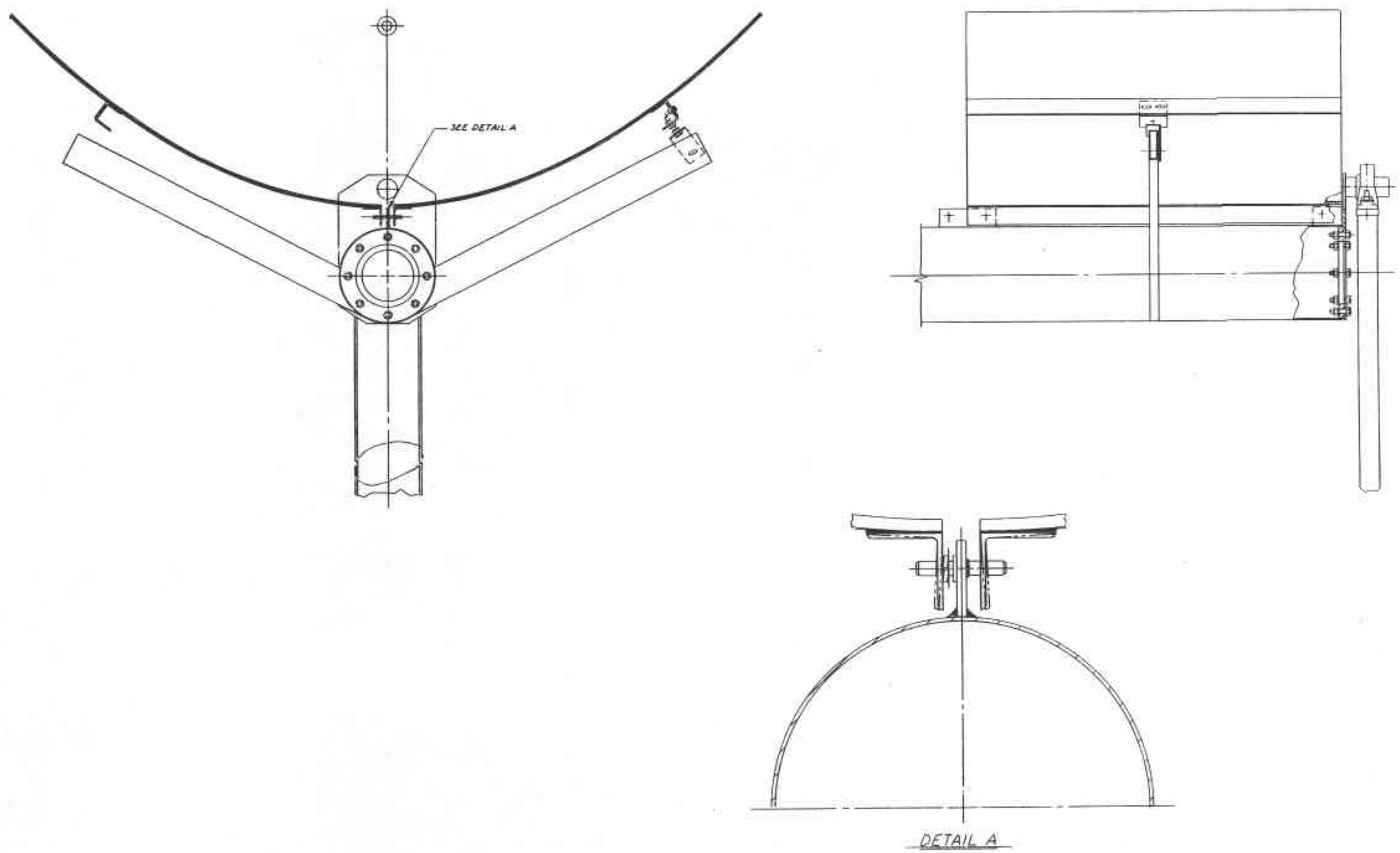

FIGURE 2 - GLASS LAMINATE - THREE POINT ADJUSTABLE

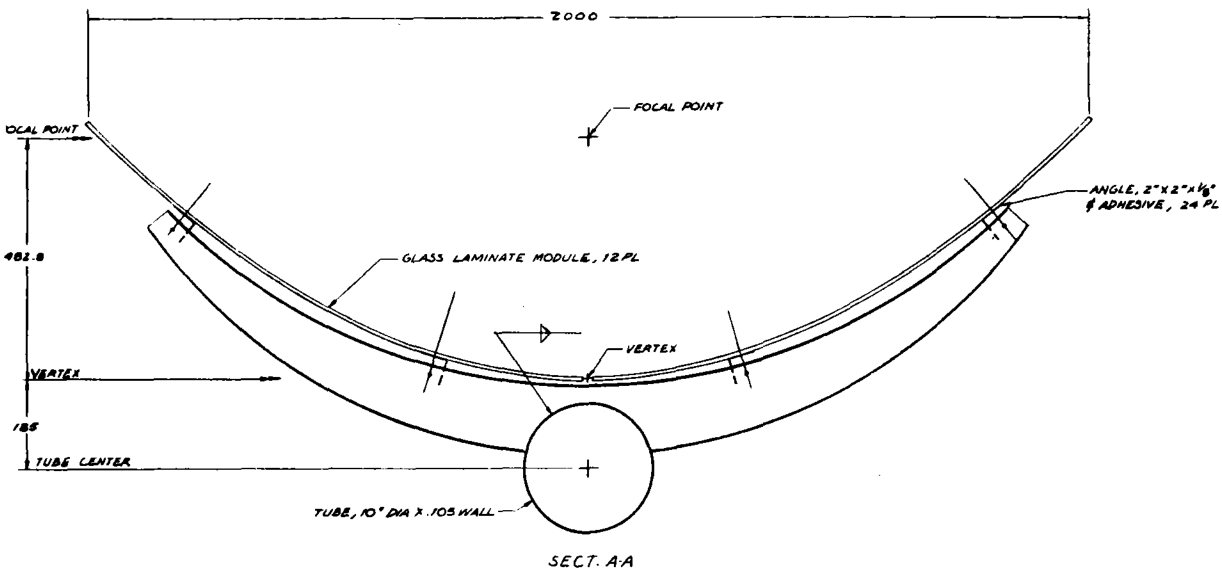

Figure 3. Glass Laminate - Longitudinal Stringer

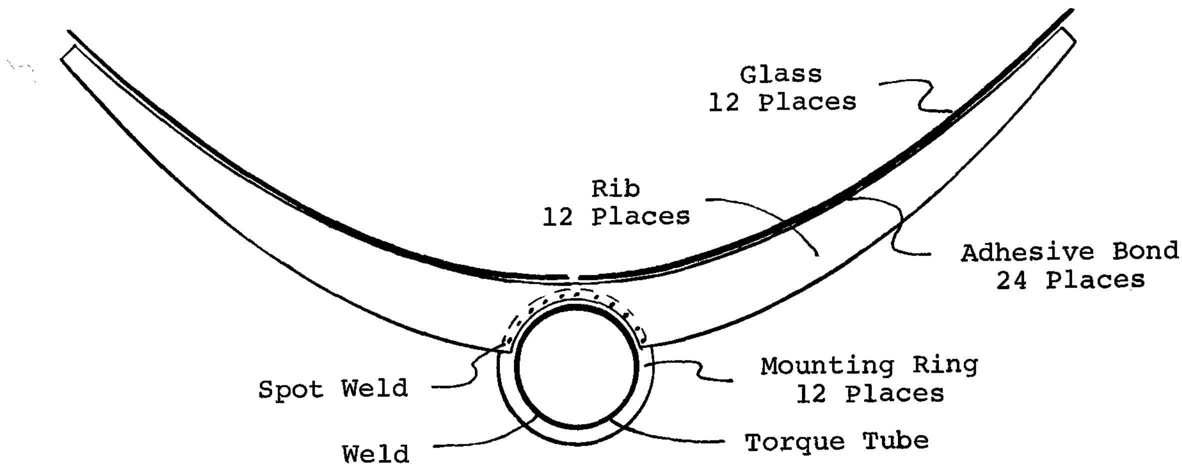

Figure 4. Glass Laminate - Rib Mounting

THERMALLY FORMED PARABOLIC GLASS PANELS

I. Earl Lewis
Western Development Laboratories Division
Ford Aerospace & Communications Corporation
Palo Alto, California

Introduction

This paper briefly presents the results of a contract between Ford Aerospace & Communications Corporation and Sandia Laboratories, Albuquerque, N.M., covering the manufacture of prototype solar panels and a related manufacturing analysis.

Ford Motor Company offers a unique complement of expertise whereby its production and manufacturing experience is combined with the systems, engineering and program management capabilities of Western Development Laboratories Division of the Ford Aerospace & Communications Corporation, a wholly owned subsidiary of the Ford Motor Company. The Ford Glass Division, second largest producer of glass in the world, maintains extensive Research and Development Laboratories along with a Technical Center, both of which are devoted to analyzing and evaluating new manufacturing techniques and products.

By far the most important barrier to the development of industrial solar energy apparatus on a large scale is the adaptibility of the solar hardware to high volume production techniques and processes. Many of the collectors available today use reflector surfaces that are not durable enough to withstand the rigors of day-in, day-out operation in changing weather conditions over a significant number of years. It is today's concensus of those working in the collector field that the only suitable surface for a truly long-life solar concentrator is glass, curved as required to form the overall concentrator surface.

To date there has been little development of a production scheme for forming flat glass into the curves needed to fashion a solar trough concentrator. This paper addresses certain manufacturing technology applicable to the cost-effective production of formed glass panels for use in parabolic trough line focus concentrating solar collectors.

Objectives

The purpose of this contract was to meet the following key objectives for the Sandia Advanced Trough Development Program:

- Develop an understanding of the optical and mechanical quality of parabolic glass panels for line-focus solar collectors by manufacturing prototype collector panels using high volume production manufacturing techniques.

- Investigate tooling and manufacturing techniques in order to assist in the development of specifications for future mass procurement activities.

- Establish cost estimates for mass produced sagged glass for trough applications.

Study Overview

Under the terms of this contract, 32 parabolic prototype panels of Ford Powerlite Plus low-iron glass (.090" thick) were fabricated at the Glass Division's Glass Technical Center located in Lincoln Park, Michigan. In addition, Corning 0317 fusion glass (.058" thick) was supplied by Sandia Laboratories, and 8 panels were fabricated on a "best efforts" basis. Each panel contour was a half parabola of one meter aperture (total trough aperture two meters) with a rim angle of 92^{o} and a focal length of 0.48 meter. The width of each panel was 1.2 meters (48 inches).

The half-parabola troughs fabricated under this contract were more complex than typical automotive parts, such as windshields, in that precise control of the entire panel surface contour was required. Therefore, to meet this requirement, forming techniques were modified but were still based on known windshield technology. The present windshield peripheral forming ring concept was modified by the addition of an internal "egg-crate" grid to produce the forming fixture for required panel contour.

Utilizing automotive practice, tooling masters and tooling aids were accurately fabricated. Solid surface mahogony models were developed from the Sandia master contour templates. From one mahogony model, a plastic solid surface male spotting model was poured and used for fabrication of the hinged forming fixture. From the other mahogony model, a plastic male skeleton gage was poured for use in final contour gaging.

The bending technique is essentially a gravity sag process. The solar glass is paired with a back-up glass sheet and passed through a bending furnace at preset speeds on an individual forming fixture. The panel is heated to the forming temperature, sagged, and cooled back to ambient temperature at a controlled rate.

Panel inspection measurements were made with the contour gage mechanical tooling and with zebra board reflective optical techniques. These measurements allowed on-line evaluations of the forming procedures and incorporation of processing changes. The final panel contour accuracies were determined by laser measurements at Sandia Laboratories.

The manufacturing analysis included: (1) manufacturing process selection, (2) manufacturing facilities and tooling expenditure estimates, and (3) directional product pricing assuming annual collector panel surface area markets of 10 thousand, 1 million, and 50 million square feet.

Conclusions and Recommendations

It is concluded that the adaptation of windshield forming technology utilizing a gridded fixture design concept is a viable process for continued short-term production of prototype quantities of presently-known configurations of solar trough panels requiring average panel slope errors less than 2.5 to 3.5 milliradians.

Based primarily on the additional complexity of this forming tool over present technology tooling and certain process limitations, it is judged that to accomplish large-volume capability will require development of new forming technology, i.e., solid ceramic mold fixtures. Ford Glass has a high confidence level that a manufacturing technique similar to that used for the prototype panels is a viable method for high-volume parabolic trough panel production.

For long-range, high-volume production of these panels, it is also recommended that the air float gas hearth process, a technique currently used to form automotive side glass, be studied as an alternate method of forming parabolic trough panels. Assuming manufacturing feasibility could be established, it is concluded that this process would be the most cost effective method of forming these panels in large volumes.

Product price was found to be highly sensitive to the level of production volume, particularly at the low volume end of the market spectrum under study. The economies of scale are particularly significant in the production of the raw material (low iron glass) and although less significant, there are substantial economies of scale in the fabrication area. For example, as a result of this study, it was concluded that product pricing per square foot of collector surface would be approximately: (1) $31.00 at the 10,000 square foot annual volume level, (2) $7.14 at the 1,000,000 square foot annual volume assuming that the qualified glass fabricator invested in a dedicated panel fabricating facility on a new site referred to as "Greenfield", (3) $2.96 at the 1,000,000 square foot annual volume level assuming existing capacity is available, and (4) $1.42 at the 50,000,000 sq.ft. annual volume level assuming that the qualified fabricator invested in a dedicated panel fabricating facility on a "Greenfield" site.

UNLOADING THERMALLY SAGGED PANEL
FROM FORMING FIXTURE

ANALYTICAL AND EXPERIMENTAL STUDIES OF SOME PARABOLIC LINE CONCENTRATOR DESIGN CONCEPTS

J. Richard Koteras
Brett A. Lewis
Applied Mechanics Division III, 5523
Sandia National Laboratories
Albuquerque, New Mexico 87185

Introduction

The finite element method is being used as part of the evaluation process for prototypical design concepts for parabolic line concentrators. The finite element studies are used to calculate stresses in line concentrators arising from various load conditions and to examine optical performance. This paper will discuss the analysis procedure which is being used. It will also discuss some experimental work being carried out in conjunction with the analyses to evaluate the numerical models.

Requirements for Finite Element Code

In order to efficiently analyze parabolic line concentrators, the finite element code used for the analysis must have certain capabilities. These capabilities become evident when one examines the nature of line concentrators and some of the objectives of the analyses.

The present line concentrators are basically shell-structures supported at a discrete number of points. Stress concentrations arise at these support points, and any finite element model of a line concentrator must be fairly detailed in the support region if the magnitudes of the stress concentrations are to be estimated with some reasonable accuracy. The need for detailed models makes a number of code capabilities important. One very important code feature for large models is some type of mesh generation. It is difficult, if not impossible, to correctly generate a model with a large number of nodes and elements without some type of mesh generation. Working with parabolic geometries can present some especially difficult problems, and it is desirable to shift as much of the burden of geometry definition as possible to the mesh generator. Another important feature required for detailed models is a large element library. Models of line concentrators usually require some combination of beam, plate, and constraint elements. Experience has shown that another important feature for detailed models of line concentrators is substructuring. Substructuring can allow the creation of an extremely detailed model while still maintaining a computationally tractable problem. One difficulty encountered with substructuring line concentrators is that they tend to lend themselves more to the generation of a small number of large substructures. Ideally, one would like to work with a medium or large number of small substructures. This is not too severe a problem if one has access to a computer system with a large mass storage system. In spite of this one difficulty, substructuring is an extremely valuable computational tool for the analysis of line concentrators. Finally, any code to be used for detailed models should be written to handle large problems, and it should handle them efficiently.

One objective of any analysis is to be able to easily examine the various load conditions that a line concentrator may experience. Because of this, it is desirable to use a code with flexible schemes for input of loads and flexible coordinate system definition. Flexible coordinate system definition is desirable since one may want to rotate parts of a collector model in regard to other parts for certain load cases.

Another objective is to evaluate the optical performance of the line concentrator. Since optical quantities are not standard output from finite element codes, it is necessary to write post-processors to compute quantities of interest. Calculation of optical quantities requires both geometric and displacement data. Any code used for the study of line concentrators should have, therefore, provisions which allow the user to easily access all tables and matrices needed for calculation of optical quantities.

Present Analysis Work

The code MSC/NASTRAN[1] is being used for the present analysis work. It has all of the features which are desirable for working with large models of line concentrators, and its substructuring capabilities can be described as highly automated. MSC/NASTRAN has been interfaced with a post-processor which will calculate equivalent slope errors. The equivalent slope error is a quantity which is useful for measuring the optical performance of parabolic concentrators.

Figures (1) through (3) show finite element models which have been developed with MSC/NASTRAN. Figures (1), (2), and (3) show models for a stamped sheet metal design, a sheet molding compound design, and a design which employs a laminated glass reflector supported by a space frame, respectively. The structures are not pictured in their entirety since substructuring is used. In Figure (1), for example, one quarter of the reflective panel has been modeled as a primary substructure. The rest of the panel is modeled as mirror image substructures of the primary substructure. These finite element models are being used to investigate stresses arising from wind loads and optical performance under gravity load conditions.

Experimental testing has been carried out on a prototype of a sheet metal concept. The purpose of the tests have been twofold. First, extensive testing of parabolic line concentrators has not been done before, and it is important to gain some insight into the structural behavior of line concentrators from actual experimental data. Second, there is a need to determine the accuracy of the results obtained by numerical methods.

The actual test was done on a module without a face sheet of glass. A sketch of the test module and its stand is shown in Figure (4). The test stand was designed to facilitate examination of a number of load cases; it roughly approximates the actual support structure the module would see in the field. Strain gages were placed on both the front of the sheet metal face and on the ribs in back. The gages were placed so that stress profiles could be drawn in both longitudinal and transverse directions (see Figure (5)). The preliminary finite element results showed high concentrations over the support points, and strain gages were concentrated in those areas. Deflection gages were also used to monitor the module.

Loading of the test module was done to simulate some net wind loads experienced by the line concentrator in wind tunnel tests. Sheets of lead were used to simulate uniform loads over portions of the panel. A total of four load cases were examined. These were used to study a survival wind load condition and a torsional loading that arises from wind loads. Measurements were taken during a stepped loading and unloading in order to determine if there were any hysteresis effects in the adhesive that bonds the ribs to the front sheet metal. A long term loading was applied to determine if there was any significant creep of the adhesive.

Some of the results from the experimental testing are shown in Figures (6) and (7). These are for the case of a twenty pound per square foot uniform loading over half (vertex to edge rim) of a panel. Figure (6) shown stress in the transverse direction at about two inches from the edge of the panel, z = 2.0 in. A high stress concentration near the attachment point is evident. Figure (7) shows stresses in the transverse direction at z = 18.8 in. Initial inspection of the results does not indicate any significant creep or hysteresis effects in the module.

Work has begun on correlating experimental and finite element data. Some of the displacement data correlates to within ten percent if an apparent rigid body motion of the test apparatus is accounted for. Correlation of the stress data varies widely over the surface of the panel. Some of the stress predictions near the support point show reasonable agreement. For regions of low stress (midway along the longitudinal axis of the trough) the finite element model is under-predicting stresses by a large amount.

Conclusions and Recommendations

The task of correlating finite element and experimental results has only just begun, and it is difficult to draw too many inferences concerning correlation. It is known that the present model is too stiff, and refinements will have to be made to produce better correlation. Some initial adjustments to the mesh indicate that, whenever significant approximations must be made, the approximations should be oriented toward the most flexible approach available within reason.

When doing refinements on a mesh, one hopes to avoid arbitrary fixes in order to achieve agreement between a finite element model and experimental results. If the present model for the sheet metal concept cannot be brought into overall agreement with some reasonable modifications, use of curved plate elements for modeling parabolic line concentrators should probably be investigated. The present models use flat plate elements to approximate the concentrators. When the angles between flat plate elements are small, the overall solution accuracy for a problem tends to decrease. Since some parts of the concentrators under study do have a very large radius of curvature, there are regions in the models which do have flat plate elements coming together at very shallow angles. Curved plate elements are a way to eliminate this problem.

The sheet metal design is the most complicated geometrically and the most difficult to model in great detail in all aspects. It may be difficult to transfer all of our findings in regard to the sheet metal design to designs which are geometrically simpler (such as the one shown in Figure (3)). For geometrically complicated designs, it may be necessary to use a finite element model for some preliminary predictions, build a prototype to provide experimental results, and then make refinements on the finite element model to correlate it with the actual structure. The verified model could then be used to investigate a wide range of load conditions. For geometrically simple designs, a rational approach to the model may be all that is required for a good representation of the actual structure.

There has been some concern about using finite element analysis to a larger extent in the initial design process. This has not been done up to now because of the long periods of time required to generate meshes. This long lead time has arisen because a mesh generator which runs in batch mode has been used. To speed up model generation, an interactive mesh generator is required which uses geometry definition as a precursor to mesh generation. As indicated earlier, working with parabolic geometries is a difficult task. If an interactive mesh generator with sophisticated procedures for geometry definition is used, much of the work of describing the structure can be transferred to the generator. If curved plate elements are to be used effectively in models, an interactive mesh generator is mandatory. In addition to interactive mesh generation, interactive post-processing is also required to bring finite element analysis into the initial design period.

Some consideration should be given to more fully exploiting the substructuring capabilities of MSC/NASTRAN. MSC/NASTRAN has the ability to do multilevel substructuring. This would allow the user to create a substructure model of a single reflector panel which is described by the degrees of freedom at its attachment points. This substructure could be used as part of a model of an entire array of panels mounted on a support structure. One could obtain a very accurate model of the entire array and support with a very economical computer model.

References

[1] McCormick, C. W., MSC/NASTRAN User's Manual, Volume I and II, The MacNeal-Schwendler Corporation, Los Angeles, California, 1976.

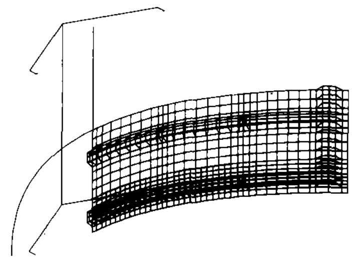

Figure 1. Finite element mesh for stamped sheet metal concept for parabolic line concentrator.

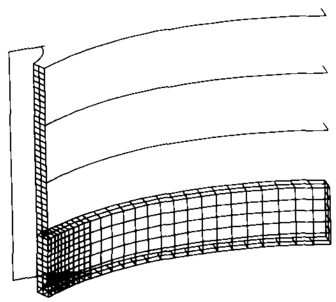

Figure 2. Finite element mesh for sheet molding compound concept for parabolic line concentrator.

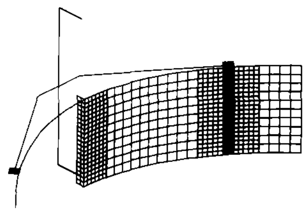

Figure 3. Finite element mesh for glass laminate concept for parabolic line concentrator.

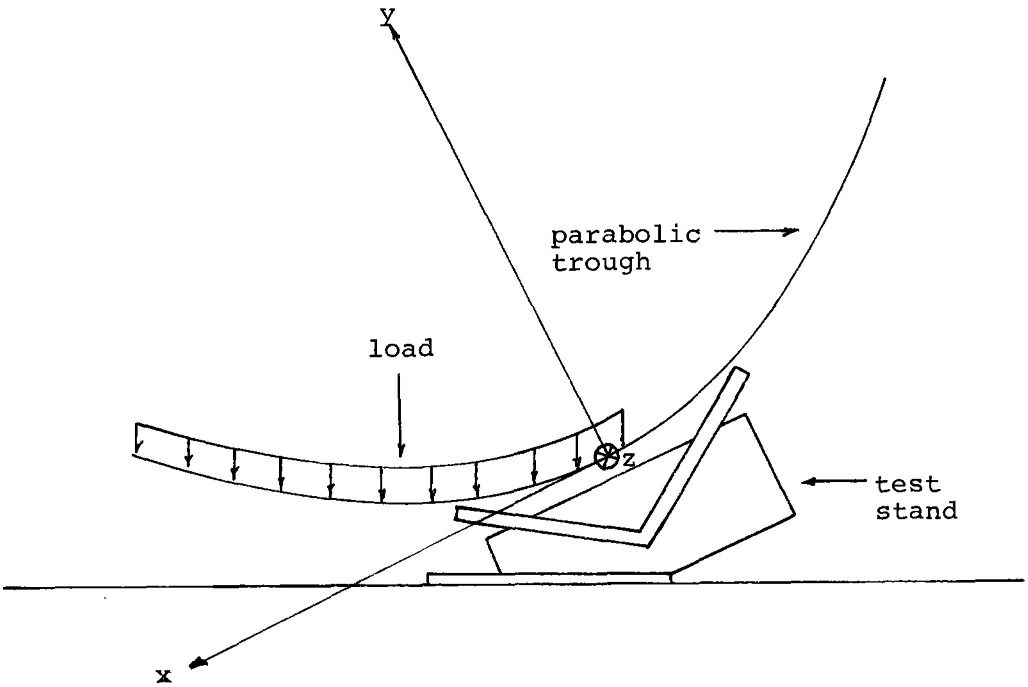

Figure 4. Test apparatus for measurement of stress and displacement data.

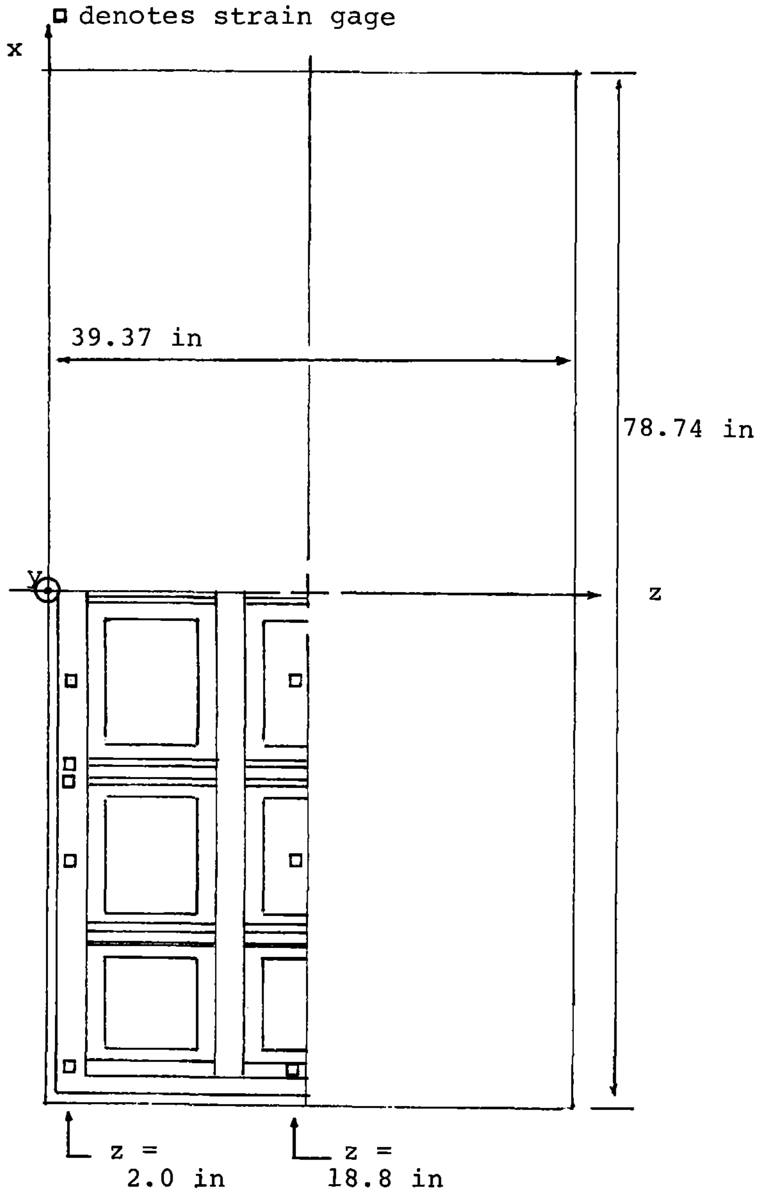

Figure 5. Location of strain gages on test panel. This figure shows the location of the strain gages on the front face of the parabolic line concentrator. Stamped sheet metal ribs on the back surface of the panel are shown in one of the quarter sections in order to give the locations of the gages relative to the ribs.

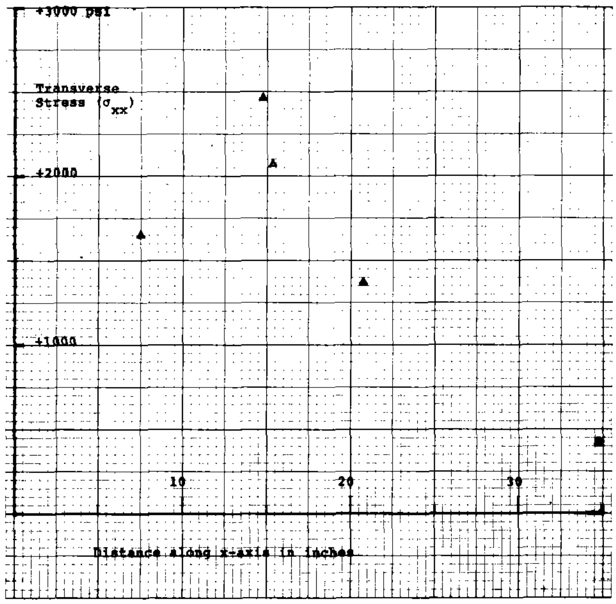

Figure 6. Transverse stress component on test apparatus at z = 2.0 inches.

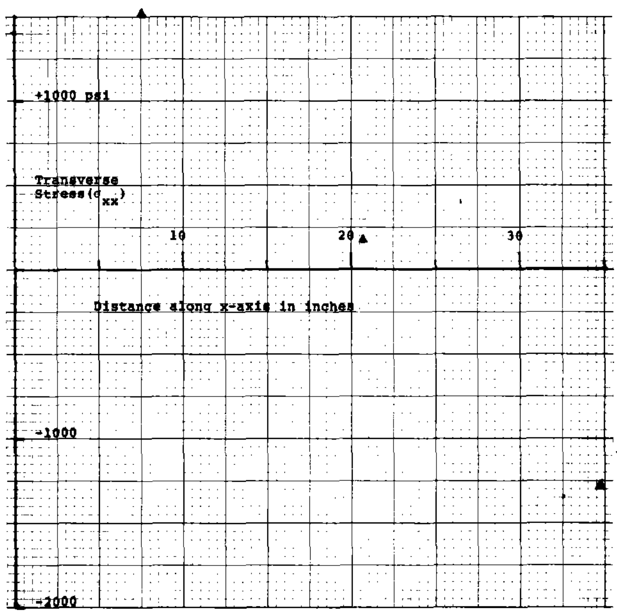

Figure 7. Transverse stress component on test apparatus at z = 18.8 inches.

INTEGRATED SOLAR FIELD CONTROL SYSTEMS

Brandon Ahrens
Component and Subsystem Development Division 4722
Sandia National Laboratories
Albuquerque, New Mexico

Introduction

Safe, high performance operation of a concentrating trough solar collector field requires that three control functions be accomplished. The troughs must be driven to stay in focus throughout the day. The flow of coolant must be controlled to maintain a desired output temperature, and, since the troughs are capable of heating their receivers far past the point of destruction if cooling is insufficient, safeguards must be provided to ensure that the system doesn't destroy itself in the event of low fluid flow. Additionally, information on the status of the field should be provided to an operator or service technician. Solar fields present some unusual problems to a controls designer. The field covers a large area making communications difficult and expensive. Components are sheltered only by a junction box and still must function reliably for many years. Many systems fielded to date have not accommodated these considerations nearly as well as they might. Controllers have too often been custom designed for one site only (a problem certainly not restricted to controllers), and designs have not always shown proper attention to high reliability. Relay logic is not uncommon and there has been poor integration of the circuitry required for different functions. An essential aspect of this system is that it integrates all control functions, tracking, flow control and safety, as well as status display into one control unit, drastically reducing wiring cost and complexity. Additionally, having one collector controller perform several functions justifies the use of a microprocessor which if used properly, reduces the size, cost and complexity of the circuitry while it increases its flexibility and capability. The result is a simpler system that should be more reliable as well as easier to maintain.

Honeywell has been contracted to develop prototype hardware combining their manufacturing and control system expertise with

Sandia's solar experience and fail safe design philosophy. Their system is presented in the following paper.

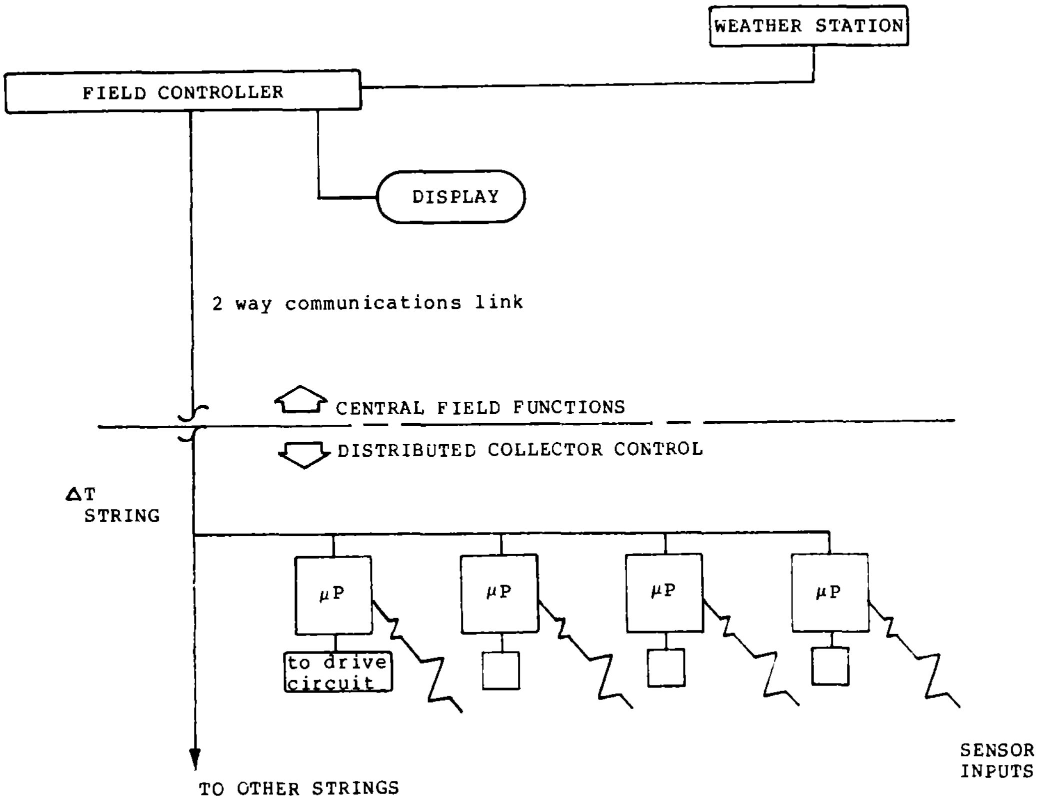

FIGURE 1
FIELD CONTROL BLOCK DIAGRAM

Configuration

The system is structured into two levels of logic (Figure 1) with an overall field controller supervising multiple collector controllers. The unit being controlled is a ΔT string which is the length of collector required to raise fluid to the desired temperature. ΔT strings are composed of several collector modules called drive strings with a collector controller for each drive string module. ΔT strings might have as few as one or two drive strings or as many as six or eight. This design easily accommodates any reasonable number of drive strings per ΔT string.

Functions

Suntracking

Of the three control functions, suntracking has probably received the most attention, though the majority of trackers that are presently in the field are variations on the conceptually simple shadow band tracker. A shadow band tracker has a bar or plate that shades a pair of optical or thermal sensors. The device is tilted so that the detectors are equally shaded and the tracker is pointed directly at the sun. Shadow band trackers have a fundamental problem in that they must be alligned with the trough. This is extremely difficult and often requires excessive maintenance. Sandia is currently experimenting with trackers that avoid this problem. One such experimental tracker uses optical fibers in a novel way to directly sense the sun's image all along the receiver. There are other types of trackers but those that meet the rather stringent precision and accuracy requirements of concentrating troughs are often very expensive, somewhat erratic or both. Many trackers that accurately detect the sun's position are easily fooled, especially if they are not close to the right position when they are enabled. In other words, they will track well once they've locked onto the sun, but they have trouble finding it. This is especially true under partly cloudy conditions. One approach that has met with some success is to use a shadow band or other limited aperture tracker, and supervise it with some coarse but reliable sun following device. The rough tracker places the sensitive one in the general region it should be and makes sure there are no gross excursions from nominal. Unfortunately, most schemes used at the present have not taken advantage of simple coarse trackers, but rather use a combination of expensive optical devices.

The design presented here uses any of a number of sensitive, small aperture trackers and constrains the trough to operate near a nominal sun angle simply and inexpensively. The field controller calculates the approximate position of the sun relative to each drive string and sends that information to the appropriate collector controller. The collector controller receives position information from an inexpensive but reasonably accurate inclination sensor on the collector and compares it with the calculated position. If there is good agreement, the accurate tracker is allowed to continue tracking (which it does to within a tenth of a degree or so). If not, the trough is moved to the correct location and the sequence repeated. Position sensors that are accurate to within the capture angle of the tracker (usually a few degrees at most) are much less expensive than those that would be required to track by themselves according to calculated sun angles alone as in the so-called computer track technique.

The difference between this tracker and those presently deployed is that a calculated sun angle is used for coarse tracking rather than a combination of sensor outputs from segmented heliometers or other optical devices. It has been argued that the optical sensors track the sun directly and are therefore better, but in practice it is difficult to track the sun unambiguously, (which, in large part, is why coarse tracking is necessary; the fine tracker is easily fooled) and relying on an independent indication of sun angle is much more reliable. It also turns out to be much less expensive.

Many different optical sensors can be used with this approach while inadvertant defocusing and incorrect pointing of the collectors are avoided.

Flow Control

The system defined herein is capable of highly accurate fluid control such as would be required for applications involving power conversion heat engines. The heat engine typically has tight tolerances on its inlet temperature to operate efficiently. Other applications require much simpler fluid control which would mean that the controller could be simpler though there is little penalty in electronics for tight fluid control. In the design discussed here fluid temperature is sensed at the outlet of each ΔT string and a control valve on the inlet to the string is driven to the correct position to regulate the outlet temperature. Calculations are done in the collector controller that is physically nearest the valve. The field controller regulates nominal flow for the whole field based on the solar energy available. This saves pumping power and allows the control valves to operate in the most favorable part of their range. The expensive component in this precision fluid control system is the control valve and while this configuration works very well, many applications would permit the use of simpler and less costly fluid control.

The paper on "Fluid Control for Parabolic Trough Collectors" presented earlier by Rudolf Schindwolf of SNLA describes the fluid control problem in depth.

Safeties

Parabolic trough collectors are capable of achieving temperatures far in excess of those the receiver can tolerate. If sufficient fluid flow is not provided a collector in focus will damage its receiver extensively. The heat transfer fluid in systems that don't use water will deteriorate rapidly above a certain temperature. Receiver tubes will overexpand, buckle and can break the glass envelopes around them, and the selective surface on the receivers will be ruined if it overheats.

On a clear day, significant damage will occur in less than a minute after loss of fluid flow.

To prevent damage the collector controllers are configured so that the collectors will remain in focus only if everything is functioning within prescribed bounds. That is, active intervention on the part of the controller is needed to keep the collectors from going to the stow position. A contactor in parallel with the solid state motor drive is set so that in the absence of a signal from the controller, it supplies current to stow the collector. The signal from the controller is given only after it has been determined that a variety of sensors are sending proper signals. Sensors that are used include fluid temperature measuring devices, flow switches, and receiver length sensors that trip if the receivers get too hot and expand past a set point. The controller is also able to sense if the power has failed and the system is being run by a backup power source. Thus if any of four failures occur, loss of flow, overtemperature, loss of power or overtravel of the receiver, the collector will stow.

The controller also checks the integrity of the communications link and whether or not adjacent controllers are functioning. If any safety device in a ΔT string trips, the controllers will stow the entire string. If weather becomes a problem, if there is a pump failure or if any other failure occurs that affects the whole field, the field controller will instruct the collectors to stow.

Display

Providing information about the status of the field is an important function of the field controller though not technically a control operation. In existing fields there has been only haphazard emphasis placed on effective display of system functions. Most installations have very crude display systems, though some try to display everything everywhere. Sandia's approach is to divide the display into levels according to who is looking at it. A field operator will be able to easily access basic information useful to him, but he will not have any control inputs beyond simple manual overrides to handle unusual situations or to shut the field down. Even this restricted control access will be limited by the use of a password to prevent casual visitors from being able to affect the system since it will be unattended most of the time.

The operator's display will be a fairly simple inexpensive device such as a plain black and white CRT or alphanumeric panel with an alarm that would signal a malfunction.

Unrestricted control access will be available to a service technician who will have display with greater capability that he will bring with him to the site. The service tech will be able to command any condition of which the system is inherently capable. He will also be able to extract detailed diagnostic information.

In addition to the central display there are a minimum number of indicator lights built into the collector controller circuit boards. These aid in maintenance of the controller. Since repair of these boards will consist of in field replacement of the whole board, there aren't many display states required.

This simple layered display philosophy effectively provides useful information at the appropriate level while reducing cost and enhancing reliability.

TABLE 1

System	Voltage to Field	Voltage at ΔT String To Drive Circuit	Motor	Backup	Control Wire
1	480 3Ø	480 1Ø	24DC	2 Central generators	Wire
2	480 3Ø	480 1Ø	24DC	2 Central generators	Optics
3	240 3Ø	240 3Ø	240 3Ø	2 Central generators	Wire
4	480 3Ø	480 1Ø	24DC	Batteries	Wire

Related Topics

There are two areas of continuing investigation that deal with controls under special circumstances. Startup on very cold mornings when the system is at ambient temperature is not well understood. Also, the controller should interact properly with a variety of backup power sources. Automatic cold temperature startup is poorly characterized since most systems in the field today are started manually. Also fluids with widely differing viscosities are used so there are significant differences from one field to the next.

Providing backup power presents another problem without an obvious solution. The best source of backup power to stow the collectors in the event of a power failure depends heavily on the location and application of the field and to a large extent on the exact configuration of the field. In a heavily industrialized area there is generally much better electrical service than in remote areas. Also many factories have their own power systems that would be suitable to stow the field upon loss of grid power.

The best use of backup power is affected by the wiring, collector drives and the size of the field. Hydrualic collector drives with accumulators, for instance, would not require emergency power.

Jacobs Engineering is studying several different power configurations a field might have to determine what each would cost. The options under consideration are listed in Table 1. Whatever choice is made, the controller must function correctly. This controller will work properly with all the options in Table 1 as well as with any number of other possible configurations.

SUMMARY

A distributed, microprocessor based solar field control system provides great flexibility and capability at moderate cost. Many different sun trackers can be used and fields of widely differing sizes can be controlled. Substantial savings both in wiring and electronics are realized by combining control functions in a single electronics package. Also, effective display functions are possible inexpensively. A detailed design review is presented in the following paper.

SANDIA SOLAR COLLECTOR FIELD CONTROL SYSTEM DETAILED DESIGN REVIEW

Jim Williams
Roger Steen
Honeywell Inc.
Technology Strategy Center
Sensors and Communications Group
1700 West Highway 36
Roseville, Minnesota 55113

Introduction and Background

Honeywell began working on solar collector tracker controls in 1978; this effort has led to the development of the Honeywell Flux-Line Suntracker (FLST) System. The FLST system consists of a solar field master controller and local collector controllers with flux-line sensors. There are presently 122 collector controls installed at various sites--45 local collector control units and a master controller at the White River Apache Indian Health Center in White River, Arizona; 20 local controllers at the Army proving ground in Yuma, Arizona; 11 local controllers at the Columbia Gas facilities in Columbus, Ohio; 42 local controllers at Honeywell's General Offices (Honeywell Plaza) in Minneapolis, Minnesota; and 4 local controllers and a master controller at the Arizona Public Service Visitor Center in Palo Verde, Arizona.

Sandia Solar Control System Development

In April 1980, Honeywell was awarded a contract by Sandia National Laboratories to develop a solar collector field control system with improved features.

The Sandia solar collector control system will consist of a field controller and up to 96 collector controllers. Significant feature improvements of this program are:

- Two-way serial data communication between the field controller and each collector controller.

- A total sun tracking technique that is a combination of calculated coarse synthetic tracking and accuracy of flux-line electro-optical sensing.

- Sun angle calculations performed only in the field controller and transmitted via serial data communications to the collector controllers.

- Addition of coarse position feedback at each collector controller.

- Complete field status displayed at field controller.

- A field controller that provides selective control of individual collectors.

- A power adapter module for flexibility of input power accommodations.

The Sandia system is designed for a 50,000-square-foot solar field (Figure 1). This field will contain 96 collectors. Each ΔT string will consist of four collectors with collector controllers and a single fluid temperature control valve. The collector controller nearest the control valve will provide electronic valve control based on maintaining the output temperature of the string at a specified temperature.

A single data communication line will be positioned on the edge of the solar field from the field controller. Data signal repeater capability will be utilized in each collector controller along the edge of the field. This layout minimizes the number of control wires required for the field and lowers installation costs.

Collector Controller

Each collector controller will contain a Zilog-Z8 microprocessor (Figure 2), which will be interfaced with appropriate sensors to monitor fluid temperature, tube expansion, fluid flow, collector overtravel, and collector position by position feedback and electro-optical sensing. Also connected will be a microprocessor "running" or watch dog timer, an address switch and a manual/automatic select switch panel.

The collector controller will provide outputs for control of the collector drive motor and, if selected, the flow control valve. The Sandia system will be configured to drive a 24-volt DC motor, but it will be possible to configure the collector controller to drive either DC or AC motors.

The collector controller will calculate error position between the collector feedback device and the sun angle transmitted from the field controller and, if selected, will provide for the ΔT flow valve control algorithm.

The Z-8 microprocessor contains an on-board universal asynchronous receiver transmitter to provide for data communications with the field controller. The collector controller communicates with the field controller, with its own status/switch panel and with other collector controllers in the same string via a separate stow interlock line.

The collectors are protected from a lack of fluid flow, overtemperature, loss of communication, tube expansion and collector position overtravel.

The collector controller status panel will provide indicators for program running, motor direction, overtemperature, auto/manual selection, overcurrent, loss of flow, tube expansion and loss of communication.

The collector controller is powered by 24 volts DC provided by the power adapter. The power adapter is capable of generating 24 volts DC from either 277 volts AC or 120 volts AC.

Field Controller

The field controller will contain a Motorola 6802 microprocessor (Figure 3). The field controller will be interfaced with sensors to enable it to monitor direct normal insolation, wind speed, ambient air temperature, precipitation, Btu demand, field fluid temperature, field flow rate and loop pressure.

Sun angle calculations will be performed with an AM9511 arithmetic processor unit. The field controller will interface with an alphanumeric display, keyboard, switch and display panel and a real-time clock that will have battery backup.

Outputs from the field controller are maintained for a diverting valve control and a variable speed field pump.

Electric power required for the field controller is 24 volts DC provided by a power adapter to accommodate various power systems.

Serial communications will be provided downward to the collector controllers and also upward to some type of master control if multiple 50,000-square-foot fields were to be controlled and monitored (Figure 4).

Summary

An improved line-focus solar collector control system has been described. The system is aimed at providing cost-effective, and reliable sun tracking and control. The system provides the required control and safety features while minimizing the all-important costs for installation and operation. The control system design is compatible with the solar field modular concept and is easily extended to a larger field of multiple solar field modules.

The system development is currently in the breadboard phase and a production prototype system will be completed in April 1981.

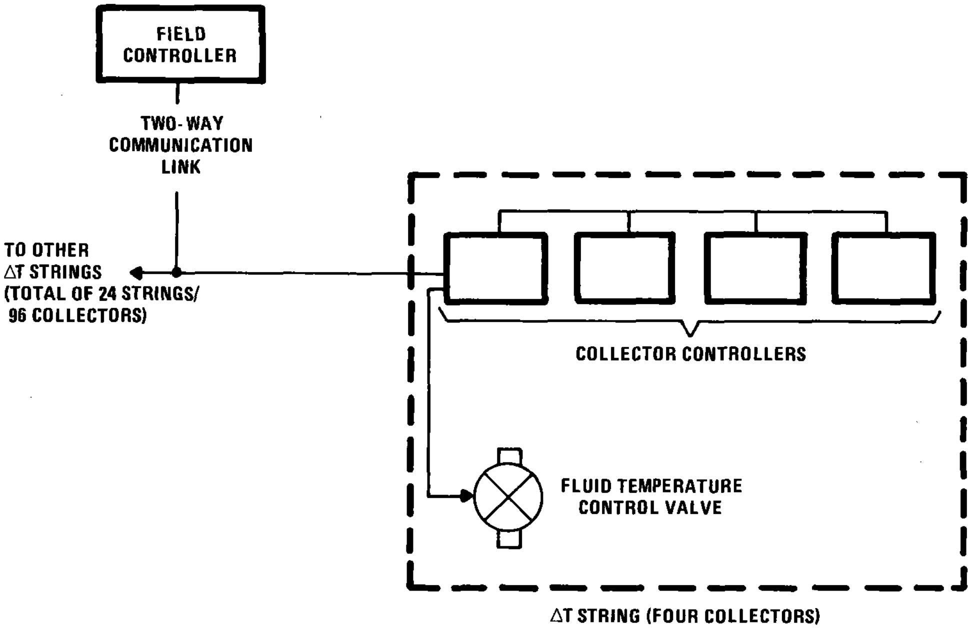

Figure 1. Solar Field

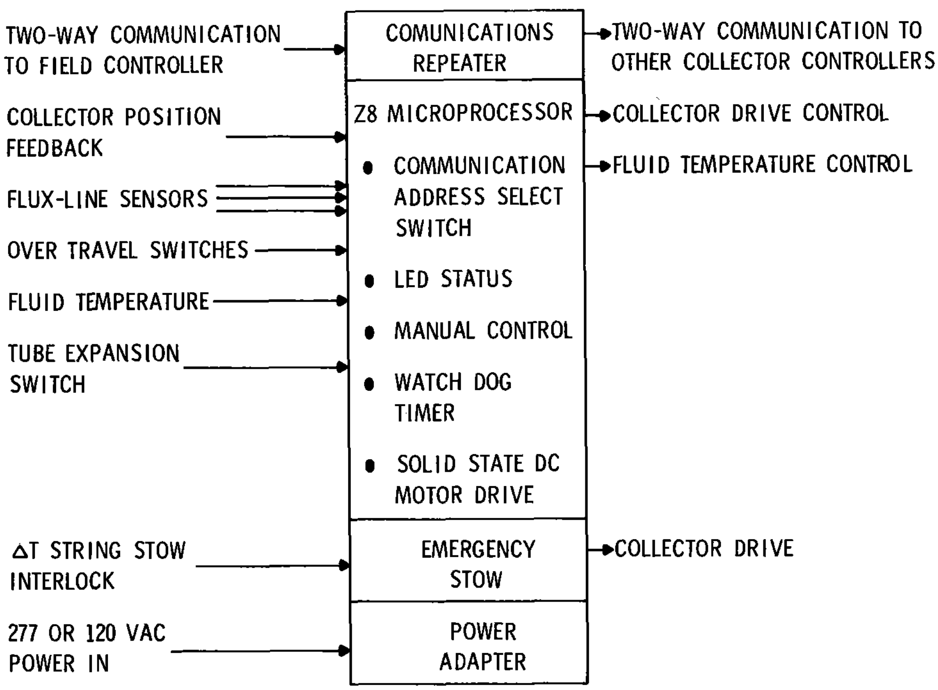

Figure 2. Collector Controller

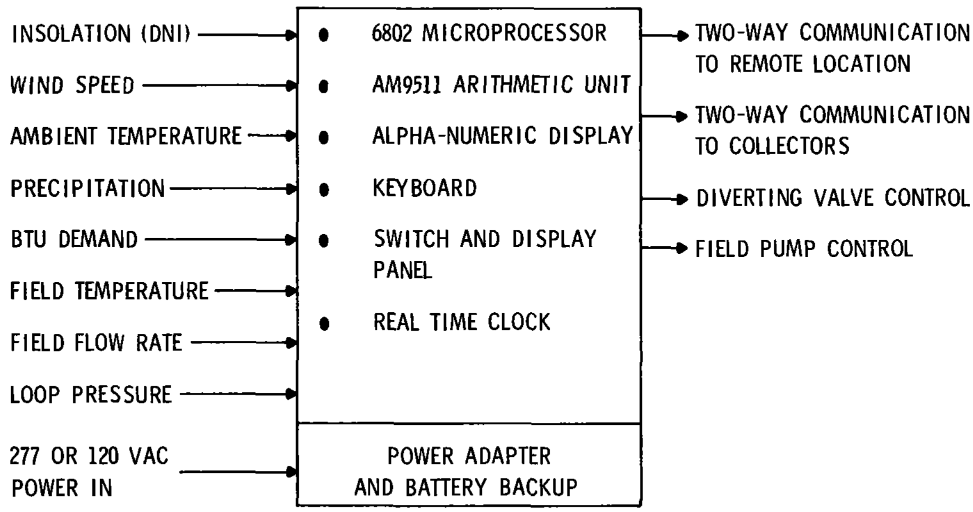

Figure 3. Field Controller

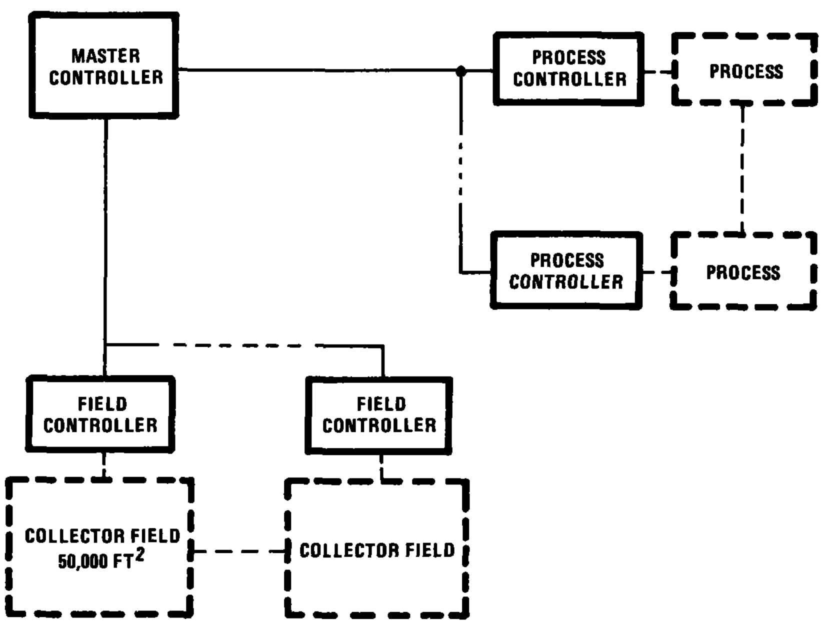

Figure 4. Extended Control System

DRIVE SYSTEM FOR LINE-FOCUS COLLECTORS

Robert A. Randall
Electromechanical Subsystems Division 2323
Sandia National Laboratories
Albuquerque, NM 87185

Introduction

In any collector system that tracks the sun, a drive mechanism is required to move or rotate parts of the system in order to maintain focus on the receiver during operation, and to move the assembly to and from the stowed condition. Stowage is required to preclude inadvertent focusing and to minimize mirror contamination. Such a drive system must provide enough force, or torque, to operate the system under all expected wind conditions, have sufficient precision of operation for accurate tracking, and have sufficient speed to provide stowage in a reasonably short time.

System Configuration

In a prototype system being studied, the driver operates a drive string of four parabolic trough type collectors (see Figure 1). The driver is centrally located in the drive string, being mounted on the central pylon. Each of the four collectors is 6 meters long by 2 meters wide. Since each driver rotates four collectors, the total collector area rotated by each driver is 48 square meters. Since half of the collectors are on each side, the driver is required to have a double extended output shaft--each extension driving half the collector

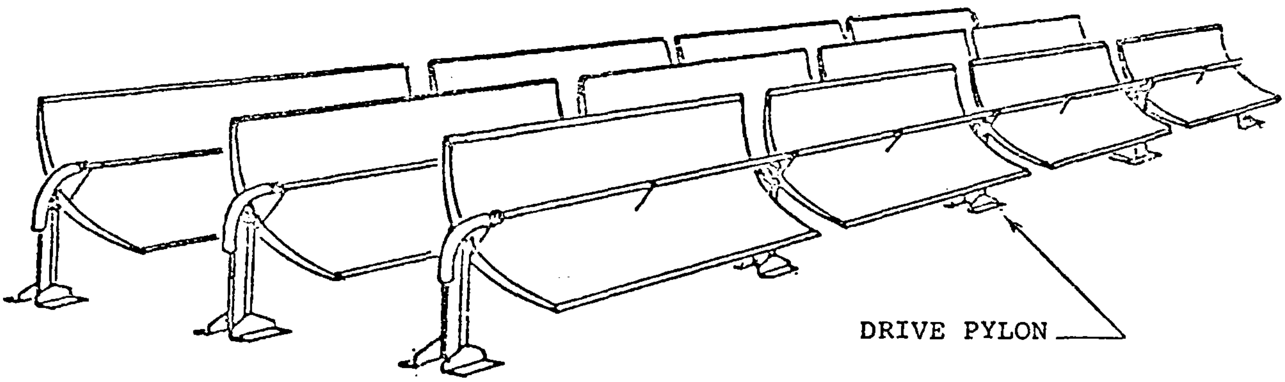

FIGURE 1

load. The collectors are required to track from horizon to horizon, and stowage requires rotation 45° beyond that, to bring the entire surface of the collector mirrors past the vertical to minimize accumulation of contaminants on the surface while stowed. Therefore, the driver is required to rotate the collector system over a range of $180^{\circ} + 45^{\circ}$, or 225°. Limit switches are provided in case the normal control circuitry fails to stop the rotation at the extremes of movement.

The drive assembly must meet certain spatial requirements; particularly, it must fit inside a 15 3/4" width and must not interfere with the receiver tube, which is slightly more than 15 inches from the shaft center (see Figures 2 and 3).

Design Goals

Certain design goals have been established, which are considered necessary for the proper function of the system, and to assure economic viability. These are as follows:

Accuracy: Positioning capability should be better than 0.25°.

Backlash: Backlash should be less than 0.1°, but more may be tolerated if cost, service life, or efficiency is significantly affected.

Cost: Ultimate cost of driver should be less than 15% of the cost of the uninstalled collector system. This is estimated to be less than $20.00 per square meter. Thus, for a 48 square meter drive string, the driver cost should be less than $960.00. Included in this cost is all of the drive assembly between the pylon mounting surface and the interface with the torque tube, and includes such things as drive motors.

Torque Loads

The torque loads on the driver come from two principal sources: wind loads and gravity loads. The torque loads due to gravity arise because the center of gravity of the collector system does not coincide with the pivot axis. This minimizes the effect of backlash in the drive system, since the driver is always loaded in one direction

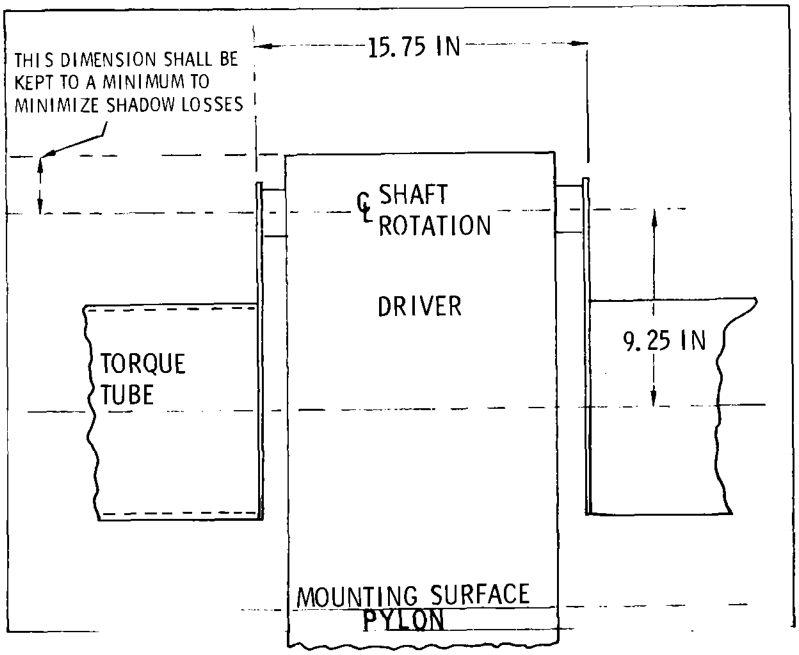

FIGURE 2 DRIVER INSTALLATION - FRONT VIEW

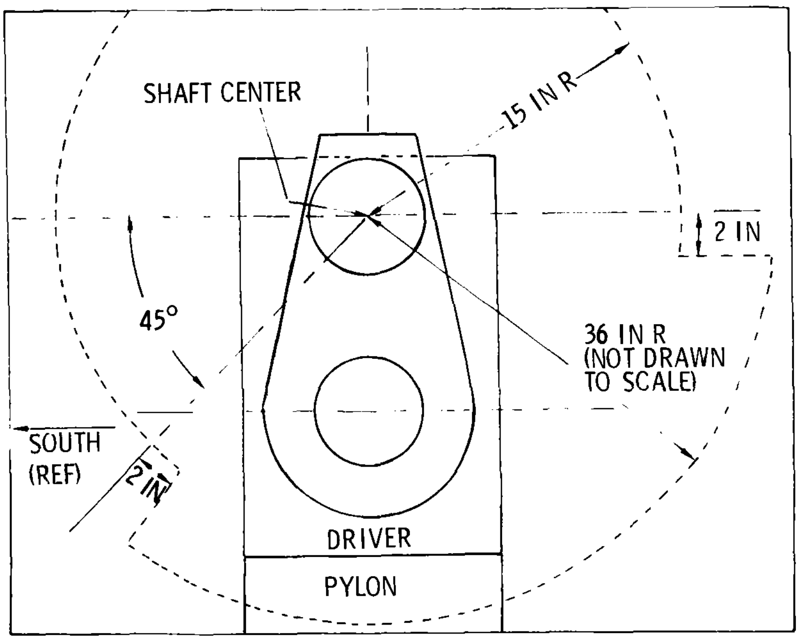

FIGURE 3 DRIVER INSTALLATION - SIDE VIEW

or the other, except when the collectors are pointing directly upward. Since the pivot axis of this system is between the center of gravity and the apex of the collector, the torque developed by gravity tends to rotate the system to a downward facing orientation. The maximum torque developed by gravity is when the collectors are facing horizontal and amounts to approximately 361 Newton-meters (3200 lb-in), the exact amount depending on the individual collector design.

Wind forces account for the greatest amount of torque load. The system described previously can operate in an 11.2 meter/sec (25 mph) average wind, with gusts to 16.5 meter/sec (37 mph). When the wind speed reaches this value, stowage is initiated. Wind tunnel analysis indicates that a 16.5 meter/sec (37 mph) wind can cause a torque in either direction of 3220 Newton-meters (28,500 lb-in) for the drive string. This represents the highest wind load under which the driver must track the sun.

Once stowing is initiated, a time interval is required to complete the stowing operation, which depends on the speed of rotation and the initial orientation of the collectors. This means that, in a rising wind situation, before stowage is completed, collectors can experience a wind significantly higher than that required to initiate stowage. Records of wind speeds show that average wind speeds increase at a maximum rate of 2.9 meters/sec/minute (6.5 mph/minute), although transient conditions can exceed this. This means that, if stowage can be completed within one minute, the driver may be required to operate in a wind with gusts of 19.5 meters/sec (43.5 mph). This translates into a torque of 4451 Newton-meters (39,400 lb-in). For a stowage completion time of five minutes, the torque due to wind could reach 11,400 Newton-meters (100,500 lb-in). These torque values for stowing determine the maximum values that the driver must operate against, and show the desirability of stowing in minimum time, since a driver with a high speed ratio and higher torque capability would be more costly, and would require more space.

After stowing, the system must withstand, but not operate in a wind of 35.8 meters/sec (80 mph). This results in a torque load of 15,000 Newton-meters (133,000 lb-in), in either direction. It is desirable that the driver not permit movement of the collectors under these conditions to preclude the possibility of the collectors drifting out of the stowed condition in a high wind. Early test results, performed on commercial worm gear type speed reducers having 3000:1 speed reduction indicate that locking does take place for this type of device. Further testing is planned; and, in the event that the driver chosen for use in the collector system does not provide locking, a separate locking mechanism will be provided.

Other torque loads include starting and stopping inertia, friction, and flexure loads. The moment of inertia of the drive string is approximately 400 kg-m^2. The torque load this imposes during starting and stopping depends upon the design details of the collector system, and is difficult to assess. However, due to the low rotation rates involved, it is expected to be small. The friction and flexure loads also depend on the design details of the individual collector system and are expected to be small compared with the wind and gravity loads. However, these factors can be of sufficient magnitude to affect the optimum electrical pulse duration for tracking.

The total torque loads then, are essentially a combination of wind and gravity loads. For normal tracking, both loads can operate in either direction; and the total possible torque load will be the sum of the two loads, or 3581 N-m (31,700 lb-in). For stowing, the torque due to gravity would add to the resisting torque only in the early portion of the stow cycle, before the wind could rise to its maximum value during stowage. During the latter part of the stow cycle, when the wind has had time to rise to its maximum expected value, the torque due to gravity will act as an overrunning load. Thus, for stowage, the resisting torque could be as high as 4090 N-m (36,200 lb-in), and the overrunning torque could be as high as 4812 N-m (42,600 lb-in). For torque loads while not operating, the load due to wind is 15,000 N-m (133,000 lb-in) in either direction. In this case, the torque due to gravity is small in comparison and can be neglected. It should be kept in mind that the above loads refer to the entire drive string and would be divided between the two shaft extensions.

Driver Design

It was decided to consider only single unit, enclosed drivers.

Two design approaches are being pursued. These are the electromechanical, consisting of a gear type speed reducer driven by an electric motor, and the hydraulic, consisting of a linear hydraulic actuator with a mechanism for translating to rotary motion. Both approaches are required to have an emergency energy source to stow the collector when normal power is not available. At this stage, each approach appears to have certain advantages over the other. There is more experience on the electromechanical approach. It also seems to require simpler controls and may provide both the high torque and sensitivity needed in a reasonably small package. The hydraulic approach offers possible cost savings and a simpler means of energy storage for emergencies (an accumulator).

The electromechanical approach is currently under investigation. This drive system concept utilizes AC electrical power to the drive pylon, and this will be rectified and stepped down to 24 volts DC to optimize personnel safety. An auxiliary power unit will be used to provide power for emergency stowage, and a second, smaller APU will provide backup emergency power to circulate cooling liquid through the receivers. A 1200 rpm permanent magnet DC motor rated at 1/2 hp will be used as the drive motor and will be operated in a pulse mode.

In order to provide adequate torque and output speed with this size motor, the speed ratio for the driver must be between 3000:1 and 5000:1. Under certain wind conditions, the 3000:1 ratio requires more input torque than the drive motor is rated for, but it is expected that the motor will be able to develop the required torque in the low duty cycle required of it. In normal tracking operation, the drive will normally operate for less than a second at approximate 30 second intervals. For stowage, the driver will operate for around one minute, once or twice per day. Since this motor has a high stall torque, the current into the motor will be limited to a value that will prevent the driver from being overstressed in a stall condition. Since the low duty cycle, high torque requirements are different from those normally required of gear type speed reducers, extensive testing will be performed.

Tester

A driver tester has been designed and built. This tester, shown in the illustration, can produce resisting or overrunning torques for loading the driver, and also has an inertia wheel which duplicates the moment of inertia of a drive string. Rotational position, torque, and input energy can be measured. Drive systems having a variety of shapes and sizes can be tested for efficiency, torque output, rotation speed, static torque resistance, starting and stopping characteristics, and service life on this tester. Also, the tester will provide a way of testing control systems in conjunction with the driver.

Three commercial speed reducers have been procured and are being tested on the driver tester. These units will also be overtested to the point of degradation or destruction to obtain information on their ultimate capability and to gain information on the requirements for special design drivers which will be evaluated later in the program.

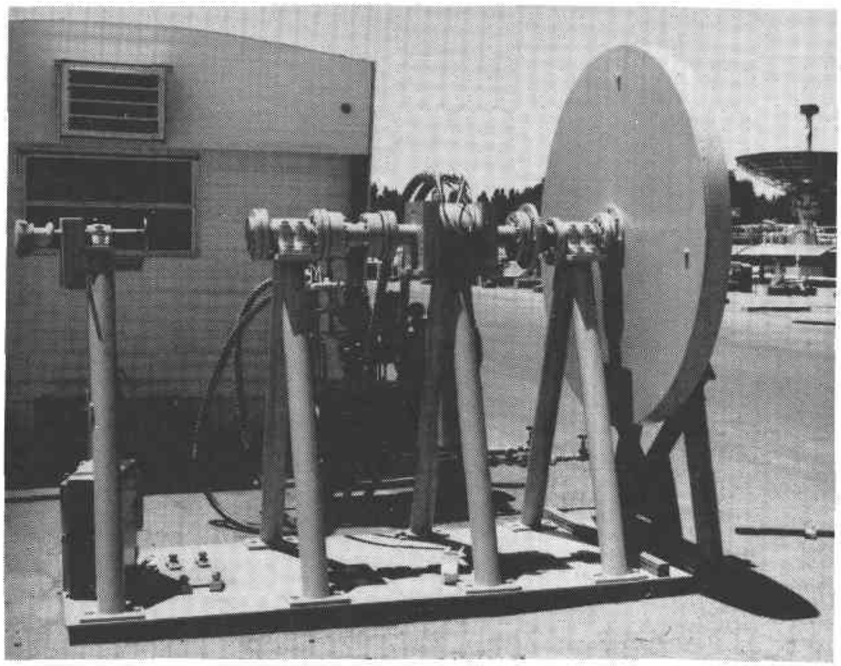

FIGURE 4

NON-EVACUATED RECEIVERS

George Treadwell
Component and Subsystem Development Division 4722
Sandia National Laboratories
Albuquerque, New Mexico 87185

Introduction

A properly designed evacuated-annulus receiver can, in theory, provide a performance enhancement of about 10%. However, the construction complexity and attendant fabrication and replacement cost limits the desirability of developing such a design for the immediate future. Non-evacuated receivers can be developed and adopted in a much shorter time period so their basic design alternatives will be described in this paper. The results of the design selections will be described.

Function

As described in a previous paper in these proceedings, (Thermo-optical Considerations ...) the receiver is the component which converts the optical energy into thermal energy. In accomplishing this function, consideration must be given to the major factors influencing performance and cost such as effective heat transfer to the fluid, accommodation of linear expansion, mechanical deflection, thermooptical design, durability, reliability, and cost of construction and replacement.

Design Alternatives

The first alternatives to consider are the receiver metal and shape. Because of temperature, pressure, and mechanical deflection requirements (up to 315°C), the choice narrows to low carbon or stainless steel. Low carbon steel is selected because it is 1/3 the cost of stainless, its elastic modulus is 10% greater, and it has higher conductance. A 1.25 inch OD receiver should nominally have a 1/8 inch wall thickness to minimize mechanical deflection between supports. The cross-section should be circular because, for a proper thermooptical design, the cost of swagging to non-circular is difficult to balance by the nominal thermal loss decrease and the moment of inertia is non-symmetric and more mechanical deflection will result. A reasonable maximum unsupported length to use is 12 feet since mechanical deflection increases as the cube of the length and glass jackets are also limited to 12 feet. The receiver has no turbulence enhancers so radial temperature gradients are controlled by flow velocity. For proper energy transfer, the Reynold's Number should be ~30,000 for a normal sun. For proper performance, electrodeposited black chrome over an undercoat of nickel is quite adequate from a thermooptical standpoint. Other selective coatings exist but are relatively expensive and are not yet at the same state of development.

The glass jacket alternatives should be limited to those glasses which can withstand thermal shock (i.e., low expansion glass), are available in approximately 12 foot lengths for reasonable cost, have high transmittance, can be readily thermally formed, and have reasonable as-drawn tolerances. The glass selected is Corning Code 7740 (Pyrex^{tm}).

Several methods are available to support the glass over a nominal 12 foot span. Intermediate supports need not be used if the annulus gap is maintained for thermal loss reasons (~1 cm) since the glass diameter has a relatively large moment of inertia. The support method must accommodate the relative expansion between the glass and steel since the steel could be at 650°F and the glass at 180°F. It is undesirable to use metal bellows and glass-to-metal seals because of the expense (and graded glasses possibly required). The glass could be supported by external sleeves or internal sleeves. External sleeves expose joints to high temperature and have potential alignment problems. The internal sleeve has been chosen. Figure 1 portrays the cross section of an internal sleeve. A model of such a design is portrayed in Figure 2. The silicone ring acts as a dust screen. To protect the silicone ring from the hostile thermal environment, the stainless steel collar is thin to form a tortuous conduction path from the 650°F receiver. The stainless steel reflects a large amount of the radiation, and convection cooling in the cavity cools the ring. Laboratory tests and analytical calculations project exposure temperatures of less than 350°F for the ring.

Because the collar is circular, a good seal is obtained by circularizing the as-drawn tubing by a carbon plug. The end cross-sectional thickness is increased to enhance strength and a platinum overcoat is used to protect the ring from ultraviolet exposure. These features are shown in Figure 3.

For ease in replacement of broken glazings (although 3/4 inch hail has been survived), Swagelok fittings are used at joints of the 10-12 foot receiver. Welded double length receivers (current electro-deposition tanks are limited to 12 feet) are difficult to handle.

Linear Expansion and Rotation Devices

One expansion compensator is shown on Figure 3. It consists of molycoated steel surfaces to accommodate expansion. Another expansion compensator is shown in Figure 4. The compensation is accomplished by the rotation of the wire support.

Both mechanisms have been subjected to a simulated 20-year life cycle by means of the tester shown in Figure 5. The axial movement is 2-1/2 inches. At periodic intervals, sand is blown at the mechanisms to simulate dust storms. At other intervals, CO_2 freezing is used to form ice on the surfaces to simulate winter storms. No failures were observed during the first 20-year cycle in the attitude shown. The positions were reversed, and it was immediately noticed that the upper wire rod foot ratcheted out of its position in a few cycles. Further development is required to eliminate this problem.

Because of some concern for hose failures caused by torsional loads, the pivoting expansion compensator is also designed to permit receiver rotation so that hose torsional loads are minimized. This feature is shown in concept in more detail in Figure 6.

Performance Testing

A baseline of performance has been obtained with a series of receivers used in conjunction with the reflectors provided by

Custom Engineering Inc. as shown in Figure 7. It should be noted that the CE reflectors are very accurate (σ slope $\approx$2.5 mrad) and focus the energy quite uniformly on the receiver, as shown in Figure 8, when compared with other reflectors. The Engineering Prototype Trough image is shown in Figure 9 for comparison. From an energy transfer standpoint, such flux variations have a modest downward influence (~2%) on performance.

The performance results are shown in Figures 10 and 11 for standard glass. It should be noted that the receiver diameter of the proto-typical performance curve is the same as the EPT-2 curve although the CE aperture is 3/4 meter wider. From the slope of the performance curve, it can be observed that the thermal design is quite adequate.

A set of Pyrex tubes was coated with an anti-reflection coating and tested on the south CE string. The results from this evaluation are shown on Figures 12 and 13. The enhancement expected from a good AR coating has not been achieved. Several reasons are suggested for consideration. The tubes are oval as a result of processing difficulties, and therefore, thermal losses are presumed to be higher because of a non-uniform annulus gap; the AR coating is not of a consistent quality; and the incidence angle effects are more pronounced because of the shape. The production cost of an AR coating remains to be determined.

Nevertheless, the efficiency of 64% at 315°C output comes very close to meeting the long-term goal of 65% shown on the figures.

Future Changes

As a result of these evaluations, several modifications to the design will be made. The plastic ring cross section will be examined for size increase. One ring was observed to split as shown on Figure 14. The platinum has eroded on many collars so a glass frit cover will be evaluated. All tubes will be cleansed of SiO_2 contamination since the silica reacts to the sun and temperature combination and turns milky white.

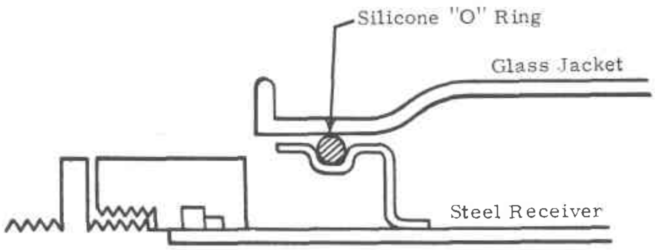

Figure 1. Receiver Glazing Support

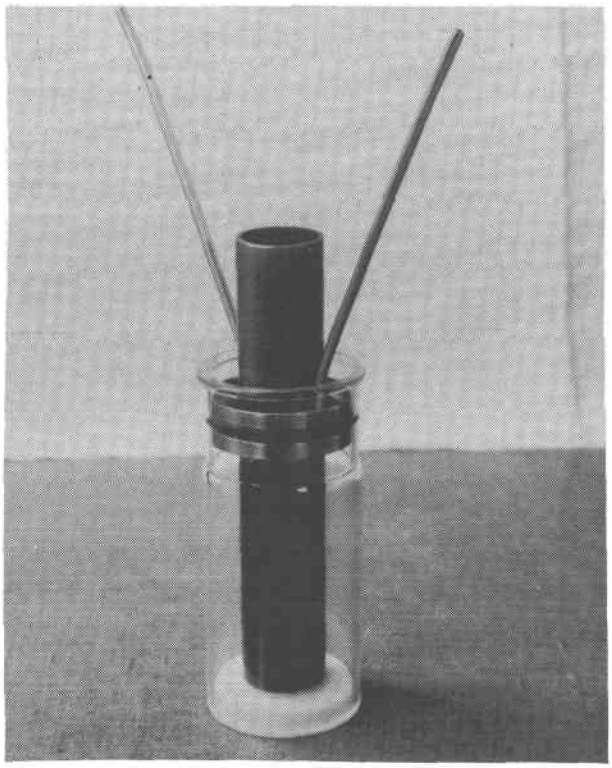

Figure 2. Receiver Glazing Support Model

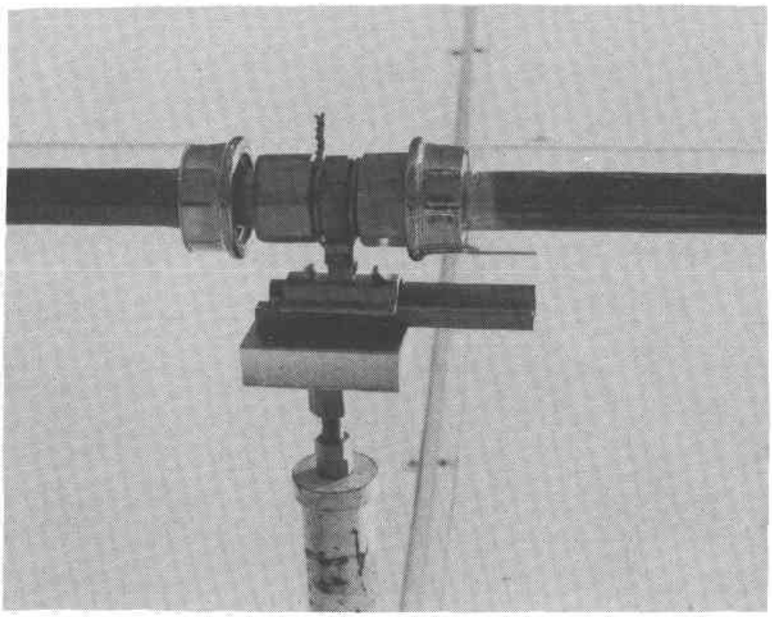

Figure 3. Receiver End Configuration

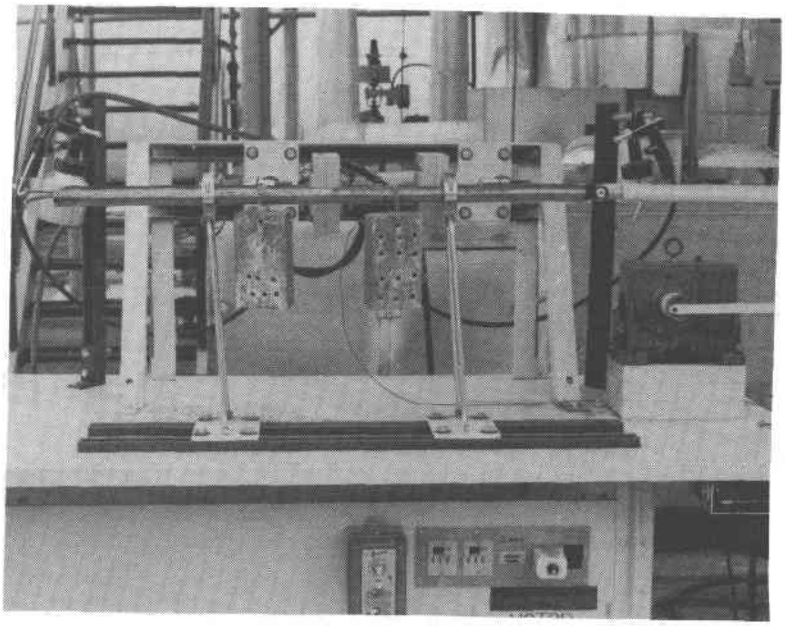

Figure 4. Expansion Compensator

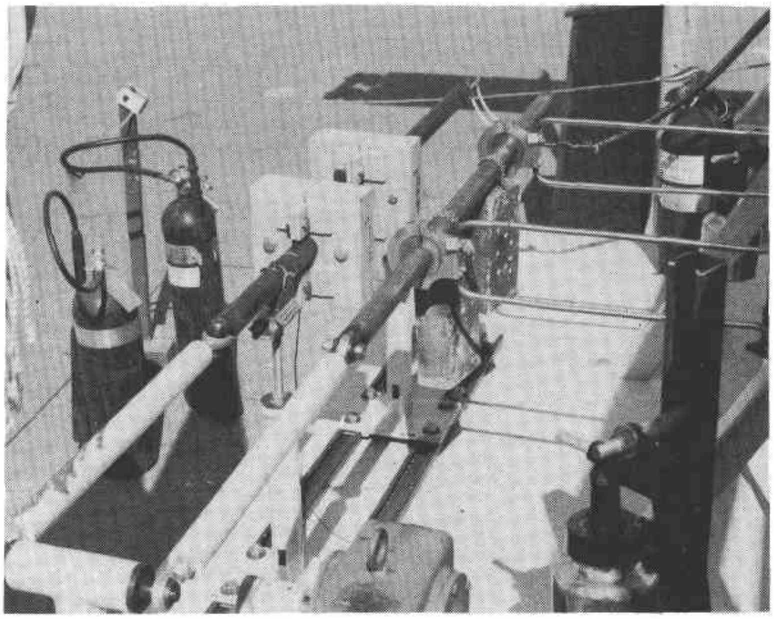

Figure 5. Expansion Mechanism Tester

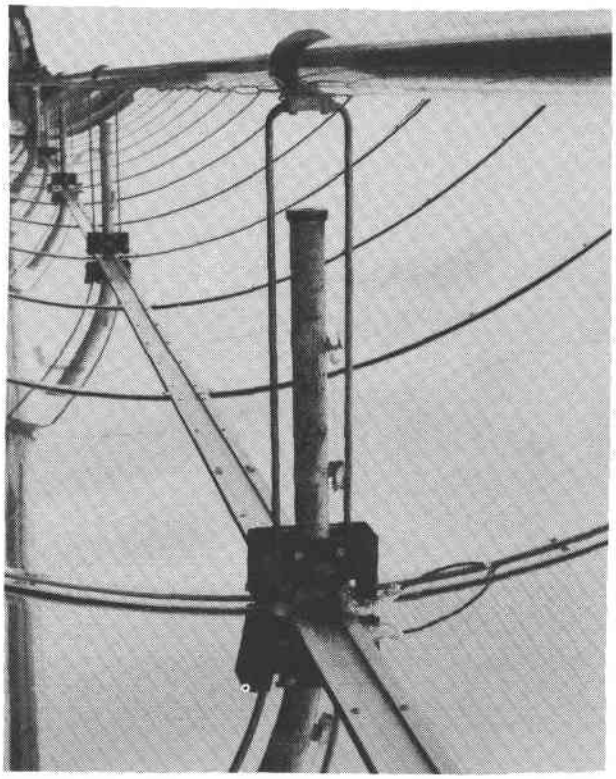

Figure 6. Rotating Expansion Compensator

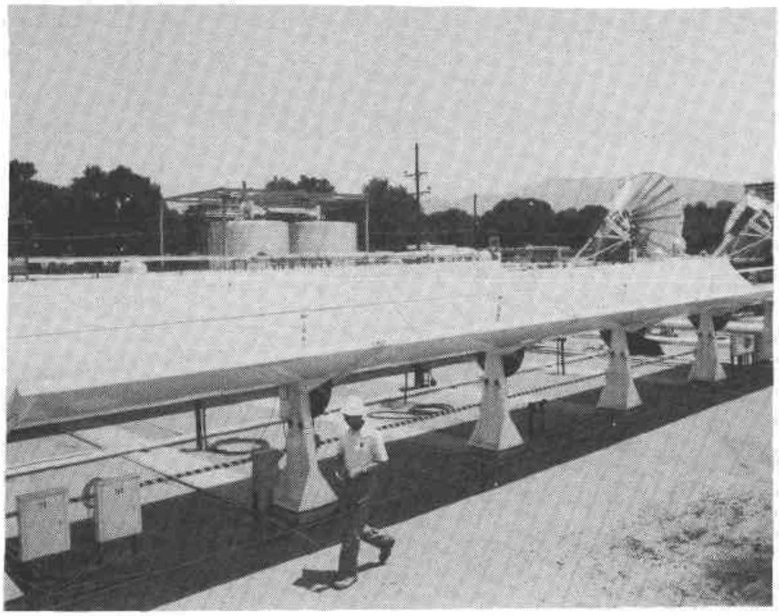

Figure 7. Custom Engineering Glass Reflectors

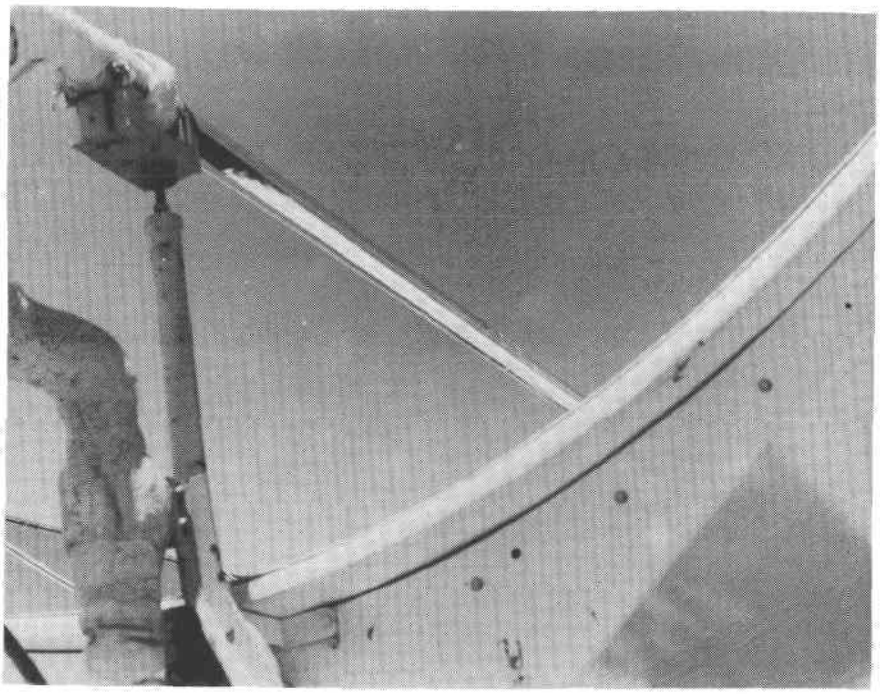

Figure 8. Custom Engineering Reflected Beam Pattern

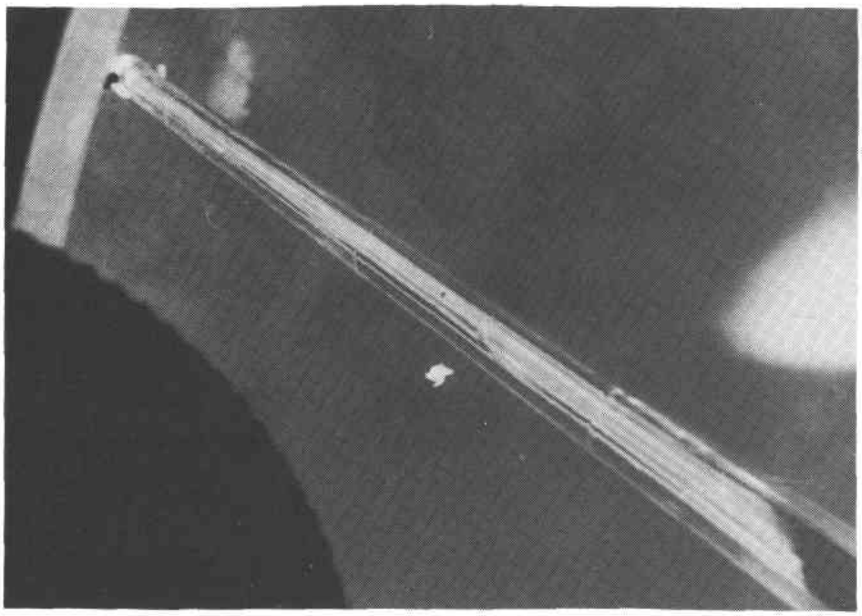

Figure 9. Engineering Prototype Trough
Reflected Beam Pattern

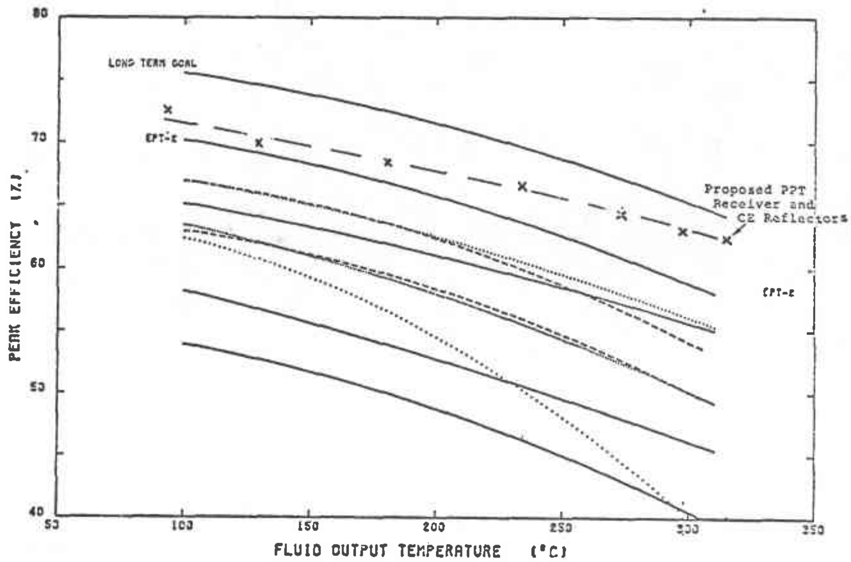

Figure 10. Non-AR Coated Receiver Efficiency
vs. Output Temperature

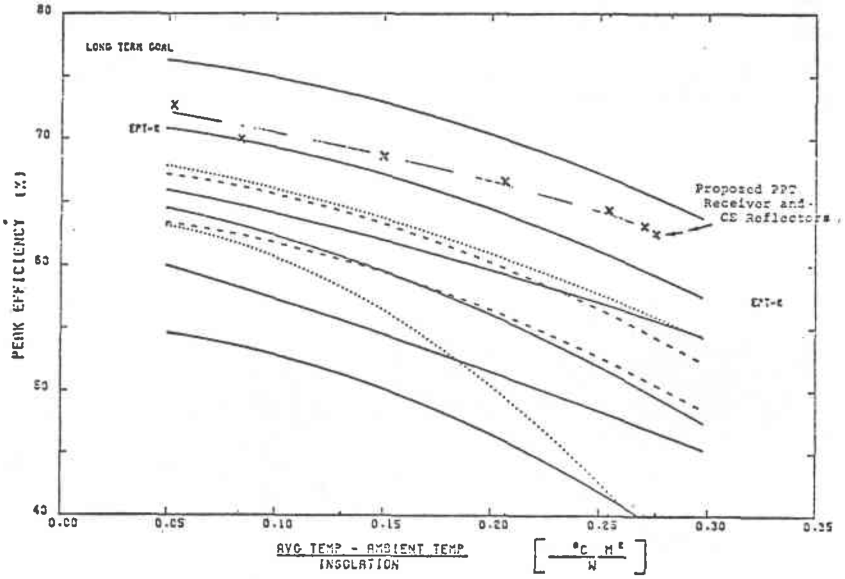

Figure 11. Non-AR Coated Receiver Efficiency vs. Semi-Normalized Weather

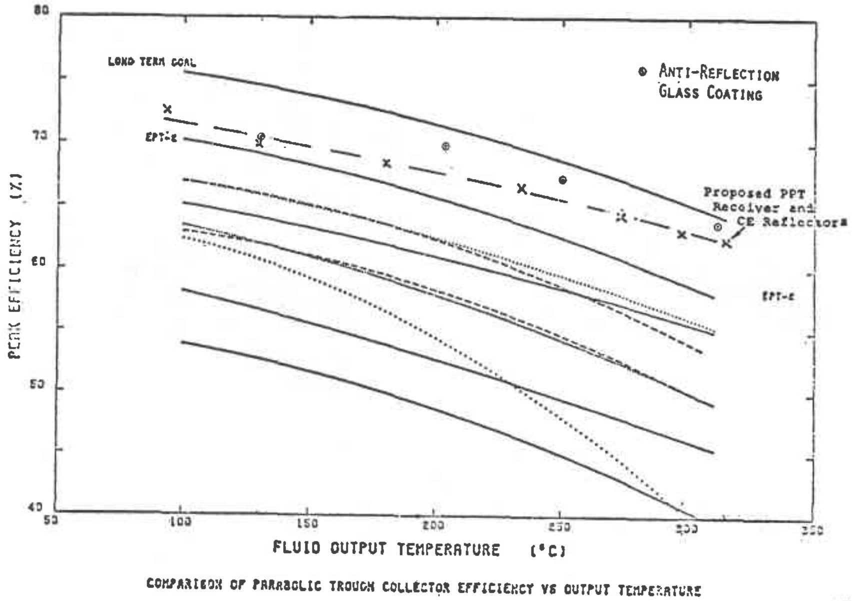

COMPARISON OF PARABOLIC TROUGH COLLECTOR EFFICIENCY VS OUTPUT TEMPERATURE

Figure 12. AR Coated Receiver Efficiency vs. Output Temperature

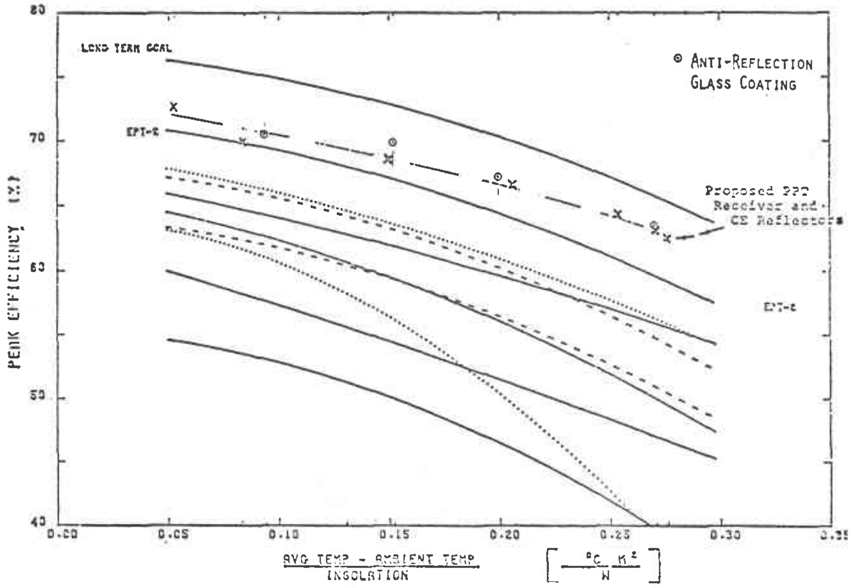

Figure 13. AR Coated Receiver Efficiency vs. Semi-Normalized Weather

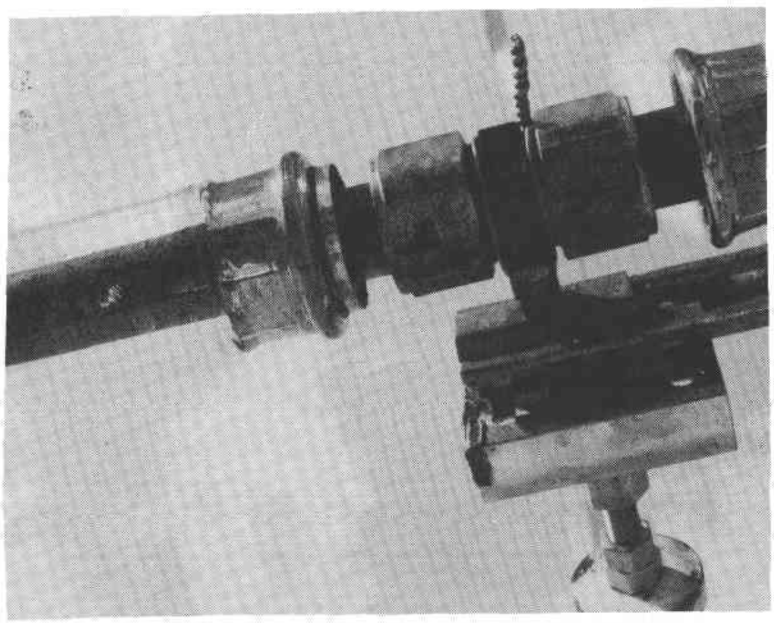

Figure 14. Receiver Split Dust Seal

PASSIVELY EVACUATED RECEIVERS

Leroy E. Torkelson
Experimental Systems Operations Division 4721
Sandia National Laboratories
Albuquerque, NM 87185

Introduction

Evacuated receivers for line-focus solar collectors contain a vacuum between their glass envelope and absorber tube. A passively evacuated receiver is a hermetically sealed assembly which maintains its vacuum without the assistance of a vacuum pump.

This paper will present an analytical comparison of the heat loss from a passively evacuated receiver and non-evacuated receiver. These results will be compared to experimental measurements made in the laboratory.

The design and construction of the laboratory model and those placed on parabolic troughs at the Midtemperature Solar System Test Facility (MSSTF) will be discussed. Lessons learned during the construction and initial testing at the MSSTF will be presented along with a discussion of the test data available to date.

Analytical and Laboratory Results

The two curves shown on Figure 1 compare the predicted heat loss from a non-evacuated receiver to that of an evacuated receiver. The attraction of the evacuated receiver concept is that receiver heat losses can be cut in half for absorber temperatures in the neighborhood of 260°C (500°F). The five data points shown on Figure 1 represent laboratory test results for a passively evacuated receiver which confirm the analytical predictions. The author has confirmed the analytical prediction for the non-evacuated receiver using test data from the MSSTF for an absorber temperature around 260°C (500°F).

Design and Construction

Figure 2 is a picture of the 30-inch long receiver tested in the laboratory. The design parameters for the computer models and the laboratory model are as follows:

Absorber tube
- 1-5/8 inch O.D. steel tube with a .065 wall thickness
- Absorptivity of .945
- Emissivity of .25 at 300°C (572°F)

Glass envelope
- 63 mm (2.480 in.) O.D. x 59 mm (2.323 in.) I.D.
- Type 7052 Kovar Sealing Glass
- An ion type vacuum gage was attached for the laboratory model

The laboratory model was assembled as shown in Figure 3 utilizing the components in the illustration. Prior to assembly, the absorber tube was baked in air at 350°C (662°F) for 24 hours. After assembly, a vacuum pump was connected to its copper pinchoff tube. In this configuration the assembly was baked for 48 hours at 200°C (392°F), 8 hours at 275°C (527°F), 16 hours at 300°C (572°F), and finally 24 hours at 350°C (662°F). The assembly was then allowed to cool slowly and the liquid N_2 condenser of the vacuum pumping system was activated. When the assembly had cooled, the copper tubulation was pinched off. The ion gage on the receiver then read 1.8×10^{-7} mm Hg.

The 30-inch long receiver assembly was then subjected to 50 temperature cycles in the laboratory. Each cycle consisted of heating the receiver to 316°C (600°F) and holding the temperature for four hours using a Calrod heater at the center of the absorber. At the end of the four hours, the heat was removed and the receiver returned to ambient temperature. At the end of the 50 cycles, the ion gage reading had risen to 5.6×10^{-7} mm Hg. Analytical predictions indicate a pressure of 1×10^{-4} mm Hg or less must be maintained to ensure the desired effect. These results indicated it should be possible to construct full sized long life passively evacuated receivers for long-term testing at the MSSTF.

Receivers for the MSSTF

The decision was made to construct eight receiver assemblies, each 12 feet in length, using the procedures outlined above. The steel absorber tubes were plated by Hyland Plating Co. During their bakeout in air at 350°C (662°F), the black chrome was damaged by the heat and the tubes were returned for replating. The plating procedure was modified by increasing the length of time in the plating bath and increasing the plating current. After replating and bakeout at 350°C (662°F) for 24 hours, their average absorptivity and emissivity readings were .97 and .38 [at 300°C (572°F)], respectively.

In the interest of maintaining a high quality vacuum in the receivers for the longest possible time, various chemical getter materials were examined for use inside the glass envelope. A getter is a device that will absorb and trap gas molecules that may enter an evacuated volume either through a small leak or by the outgassing of the container materials. A non-evaporable Zr-Al getter in the form of a ribbon was chosen. SAES Getters/USA, Inc., provided samples of their St101/CTS/Ni/8D getter strip for our evaluation. A technique for spot welding pieces of this ribbon to the absorber tube was developed and ribbons were fastened to half of the tubes.

The eight receivers were then assembled, baked under vacuum, and their copper tubulation was pinched off. The baking process lasted for 48 to 72 hours at 330°C (626°F) for each tube. A residual gas analyzer indicated H_2 and H_2O were being removed during the long bakeout periods.

Five of these receivers were installed on parabolic troughs supplied by Custom Engineering at the MSSTF, as illustrated in Figure 4. The test data for these receivers showed poorer than expected results due to high heat losses. The receiver hardware and test results are being examined to determine the cause of these heat losses.

Lessons Learned

The lessons learned to date from this program are listed below:

1. It is possible to build a passively evacuated receiver that will perform as predicted by the analytical model and retain its vacuum very well.

2. Assembling a receiver that will retain its vacuum is very difficult. In order to improve the success rate, the number of penetrations into the vacuum for instrumentation purposes must be kept to a minimum.

3. These receivers have shielded thermocouples penetrating into the vacuum that are attached to the outside of the absorber tubes. Some of the shields developed small leaks into the vacuum that were extremely hard to pinpoint. It became necessary to leak check each shielded thermocouple prior to assembly and attach it to the absorber tube by crimping it into a small tube which had been welded to the absorber's surface earlier.

4. During the few days the five receivers were being tested at the MSSTF, two of them developed cracks in the glass at the glass to kovar seal, causing an immediate vacuum loss. The glass to metal seal has proven to be a sensitive area and will require more development work.

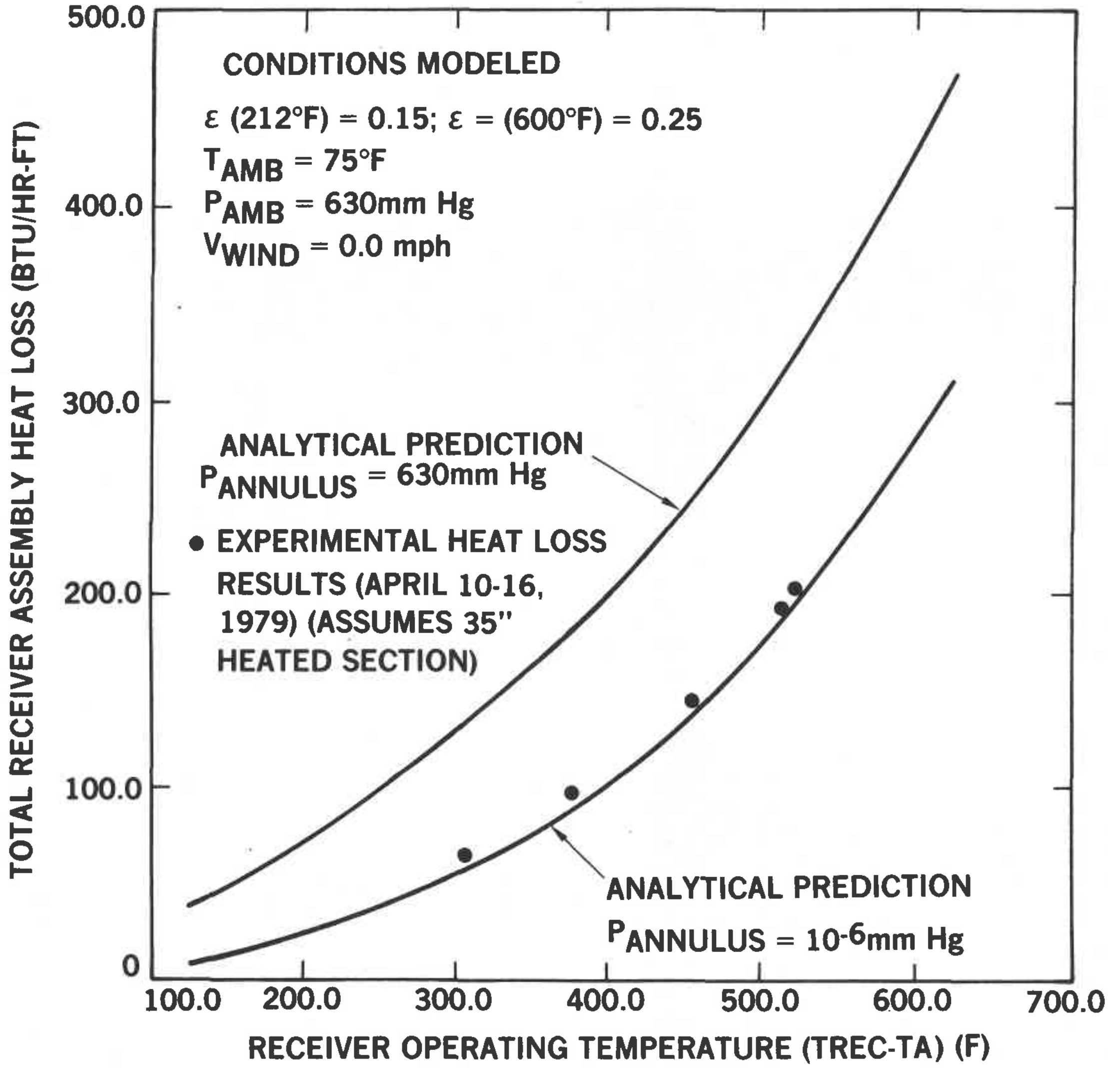

Figure 1. Receiver Assembly Heat Loss Characteristics

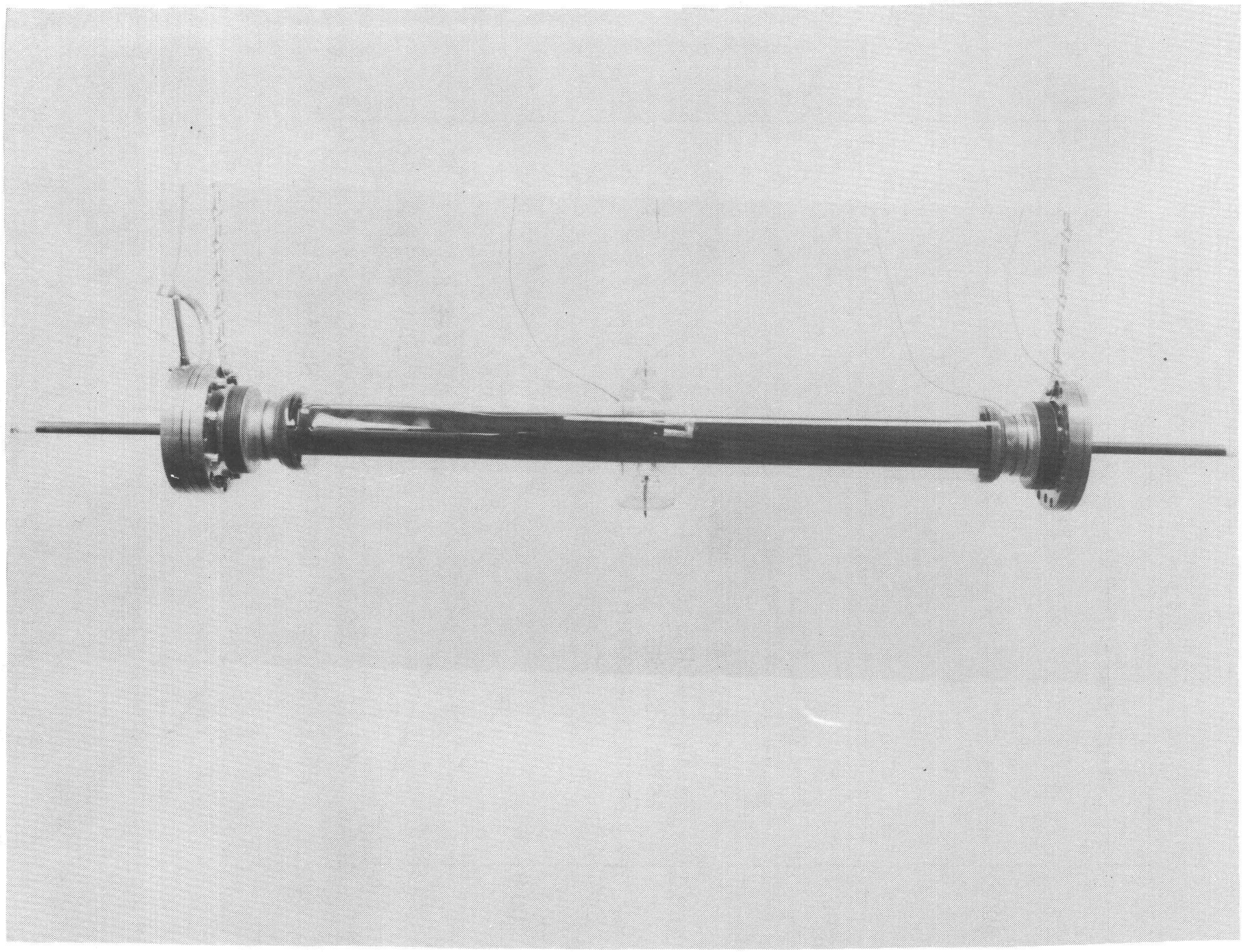

Figure 2. Laboratory Model Under Test

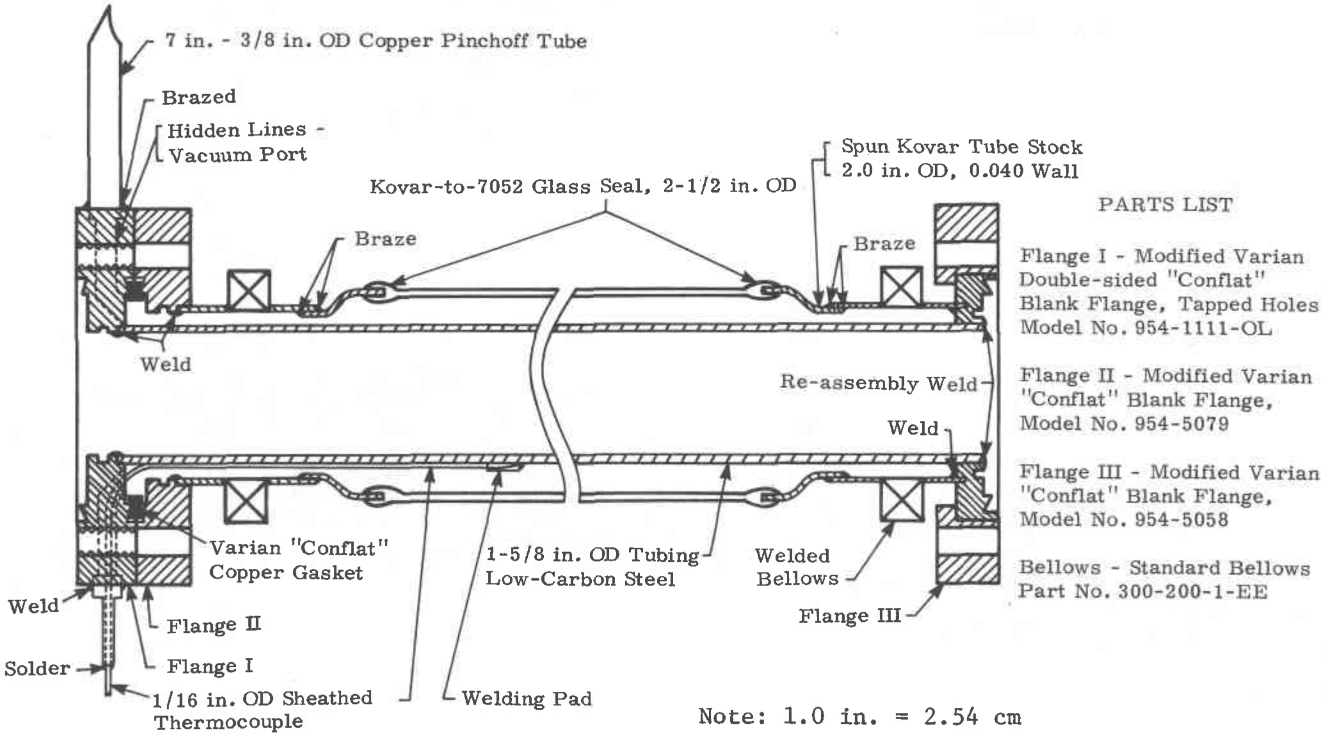

Figure 3. Assembly Details of Passively Evacuated Receiver Design

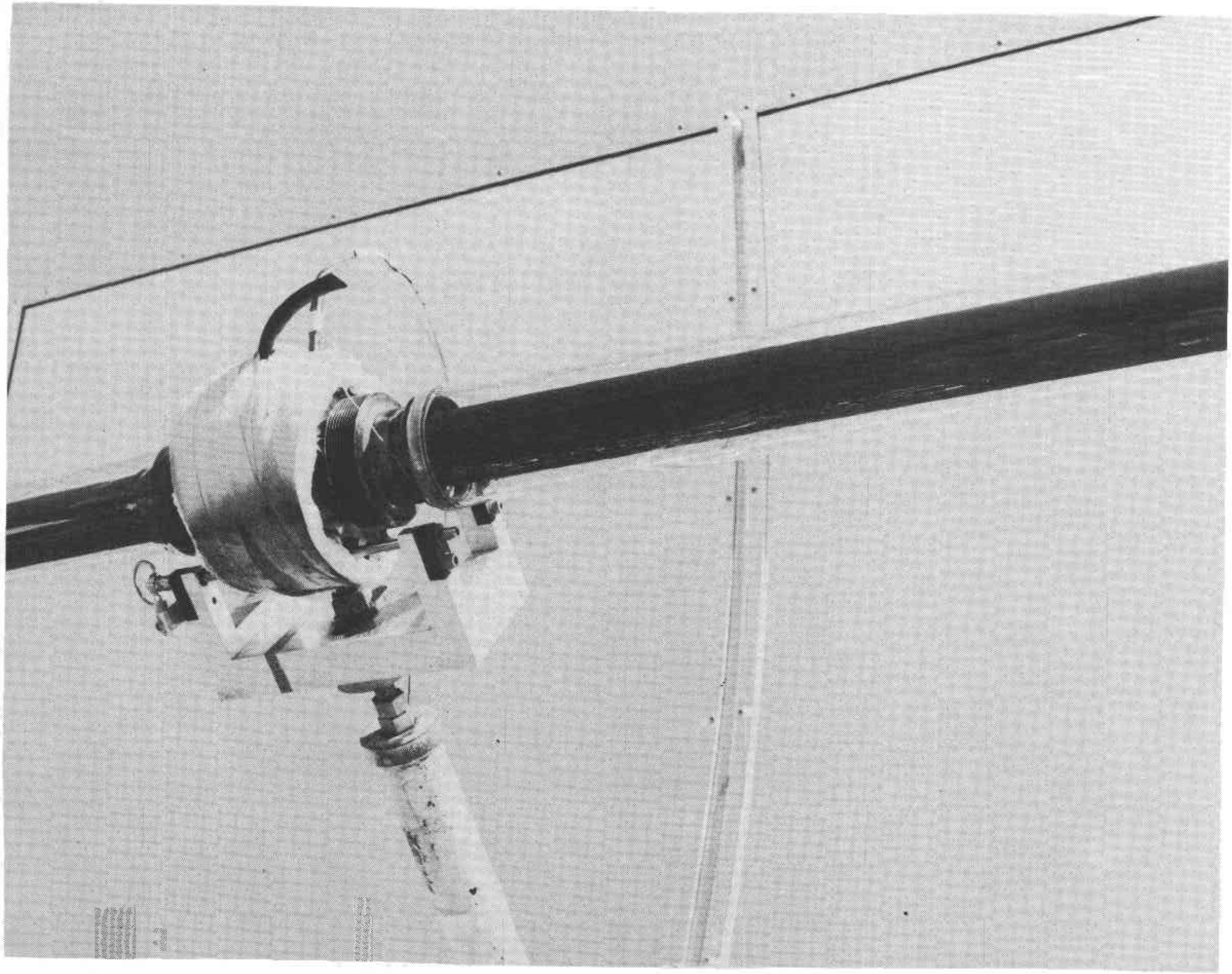

Figure 4. Full-Size Receivers Installed at MSSTF

INSULATED METAL HOSE FOR TRACKING RECEIVER APPLICATION

Wilbur E. Boyd
Component and Subsystem Development Division 4722
Sandia National Laboratories
Albuquerque, NM 87185

Introduction

Heat transfer fluid must be conveyed between the solar receiver and the field distribution manifold in a field of parabolic trough solar collectors. The devices to accomplish this task must:

- o Accommodate motions of collector, receiver, and manifold
- o Minimize pressure drop
- o Conserve collected energy
- o Minimize cost.

The motions to be accommodated, and the mechanisms considered for each are:

A. Collector rotation - by flexible hose or rotary joint
B. Receiver thermal expansion - flexible hose or linear bellows device
C. Manifold thermal expansion - flexible hose or linear bellows device.

Del Manufacturing Company has demonstrated the concept of a stationary receiver with the collector pivoting about the focal line, which would only have to contend with B and C above. This paper will deal with the approach in which the receiver moves through an arc.

Since a rotary joint approach requires three discrete components to satisfy A, B, and C above, and since the hose is the common element in A, B, and C, a single hose approach seems the obvious choice to minimize cost.

The purposes of this paper are to:

1. Describe the interface requirements
2. Describe the conceptual design of an insulated metal hose
3. Describe some hose deployment concepts
4. Describe a hose test program.

Interface Requirements

A collector must be capable of tracking the sun from one horizon to another, plus further rotation to stow with its mirror surfaces facing downward. The total rotation required is about 225° minimum; some collector manufacturers use as much as 270° of rotation.

The receiver for a typical 80 ft long drive string grows approximately four inches longer when heated to near 700°F to achieve 600°F $\pm$ 50°F operating temperature for the heat transfer oil. By anchoring the receiver at the mid-point of the drive string, we can distribute this four inches of thermal expansion equally, two inches at each end of the receiver.

The manifold piping, which runs at right angles to the receiver, is also subject to thermal cycling. Therefore the location of each attachment point along the manifold is temperature dependent, in addition to tolerances on location at initial installation. These can easily add up to a plus or minus one inch (two inch total) uncertainty of location for these points.

The thermal deflections of the receiver and the distribution manifold, superimposed upon the hose flexure, impart torsion to the hose. Torsion is detrimental to hose life. We are investigating various deployments and testing hoses under actual use conditions to determine if a hose so used can have an acceptable life expectancy.

Insulated Metal Hose

A metal hose is essentially a long thin-walled bellows of corrugated convolutions, usually of stainless steel, covered by a stainless steel wire braid (see Figure 1). The braid jacket restricts the bellows from elongating under pressure. It also stabilizes and adds hoop strength to each convolution to limit its deflection outward under pressure.

As the hose is flexed, each individual convolution deflects. These individual deflections must be kept small and uniform to stay within the elastic limit of the material. The elastic limit is low because hoses are usually formed from annealed material. Each manufacturer publishes tables of minimum allowable bend radii for each hose size (diameter) for intermittent flexure applications. If the minimum allowable bend radius is seriously violated, the hose is "kinked"--that is, the elastic limit of the material is exceeded in a localized area and the material takes a permanent set. If such a hose is continued in use for intermittent flexure, it will fail prematurely. This has probably been the dominant mechanism in most of the early hose failures which have been experienced in solar fields during their short history. The hoses have not been protected against flexing at too small a radius of curvature. Until hose designs are available which protect the hose from flexing at too small radius, we cannot separate the effect of this mechanism from that of torsion in causing hose failure.

Since the hose must be insulated to prevent excessive heat loss, the insulation and the outer cover can work to distribute deflection uniformly over the entire length of the hose and prevent local over-bending. For example, a "stripwound" metal hose (Figure 2) can be used for the outer cover, as in the hoses on the right of Figure 6. This type of hose has the useful characteristic of flexing to a certain radius of curvature, depending upon its diameter, and no further. Thus the working hose, lying coaxially within the insulation inside the cover is protected if its allowable bend radius is smaller than that of the cover. The outer cover must be a material which can withstand the concentrated sunlight which spills off the end of a parabolic trough at certain sun angles, which probably implies a metal cover.

Two other considerations which can have a major impact upon hose life are (a) the basic hose deployment, and (b) whether or not the receiver is free to rotate. A receiver which can rotate (Figures 3 and 4) does not force the hose to flex to as small a radius of curvature at the extremes of travel.

A deployment such as in Figure 3 which supports the hose against sagging from gravity, and does not require the hose to flex through a neutral plane, should have advantages.

A deployment as in Figure 4 would have the advantage of not requiring a cradle for the hose, if the effects of gravity on the hose are not detrimental. Both the Figure 3 and Figure 4 deployments require a receiver which can rotate.

Figure 5 is another example of how deployment can be chosen to aid the hose. By bisecting the angle of rotation, the hose is not worked as hard as it would be if brought up vertically from a lower attachment near the collector pylon. The Figure 5 deployment will function with either a rotatable or non-rotatable receiver.

Hose Test Program

A hose test machine (Figure 7) which can duplicate the motions of collector, receiver, and manifold has been assembled at SNLA. A fluid conditioning loop which will allow testing at temperature and pressure is nearing completion. A test program will be initiated in October 1980 to evaluate hoses in various deployments, starting with those of Figures 3, 4, and 5. Hoses will be cycled in pairs while oil is circulated through them at temperature, pressure, and flow conditions simulating actual use conditions. Hoses from various manufacturers will be evaluated.

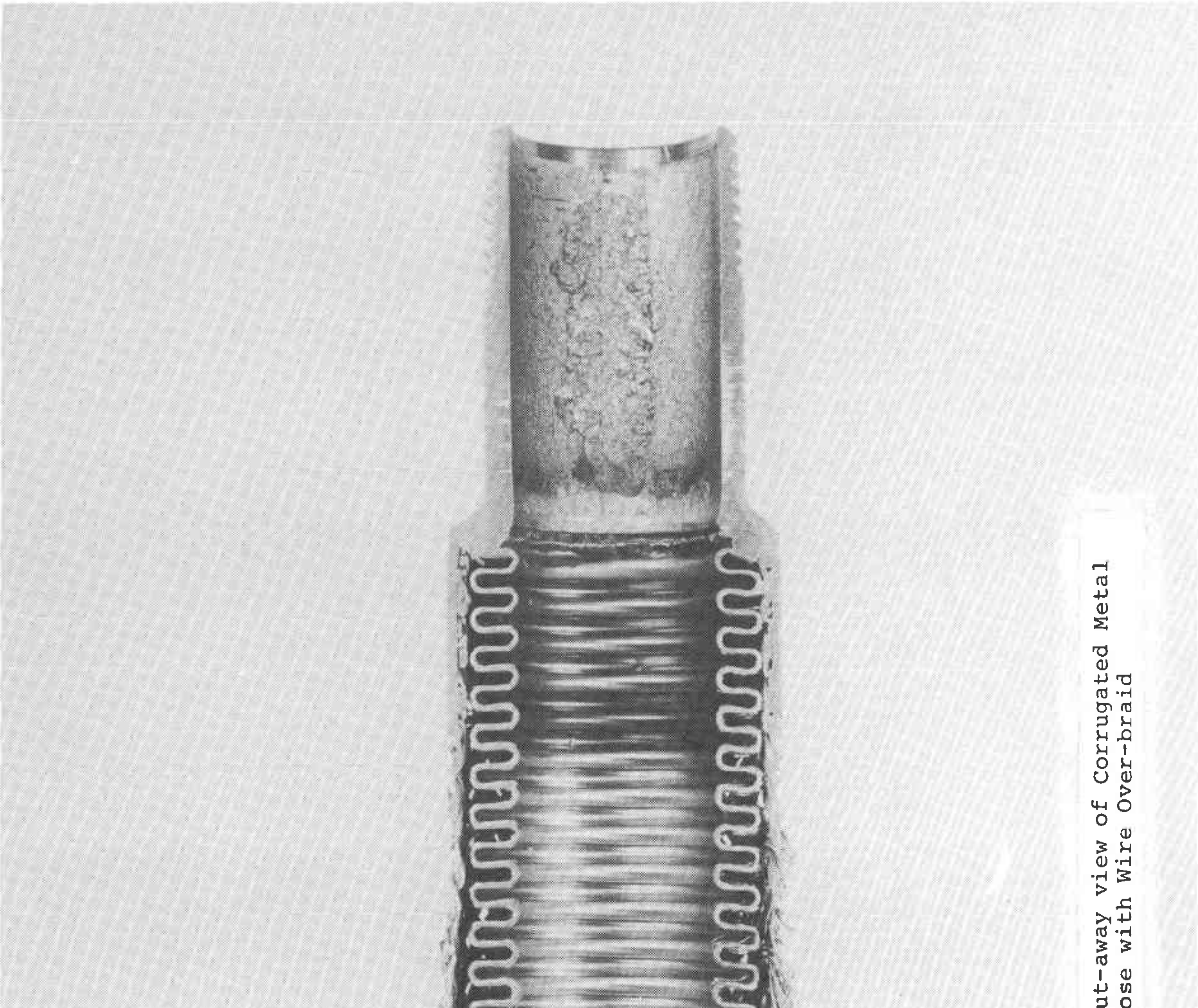

Figure 1. Cut-away view of Corrugated Metal Hose with Wire Over-braid

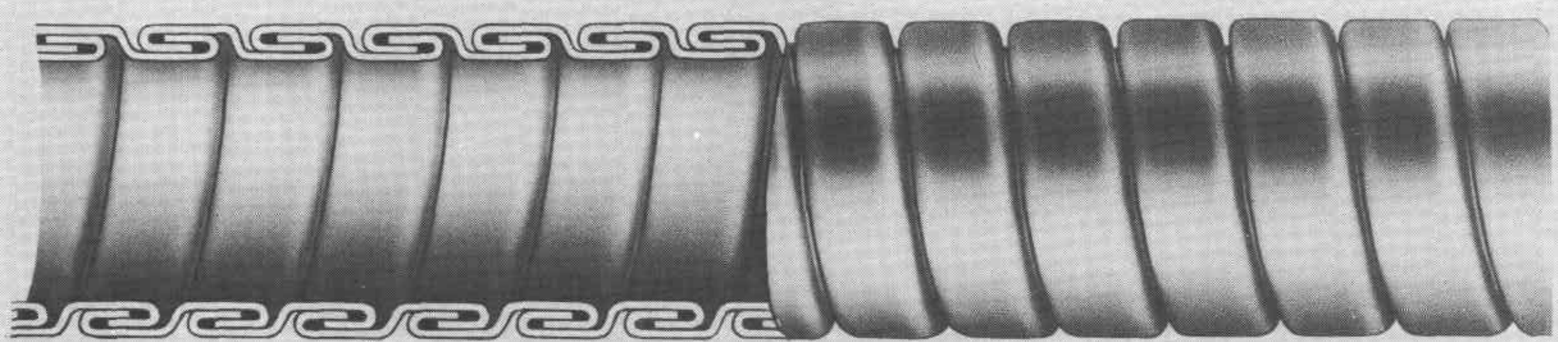

Figure 2. Cut-away view of Strip-wound Metal Hose

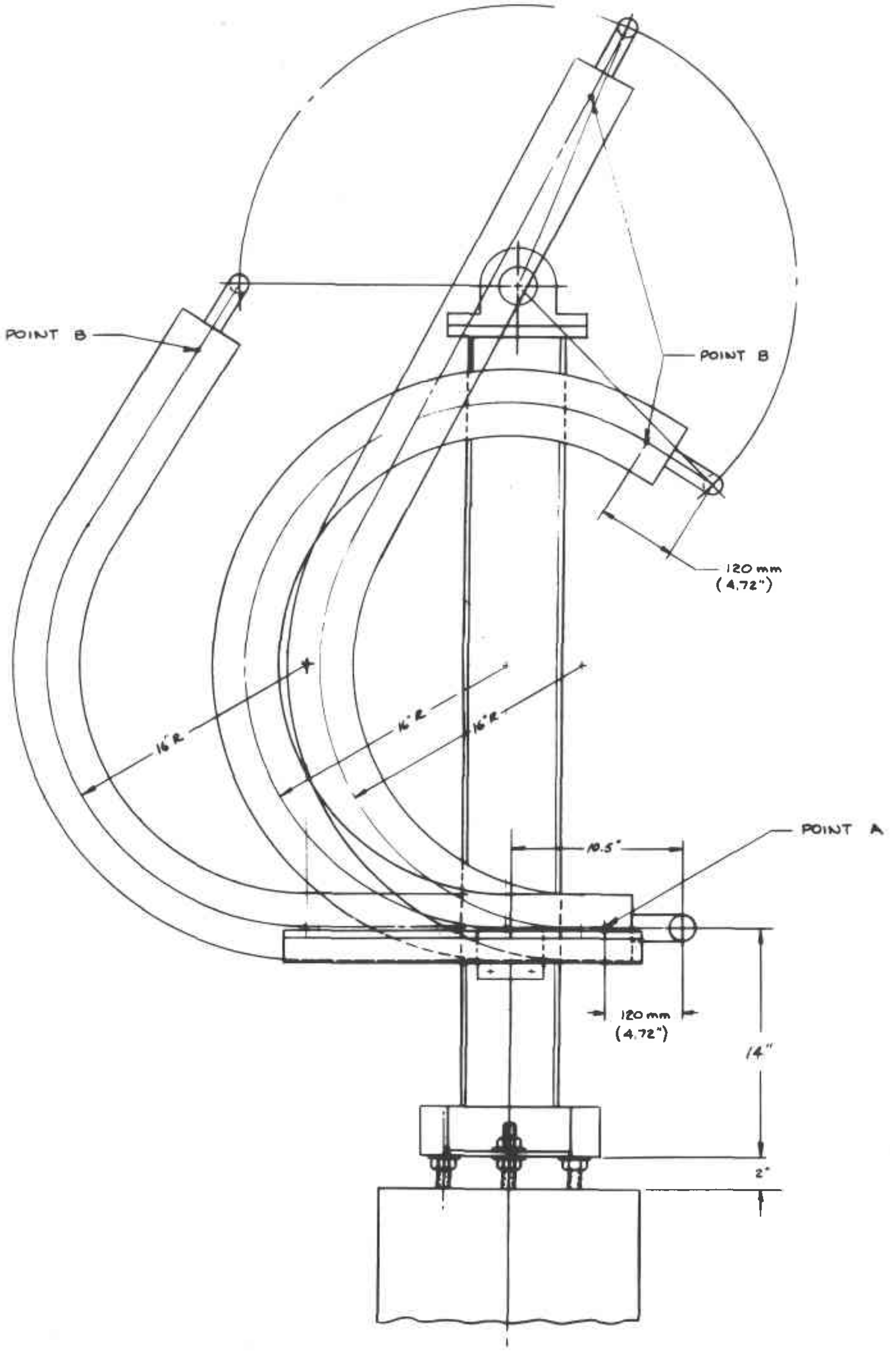

Figure 3. Hose Deployment for Use With Rotatable Receiver.
Hose Rolls on Support Cradle.

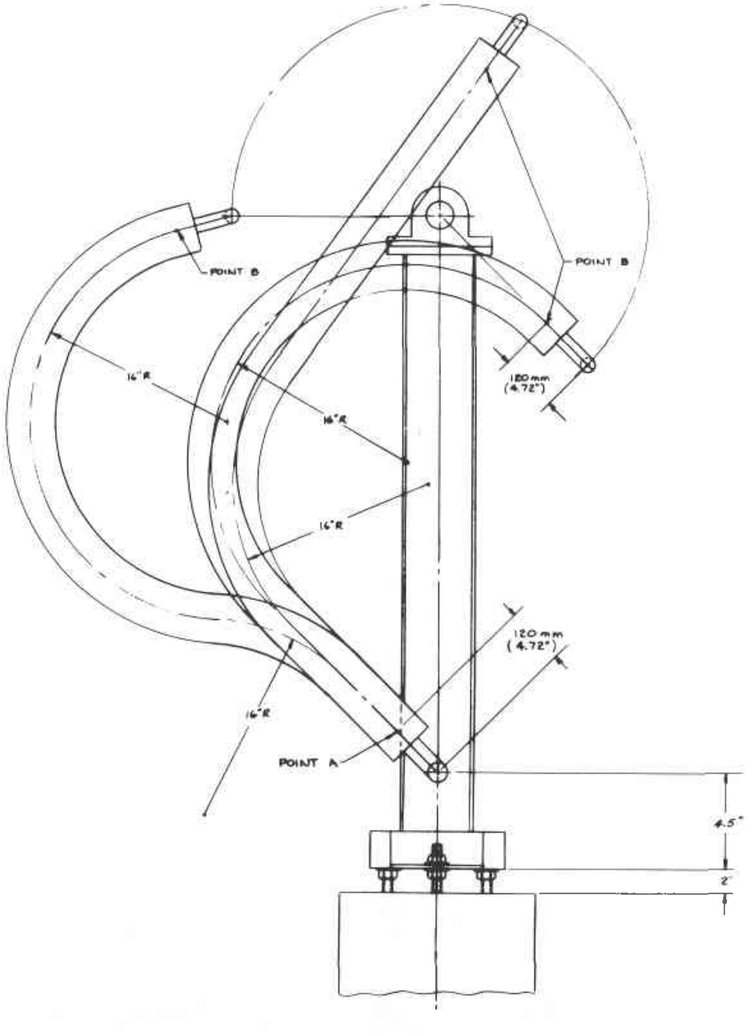

Figure 4. Hose Deployment for Use With Rotatable Receiver

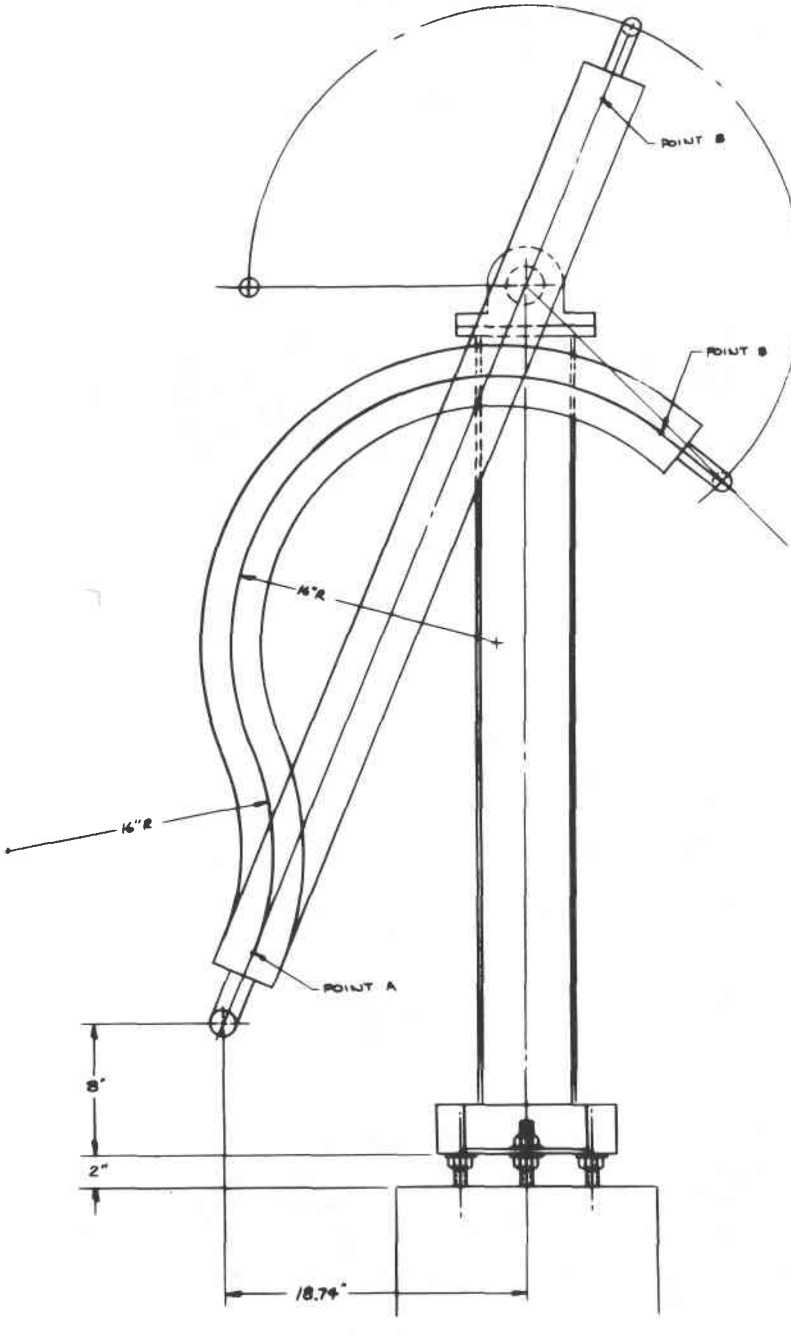

Figure 5. Hose Deployment Which Can Function With Rotatable or Non-rotatable Receiver

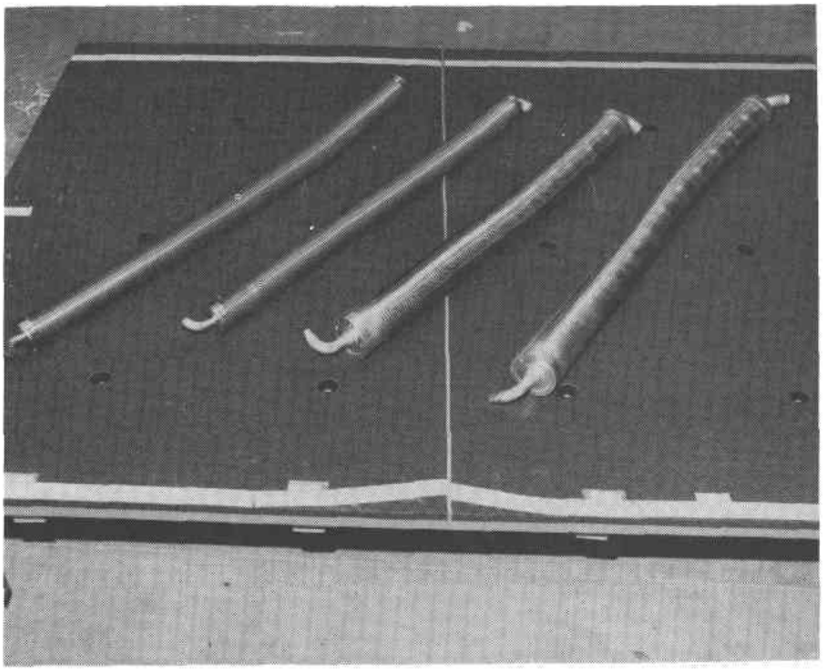

Figure 6. Insulated Metal Hoses of Two Manufacturers

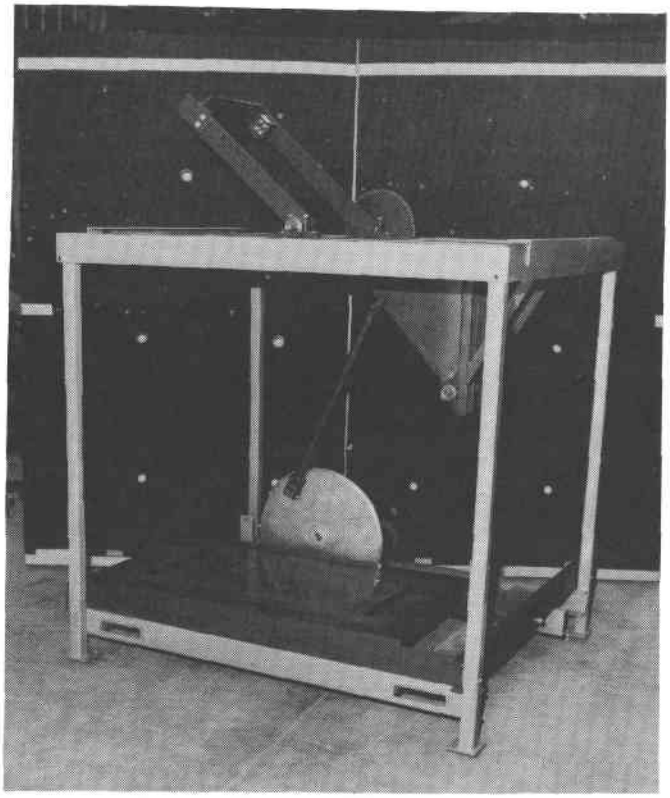

Figure 7. Hose Testing Machine

Session VI - Materials Development

Nancy Clark, Chairwoman
Energy Components and Materials
Compatibility Division 1415
Sandia National Laboratories

BLACK CHROME SOLAR SELECTIVE COATING

R. B. Pettit and R. R. Sowell
Thermophysical Properties Division 5824
Sandia National Laboratories
Albuquerque, New Mexico 87185

Introduction

Electrodeposited black chrome solar selected coatings obtained from the Harshaw Chromonyx Bath[1] have been a prime candidate for use in concentrating solar collector systems. The black chrome coating is applied to a mild steel receiver tube that has been electroplated with ~25 μm (0.001") of nickel. Initial studies[2] demonstrated that with proper substrate and plating control, as plated optical properties with solar absorptance values (α_s) greater than 0.95 and corresponding emittance values at 300°C ($\varepsilon(300)$) less than 0.25 could be obtained in the laboratory and a commercial plating facility with relative ease and at reasonable cost. Although some initial results indicated that the coating was stable in air at 350°C,[2] subsequent detailed studies demonstrated that the solar absorptance frequently decreased 6-10% within a few tens of hours when the coatings were heated above approximately 250°C in air.[3] Because a few coatings remained stable after heating to 350°C in air, a program was initiated to improve the thermal stability of plated coatings by careful control of the plating process.

This report summarizes our progress in improving the thermal stability of these coatings and problems encountered in scaling up the laboratory studies to a commercial plating facility. Finally, our current program is outlined.

Trivalent Chromium Concentration

The nominal composition of the Harshaw Chromonyx Bath (standard bath) was determined to be 332 g/l chromic acid (CrO_3), 226 g/l acetic acid, 16 g/l trivalent chromium (Cr^{+3}) and, 8 g/l iron (Fe^{+3}). All coatings plated from the standard bath were thermally unstable when heated to 300°C and above (see Table I). However, upon reducing the Cr^{+3} concentration from a nominal value of 16 g/l to 12 g/l or less, coatings were obtained which were stable after thousands of hours at 350°C in air (see Table I).[4,5] As the Cr^{+3} concentration was reduced, slightly longer plating times were required in order to obtain coatings with solar absorptance values greater than

0.95. This also resulted in higher 300°C emittance values for these coatings (0.35 to 0.40) which decreased significantly after heating to 350°C and above (0.25 to 0.30).

Detailed microscopic analysis of the stable and unstable coatings indicated that the as-plated stable coatings have a slightly increased metallic chromium content as compared to the unstable coatings.[5,6] However after heating, the stable coatings exhibit significantly less oxidation compared to the unstable coatings. Scanning electron microscopy studies show that the black chrome coating is composed of layers of nearly spherical particles.[5] For coatings obtained from a nominal 16 g/l Cr^{+3} bath, the particles range in size from 65 to 90 nm. When the Cr^{+3} concentration is reduced to 10 g/l, these particles agglomerate together to form clusters that are typically 150 to 200 nm in size. Thus the reduced amount of oxidation in the stable films appears to result from the larger effective particle size of these films.

Plating Demonstration

In order to demonstrate the improved plating formulation in a commercial facility, a low trivalent chromium bath (10 g/l Cr^{+3}) was set up at Highland Plating Company, Los Angeles, CA. The demonstration was coordinated with the plating of 600 receiver tubes for use in the Solar Irrigation Project at Cooledge, AZ. During the production plating, several "dummy" tubes were plated and tested for thermal stability in air at 400°C. After only 120 hours at temperature, solar absorptance values had decreased an average of 10% to values as low as 0.82. Thus the bath produced unstable coatings even though the low trivalent chromium level was maintained throughout the production plating. Therefore it appeared that additional plating variables needed to be controlled in order to obtain thermally stable coatings.

Several months after the production plating, several tubes were sent back to Highland for replating. Certain plating conditions were changed in the hope of improving the coating stability: (1) the current density was increased from 161 ma/cm^2 to 215 ma/cm^2; (2) the plating time was increased from three minutes to five minutes, and (3) the spacing between the tubes was increased in order to improve the coating uniformity. Although the initial emittance values of the coated tubes were high, the coatings were stable after heating at 400°C in air for over 600 hours (see Table II). Unfortunately, subsequent plating at Highland from the same bath again produced unstable coatings. As in the previous cases, the bath chemistry indicated a bath composition identical to baths used in earlier laboratory studies.

Because of the limited success in plating the improved black chrome coating in a commercial environment, a scaleup of the laboratory studies was initiated in Sandia's plating shop facility. Two plating baths were successful in producing stable black chrome coatings, but only for the initial 15-20 samples plated. Subsequent samples plated were thermally unstable. Changes in the bath chemistry were not detected using conventional chemical analysis or emission spectroscopy. For one black chrome bath, results obtained using a gas chromatograph/mass spectrometer indicated the presence of a small amount of organic material from the nickel plating solution. Microscopic analysis of the deposited coatings indicated the presence of small isolated particles in the unstable coatings while the stable coatings obtained from the same bath were composed of large clusters. A positive identification of the organic material as the cause of the unstable coatings will be confirmed by adding small quantities of the nickel plating solution to a "good" bath.

In summary, it is our current belief that difficulties in reproducing our laboratory results for stable black chrome coatings resulted from either (1) improper sample surface preparation, (2) inadvertent plating bath contamination, or (3) improper plating conditions (unknown current density, bath temperature, bath agitation, etc.).

Statistical Study of Plating Variables

Although the role that the trivalent chromium concentration plays in the thermal stability of deposited coatings has been established, the effects of the other bath constituents and plating parameters have not been determined. In addition, the entire process has not been optimized for solar applications. Therefore, a series of detailed experiments has been planned to obtain this information. The experiments will be used to determine the optimum process parameters and to set bath and plating control limits on this process. The variables to be studied include: chromic acid concentration, acetic acid concentration, trivalent chromium concentration, iron concentration, plating time, current density, bath temperature, bath agitation and substrate. The experiments are being designed and analyzed using statistical techniques. Initial results from these experiments indicate that with careful control the plating process has excellent reproducibility both for coatings plated from the same bath and for coatings plated from different baths of the same composition.

Plating Process Specification

A preliminary process specification for electroplating mild steel substrates with the stable black chrome coating is listed in the Appendix. The specification includes instructions for substrate preparation, nickel electroplating and black chrome electroplating as well as recommended optical and chemical inspection techniques. Careful attention was given to surface cleanliness through a thorough rinsing/cleaning procedure and minimization of bath contamination. It should be noted that the specification is only preliminary and that it is anticipated changes will result from the detailed study of the plate bath variables outlined above.

Conclusion

While thermal degradation of black chrome coatings electrodeposited from the standard bath occur above 250°C in air, the thermal stability can be significantly improved by decreasing the trivalent chromium concentration in the plating bath. With this reduction, coatings have experienced only a 3% decrease in solar absorptance after laboratory tests to 3600 hours at 400°C. Reproduction of the improved coating in a commercial environment has met with failure that appears to be related to either inadequate sample surface preparation, inadequate plating process control, or bath contamination. A program has been initiated to more fully understand the effect of a variety of plating variables, including all bath constituents, on the optical properties and thermal stability of plated coatings. With these studies, we hope to optimize the plating process for solar applications and to set reasonable process limits for the various bath constituents. A preliminary process specification has been developed which carefully controls the sample surface preparation and cleaning throughout the plating sequence. At the completion of this study, a full scale demonstration, utilizing a 3.66 m long receiver tubes plated in a production facility, is planned. Results for this demonstration should verify the feasibility of plating the improved coating on full size solar hardware.

Acknowledgement

The authors wish to acknowledge the assistance of A. R. Mahoney in performing optical measurements and thermal aging tests, P. J. Rodacy for the gas chromatograph/mass spectrometry analysis and S. L. Erickson, R. V. Whiteley and R. J. Kottenstette for bath chemical analysis.

Appendix

PROCESS FOR ELECTROPLATING MILD STEEL RECEIVERS FOR CONCENTRATING SOLAR COLLECTORS

I. General

This procedure defines requirements for electroplating nickel and black chrome on mild steel tubular solar receivers. All phases of surface preparation, cleaning and plating are critical to efficient perfomance and durability of receivers operating at temperatures above 250°C. Solar absorptance, thermal emittance, and stability at operating temperatures to 350°C in concentrated sunlight, are of primary importance.

This process is outlined for the plating line dedicated to producing high temperature black chrome solar selected coatings. Cleaning and rinse tanks should be single-duty, i.e., tanks shall be used only for the specified step in cleaning the sequential and plating operations.

II. Equipment

1. Steel cleaning, rinsing and plating tanks should be 0.6-0.9 m by 1.5 m by 4.0 m.

2. Materials for lined tanks shall be nonreactive and noncontaminating to cleaning and plating solutions. Rigid PVC is recommended for the black chrome bath.

3. The temperature of heated tanks should be controlled to ± 2.5°C during plating.

4. Rack materials should be nonreactive and noncontaminating in all baths. Racks should provide adequate spacing (typically greater than three pipe diameters) to give unifom coatings around the entire circumference of receiver tubes.

5. Mechanical or air agitation should be used in all plating baths. If air agitation is used, the air should be free of oil and other contaminants.

6. Constant current DC plating power supplies should have no greater than 5% AC ripple under plating conditions and should be instrumented to control and monitor a current to ± 1%.

7. For thermal aging tests, a dedicated tube furnace should maintain temperatures to ± 5°C in the test zone.

III. Surface Preparation and Cleaning

1. Vapor degreased parts with trichloroethylene or equivalent.

2. Fine bead blast the entire outer surface uniformly. The glass bead diameter size shall be 0.178-0.124 mm (0.0070-0.0049 inches).

3. Tube should be plugged at each end to prevent entry of cleaning and plating solutions.

4. Soak in low pH (pH less than 10) borax base agitated cleaner for a minimum of 15 minutes.

5. Anodically clean in a 50% caustic soda, (nominal concentration 71 g/l (9.5 oz. per gallon)) at 54-108 ma/cm^2 (50-100 amps per square foot) at a temperature of 65-80°C for one to two minutes.

6. Tap water rinse by immersion. If rinse tank is not agitated, part should be dipped at least two times with a minimum dwell time of one minute. If agitated, part should be rinsed a minimum of two minutes. The tank should be an overflow type with a flow rate adjusted to minimize buildup and dragout.

7. Cathodic acid cleaned in room temperature bath with sulfuric acid concentration maintained between 120-135 g/l (16-18 oz. per gallon). Electric clean shall be at 5 ma/cm^2 (5 amps per foot) for 1-3 minutes. (An acid salt bath with bifloride wetting agent is recommended.)

8. Tap water rinse same as #6.

9. Repeat anodic clean except caustic soda concentration shall be 60-64 g/l (8-8.5 oz. per gallon).

10. Mild acid rinse (10 volume percent H_2SO_4).

11. Tap water rinse same as #6. Note: Do not allow tubes to dry between cleaning and nickel plating processes.

IV. Nickel Plating

12. Nickel plate per MIL-QQ-N-290 class 1, 25 μm to 38 μm (0.001 inches to 0.0015 inches) thick (25 μm (0.001 inches) minimum). Mat or semibright finish. Note: No copper strike should be used.

13. Water rinse as in #6 but use deionized (DI) water with a minimum resistivity of 250,000 ohm-cm and passed through a charcoal filter.

14. Spray rinse with deionized water.

15. Water rinse same as #6 but with deionized water. Note: Do not allow tubes to dry between nickel plating and black chrome plating.

V. Black Chrome Plating

16. Black chrome plate with Harshaw Chemical Co. Chromonyx bath at 188 ma/cm^2 (175 amps/sq. ft.) for 3-5 min. at 18-26°C. The black chrome bath composition should be maintained as follows:

CrO_3	332 ± 4 g/l
Plating Addition Agent	27 ± 1 volume percent
Cr^{+3}	8 ± 0.5 g/l
Fe^{+3}	7.5 ± 1 g/l

The anode should be mild steel. The anode cathode ratio should be 2:1. Mild agitation should be used.

17. Water rinse same as #6 but use deionized water.
18. Spray rinse with deionized water.
19. Water rinse same as #6 but use deionized water.
20. Dry parts by one of the following methods:
    a. Blow dry with clean dry nitrogen or hot air filtered to remove dust particles, oil and other contaminates.
    b. Oven dry in forced air furnace.

VI. Requirements and Specifications

1. Solar absorptance should be a minimum of 0.96 and should be measured at two locations on each receiver tube using a Gier Dunkle Model MS 251 Solar Reflectometer[7] or a Devices and Services Solar Spectrum Reflectometer.[8]

2. Emittance at 300°C should be between 0.25 and 0.38 as measured with a Gier Dunkle DB 100 infrared reflectometer modified for 300°C measurements.[7]

3. Analysis of all plating baths should be perfomed daily. Analytical procedures for the black chome bath should have the following accuracies:

CrO_3	± 2 g/l
Addition Agent	± 1 volume percent
Cr^{+3}	± 0.5 g/l
Fe^{+3}	± 0.5 g/l

The analytical methods have been previously developed.[9,10]

4. Sections of tubes should be heated at 400 ± 5°C for 100 hrs in air. A decrease in solar absorptance of greater than 2% after heating will indicate an unacceptable coating.

VII. Handling and Packaging

1. Critical surfaces should not be touched or mechanically damaged.
2. Receiver should be handled only at the ends with clean white cotton work gloves and should be packaged so as not to damage the coating during shipment.

Table I. Thermal Aging Results for Black Chrome Coatings on Electrodeposited Nickel Substrates

Plating Conditions	Time Temperature	Test Time (hr)	α_s	ε(300°C)
16 g/l Cr^{+3}	As plated	0	0.95	0.15
3.5 minutes	250°C	64	0.93	0.14
	350°C	64	0.89	0.12
8 g/l Cr^{+3}	As plated	0	0.97	0.40
5 minutes	350°C	40	0.97	0.32
		752	0.98	0.31
		3908	0.98	0.31
	400°C	0	0.97	0.40
		40	0.97	0.29
		755	0.96	0.27
		3650	0.94	0.23

Table II. Optical Properties of Replated Black Chrome Coatings from Highland Plating Co. after Heating at 400°C in Air

Time (hrs)	α_s	ε(300°C)
0	0.97	0.53
25	0.97	0.38
115	0.97	0.37
277	0.97	0.35
670	0.97	0.33

References

1. Harshaw Chromonyx Black Chrome Bath Covered by U.S. Patent No. 3,620,935, Harshaw Chemical Co., Cleveland, OH 44106
2. R. B. Pettit and R. R. Sowell, J. Vac. Sci. and Tech. 13, 596 (1976).
3. R. R. Sowell and R. B. Pettit, Sandia Labs Report SAND 78-0554 (April, 1978).*
4. R. R. Sowell and R. B. Pettit, Plating and Surface Finishing 65 (#10), 42, Oct. 1978.
5. R. B. Pettit and R. R. Sowell, Proceedings 1979 International Solar Energy Society Congress, May 28-June 1, 1979, Atlanta, GA.
6. P. H. Holloway, K. Shanker, R. B. Pettit and R. R. Sowell, to be published Thin Solid Films.
7. R. B. Pettit, Engineering For Power 100, 489 (1978).
8. R. B. Pettit and A. R. Mahoney, Proceedings Line-Focus Solar Thermal Energy Technology Development Conference, Albuquerque, NM, Sept., 9-11, 1980.
9. S. L. Erickson, Sandia Labs Report SAND 78-1466-OUO (Aug., 1978).
10. R. V. Whiteley, Jr., Analy. Chem. 51, 1575 (1979).

*Available: National Technical Information Services
U. S. Dept. of Commerce
5285 Port Royal Rd.
Springfield, VA 22161

GLASS FIBER REINFORCED CONCRETE FOR PARABOLIC TROUGHS

Arthur J. Slemmons
Dale W. Ploeger
Engineering Sciences Laboratory
SRI International
Menlo Park, CA 94025

Introduction

The successful commercialization of solar thermal energy depends largely upon developing a system having a low enough energy cost to be competitive with energy from conventional fuels.

A major cost of any solar thermal system will be the collection subsystem. In the central power concepts, the collection subsystem is the heliostat field. In the distributed systems, it is the parabolic dish or parabolic trough collectors.

Martin Marietta* has estimated that, depending on heliostat costs, from 59 to 67 percent of the total solar plant investment cost is in the collection equipment. A recent study completed by General Motors Corporation† showed that the cost of purchased materials can amount to 81 to 85 percent of their factory cost, or about 64 percent of their installed cost, based on SERI's installation costs.‡ Taking these estimates into account, the collector subsystem purchased material costs from 38 to 43 percent of the total solar thermal power plant.

SRI International has proposed that a key to lowering the cost of solar thermal power lies in reducing the material costs of the collection subsystem through the use of glass fiber reinforced concrete (GRC). Figure 1 shows the relative production energy requirements for several common engineering materials on a basis of Btu per ton of raw material produced. These data show that plastic and aluminum are highly energy intensive materials, requiring a significantly greater amount of energy to produce than steel, glass, or portland cement. These data are for 1975 rates, but it is easy to see that as the cost of energy increases, the energy cost differences between these materials will increase at the same rate. The cost of cement is the lowest, even though these data are for the wet slurry process with uninsulated kilns currently in general use in the U.S. Figure 1 does not take into account the additional energy

---

*Martin Marietta Corporation, Denver, Colorado, "Conceptual Design of Advanced Central Receiver Power System," Final Report DOE/ET/20314-1/2, pp. II-278-280.

†J.F. Britt et al., "Heliostat Production Evaluation and Cost Analysis," SERI/TR-8052-1, p. 132.

‡Ibid., p. vi.

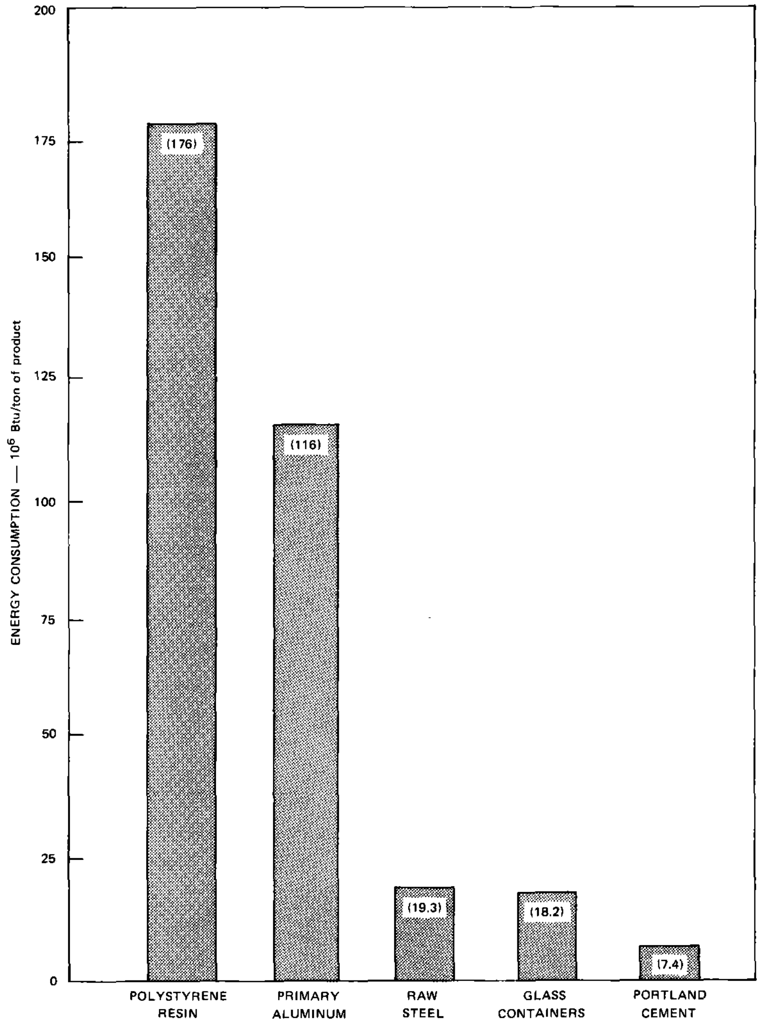

SOURCE: *Energy Sourcebook:* Aspen Publication (1975 FEA Data)

FIGURE 1 RELATIVE PRODUCTION ENERGY REQUIREMENTS FOR FIVE COMMON ENGINEERING MATERIALS

required to form usable shapes from the metals, nor the differences in strength, density, and minimum practical thicknesses of these materials.

The reinforcement of clay products with fibers has a long history. Early methods used natural fibers such as straw. More recently, investigations have been made of concrete reinforcement using manmade fibers such as plastic, steel, and glass fibers. Plastic fibers are expensive and have a low modulus; steel fibers are expensive and they rust; and conventional glass fibers are destroyed by the alkalinity of the concrete. In 1967, the British developed a glass from zirconia sands that gives a commercially feasible alkali-resistent glass fiber that is sold under the trade name Cem-Fil.

Reinforcing a sand/cement concrete with these chopped glass fibers produces a durable concrete and allows the use of thin ($\sim$3/16 inch), strong and resilient sections. SRI is now investigating under contract to Sandia Laboratories the potential of this relatively new and very low-cost material for use as a construction material for solar collectors.

Objectives

The SRI program objective is to investigate the use of GRC as a material for the construction of heliostats and parabolic trough collectors. Initial efforts have emphasized the utilization and suitability of GRC for parabolic trough collectors and the development of a low-cost design. GRC material properties are being determined with various sands and sand/cement ratios. The construction of a single 2 m x 6 m parabolic trough collector module is planned. It will be tested at Sandia's Solar Thermal Test Facility at Albuquerque.

Present Status

Prior to initiation of the contract, SRI had made an extensive literature search on fiber-reinforced concrete. Of all the candidate fibers, the British-developed zirconia-sand glass-fiber Cem-Fil appeared to be the most promising on both a cost and performance basis.

Testing

The first contractual task was to develop a GRC Test Plan to determine the material properties necessary to design a GRC solar collector.

(1) Tests on small GRC coupons to determine basic material properties such as:
- Proportional Elastic Limit (PEL)
- Modulus of Rupture (MOR)
- Elastic Modulus (E)
- Shrinkage during cure
- Flatness
- Thermal expansion.

(2) Tests on large hat-section beams to evaluate the proposed production techniques, the strength and flatness of complex sections, and the effects of freeze/thaw cycling.

The small coupons were 2 inches x 12 inches x 1/4 inch thick and were cut from 12-inch x 36-inch panels. Two sand types, Monterey and Quarry, were tested and three sand:cement ratios were tried--0.50:1, 0.66:1, and 0.80:1. All samples contained 5 percent by weight glass fiber. The coupons were made in five configurations:

- Plain
- Bonded to glass when wet
- Bonded to FEK* when wet
- Bonded to glass when dry
- Bonded to FEK when dry.

An epoxy that cures with the concrete and bonds to it was used on the wet-bonded samples. Dry bonding was done using a spray adhesive. All the samples were cured in individual plastic bags.

The PEL, MOR, and E values were obtained from a standard third point flexural test. Coupons made with Monterey sand at 0.66:1 sand:cement ratio were tested 1, 7, and 28 days after spray-up. All other coupon types were tested at 28 days. The results of these tests are summarized in Tables 1 and 2.

Table 1

RESULTS OF FLEXURAL TESTS ON GRC SAMPLES
MADE WITH MONTEREY SAND AT 0.66:1 SAND:CEMENT RATIO

Elapsed Time (days)	PEL		MOR		E	
	psi	σ	psi	σ	psi	σ
1	789	167	1574	429	1.98×10^6	0.51×10^6
7	1092	108	3003	962	1.72×10^6	0.14×10^6
28	1317	71	2549	564	1.96×10^6	0.08×10^6

Table 2

TWENTY-EIGHT DAY STRENGTHS OF GRC SAMPLES

Sand	Ratio	PEL		MOR		E	
		psi	σ	psi	σ	psi	σ
Monterey	0.66:1	1317	71	2549	564	1.96×10^6	0.08×10^6
Monterey	0.50:1	1521	502	3164	1221	2.73×10^6	1.22×10^6
Monterey	0.80:1	1256	186	2512	736	1.83×10^6	0.32×10^6
Quarry	0.66:1	1402	172	2830	460	2.19×10^6	0.40×10^6

Shrinkage and flatness were measured 2, 7, 14, 21, and 28 days after spray-up. As seen in Figure 2, the samples made with Quarry sand shrunk approximately one-half as much as samples made with Monterey sand. In all samples tested, most of the shrinkage occurred in the first 14 days after spray-up.

*FEK is the trademark for an aluminized acrylic film manufactured by 3M Corporation.

The small coupons, both with and without glass, warped during curing. Typical warping histories are shown in Figure 3. We believe that the warping is primarily due to differential drying and shrinkage of the coupon across its thickness. The differential drying is the result of a vapor barrier on one surface preventing the drying of that surface. The epoxy and mirror form the vapor barrier on the wet-bond samples. The "glassy" surface produced on the form side of the coupon would form a vapor barrier on the plain samples. To test this hypothesis, a set of coupons was made with both sides smooth, resulting in a vapor barrier on both sides. In 14 days, these samples have shown no signs of warping.

The thermal expansion tests over a temperature range from 122°F to -33°F were performed on specimens cut from dry samples 56 days old. The results are given in Table 3.

Table 3

COEFFICIENT OF THERMAL EXPANSION
FROM 122°F TO -32.8°F

Beam Composition	Expansion
Monterey Sand 0.66:1	$\alpha = 4.3 \times 10^{-6}/°F$
Monterey Sand 0.50:1	$\alpha = 4.8 \times 10^{-6}/°F$
Monterey Sand 0.80:1	$\alpha = 5.3 \times 10^{-6}/°F$
Quarry Sand 0.66:1	$\alpha = 5.3 \times 10^{-6}/°F$
Glass Mirror	$\alpha = 3.0 \times 10^{-6}/°F$

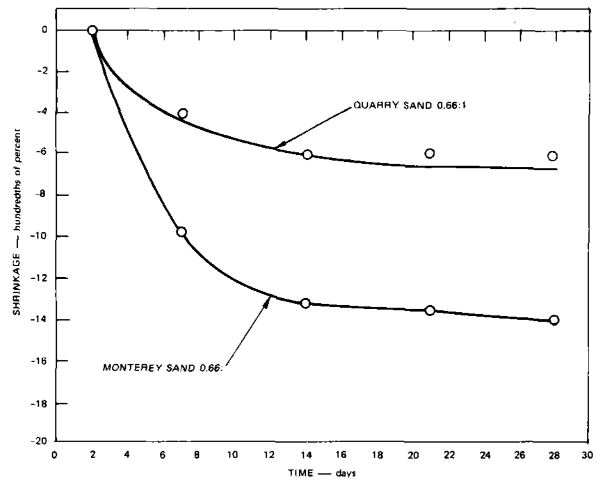

FIGURE 2 GRC DURING WET CURE

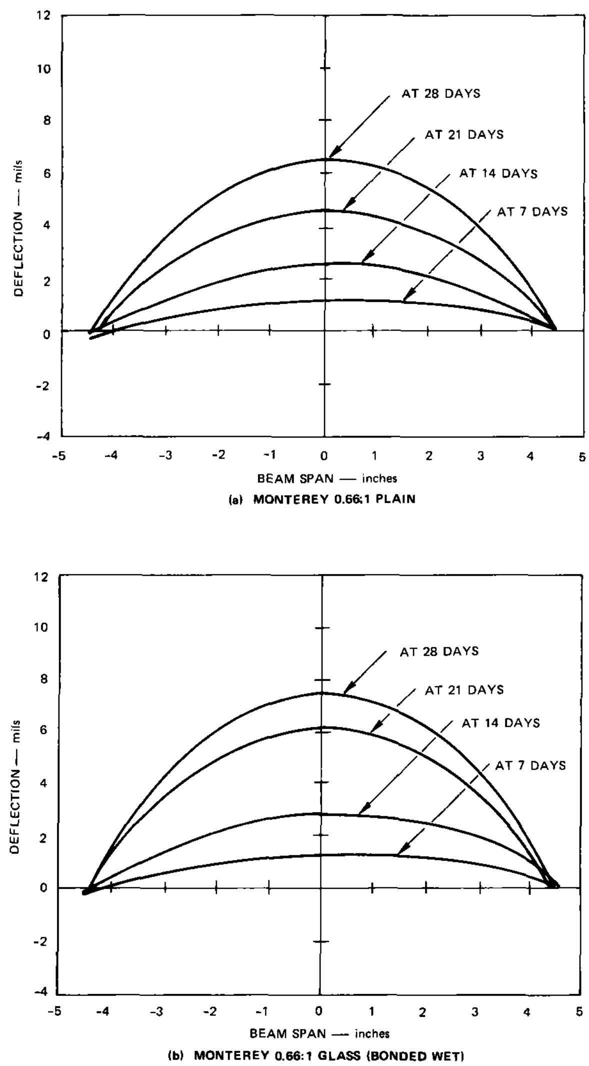

FIGURE 3 GRC WARPING DURING WET CURE

The large hat-section beams were 12 inches x 36 inches with a 2-inch deep hat section following the long axis. The wall thickness was 1/4 inch. All the beams were made with Monterey sand at 0.66:1 sand:cement ratio and 5 percent by weight glass fibers. Beams were made without reflective surfaces bonded wet to glass, and bonded wet to FEK configurations. Each beam was stored in a plastic bag during curing.

Beams were tested for strength at 1, 7, and 28 days by supporting them at each end while applying a uniform load. The load-deflection curves for plain beams are shown in Figure 4. The plain, one day old beam yielded at a bending moment 1.73 times greater than the maximum bending moment calculated for a 2-m collector subjected to a 90-mph wind in the "stand-alone" configuration. The 7- and 28-day old beams did not fail in our test.

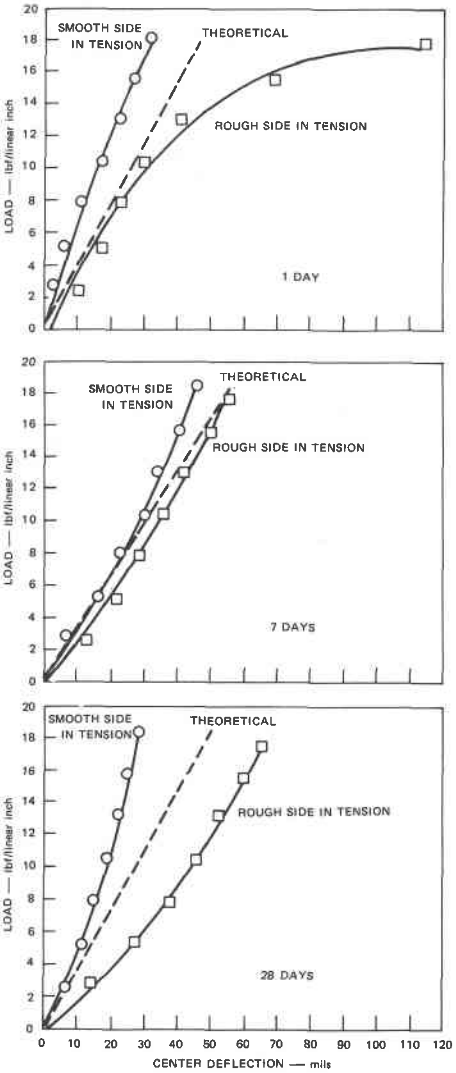

FIGURE 4 GRC BEAM TESTS WITH UNIFORM LOADING — MONTEREY 0.66:1 PLAIN

Flatness tests of the large beams were performed at 1, 7, 14, 21, and 28 days. These measurements have revealed no measurable changes in flatness of the plain beams. The glass beams warped a maximum of 0.012 inch in their 36-inch length.

Thermal cycling of the beams has been initiated. Cycling is from 0°F to 40°F to 0°F in 12-hour cycles. The results of the Phase A tests can be summarized as follows:

- Good 28-day strength.
- Good 1-day strength--possible to strip mold in one day.
- Shrinkage of samples made with Quarry sand was approximately one-half of those made with Monterey sand.
- Indications that warping can be controlled.
- Thermal expansion is approximately 5×10^{-6}/°F.
- The complex beams performed as predicted.
- The 2-inch hat section withstood the bending movement predicted for a stand-alone collector in a 90-mph wind.

Design

The preliminary conceptual design of a 2 m X 6 m GRC parabolic trough collector is shown in Figure 5. The structure is 3/16 inch thick GRC throughout and is a sprayed-up monolithic structure made of three integrated parts: the triangular torque tube extending the 6-m length of the collector, the module parabolic substrate with bonded second-surface mirrors, and a series of support ribs on 1-m centers along the axis under the parabolic mirror substrate. Figure 6 is a photograph of a scale model of this structure. This entire GRC structure is supported by a stamped-steel end-plate "hub" that pilots on the inside surfaces at each end of the triangular torque tube. These dished hubs are attached by three 3/8-inch bolts that extend inside the

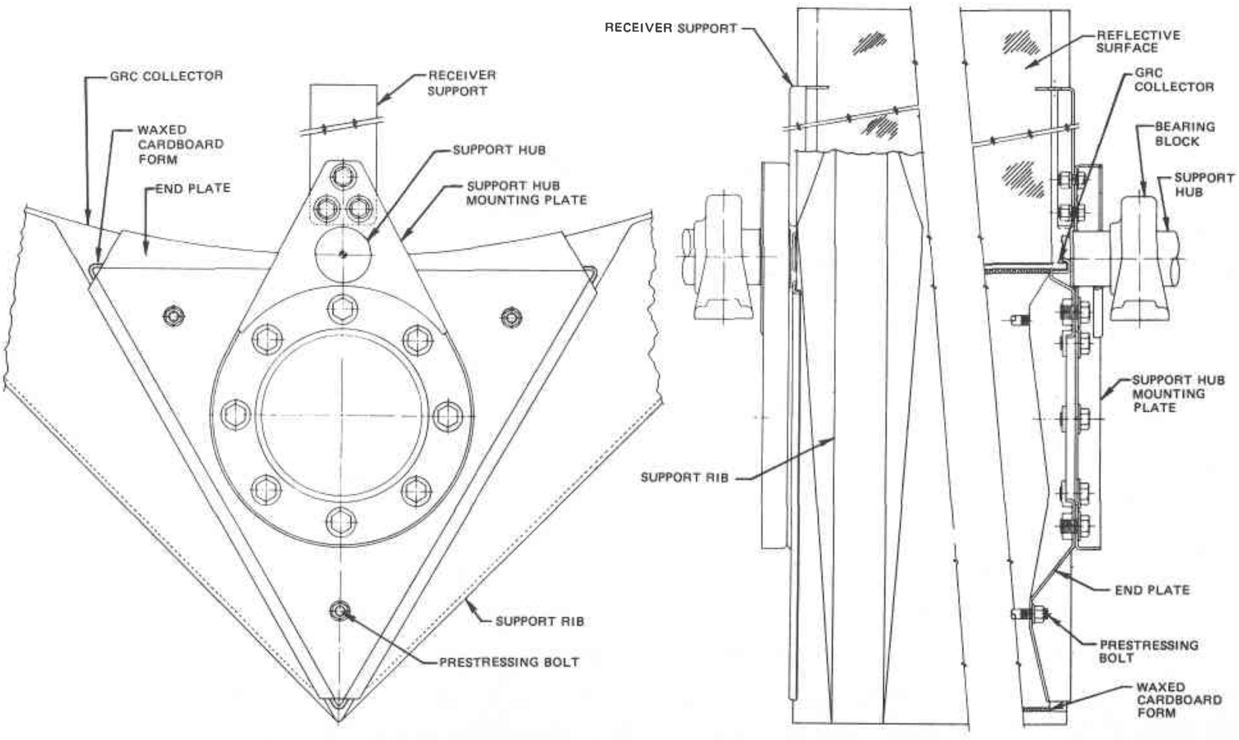

FIGURE 5 CONCEPTUAL DRAWING OF THE GRC PARABOLIC THROUGH COLLECTOR

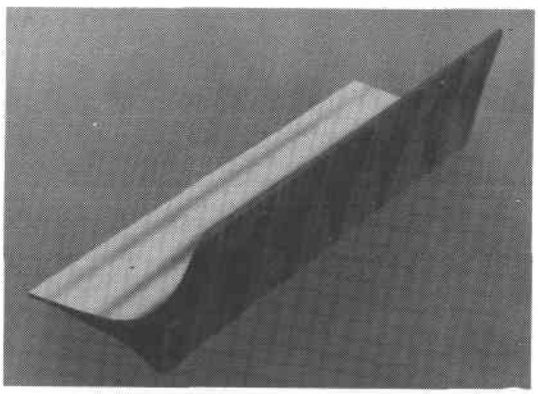

FIGURE 6 SCALE MODEL OF GRC PARABOLIC THROUGH COLLECTOR

length of the torque tube and prestress the GRC in compression. Differential tensioning of the three bolts can be used to compensate for any long-term creep deflections. Plastic inserts between the steel hubs and the concrete torque tube act as cushions and corrosion inhibitors.

The reflective surfaces currently under consideration are FEK and sagged or chemically strengthened 0.058-inch second-surface silvered glass. The conclusions of the preliminary conceptual design study can be summarized as follows:

- The monolithic design appears practical
- The wet bonding of glass appears practical
- The end hub plates can be used for prestressing
- There is a 90-mph wind resistance capability
- Curvature due to shrinkage should be predictable
- The 3/16 thickness has adequate strength.

Proposed Manufacturing Process

The manufacturing process proposed for the 2-m X 6-m modules takes advantage of automated GRC spray-up techniques. The proposed process also utilizes a novel concept for installation of the reflective surface with the GRC integral substrate/support structure during spray-up.

In Figure 7, the reflective surface shown is a second-surface mirror that is first placed over a parabolic male mold. Suction is used to secure the second surface mirror pieces to the mold. 3M's FEK-163 aluminized acrylic film could be stretched over the mold in place of the glass. The mold is shaped to take into account any curvature changes due to shrinkage of the GRC. An epoxy adhesive is sprayed onto the back of the mirror and GRC is sprayed to a specified thickness by a programmed cement/glass gun traversing mechanism. After spraying this first layer of GRC, a vibrating expanded metal form, shaped to the desired contour, is lowered over the wet GRC to ensure close contact of the fibers and concrete and to eliminate air bubbles.

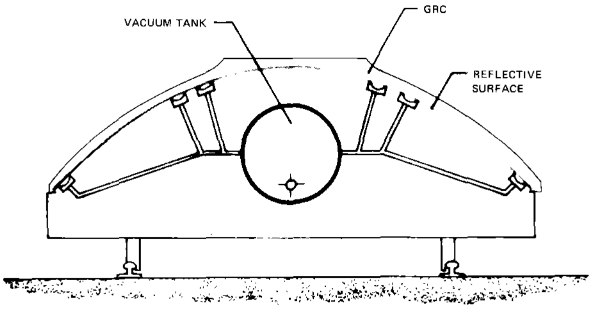

FIGURE 7 APPLICATION OF FIRST LAYER OF GRC

As shown in Figure 8, the next operation is to place a triangular, waxed corrugated cardboard torque section 6 m long on the newly formed GRC parabolic trough. End plate positioners and over-spray shields locate and support the section as the GRC is next automatically

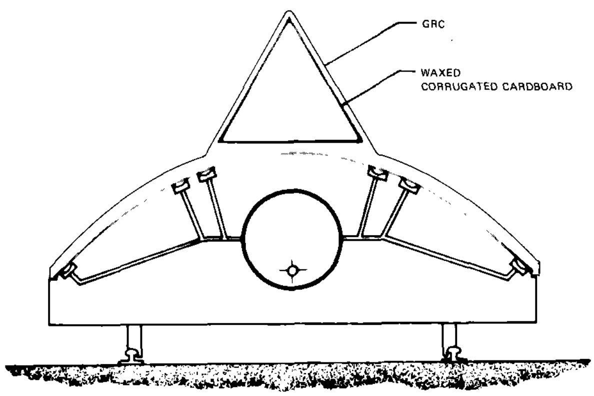

FIGURE 8 SPRAY-UP OF GRC PARABOLA AND TRIANGULAR TORQUE SECTION

sprayed onto the two top surfaces of the cardboard to a thickness of 3/16 inch. Subsequently, a vibrating expanded metal form is lowered over the two top surfaces to ensure bonding of the glass fibers with the concrete. Finally, waxed corrugated beam inserts are placed on the GRC as shown in Figure 9. GRC is automatically sprayed over the beam inserts to a thickness of 3/16 inch. Again, vibrating expanded metal forms are lowered sequentially over the newly sprayed beams to assure structural integrity and elimination of air bubbles.

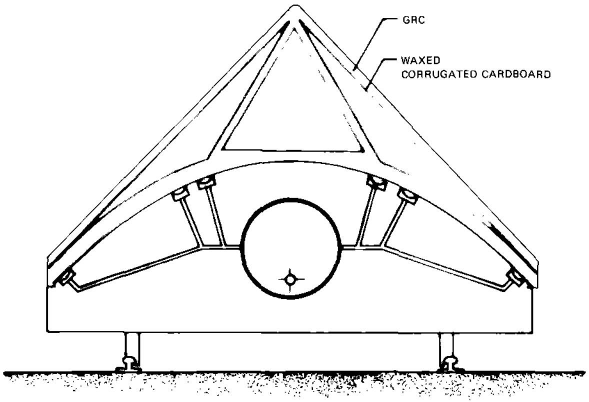

FIGURE 9 PLACEMENT OF STIFFENING RIBS

The entire assembly is cured in a fog room for 24 hours. At that time the end mold pieces are swung out of the way and the end plate hubs and tensioning bolts are assembled. At one day, GRC has a proportional elastic limit of not less than 600 psi, so the completed parabolic trough can be de-molded and moved outside where it will be cured for 28 days, mirror facing downwards, under a continuously operating water sprinkler system. The water is collected, filtered, and reused, as in commercial concrete pipe curing practice. When ready for shipment the tensioning bolts are given the final tension and the 2-m x 6-m collector is optically inspected. The collectors will be shipped face downwards on trucks. The completed beam is shown in Figure 10.

These manufacturing steps are summarized in the Process Flow Chart in Figure 11. Preliminary estimates indicate a facility with a 20,000 ft^2 manufacturing and one-day cure building and a 5-acre wet curing yard will be required to build 25,000 2-m x 6-m modules per year on a one-shift basis. A preliminary cost estimate, including labor, overhead, materials, G&A, equipment, building, and yard with a three-year depreciation indicates a cost of \$1.23 per ft^2 for the 550-lb, 2-m x 6-m GRC module. The reflective surface, receiver, tracker system, support foundations, field piping and electrical, and installation costs are additional. The material cost of \$93.50 for each 2-m x 6-m GRC module is 60 percent of the total production cost. Table 4 shows the material cost breakdown.

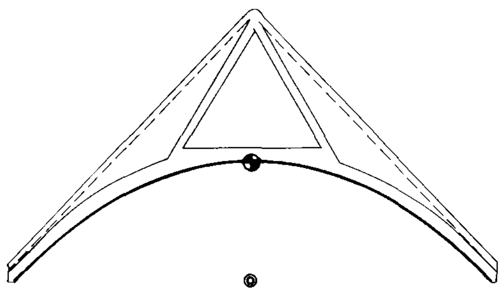

FIGURE 10 COMPLETED GRC PARABOLIC THROUGH COLLECTOR

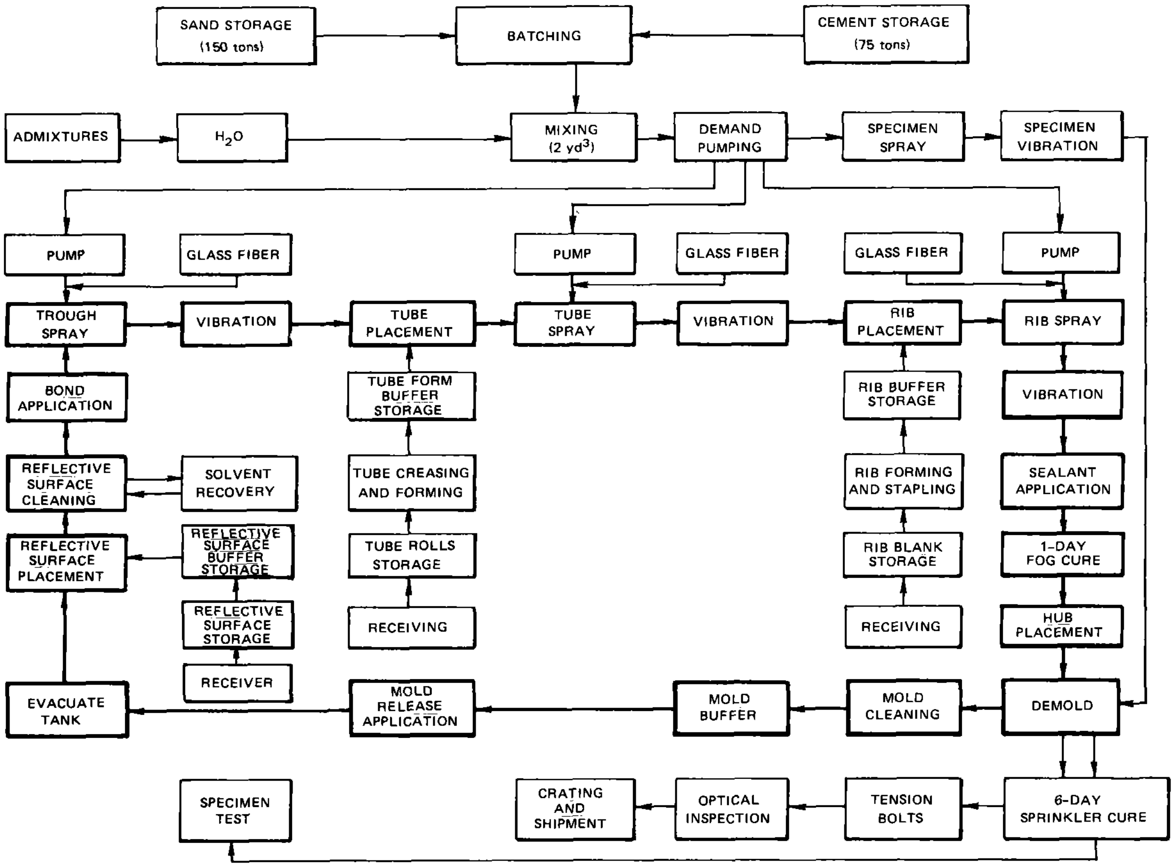

FIGURE 11 FLOW CHART OF THE GRC SOLAR COLLECTOR MANUFACTURING PROCESS

Table 4

GRC COLLECTOR
PRODUCTION MATERIAL COSTS
(Per 2-m x 6-m module)

Material	Cost
GRC (550 lbs)	$38.50
Paper molds	12.00
End plates	30.00
Tension rods and nuts	6.00
Concrete sealer	7.00
Total*	$93.50

*60 percent of total production cost.

The conclusions of the preliminary production analysis can be summarized as follows:

- The production process flow has been developed.
- The wet bonding process lends itself to automation.
- The end hub plates can be used for handling collectors after one day.
- The multi-spray buildup process has been proven and can be automated.
- The 3/16 thickness is practical with automation.
- The monolithic design appears to offer low cost advantages.

In summary, since the GRC spray process lends itself to automation, the labor costs are low. The GRC material costs are also low. This combination promises a significant reduction in collector field costs, which will be necessary for low-cost thermal energy production.

Future Plans

We are planning to complete the freeze/thaw tests. The conceptual design will also be completed. The construction of a 2-m x 6-m collector is planned and will be tested at Sandia's Thermal Test Facility at Albuquerque.

MATERIAL DESIGN CONSIDERATIONS FOR SILVERED GLASS MIRRORS

Nancy H. Clark
Components and Materials Compatibility Division 1415
Sandia National Laboratories
Albuquerque, New Mexico 87185

Introduction

The application of silvered glass mirrors as the reflective surface in solar concentrating collectors is relatively new. As shown in Figure 1, a reflector consists of several materials and material interfaces. The purpose of this paper is to outline the material design considerations for using silvered glass mirrors in solar concentrating collectors. The review is based on not only completed work but also on-going research among several organizations: Battelle-Pacific Northwest (PNL), Jet Propulsion Laboratory (JPL), Solar Energy Research Institute (SERI), Sandia National Laboratories-Albuquerque (SNLA), and Sandia National Laboratories-Livermore (SNLL).

Generic Design	Option
Glass	thin, chemically strengthen, sagged
Silver............................	wet chemical process only
Copper	" " " "
Paint	none, standard mirror paint, double paint (mirror paint/acrylic, mirror paint/epoxy)
Adhesive	none, epoxy, urethane, PVB
Substrate	glass, steel, sheet molding compound (SMC)

Figure 1. Generic Mirror with Material Listed from Outer Glass Layer to Substrate

Reflector Concepts

Fabricating glass mirrors into the curved shape required for concentrating collectors has lead to three potential concepts: chemically strengthened, thermally formed glass, and thin glass laminates.

Chemical strengthening, achieved by an ion exchange process, provides a high compressive stress state at the surfaces of the glass sheet. Typical modulus of rupture (MOR) of 40,000 psi and depth of penetration of 6-8 mils have been achieved in Corning Chemcor^{R}. Schott glass chemically strengthening by Artistic has MOR of 20-30,000 psi but a depth of penetration that is less than 1 mil.

Thus, in this concept, chemically strengthened glass can be elastically deformed into the solar collector to form the reflective surface. Mirroring can be accomplished with the glass in a flat configuration thus making use of the current mirroring industry.

Thermal forming of glass to the required reflector shape can be accomplished by gravity sagging and press forming techniques which were described in earlier papers by Martin and McDowell. Both Ford and PPG have produced thermally formed glass (prototypes) with surface slope errors of 3 mrad using production processes. A key process development problem with this concept as yet unadressed is the mirroring of curved glass.

Thin glass laminates consist of a relatively thin (~ 10-40 mil), sheet of silvered glass bonded to sheet steel. The neutral axis can be placed in the steel allowing the glass to remain in compression when elastically deformed. Mirroring can advantageously be achieved with the glass flat. Prototype laminates have been fabricated by Glaverbel, Solar Kinetics and SNLA.

Optical Performance

The optical performance of any reflector is dependent on the performance of both the glass and the reflective material.

The glass performance depends on it's ability to transmit light in the solar spectrum and it's specularity. Data from Pettit and Freese of SNLA show that transmission depends on the composition of the glass and it's thickness.

As can be seen in Table 1, the aluminosilicates and bososilicates show high reflectance values of approximately 94%, which is independent of glass thickness. Float glasses have reflectances of 84% for standard ion content of .1% and 90% for low ion content of .06% for equivalent thickness. However, it can be seen that as the thickness goes from .118 to .244 inches, the reflectance goes from 71% to 84%. Thus, in the case of thin glass (.010-.040) absorption losses will be minimal,and thereby, transmissions of 94% can be achieved. It appears that the transmissivity is dependent on the amount of iron in the ferrous or Fe+2 valance state. Table 1 shows that even though the aluminosilicate has considerable iron, it is in the +3 state, and thus, does not hinder transmission. A bonus of this +3, +2 iron shown in work done by Shelby and Vitko of SNLL(1) is that UV light apparently causes iron in the +2 state to behave as if it were in the +3 state, and thus, with time transmission improves outdoors.

The specularity, of glasses for trough applications requires low mechanical distortion in the glasses. Work by Beauchamp(2) and others show that most glasses considered for solar application are float and fusion glasses that have less than a 2 mrad slope errors. (Figure 2.)

The other parameters in optical performance is the choice of reflecting material. If one considers the solar averaged reflectance of the three most reflective metals, silver, aluminum and gold as shown in Figure 3, one can see that the solar averaged reflectance for silver is 6% greater than for aluminum and 13% greater than for gold.

Mechanical Performance

In trough designs, glass mirrors are also structural members, thus their mechanical behavior is important. Major concerns include the tensile stress in the glass under stress, fracture of the glass, and failure of the mirror laminate at one of the interfaces.

Glass normally has a design limit of 1000 psi in tension; stresses greater than this will cause glass fracture. In addition, flaws in the glass, which is under some stress, will cause fracture at lower tensile stress values. These flaws can be inherent in the glass, or environmentally induced by blowing sand, hail or human handling. Inherent flaws can be reduced by proper cutting techniques and quality control in manufacturing. Experience with realtime exposures indicate inherent flaws should not be a problem.

Environmentally induced flaws and their propagation are in a stage of preliminary study by J. Mecholsky of SNLA to determine the magnitude of this problem. Sand abrasion may result in these subcritical flaws. It is thought that in some designs like the thin glass laminates where there is continuous stress, these subcritical cracks may result in failure with time. This is of particular concern where chemically strengthened glass is used since the failure is catastrophic. Work by Miller, Baca and Rainhart SNLA have shown that Corning chemically strengthened glasses, thin glass laminates without adhesive voids, 1/4" or greater plate glasses, and glass molded to SMC can survive 3/4" hail balls at about 50 feet/second.

Work to determine the strength of the mirror interfaces is also in progress. Allred(4) found in shear tests using SMC and silvered glass mirrors that the paint failed cohesively at a lower bound of 2300 psi. Burolla at SNLL found in shear tests with mirrors bonded to sheet metal that an adhesive failure occurred between copper and paint at 1500 to 2000 psi. Lind at Battelle and Burolla at SNLL SNLL have done a range of tensile pull tests. Preliminary results give a range from 50-1000 psi with very little reproducibility. A tentative conclusion is that results may be due to lack of consistances in mirror manufacturing.

Environmental Performance

The environmental stability, particularly of the glass/silver and the paint/adhesive interfaces,is the subject of a broad range of studies.

Real time data of long-term aging looks promising. JPL(5) has studied automobile mirrors from the twenties and thirties and many of them show no degradation. Battelle[6] has investigated 15-20 year old mirrors silvered and stored by the Carolina Mirror Company, and those which were not exposed to standing water show very little degradation. On the other hand, some mirrors exposed to an outdoor environment at SNLL for less than 1 year show large amounts of corrosion. At Albuquerque, mirrors laminated to painted steel exposed for less than 3 months outdoors and less than 3 weeks in a temperature/humidity environmental test chamber show significant degradation.

An understanding of the causes of mirror corrosion is beginning to form. In general, it has been found by Vitko et al., that areas of corrosion contain primarily silver agglomerates as seen in Figure 4. The cause(s) of this agglomerates are not known, but, may be high temperatures, standing water, or outgassing of adhesives. Preliminary results show agglomeration as a result of aging at 100°C may result in a maximum irreversible loss of about 2% in reflectance (Figure 5). This question is being pursued by SNLL.

Corrosion due to the presence of standing water and the presence of certain adhesives has been documented by Burolla and Roche[7] of SNLL. These effects can be minimized in several ways. Designs which don't allow water to collect or which have edge seals designed to exclude water, but which do not outgas sulfides which are corrosive to silver have been successful[8]. Adhesive choices like polyol cured polyurethane or PVB which are unreactive with silver, minimize adhesive corrosive effects. If designs do allow for some moisture to be present or corrosive adhesives are necessary for structural reaons, heliostat designers and foreign mirror manufacturers as Schott and Glaverbell have double painted and/or single painted their mirror with outside coating or essentially impervious paints with good results.

The environmental stability of silvered glass mirrors looks promising but, to date even environmental qualifications for ten-year life have yet to be accomplished.

Table 1 - Total Solar Hemispherical Reflective for Silvered Glass Mirros (Air Mass 1.5)

Glass	Type	% Iron	Thickness (inches)	Reflectance (% + 1%)	Silvered by
Corning 0317*	Aluminosilicate	.09	.056	94	Falconer
Corning 0317*	"	-	.070	94	Falconer
Corning 0317*	"	-	.061	95	Sinclair
Corning 7809*	Borosilicate	-	.060	95	Falconer
Ford **	Regular Float	.09-.10	.118	85	--
Ford **	" "	" "	.185	78	--
Ford **	" "	" "	.244	71	--
Ford **	Low Iron Float	.06	.118	90	Falconer
Schott B270*	Soda Lime	-	.250	94	Schott

* Data from J. M. Freeze - SNLA

** Data from Taketani and Arden, Mirrors for Solar Energy Application, MDC G7213, September 1977.

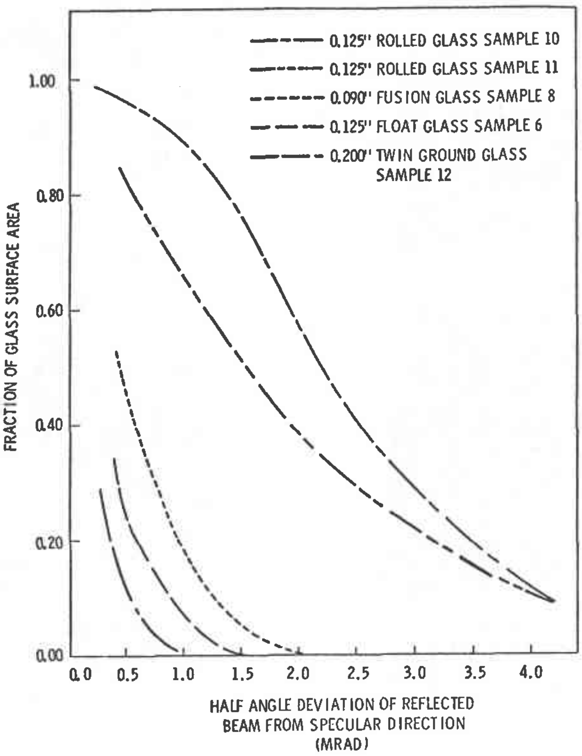

Figure 2. Specularity of Glasses
Used in Solar Applications

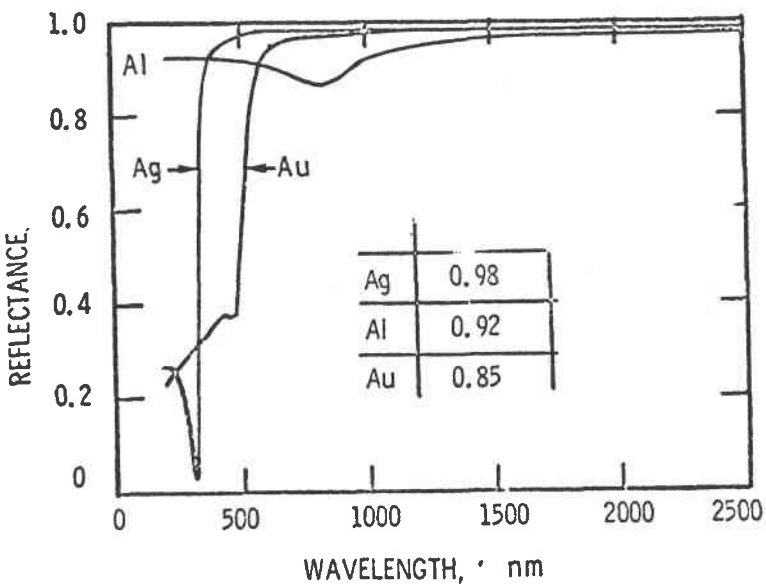

Figure 3. Reflectance properties of silver (Ag), aluminum (Al), and gold (Au) as a function of wavelength for the metal/vacuum interface.

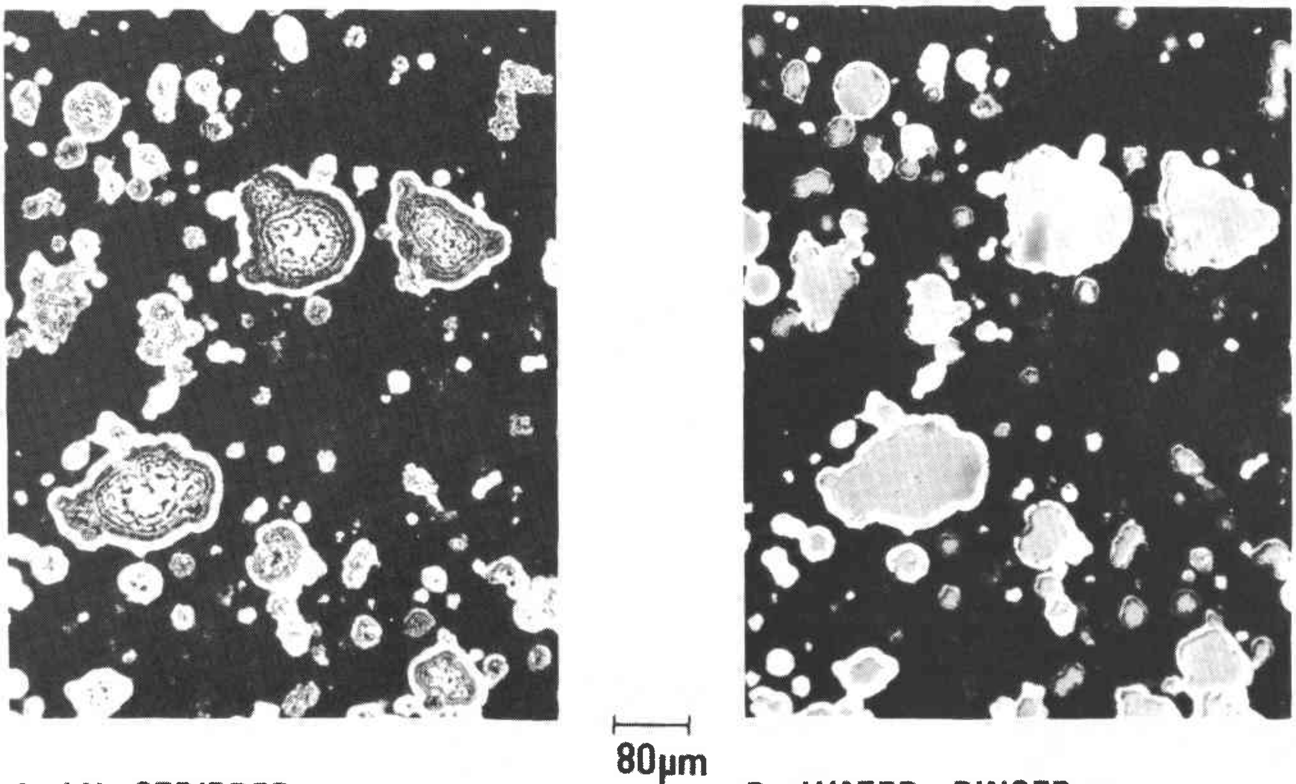

Figure 4. Agglomerates of Silver in the Corrosion Sites of a Silvered Glass Mirror

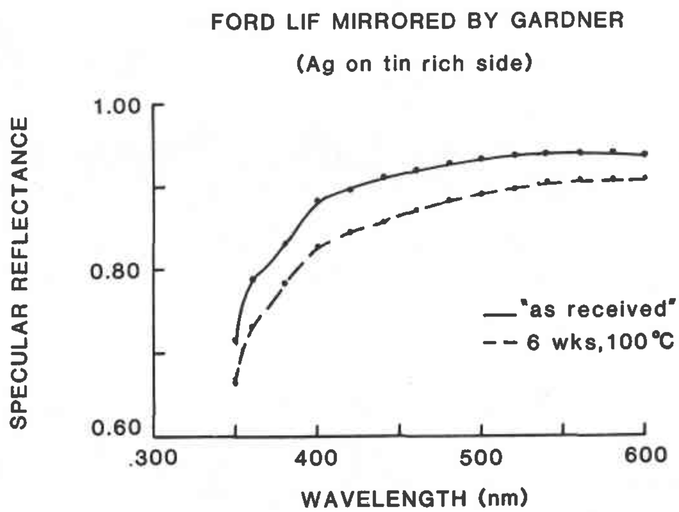

Figure 5. Loss of Specularity in Silvered Glass Mirrors as a Result of 6 Weeks at 100°C.

References

1. J. Vitko, Jr. and J. E. Shelby, Solarization of Heliostat Glasses, SAND79-8754 (Livermore - Sandia Laboratories, 1979).
2. E. L. Beauchamp, Glass Technology Needs for Solar Energy. Glass Division, American Ceramic Society Conference, October 1979.
3. R.B. Pettit and E. P. Roth, Solar Mirror Material: Their Properties and Uses in Solar Concentrating Collectors, SAND 79-2190 (Albuquerque: Sandia Laboratories, 1980)
4. R. L. Champion and R. Allred, Development of Sheet Molding Compound Solar Collector with Molded-In Silvered Glass Reflector Surface, Society of Manufacturing Engineers Composite Conference, June, 1980.
5. F. L. Bouquet, Glass for Solar Concentrator Applications, 5102-105 (Pasadena: JPL, 1979)
6. M. A. Lind et al., Heliostat Mirror Survey and Analysis PNL-3194 UC-62 (Richland: Battelle, 1979).
7. V. P. Burollo and S. L. Roche, Silver Deterioration in Second Surface Solar Mirrors, SAND79-8276 (Livermore, Sandia Laboratories, 1980).
8. K. Wishman, M. H. Gonzales, Protective Coating and Sealants for Solar Applications SAND80-0808 (Albuquerque:Sandia Laboratories, 1980).

DEVELOPMENT AND TESTING OF POLYMER REFLECTORS

Roger A. Assink
Chemistry of Organic Materials Division 5811
Sandia National Laboratories
Albuquerque, New Mexico 87185

Introduction

Metallized polymer sheets and films offer the potential of providing a low cost, light weight and easily installed solar reflector surface. Metallized polymers presently available, however, suffer from three disadvantages: 1) low initial reflectance, 2) UV degradation and 3) surface abrasion. The solar reflectance properties of commercially available aluminized polymers are typically 0.06 to 0.10 reflectance units (1.00 reflectance units = 100 percent reflectance) lower than the solar reflectance properties of high quality silvered glasses (1). This difference results from the inherently lower solar reflectance of aluminum as compared to the solar reflectance of silver. Efforts to deposit and protect silver on a polymer surface have not been successful. UV degradation of polymers can affect the material's optical and mechanical properties. Recent studies, however, indicate that UV degradation may not be a serious problem for acrylic materials (2,3). Abrasion of the polymer surface by wind blown sand or contact cleaning methods can cause a substantial reduction in the specularity of the reflector (2).

The purpose of this study is to develop and evaluate several abrasion resistant aluminized polymer reflectors suitable for solar applications. The lower initial reflectance of aluminized polymers may then be offset by the advantages previously mentioned.

Materials

Acrylic Film/Q9-6313

FEK-244 is an aluminized acrylic film with an adhesive backing manufactured by the 3-M Company (Minneapolis, Minnesota). This material has exhibited excellent UV stability and mechanical integrity when used as a solar reflector (2). FEK-244 was flow coated with Dow Corning's (Midland, Michigan) Q9-6313 experimental abrasion resistant resin and cured for 16 hours at 82°C. The coating thickness was estimated to be 3 to 5 μm thick. Coated film had a tendency to wrinkle during cure, probably due to differences in the coefficients of thermal

expansion of the various components. The wrinkles did not appear to be permanent as they disappeared when the film was applied to a smooth surface. The coating exhibited some nonuniformity in thickness particularly around the edges, probably due to the method of application.
Coated FEK-244 was applied to glass microscope slides by the detergent and water method recommended by 3-M (4).

Acrylic Film/Plasma Deposition

FEK-244 was protected with plasma deposited hexamethyl disiloxane by Leybold-Heraeus, Inc. (Enfield, Connecticut). Coating thicknesses of 0.17 μm and 0.5 μm were provided. Only the 0.5 μm coating will be discussed in the following sections since the thinner coating did not appear to enhance abrasion resistance.

Ion Plated Acrylic Sheet

Lucite SAR, manufactured by E. I. duPont Company (Wilmington, Delaware), is an acrylic sheet coated on both sides with a silica based abrasion resistant resin. A 0.16 cm thick sheet was ion plated (5) with aluminum by Endurex Corporation (Dallas, Texas) after being cleaned with fluorinated solvent. The aluminum surface of some of the samples was protected from the environment with a spray coating of polystyrene/butadiene block copolymer manufactured by Shell Chemical Co., (Houston, Texas). Attempts to deposit aluminum by thermal evaporation were unsuccessful because of poor adhesion between the aluminum and abrasion resistant coating.

First-Surface Aluminum/Vestar

An aluminized polyimide film was provided by Sheldahl Company (Northfield, Minnesota). Polyimide film was chosen because it can withstand the high cure temperatures used in the application of an abrasion resistant resin, Vestar, manufactured by Dow Corning. The polyimide film was laminated, with the aluminum surface exposed, to a glass microscope slide with 2 layers of 0.0025 cm thick high temperature nylon epoxy adhesive film, 1041R, manufactured by American Cyanamide Company (Wayne, New Jersey). The adhesive was cured at 175°C and 2.0 MPa for 90 minutes. The aluminum surface was then cleaned with a 1 liter water solution containing 47 cm^3 85 percent phosphoric acid and 20 gm chromic acid as described in MIL-A-8625. These samples were placed in the cleaning solution at 94°C for 5 minutes and then dip coated with the Vestar resin and cured at 175°C for 2 hours. The coating was estimated to be 5 to 8 μm thick.

Experimental Procedures

Reflectance Properties

The hemispherical reflectance properties were measured over the wavelength range 350 to 2500 nm with a Beckman DK-2 spectroflectometer (6). Solar average hemispherical reflectance values, $R_s(2\pi)$, were calculated by averaging the hemispherical reflectance values over the air mass 1.5 solar energy spectrum of Thekaekara (7). Hemispherical reflectance values are accurate to $\pm$ 0.01 reflectance units.

The specular reflectance properties were determined for angular apertures from 1 to 15 milliradians (mrad) using a specially constructed bidirectional reflectometer (6). A wavelength of 500 nm and an incident angle of 22.5° were chosen for these measurements. Specular reflectance values are accurate to $\pm$ 0.01 reflectance units.

Abrasion Resistance

A falling sand apparatus as described by ASTM-D968-51 was used with 100 cm^3 of 80 mesh silicon carbide to abrade the reflector surfaces. In this apparatus the silicon carbide falls approximately 95 cm and impacts at a 45° angle with the reflector surface. The abrasion resistance of a reflector surface was determined by measuring its specular reflectance before and after exposure to this test.

Weatherability

Samples were tested for weatherability using a cycling environmental test chamber. A cycle consisted of 2 hours at -29°C, a 2 hour ramp to +55°C, 2 hours at +55°C and a 2 hour ramp back to -29°C. The relative humidity was 50 percent at ambient temperature, and the chamber passes through a freeze-thaw and a thaw-freeze situation during each cycle.

Results and Discussion

Reflectance Properties

The solar averaged hemispherical reflectance values are summarized in Table I. Reflectance curves for FEK-244, FEK-244/Q9-6313 and FEK-244/plasma are shown in Figure 1. The Q9-6313 introduces several small absorption peaks between 1000 and 1500 nm while the plasma coating reduces the reflectance values between 400 and 500 nm. These effects are small, however, as the solar averaged hemispherical reflectances range from 0.86 to 0.87 reflectance units for each of these materials.

The hemispherical reflectance properties for aluminized Lucite SAR sheet are shown in Figure 3. Below 1000 nm the reflectance curve is very similar to the reflectance curve of the FEK-244 film. Above 1000 nm the reflector exhibits several strong absorption lines due to the acrylic sheet. These lines lower the solar averaged hemispherical reflectance to 0.80 reflectance units, a significant decrease in performance compared to the FEK-244 reflector. Presumably, the solar reflectance could be increased by reducing the thickness of the acrylic sheet, although thinner sheets are not now commercially available.

Figure 3 shows the reflectance properties of aluminized polyimide (first-surface) both with and without a Vestar coating. The solar averaged hemispherical reflectance for the Vestar coated sample is 0.86 reflectance units compared to 0.89 reflectance units for the uncoated sample.

The specularity of a reflector is defined as the amount of radiation that is reflected into a specific solid angle in the specular direction (1) The reflected beam profiles for the three FEK-244 reflectors and aluminized Lucite SAR were characterized by a normal angular distribution (6) and their dispersions are given in Table I. Application of the Q9-6313 coating to FEK-244 resulted in a slight increase in the beam dispersion. Specular reflectances for the FEK-244 reflectors and for aluminized Lucite SAR at a 15 mrad angular aperture and 500 nm were 0.02 to 0.03 reflectance units less than the hemispherical reflectances at 500 nm, indicating some large angle scattering in the reflected beam.

The aluminized polyimide reflectors exhibited the greatest dispersion. Their reflected beam profiles could not be accurately described by a single normal distribution (6). Specular reflectances for the aluminized polyimide reflectors at a 15 mrad angular aperture and 500 nm were 0.04 to 0.06 reflectance units less than the hemispherical reflectance at 500 nm. A significant portion of the beam spreading for these laminated films may be due to irregularities in adhesive thickness. To determine the intrinsic specularity of the aluminized film, a portion of film was stretched and held in position by a fixture specifically designed for thin, unmounted films. The specular beam profile for this sample is characterized by a normal distribution with a dispersion of less than 0.2 mrad. Presumably, with improved or automated methods of lamination, the specularity of mounted film could approach that of the stretched film. Because Vestar could only be applied to a mounted film, the effect of applying Vestar to the film's dispersion could not be determined.

Abrasion Resistance

The primary effect of surface abrasion is to reduce the intensity of the specular beam while maintaining approximately the same beam dispersion (1). The decreases in specular reflectance values at 500 nm and a 15 mrad angular aperture are summarized in Table II. Unprotected FEK-244's specular reflectance was reduced 0.22 reflectance units by abrasion. The abraded area appeared covered with microscopic surface scratches. The specular reflectance of the FEK-244/Q9-6313 and FEK-244/plasma samples decreased 0.01 and 0.08 reflectance units respectively, while that of Lucite SAR showed no measurable decrease.

As expected, unprotected first-surface aluminum on polyimide shows a substantial loss in specularity after abrasion. When the surface was protected with a Vestar coating, the loss was reduced to 0.08 reflectance units. This surface did not appear to be scratched but rather covered with a network of cracks having approximately a 0.02 cm spacing. This feature is believed to depend on the hardness of both the polymer substrate and adhesive layer.

Weatherability

The weatherability of the reflectors was tested in the environmental test chamber. The FEK-244 and FEK-244/Q9-6313 were tested for 10 months and the FEK-244/plasma was tested for 2 months. All of the samples showed no visible sign of degradation. The metallized Lucite SAR exhibited severe degradation after 1 month. Large areas of metallization had been completely removed. Samples for which the aluminum surface was protected with a coating of polystyrene/butadiene block copolymer retained much more, but not all, of their metallization. The delamination appears to be related to the pattern of moisture condensation. The unprotected first-surface aluminum on polyimide experienced substantial degradation after 1 month. Approximately 5 percent of the aluminum surface had either been removed or discolored. Vestar protected aluminum showed no visible sign of degradation after 2 months. After 3 months several of these samples had delaminated from the glass slides. The unmounted film curled and much of the Vestar separated from the aluminum surface.

Conclusions

FEK-244 coated with either Dow Corning's Q9-6313 resin or protected by Leybold-Heraeus's plasma deposition process appears to be a promising candidate for an abrasion resistant polymer solar reflector. The coatings had little affect on the solar averaged hemispherical reflectance properties, the specular reflectance or the weatherability. Both coatings reduced abrasion losses significantly.

The solar averaged hemispherical reflectance of aluminized Lucite SAR sheet was substantially lower than that of the other reflectors studied. This material exhibited excellent abrasion resistance although weatherability appears to be a severe problem. The reflector's low initial reflectance and poor weatherability are major obstacles to serious consideration of this material for solar applications.

The solar averaged hemispherical reflectance of Vestar coated aluminized polyimide was excellent, although the reflector's specularity and weatherability were poor. Further investigation of this reflector is warranted, however, since these problems appear to be related to the techniques and materials used to laminate the film.

Acknowledgements

The technical assistance of F. T. Gurule in the preparation of samples is gratefully adknowledged. The author is indebted to R. B. Pettit and J. M. Freese for assistance with the optical measurements and to K. B. Wischmann and M. H. Gonzales for assistance with the abrasion test apparatus.

References

1. R. B. Pettit and E. P. Roth in "Solar Materials Science," edited by L. E. Murr, Academic Press (1980) and Sandia Report SAND79-2190 (June, 1980).*

2. Solar Total Energy Test Facility Project Semiannual Report, October 1976-March 1977, SAND77-0738, p. 52.*

3. R. B. Pettit and J. M. Freese, personal communication.

4. 3-M Company Product Bulletin 206, September 1978.

5. G. J. Hale, G. W. White, D. E. Meyer, Electronic Packaging and Production, 15, (5), p. 39 (1975).

6. R. B. Pettit, Solar Energy 19, 733 (1977).

7. M. A. Lind, R. B. Pettit and K. K. Masterson, to be published, J. Solar Energy Eng. 102, 34 (1980).

* Available from National Technical Information Service, U. S. Department of Commerce, Springfield, VA 22161.

Table I. Solar averaged hemispherical reflectance values and the reflected beam dispersion at 500 nm.

Reflector	$R_s(2\pi)$	σ (mrad)
FEK-244	0.86	<1.0
FEK-244/Q9-6313	0.87	<1.5
FEK-244/plasma	0.86	<1.0
Aluminized Lucite SAR	0.80	<1.0
Aluminized Polyimide	0.89	(<0.3)*
Aluminized Polyimide/Vestar	0.86	

*Beam dispersion for a stretched sample; see text for explanation.

Table II. Specular reflectance properties at 500 nm and a 15 mrad angular aperture before and after abrasion testing.

Reflector	Initial	Abraded	Loss
FEK-244	0.85	0.63	0.22
FEK-244/Q9-6313	0.85	0.84	0.01
FEK-244/plasma	0.87	0.79	0.08
Aluminized Lucite SAR	0.82	0.82	0.00
Aluminized Polyimide	0.85	0.60	0.25
Aluminized Polyimide/Vestar	0.78	0.70	0.08

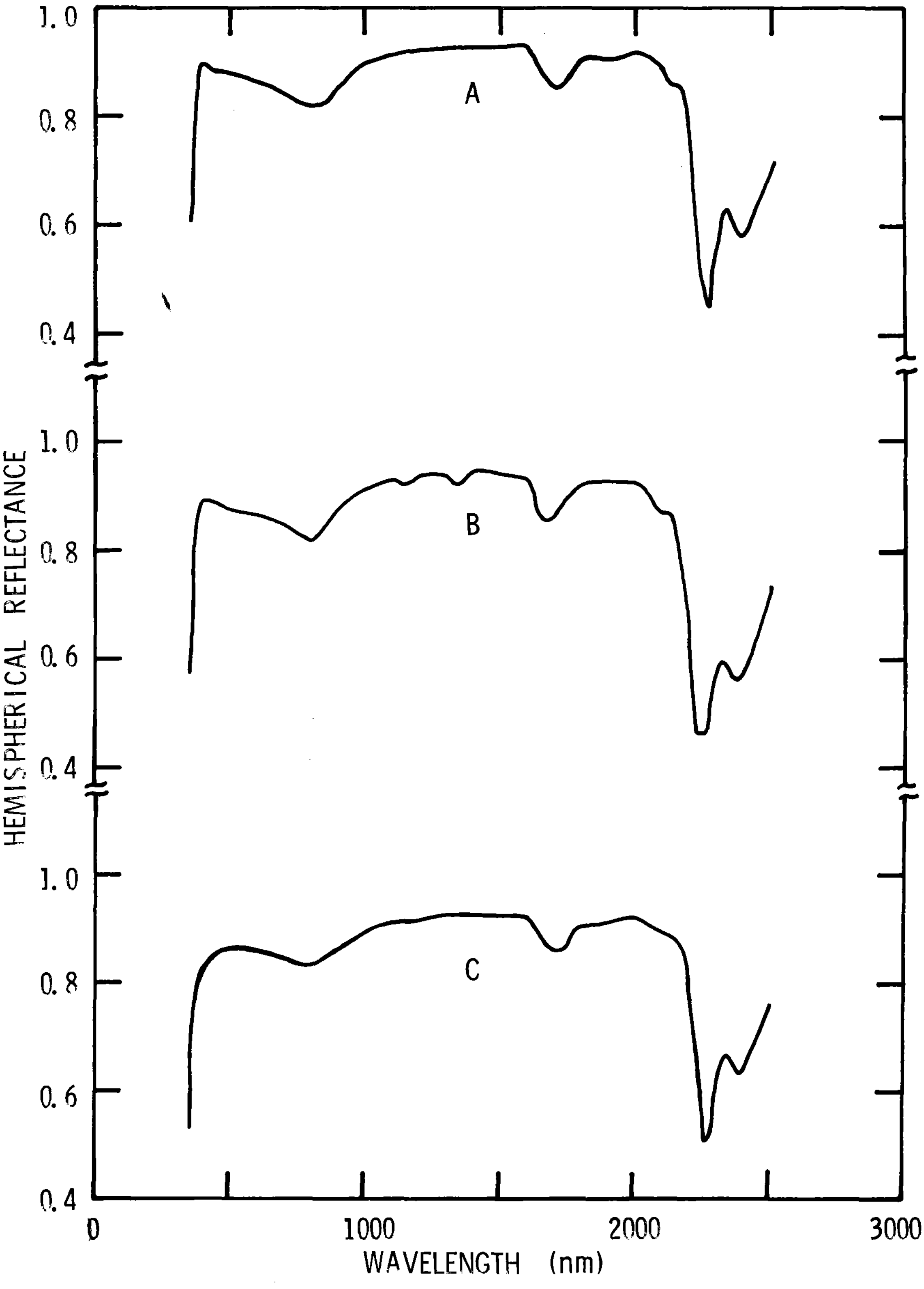

Figure 1. Spectral hemispherical reflectance properties of FEK-244 (A), FEK-244/Q9-6313 (B) and FEK-244/Plasma (C)

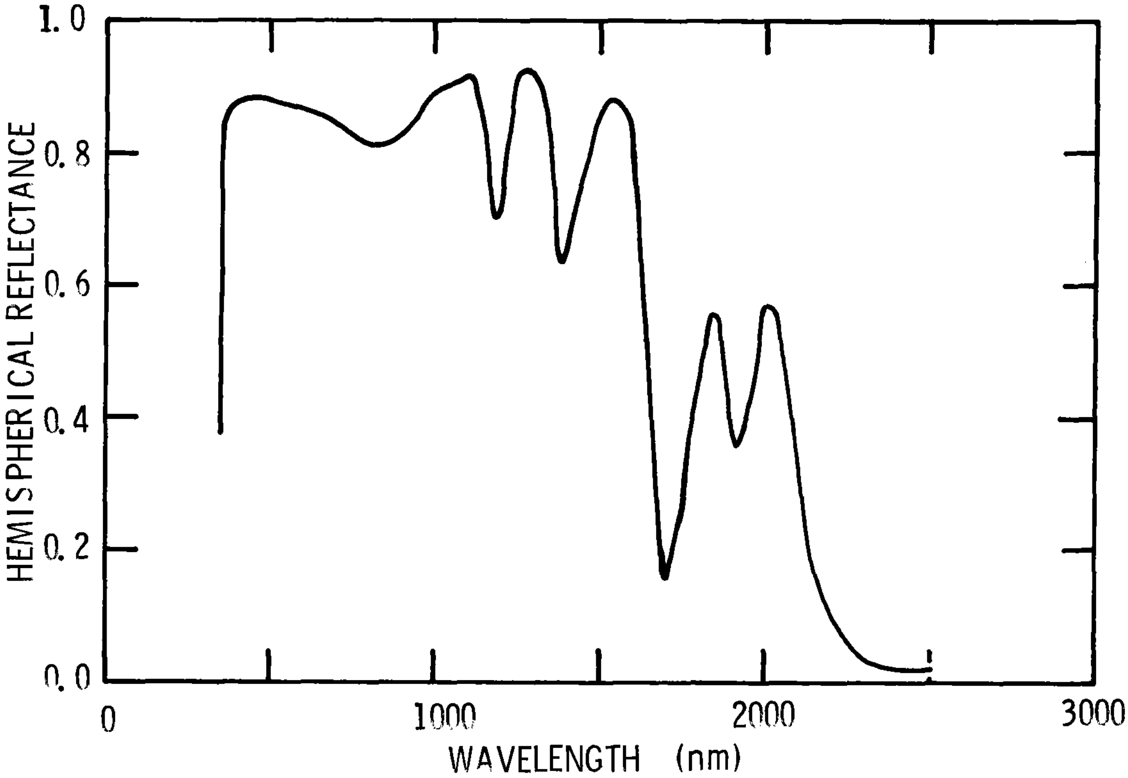

Figure 2. Spectral hemispherical reflectance properties of aluminized Lucite SAR sheet, 0.16 cm thick.

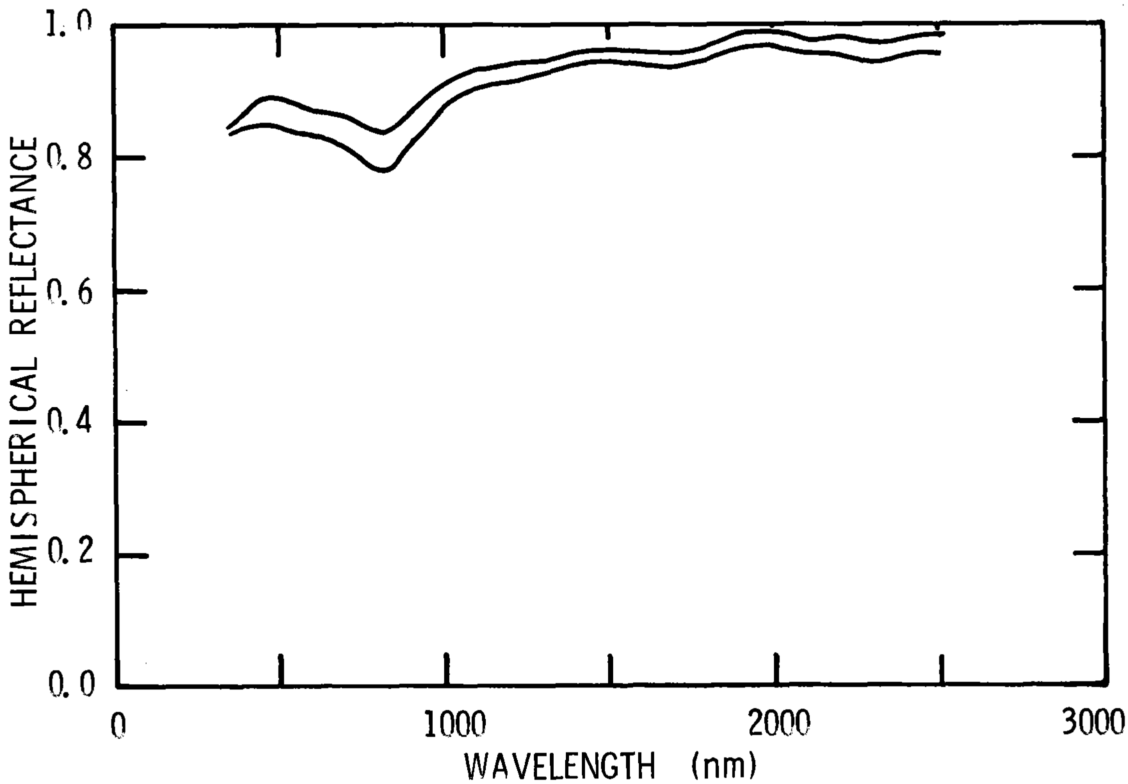

Figure 3. Spectral hemispherical reflectance properties of aluminized polyimide (A) and aluminized polyimide coated with Vestar (B).

MATERIALS COMPATIBILITY/LIFE PREDICTIONS

Nancy Clark
Energy Components and Materials Compatibility Division 1415
Sandia National Laboratories
Albuquerque, New Mexico 87185

Introduction

Studies of the economics of solar energy suggest that system lifetimes of 10-20 years are required. Since solar system and component technologies are in relatively early stages of development, accelerated aging methods are required to make reliable life predictions. Traditionally, testing has been done using a combined temperature, humidity cycle of 2 hours at low temperature/low humidity, 2 hours transition, 2 hours at high temperature/high humidity, 2 hours transition. Although this method has produced failures in systems, interpretation of the failure in terms of cause is very difficult since we have at a minimum 3 effects - temperatures/humidity/mechanical cycling stress-operating simultaneously. In some cases, especially in diffusion controlled processes, failures can occur in such testing that do not appear in actual application. In order to improve accelerated aging techniques, Sandia National Laboratories has initiated a project to predict lifetimes of solar collector components based on an approach developed by Gillen and Mead of Sandia National Laboratories. This method deals with identification of material incompatabilities and failure modes followed by an Arrhenius type kinetic analysis to predict lifetimes. Details of the general method can be found in Predicting Life Expectancy and Simulating Age of Complex Equipment Using Accelerated Aging Techniques by Gillen and Mead (SAND79-1561). The purposes of this paper are to briefly describe the method and to describe an experimental plan which will be applied to parabolic trough solar collector/reflector/structures.

Material Incompatabilities/Failure Mode Testing

Accelerated aging programs require the identification of the stresses that are most likely to damage the performance of this system. Data is frequently not available on the performance of a system under a particular stress. When this is the case, it becomes necessary to make predictions of those stresses most likely to cause degration and then test to see if the stresses selected are dominant.

Stresses are herein defined as conditions that will degrade system performance. For solar systems these stresses can include temperature, humidity, UV radiation, and temperature cycling. Once stresses are identified then tests are designed to subject the system to each particular stress. The results of these tests can lead to the conclusions that the stress does not produce a system failure or that one has a material incompatibility which can be accommodated by either design changes or, although the stress results in failure, an acceptable level of performance has been achieved. A failure mode is identified when stress results in a failure but at an acceptable level of performance, once a failure mode has been identified, a damage parameter, P, which correlates in an empirical fashion with the expected failure mode must be identified as well. It is important to realize that more than one environmental stress can be responsible for the degradation; however for our current study only single stress environments will be considered.

Kinetic Analysis

Following failure mode identification, (i.e. the material suspected of significant aging, the stress implicated in its aging, and the appropriate damage parameter, P, which correlates to the expected failure mode) the kinetic analysis for the predictions of lifetimes is conducted. The analysis attempts to establish that under an overstress condition over a given period of time the damage parameter has some simple functional form and under different stress conditions the simple functions are interrelated by an acceleration factor, A_S. It is possible to check this by plotting P vs. log time for example for 3 or more stress levels (Figure 1)

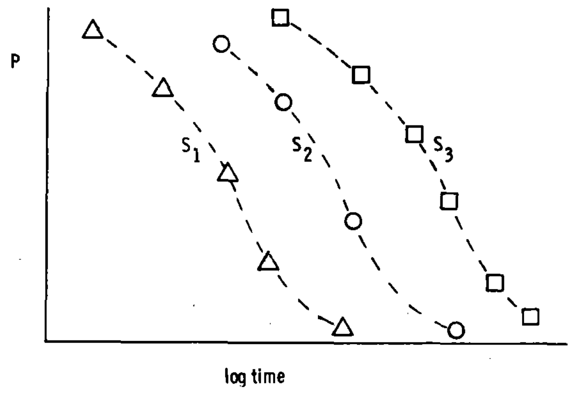

Figure 1. Hypothetical accelerated aging data, where the damage parameter, P, is followed vs. time at 3 different stress levels, S_1, S_2, and S_3.

and then multiplying S_2 and S_3 by the $A_s$to see how accurately they superimpose on S_1 (Figure 2).

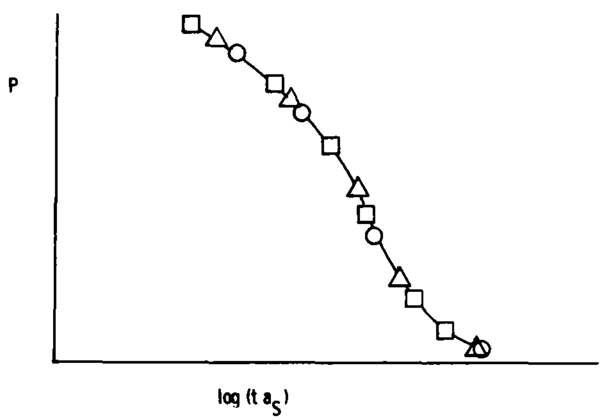

Figure 2. The data of Figure 2 after time-stress superposition a_s is the shift factor.

Superposition is necessary to show constant acceleration. For thermal stresses it often turns out that A_s is related to the Arrhenius term

$$A_s \alpha \exp(-E_a/RT)$$

Where E_a is the Arrhenius activiation energy, R = the gas constant and T is the Temperature in ^{o}K. If this is in fact the case then one can plot 1/T vs $\ln a_T$ (Figure 3).

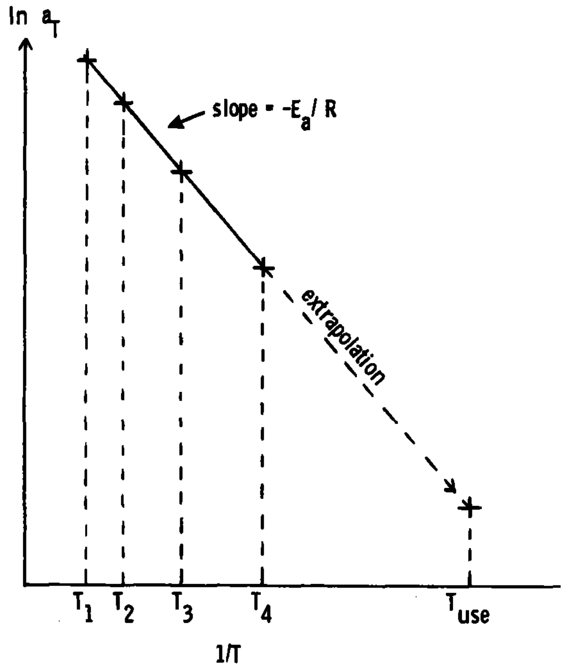

Figure 3. Arrhenius plot of In of the thermal shift factor, a_T, vs. inverse temperature ($^{o}K^{-1}$) for the 4 temperatures, T_1, T_2, T_3, and T_4. The resulting straight line behavior is extrapolated to the use temperature, T_{use}.

With $\ln a_T$ known for the use temperature, one can estimate the degradation with time at the use temperature. If one has set a valid failure criteria, it becomes possible to estimate the expected life of the system.

It must be expected that in some cases failure modes are a result of synergisims, and that sometimes time-stress superposition is not possible using a particular P factor. It can also be seen that to do even single failure mode/single stress analysis can be time consuming and expensive.

Preliminary Plan for PPT's

In the production Prototype Program, a test plan is being developed based on the proceeding concepts. Table 1 indicates how we are proceeding to do failure mode analysis. Table 2 shows how we anticipate determining of A_s given that the failure mode is loss of mechanical strength in adhesive, the stress is temperature; and the damage parameter P, is loss of shear strength. Initial failure mode testing is anticipated to take 6-9 months with the determination of A_s taking another 9-12 months.

Acknowledgements: The author wishes to thank Keith Mead for his efforts in helping define the methods and matrixes used in this system.

	Interface	Stress	Tests	Damage Parameter
1.	Mirror/ Adhesive (PVB, Epoxy, Urethane)/ Substrate (Steel, glass or SMC)	Temperature (Humidity or Temperature Cycling)	a. Hold full size in oven for 6 months at 200°F (200°F,95%RH or cycle from -40°F to 150°F) Test reflectance at 0, 1, 3 and 6 months (or Laser Ray Trace.)	a. Loss of Reflectance
			b. Hold lap shear Samples at 200°F and test 5 at 0, 1, 3 and 6 months	b. Loss of mechanical strength of adhesive
			c. Hold 10" x 20" samples in oven at 200°F, (200°F 95%RH, cycle from -40°-150°F), ultra sound test 0,1,3, and 6 months.	c. Loss of mechanical strength of adhesive
			d. Hold samples of adhesive only at 200°F (200°F, 95% RH) test T_g at 0, 1,3 and 6 months	
2.	Copper/Mirror Paint/Adhesive	UV radiation	a. Irradiate adhesive blocks with UV light, measure change in T_g	a. Loss of mechanical strength of adhesive
			b. Irradiate minor samples with UV pull Tensile plugs on paint only	b. Loss of mechanical strength
			c. Irradiate mirror samples bonded with adhesive of choice to substrate - pull tensile plugs	c. Loss of mechanical strength

TABLE 1
Failure Mode Analysis Test Matrix

Interface	Stress	Test
Mirror/Adhesive/ Steel	Temperature	Hold samples of adhesive at 180^{o}, 190^{o} and $210^{o}F$ ovens. Measuring the shear stress at 0, 1, 3 and 6 months

Table 2

Test Matrix To Determine the A_s for the Loss of Mechanical Strength in the Adhesive at the Mirror/Adhesive/Steel Interface.

Session VII - Instrumentation Development

Lewis M. Larsen, Chairman
Component and Subsystem
Development Division 4722
Sandia National Laboratories

PORTABLE INSTRUMENTATION FOR SOLAR ABSORPTANCE AND EMITTANCE MEASUREMENTS

R. B. Pettit and A. R. Mahoney
Thermophysical Properties Division 5824
Sandia National Laboratories
Albuquerque, New Mexico 87185

Introduction

In many solar collectors, the optical properties of various components must be carefully controlled since they are important for the proper operation of the collector. Primary optical properties include the solar absorptance and emittance of absorbing coatings,[1] the reflectance of mirrors and the transmittance of glazing. In addition to obtaining optical property measurements using laboratory equipment, it is often necessary and useful to be able to measure these properties in the field using portable instrumentation. Such instrumentation can be utilized at a manufacturing facility, during assembly of a collector, or before and after collector installation. Optical instrumentation which is primarily used for measuring the solar absorptance, α_s, and emittance, ε, of solar selective coatings are evaluated in this paper.

While almost all of this type of instrumentation is designed to accommodate flat samples, special measurement procedures have been developed to measure the optical properties of coatings applied to cylindrical samples. These procedures are also outlined. In addition, this instrumentation can be utilized to determine the hemispherical solar reflectance properties of mirror materials. However, significant errors can result depending upon the thickness of the mirror and the characteristics of the portable instrumentation.

At the present time, we are aware of three manufacturers who provide portable equipment for α_s and ε measurements: (1) Devices and Services Co., Dallas, TX; (2) Gier-Dunkle Instruments, Inc. (Dynatech), Santa Monica, CA; (3) International Technology Corp., Sattelite Beach, FL (formerly Willey Corp.). Important characteristics of this instrumentation, including samples size, cost, etc., are listed in Tables 1 and 2.

We have previously evaluated the Gier-Dunkle Solar Reflectometer and Willey Alpha Meter (Model 2150) for α_s measurements; and the Gier-Dunkle Infrared

Reflectometer and Willey Ambient Emissometer (Model 2158) for ε measurements.[2] The important results of that investigation are listed in Tables 1 and 2.

The operation and accuracy of the Devices and Service (D & S) Solar Spectrum Reflectometer and Model AE Emissometer are presented in this paper.

D & S Solar Spectrum Reflectometer

Operation and Accuracy

The D & S Solar Spectrum Reflectometer is designed to measure the solar reflectance (or absorptance) of flat, opaque samples for an air mass two (AM2) solar spectral distribution.[3] This measurement is accomplished by hemispherically illuminating a sample placed over the measurement port and determining the amount of radiation reflected at an angle of 20° from normal using four different detector/filter combinations. Measurements are referenced to a calibrated white reflectance standard. The weighted output of each detector/filter combination is summed to give a reading of the solar averaged hemispherical reflectance.

The approximate spectral response of each detector/filter combination is shown in Figure 1 (data obtained from manufacturer). Note that the four detector/filter combinations cover the approximate wavelength intervals 330-420 nm (UV); 370-700 nm (Blue), 520-950 nm (Red), and 850-2500 nm (IR). The weighting of each detector output is chosen for a close match to an AM2 solar spectral distribution. The two absorption bands (at 1400 nm and 1900 nm) for the IR detector/filter combination are produced by a thin, internally mounted water filter. Potential problems with this filter are discussed later.

The accuracy of the D & S Solar Spectrum Reflectometer was determined by measuring the solar absorptance properties of a variety of solar coatings including several black chrome electrodeposited coatings on nickel substrates. The AM2 solar absorptance of each coating was calculated from spectral hemispherical reflectance data measured using a Beckman Model 5270 spectroreflectometer over the wavelength range 300-2400 nm.[3] The accuracy of the calculated values is $\pm$ 0.01 absorptance units (100% absorptance = 1.00 absorptance units). The results for the black chrome samples are shown in Figure 2. Two different nickel substrates were used: (1) Zodiac nickel, which has a bright, shiny surface, and (2) Perflow nickel, which has a dull, rough surface. For the samples studied, the α_s values ranged from 0.85 to 0.96. The average difference between the calculated solar absorptance and the solar absorptance values measured with the D & S Solar Spectrum Reflectometer was $\pm$ 0.005 absorptance units while the maximum deviations were less than $\pm$ 0.010 absorptance units.

In addition to the black chrome samples, several additional solar coatings were measured including black paint, metal oxide coatings, etc. as shown in Table 3. The results for these surfaces indicate an average deviation in α_s from the calculated values of only $\pm$ 0.01 absorptance units and a maximum deviation of less than $\pm$ 0.02 absorptance units.

Measurement of Mirror Samples

The solar averaged hemispherical reflectance properties, $R_s(2\pi)$, of several mirror materials were measured using the D & S Solar Spectrum Reflectometer; the results obtained for a variety of mirror materials are listed in Table 4. The solar average hemispherical reflectance of each sample was determined by solar averaging the spectral hemispherical reflectance properties measured using a spectroreflectometer. All measurements were referenced to a calibrated NBS mirror standard; the accuracy of the calculated values is $\pm$ 0.01 reflectance units (100% reflectance = 1.00 reflectance units).

The results obtained with the D & S reflectometer are within $\pm$ 0.02 reflectance units of the calculated values but only for mirror materials in which the reflecting layer is covered by a thin protective film, such that the reflecting layer is sufficiently close to the measurement port. For the materials where the reflecting layer is displaced away from the measurement port due to the thickness of a protective coating, the measured solar reflectance values are much lower than the calculated values. Thus the instrument underestimates $R_s(2\pi)$ for second-surface mirrors.

The effect of spacing the reflecting surface away from the measurement port was determined by measuring the solar reflectance of a first surface mirror as the mirror was displaced away from the measurement port. The results, shown in Figure 3, indicate that a mirror displacement of only 1 mm results in a decrease in reflectance of 5%. Therefore, for the error introduced by second-surface mirrors to be less than $\pm$ 0.01 reflectance units, the protective front surface layer should be less than 0.2 mm thick. We are currently investigating the cause of this effect for second-surface solar mirrors and examining ways to eliminate it.

Receiver Tube Measurements

Measurement of the solar absorptance properties of coatings applied to cylindrical parts (receiver tubes) can be easily accomplished using the D & S Solar Spectrum Reflectometer if properly calibrated. As with the other portable solar reflectometers,[2] the main source of error results from radiation that is reflected by the sample but which misses the detector/filter optics. The amount of lost radiation will be a function of the sample curvature, the angular distribution of reflected radiation from the sample, the distance between the sample and the measurement port, and the orientation of the sample with respect to the measurement optics.[4]

The calibration procedure consists of first measuring the reflectance of a flexible, opaque calibration sample when it is flat, R_f, and when it is wrapped around the curved surface to be measured, R_c. We have found that heavy white paper, backed with thin aluminum foil (which prevents any transmitted radiation) is an adequate diffusely reflecting calibration sample. If enough gain is available, the reflectance value R_c can be adjusted to the value R_f. In this case, the reflectance value of an unknown surface is read directly on the instrument panel meter. Alternatively, a correction factor, C, can be calculated for the ratio

$$C = R_f/R_c \ .$$

The value of C should always be ≥ 1.0. The reflectance value measured for an unknown curved sample is then multiplied by C in order to obtain the corrected reflectance value. We have found that both procedures gave the same results.

Water Filter

As previously mentioned, there is a water filter (a thin layer of water between two glass plates) located in front of the detector assembly. This filter is primarily used to reduce the response of the IR detector (lead sulfide) at wavelengths above ~1800 nm. If the water should leak out of the filter, the measurement spectrum in the infrared will be significantly changed. Since the gain adjustments available on the IR detector electronics allow the output to be set at the recommended value with or without the water filter, proper functioning of this filter is difficult to determine. Therefore, it is recommended that the individual detector response values (as described in the instruction manual) should be frequently checked. If significant (> 10%) changes in the set value are observed, particularly for the IR detector, the water filter should be removed and checked.

D & S Model AE Emissometer

The D & S model AE Emissometer is designed to measure the total hemispherical emittance for a 80°C (180°F) blackbody. The measurement head is heated, while the sample remains at room temperature. Calibration of the instrument is accomplished by comparing readings of both high ($\varepsilon = 0.92$) and low ($\varepsilon = 0.04$) emittance standards that are supplied with the instrument. A primary requirement for accurate measurements is to ensure that the standards and the unknown sample are maintained at the same temperature. This is accomplished by placing all materials on a large heat sink.

In order to check the accuracy of the instrument, the emittance properties of a series of black chrome coated samples, as well as a variety of other materials, were measured. The measured emittance values [ε(D & S)] were compared to the total hemispherical emittance determined from calorimetric measurements at 100°C [$\varepsilon_{t,H}$(100°C)].[5] Although the calorimeter data were measured at 100°C, the change in emittance measured at 80°C is much less than the measurement error[5] (see Table 5).

The comparison of these results is shown in Figure 4, where the error bars represent the error in the measured $\varepsilon_{t,H}$(100°C) values. The average difference between the emittance values for all coatings was $\pm$ 0.02 emittance units, with the largest difference of 0.06 emittance units occurring for a high emittance porcelain enamel sample. For the black chrome samples, the difference was less than $\pm$ 0.03 emittance units. Note that at low emittance values, $\varepsilon_{t,H}$(100°C) is greater than ε(D & S) while at high emittance values the reverse is true. This behavior follows the theoretical relationship between the total hemispherical emittance and total normal emittance for metallic and insulating surfaces[6] as shown by the solid line in Figure 4. Thus the emittance values measured with the AE emissometer more accurately follow the behavior of the total normal emittance.

Because of the design of the measurement head, the emittance properties of cylindrical surfaces could not be adequately measured.

Conclusions

The operation and performance of portable, optical instrumentation for α_s and ε measurements have been evaluated. The optical instruments, manufactured by Devices and Services Co., included a Solar Spectrum Reflectometer for α_s measurements and a model AE Emissometer for $\varepsilon(80°C)$ measurements. The accuracy of the Solar Spectrum Reflectometer was better than $\pm$ 0.02 for a variety of solar coatings, including black chrome solar selective coatings. With proper calibration, the instrument can measure the solar absorptance properties of coatings applied to cylindrical surfaces. The accuracy of the $\varepsilon(80°C)$ values measured with the model AE Emissometer was better than $\pm$ 0.03 emittance units for black chrome solar coatings and better than $\pm$ 0.06 emittance units for all coatings studied. The measured values corresponded more closely with total normal emittance values than total hemispherical emittance values. Because of the design of the instrument, measurement of the emittance properties of cylindrical surfaces is not practical.

References

1. P. J. Call, "National Program Plan for Absorber Surfaces R & D," Solar Energy Research Inst. Report SERI/TR 31-103 (Jan, 1979).*
2. R. B. Pettit, Engineering For Power, 100, 489 (1978).
3. M. A. Lind, R. B. Pettit and K. D. Masterson, J. of Solar Energy Eng. 102, 34 (1980).
4. R. B. Pettit, Solar Energy, 21, 247 (1978).
5. R. B. Pettit, "Total Hemispherical Emittance Measurement Apparatus for Solar Selective Coatings," Sandia Labs Report SAND 75-0079 (June, 1975).*
6. See Thermal Radiative Properties - Metallic Elements and Alloys, ed. Y. S. Touloukian and D. P. Dewitt, Plenum, 1970, p. 259.

*Available from: National Technical Information Services
U.S. Dept. of Commerce
5285 Port Royal Rd.
Springfield, VA 22161

TABLE 1. Characteristics of Currently Available Instrumentation For Solar Absorptance Measurements

Manufacturer	Cost	Model	Minimum Sample Size	Radiation Source	Detector	Comments
Devices & Service Co.	$ 7,245	SSR-ER	2 cm dia.	Tungsten-Halogen Lamp	Four Detector/ Filter Comb	$\pm$ 0.02 absorptance units all coatings
Gier-Dunkle, Inst. (Dynatech)	$15,000	MS-251	1.3 cm dia.	Xenon Lamp	Thermopile	$\pm$ 0.03 absorptance units for black chrome[2]
International Technology Corp. (Willey Corp.)	$ 1,825	Alpha Meter Model 2150	1.2 cm dia.	Projector Lamp	Silicon	Errors as large as 0.11 absorptance units for black chrome[2]

TABLE 2. Characteristics of Currently Available Instrumentation For Emittance Measurements

Manufacturer	Cost	Model	Minimum Sample Size	Radiation Source	Detector	Comments
Devices & Services Co.	$ 1,000	AE	6 cm by 6 cm plate	Heated Cavity	Differential Thermocouple	80°C emittance $\pm$ 0.03 emittance units for black chrome
Gier-Dunkle Inst. (Dynatech)	$20,000	DB-100	2 cm dia.	Heated Cavity	Thermocouple	100°C emittance $\pm$ 0.02 emittance units for black chrome[2]
International Technology Corp. (Willey Corp.)	$ 5,000	Ambient Emiss. Model 2158	3 cm dia.	Heated Cavity	Thermocouple	Linear relationship for black chrome[2]

TABLE 3. Solar Absorptance Values Measured with the D & S Solar Spectrum Reflectometer Compared to Calculated Values

Material	Calculated α_s	Measured D & S
Copper Oxide on Cu/5% Al	0.75	0.74
Zirconium Oxide on Zircaloy	0.86	0.86
Oxidized Cu/Ni alloy	0.84	0.83
Chemically Treated Silver	0.88	0.86
3M-401 C10 Black Velvet Paint	0.97	0.97
Pyromark Paint	0.97	0.97
Porcelain on steel:		
R-5	0.83	0.84
R-10	0.73	0.72
R-15	0.70	0.70

TABLE 4. Comparison of Measured and Calculated Solar Averaged Hemispherical Reflectance Values for Several Solar Mirrors

Material	Calculated Reflectance	D & S	Thickness of Protective Coating
Roll Polished Aluminum	0.92	0.92	None
5657 Alloy Aluminum	0.82	0.84	None
Alzak (Type I)	0.85	0.87	0.002 mm
3M5400	0.86	0.88	0.10 mm
Aluminized Quartz	0.88	0.85	1.52 mm
Silvered 0317 Glass	0.94	0.90	1.52 mm
Silvered Float Glass	0.83	0.64	3.0 mm
Silvered Low Iron Float Glass	0.90	0.81	3.02 mm

Table 5. Comparison of the Total Hemispherical Emittance at 100°C, $\varepsilon_{t,H}(100°C)$, with Emittance Values Measured with Model AE Emissometer, $\varepsilon(D \& S)$, for a Variety of Materials

Material	$\varepsilon_{t,H}(100°C)$	$\varepsilon(D \& S)$
Electroplated Gold	0.025 ± 0.01	0.012
Electroplated Nickel	0.06 ± 0.01	0.03
Black Chrome	0.10 ± 0.01 0.15 ± 0.01 0.22 ± 0.01	0.08 0.12 0.20
AMA Solar Selective Coating	0.35 ± 0.02	0.35
Ebanol "C" Treatment of Copper	0.65 ± 0.03	0.71
Ge Pigmented DC-805 Silicone Paint	0.76 ± 0.03	0.78
Black Porcelain Enamel on Steel	0.80 ± 0.03	0.86
3M 401-C10 Black Paint	0.90 ± 0.04	0.91

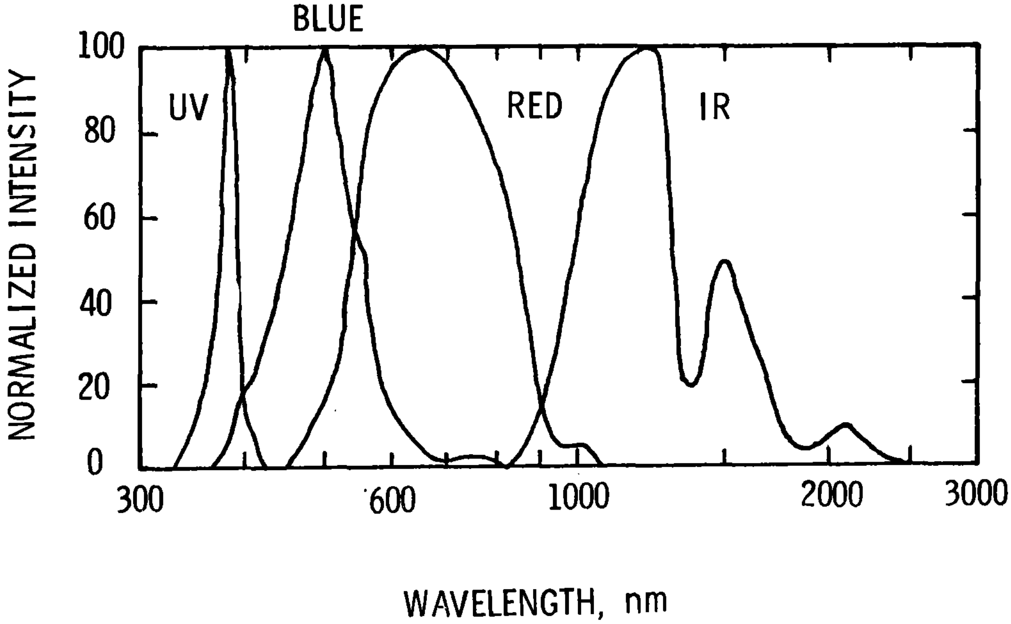

Figure 1. Normalized measurement spectrum vs. wavelength for the four detector/filter combinations in the D & S Solar Spectrum Reflectometer.

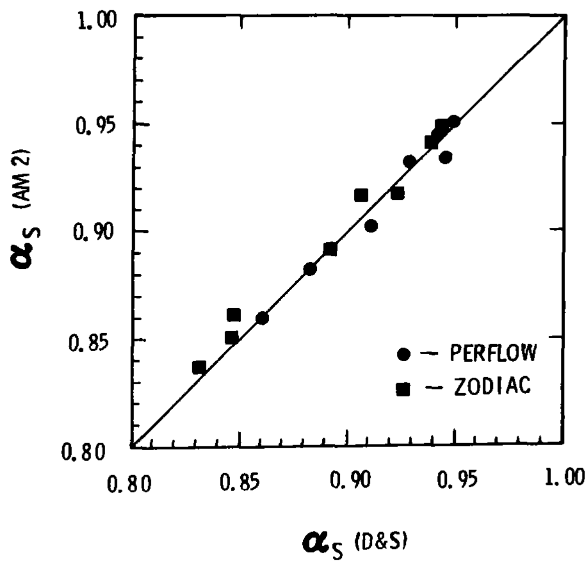

Figure 2. Comparison of calculated AM2 solar absorptance, α_s(AM2) with the solar absorptance measured with the D & S Solar Spectrum Reflectometer, α_s(D & S) for several black chrome coatings on both Zodiac and Perflow nickel substrates.

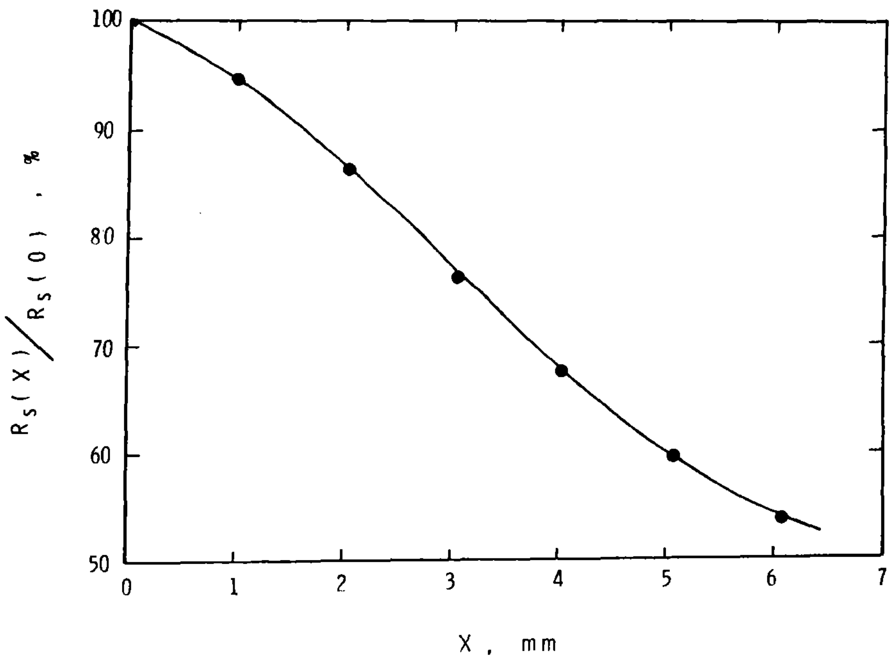

Figure 3. Normalized solar reflectance values, R_s, measured for a first surface mirror as a function of its displacement, X, away from the measurement port of the D & S Solar Spectrum Reflectometer.

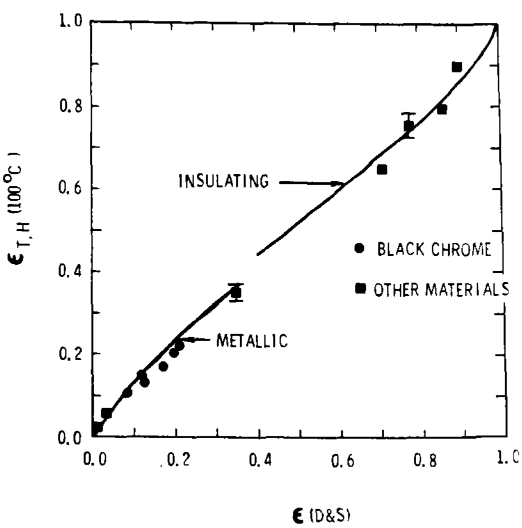

Figure 4. Comparison of the total hemispherical emittance at 100°C, $\varepsilon_{t,H}$(100°C), with the emittance values measured with the D & S model AE emissometer, ε(D & S), for a variety of materials. Also shown is the theoretical relationship between $\varepsilon_{t,H}$ and the total normal emittance ($\varepsilon_{t,N}$), for metallic and insulating surfaces.

OPTICAL TESTING OF LINE-FOCUS SOLAR CONCENTRATORS BY LASER RAYTRACE

Robert L. Hughes
Photometrics & Optical Development Division 1556
Sandia National Laboratory
Albuquerque, New Mexico 87185

The classical optical tests for evaluating mirrors are too sensitive and precise for use in the testing and evaluation of solar collector mirrors. Such tests are sensitive to fractions of a wavelength of light while solar collectors have errors of hundreds to thousands of wavelengths. Sandia National Laboratories started a program to develop methods and test equipment suitable for evaluation of solar collector mirrors in 1974.

The ideal cross section of a line-focus collector is a parabola. The parabola, a member of the family of geometric curves called conic sections, has the unique optical property of reflecting all light rays, which enter parallel to the optical axis, into a single focus. The right side of Figure 1 shows a family of rays reflected by a parabola.

The well known equation of a parabola in the X-Y coordinate system is:

$$Y = X^2/4F$$

where F is the distance from the X-Y origin to the focal point. The slope (M) of the parabola at any point is:

$$M = \tan \alpha = X/2F$$

For each small area of a mirror the law of reflection is obeyed. This law states that the angle of reflection (α) is equal to the angle of incidence. The geometry of Figure 1 shows that $\tan \alpha$ is the slope of the parabola at the point of incidence of the light ray. Errors in the slope of the surface cause the reflected ray to miss the focal point and a measure of this miss distance is a measure of the slope error.

The left side of Figure 1 shows the effect of an error (E) in the slope angle. This error increases the angle ($B > \alpha$) between the incident ray and the normal to the surface. Since the angle of reflection equals the angle of incidence, the reflected ray is deviated through an angle two times E and misses the focal point. If we measure angles in radians and approximate the small error angles by the trigonometric tangents of those angles, we can measure the linear distance of a ray from the focus and calculate the slope error at any given point on the mirror. For a slope error at the mirror of only one thousandth of an inch per inch (one milliradian) the reflected ray is deviated two milliradians. A typical line-focus collector with a focal length of about 20 inches, and with a mirror surface error of one milliradian near the vertex would cause the reflected ray to miss the focus by 0.040 inches. Thus the light beam serves as an optical lever to magnify any small slope error.

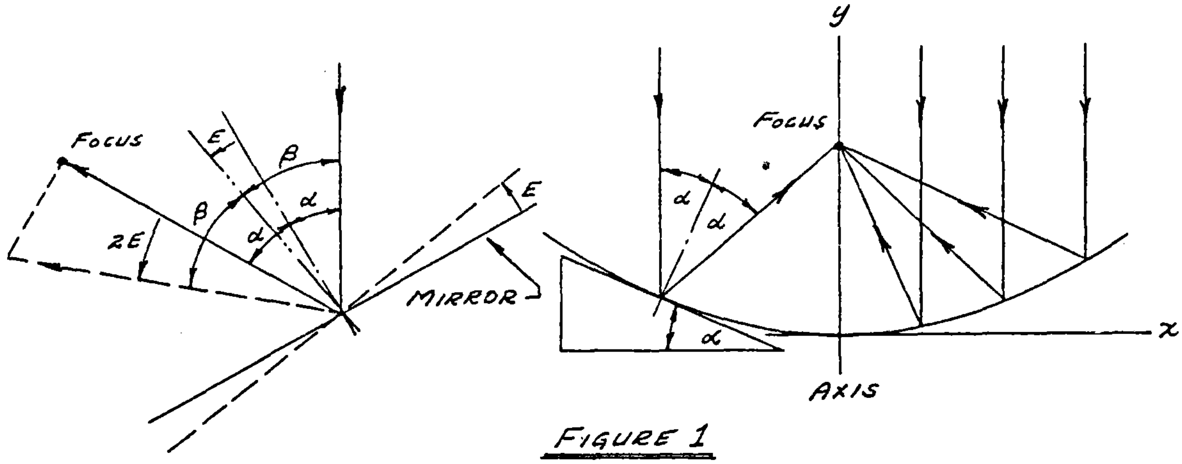

FIGURE 1

A laser produces a small beam of light which can be used to study the path of individual light rays. If a laser is mounted on a rail so that its ray remains parallel to the optical axis of a parabola, the offset of the reflected beam from the intended focus is a measure of the quality of a collector. The Laser Ray Trace Tester developed at Sandia Laboratories implements this simple geometry.

The Laser Ray Trace Tester has a helium-neon laser suspended vertically in a gimbaled mount on a carriage which moves along on overhead gantry. The collector to be tested is mounted with its focal line at a right angle to the gantry axis on a movable table on the floor. A 4-inch long linear detector is mounted on a rotating stage at the collector focal line so that any deviation of the reflected light beam is measured along the detector. The stage rotation is controlled so that the detector is always normal to the reflected beam from the collector. A computer controls the motions of the system, reads the beam position on the detector, stores the data for each scan, reduces the data into slope error at each position, and plots the slope error curve for each scan. The collector is scanned in raster fashion from rim-to-rim and from end-to-end. A practical sample interval generally used is about 1 inch. Figure 2 is a copy of the plotted results from one mirror test. The deviation of the individual lines, from a straight line, shows the difference between the collector surface and a true parabola. From the known geometry of the test and the experimental data, a best fit parabola and two focal point offsets are computed. The slope errors plotted are deviations from the best fit parabola for each scan. A second plot (Figure 3) is produced showing the focal line offsets for each scan. Statistics of the errors are accumulated using the whole test and the RMS slope-error and average focal length are included in the output.

It is not necessary to use a laser to test solar collectors. A small light source at the focus of a parabolic mirror will reflect a parallel beam of light just as a searchlight does. A grid placed in the parallel light beam will cast the grid's shadow on a screen placed along and normal to the beam. If we know the distance from the grid to the screen and measure the distortions of the grid shadow at the screen, we can calculate the deviations of the light rays which form the shadow. These deviations are caused by slope errors of the mirror. This is called a Projected Grid Test and has been used to evaluate collector mirrors. The evenness of the distribution of light on the screen gives a subjective view of the mirror quality and measurement of the grid shadow can give quantitative measures of the slope errors.

Sandia Laboratories has developed and has in operation a system for measuring the accuracy of line-focus solar collectors. Test data, derived from use of the Laser Ray Trace Tester, are being used in current programs to develop and evaluate line-focus solar collector systems.

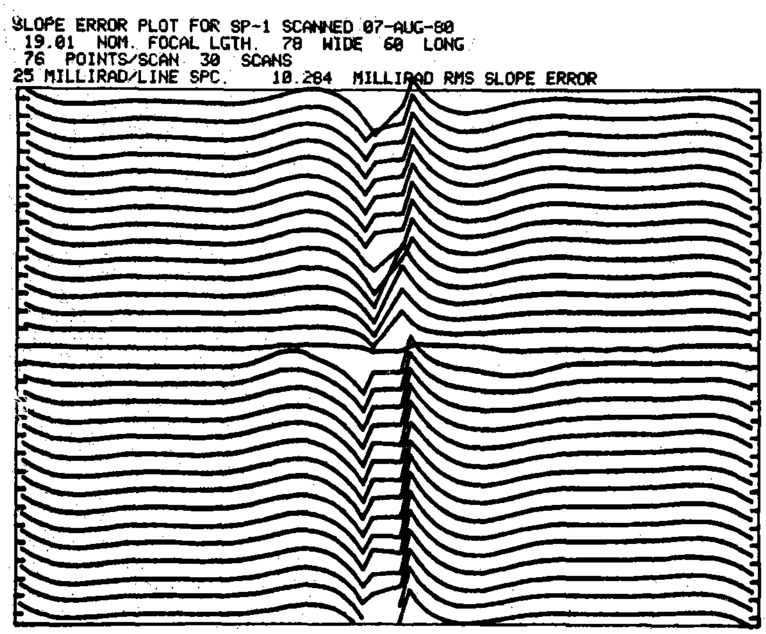

Figure 2

FOCAL LINE OFFSETS FOR SP-1 SCANNED 07-AUG-80
19.01 NOM. FOCAL LGTH. 78 WIDE 60 LONG
18.9959 AVG. FOCAL LGTH
UPPER PLOT X OFFSET (IN.), LOWER FOCAL LGTH.

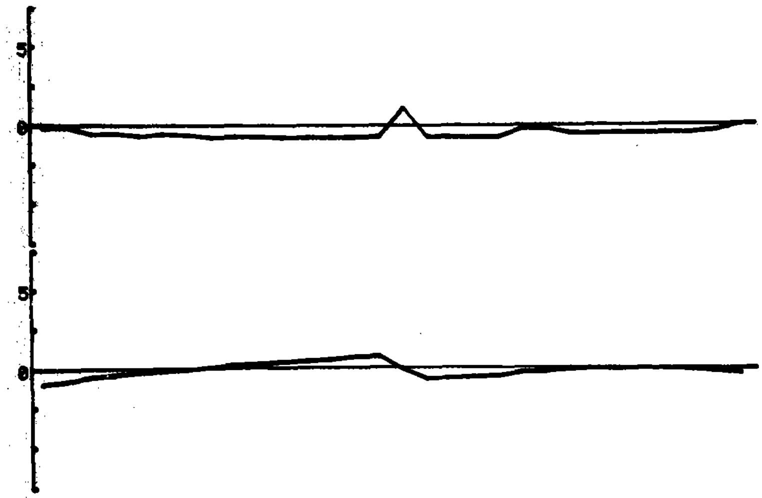

Figure 3

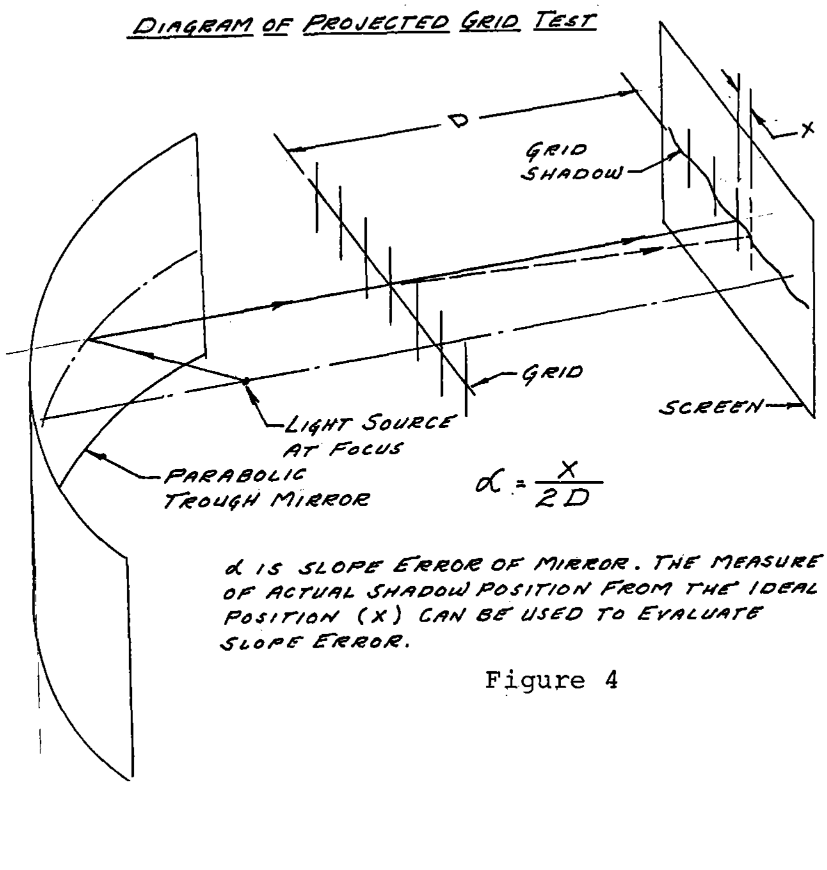

$\alpha = \frac{X}{2D}$

α IS SLOPE ERROR OF MIRROR. THE MEASURE OF ACTUAL SHADOW POSITION FROM THE IDEAL POSITION (X) CAN BE USED TO EVALUATE SLOPE ERROR.

Figure 4

FIELD LASER RAY TRACE TESTER

Bruce D. Hansche
Nondestructive Testing Technology Division 1552
Sandia National Laboratories
Albuquerque, NM 87185

Introduction

Ray trace testing of a parabolic trough solar reflector consists of shining a ray of light on the reflector, and measuring its angle of reflection by detecting the position of the reflected ray as it strikes a surface - usually a detector of some sort. A laser is usually used as a convenient source of a light ray. In the laboratory ray trace tester (LRTT) the input ray is maintained parallel to the parabola focal plane, which causes the reflected ray to pass somewhere near the theoretical focal line, as in Figure 1. This method has the advantages of minimizing necessary detector size, and testing the device in a manner which is optically similar to its intended use.

Hardware

Generating a scan ray parallel to the focal plane requires hardware of the same size as the aperture of the parabola under test, and also requires a detector at the focal line. Neither of these requirements is easy to meet for a portable instrument capable of testing reflectors as installed in the field - the size impairs portability, while the focal line is often occupied by receiver hardware. Therefore the decision was made to use a "finite conjugate" geometry, as shown in Figure 2. The laser ray pivots about a point, so the theoretical return rays do not come to a single focus, but follow a predictable curve. Reflector slope error at any point can be measured by comparing the actual return position of the rays to the theoretical return position from that point on the reflector.

An instrument to perform these in-situ tests has been developed at Sandia. A prototype device has been in use, in various stages of development, for approximately two years, and an improved version is nearing completion. Both consist of a track which sits on tripods, along which a carriage rides. Figure 3 shows the prototype aligned to a reflector, and Figure 4 shows the new system. A laser shines along the track, and is reflected off a pivoting mirror on the carriage. Thus a raster pattern can be made - a scan is made by pivoting the mirror to move the laser beam vertically, perpendicular to the mirror axis, then the carriage is moved along the track and a new scan is made. A microprocessor controls the test. For a typical reflector, the reflected rays form a caustic or smallest focus of about 0.5 meter in extent (see Figure 2). No position sensitive detectors with that aperture were available, so one was developed. It consists of 512 discrete phototransistors on 2.5 mm (0.1 inch) centers - Figure 5. The phototransistors are interrogated one at a time under control of the microprocessor, and the one with the largest signal is taken to represent the return position of the ray. For a typical working distance of 2 meters, this implies a ray slope resolution of 1.3 milliradians, or a surface slope resolution of 0.65 milliradians.

The laser is modulated and synchronously detected to discriminate against ambient light, which may be significantly more intense than the laser return ray. To save time, only a small subset of the detectors is interrogated for each data point, centered on the theoretical return position for that data point.

The raw data, consisting essentially of a list of ray return positions, one for each data point on the reflector, is digitally recorded on cassette tape by the microprocessor for later processing on the large time-share system (NOS). A typical test generates approximately 200 data points per vertical scan, with approximately 100 scans. It takes roughly one hour to align (once the alignment technique for a particular reflector is determined and necessary hardware made), and one hour to take the data. The device works in daylight, but off axis reflected sunlight can saturate the detectors and present a hazard to operating personnel. Alignment is also easier at night or under overcast conditions, so bright sunlight is avoided for testing if possible. This policy has the added convenience of minimizing interference with operation tests being conducted.

Data Reduction

The basic information sought in these tests is the deviation of the slope of the actual reflector surface from that of a theoretical parabolic surface, as shown in Figure 6. The definition of this theoretical reference surface is not as simple as it might seem, and there are choices to make in selecting it, depending on what part of the total system is actually being tested. Alignment of the field LRTT is often made difficult by lack of proper fiducials or alignment points. The edges or rims of a typical trough are often the most misshapen parts, while the vertex is often undefined. Designers contemplating a reflector which might undergo ray trace testing in the future should consider including some fiducial points such as pins, drill holes, etc. at known locations, accessible from the front of the reflector when it is in the test configuration.

Often, the position of the reflector relative to anything else in the world is irrelevant, such as when comparing glass bonding methods, checking focal lengths or molding techniques, etc. In these cases, a rough alignment is made, then a parameter estimation technique is used to fit, in a least squares sense, a reference parabola to the data as shown in Figure 6. Even in this case, the exact reference surface used, (and hence the numerical test results), depends on some choices of weighting factors and initial assumptions. The analysis program currently in use assumes no error in location of the vertex, and fits two orthogonal focal point parameters. A focal length error is represented by ΔF, and a tilt by ΔY, as indicated in Figure 6. These parameters are found for each scan, then are adjusted to occupy a straight line in space. This line defines the focal line of the reference surface. In other words, the reference surface is a quasi-parabolic cylinder, whose focal length and twist or tilt are linear functions of the axial position.

Sometimes an entire system must be tested, such as a reflector with fixed collector, without provision for adjustment. In this case, the tester must be aligned relative to the assumed focal line, and the reference surface taken to be the design parabola. If there is indeed some tilt to the reflector, or if the tester is misaligned, the data will show a non-zero mean in slope error.

Once the data is reduced to slope error, many options exist for data presentation. Typical data formats include focal line position (position of reference surface focal line relative to the position of the aligned LRTT), slope error as a function of position on the reflector (Figure 7), slope error statistics (Figure 8), or ray projection (Figure 9). Usually an rms slope error number is given, and taken as an overall figure of merit. Caution must be advised in attaching too much significance to this number, since it is a function of various choices in how the reference parabola is defined. For a series of tests done in the same way, with identical analysis procedures, the rms slope error should be a valid comparison.

Conclusion

An instrument has been developed to measure slope error of line focus reflectors in-situ. The major difficulties in using the device are alignment to the reflector and complexities in analysis made necessary by possible misalignment. To date, approximately 50 tests have been made with the prototype device, and an improved model is expected to be on line by fall 1980.

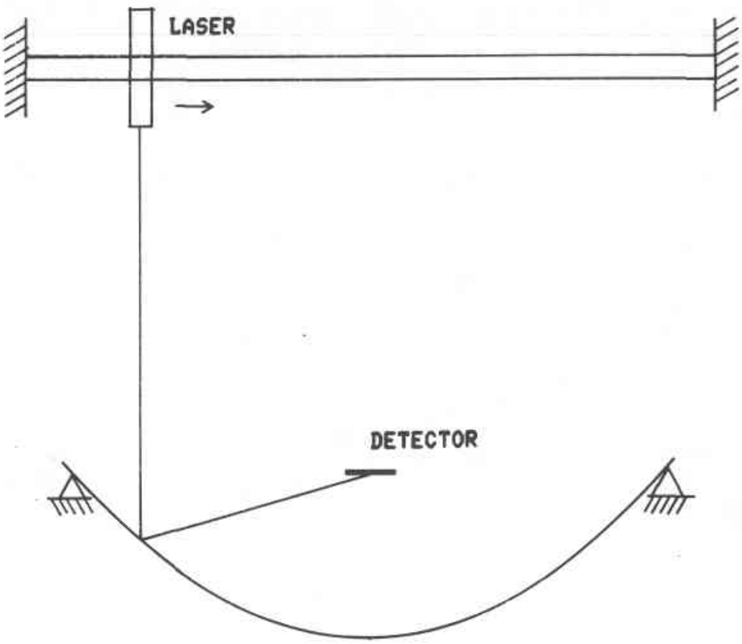

Figure 1 Laboratory Tester Geometry

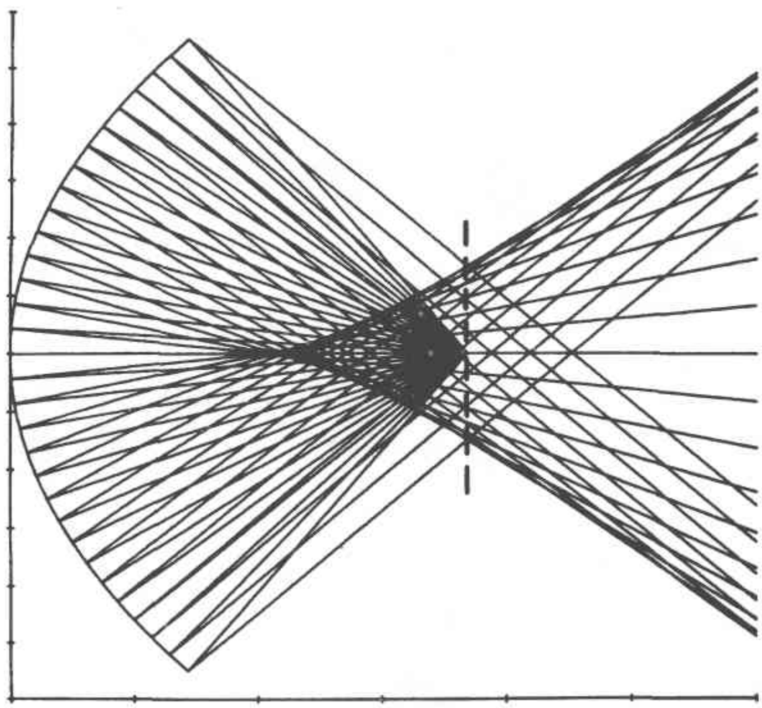

Figure 2 Finite Conjugate Ray Trace Pattern.
Dotted line represents detector position.

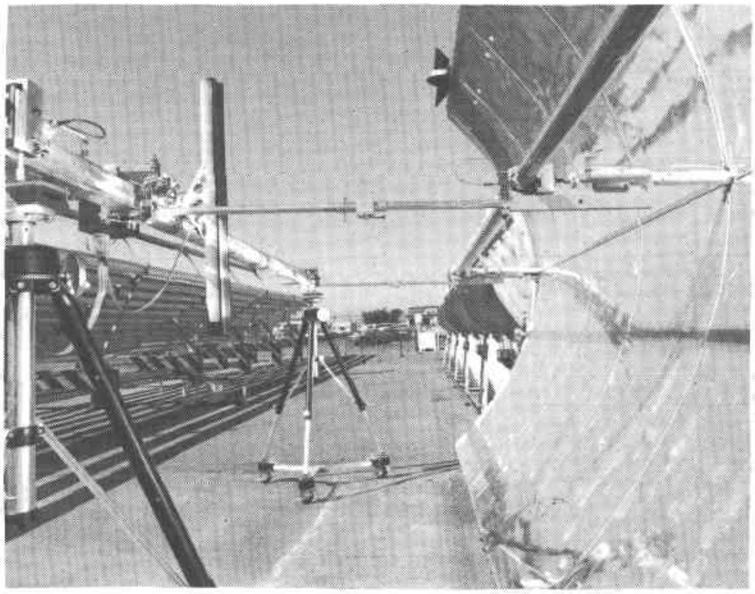

Figure 3. Prototype Field Laser Ray Trace Tester. Shown sligned to a reflector in the field.

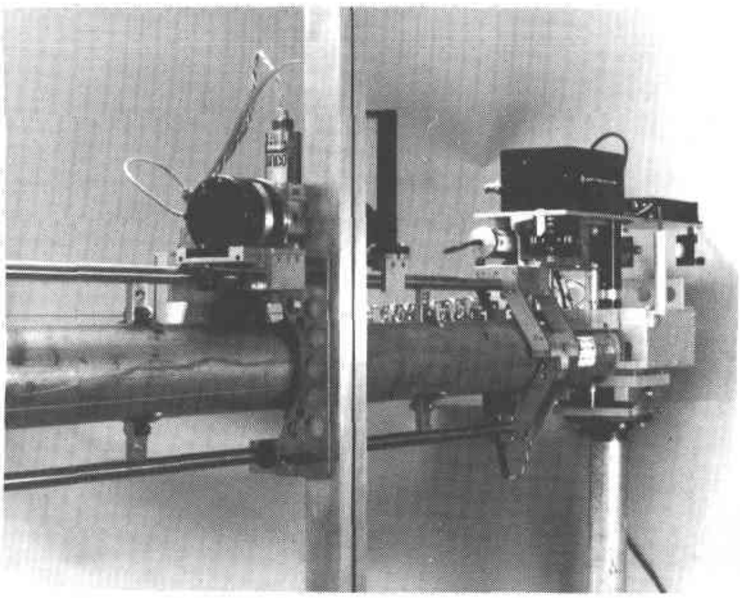

Figure 4. New Field Laser Ray Trace Tester. Closeup of fixed laser and moving carriage.

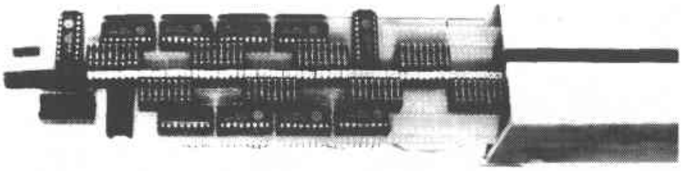

Figure 5. Closeup of Detector Assembly.

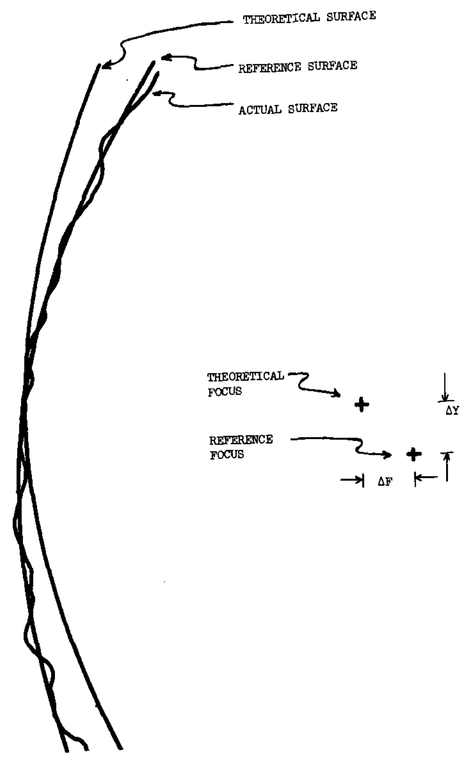

Figure 6. Relationship of Theoretical, Reference, and Actual Reflector Surfaces and Focal Points.

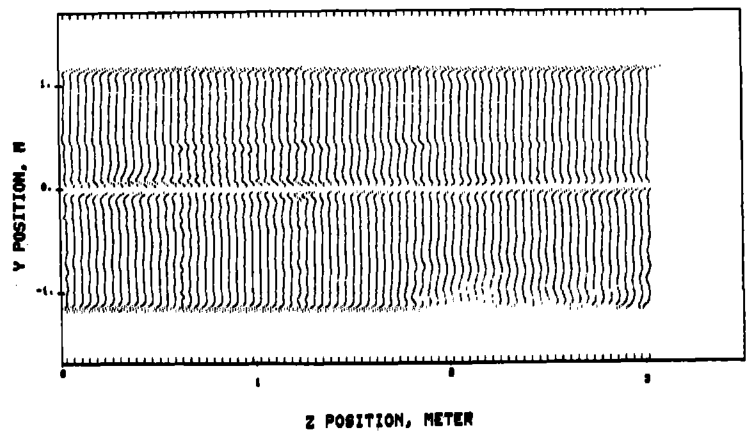

Figure 7. Slope Error. Each tic mark represents 2Ø milliradians in this "isometric" display.

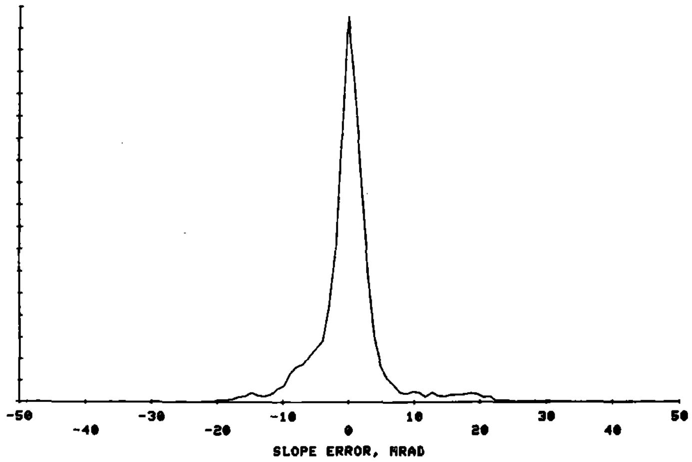

Figure 8. Histogram of Slope Errors.

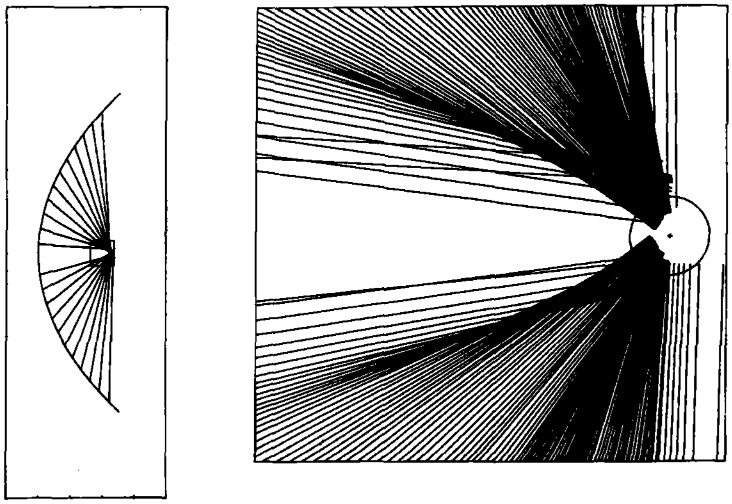

Close-Up of Collector Area

Figure 9. Ray Projection Plot

SOLAR PROFILE INTENSITY GAUGE FOR RECEIVER TUBE SUBSYSTEM OPTIMIZATION IN CONCENTRATING COLLECTORS

Michael G. Semmens
Energy Systems Design
The BDM Corporation
Albuquerque, NM 87106

Background

Component and material optimization are important issues in developing optimal collectors for both solar thermal and photovoltaic applications. The optimization of linear parabolic troughs (LPT) was addressed in a DOE contract for the "Conceptual Design and Analysis of a 100 MW Line Focus Solar Central Power Plant" (Contract Number ET-78-C-03-2073) where a large aperture trough with a D-shaped receiver tube subsystem (RTS) was determined to provide both improved performance and lower cost for large solar thermal electric power applications. Sandia National Laboratories in Albuquerque is currently developing the large apeture trough and has contracted The BDM Corporation to provide the necessary receiver tube subsystem optimization by expanding and completing the work performed in the above referenced contract. During the Line Focus Power Plant (LFPP) contract, BDM conservatively calculated that a total of four points (6 to 7 percent) improved net collector performance could be gained by utilizing a D-shaped receiver tube with a D-shaped glass annulus. This alternative geometry reduced thermal energy losses while maintaining the intercept integrity of the collector. Preliminary measurements performed at the BDM Solar Test Facility on a prototype of a D-shaped tube with a circular glass annulus showed about 5 percent improved performance using the same concentrating mirror. Other receiver tube geometries offer even greater thermal energy savings.

The same characteristics of light "crowding" in regions around the receiver tube in line focus troughs also will effect the photovoltaic system performance. BDM, under DOE contract for the "Commercial Application of a Photovoltaic Concentrating System" (Contract Number ET-78-C-04-5313), has demonstrated that more cost effective power can be produced with the use of smaller photovoltaic cells and larger LPTs. The optimization, the photovoltaic cell size and trough size promise significant cost reductions in the use of line focus photovoltaic systems.

Program Purpose and Objective

The optimization of either a thermal or a photovoltaic RTS when used in line focusing concentrating solar collectors requires detailed definition of the positional intensity of concentrated insolation around the focal area of the concentrator. Once detailed emperical data concerning the intensity profile is provided, the optimal receiver can be designed with the use of detailed engineering design models and calculations. These models and calculations will, of course, determine the optimal geometry and dimensions of the RTS for any given solar concentrator.

As part of the program described within this paper, BDM will address three specific objectives which are summarized in Figure 1. First, the program will develop a solar profile intensity gauge (SPIG) to support the engineering design trade-off and optimization analyses of receiver tube subsystems. The second objective will be to verify improved performance of optimized RTS through prototype test and evaluation. Assuming positive performance gains in the optimized prototype receiver tube are demonstrated, the final objective of the program will be to identify and prepare for the application of the SPIG and receiver tube optimization analysis to advance linear concentrators and other existing concentrator technology.

Program Approach

To achieve these program objectives, the initial project has been divided into 2 phases as shown in Figure 2. The first phase is directed towards the development of the solar profile intensity gauge (SPIG), and the second phase encompasses the design, construction, and testing of an RTS which has been optimized with the use of the SPIG data and BDM design efforts for an existing LPT.

At this time the design of the SPIG has been completed and the materials and hardware are being procured. The SPIG will be completed and tested by November 1, 1980.

The BDM design codes are currently being prepared for the optimization of the receiver tube subsystem on a Solar Kinetics T-700 linear parabolic trough. These codes will be applied in the final optimization after the emperical SPIG data is available. In an effort to verify the initial SPIG data collection effort, laser scans of the T-700 will be taken to characterize the focal pattern of the collector. These laser scans will be used in conjunction with the flux profiles mapped by the SPIG to insure that relative intensities are being measured by the gauge.

SPIG PROGRAM PURPOSE/OBJECTIVES

(1) DEVELOP A SOLAR PROFILE INTENSITY GAGE TO SUPPORT ENGINEERING DESIGN TRADE-OFF AND OPTIMIZATION ANALYSES OF RECEIVER TUBE SUBSYSTEMS (RTS) ON CONCENTRATING SOLAR COLLECTORS.

(2) DESIGN, CONSTRUCT, AND EVALUATE AN OPTIMAL RTS FOR EXISTING LINEAR PARABOLIC TROUGH COLLECTOR USING SPIG EMPIRICAL DATA AND APPROPRIATE ENGINEERING DESIGN ANALYSIS.

(3) IDENTIFY AND PREPARE FOR THE APPLICATION OF THE SPIG TO ADVANCED LINEAR CONCENTRATORS AND OTHER (EXISTING) CONCENTRATING COLLECTOR TECHNOLOGY.

Figure 1

SPIG PROGRAM SCHEDULE

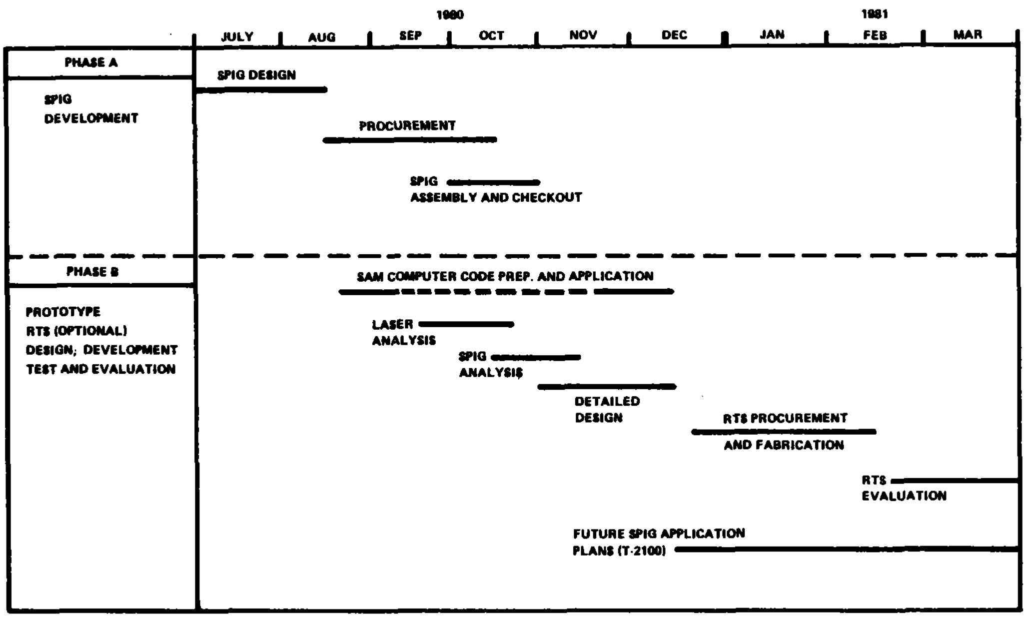

BDM/TAC-80-183-BR

Figure 2

After the emperical data is made available from the SPIG, the final engineering calculations will be made to define the optimal receiver tube geometry and dimensions. Once defined, procurement of the receiver tube and annulus will be initiated immediately and will take about 10 weeks. The final test and evaluation of the optimized RTS will occur in late February and early March, 1981.

The SPIG and RTS optimization analysis will be applied to the large 21 foot apeture linear parabolic trough being developed by Solar Kinetics for Sandia National Laboratories, subsequent to the successful demonstration of improved receiver tube performance. As the final effort in Phase B of the program, specific plans for the application of the SPIG and the test of the optimal T-2100 RTS will be defined.

Receiver Tube Subsystem Optimization

The BDM procedure for the optimization of the RTS will involve separate measurement and modeling efforts as shown in Figure 3. First, the SPIG will be used to map the solar intensity about the focal region of the cencentrator. The flux density will be automatically integrated and digitized by microprocessor for the use in the design model.

The BDM Solar Analysis Model (SAM) has been used in the DOE LFPP program described above and will be used to perform design trade-offs for the receiver tube subsystem. The receiver tube model is an electrical network equivalent thermal grid model of the receiver tube and annulas. The insolation defined by the SPIG will be entered as current sources, and the detailed grid will provide adequate resolution and nodal temperatures and heat flows to model the thermal dynamic characteristics of the solar thermal RTS. The key trade-off between the collector intercept and thermal energy losses will be performed within the design computer code and the geometry and dimensions of the RTS which provides the maximum thermal energy gains will be defined. This process can be repeated quickly and efficiently for all line focus collectors and a variety of Fresnels and point focus collectors as well. (The BDM SAM computer code has been described in detail in Appendix C of the LFPP Topical Report and Final Report.)

SPIG Description

The first application of the SPIG will be on a linear parabolic trough. This configuration is shown in Figure 4. The basic components of the SPIG will include:

PROCEDURE FOR RTS OPTIMIZATION

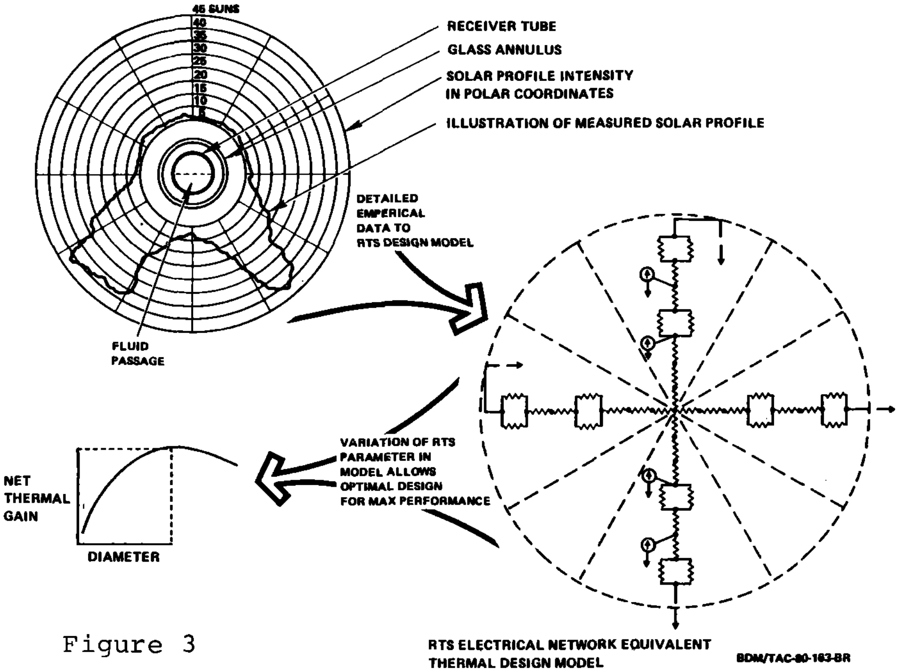

Figure 3

TRACK ASSEMBLY

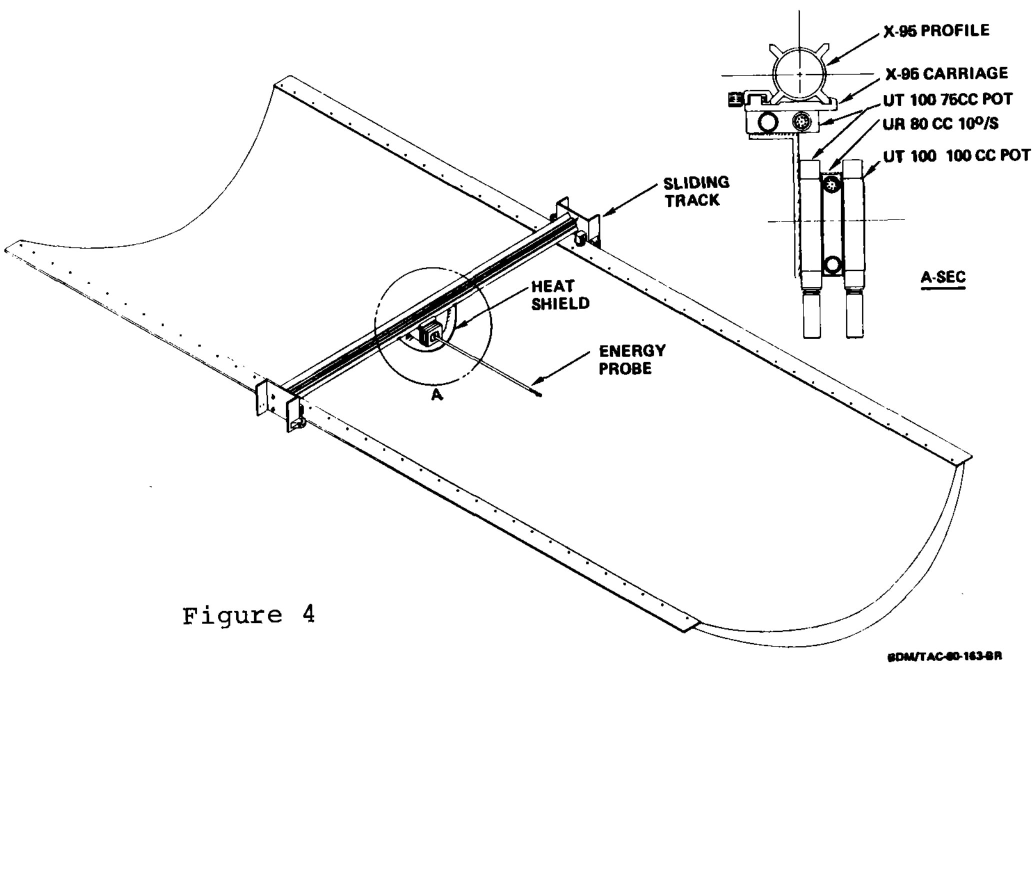

Figure 4

1. The collector mounting
2. The SPIG structure
3. Translators and controls
4. Insolation sensor

The collector mount is designed to traverse the collector and stay centered on the axis. A plate is bolted on to the wings of the trough which is used as a guide for the mount. The mount has opposed castors to allow free movement along the axis and to prevent any vertical movement of the structure. To prevent any horizontal movement, opposed castors will ride the edges of the plates. All castors are adjustable to allow proper alignment on the concentrator.

The cross structure is a commercially available aluminum extrusion normally used as an optic bench. Vertical deflection of .005 inch for a seven foot span with 20 pounds of force centered in the beam are projected. A sliding mount is also available commercially which will be used to center the translators and energy sensor. The cross structure will be bolted to the collector mount which will provide a rigid, solid base for the translators.

The solar intensity will be measured over 360° of rotation. This is accomplished with a rotational translator driven by a reversible DC motor. A potentiometer will be coupled with the translator to provide a measurement of angular displacement. To vary the radius of rotation, a linear translator will be attached to the rotational translator. An effective diameter of 30 cm can be measured. To measure intensity, both vertically and horizontally about the axis centerline, linear translators will be mounted to the cross structure and will provide a 75 mm displacement in each direction. All linear translators have built-in potentiometers for displacement measurement. A constant voltage source provided by the HP-85 data acquisition system will be used to measure the voltage drop across the pots.

To measure the solar intensity, a calorimeter will be mounted on a shaft which extends from the rotational translator. This calorimeter has a thermal sensing area of 3.2 mm (1/8 inch) diameter. Full scale output of 10 mV for 0-5.68 w/cm^2 (0-5 Btu/ft^2-sec) is provided by the sensor. The sensor has a threaded body for easy removal and replacement. A temperature sensor will be mounted on the calorimeter to protect against over temperatures. A schematic of the SPIG controls and measurements is provided in Figure 5.

The HP-85 microprocessor and signal conditioning system will be used for data acquisition and SPIG control. Each measurement processed will be preprogrammed on the

CONTROL AND MEASUREMENT SCHEMATIC DIAGRAM

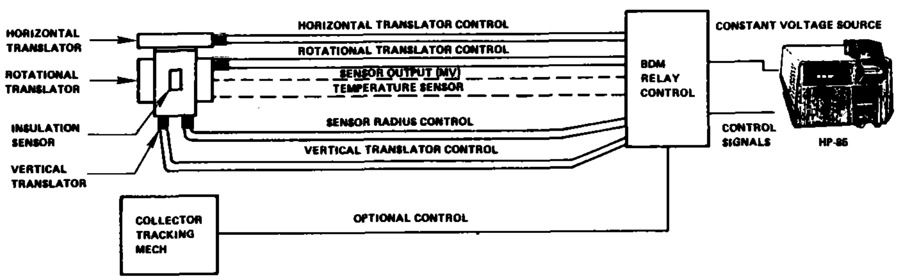

Figure 5

BDM/TAC-80-163-BR

HP-85 software and will be conducted automatically producing complete solar intensity profile, integrated energy, and necessary digitized data and graphical output.

Summary

Significant improvements in the performance of solar thermal collectors and photovoltaic concentration collectors have been demonstrated with alternative receiver tube configuration designs. Optimal design for each collector produced by the variety of manufacturers involved in solar thermal or an solar photovoltaic systems needs a quick and efficient means of providing the emperical data necessary to perform receiver tube optimization engineering analysis. The solar profile intensity gauge being produced by BDM for Sandia will provide the capability required by manufacturers and design engineers. Further, the SPIG and variety of receiver tube models can be applied to the optimal design of either thermal or photovoltaic receiver tubes and linear parabolic troughs, linear Fresnels, fixed aperture line focus collectors, circular Fresnels, and parabolic dishes. The application of the SPIG and the appropriate engineering analysis will produce maximum net thermal gains and solar thermal applications allowing for minimum materials and receiver tube shadowing. In addition to improved performance, the optimal receiver tube design will provide enhanced film convective heat transfer coefficients, while minimizing pressure drops in receiver tubes and enhance parasitic powers.

Optimization of photovoltaic receiver tubes will identify optimum cell size, minimizing the cost of of photovoltaic cells while optimizing the cell concentration ratio. The appropriate cell design and cell/collector matchup will also reduce such problems as current crowding, intensity variations on cells causing current restrictions, and will also allow improved thermal designs of photovoltaic/thermal hybrid and concentrating passive photovoltaic systems. The improved performance and implied reduced cost which are achievable with the capability described above will substantially enhance the commercialization of solar energy.

THE DEVELOPMENT OF A SECOND GENERATION PORTABLE SPECULAR REFLECTOMETER

J. M. Freese
Thermophysical Properties Division 5824
Sandia National Laboratories
Albuquerque, New Mexico 87185

Introduction

A second generation portable specular reflectometer has been developed at Sandia National Laboratories (SNL) in response to an increasing demand for a portable instrument to measure a variety of mirror materials in the field.[1] Utilizing the talents of a design draftsman, a second generation instrument was developed and two prototype instruments were fabricated at SNL. After final assembly and alignment both instruments were tested by measuring the specular reflectance properties of several mirror materials. The results were found to be within ± 0.012 reflectance units of those obtained by appropriately averaging reflectance versus wavelength data taken with a laboratory bi-directional reflectometer. The instruments were then released to the Midtemperature Solar Systems Test Facility (MSSTF) and the Central Receiver Test Facility (CRTF) located at Sandia National Laboratories. The specular reflectance measurements have been made on a number of systems in the field, including the CRTF heliostats, the advanced troughs, Suntek slats, Raytheon Petal, G. E. 7 meter dishes, the Martin Marietta and McDonnell Douglas prototype heliostats for the Barstow plant, and the parabolic troughs at the Willard, New Mexico and Coolidge, Arizona sites. In addition, the instrument has been used extensively in a cleaning study for the advanced parabolic trough design. Phase three of the instrument design is in progress with Sandia requesting assistance from optical instrument manufacturers in evaluation of the reflectometer from a design and manufacturability standpoint.

Instrument Description

The portable specular reflectometer essentially consists of two parts: collimation optics and collection optics, as shown in the photograph in Fig. 1 and the schematic in Fig. 2. The collimation optics consist of a tungsten filament lamp, filter, focusing lens, source aperture, collimating lens, and a variable beam aperture. The filter (Corion Corporation IRS-2) passes only a beam of radiation with wavelengths from 350 to 750 nm with the peak transmission occurring at 560 nm

(Figure 3). This radiation is imaged onto a 0.25 mm diameter source aperture with a 17 mm focal length lens. The circular source aperture is positioned at the focal point of the collimating lens (55 mm focal length) so that the collimating optics produce a beam of radiation whose divergence is θ_s = 4.5 mrad (0.25 mm/55 mm). A beam aperture permanently positioned in front of the collimating lens limits the beam diameter to 10 mm. This beam aperture insures that all of the specularly reflected radiation from the sample mirror surface is collected by the 22 mm diameter collection lens.

The collection optics consist of a collection lens, identical to the collimating lens, a collection aperture, filter and viewing optics or silicon detector. The collection lens is positioned to produce an image of the source aperture at the plane of the collection aperture. The collection aperture diameter can presently be varied from 1.02 mm to 3.51 mm by using removable aperture discs. Table I shows the size of the apertures (in mm and inches) made for the instrument and the corresponding angular opening, θ_c. The size of the aperture selected will depend upon the reflectance properties of the mirror material to be measured[2] and the optical requirements of the solar collector. However it should be larger than the source aperture for most applications. The currently used aperture of 1.27 mm diameter was chosen for easy positioning and alignment of the reflectometer. The collection filter is identical to the collimating filter and is used at this location to reduce the effect of stray light. Either the detector or viewing optics can be positioned behind the filter. The viewing optics allow observation of the reflected beam shape and its position relative to the collection aperture. The viewing optics can be replaced with a silicon detector (United Detector Technology Inc., Model 500) which converts the radiation that is passed through the collection aperture to an electrical current. The current is then converted to an output voltage by a built-in operational amplifier and the output is read directly from a liquid crystal digital voltmeter. The output signal from the detector can also be fed to a small microprocessor which will average up to 100 reflectance readings and give a mean and standard deviation of these readings.

Improvements

The second generation portable specular reflectometer has incorporated many improvements over the first instrument.[1] One of the major improvements was achieved by increasing the beam diameter of the optics from 5 mm to 10 mm. This allows the instrument to average a larger surface area of a reflecting surface and reduces the number of measurements on a mirror required for obtaining the averaged specular reflectance. By using nylatron and aluminum parts throughout, the weight of the reflectometer was reduced from 6 1/2 pounds to 3 1/2 pounds; this improves the field operating ability of the instrument. The removable beam stops used on the first instrument were replaced with adjustable apertures to considerably aid alignment of the instrument. The X and Y tilting adjustments were redesigned to permit greater travel and improve the ability to measure short radius of curvature surfaces (e.g., parabolic troughs). The mount for the collimation and collection tubes was also redesigned to allow a straight-through beam configuration to obtain a 100% intensity value. In this configuration, the instrument can be used to measure the specular transmittance of materials. This redesign, however, created a problem with stray light in an outdoor environment. The problem was solved by placing removable covers on the front, back, and sides of the reflectometer head. Finally, batteries used in the detector were replaced with a small power supply giving the instrument output better stability and eliminating the need of frequent battery changes. A complete set of drawings on the instrument has been completed and is available upon request.

The Microprocessor

To further improve the operating convenience of the portable reflectometer, a small microprocessor was added to the output of the detector. The microprocessor has the capability of displaying the percent reflectance for each measurement, the number of measurements taken, and the mean and standard deviation of the total number of measurements made. This eliminates the need to manually record each reflectance value and reduces operator error. In future models of the instrument, it would be desirable to place the power supplies and microprocessor in one chassis. A very small printer could also be added to provide the operator with a hard copy of individual data points.

Performance

The spectral bandwidth curve for the first portable specular reflectometer was calculated[1] using the spectral transmittance properties of the Corion filters and the detector response curve. However, actual measurement of the spectral bandpass curve for the second generation instrument was obtained with the new instrument in the straight-through beam configuration. Narrow band pass filters were placed in the beam path and the percent transmission was measured. A spectral bandwidth curve was then generated by plotting these normalized transmittance values as shown in Figure 4. In order to compare the reflectance values obtained with the portable reflectometer and the laboratory bi-directional reflectometer, a weighted specular reflectance value was calculated for the laboratory instrument. For this calculation, the spectral bandwidth curve of the portable instrument was divided into three regions: (I) below 550 nm, (II) 550 to 650 nm, and (III) 650 and above. The fractional area of each region was then determined ((I) 0.13, (II) 0.58, (III) 0.29). Next, the reflectance of a material was measured at the center wavelength of each region with the laboratory bi-directional reflectometer (i.e., 500, 600 and 700 nm). These values were then multiplied by the respective fractional area and summed to produce a weighted specular reflectance value. These values are shown in Table II for several mirror materials.

Also shown in Table II are the specular reflectance properties measured using the three portable specular reflectometers (one 1st generation and two 2nd generation instruments). The mirror samples selected for these measurements were as follows: (1) second-surface aluminized quartz flat calibrated by NBS (this was used as the reference sample), (2) second surface silvered float glass, (3) aluminized acrylic manufactured by 3M (special Scotchal 5400), (4) polished aluminum sheet manufactured in France (without any protective coating), and (5) Alcoa type I specular reflector sheet without Alzak® anodized coating. The differences between the laboratory bi-directional reflectometer and the portable reflectometers have been previously discussed.[1] The reflectance values determined using the portable instruments are all within ±0.012 reflectance units of the calculated values obtained from the laboratory bi-directional reflectometer.

A check was made on the reflectance properties of the second surface aluminized quartz flat calibrated by NBS using the straight-through beam configuration of the second generation portable instruments. The reflectance values for the NBS standard obtaned in this manner deviated less than 0.005 reflectance units from the value obtained by the calculated method using the laboratory bi-directional reflectometer.

Temperature Effect

The operation of the instrument in the outdoor environment has been successfully demonstrated over a wide temperature range (32°F to 100°F). However, when the outdoor temperature reached 100°F the reflectometer output decreased dramatically. Because the reading drifted with respect to time continuously, it was difficult to stay within the measuring error of the instrument. The problem was finally traced to either the detector or the detector preamplifier. This problem can be solved if a detector and preamplifier with a higher temperature range can be found.

Outside Procurement

Interest in the portable specular reflectometer has been expressed by other government laboratories, universities, and industrial companies involved in solar work. In order to provide the most economical and efficient instrument possible, Sandia is seeking the assistance of American optical instrument manufacturers to evaluate the reflectometer from a design and/or manufacturability standpoint and to incorporate any improvements resulting from their evaluation in the instrument design. The manufacturer would then fabricate several instruments confirming the design changes. It is hoped that this phase of system development will be completed by May, 1981.

Conclusions

A second generation portable specular reflectometer has been developed and two prototypes have been constructed. Improvements, including larger sampled area, reduction of reflectometer weight, addition of adjustable beam stops and the capability of a straight-through beam configuration, were incorporated in the second generation instrument. Convenience of operation was further enhanced with the addition of a small microprocessor. The specular reflectance properties of several mirror materials were measured with the new instruments and the results compared within ± 0.012 reflectance units of the calculated specular reflectance values determined from the laboratory bi-directional reflectometer. The instruments were also tested in the field on several reflector systems and over a wide range of outdoor temperatures with good results up to 100°F. Above this temperature, the detector and preamplifier output decreased significantly, resulting in reduced accuracy.

The instrument is presently being evaluated by over thirty American companies and a contract will be placed with one of these companies to commercialize and fabricate several instruments.

Acknowledgement

The author would like to thank R. B. Pettit for his helpful discussions concerning the portable reflectometer, Howard Seltzer for his design drafting assistance and Bob White for his programming expertise on the microprocessor.

References

1. J. M. Freese, "The Development of a Portable Specular Reflectometer for Field Measurements of Solar Mirror Materials," SAND Report 78-1918, Oct. 1978.

2. R. B. Pettit, "Characterization of the Reflected Beam Profile of Solar Mirror Materials," Solar Energy 19, pp. 733-741, Nov. 1976.

Table I. Collection Aperture Sizes and Acceptance Angles

Diameter		θ_c
mm	(inches)	mrad
1.02	(0.040)	18.5
1.27	(0.050)	23.1
1.50	(0.059)	27.3
1.75	(0.069)	31.9
2.01	(0.079)	36.6
2.64	(0.104)	48.0
3.51	(0.138)	63.7

Table II. Specular Reflectance Values of Mirror Materials on the Laboratory Bidirectional Reflectometer and the Portable Specular Reflectometers

Mirror Description	Reflectance Measured on Laboratory Bidirectional Reflectometer 500 nm	600 nm	700 nm	Calculated Reflectance from Laboratory Bidirectional Reflectometer	Reflectance of Portable Reflectometer #1	#2	#3[c]
Aluminized Quartz Flat[a]	0.882	0.869	0.848	0.865	--Assumed--[d]		
(Polished Aluminum) Special Alzak (Parallel to Roller Marks)	0.863	0.862	0.853	0.860	0.828	0.841	0.838
				0.840[b]			
Special Alzak (Perpendicular to Roller Marks)	0.810	0.822	0.822	0.820	0.828	0.841	0.838
French Reference #6	0.888	0.885	0.871	0.881	0.879	0.885	0.881
(Metallized Plastic) SCS 1790 (3M Scotchcal 5400)	0.851	0.844	0.826	0.840	0.841	0.845	0.847
(Silvered Glass) R119 Float	0.919	0.904	0.825	0.883	0.889	0.894	0.889

(a) Standard Mirror

(b) Averaged Value

(c) #1 - First Generation Instrument
#2 & #3 - Second Generation Instruments

(d) Although instruments #2 and #3 can make 100% readings, for comparison purposes, the Aluminized Quartz Flat was used as a standard.

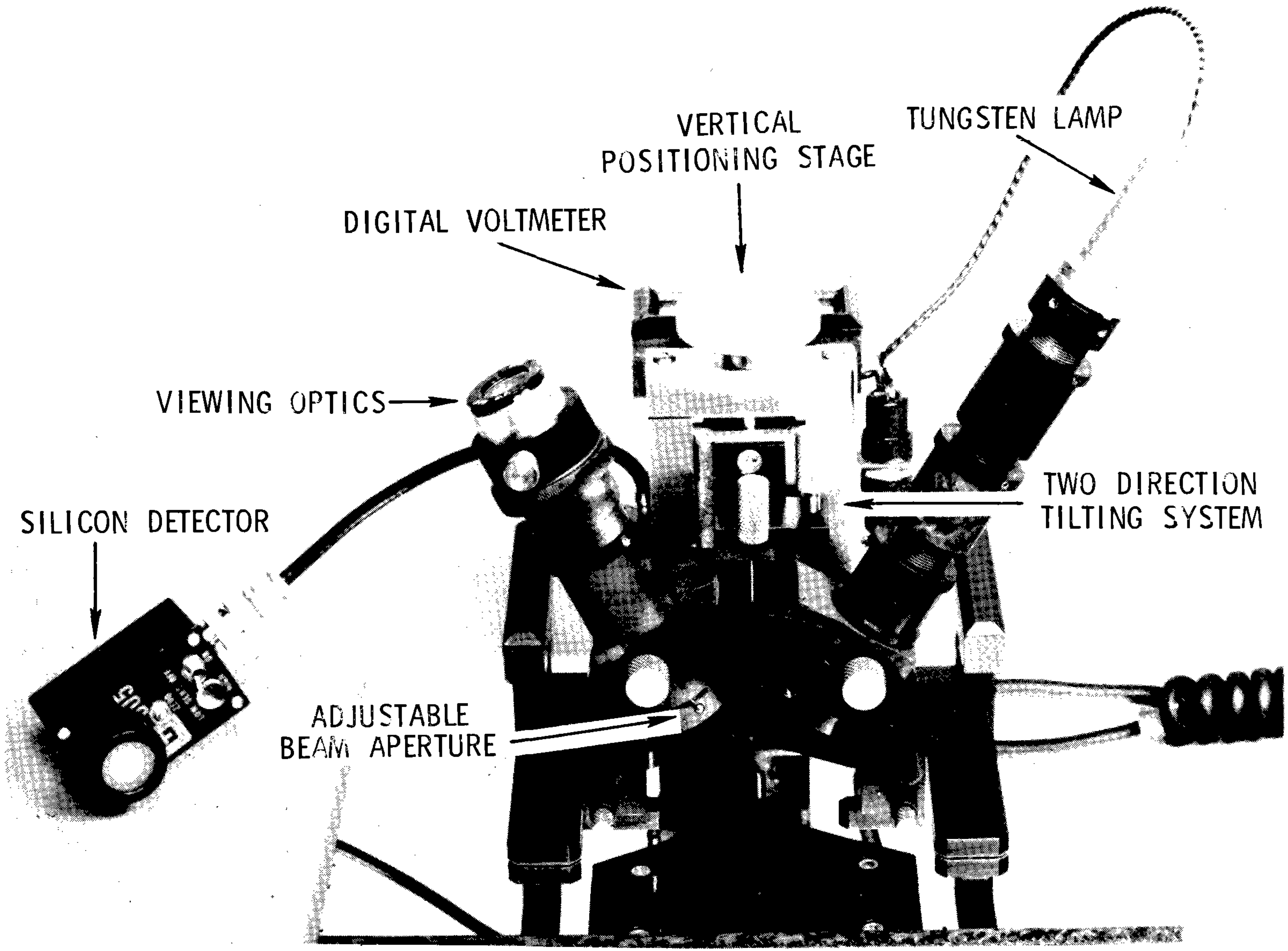

Figure 1. Photograph of Portable Specular Reflectometer

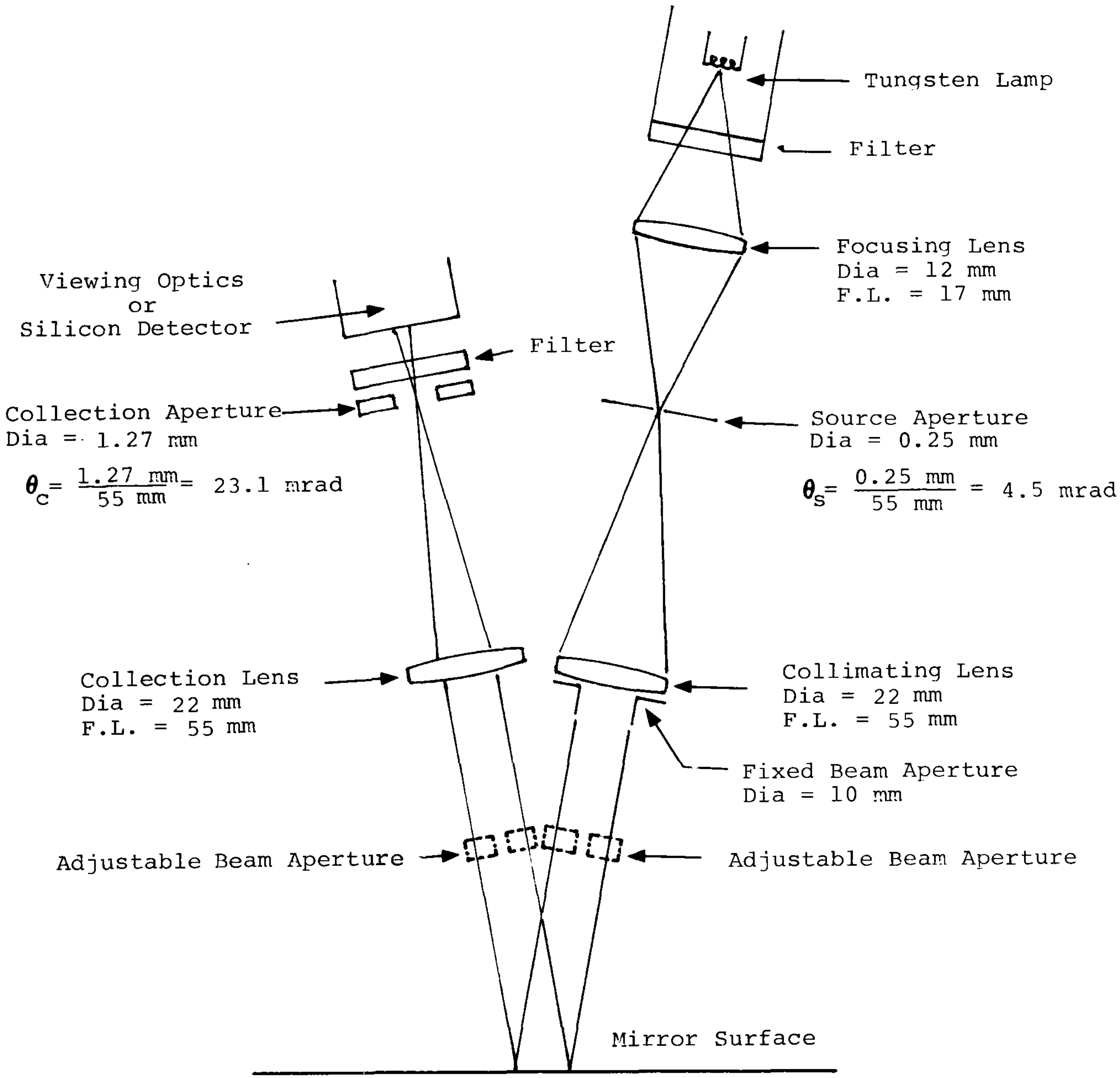

Figure 2. Schematic Diagram of Portable Specular Reflectometer

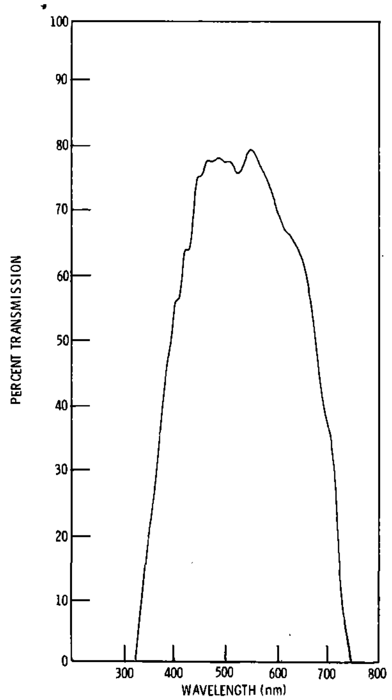

Figure 3. Transmission Curve for Corion Corporation Filter (IRS-2)

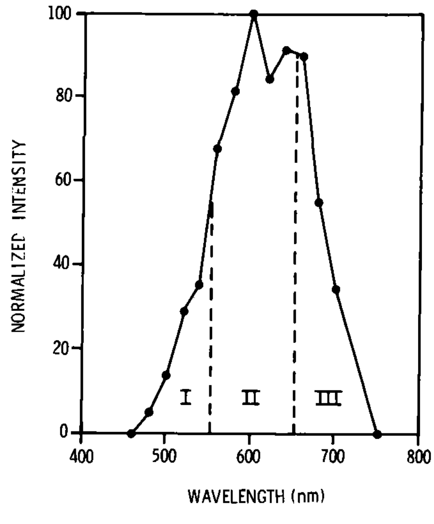

Figure 4. Instrument Spectral Bandwidth Curve

Joe Abbin
Div. 2324
Sandia National Labs
Albuquerque, NM 87185

James C. Adams
Production Engineer
Raymond Engineering
217 Smith Street
Middletown, CT 06457

Brandon Ahrens
Div. 4722
Sandia National Labs
Albuquerque, NM 87185

D. J. Allen
Research Assoc.
Foster Wheeler
12 Peach Tree Hill Rd.
Livingston, NJ 07039

Robert Alvis
Division 4725
Sandia National Labs
Albuquerque, NM 87185

Roger Assink
Division 5871
Sandia National Labs
Albuquerque, NM 87185

Harry Auld
Higgins, Auld & Assoc.
2601 Wyoming Blvd. NE
Albuquerque, NM 87112

F. L. Baker
Division 1473
Sandia National Labs
Albuquerque, NM 87185

James F. Banas
Division 4722
Sandia National Labs
Albuquerque, NM 87185

William J. Barattino
Chief DOE-USAF Liaison
AF Energy Liaison Office
USAF
DOE/ALbq. Ops. Ofc.
P.O. Box 5400
Albuquerque, NM 87115

Ralph Barber
Director
Wyle Laboratories
7800 Governors Drive
Huntsville, AL 35807

Gail Barton
EMA
615 Wyoming SE
Albuquerque, NM 87123

Carlo Bellecci
Cons. Engr.
CIRAES UNICAL
P.O. Box 379
Cosenza, Italia

Welcome W. Bender
Frank B. Wiens & Assoc.
2805 South Tejon St.
Englewood, CO 80110

Rick Bennett
Albuquerque TVI
525 Buena Vista SE
Albuquerque, NM 87106

Bud A. Benson
Sr. Prod. Dev. Spc.
3M
3M Center Bldg. 209-2N
St. Paul, MN 55101

Ken Bergeron
Division 4723
Sandia National Labs
Albuquerque, NM 87185

J. S. Bichler
Programs Mgr.
CSERC
328 Exec. Plaza
1200 Sixth Street
Detroit, MI 48236

A. W. Biester
Budd Company
Technical Center
375 Commerce Drive
Ft. Washington, PA 19034

P. M. Baca
Division 1472
Sandia National Labs
Albuquerque, NM 87185

William L. Bigelow
Proj. Engr.
ETEC
P.O. Box 1449
Canoga Park, CA 91304

Robert Bivens
Water Commissioner
City of San Bernardino
300 "D" St.
San Bernardino, CA 92401

Mark Bohon
Black & Veatch
11401 Lamar
Overland Park, KS 66212

Wilbur Boyd
Division 4722
Sandia National Labs
Albuquerque, NM 87185

Richard G. Brady
Vice President
Olympic Solar Corp.
208 15th St. SW
Canton, Ohio 44707

Kenneth Brakebill
Comm. Dev. Mgr.
Monsanto Company
800 N. Lindbergh Blvd.
St. Louis, MO 63166

Gregg Brucker
Suntec Systems
2101 Wooddall Drive
St. Paul, MN 55119

Robert Bullemer
Associate
TBA
1520 Wilshire Blvd.
Los Angeles, CA 90017

Kenneth Busche
President
Progress Industries
7290 Murdy Cr.
Huntington Beach, CA 92647

Larry Bush
Division 4714
Sandia National Labs
Albuquerque, NM 87185

Barry Butler
Div. Mgr.
SERI
1617 Cole Blvd.
Golden, CO 80401

Delmar Calhoun
Director
NMERI-UNM
Box 25 UNM
Albuquerque, NM 87109

Jack E. Cannon
Division 4721
Sandia National Labs
Albuquerque, NM 87185

Don Carroll
Physicist
Alpha Solarco
Suite 2230 1014 Vine St.
Cincinnati, OH 45202

Roscoe Champion
Division 4722
Sandia National Labs
Albuquerque, NM 87185

Hu Chung-Chang
Dept. of Mechanical Engr.
UNM
Albuquerque, NM 87131

Dave Chenault
President
Toltec Ind. Inc.
40th & East Main
Clear Lake, IA 50428

J. Cherng
New Mexico State Univ.
Box 350L
Las Cruces, NM 88003

G. Ronald Christ
Design Engr.
AAI Corporation
P.O. Box 6767
Baltimore, MD 21204

Ken Clark
Prod. Mgr.
Toltec Ind. Inc.
40th & East Main
Clear Lake, IA 50428

Nancy Clark
Division 1415
Sandia National Labs
Albuquerque, NM 87185

Clement Chiang
Division 4723
Sandia National Labs
Albuquerque, NM 87185

Bill Coady
Applied Solar Reso.
490 E. Pima Street
Phoenix, AZ 85004

Leon Cooper
Tech. Director
Solar America
2620 San Mateo NE
Albuquerque, NM 87110

Mike Dahl
Gen. Engr.
Water & Pwr Reso. Svc.
P.O. Box 25007
Denver Fed. Ctr.
Denver, CO 80225

Raymond L. Degner
Eng. Mgr.
Acurex Corp.
485 Clyde Avenue
Mountain View, CA 94040

Hans Dehne
Acurex Corporation
485 Clyde Avenue
Mountain View, CA 94040

Theodore A. Dellin
Division 4723
Sandia National Labs
Albuquerque NM 87185

Carl J. D'Haene
Manager
Glaverbel Belgium
Chaussee de la Hulpe 166
B. 1170
Brussels, Belgium

Nicholas DeLollis
Sandia National Labs
Division 4722
Albuquerque, NM 87185

Stephen C. Diamond
Staff Member
LASL
Box 1663 MS 985
Los Alamos, NM 87545

Bill Dickhart
Asst. Tech. Dir.
Budd Company
375 Commerce Drive
Ft. Washington, PA 19034

Vince DiNenna
Proj. Engr.
General Electric
King of Prussia, PA 19406

Fred Downum
Instructor
Albuquerque - TVI
525 Buena Vista SE
Albuquerque, NM 87106

Vern Dudley
EG&G
Div. 4721
Albuquerque, NM 87185

Don Duffy
Mgr. Sys. Anal. & Des.
Acurex Corporation
485 Clyde Ave.
Mt. View, CA 94042

Virgil L. Dugan
Division 4720
Sandia National Labs
Albuquerque, NM 87185

Mike Edenburn
Division 4723
Sandia National Labs
Albuquerque, NM 87185

Robert Edwards
Marketing Mgr.
Baird Corp.
125 Middlesex Turnpike
Bedford, MA 01730

Walter Eggert
Chief Des. Engr.
The Budd Tech. Center
375 Commerce Drive
Ft. Washington, PA 19034

Mel Eisenstadt
Mel Eisenstadt & Assoc.
7800 Phoenix Ave. NE
Albuquerque, NM 87110

John Erins
Engineer
Bituminous Mat'l Co.
444 S. 6th St.
Terre Haute, IN 47808

Rob Farrington
SERI
1617 Cole Blvd.
Golden, CO 80401

Max T. Faeth
President
Highland Plating
1128 N. Highland Ave.
Hollywood, CA 90038

David Feldman
Vice President
Texfel Corp.
10889 Wilshire Blvd.
Ste. 1460
Los Angeles, CA 90024

Dr. K. Thomas Feldman
President
Energy Engineering Inc.
1704 Stanford Dr. NE
Albuquerque, NM 87106

Don Fenton
New Mexico State Univ.
Las Cruces, NM 88003

Merton Fewell
Division 5513
Sandia National Labs
Albuquerque, NM 87185

Richard D. Franzen
Consultant
5717 Aspen Ave. NE
Albuquerque, NM 87110

Jim Freese
Division 5824
Sandia National Labs
Albuquerque, NM 87185

Stuart E. Friesema
Energy Prog. Mgr.
Jet Propulsion Lab
4800 Oak Grove Dr.
MC 264-801
Pasadena, CA 91103

Robert Gall
Division 3161
Sandia National Labs
Albuquerque, NM 87185

Dave Ganoung
Division 4714
Sandia National Labs
Albuquerque, NM 87185

Randy Gee
SERI
1617 Cole Blvd.
Golden, CO 80401

Roland Glatt
Chief Engr.
Eaton Corporation
I.D.O. Cleveland Div.
3249 E. 80 St.
Cleveland, OH 44104

Constance Golden
Ford Aerospace
300 Renaissance Ctr.
Detroit, MI 48243

Norman Grandjean
Division 4722
Sandia National Labs
Albuquerque, NM 87185

Vito Grasso
Proj. Engr.
Budd Company
375 Commerce Drive
Ft. Washington, PA 19034

Donald C. Gray
Black & Veatch
11401 Lamar
Overland Park, KS 66212

Conway Grayson
Off. of Energy & Consv.
DOE-NV
P.O. Box 14100
Las Vegas, NM 89114

Robert Gross
Division 5513
Sandia National Labs
Albuquerque, NM 87185

Bruce Hansche
Division 1552
Sandia National Labs
Albuquerque, NM 87185

E. L. Harley
Division 4725
Sandia National Labs
Albuquerque, NM 87185

Ray Harrigan
Division 4722
Sandia National Labs
Albuquerque, NM 87185

Thomas D. Harrison
Division 4721
Sandia National Labs
Albuquerque, NM 87185

Dr. Michael G. Heaviside
Mgmt/Tech Asst. Ofc. Clearing
House Coordinator
Dept. of Commerce
341 W. 2nd St.
San Bernardino, CA 92408

W. Heller
V. P. Sales
Winsmith
172 Eaton Street
Springville, NY 14141

Ronald W. Herman
Staff Scientist
Science Applications
200 Lomas NW
Suite 600
Albuquerque, NM 87102

Jim Higbie
BDM Corporation
2600 Yale SE
Albuquerque, NM 87106

James T. Hillman
Division 1415
Sandia National Labs
Albuquerque, NM 87185

Steven L. Hudson
Vice President
Energetics
833 E. Arapaho #202
Richardson, TX 75081

Robert L. Hughes
Division 1556
Sandia National Labs
Albuquerque, NM 87185

Gerald D. Hunter
Sr. Dev.
Honeywell
724 NE Harding
Minneapolis, MN 55413

Gus Hutchison
Solar Kinetics
8120 Chancellor Row
Dallas, TX 75247

Edward L. Klopfer
Vice President
WEBA Supply, Inc.
1570 A. Pacheco St.
Santa Fe, NM 87501

Joseph Jablonsky
Electro Magnetic Applic.
1025 Hermosa SE
Albuquerque, NM 87108

Dov Jacobs
Luz Engr/Kimcorp Inc.
3928 Montclair Rd.
Birmingham, AL 35213

Marcia Jenkins
Applied Solar Reso.
490 Pima Street
Phoenix, AZ 85004

Ronald Jenkins
Applied Solar Reso.
490 Pima Street
Phoenix, AZ 85004

Kenneth R. Johnson
Proc. Des. Engr.
Jacobs Engr. Group
251 S. Lake Street
Pasadena, CA 91104

Jeff Johnston
Solar Kinetics
8120 Chancellor Row
Dallas, TX 75247

Pat Joy
Solar Thermal Systems
200 Park Avenue
Florham Park, NJ 07932

Michael Kast
Engineer
Pacific Sun Inc.
439 Tasso St.
Palo Alto, CA 94301

L. F. Kautz
Kaiser Aluminum
P.O. Box 877
Pleasonton, CA 94566

M. I. Kazimi
Dir. Marketing
Parsons of CA
3437 S. Airport Way
Stockton, CA 95206

David D. Kenney
Dept. of Mech. Engr.
UNM
Albuquerque, NM 87131

C. Edward Kepler
Sr. Res. Engr.
UTRC
Silver Lane
East Hartford, CT 06108

Sol Kimerling
President
Luz Engineering
3928 Montclair Rd.
Birmingham, AL 35213

John C. Kiminas
CEO
Olympic Solar Corp.
208 15th Street SW
Canton, OH 44707

George S. Kinoshita
Division 4725
Sandia National Labs
Albuquerque, NM 87185

Paul Kirsch
Budd Company
Tech Center
375 Commerce Drive
Ft. Washington, PA 19034

James Knister
Vice President
Donnelly Mirrors
49 W. 3rd
Holland, MI 49423

Richard Kocinski
Analytic Services Inc.
400 Army Navy Dr.
Arlington, VA 22202

James Koteras
Division 5523
Sandia National Labs
Albuquerque, NM 87185

George Krivokopich
New Mexico State Univ.
Las Cruces, NM 88003

Ben Kunz
Secretary
Parabolite Inc.
1609 Cagua NE
Albuquerque, NM 87110

Lewis M. Larsen
Division 4722
Sandia National Labs
Albuquerque, NM 87185

Dennis L. Larson
University of Arizona
Tucson, AZ 85721

Gerald Leigh
NMERI-UNM
Box 25 UNM
Albuquerque, NM 87109

James A. Leonard
Division 4725
Sandia National Labs
Albuquerque, NM 87185

Allan Lewandowski
Staff Engr.
SERI
1617 Cole Blvd.
Golden, CO 80401

Brett Lewis
Division 5523
Sandia National Labs
Albuquerque, NM 87185

I. Earl Lewis
Prin. Engr.
Ford Aerospace
3939 Fabian Way
Palo Alto, CA 94303

Glen E. Loeppke
Division 4722
Sandia National Labs
Albuquerque, NM 87185

Robert E. Losey
Director - Solar Prog.
Wyle Laboratories
7800 Governors Dr. West
Huntsville, AL 35807

Norman F. Ludtke
Director
Research & Devlop.
Pioneer Engr. & Mfg. Co.
2500 East Nine Mile Road
Warren, MI 48091

Ron Lundgren
Division 4721
Sandia National Labs
Albuquerque, NM 87185

Alan R. Mahoney
Division 5824
Sandia National Labs
Albuquerque, NM 87185

Robert Maraschin
Sr. Mech. Engr.
Acurex Corp.
485 Clyde Ave.
Mt. View, CA 94042

P. L. Marjon
BER FEC 124
UNM
Albuquerque, NM 87131

Michael Marlow
Toltec Ind.
614 N. Johnson
Algona, IA 50511

Sam Martin
Division 2323
Sandia National Labs
Albuquerque, NM 87185

Bisagni Massimo
Engineer
AMN
via g. D'Annunzio 113
Genoa Italy 16121

Clayton L. Mavis
Division 8451
Sandia National Labs
Livermore, CA 94550

Don H. May
Solar Consultant
Highland Plating
1128 North Highland Ave.
Los Angeles, CA 90038

C. J. Mead
Vice President
Bohannan-Huston
4125 Carlisle Blvd. NE
Albuquerque, NM 87107

Jo Meglen
Associate
PRC/EAC
7600 Old Springhouse Rd.
McLean, VA 22102

Allen Monasmith
Proj. Engr.
Jacobs Engineering
251 S. Lake Ave.
Pasadena, CA 91101

Jim Moore
Sales Mgr.
Tona-West Inc.
1243 E. Beamer St.
Woodland, CA 95695

George T. Morin
Sr. Technologist
EG&G
Box 4339 Sta. A
Albuquerque, NM 87196

Robert Morton
Sr. Process Engr.
Jacobs Engineering
251 S. Lake Ave.
Pasadena, CA 91773

Charles Moyers
Dept. of Mech. Engr.
UNM
Albuquerque, NM 87131

Prem K. Munjal
Project Engineer
The Aerospace Corp.
P.O. Box 92957
Los Angeles, CA 90009

Karl D. McAllister
Section Head
EG&G
Box 4339 Sta. A
Albuquerque, NM 87196

William McCulloch
Division 4725
Sandia National Labs
Albuquerque, NM 87185

A. J. McDanal
E Systems
P.O. Box 226118
Dallas, TX 75266

Joseph McDowell
Division 2323
Sandia National Labs
Albuquerque, NM 87185

Ron McFayden
Mech. Sys. Engr.
Applied Solar Energy Co.
P.O. Box 1212
City of Industry, CA 91749

William R. McIntire
Physicist
Argonne Nat'l Lab
9700 S. Cass Ave.
Argonne, IL 60439

Ray McVeety
Division 4721
Sandia National Labs
Albuquerque, NM 87185

Douglas C. Nelson
Mgr. Prod. Engr.
Raymond Engineering
217 Smith Street
Middletown, CT 06457

Rick Nelson
Mgr. Dev. Progs.
Acurex Solar Corp.
485 Clyde Ave.
Mt. View, CA 94042

William D. Nettleton, Jr.
Proj. Mgr.
Dept. of Energy
1333 Broadway
Oakland, CA 94598

Janet Neville
Prog. Coordinator
DOE/SAN Ops. Ofc.
Consv. & Sol. Apps. Div.
1333 Broadway
Oakland, CA 94612

Alan O'Brien
Solar America
2620 San Mateo NE
Albuquerque, NM 87110

Joseph O'Gallagher
Sr. Res. Assoc.
Univ. of Chicago
Enrico Fermi Inst.
5630 S. Ellis Ave.
Chicago, IL 60637

Stephen Olah
Applied Solar Energy Corp.
15251 E. Don Julian Rd.
City of Industry, CA 91746

John Otts
Division 4721
Sandia National Labs
Albuquerque, NM 87185

George Pappas
DOE/ALO
Albuquerque, NM 87185

Larry Payne
Engineer
LaJet Energy Co.
301 S. Pioneer
Suite 111
Abilene, TX 79605

Y. K. Pei
Tech. Director
Owens-Illinois
1020 N. Westwood
Toledo, OH 43614

Ralph Peters
Division 4723
Sandia National Labs
Albuquerque, NM 87185

William E. Platt
Designer
Fletcher Const.
P.O. Box 764
Gunnison, CO 81230

Dale W. Ploeger
Mech. Engr.
SRI International
333 Ravenswood Ave.
Menlo Park, CA 94025

Marshall Prothero
Engineer
Bituminous Mat'l Co.
444 S. 6th
Terre Haute, IN 47808

William Putman
DSET Labs
Box 1850
Phoenix, AZ 85029

Duane Randall
Division 4725
Sandia National Labs
Albuquerque, NM 87185

Robert Randall
Division 2323
Sandia National Labs
Albuquerque, NM 87185

James Rannels
DOE/HQ
600 E Street NW
Washington, DC 20585

Theodore H. Reed
Division 2323
Sandia National Labs
Albuquerque, NM 87185

L. W. Rees
Suntec Systems
2101 Wooddall Dr.
St. Paul, MN 55119

John D. Reichert
Dept. of Electrical Engr.
Texas Tech Univ.
Lubbock, TX 79409

R. D. Reid
Proj. Manager
Ford Aerospace
Ford Road
Newport Beach, CA 92660

Tom Reitter
Engineer
LLNL
P.O. Box 808 L-46
Livermore, CA 94550

R. C. Reuter
Division 5523
Sandia National Labs
Albuquerque, NM 87185

Jack Roberts
Energy Tech Engr.
P.O. Box 1449
Canoga Park, CA 91304

Phil Rowe
Division 4714
Sandia National Labs
Albuquerque, NM 87185

Vincent Rubano
Chem. Engr.
Burns & Roe
185 Crossways Park Dr.
Woodbury, NY 11797

Earl Rush
Division 4722
Sandia National Labs
Albuquerque, NM 87185

Kenneth B. Sales
Adv. Engr.
General Electric Co.
Spartanburg Hwy
Hendersonville, NC 28739

Walt Schimmel
Division 4723
Sandia National Labs
Albuquerque, NM 87185

Rudolph Schindwolf
Division 4722
Sandia National Labs
Albuquerque, NM 87185

Edward Schmidt
Exec. Vice President
Alpha Solarco
Suite 2230
1014 Vine St.
Cincinnati, OH 45202

Robert J. Schnell
Dev. Engr.
Honeywell
724 Harding St. NE
Minneapolis, MN 55413

Larry Scott
President
SEMCO
2821 Eagle Dr.
Ft. Collins, CO 80526

Tony Schraub
Acurex Solar Corp.
485 Clyde Ave.
Mt. View, CA 94042

Joe Schrauth
Schott America
11 E 26th Street
New York, NY 10010

R. Schroter
Proj. Mgr.
Kaiser Aluminum
P.O. Box 877
Pleasanton, CA 94563

Dorner T. Schueler
DOE/ALO
Albuquerque, NM 87185

James Scott
Division 4700
Sandia National Labs
Albuquerque, NM 87185

Clifford S. Selvage
Division 8420
Sandia National Labs
Livermore, CA 94550

Michael G. Semmens
Director, Energy Sys.
The BDM Corporation
1801 Randolph Road SE
Albuquerque, NM 87106

Harold Sexson
Prod. Mgr.
Hexcel
Box 66
Casa Grande, AZ 85222

John Sharp
Division 4723
Sandia National Labs
Albuquerque, NM 87185

Jeanette Sharpless
Prog. Analyst
DOE/NV Op. Ofc.
2753 Highland Ave.
Las Vegas, NV 89102

Mark Sherwood
Exec. Director
Kingston Industries
205 Lexington Ave.
New York, NY 10016

Walter E. Shipp
National Bureau of Stds.
Washington, DC 20234

Travis Simpson
Texas Tech Univ.
Crosbyton Solar Pwr. Proj.
Lubbock TX 79409

Thomas A. Sinagra
Sr. Engr.
Bechtel National Inc.
P.O. Box 3965
San Francisco, CA 94119

Arthur J. Slemmons
Sr. Res. Engr.
SRI International
333 Ravenswood Ave.
Menlo Park, CA 94025

Martin E. Sorkin
Sr. Tech. Spec.
Dow Corning Corp.
18008 Skypark Blvd.
Suite 145
Irvine, CA 92714

Ram Srinivasan
Dept. of Mech. Engr.
UNM
Albuquerque, NM 87131

Roger Steen
Tech Strategy Ctr.
Honeywell Inc.
Roseville, MN 55113

Benno Steinmetz
Tona Midsouth
Box 22
Poplar Bluff, MO 63933

Ray Stiles
Proj. Engr.
Honeywell, Inc.
1700 W. Highway 36
Roseville, MN 55113

R. N. Stillwell
Dow Corning Corp.
Salzburg Road
Midland, MI 48640

William B. Stine
Professor
Cal Poly St. Univ.
Aero & Mech Engr. Dept.
San Luis Obispo, CA 93407

Robert Stromberg
Division 4714
Sandia National Labs
Albuquerque, NM 87185

Chris Thompson
Sales Engineer
Lynn Ind. Inc.
Wyandanch, NY 11743

Sig Thunborg
Division 4722
Sandia National Labs
Albuquerque, NM 87185

George Treadwell
Division 4722
Sandia National Labs
Albuquerque, NM 87185

Robert L. Treiber
Anaconda Metal Hose
698 S. Main Street
Waterbury, CT 06723

Samuel Tobias
Solar Kinetics
8120 Chancellor Row
Dallas, TX 75247

Leroy Torkelson
Division 4722
Sandia National Labs
Albuquerque, NM 87185

Roberto Visentin
Director Sol En Res Prog
CNR
PFE-CNR Via Nizza 128
Roma, Italy

Warren G. Votaw
Design Engineer
Morse Div. Borg-Warner
4650 Steele St.
Denver, CO 80216

Karl Wally
Division 4725
Sandia National Labs
Albuquerque, NM 87185

George Walters
Solar Kinetics
8120 Chancellor Row
Dallas, TX 75247

Jim Ward
President
Tona-West Inc.
1243 E. Beamer St.
Woodland, CA 95695

S. D. Warner
Euro Drive Inc.
2001 W. Main St.
Troy, OH 45373

A. D. Watt
President
Watt Engr. Ltd.
2142 T. 50 Road
Cedaredge, CO 81413

Herb Wessel
General Mgr.
City of San Bernardino
300 "D" St.
San Bernardino, CA 92401

Rodney V. White
Corp. Engr.
Owens-Illinois
1700 N. Westwood Ave.
Toledo, OH 43560

J. Weisiger
DOE/ALO
Albuquerque, NM 87185

Harold Wilkening
AAI Corporation
P.O. Box 6767
Baltimore, MD 21204

Frank Wilkins
Prog. Mgr.
DOE
600 E St. NW
Washington, DC 20585

Howard E. Wilkins
President
Applied Solar Reso.
490 E Pima St.
Phoenix, AZ 85004

Ronald Wilks
Manager
Lavelle Aircraft Co.
Sterling Street
Newtown, PA 18940

Carl Williams
President
LaJet Energy Co.
301 South Pioneer
Suite 111
Abilene, TX 79605

Jim Williams
Honeywell Inc.
1700 West Highway 36
Roseville, MN 55113

John H. Williams
Insights West
900 Wilshire Blvd.
Los Angeles, CA 90017

Lee E. Wilson
Manager
Energetics
833 E. Arapaho #202
Dallas, TX 75428

Gordon Winders
President
SunTrac Ind. Inc.
113 Flint Road
Oak Ridge, TN 37830

Mark Witkofsky
Dept. of Mech. Engr.
UNM
Albuquerque, NM 87131

George Witt
Mayor
City of Crosbyton
119 S. Ayrshire
Crosbyton, TX 79322

John Witt
Solar Kinetics
8120 Chancellor Row
Dallas, TX 75247

Doug Wood
Solar Steam
Fox Island, WA 98333

Richard L. Wood
Engineer
Lawrence Livermore Lab
P.O. Box 808
Livermore, CA 94550

Robert Workhoven
Division 4721
Sandia National Labs
Albuquerque, NM 87185

Albert Wright
Eng. Scientist
ONERSOL
222 Maple NE
Apt. 20
Albuquerque, NM 87106

☆U.S. GOVERNMENT PRINTING OFFICE: 1980—777-023/567